AFRL-RB-WP-TR-2011-3102

AIR VEHICLE INTEGRATION AND TECHNOLOGY RESEARCH (AVIATR)

Delivery Order 0013: Nonlinear, Low-Order/Reduced-Order Modeling Applications and Demonstration

Salvatore L. Liguore, Dale M. Pitt, Michael J. Thomas, and Nicholas Gurtowski

The Boeing Company

DECEMBER 2011
Final Report

AIR FORCE RESEARCH LABORATORY
AIR VEHICLES DIRECTORATE
WRIGHT-PATTERSON AIR FORCE BASE, OH 45433-7542
AIR FORCE MATERIEL COMMAND
UNITED STATES AIR FORCE

NOTICE AND SIGNATURE PAGE

Using Government drawings, specifications, or other data included in this document for any purpose other than Government procurement does not in any way obligate the U.S. Government. The fact that the Government formulated or supplied the drawings, specifications, or other data does not license the holder or any other person or corporation; or convey any rights or permission to manufacture, use, or sell any patented invention that may relate to them.

This report was cleared for public release by the USAF 88th Air Base Wing (88 ABW) Public Affairs Office (PAO) and is available to the general public, including foreign nationals. Copies may be obtained from the Defense Technical Information Center (DTIC) (http://www.dtic.mil).

AFRL-RB-WP-TR-2011-3102 HAS BEEN REVIEWED AND IS APPROVED FOR PUBLICATION IN ACCORDANCE WITH THE ASSIGNED DISTRIBUTION STATEMENT.

*//Signature//

LEONARD L. SHAW, Program Manager
Experimental Validation Branch
Structures Division

//Signature//

JOSEPH P. NALEPKA, Chief
Experimental Validation Branch
Structures Division

*//Signature//

DAVID M. PRATT, PhD
Technical Advisor
Structures Division
Air Vehicles Directorate

This report is published in the interest of scientific and technical information exchange, and its publication does not constitute the Government's approval or disapproval of its ideas or findings.

*Disseminated copies will show "//Signature//" stamped or typed above the signature blocks.

REPORT DOCUMENTATION PAGE

Form Approved
OMB No. 0704-0188

1. REPORT DATE *(DD-MM-YY)*	2. REPORT TYPE	3. DATES COVERED *(From - To)*
December 2011	Final	01 November 2009 – 07 November 2011

4. TITLE AND SUBTITLE
AIR VEHICLE INTEGRATION AND TECHNOLOGY RESEARCH (AVIATR)
Delivery Order 0013: Nonlinear, Low-Order/Reduced-Order Modeling Applications and Demonstration

5a. CONTRACT NUMBER
FA8650-08-D-3857-0013

5b. GRANT NUMBER

5c. PROGRAM ELEMENT NUMBER
62201F

6. AUTHOR(S)
Salvatore L. Liguore, Dale M. Pitt, Michael J. Thomas, and Nicholas Gurtowski

5d. PROJECT NUMBER
2401

5e. TASK NUMBER

5f. WORK UNIT NUMBER
A0F20C

7. PERFORMING ORGANIZATION NAME(S) AND ADDRESS(ES)
The Boeing Company
P.O. Box 516
St. Louis, MO 63166-0516

8. PERFORMING ORGANIZATION REPORT NUMBER

9. SPONSORING/MONITORING AGENCY NAME(S) AND ADDRESS(ES)
Air Force Research Laboratory
Air Vehicles Directorate
Wright-Patterson Air Force Base, OH 45433-7542
Air Force Materiel Command
United States Air Force

10. SPONSORING/MONITORING AGENCY ACRONYM(S)
AFRL/RBSVA

11. SPONSORING/MONITORING AGENCY REPORT NUMBER(S)
AFRL-RB-WP-TR-2011-3102

12. DISTRIBUTION/AVAILABILITY STATEMENT
Approved for public release; distribution unlimited.

13. SUPPLEMENTARY NOTES
PAO Case Number: 88ABW-2012-1349; Clearance Date: 14 Mar 2012.
Report contains color.

14. ABSTRACT
Dynamic response analysis tools used by the aerospace industry rely heavily on linear modal frequency response finite element methods. These linear methods are straight forward to use even in the analysis of a complex structural component that require a large number of degrees-of-freedom to model. However, this approach is not suitable for predicting the response of highly loaded thermal/acoustic aircraft structures that may respond in a nonlinear geometric manner. This type of problem requires a nonlinear transient analysis. The nonlinear analysis of a complex structural component is computationally prohibitive, especially for random acoustic response prediction which requires long duration time simulations. To overcome these computational deficiencies, nonlinear reduced order modeling (NLROM) methods have been developed. The objective of this effort is to further refine the NLROM methodology and validate it in the design and lab testing of a representative aircraft structural component. The final product of this program is a validated method and the quantified benefits of using the NLROM methodology.

15. SUBJECT TERMS
thermal, acoustic, nonlinear, dynamic, reduced order models

16. SECURITY CLASSIFICATION OF:			17. LIMITATION OF ABSTRACT:	18. NUMBER OF PAGES	19a. NAME OF RESPONSIBLE PERSON (Monitor)
a. REPORT	b. ABSTRACT	c. THIS PAGE			Leonard L. Shaw
Unclassified	Unclassified	Unclassified	SAR	274	19b. TELEPHONE NUMBER *(Include Area Code)* N/A

Table of Contents

List of Figures

List of Tables

Acknowledgements

This work is funded by the United States Air Force (USAF) Air Force Research Lab (AFRL/RB). The authors would like to acknowledge the technical support and guidance of AFRL/RB Leonard Shaw, Robert Gordon, Joseph Hollkamp, and Travis Wyen (AFRL/RBSVA). We also like to acknowledge the contribution of many Boeing teammates. First our Boeing Test and Evaluation teammates: Dale Schroeder, Bob Dieckelman, Tony Hauenstein, Brian Nelson, Matt Kardell, John Simms, Paul Crnic, Ken Stabenow, and Arnaldo "Cat" Aleman. The Manufacturing Team: Ryan Hanks, Tom Talley, Kevin Waymack, and Gregg Miltenberger. Also, we like to acknowledge analysis and design support for BR&T teammates Nick Eckstein and Bob Keeler. Finally, we'd like to acknowledge the assistance of NASA/LaRC; Steve Rizzi and Adam Przekop.

1.0 Executive Summary

Acoustic fatigue is an important design consideration for high speed jet aircraft. High acoustic loads often crack or damage skins and substructure of aircraft. This fatigue damage is due to the resonant bending response of lightly damped, stiffened skins exposed to extreme aero-acoustic environments. Cracks typically occur in minimum-gauge structures like flaps, fairings, and leading and trailing edges. Repair of this nuisance cracking is costly. It has been estimated that the total repair cost of sonic fatigue cracking in USAF aircraft exceeds $20M/year, Ref. (1).

The design of an acoustically loaded structure is complicated by the fact that high-intensity acoustic loading often causes nonlinear resonant response of aircraft structures. Other loading such as thermal and pressure only exacerbates the nonlinear response. Currently, the only nonlinear analysis approach for realistically complicated aircraft structure is based on full order time domain Finite Element Method (FEM) transient analysis. The nonlinear, fully coupled, full order FEM equations of motion must be integrated numerically over long time periods in order to capture the steady-state statistics of the random response. This is computationally prohibitive for all but the smallest and simplest models. As a result, even though it is known that important nonlinear response is missed, linear analysis methods are typically used in aircraft design to both reduce the problem order and uncouple the equations of motion. Aircraft designers and manufacturers know that these linear methods tend to over predict response in most parts of the structure resulting in the design of overweight structure. These linear methods have also been known to entirely miss localized areas of high response that later suffer fatigue cracking. The existing nonlinear FEM methods are computationally prohibitive as design tools.

To address this problem, the USAF Research Laboratory (AFRL) has internally developed a Nonlinear Reduced Order Modeling (NLROM) method that overcomes the computational burden of full order analysis while preserving its accuracy, Ref. (2) through (6). AFRL has successfully validated the NLROM method for relatively simple geometries. In the Phase I contracted research program with The Boeing Company, the NLROM methods was implemented in Matlab/NASTRAN and evaluated for its efficiency, practicality, and accuracy, Ref. (7). The NLROM method was found to be accurate and computationally efficient enough to be used in an aircraft design environment. This key Phase I conclusion indicated that the NLROM method could be used to improve aircraft design by enabling more trade studies, earlier in the design cycle resulting in better optimized aircraft designs. The Phase I evaluation was strictly analytical. One shortcoming in practicality, previously recognized by AFRL, is that the method requires selection of the important structural modes to be retained in the analysis. Currently, this selection is performed by the analyst, using engineering judgment with limited quantitative aids. The mode selection shortcoming was evaluated in the Phase II research effort as documented in this report. Additionally, Phase II implemented enhancements to the NLROM technique, and finally provided validation of the method against test data for a representative aircraft structure. Validation of the NLROM method will ultimately provide USAF life cycle cost savings through reduced repairs, better aircraft availability, and weight savings by making airframe structure more efficient. **The technology readiness of the NLROM methodology has been increased as a result of this research. Future suggested improvements to the methodology are put forth in Section 10.0 of this document.**

2.0 Introduction

Next generation advanced aircraft will use high strength and lightweight materials that are designed to endure combinations of extreme thermal, static, and acoustic loading. These severe loadings can produce nonlinear structural behavior. To better evaluate potential designs, nonlinear finite element analysis methods need to be used to evaluate structures under these extreme loads. Current acoustic fatigue design methods are based on linear structural analysis with empirical corrections to account for nonlinear behavior. But, these linear analysis methods have been found to be conservative, often resulting in over designed structures. These linear methods are inaccurate and often unable to capture the correct magnitude or spatial distribution of internal loads and stresses in structures. Acoustic fatigue is an important design consideration for high speed jet aircraft where high-intensity acoustic loading can cause nonlinear resonant response of aircraft structures. Hence, there is a need for an accurate, efficient nonlinear prediction method to design acoustic fatigue resistant structures.

The current aerospace industry state of the art in dynamic response analysis relies heavily on a linear approach. Commercial finite element codes make a linear modal frequency response of a complicated structure straightforward, even for large degree-of-freedom (DoF) systems. Experience has shown that this approach is not suitable for predicting the response of aircraft structures when they respond to high dynamic loading in a geometrically nonlinear manner. A nonlinear dynamic analysis in physical DoFs is computational prohibitive, especially for nondeterministic problems involving long simulation times. It is common practice to reduce the system size by modeling just a portion of the structure, e.g., a single bay in a multi-bay panel. However, with such an approach, important global dynamics are lost because the boundary conditions cannot be accurately modeled in a nonlinear dynamics analysis. To overcome these deficiencies, there has been significant effort in recent years in the development of the finite element based reduced-order analysis methods. The results of these recent advances were exploited in the current effort.

Acoustic fatigue is the dynamic loads problem most often encountered in-service especially on high performance aircraft. This was previously documented in Boeing's Aircraft Vehicle Technology Integration Program (AVTIP) Delivery Order No 27, "Identification of Dynamic Loads Problems and Solutions", Ref. (8). Although a large amount of effort is directed to sonic fatigue analysis during airframe development, a number of problems have historically appeared after aircraft are in service. In the past, design development analysis methods only considered the skin panels with idealized boundary conditions and plane wave excitation. The adjacent substructure was not included which not only affected the response through inaccurate modeling of boundary conditions, but often experienced failures itself. Based on experience, adequate analysis methods must include:

1. Spatially correlated loading with the proper coherence
2. Static pressure and thermal loads
3. Accurate boundary conditions and modeling of the adjacent substructure
4. Determination of the critical vibration modes that are not necessarily the first or lowest-frequency modes

Quick linear methods for predicting acoustic fatigue are in widespread use, and are relied upon because of schedule and cost constraints common to all programs, and because the methods were

thought to be generally conservative. However, these quick methods are generally inaccurate for highly nonlinear acoustic response applications.

Linear response methods have traditionally been used to analyze for acoustic fatigue. In the late 1980's and early 1990's, the development of the hypersonic NASA/USAF National Aerospace Plane (NASP) Program presented new challenges for thermal-acoustic fatigue. The use of new materials, high temperatures, and very high acoustic loads meant that linear methods of analysis were no longer valid. Research was initiated in the area of nonlinear acoustic response analysis and performed as part of cooperative R&D programs with NASA-LaRC, Old Dominion University (ODU) and AFRL. Boeing implemented its first nonlinear response method (called TAPS, for Thermal Acoustic Post-buckled response of Structures) based on the method developed by James Locke (Ref. (9)), and a panel code called Nonlinear Response of Panels (NRAP), based on early work by Professor Chuh Mei, Ref. (10). In the mid 1990's, Boeing evaluated the NASA-LaRC Equivalent Linearization (EL) method which was implemented in NASTRAN using DMAP alters, Ref. (11). This research was primarily driven by the new requirements for High Speed Civil Transport (HSCT) and the High Speed Research (HSR) programs. Boeing worked with NASA on the development of new methods and test techniques for acoustic fatigue. In 2001, Boeing provided NASA-LaRC with an evaluation of the Equivalent Linearization using a Stiffness Evaluation Procedure (ELSTEP) method. ELSTEP was used to predict strains in the Durability Patch test panel, Figure 1. This assessment discussed how the method operated, relayed some user experiences, and compared measured response to that predicted by the method. Although, the method was more accurate than the linear methods, it was in fact difficult to use. There was a steep learning curve to the ELSTEP procedure. There are approximately 40 files to be generated and tracked throughout the process.

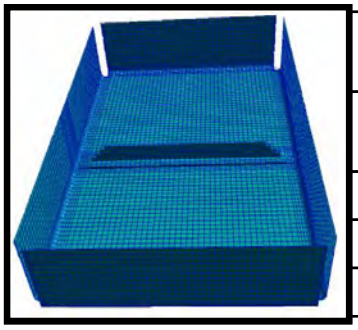

OASPL of Load	**Measured Strain**	**Predicted Strain** *nonlinear*		**Predicted Strain** *linear*	
dB re 0.0002 μbar	μin/in	μin/in	error	μin/in	error
165	956	848	-11%	2415	153%
156	472	476	0.8%	857	82%
144	165	186	13%	215	30%

Figure 1 – NASTRAN FEM and results from the ELSTEP evaluation

Acoustic fatigue analysis requires a good understanding of the variables used to perform the analysis. The input loads need to be well defined because they can be a combination of acoustic (noise), structural vibration, shock, thermal, static pressure, or in-plane loads. It's important to understand the static response as well as the dynamic response. Some acoustic fatigue problems consist of high static loads with relatively low acoustic loading, where the acoustic loads alone would not cause fatigue. Static or thermal loads causing buckling instabilities in the presence of moderate to high acoustic loads have created cracking problems. Very high acoustic loads cause a majority of acoustic fatigue problems. Linear dynamic frequency response methods are inadequate for these problems. There is a need for nonlinear reduced order methods that execute in an efficient and timely manner in a design environment.

The acoustic fatigue design process is shown in, Figure 2. In the early development phase of new aircraft, the first step in the acoustic fatigue design process is the definition of the internal and

external acoustic environment. If the aircraft is not a derivative aircraft, then the acoustic environment is defined using (a) measured data from similar aircraft, (b) empirical data, (c) wind tunnel testing, or (d) computational aero-acoustic (CAA). The second step in the process is to evaluate all structure in the affected high acoustic zones. This evaluation typically involves using simplified handbook or spreadsheet analysis methods. These methods are all linear in nature. These methods are essentially quasi-static response methods that use RMS based fatigue approaches. Regardless of the method, the objective is to quickly screen a large portion of the aircraft for potential acoustic fatigue issues. The methods typically rely on conservative design requirements (i.e., adding 3.5dB to maximum expected acoustic loads, conservative s-N curves and structural Kt's, and two to four times factor on Design Life requirements). This is meant to account for the uncertainty in the measured acoustic loads, s-N properties, nonlinearities, and the modal damping. In parallel with the analysis screening, there is a high cycle fatigue allowables test program to generate data for use with detailed finite element analysis.

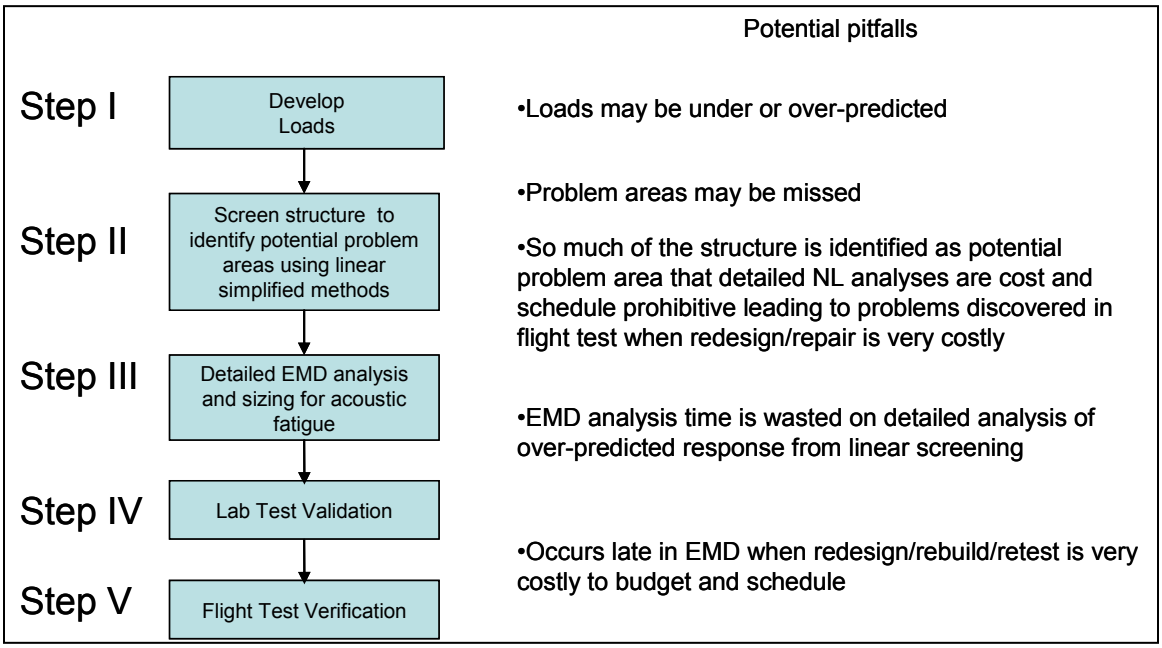

Figure 2 – Acoustic fatigue design process

The third step in the process is to evaluate any structure determined to be critical in Step II. This evaluation most likely is a detailed linear random frequency response finite element analysis (FEA) of the structure. This analysis process is used to finalize the design of the structure. This type of analysis is only performed on a few select critical panels. The effort involved in doing this type of analysis on a new development program is limited by schedule.

The fourth step in the process is to validate the analysis in Step III, typically using acoustic chamber testing of selected critical structure. This accelerated test will simulate the acoustic levels and durations expected in service. If the test article fails the validation test, then the process starts over with Step III. The fourth step validates the analysis process and design.

The fifth step is flight test validation of the preliminary acoustic design loads. The internal and external noise and vibration environment will be measured for the entire flight envelop and under realistic missions and flight maneuvers. These loads are stored in a database for retrieval and

comparison to the preliminary loads. If the loads from Step V are higher than expected, the acoustic fatigue design process would restart from Step II.

Acoustic fatigue problems that are identified during the development of an aircraft are not as costly as those experienced in service, because design changes can be incorporated during the on-going design activity. The process shown in Figure 2 emphasizes the need for better structural dynamic response prediction, better loads prediction, and better fatigue life calculation methods. Problems caught after large numbers of aircraft are in service are very costly, and can cost over $100M over the life of the fleet, Ref. (8).

Even with a well-documented acoustic fatigue design process, there can always be unexpected fatigue problems. The cause of these fatigue problems varies, but a major reason is a screening (Step II) or detailed (Step III) analysis process that incorrectly predicted the response stresses and fatigue life. Linear response analysis methods are not always conservative in the prediction of stresses in the substructure. All analysis methods need models that can accurately predict the correct stress distribution within the structure. Acoustic fatigue typically occurs near the edge of a panel or in the attachment structure at a stress concentration (Kt) detail. These Kt details may be fastener holes, bend radii, machined steps, welds, etc. These allowables are random s-N curves of new materials (Kt=1, R=-1), and allowables of joints (bonded, bolted, welded, etc.) using a test specimen like the one shown in Figure 3. Hence, a detailed FEA needs to model the structure accurately to be used with the allowables that are available. For instance, if there are joint allowables then the finite element model (FEM) does not need to model the joint in detail, but it needs to predict accurately the reference stress (note: the reference stress is a stress near the failure point in a low stress gradient location that is easily predicted in an analysis model, and which coincides with the placement of the strain gauges on the specimens). The model may also need to predict the correct loads at a stress detail, and then a “break-out” model with internal (element, grid point or constraint) loads may be used to predict stress in the detailed part.

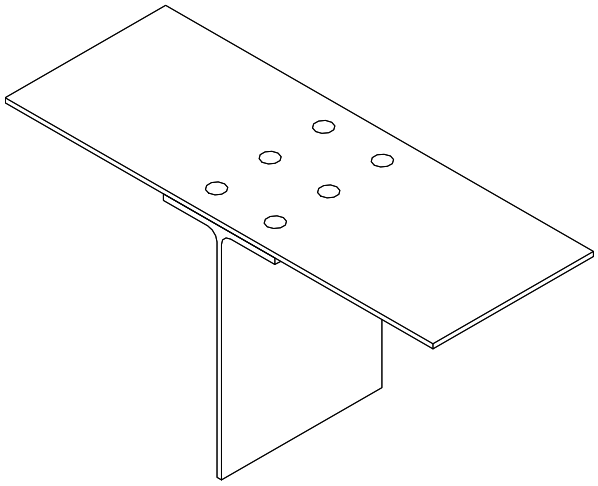

Figure 3 – Typical high cycle fatigue joint specimen

Another source of error in the detailed dynamic response analysis is a model that does not correctly predict the stress and internal loads distribution due to nonlinearities. When a panel undergoes nonlinear membrane response, the linear normal mode response is no longer a good approximation of the internal stress and loads distribution. Membrane response has the effect of increasing the loads transferred into the attachment structure. Although linear analysis may over

predict response and appears to be conservative, it could in fact predict the incorrect stress distribution which leads to an incorrect fatigue prediction because the stress hot spot is missed as demonstrated in Figure 4. The acoustic response simulation of the AFRL Durability Patch panel is depicted in the figure. The two analyses shown are a linear random frequency analysis, and the other is nonlinear reduced order method using two modes, both at an acoustic loading of OASPL=165dB. The figure clearly shows that the linear response method did not predict the correct internal distribution of loads and stresses. The nonlinear reduced order analysis correctly predicted the failure location and the magnitude of the measured RMS strain, as verified by test.

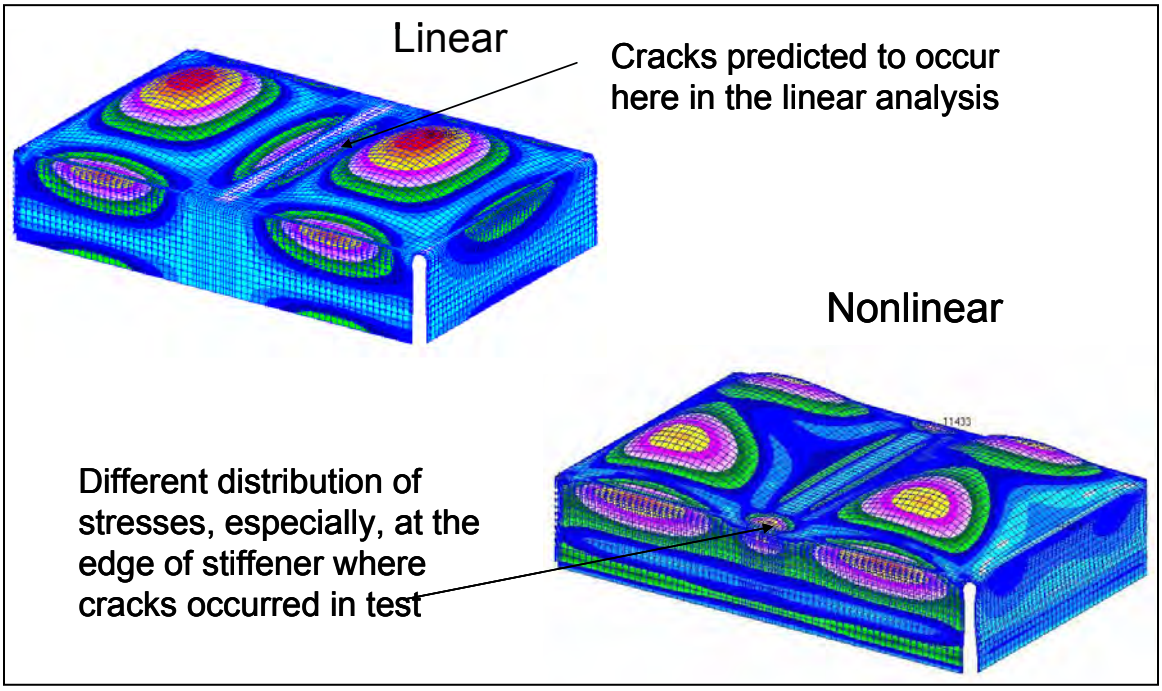

Figure 4 – Comparison of linear and nonlinear RMS stresses

The nonlinear analyses are required when large static loads are present which might be causing buckling or nonlinear static response. The presence of large static loads also affects the linear mode shapes and stress distribution.

These types of complex acoustic fatigue problems can only be analyzed using nonlinear geometric transient response analysis. Nonlinear response analysis have been shown to be a costly and time consuming analysis; especially, when a detailed FEM is used that may require a 100,000+ DoF to predict stress concentrations near holes, in shear clips, or in integrally machined multi-stepped flanges. The reduced order response approach allows for larger models with more refined mesh in the fatigue critical details. The mesh density (and element size) limits the use of a full-order physical degree of freedom analysis, since the stable time integration step is dependent on the size of the smallest (stiffest) element in the model. The reduced order modal methods avoid this limitation of time integration step size.

High acoustic loading can come from many sources: engine near field noise, engine exhaust, separated turbulent boundary layer (TBL), shock waves, vortices generated from lift improvement devices, rocket thrust, and high rate gun fire, Figure 5. For acoustic fatigue analysis, it's important to understand how the acoustic loads are distributed (amplitude) and correlated (phase) over the surfaces being analyzed. Some acoustic load sources are well

correlated over a large area (vortex-sheet or explosive blast), while others are not correlated at all (high rate gun fire), and still others are considered partially correlated (or correlated over a small area such as a single panel) with the degree of correlation degrading with distance (separated flow, exhaust impinged flow).

Figure 5 – Acoustic noise sources

Another important aspect of the acoustic panel response is the definition of the structural model. The boundary conditions of the model are very important. Many acoustic fatigue problems are actually in the substructure, so it's important to accurately model the substructure stiffness, since the stiffness is important in the development of nonlinear membrane response of thin skin panels. Correctly modeling the substructure is vital to predicting the correct "Hot Spot" for acoustic fatigue. However, to accurately capture these details requires the use of large models that are not practical for full nonlinear analyses in a production engineering environment. This is another advantage of using a nonlinear reduced order method. Transforming the problem into modal space to perform the time integration causes the size of the actual model to become less relevant.

The damping of the structure is also an important variable in the structural response of the panel. The damping comes from different sources, such as from the boundary conditions in the form of frictional damping, air pumping from high amplitude response, aerodynamic damping from high speed TBL or vortex flow, and material damping. All of these damping sources need to be accounted for in the acoustic fatigue analysis. For aero-acoustic applications, the aerodynamic damping (and mass and stiffness) can be best predicted using a coupled aeroelastic model (i.e., Solution 146 in MSC/NASTRAN.) Measured lab and flight damping levels in all types of metallic and composite structures, Figure 6, shows that the damping can vary considerably, Ref. (11). The reference level of ζ=0.016 is also shown.

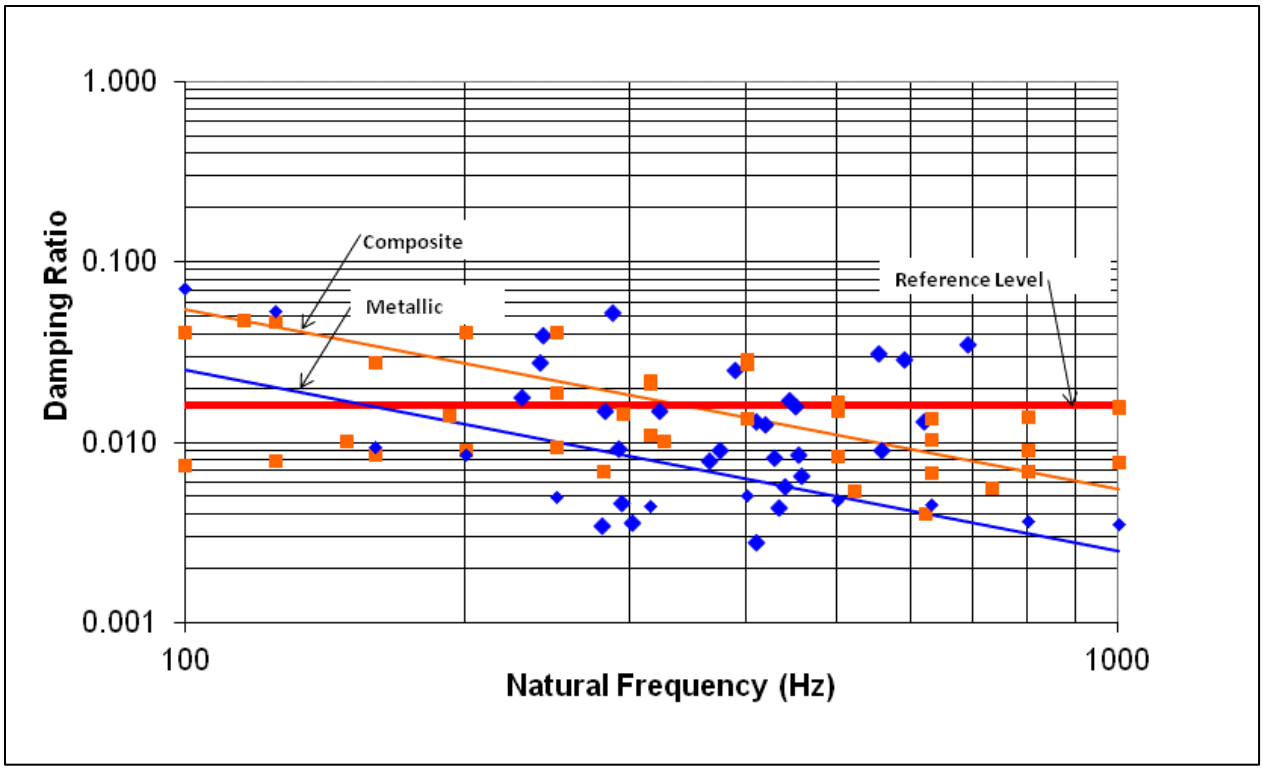

Figure 6 – Measured damping levels in all types of metallic and composite structures

Lastly, while predicting the correct acoustic response is very important, the ultimate objective is correctly predicting the fatigue life. Acoustic response is a random amplitude high cycle fatigue problem. Most fatigue data is generated from round bar axial constant amplitude test data at very high loads and low cycles. It's important to understand how to correctly apply the available fatigue data to the nonlinear acoustic fatigue problem. Most linear acoustic fatigue problems use random amplitude RMS beam bending fatigue data, which is directly applicable to most acoustic fatigue problems. However, nonlinear problems use constant amplitude fatigue data and apply cycle counting fatigue methods. It is felt that this later method produces a more accurate fatigue life prediction.

3.0 Methods, Assumptions, and Procedures

In this section, the Nonlinear Reduced Order Modeling (NLROM) method and its implementation is described. The first sub-section provides some background on Implicit Modal Condensation Method with Expansion (ICE). The second sub-section provides a description of the implementation of the method, while the third sub-section describes the Matlab NLROM tool. The final sub-section describes the acoustic fatigue analysis process and insights to using the NLROM method in a design application.

3.1 Background on Reduced Order Modeling Methods

A linear finite element model produces a system of equations as shown in Eq. (1), where *x* is the time varying vector of nodal displacements; *M*, *C* and *K* are the linear mass, damping, and stiffness matrices. The vector, *f(t),* represents the nodal force vector as a function of time.

$$[M]\{\ddot{x}(t)\}+[C]\{\dot{x}(t)\}+[K]\{x(t)\}=\{f(t)\} \quad (1)$$

The linear equations of motion can be uncoupled by transforming the physical coordinates, *x*, to modal coordinates, *p*, where *N* is the number of DoF in the finite element model.

$$\{x(t)\}=\sum_{i=1}^{N}\{\phi_i\}p_i(t) \quad (2)$$

Finite element models with a large number of degrees of freedom (DoF) can be reduced to a low order system of modal equations through a modal transformation. The normal mode shapes (eigenvectors), ϕ_i, are the basis vectors, and are computed from the eigenvalue solution of Eq. (1) when f(t)=0. The solution also produces the natural frequencies, ω_i. The mode shapes are scaled so that

$$\begin{aligned}&\{\phi^T\}[M]\{\phi\}=[I], \quad \{\phi^T\}[C]\{\phi\}=[\overline{C}]=diag(2\zeta_1\omega_1,2\zeta_2\omega_2,...2\zeta_n\omega_n)\\&\{\phi^T\}[K]\{\phi\}=[\overline{K}]=diag(\omega_1^2,\omega_2^2,...\omega_N^2)\end{aligned} \quad (3)$$

Typically only a few modes are retained and the displacement vector is approximated.

$$[\overline{M}]\{\ddot{p}\}+[\overline{C}]\{\dot{p}\}+[\overline{K}]\{p\}=\{\phi^T\}\{f(t)\} \quad (4)$$

For a nonlinear problem, the equation for r^{th} arbitrary mode can be written where θ_r represents the nonlinear stiffness part of the model.

$$[\overline{M}]\{\ddot{p}_r\}+[\overline{C}_r]\{\dot{p}_r\}+[\overline{K}]\{p_r\}+\lfloor\theta_r(p_1,p_2,...p_N)\rfloor=\{\phi_r^T\}\{f(t)\} \quad (5)$$

The nonlinear modal equations differ from linear modal equations in that they are coupled through the nonlinear function. Typically for structural applications, the nonlinear function is approximated by quadratic and cubic terms. The general form of the nonlinear function is

$$\theta_r = \sum_{j=l}^{L}\sum_{k=j}^{L} B_r^{jk} p_j p_k + \sum_{j=l}^{L}\sum_{k=j}^{L}\sum_{l=k}^{L} A_r^{jkl} p_j p_k p_l \qquad 6$$

Note that only L modes have been retained in the modal expansion. The general form of the nonlinear function is where the quadratic coefficients, B_r, and the cubic coefficients, A_r, belong to the ‘‘rth’’ modal equation and have indices to denote which group of terms they multiply. The reduced-order system of nonlinear modal equations can be solved by direct time integration, and time histories of the modal displacements result. Time histories of physical displacements are computed from the nonlinear modal displacements.

The nonlinear stiffness terms are evaluated using applied modal load solutions, Ref. (2). First, generate a set of force vectors, $\{F_k\}$, as physically-scaled combinations of the modal basis vectors, and compute nonlinear static solutions for the set of forces,

$$\{w_k\} = \left([K_{Lin}] + [K_q(w_k)] + [K_C(w_k)]\right)^{-1}\{F_k\} \qquad 7$$

Convert each $\{w_k\}$ and $\{F_k\}$ to the modal domain,

$$\{p_k\} = [\phi]^{-1}\{w_k\} \quad \{f_k\} = [\phi]^T\{F_k\} \qquad 8$$

Each modal equation has the form (only showing the cubic terms for clarity),

$$\ddot{p}_1 + \omega_1^2 p_1 + A_1^{111} p_1^3 + A_1^{112} p_1^2 p_2 + A_1^{122} p_1 p_2^2 + A_1^{222} p_2^3 = f_1 \qquad 9$$

Considering only the static response (ignoring the inertia term) and rearranging,

$$A_1^{111} p_1^3 + A_1^{112} p_1^2 p_2 + A_1^{122} p_1 p_2^2 + A_1^{222} p_2^3 = f_1 - \omega_1^2 p_1 \qquad 10$$

Considering all static modal load cases, a set of equations can be formed for each mode,

$$\begin{array}{l}\text{Load Case 1}\\ \text{Load Case 2}\\ \\ \text{Load Case n}\end{array}\begin{pmatrix} {p_1}^3 & {p_1}^2 p_2 & p_1 {p_2}^2 & {p_2}^3 \\ {p_1}^3 & {p_1}^2 p_2 & p_1 {p_2}^2 & {p_2}^3 \\ \cdots & & & \\ {p_1}^3 & {p_1}^2 p_2 & p_1 {p_2}^2 & {p_2}^3 \end{pmatrix} \begin{Bmatrix} {A_1}^{111} \\ {A_1}^{112} \\ {A_1}^{122} \\ {A_1}^{222} \end{Bmatrix} = \begin{Bmatrix} f_1 - {\omega_1}^2 p_1 \\ f_1 - {\omega_1}^2 p_1 \\ \cdots \\ f_1 - {\omega_1}^2 p_1 \end{Bmatrix} \qquad 11$$

This set of equations can then be solved using least squares for the nonlinear coefficients. These coefficients are then substituted back into the nonlinear modal equation, Eq. (5). This nonlinear modal equation is then solved using direct time integration. For the time integration, the model has the form below (for a two mode example),

$$\begin{Bmatrix} \ddot{p}_1 \\ \ddot{p}_2 \end{Bmatrix} + \begin{pmatrix} 2\zeta_1\omega_1 & 0 \\ 0 & 2\zeta_2\omega_2 \end{pmatrix} \begin{Bmatrix} \dot{p}_1 \\ \dot{p}_2 \end{Bmatrix} + \begin{pmatrix} \omega_1^{\,2} & 0 \\ 0 & \omega_2^{\,2} \end{pmatrix} \begin{Bmatrix} p_1 \\ p_2 \end{Bmatrix} + \begin{pmatrix} A_1^{111} & A_1^{112} A_1^{122} A_1^{222} \\ A_2^{111} & A_2^{112} A_2^{122} A_2^{222} \end{pmatrix} \begin{Bmatrix} p_1^{\,3} \\ p_1^{\,2} p_2 \\ p_1 p_2^{\,2} \\ p_2^{\,3} \end{Bmatrix} = \begin{Bmatrix} f_1(t) \\ f_2(t) \end{Bmatrix} \qquad 12$$

The modal transformation is then used to calculate the physical displacements. Nodal response quantities like velocity and acceleration can easily be calculated. But other response quantities like element stress, strain, or internal loads, are calculated in the original FEM. The physical displacements are used as enforced displacements to calculate the element stresses and loads. This operation can be performed on an element by element basis or on the whole model.

Note, only the bending modes are retained in the modal basis set. Nonlinear static load solutions obtained through nonlinear static finite element analysis are used in the estimation process. The effects of membrane stretching on the bending displacements are contained in the static cases and are incorporated into the estimated nonlinear terms for the bending modes. That is, the effects of stretching are implicitly condensed into the nonlinear terms of the bending mode equations. This approach has been referred to as the Implicit Modal Condensation (IC) method.

Modal bending amplitudes are computed directly from integrating the model. Physical bending displacements can then be computed from the modal amplitudes. However, physical membrane displacements cannot be obtained. As a result, linear membrane stresses and strains which depend on membrane displacements cannot be recovered using the finite element strain-displacement equations. An expansion process is sought to expand the modal bending amplitudes into membrane displacements.

The process requires a transformation matrix or membrane basis set. A procedure was implemented to estimate the membrane basis set from the static nonlinear solutions. This process is referred to as the Implicit Modal Condensation Method with Expansion (ICE), Ref. (3).

3.2 Implementation of the NLROM Method

For this study, the NLROM method was implemented based on the MSC/NASTRAN commercial finite element analysis software. NASTRAN is a standard FEA tool used within the aerospace industry. Hence, NASTRAN was chosen to demonstrate the practicality of NLROM, but the implementation could use any nonlinear FEA code. This implementation required writing a Matlab interface that could read and write results to and from NASTRAN bulk data and output (punch) files. Matlab was then used as the primary tool for computation of the nonlinear stiffness coefficients, the integration of the nonlinear modal equations, and for the computation of the inverse transformation of the results back to physical coordinates. The Matlab interface is also used to setup element stress post-processing operations.

The entire simulation procedure is shown in the Figure 7. First, a finite element model is developed in PATRAN, and linear static (SOL 101) is run to get the applied load nodal forces. Then, the normal mode solution (SOL 103) is calculated in NASTRAN. The mode shapes, frequency table, and grid point force balance is output. The grid point forces are a linear scalar of the eigenvectors. These loads cases are then used in the nonlinear static solutions (SOL 106).

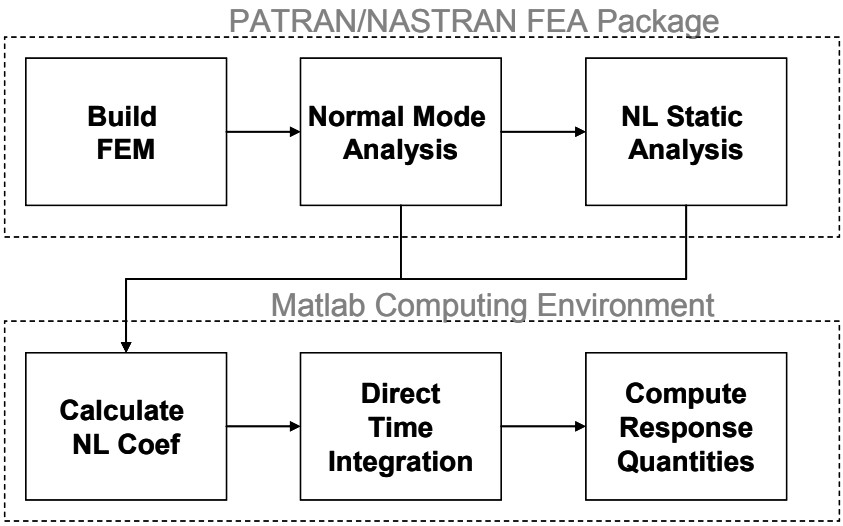

Figure 7 – NLROM simulation procedure, modified from Ref. (2)

The first step is to setup the FEM with the acoustic excitation load cases. This is done in PATRAN using the Load/BCs menu. The acoustic loading is defined as a distributed pressure loading over the face of CQUAD4 elements. An example of this technique is demonstrated for the curved aluminum beam test case. The beam is 18 inch long by 1 inch wide, 0.09 inch thick, and with an 81 inch radius of curvature. The acoustic loading is defined as two uncorrelated pressure load cases, as shown in Figure 8. These are unit pressure loads, 1 psi. This step is required in order to get the nodal distribution of the applied loads for the modal response calculation. The easiest way to get these nodal forces is by setting up a linear static solution (SOL 101), and requesting the applied loading at the nodes, OLOAD = ALL.

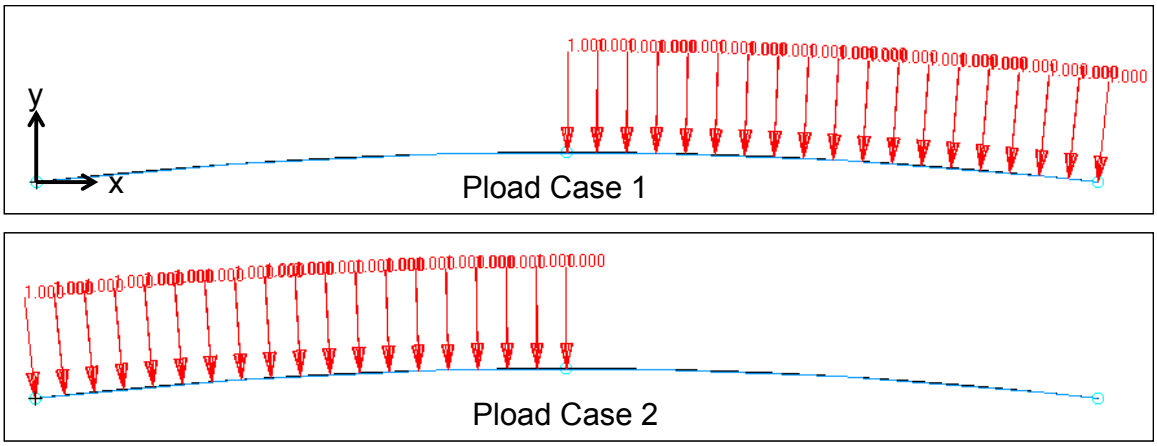

Figure 8 – Acoustic pressure load cases

The next step is the setup and solution of the linear normal mode solution (SOL 103). From this solution, the eigenvectors (VECTOR = ALL), frequencies (eigenvalues), and the grid point forces (GPFORCES = ALL) are requested in the CASE CONTROL. The eigenvectors and frequencies are used in the modal transient response solution and in the evaluation of the nonlinear stiffness coefficients. The grid point forces are used in the nonlinear (modal) static solutions. The grid point forces are a linear combination of the eigenvectors, and represent the internal loads in the model, if the eigenvector was a static deflection shape. The eigenvectors are mass normalized. This is set on the EIGRL card.

```
EIGRL 1 0. 1500. 0 MASS
```

This is the initial setup process, and it is shown in Figure 9. The next step is the determination of the nonlinear stiffness coefficients.

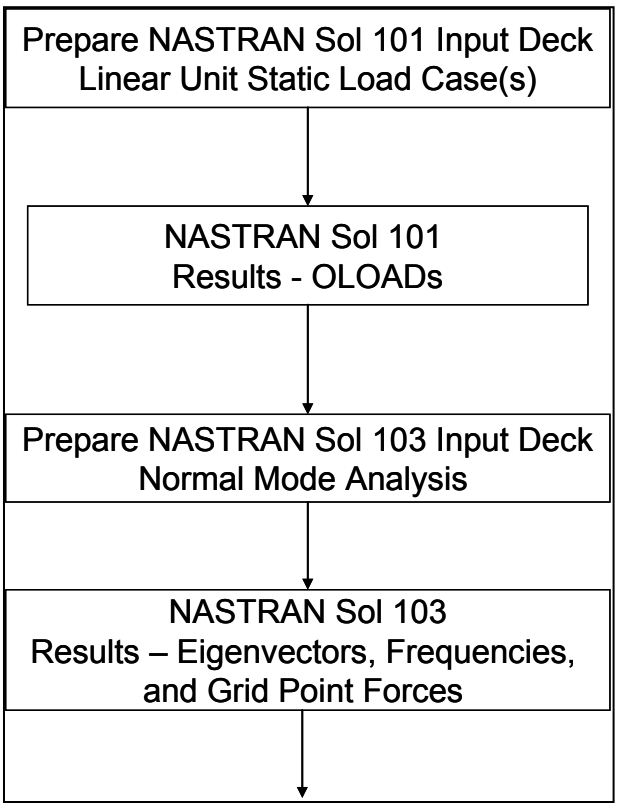

Figure 9 – Model setup steps

The number of static solutions is dependent on the number of modes. A one mode solution requires two static solutions, two modes require eight static solutions, three modes require 26 static solutions, and four modes require 64 static solutions, and so on. The number of nonlinear static solutions is given by the combination formula.

$$\binom{n}{K} = \frac{n!}{k!(n-k)!} \tag{13}$$

The total number of nonlinear static analysis is then,

$$\text{Total Number of NLStatic Solutions} = \binom{n}{1} \times 2^1 + \binom{n}{2} \times 2^2 + \binom{n}{3} \times 2^3 \tag{14}$$

The first term in Eq. 14 represents the one mode solution, the second term the two mode combination solutions and the third term all of the three mode combination solutions. The

process only requires up to three mode combination solution in order to calculate the coupled cubic nonlinear coefficients. For example, the load cases for the 3-mode model are shown below in Figure 10. These nonlinear static load cases are scaled combinations of the modal vectors, where c_1, c_2, and c_3, are scale factors to modal (grid point force) vectors (1, 2, and 3 respectively). The load scalars are chosen such that the nonlinear static solution results in physically appropriate displacements. In other words, the response has to be nonlinear in order to accurately determine the nonlinear stiffness coefficients.

	load cases												
	1	2	3	4	5	6	7	8	9	10	11	12	13
mode 1	c_1	0	0	c_1	c_1	0	c_1	c_1	0	c_1	$-c_1$	c_1	c_1
mode 2	0	c_2	0	c_2	0	c_2	$-c_2$	0	c_2	c_2	c_2	$-c_2$	c_2
mode 3	0	0	c_3	0	c_3	c_3	0	$-c_3$	$-c_3$	c_3	c_3	c_3	$-c_3$
	14	15	16	17	18	19	20	21	22	23	24	25	26
mode 1	$-c_1$	$-c_1$	c_1	$-c_1$	$-c_1$	0	0	$-c_1$	$-c_1$	0	$-c_1$	$-c_1$	0
mode 2	$-c_2$	c_2	$-c_2$	$-c_2$	0	$-c_2$	0	c_2	0	$-c_2$	$-c_2$	0	$-c_2$
mode 3	c_3	$-c_3$	$-c_3$	$-c_3$	0	0	$-c_3$	0	c_3	c_3	0	$-c_3$	$-c_3$

Figure 10 – Sample three mode problem with 26 static load cases

Note that for each mode, there is a positive and negative loading condition. This allows for fitting of the nonlinear stiffness coefficients through the entire range of structural motion. For instance consider the one mode case or load cases 1 and 18 above. Isolating these two load cases, the deflections and loads are output from the nonlinear solutions and the modal forces are calculated using Eq. 8. These modal forces and deflections are then plotted in the Figure 11. In the figure, there are five data points used to fit the nonlinear stiffness coefficients. Note the solution is forced through an intercept of zero, which is the trivial zero load case. A cubic polynomial is used to fit the load-deflection curve, and the three constants are the A_1^{111}, B_1^{11}, and K_1. Note, the frequency of this mode is $f_n = 258.4$ Hz, and $f_n = (1/2\pi)*(K_1/M_1)^{0.5}$, where $M_1 = 1.0$, mass normalized. This is the general process that is used to calculate the nonlinear modal stiffness coefficient. The process for getting the nonlinear modal terms is fairly straight forward, however, selecting the correct static load scalars and keeping the best modes for the modal solution is critical.

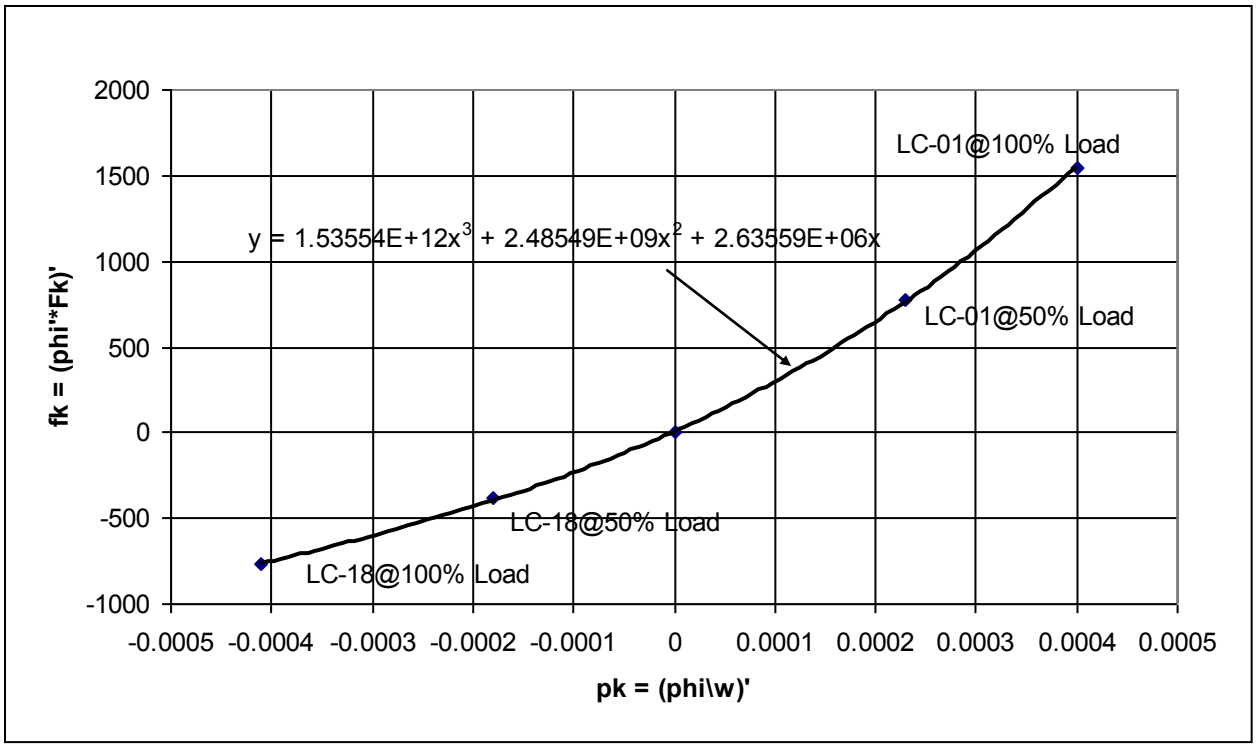

Figure 11 – Curved beam nonlinear static (modal) results for mode 2

The nonlinear static load case scalars can be approximated. As a rule of thumb, a thin shell structure will start to undergo nonlinear deformation when the deflection is ½ of the shell thickness. At one times the shell thickness the structure is nonlinear; at twice it is very nonlinear and the membrane stiffening effects should be significant. These criteria can be used as a guide for making an initial selection of the scalars. Since, the grid point forces are used to generate the load cases, and these are based on mass normalized eigenvectors. The 2*thickness divided by the max value of the mass normalized eigenvector is the approximated scale factor.

$$c_1 = \frac{2t}{|\phi_{\max}|} \qquad 15$$

For the above curved beam test case, the thickness is t=0.09 inch, and the max mass normalized eigenvector was $\phi_{max} = 102$. This yields a $c_1 = 0.0018$. For this analysis, $c_1 = 0.002$ and $-c_1 = 0.0004$. Note the scalar was not the same for the positive and negative load cases. This is because the beam would snap through (buckle) under the higher load value in the negative load case. It has not been determined if this is beneficial to the overall accuracy of the NLROM solution, but in general it's assumed that the static solutions are not allowed to buckle, since this would invalidate the cubic polynomial least squares fit of the nonlinear modal stiffness coefficients.

A few things to consider when setting up the nonlinear static solutions:

(1) The load scalars are not arbitrary, and need to produce physically significant deflection results.
(2) The loads should not produce a buckled shape. But, they should produce nonlinear deflections, otherwise, the cubic (hardening) and quadratic (softening) nonlinear stiffness terms will not be correct.

Curved structure, like this beam, is highly sensitive to snap-through on the negative loading. The snap-through response is shown in Figure 12. The intermediate results for the nonlinear solution is shown for a modal load scalar of c_1=-0.002. At 40% of this load, the model is snapping through as shown by the solid diamond symbols. The solid curve is the cubic polynomial fit, which is obviously not a good approximation.

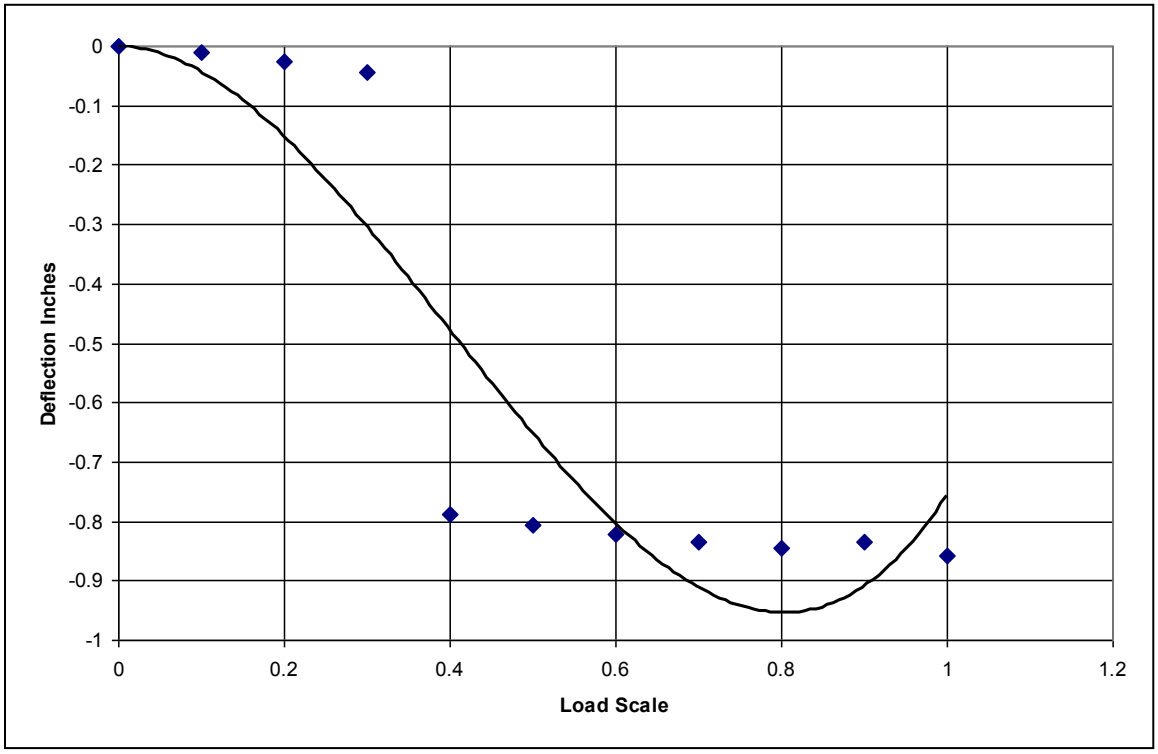

Figure 12 – Nonlinear static analysis of mode 1 loads (snap-through analysis)

The selection of the nonlinear static load scalars can be an iterative process. The user needs to be prepared for this and not initially select a lot of modes for the solution. It's best to select only the primary modal contributors first, and adjust the scalars for the modes. For the higher order modes, the load scalars can usually be set at much lower values. The nonlinear hardening and softening effects seems to diminish with increasing modal order, or at least this effect is less important. Typically, the level of acoustic energy decreases with frequency for most aero-acoustic fatigue applications. Hence, for the higher order modes, there doesn't seem to be much shifting in natural frequencies or peak broadening. This is based on observed test data, which will be presented later in this report.

The higher order modal combination load cases typically produce solution convergence problems if the load scalars are too high. It's possible to go into the input deck and change the troubling load cases on an individual basis. If running a 20 mode solution which requires 9920 combination loads cases, then this can be a daunting task. Hence, it seems best to just set the higher mode scalars at a single lower value that won't produce any solution problems. This seems best as long as those modes don't significantly contribute to the overall critical stress response.

The general rule of thumb found in this study is that the primary modal contributors should produce deflections up to one to two times the thickness, and the higher order modes can be much less but at least half the thickness.

3.3 Matlab User Interface – NLROM

The NLROM method is not a standard analysis procedure in any commercial FE code. Hence, the calculation of the nonlinear stiffness terms and the integration needs to take place outside of any standard analysis package. We chose to use Matlab for our primary computation tool because it's easy to develop a graphical user interface, matrix calculations are easily programmed, and the nonlinear equations are conveniently solved using Matlab ODE solver. The following describes the NLROM Matlab Tool that was used to perform all of the studies described in this report.

As previously mentioned, MSC/NASTRAN was selected as the structural analysis code that would be the basis for the model. NASTRAN was chosen because it is a widely used structural analysis tool, and it's a standard method for performing acoustic response calculations. Abaqus was also considered. Abaqus is a nonlinear structural analysis tool, and is primarily used for nonlinear transient response calculations. But, since we didn't require these aspects of Abaqus, we went with a tool that has the widest base of use in NASTRAN.

The setup for the Static and Normal Mode Solutions of the NASTRAN model are done in PATRAN. The models (bulk data files, or *.bdf) can be run using PATRAN's Analysis Manager or by running the NASTRAN windows executable program. The second option has been integrated into the Matlab NLROM Tool.

Below is a screen shot of the NLROM Tool, Figure 13. The tool was written for Matlab R2007b. There are MEX files compiled with the script. These MEX files are C++ programs that perform certain I/O functions. The script is generic and runs on most versions of Matlab, but the C++ functions need to be recompiled using the user MEX utility.

There are four different functions to the Matlab tool: (1) Model I/O and Solution, (2) ODE Solution, (3) Nodal Response Post-Processing, and (4) Element Post-Processing Setup. These operations will be explained as they pertain to the evaluation process.

First, there is the linear model solutions and results I/O,
Figure 14. As previously mentioned, these models are setup in PATRAN, but they can be submitted to NASTRAN from this tool. This is just for convenience. But more importantly, the PUNCH results from NASTRAN are scanned and the results are read into Matlab.

At this point, the linear modal transient response can be calculated and nodal or element post-processing can be performed. On the interface, we can select a range of modes or just a list of modes, and also a prescribed modal damping ratio, Figure 15. It's important to understand what the linear response is before running the nonlinear response, Figure 16. From the linear response, we can quickly estimate the critical modes to the structural response. This aids in the selection of modes to use in the nonlinear solution. This doesn't guarantee the best selection of modes but it does yield a good first estimate. Also, an initial estimate of the response can be compared to the nonlinear solution.

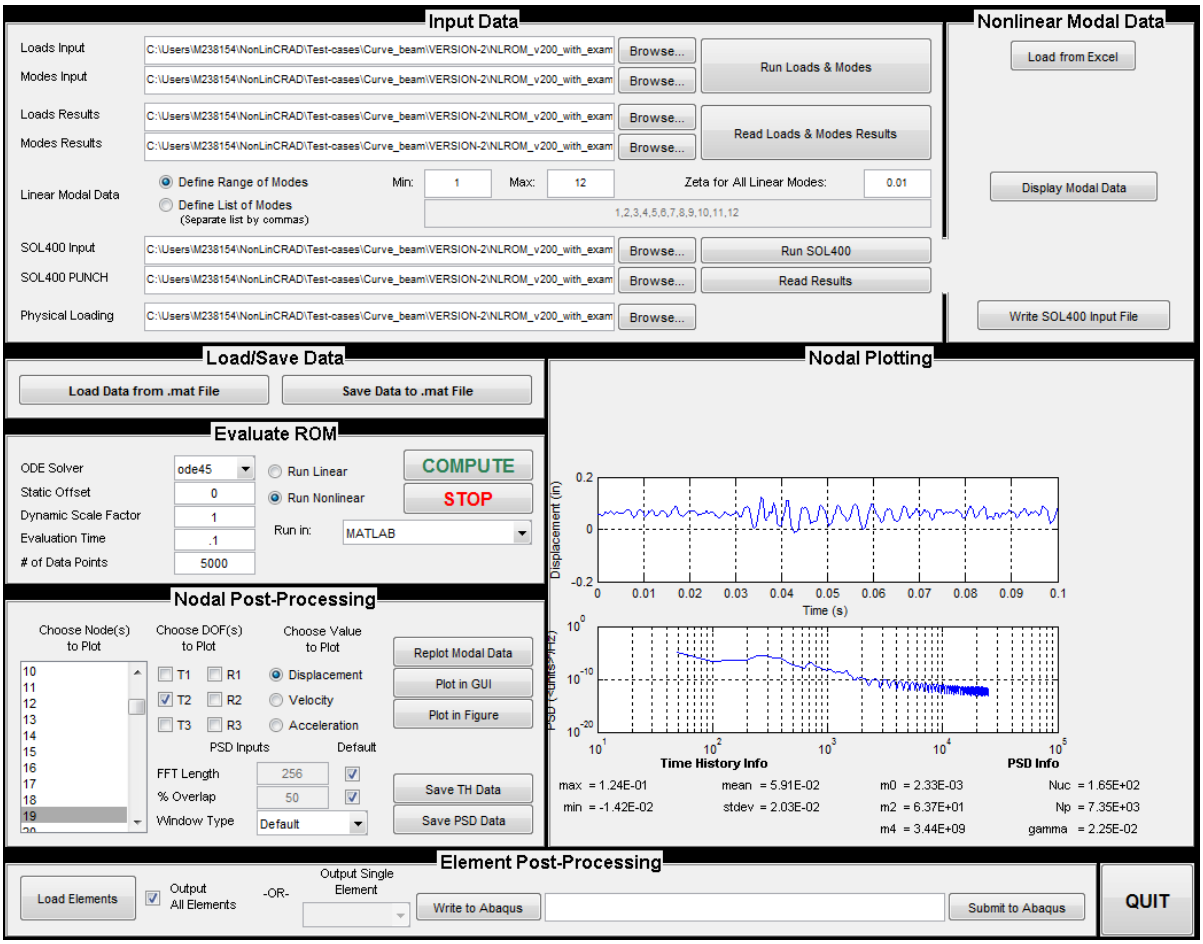

Figure 13 – Matlab NLROM tool: GUI

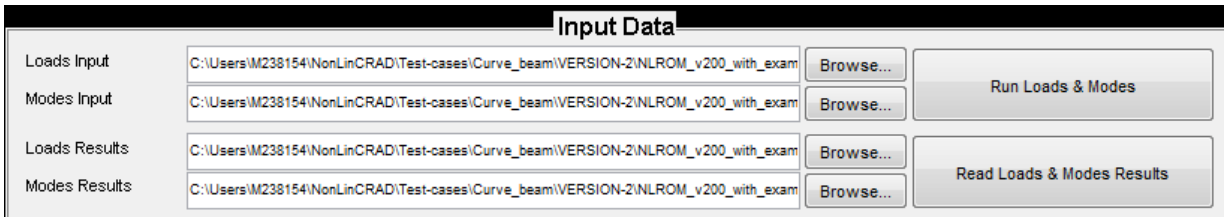

Figure 14 – Matlab NLROM tool: loads and modes model input and output

Figure 15 – Matlab NLROM tool: selection of linear modes

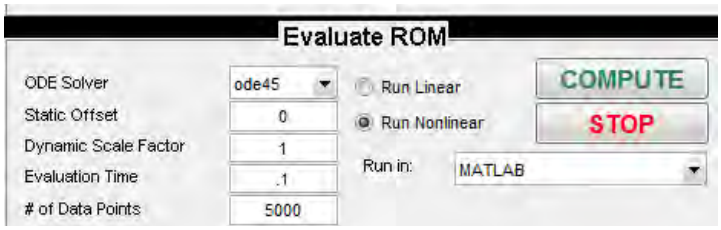

Figure 16 – Matlab NLROM tool: evaluation of linear response

The next step is selecting the modes and setting up the nonlinear static solutions, Figure 17. This is easily performed in the interface. The mode numbers, their scale factors (+ and -), and the modal damping ratio is listed in the table. Matlab sets up the NASTRAN SOL 106 model. This is a huge time saver. This could be done in PATRAN, but it would be a very tedious and error prone process. The Matlab script writes out all of the modal load cases combinations. The tool is currently limited to 10 mode solutions, and this is just because it doesn't seem practical to run thousands of nonlinear static solutions. The user can submit the job from the interface locally on the same machine, or to a network computer cluster outside of the Matlab tool. But once the solution has completed, the user reads the displacement results back into Matlab. The script also calculated the nonlinear modal stiffness terms (A's and B's), and it's ready to perform the ODE solution. A key result that comes out of the nonlinear static solution is the max displacements for each load case output to an ASCII file. The user can quickly scan this file and determine if the nonlinear solutions produced structural significant displacements.

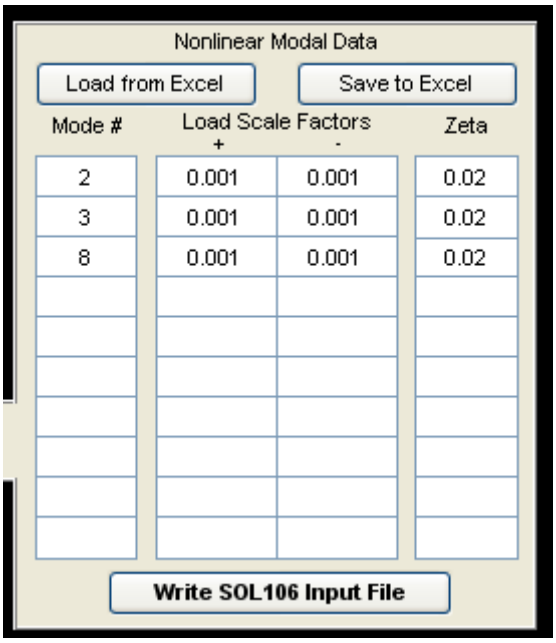

Figure 17 – Matlab NLROM tool: nonlinear static solution setup

Once the ODE solution has been performed, the user can perform post-processing of node results (Displacement, Velocity, and Acceleration) for any Node and DoF in the model, Figure 18. The physical results are displayed as a time history and a PSD. The time history statistics (Min, Max, Mean, and Standard Deviation of the time history) and PSD statistics (m_0, m_2, m_4, N_{uc}, N_p, and γ) are also given, Figure 19. The statistics m_0, m_2, and m_4 are zero, second, and fourth spectral moments, respectively. These are calculated using the WAFO routine, spec2mom. N_{uc} and N_p are the number of upward zero-crossings, and number of peaks, respectively. Gamma, γ, is the irregularity factor. A $\gamma = 1$ means that for every valley there is a corresponding peak. A sine wave or narrow band signal would produce a γ=1.0. If γ is less than 0.5, then the signal is a wide band process. If it's close to zero, then its broad band white noise process. Being able to post-process the nodal results interactively is a great asset. This allows the user to quickly scan through displacement response to make sure the solution seems reasonable. It's entirely possible at this point that the user might want to rerun the nonlinear modal static solutions, and formulate a different nonlinear modal model with different modes or based on different scalars.

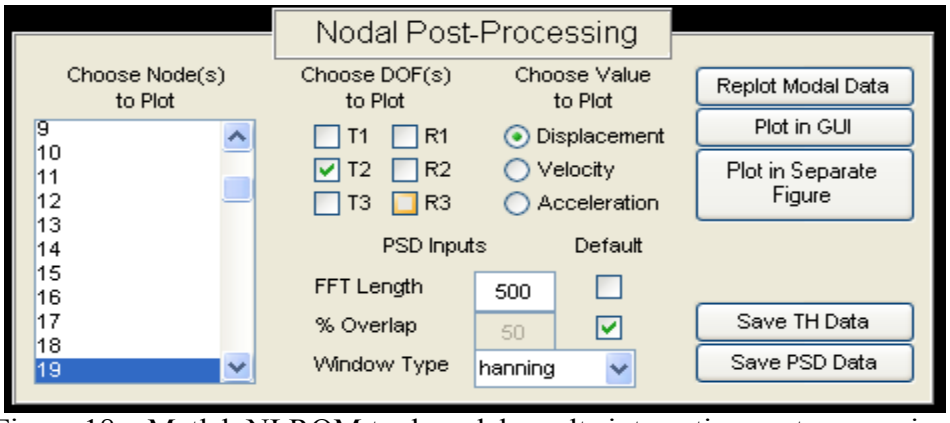

Figure 18 – Matlab NLROM tool: nodal results interactive post-processing

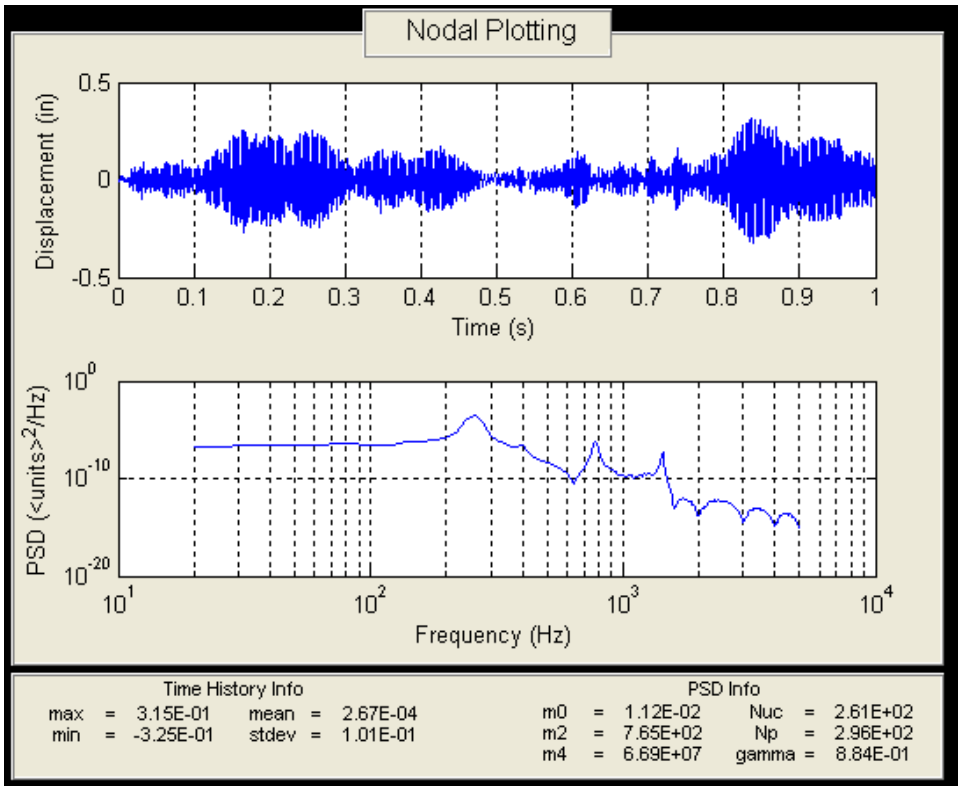

Figure 19 – Matlab NLROM tool: nodal post-processing plots

The final step is to post-process the element results, Figure 20. From the NLROM tool, the user has two options. The first option is to output displacement time histories for every DoF attached to a single element. This sets up an explicit time integration solution in Abaqus. The nodal displacement time histories are applied as enforced displacement boundary conditions. Abaqus was chosen for its convenience of setting up this type of problem. NLROM reads the SOL 101 model, and extracts out the selected element grid point and grid point coordinates. Also, the material properties and shell properties are read into Matlab, and output to the Abaqus model. The second option is to output whole model results. The method uses the original modal grid point forces, and the nonlinear static load cases. Based on the modal response, RMS response is calculated for each mode to the applied acoustic loading. When the SOL 106 model was run, the script finds the translation DoF that give the highest response. The script then calculates the time history response for these same translational DoF. These become a reference to scale the modal

load cases. The script then sets up a new SOL 106 model, with new RMS based scale factors. The user would run this model and review the results in PATRAN. The model would yield useful information related to distribution and magnitude of the stress, strains, and loads in the model. These results are not used for the fatigue calculation, but more for pin-pointing the critical stress hot spots. After post-processing the whole model results, the analyst should then post-process this critical element(s) time history solution. The final step is to take the element stress time history and calculate the fatigue life.

Figure 20 – Matlab NLROM tool: element results post-processing

There are other features to the NLROM tool that are very useful, Figure 21. The first is being able to save the current Matlab matrices in a database. This allows the user to reload this database later to auto-fill in all of the enter information and model results. The second feature is being able to scale the acoustic loading without having to generate a new loading file. A static offset can also be added to the loads. Shown in Figure 16, the integration parameters Solver Time, and number of output points can be controlled. Also, any of Matlab's ODE solvers can be chosen. This is useful if one solver is having numerical difficulties.

Figure 21 – Matlab NLROM tool: additional NLROM interface features

3.4 General Acoustic Fatigue Analysis Process

In this section, the process for using the NLROM method for acoustic fatigue analysis is described. There are several steps that are common between the linear random frequency response solution, the nonlinear full-order solution, and the reduced order solution. This includes building the FEM, defining the acoustic loading, and performing the fatigue calculations. The primary goal is to predict fatigue life using calculated element stress time histories. The problem with nonlinear analysis is that the critical stress location is not necessarily known a priori. Random transient response solutions require extensive memory if all element stress components time histories is to be output. So usually, only a small set of critical elements and nodes are included in the output request sets.

The process starts with the Model Checkout phase, as shown in Figure 22. These are the common steps between the linear methods and nonlinear reduced order methods. The analyst starts by developing the FEM. Secondly, the acoustic load case is defined (i.e., apply the pressure). Then, the normal mode and unit linear static pressure runs are performed. This is part of the standard analysis process. During this step, the analyst is checking for the rigid body modes, checking the model mass, checking the loads, etc. The analyst may also check static and modal element stresses and nodal displacements. The element stresses are scaled to the mode shapes, but it is useful to determine which elements will have the highest stresses for selected modes. Similarly, the unit static pressure (which is the acoustic load condition(s)), also yield information about which elements might have the highest response when the nonlinear transient response is run. Therefore, this process is performed first, and it determines which modes might

be important and which reference results from elements and nodes need to be reviewed during the nonlinear analysis.

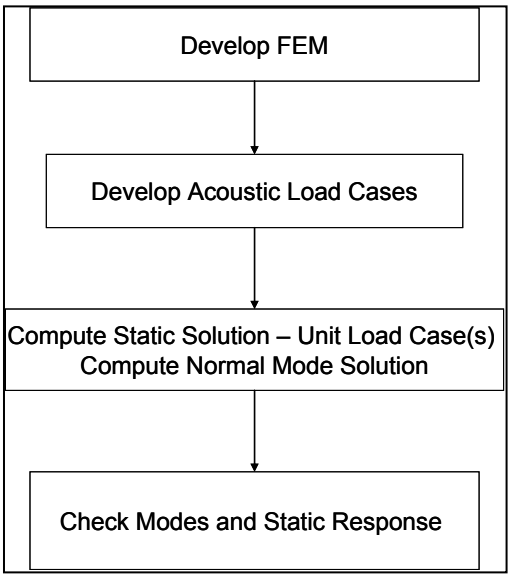

Figure 22 – Model checkout process

Once the unit static and normal modes solutions have run, then the analyst selects modes that will be within the frequency range of the acoustic excitation. Then, before setting up the NLROM, the analyst performs a linear modal transient response solution, Figure 23. This step runs the linear modal transient response with the actual acoustic load condition(s). From these results, the analyst can better determine the modes to use for the nonlinear analysis. The user has selected reference nodes and elements based on the linear normal mode solution. They will review the linear nodal displacements and element stresses at these previously identified reference locations.

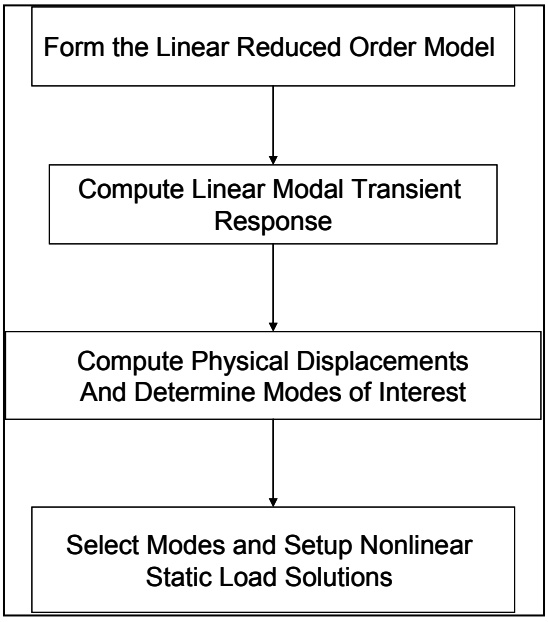

Figure 23 – Pre-NLROM process linear modal response procedure

The next steps in the process are to setup and run the nonlinear response, Figure 24. First, the analyst runs the nonlinear static solutions and calculates the nonlinear stiffness terms. Then, the analyst computes the nonlinear modal transient response. The analyst will then review the displacement (or accelerations) at the reference nodes. Based on the modal response, the analyst then selects elements to post-process for the stress time history. The analyst may also elect to review the nonlinear static solutions that were run to get the nonlinear stiffness terms. The analyst needs to scale these results to the max or RMS modal displacement based on the nonlinear response. From these results, the analyst can also determine or verify the elements initially selected for the element output reference set. The analyst performs the post-processing analysis, output the element stress time histories, and then performs the fatigue analysis. The process repeats for each element that's part of the reference set.

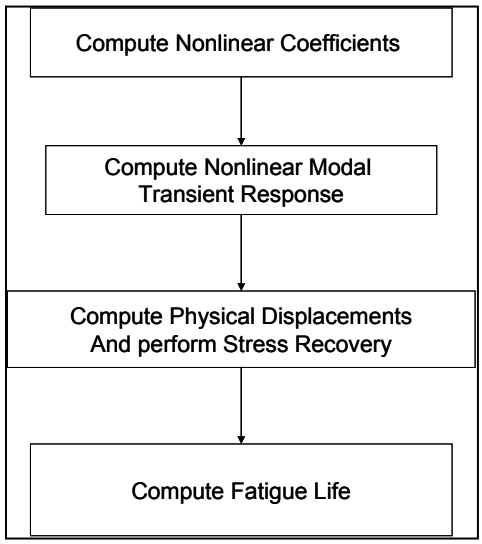

Figure 24 – NLROM analysis process

4.0 NLROM Improvements

This section of the report will document improvements made to the NLROM technique during this study.

In NLROM Phase I, the Implicit Condensation (IC) methodology, described in Section 2.1, was implemented in the analysis of simple test cases. It was demonstrated that the AFRL methodology provides equivalent accuracy to full-order nonlinear (NL) analyses; that the method is computationally efficient; and the methodology is practical for general nonlinear aero acoustic response and fatigue design studies. The Phase I analyses used realistic flight-type aero-acoustic loads that included steady (static) pressure effects.

For NLROM Phase II, the objective was to refine and validate the methodology to be able to analyze complex, multiple bay stiffened structure exposed to combined thermal, static pressure, and acoustic loads. First, the implicit condensation (IC) approach used in Phase I was updated to the more general ICE (implicit condensation with expansion) to better include the effects of in-plane membrane response. The expansion process is a post-processing operation and did not require any significant change to the basic IC process in the Matlab NLROM tool developed in the Phase I effort.

The second update/improvement was to improve the handling of static thermal and pressure loads. For the thermal loads, two approaches were studied: Cold-Modes and Hot-Modes. The final approach selected for this study was the "Hot-Mode" approach. The Hot Mode approach uses a modal basis that has been adjusted for thermal (or any static loads.) This approach requires a normal mode analysis after a nonlinear static analysis.

Third, a practical scheme to select modes to be used in the nonlinear analysis was studied. A typical large multiple bay panel will have dozens of modes in the frequency range of acoustic excitation. Most of these modes do not significantly contribute to the response of the overall or local panel structure. As with any type of modal reduction scheme, the quality and accuracy of the reduced-order solution is dictated by the modal basis selection. For the NLROM technique to be effective, a practical method to identify the most important modes to use in the analysis is required.

In this Phase II effort, the Proper Orthogonal Decomposition (POD) method was studied as a mode selection technique. POD is a well-known and reliable procedure for system identification. NASA-LaRC developed a POD based system identification guided basis selection method for reduced order nonlinear models using mode displacement, Ref. (14). NASA supplied the latest version of their POD and RanStep analysis tools for this evaluation. The NASA POD tool uses a reduced DoF set from a short time integration of an Abaqus explicit analysis to determine the Proper Orthogonal Modes (POMs). The POMs are related to the normal modes through the use of the Modal Assurance Criterion (MAC). This permits the determination of a reduced order system that remains applicable over a wide range of nonlinear response regimes. The POD tool was specifically developed for the NASA-LaRC displacement based approach, but this tool is generally applicable to the ICE method.

Lastly, various updates to the NLROM Matlab Tool were made to include improvements in the numerical integration scheme, I/O processing of input and results files, and updating to the latest MD-NASTRAN solution sequences. It was determined that the internal ordinary differential

equation (ODE) solvers in Matlab are relatively inefficient, and that the computation of reduced order models with 12 modes or greater to be significantly slow. Hence, the ODE solver was improved by using a stand-alone external code, incorporated in Matlab through a MEX (Matlab Executable) subroutine. The goal was to significantly improve the computational efficiency to more effectively run design and analysis trade studies. The NLROM methodology was also updated to work with MD-NASTRAN solutions enabling better handling of combined static/dynamic load cases; i.e., thermal and/or static pressure pre-loads. Lastly, improvements were made to the post-processing of results, which was critical to utilizing the NLROM methodology. One of the difficulties in nonlinear transient response analysis is the post-processing of long time histories results. Requesting all model data in an Abaqus/Explicit analysis can result in extremely large output database files that are difficult to post-process. The reduced order methods have the same difficulties, and there is a need for better post-processing for the use of NLROM in design studies. In Phase I, some development of whole model processing was implemented in the NLROM tool; such as, RMS and Max results.

The first refinement discussed below is the updating the NLROM Tool to work with the latest version of MD/NASTRAN and converting from the Matlab ODE solver to an external solver. The major difference was the change from SOL 106 to SOL 400, which allows for independent NL static sub-cases. The second refinement is to add the steady state thermal loads. The third refinement is updating the methodology from IC to ICE.

4.1 Matlab Solver Improvements

When changing from MSC/NASTRAN SOL 106 to SOL 400, this allows for independent NL static sub-cases. This is the correct manner in which to calculate the response that the nonlinear coefficient terms are based on. A snippet of the SOL 400 deck is shown below. Note the TEMPERATURE cards in the Case Control.

```
$ NASTRAN input file created by Matlab NLROM GUI
$ Direct Text Input for File Management Section
$ Nonlinear Static Analysis, Database
SOL 400
CEND
SEALL = ALL
SUPER = ALL
TITLE = MSC.NASTRAN Nonlinear Static Analysis
ECHO = NONE
TEMPERATURE(INIT) = 9998
TEMPERATURE(LOAD) = 9999
SPC = 2
DISPLACEMENT(PUNCH,REAL) = ALL
OLOAD(PUNCH) = ALL
SUBCASE 1
$ Subcase name : lc0001
  SUBTITLE = lc0001
  ANALYSIS = NLSTATICS
  NLPARAM = 1
  LOAD = 101
SUBCASE 2
$ Subcase name : lc0002
  SUBTITLE = lc0002
  ANALYSIS = NLSTATICS
  NLPARAM = 1
  LOAD = 102
```

Solver improvements were made to decrease the evaluation/computational time the standard Matlab ODE function required during execution. Originally, an *eval* statement was used, due to its simplicity, to evaluate the nonlinear state-space vector. This statement is generally deemed to be very costly from a CPU and time standpoint. Thus, two nested *for* loops were substituted for the *eval* statement, resulting in a noticeable computation speed improvement. In general, the improvement seemed to be roughly a factor of three or better. Additionally, to facilitate more complex models with many modes and DoFs, a C++ MEX version of the Runge-Kutta ODE45 solver with adaptive time step control was written and compiled to be used with the NLROM Matlab code. Similar to the speed improvements that were seen when implementing MEX for file input and output, the improvement to the ODE solution time was significant. The amount of improvement is dependent on the complexity of the problem and the desired evaluation interval, but it reduced computational time by at least an order of magnitude.

4.2 Thermal Load Implementation

An additional refinement to the NLROM technique involved the thermal load implementation into the NLROM interface. Initially, both the Cold Modes and Hot Modes approaches were considered. The Cold Modes approach develops the nonlinear coefficients based on the normal modes without any influence of the applied thermal loads. Conversely, the Hot Modes approach uses the thermal load adjusted normal modes. The general process for each approach is listed below.

Cold Modes Approach for NASTRAN:

1.) Run Sol 101 – Output all applied loads subcases (thermal and acoustic pressure)
2.) Run Sol 103 – output the mode shapes deflection shapes
3.) Setup and run the nonlinear static (Sol 106 or 400) modal combination runs based on the mode shapes
4.) Compute the Nonlinear Coefficients
5.) Estimate the linear K_{DT} matrix, (Note: RanStep was used in the test case, but a general process is described below.)
    a. Run Thermal Nonlinear Static, restart with a small pressure perturbation load.
    b. Output nodal applied loads {f} and displacement response {d} vectors, form the linear stiffness matrix
    c. Perform modal transformation on [K] to get $[K_{DT}]$ modal
    d. The updated stiffness matrix is $\text{diag}[\omega_n^2] - [K_{DT}]$
6.) Perform the integration of the ODE
    a. Form a Right Hand Side (applied Thermal Load vector and time history). Note; the RHS thermal load vector is determined from the Static Solution. This is a nodal loading vector for each DoF in the model. This then gets transformed into modal coordinates to form the modal load vector. The time history file is the scalar at each time step by which the applied thermal modal load vector will be multiplied by during the ODE solution.

Hot Modes Approach for NASTRAN:

1.) Run Sol 400 (nonlinear static) for the thermal load case Step. Restart into a Normal Mode Step (both the Thermal Load and Normal Mode are in the same subcase.) This produces a set of hot modes eigenvectors to be used to form the nonlinear static cases.
2.) Setup and run the nonlinear static load cases, but add an additional thermal load case (TEMPERATURE (load)) to each modal load force combination. Output the displacements.
3.) Subtract off the thermal load (only) response from the nonlinear static runs.
4.) Compute the nonlinear coefficients and Membrane Basis (Tm) vectors
5.) Perform the integration of the ODE. Note: Do not form K_{DT} linear, a Thermal Load RHS vector, or time history scalar. This is not required.
6.) Compute the nonlinear modal response, transform to physical coordinates and add the thermal load (only) physical displacements back into the response.
7.) Compute element stresses from the total physical displacements (Thermal plus Acoustic).

Cold Modes runs a SOL 101 linear static solution with the thermal loads (and the unit acoustic pressure load in a separate load case), and output the equivalent OLOADs. OLOADs are nodal forces in all 6 DoFs. This is to establish the modal load vectors in terms of the nodal DoFs normalized to a reference unit pressure load and a reference thermal load. The actual time dependent loads are scalars of these reference load cases. But, since the acoustic pressure is a unit load case, the physical load time history is in psi units. Similarly for the thermal load, the physical loading time history is a scalar of the reference load case. The reference thermal load case can be a ΔT=1 °F. Also, it's best to apply all steady state loads with an initial ramp to avoid transients in the response. Hence, the steady state loads are ramped from zero to max value (@t=0.1sec) and then held steady to the end of the integration.

4.3 Implementation of Membrane Expansion

An additional refinement to the NLROM was implementing the AFRL methodology for estimating the membrane basis vectors and updating the NLROM tool from IC to ICE. The following is the methodology as developed and documented by Dr. Joseph Hollkamp (AFRL/RB). Much work has been reported in recent years on prediction methods which reduce a finite element model to a reduced-order system of nonlinear modal equations. This body of work has shown good results for predicting the random response of flat structures. However, there have been few studies reported on reduced-order methods applied to structures with shallow curvature. Curvature complicates the analysis by introducing linear coupling of transverse and in-plane displacements. The implicit condensation and expansion (ICE) method, which eliminates the need for normal membrane vectors in the modal basis, has been shown to give accurate results for flat structures, Ref. (6).

The IC method estimates the nonlinear coefficients in Eq. (6) from a set of nonlinear static solutions obtained from NASTRAN. The applied loads for the static solutions (from SOL 400) are linear combinations of the modal basis vectors. Only bending-dominated modes in the frequency range of the acoustic excitation are needed in the basis. The IC method must be modified to compute membrane displacements. The ICE method implements this procedure. The transformation matrix from the IC method is augmented as

$$\mathbf{T} = [\Phi_b \; \mathbf{T}_m] \tag{16}$$

$\mathbf{T}_m$ is the estimated membrane basis. The subscript, b, has been added to Φ to denote that it is comprised of bending modes. Note that the columns of $\mathbf{T}_m$ are orthogonal to the columns of Φ_b. The vector of physical displacements can then be represented by

$$\mathbf{w} = \mathbf{w}_b + \mathbf{w}_m = \Phi_b \; \mathbf{p}_b + \mathbf{T}_m \; \mathbf{p}_m \tag{17}$$

$\mathbf{p}_b$ is the modal bending amplitudes, $\mathbf{w}_b$ are the physical displacements spanned by the bending modal vectors, $\mathbf{p}_m$ will be called generalized membrane amplitudes, and $\mathbf{w}_m$ are the corresponding physical displacements. The vector, $\mathbf{w}_m$, contains displacements that are not spanned by the bending mode shapes. For convenience they are referred to as the membrane displacements. The displacement vector in Eq. (16) is not partitioned; rather the displacement is separated into two additive vectors. Each physical displacement DoF has an entry in both vectors. Any general structure can be modeled. In the case of a planar structure, many of the entries will be zero in either $\mathbf{w}_b$ or $\mathbf{w}_m$. In the case of a curved structure modeled in a Cartesian coordinate system, the vectors will be fully populated. The expansion process by which $\mathbf{T}_m$, $\mathbf{p}_m$, and ultimately $\mathbf{w}_m$ are derived is summarized here. A single static solution is represented by Eq. (16). Considering many static solutions, the equation becomes

$$\mathbf{W} = \Phi_b \mathbf{P}_b + \mathbf{T}_m \; \mathbf{P}_m \tag{18}$$

The columns of $\mathbf{W}$, $\mathbf{P}_b$, and $\mathbf{P}_m$ correspond to the individual solutions. The set of generalized membrane displacements, $\mathbf{P}_m$, can be synthesized from the modal bending displacements. A single column of $\mathbf{P}_m$ is computed from

$$\mathbf{p}_m = [p_1^2 \; p_1p_2 \; p_1p_3 \; \ldots \; p_1p_n \; p_2^2 \; p_2p_3 \; \ldots \; p_2p_n \; \ldots \; p_{n-1}^2 \; p_{n-1} \; p_n \; p_n^2 \;]^T \tag{19}$$

The terms p_1 through p_n refer to the bending modal amplitudes in the corresponding single static solution. The set of generalized membrane amplitudes spans all the possible quadratic combinations of the bending modal amplitudes. The estimated membrane basis, $\mathbf{T}_m$, is then found by solving Eq. (18).

4.4 AFRL Curved Beam Example with Refined ICE Script

The first verification test case is the clamped-clamped curved beam, Figure 25, Ref. (4). The beam is 0.09 inches thick with aluminum material properties. The properties of the beam are aluminum and the boundary conditions are clamped-clamped. The acoustic pressure loading is a flat excitation spectrum from 0 to 1500 Hz, at P_{rms}=0.9 psi, or OASPL~169 dB. The applied pressure is assumed to be fully correlated. The finite element model has 74 nodes, and 36 quad elements.

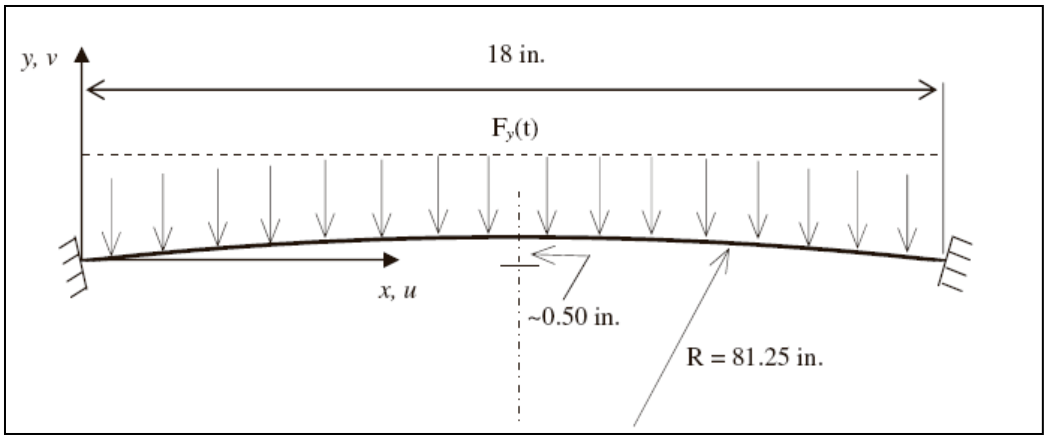

Figure 25 – Curved beam verification example

Verification of ICE implementation is to a full-order Abaqus analysis with acoustic loads only. The quarter and mid span vertical and in-plane displacements are compared. These are all 2 sec simulations at 20 KHz. Mass proportional damping is assumed. The NLROM uses the first 8 bending modes, Table 1.

Table 1 – First 8 bending modes

Mode	Freq	Type
1	158.7	Asym-2
2	258.4	Sym-3
3	440.1	Sym-3*
5	515.1	Asym-4
8	776.8	Sym-5
9	1075.2	Asym-6
11	1433.8	Sym-7
14	1839.7	Asym-8

Results are shown in Figure 26 through Figure 31 for the refined NLROM and Abaqus/Explicit. There is much better comparison for the in-plane response of the ICE approach, Figure 27 and Figure 29, over the IC method. This acoustic loading is very high at P_{rms}=0.9 psi with peak loads exceeding 3.0 psi. The static buckling load is P_b=-2 psi. Hence, there is some intermittent snap through for this curved beam example. The ICE method has improved the higher frequency response as seen in Figure 30.

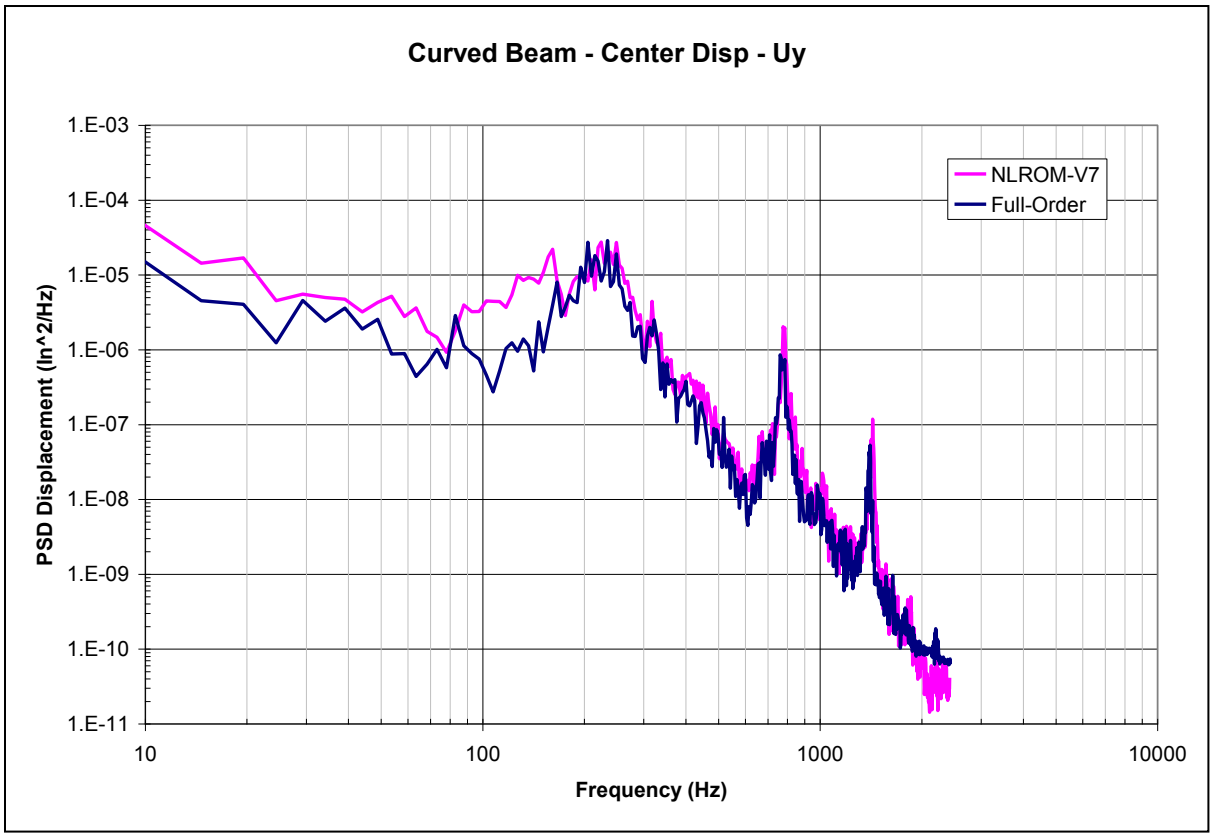

Figure 26 – Mid span vertical displacements at P_{rms} = 0.9psi

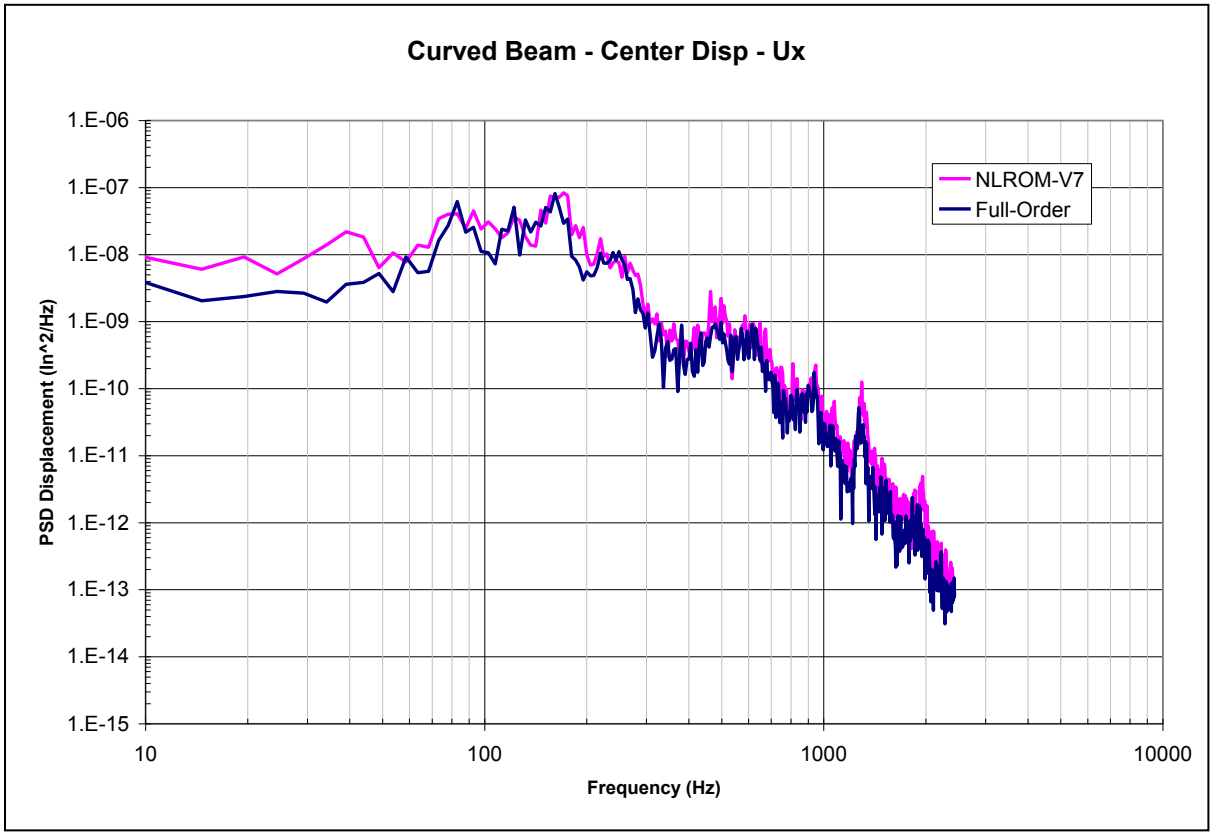

Figure 27 – Mid span in-plane displacements at P_{rms} = 0.9psi

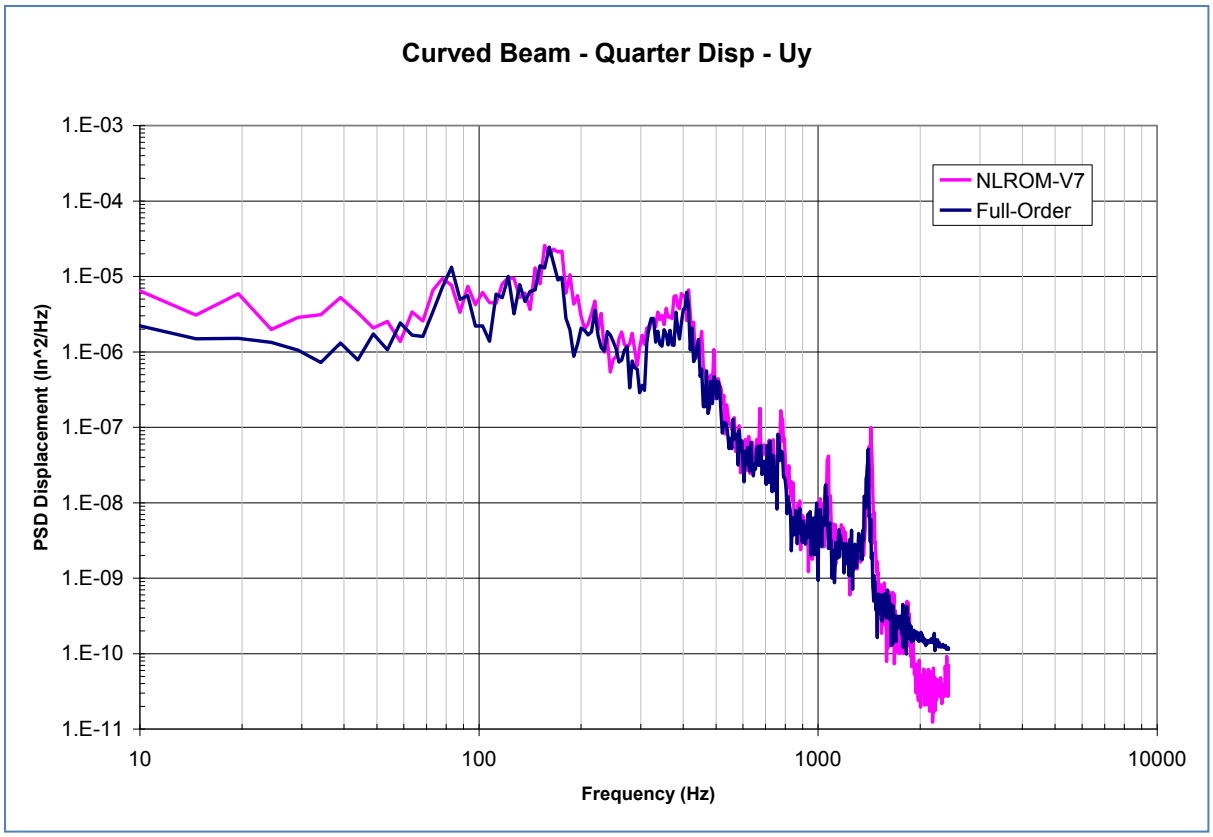

Figure 28 – Quarter span vertical displacements at P_{rms} = 0.9psi

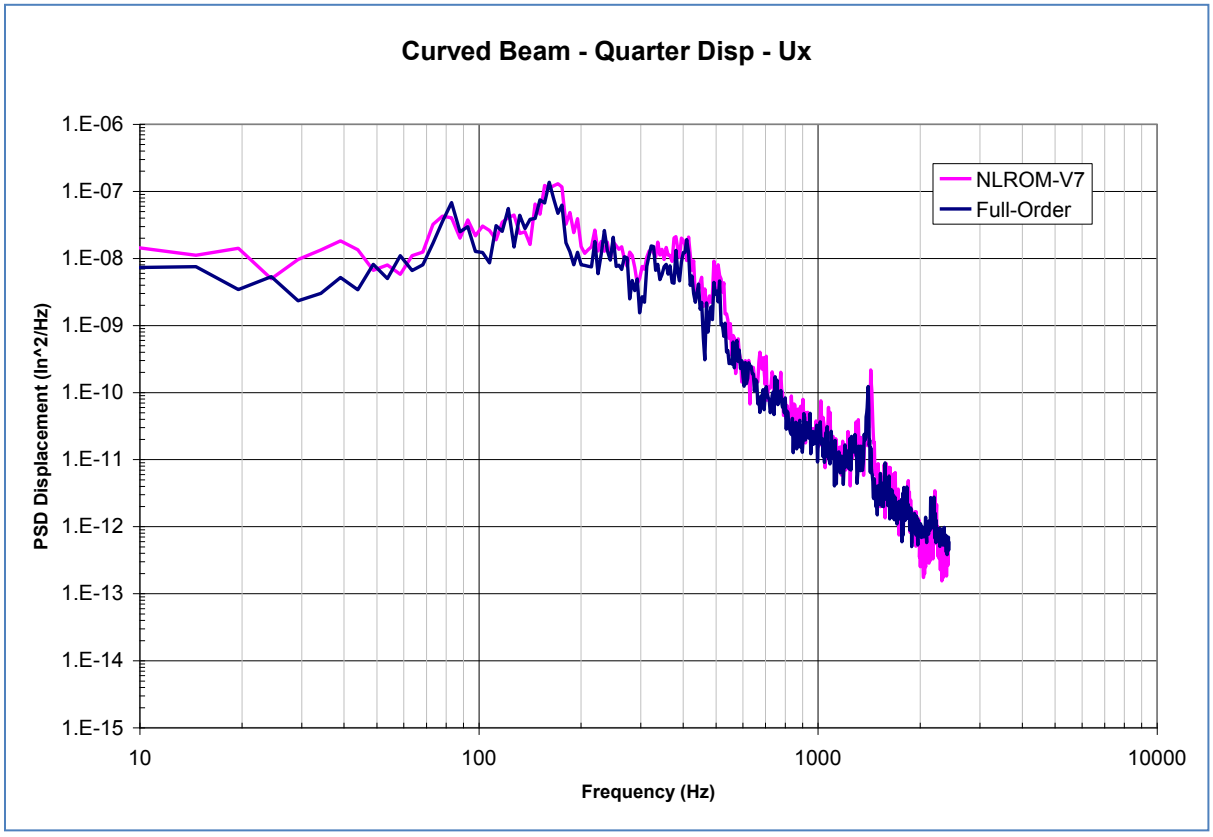

Figure 29 – Quarter span in-plane displacements at P_{rms} = 0.9psi

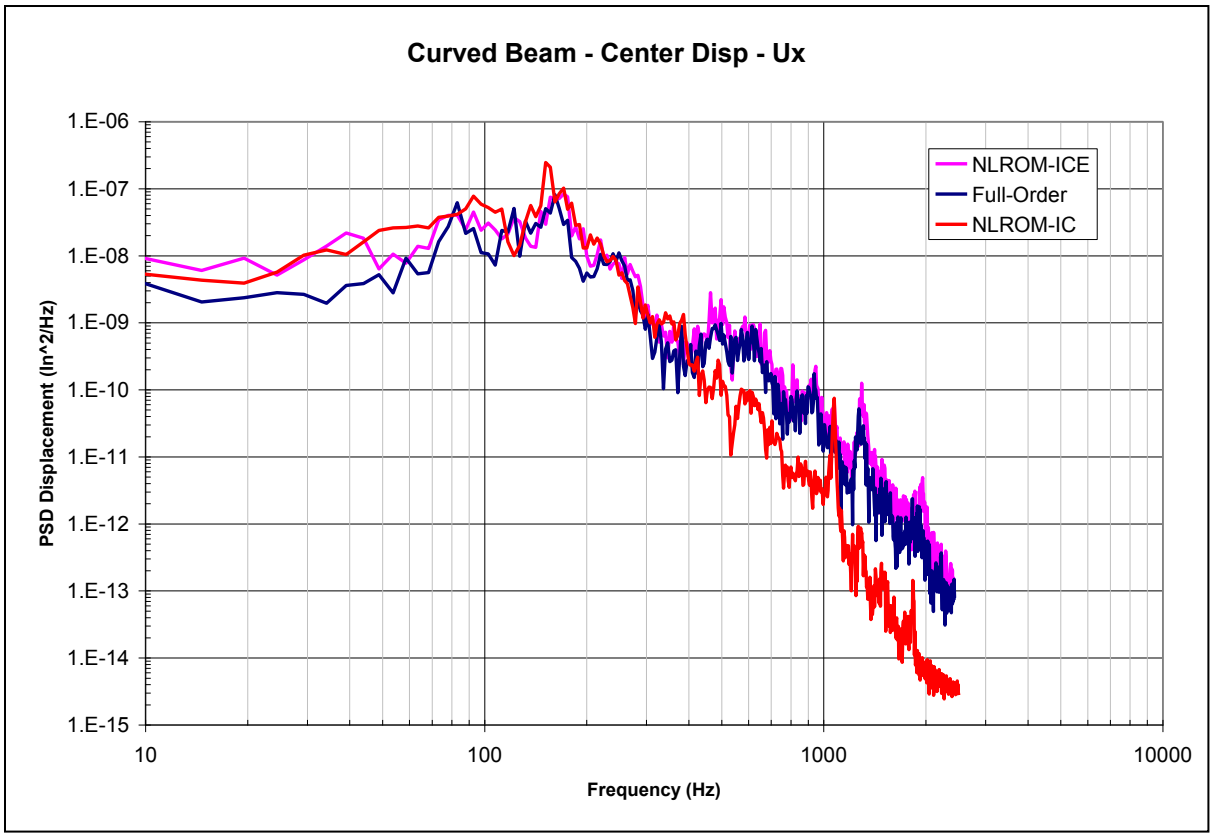

Figure 30 – Compare IC and ICE for curved beam

For the static pressure only condition, the pressure load is slowly ramped from 0psi to 5psi over 5 seconds. The Abaqus and refined NLROM results are show below, Figure 31. The pre-buckled response is the same. The buckled response in snap through is close, but the post-buckled response doesn't match as well. This might be a product of using too few modes (8) in the response.

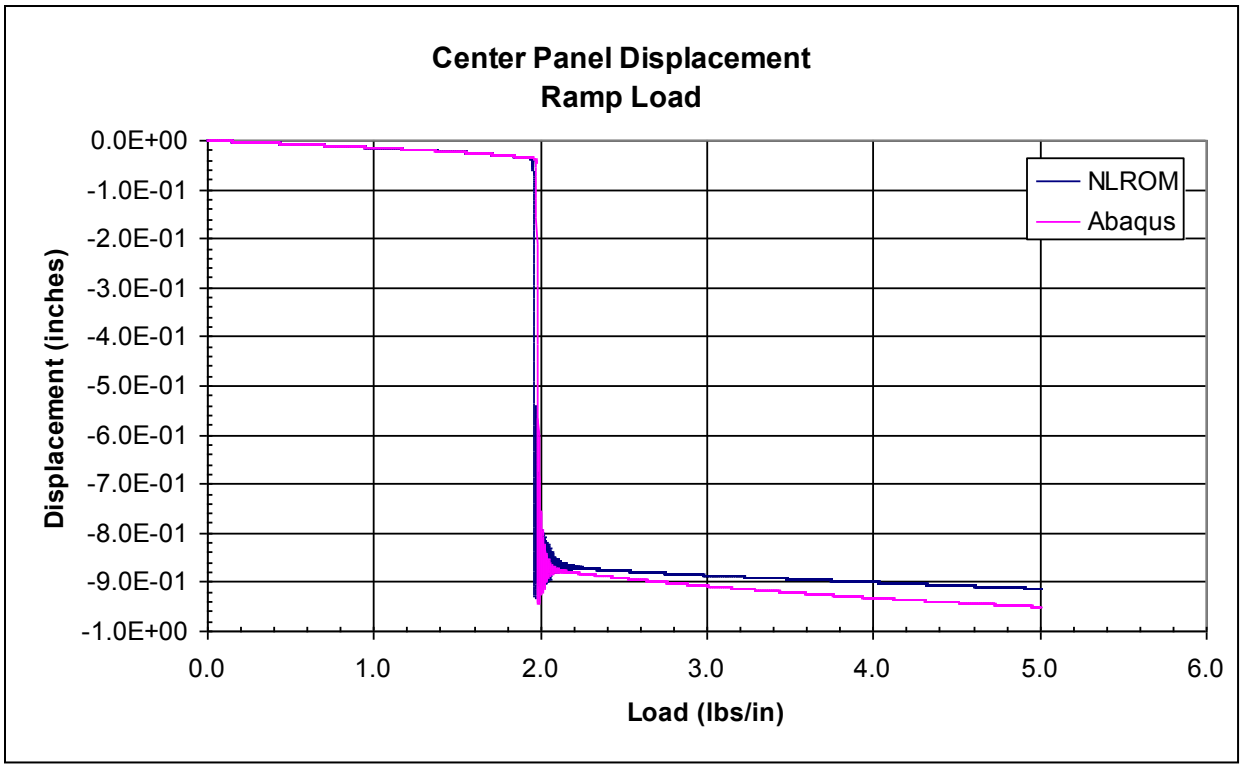

Figure 31 – Static ramp pressure 0-5psi for the curved beam example

4.5 Linear Full-Order to Linear ROM – Static Thermal

Using the cold modes approach, the linear static response is exact. Figure 32 below shows the static deflection shape of the beam, at $\Delta T=35°F$. The ROM loading was a RHS time dependent load vector was a ramp load from, 0 to 1.0, over a 1 sec. Hence, the shape below is the final shape of the beam at 1.0sec.

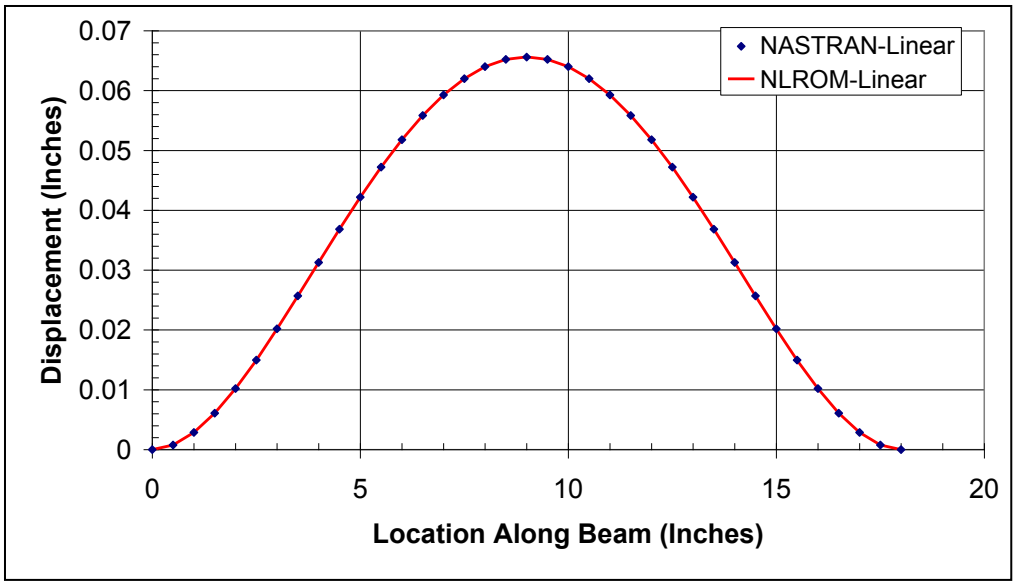

Figure 32 – Linear thermal static response

Below, we compare the full-order linear static to the nonlinear static. At this temperature, there is nonlinearity, as shown in Figure 33.

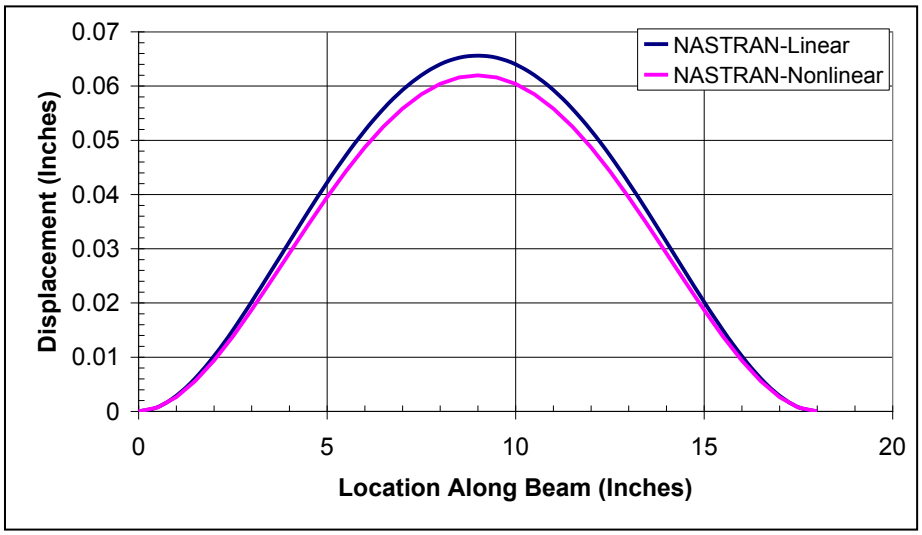

Figure 33 – NASTRAN full-order linear and nonlinear thermal static response shape

Figure 34 below shows the difference in including the LHS linear thermal stiffness term, $K_{\Delta T}$. The thermal stiffness is not required for linear analysis, but it is required for nonlinear geometric problems.

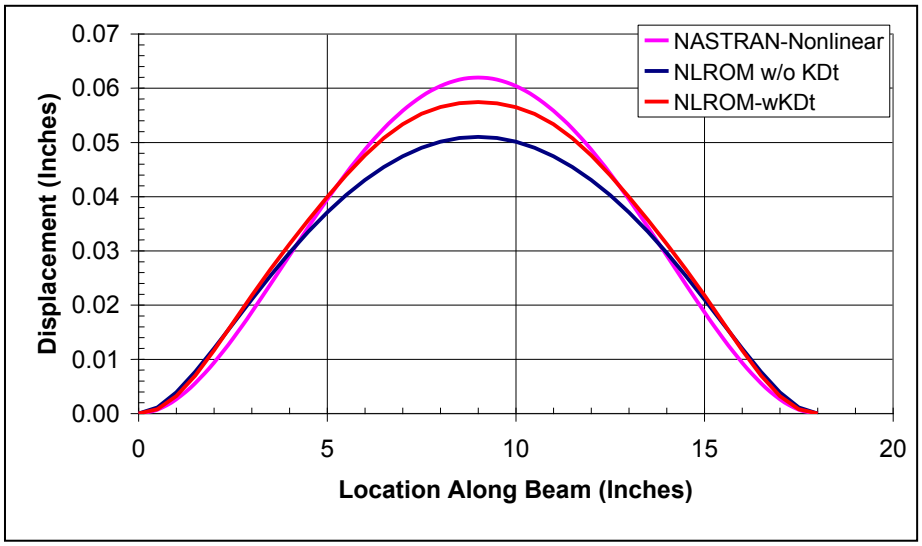

Figure 34 – Comparison of nonlinear static thermal response, influence of linear $K_{\Delta T}$

The Hot Modes approach implementation is discussed in more detail below. The procedure is to setup and run a NASTRAN SOL 400 with two independent subcases. The first subcase is a nonlinear static analysis of the thermal load. (Note: The thermal load can be zero if this is an acoustic only analysis.) The second subcase is the pressure load. (Note: There may be several pressure load cases to define an acoustic problem with several acoustic zones.) The displacements from Subcase 1 are saved for later use with the nonlinear static modal load cases. The pressure OLOADs from Subcase 2 will eventually be used to form the modal loading.

```
$ Thermal and pressure load model
SOL 400
CEND
ECHO = NONE
SUBCASE 1
       SUBTITLE = THERMAL
       ANALYSIS = NLSTATICS
       TEMPERATURE(INIT) = 9998
       TEMPERATURE(LOAD) = 9999
       NLPARAM = 1
       SPC = 2
       DISPLACEMENT(PUNCH,SORT1,REAL) = ALL
SUBCASE 2
       SUBTITLE = PRESSURE 1
       ANALYSIS = LNSTATICS
       LOAD = 3
       SPC = 2
       OLOAD(PUNCH,SORT1,REAL) = ALL
.
.
.
```

The second step is to setup and run the normal mode analysis in SOL 400. The solution is setup in two analysis Steps. The first Step is the Thermal Preload and the second Step is modal analysis. In the first Step, the temperature load is applied and static displacements are output. In the second Step, the eigenvectors are output.

```
SOL 400
CEND
ECHO = NONE
SPC = 2
TEMPERATURE(INITIAL) = 9998
SUBCASE 1
  STEP 1
    SUBTITLE = THERMAL PRELOAD
    ANALYSIS = NLSTATICS
    TEMPERATURE(LOAD) = 9999
    NLPARAM = 1
    METHOD = 1
    DISPLACEMENT(PUNCH,SORT1,REAL) = ALL
  STEP 2
    SUBTITLE = MODES
    ANALYSIS = MODES
    METHOD = 1
    RESVEC = NO
    VECTOR(PUNCH,SORT1,REAL) = ALL.
.
.
```

The third step is to form the nonlinear static load cases in SOL 400. The thermal loads are included in all modal force subcases. Next, read the SOL 400 displacements back in Matlab, and subtract off the thermal displacement (from Step 1) from each subcase. Finally, calculate the nonlinear coefficients and membrane basis vector.

```
$ NASTRAN input file created by Matlab NLROM GUI
$ Direct Text Input for File Management Section
$ Nonlinear Static Analysis, Database
SOL 400
CEND
SEALL = ALL
SUPER = ALL
TITLE = MSC.NASTRAN Nonlinear Static Analysis
ECHO = NONE
TEMPERATURE(INIT) = 9998
TEMPERATURE(LOAD) = 9999
SPC = 2
DISPLACEMENT(PUNCH,REAL) = ALL
OLOAD(PUNCH) = ALL
SUBCASE 1
$ Subcase name : lc0001
 SUBTITLE = lc0001
 ANALYSIS = NLSTATICS
 NLPARAM = 1
 LOAD = 101
SUBCASE 2
$ Subcase name : lc0002
 SUBTITLE = lc0002
 ANALYSIS = NLSTATICS
 NLPARAM = 1
 LOAD = 102
SUBCASE 3
$ Subcase name : lc0003
 SUBTITLE = lc0003
 ANALYSIS = NLSTATICS
 NLPARAM = 1
 LOAD = 103
.
.
.
-----------------------------------------------------------------------------------------------------
```

The following plots, Figure 35 and Figure 36, compare Abaqus/Explicit (full-order) to the NLROM method with thermal loads using the Hot Modes approach outlined above. These plots compare the results of the clamped-clamped curved beam with an OASPL=164dB, and uniform ΔT=35 °F. The second set of plots, Figure 37 and Figure 38, show the comparison without the thermal load (acoustic only). These are all 2 sec simulations. The damping is the same in both analyses.

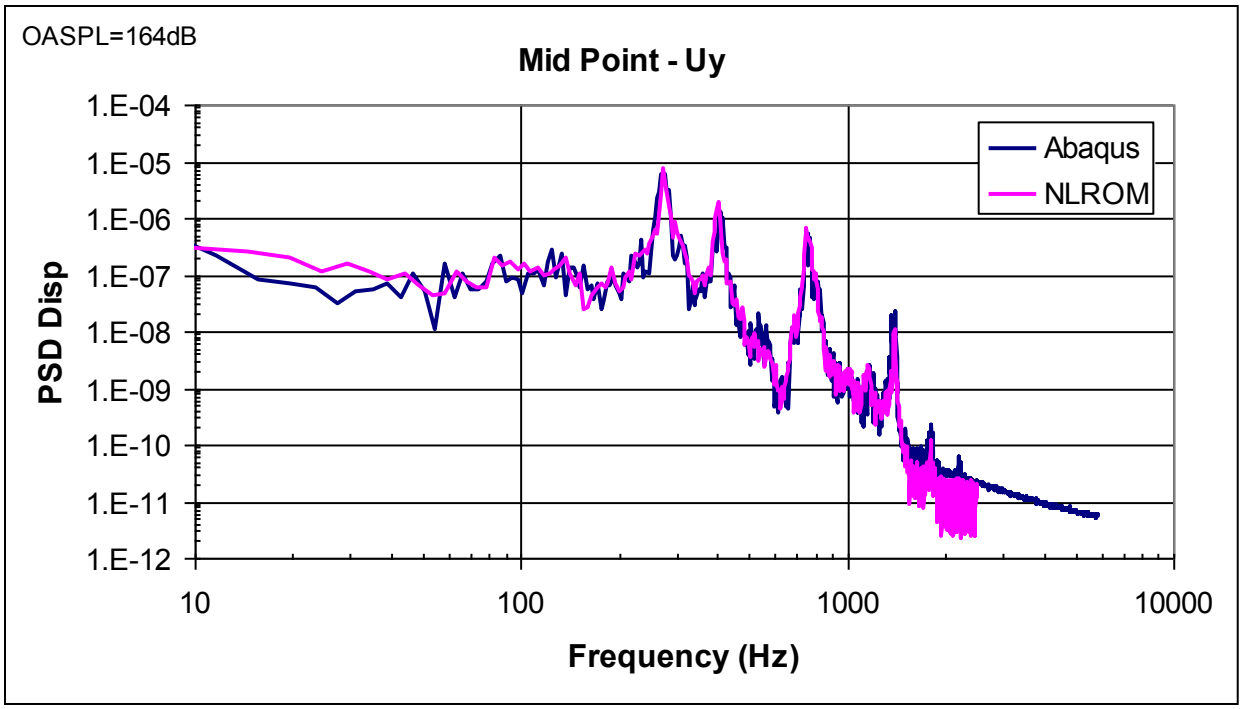

Figure 35 – Compare mid-point out-of-plane displacement PSD with thermal load

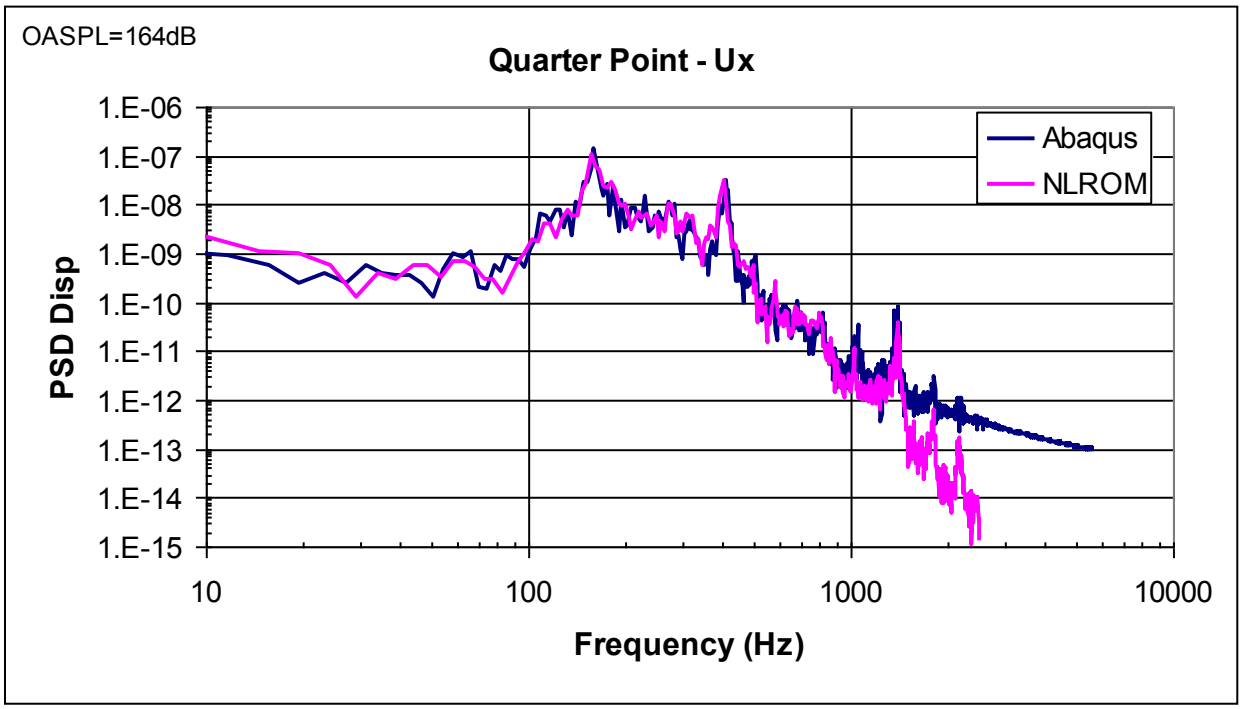

Figure 36 – Compare quarter-point in-plane displacement PSD with thermal load

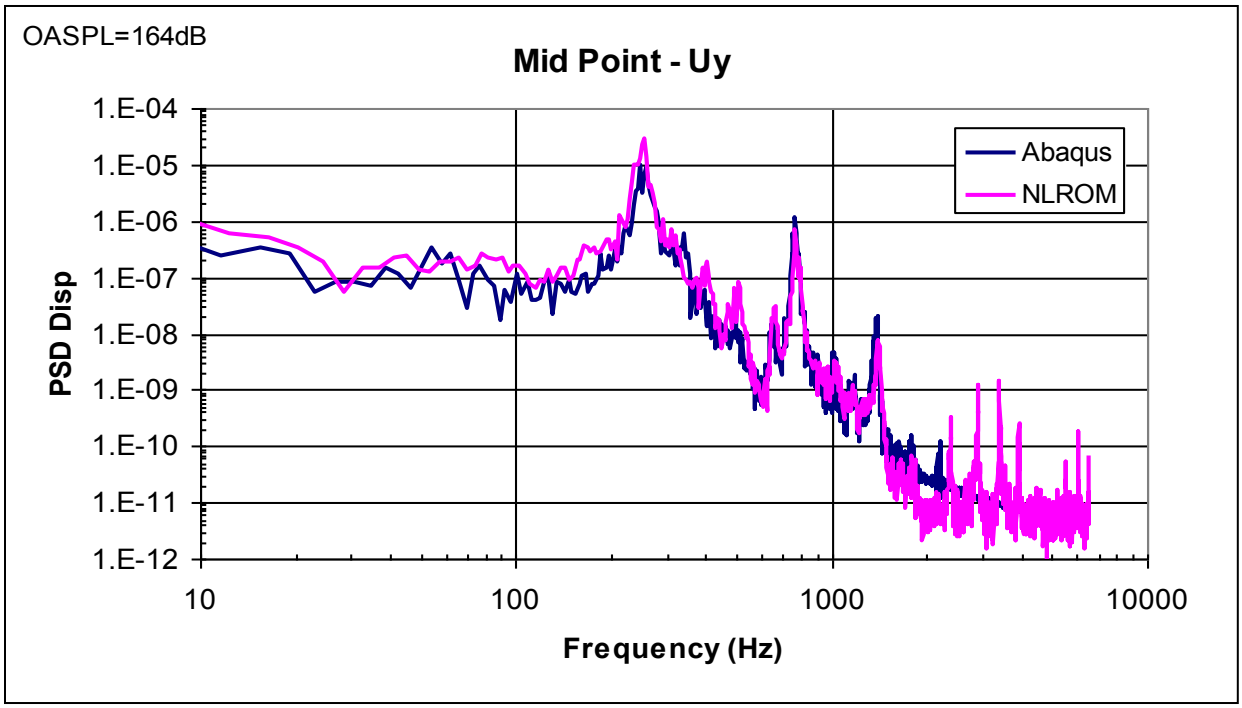

Figure 37 – Compare mid-point out-of-plane displacement PSD (acoustic only)

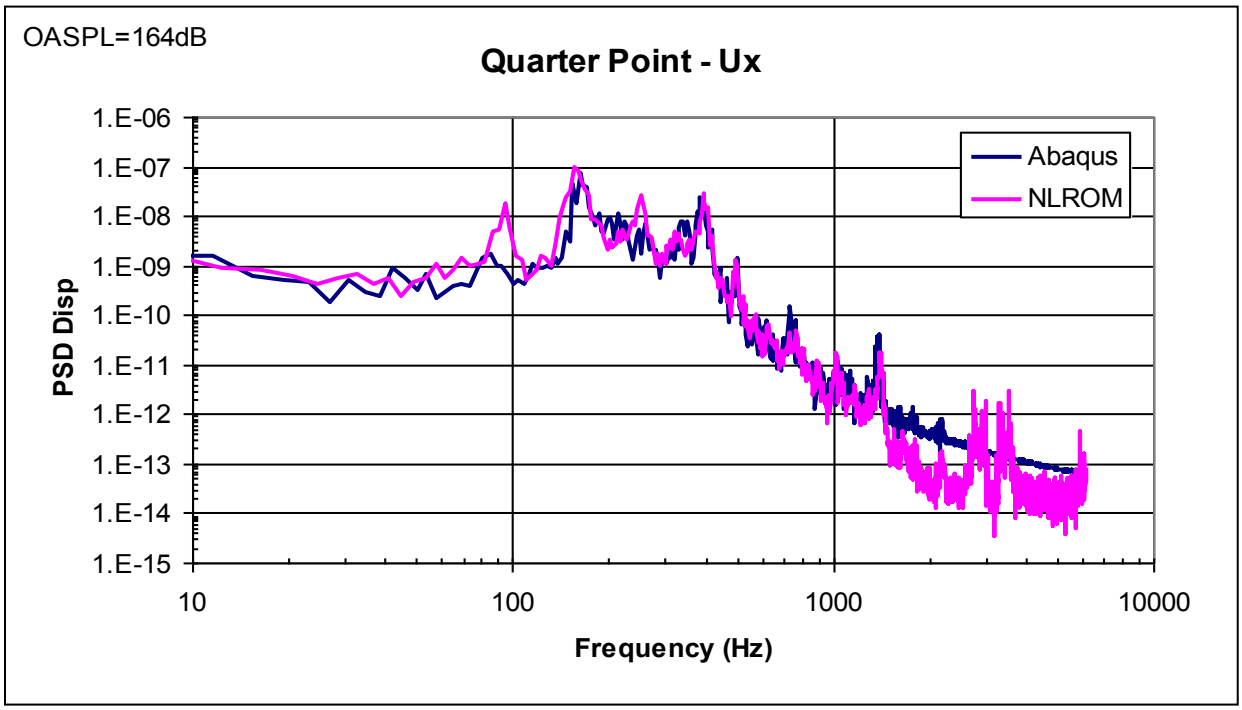

Figure 38 – Compare quarter-point in-plane displacement PSD (acoustic only)

4.6 Evaluation of the NASA/LaRC POD Technique

The Phase I study clearly identified the need to keep the number of reduced order modes to a minimum in order to realize the computational benefits of the NLROM method. As was previously stated, the number of nonlinear static solutions increases dramatically with the increase in the number of included modes. These nonlinear static solutions are a fixed cost in the development of the NLROM. If a structure has many modes, it is not easy to identify which modes are important. A trial and error process of mode selection would require repeating the nonlinear static solutions, possibly many times. Hence, a smart and practical mode selection method is required.

A large multiple bay model will have dozens of modes in the frequency range of acoustic excitation. Most of these modes do not significantly contribute to the response of the overall or local panel structure. As with any type of modal reduction scheme, the quality and accuracy of the reduced-order solution is dictated by the modal basis selection. Current techniques in use for modal basis selection are ad hoc and dependent upon the analyst's subjective judgment. It is required that a practical scheme be developed that can identify the most important modes. In Phase I, a practical scheme was demonstrated that used a combination of linear and nonlinear analyses. First a linear reduced order model (LROM) was developed. This LROM retained all of the modes in the frequency range of interest. Then, the dynamic response was predicted. The frequency response at a few key reference grids was checked and the modes that responded the most were retained for the nonlinear reduced order model. This process was sufficient for the less complex test cases used in Phase I, but this process is too cumbersome for a complex model with high modal density.

For the Phase II study, the Proper Orthogonal Decomposition (POD) based mode selection was investigated. POD is a well-known and reliable procedure for system identification. NASA-LaRC developed a POD based system identification guided basis selection method for reduced order nonlinear models, Ref. (14). The POD tool uses a reduced DoF set from a short time integration of an Abaqus explicit analysis to determine the proper orthogonal modes (POMs). The POMs are related to the normal modes through the use of the modal assurance criterion (MAC). This permits the determination of a reduced order system that remains applicable over a wide range of nonlinear response regimes. The POD tool was specifically developed for the NASA-LaRC displacement based approach, but this tool will be generally applicable to the ICE method.

The objective of the System Identification using Proper Orthogonal Decomposition is for basis selection. For the POD analysis, a short (t=0.25s) but representative sample of full-order nonlinear response in physical degrees-of-freedom (DoF) is required. Also, a subset of every 10^{th} node is used in the POD analysis. The response is output for each of these nodes. This forms the snap-shot matrix, below.

$$X^T = [x(t_1) \quad x(t_2) \quad \dots \quad x(t_n)] \tag{20}$$

From which to form the correlation matrix;

$$R = \frac{1}{n} X^T X \tag{21}$$

Then perform an eigenvalue analysis on the correlation matrix to yield the Proper Orthogonal Modes (POMs).

$$[R\lambda Ip]\cancel{\theta} \longrightarrow \underbrace{\lambda}_{\substack{\textbf{Proper Orthogonal Values} \\ \textbf{(POV's)}}}, \underbrace{P = [p_1 \quad p_2 \quad \cdots \quad p_n]}_{\substack{\textbf{Proper Orthogonal Modes} \\ \textbf{(POM's)}}} \tag{22}$$

From the eigenvalues, form the POM participation factors.

$$\chi_i = \frac{\lambda_{ii}}{\sum_{j=1}^{m} \lambda_{jj}}, \qquad i = 1, \dots, m \tag{23}$$

And the cumulative participation factors of M selected POMs.

$$\upsilon = \sum_{i=1}^{M} \chi_i\,, \qquad 0 < \upsilon \leq 1 \tag{24}$$

The cumulative participation factor is used to determine the number of rank-ordered POMs needed to achieve a prescribed value.

The POMs are load-dependent. The next step is to select normal modes (NM) representing the POMs to form a load independent basis.

There are two selection methods:

Method 1: Modal Assurance Criteria (MAC)

$$MAC(p_k, \phi_l) = \frac{|p_k^T \varphi_l|^2}{(p_k^T p_k)(\varphi_l^T \varphi_l)}, \qquad \begin{matrix} k = 1, \dots, M \\ l = 1, \dots, N \end{matrix} \tag{25}$$

Computation of MAC values for every pair of selected POMs and NMs enables identification of correlated pairs. The POD analysis establishes which POMs are required for a specified cumulative participation. Once these POMs are identified, the NMs resembling them are determined via their MAC value. This collection of NMs forms the modal basis.

Method 2: Modal Expansion (ME)

$$p_i \varphi = \sum_{j=1}^{N} c_{ij}\,, \qquad i = 1, \dots, M \qquad \longrightarrow \qquad S\Phi P^T \tag{26}$$

Select number (L) of NMs required representing M selected POMS for a given MAC/ME cutoff value (0.5 typical).

The NASA POD script was evaluated on different examples with increasing complexity. The first test case is the curved beam test case. The POD script identifies all modes that contribute the response for each DoF separately (Ux, Uy, Uz, Rx, Ry, and Rz). Then, the user needs to select a comprehensive set of modes. For this example, the comprehensive set of modes is in the table below, Table 2. The POD script identifies both the primary bending modes and the higher frequency membrane modes. A total of 23 modes have been identified based on the contribution

requirements set in the script. Note: The identification of the membrane modes is important for the RANSTEP method, but is not required for the ICE method. Also, the POD method does identify both symmetric and asymmetrical modes. Choosing the best set of asymmetrical modes is not an easy task.

Table 2 – Abaqus POD example, curved beam identified modes

Mode #	Freq	Type
1	159.6	Asym-Bending
2	260.4	Sym-Bending
4	401.9	Sym-Bending
5	524.1	Asym-Bending
7	798.4	Sym-Bending
9	1118.2	Asym-Bending
11	1510.7	Sym-Bending
14	1968.1	Asym-Bending
16	2502.2	Sym-Bending
19	3116.2	Asym-Bending
23	3820.6	Sym-Bending
26	4622.1	Asym-Bending
30	5535.4	Sym-Bending
31	5625.7	Membrane
35	6571.6	Asym-Bending
39	7745.2	Sym-Bending
50	11255	Membrane
74	22673	Membrane
85	28504	Membrane
89	34452	Membrane
92	40540	Membrane
98	53259	Membrane
99	59956	Membrane

The second test case for the POD evaluation was a curved panel, Figure 39. The outside dimensions of the panel are 17.75 inch x 11.75 inch with a 100 inch radius of curvature in the long panel dimension. The frame is 1 inch wide, so the effective dimensions of the panel are 15.75 in x 9.75 in. The thickness is 0.048 inches. The material is 304-stainless steel. The nominal properties are E=2.85 Msi, density=0.289 lb/in^3, and nu=0.29. The cap strips is 1 inch wide and 0.25 inch thick. The first nine normal modes are shown in Figure 40.

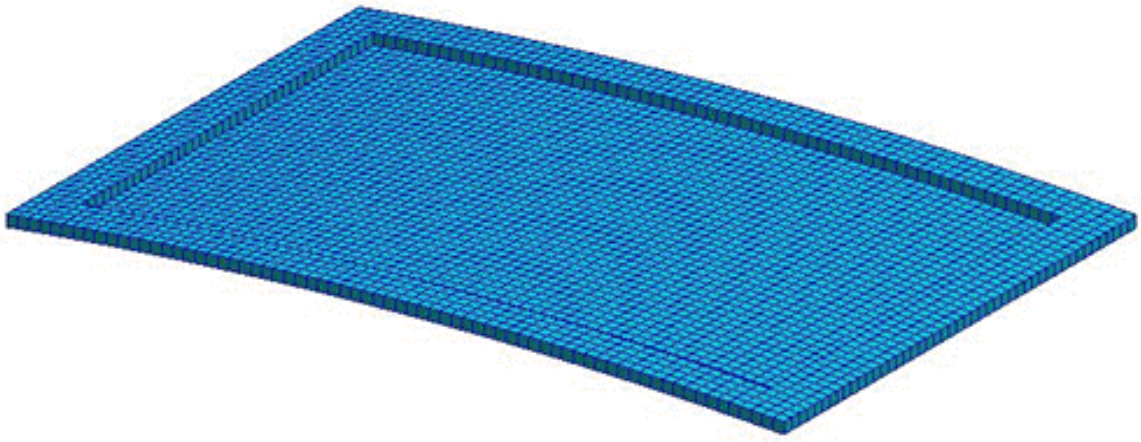

Figure 39 – AFRL curved panel

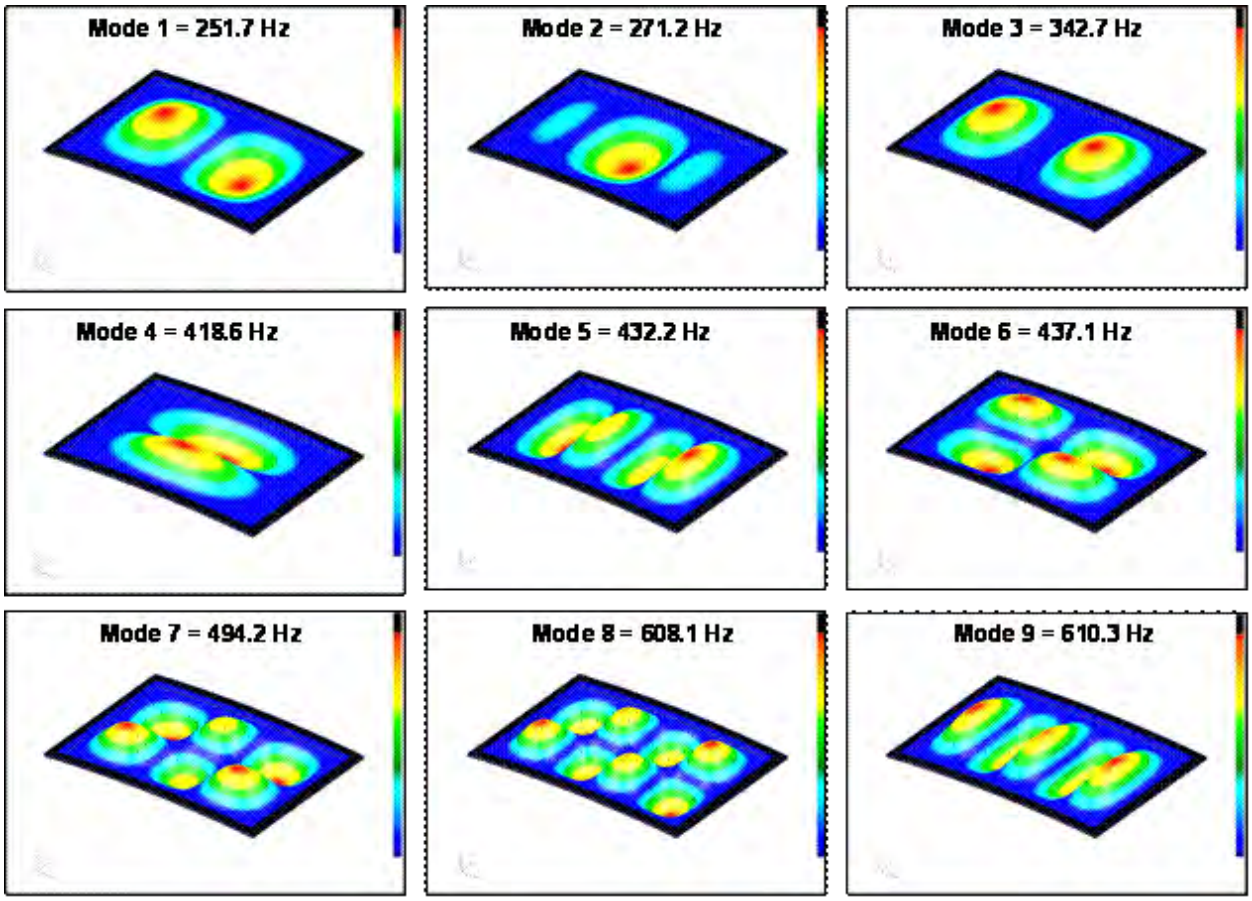

Figure 40 – NASTRAN normal modes

The NASTRAN modes match the Abaqus modes fairly well up to mode #17. The Abaqus model version is used for the POD evaluation.

Table 3 – Comparison of NASTRAN and Abaqus modes

NASTRAN Mode	Mode #			ABAQUS Mode	Mode #		Diff Hz	Diff %
						Freq		
2,1	1	251.72		2,1	1	253.64	-1.92	-0.76%
1,1	2	271.26		1,1	2	272.49	-1.23	-0.46%
3,1	3	342.69		3,1	3	347.2	-4.51	-1.32%
1,2	4	418.55		1,2	4	419.39	-0.84	-0.20%
2,2	5	432.21		2,2	5	434.46	-2.25	-0.52%
4,1	6	437.08		4,1	6	443.03	-5.95	-1.36%
3,2	7	494.17		3,2	7	498.44	-4.27	-0.86%
4,2	8	608.09		4,2	8	615.87	-7.78	-1.28%
5,1	9	610.28		5,1	9	621.2	-10.92	-1.79%
1,3	10	650.73		1,3	10	656.98	-6.25	-0.96%
2,3	11	686.31		2,3	11	694.28	-7.97	-1.16%
3,3	12	758.78		3,3	12	769.67	-10.90	-1.44%
5,2	13	771.09		5,2	13	784.55	-13.46	-1.75%
6,1	14	822.20		6,1	14	840.54	-18.34	-2.23%
4,3	15	873.44		4,3	15	889.03	-15.59	-1.79%
6,2	16	977.15		6,2	16	999.03	-21.88	-2.24%
1,4	17	991.07		1,4	17	1010.7	-19.63	-1.98%
INPL	18	1341.24		5,3	18	1053.7	287.54	21.44%
INPL	19	1600.75		2,4	19	1057.4	543.35	33.94%
INPL	20	1608.58		7,1	20	1103.5	505.08	31.40%
MEM	21	7095.04						
MEM	22	8951.81						
MEM	23	10751.35						

For this study, a total of 17 normal modes are used. A 0.9 threshold relative to max is used. The POD results for the curved panel are shown below.

Table 4 – Out-of-plane modes of interest

POM Number	POV	Cum POV %	NM Number	NM Freq
1	0.868314	86.83136	1	253.64
2	0.041447	90.9761	2	272.49
3	0.03046	94.02213	3	347.21
4	0.015404	95.56253	4	419.39
5	0.008852	96.44775	5	434.46
6	0.005735	97.02128	6	443.03
7	0.004781	97.4994	7	498.44
8	0.003726	97.87196	8	615.87
9	0.003236	98.19552	9	621.22
10	0.002003	98.39583	10	656.98
11	0.001501	98.54594	11	694.28
12	0.001479	98.69388	12	769.67
13	0.000988	98.79267	13	784.55
14	0.000835	98.87614	14	840.54
15	0.000812	98.95734	15	889.03
16	0.000466	99.00392	18	1053.7
17	0.000237	99.02759	20	1103.5

The above table only shows the lower order bending modes. However, there is a similar set of higher-order in-plane modes. These are listed below.

Table 5 – In-plane DoF modes of interest

POM	U1	U2
1	1	176
2	10	177
3	11	188
4	21	191
5	188	248
6	191	288
7	226	334
8	282	337
9	289	341
10	291	371
11	302	375
12	368	380
13	376	390
14	403	432
15	404	439
16	410	448
17	457	451
18	459	454
19	483	465
20	492	484
21	502	502
22	551	516
23	619	576
24	620	634
25	732	688
26	904	751
27		832
28		940
29		941

The next step is comparing the POD selected NLROM to a full-order (Abaqus/Explicit) analysis. The NASTRAN model and Abaqus model have similar modal characteristics up to 1000Hz. The reduced order model was based on a POD selected sub-set of these modes. Both the reduced order and full-order models were run for 5 seconds. The input load was a uniform acoustic pressure, shown as the blue line in Figure 41, while the 1/3 octave bands are shown as the pink squares. The loading time history was generated from a PSD with a constant spectrum from 20-500Hz. The reduced order model used seven POD selected modes, by criteria of importance. Both models used a damping of Alpha=64, and the same loading time history. Overall, the models yield similar results. The midpoint Z-displacement, Figure 42, looks very good with magnitude, overall RMS, and spectral content comparing well. The full-order analysis shows a mode at 780Hz in full-order. The mode is more observable in the quarter point Z-displacement, Figure 43, and in-plane displacement, Figure 44. The POD method had this mode ranked 13th. The NLROM was based on the seven highest ranked modes. So the question is: should this mode have been used in the NLROM? It would have made the ¼ point PSD comparisons better, but since the objective is overall response accuracy at all locations in the model, then we have to trust that the POD method selected those modes of most importance.

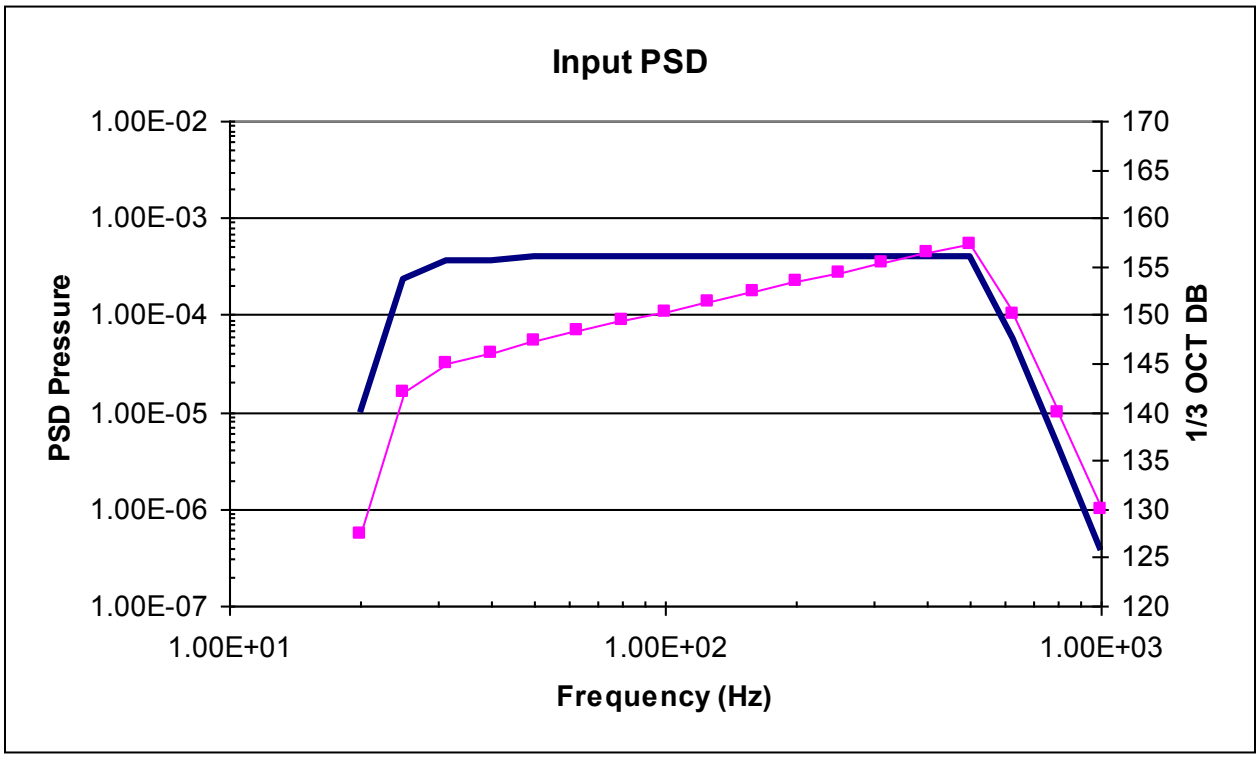

Figure 41 – Input PSD, OASPL = 164dB

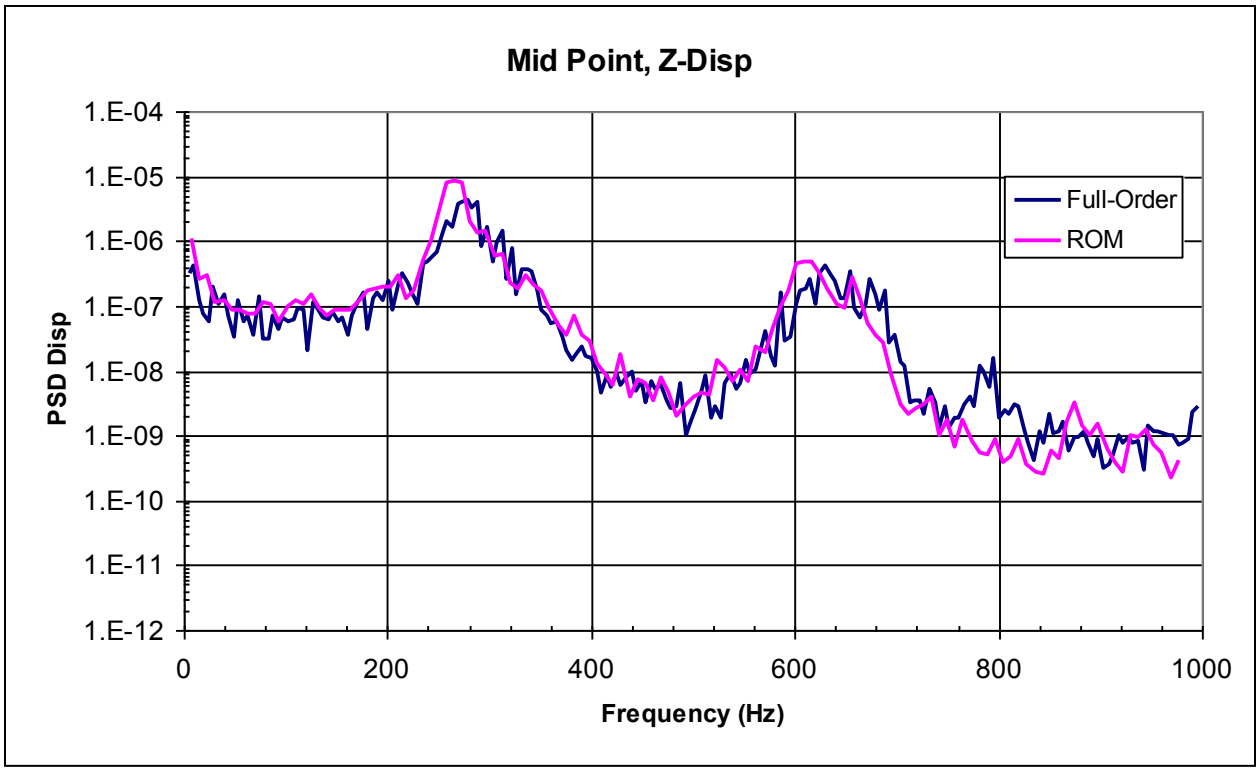

Figure 42 – Mid point z-displacement PSD

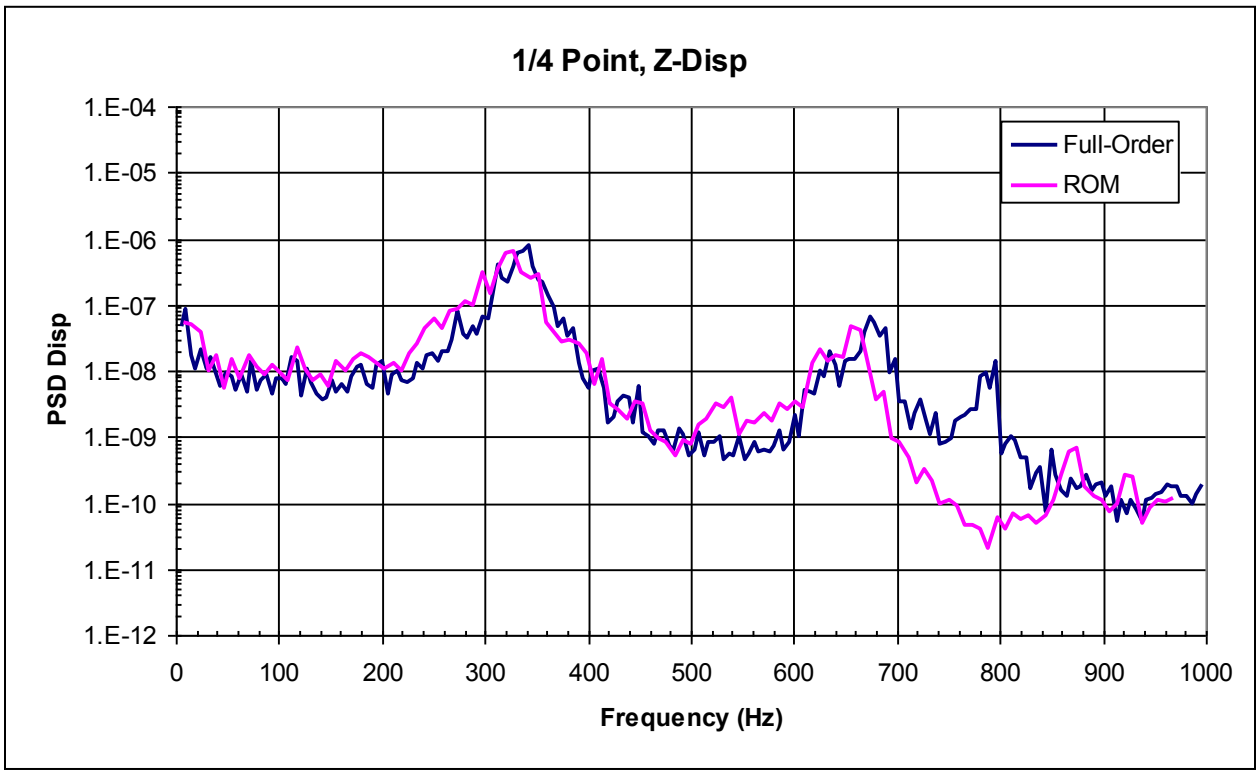

Figure 43 – Quarter point z-displacement PSD

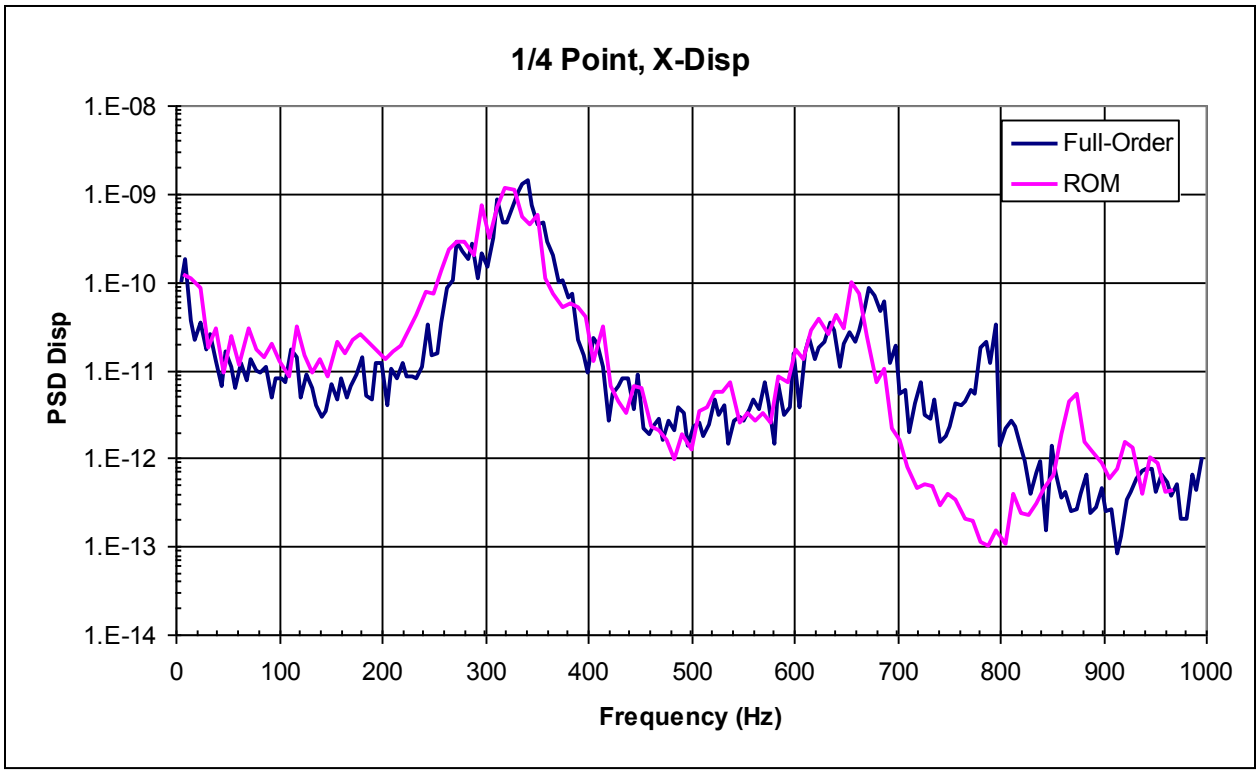

Figure 44 – Quarter point in-plane displacement PSD

The next study was to compare POD selected NLROM to Abaqus, when there is a uniform $\Delta T=100°F$ load applied. In this simulation, mode 13 is included as the 8^{th} mode. The center point results are shown below. The in-plane results don't compare very well, Figure 45 and Figure 46. However, the out-of-plane Uz results compare quite well, Figure 47. Closer inspection shows that the Abaqus and NASTRAN modes do not compare very well. (Note: The Abaqus modes come from a similar normal mode solution.) As shown in the comparison of the modal displacements across the center of the panel in the short dimension, the z-displacement matches well, Figure 48, but the y and x-displacements are not similar, Figure 49 and Figure 50. The main conclusion is that it can be difficult to judge the accuracy of the reduced order model based on a full-order solution from a different FE solver.

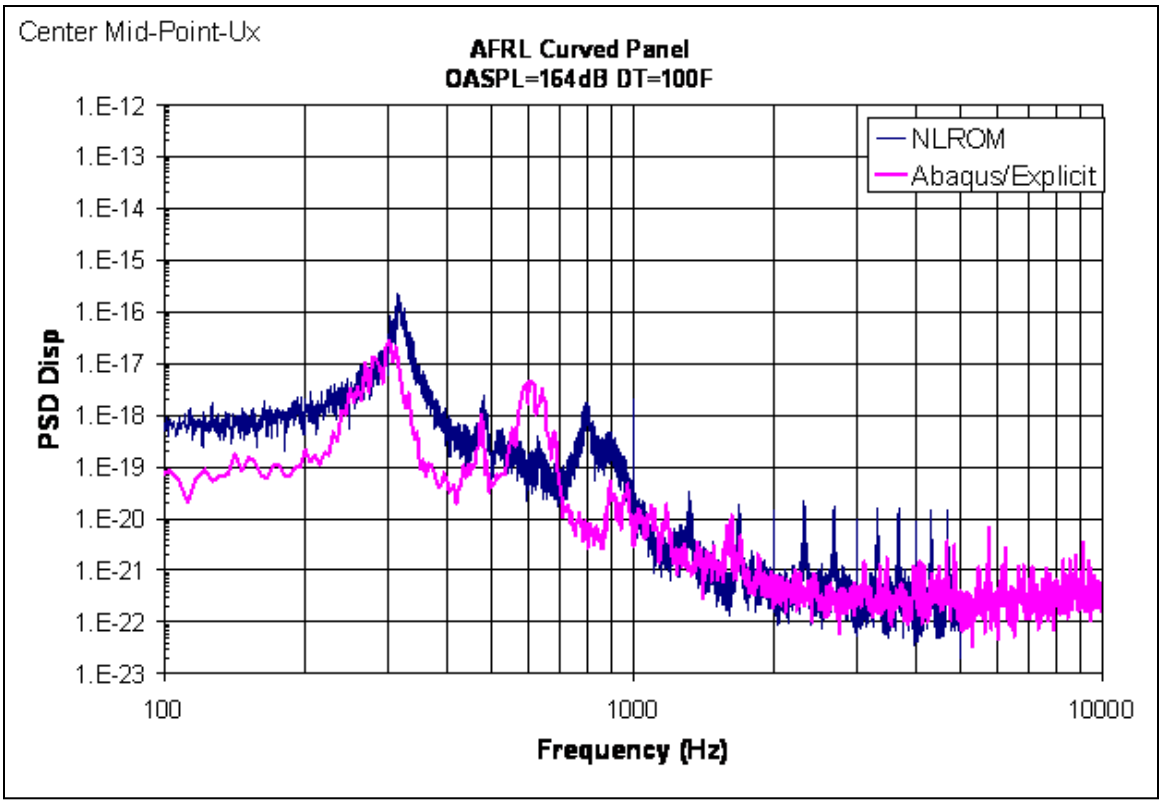

Figure 45 – Mid point Ux

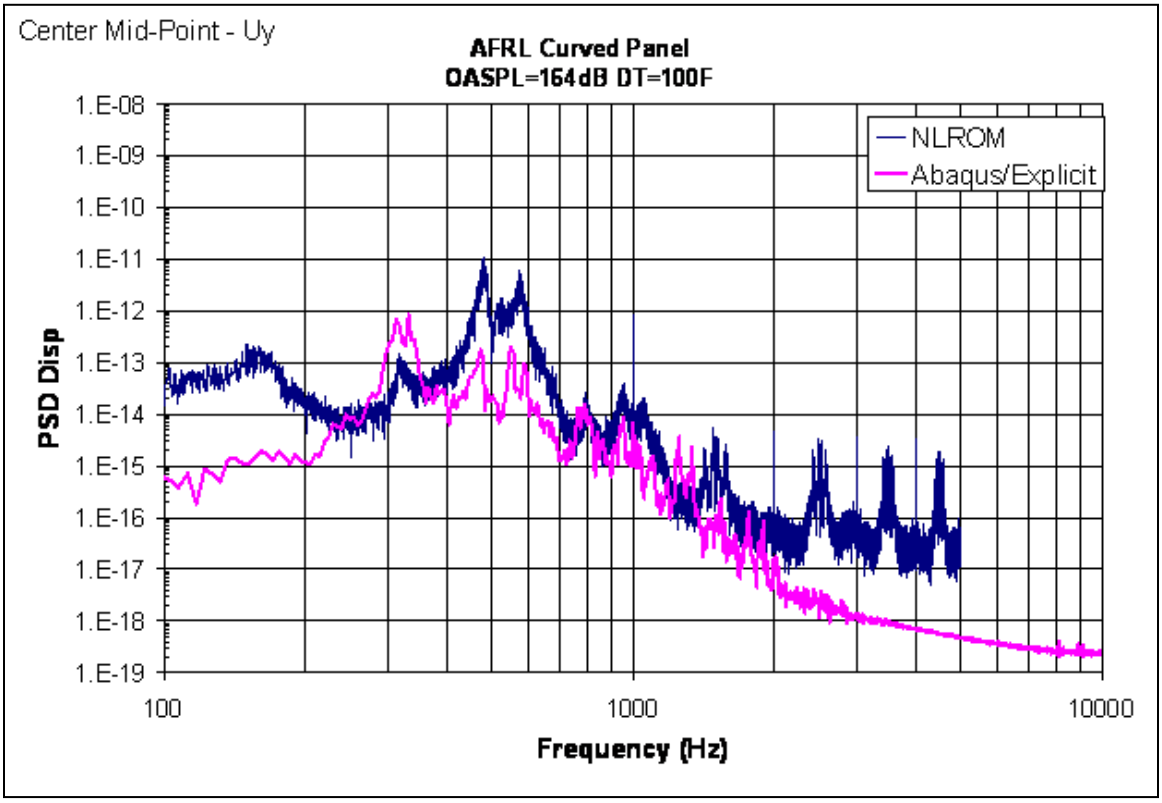

Figure 46 – Mid point Uy

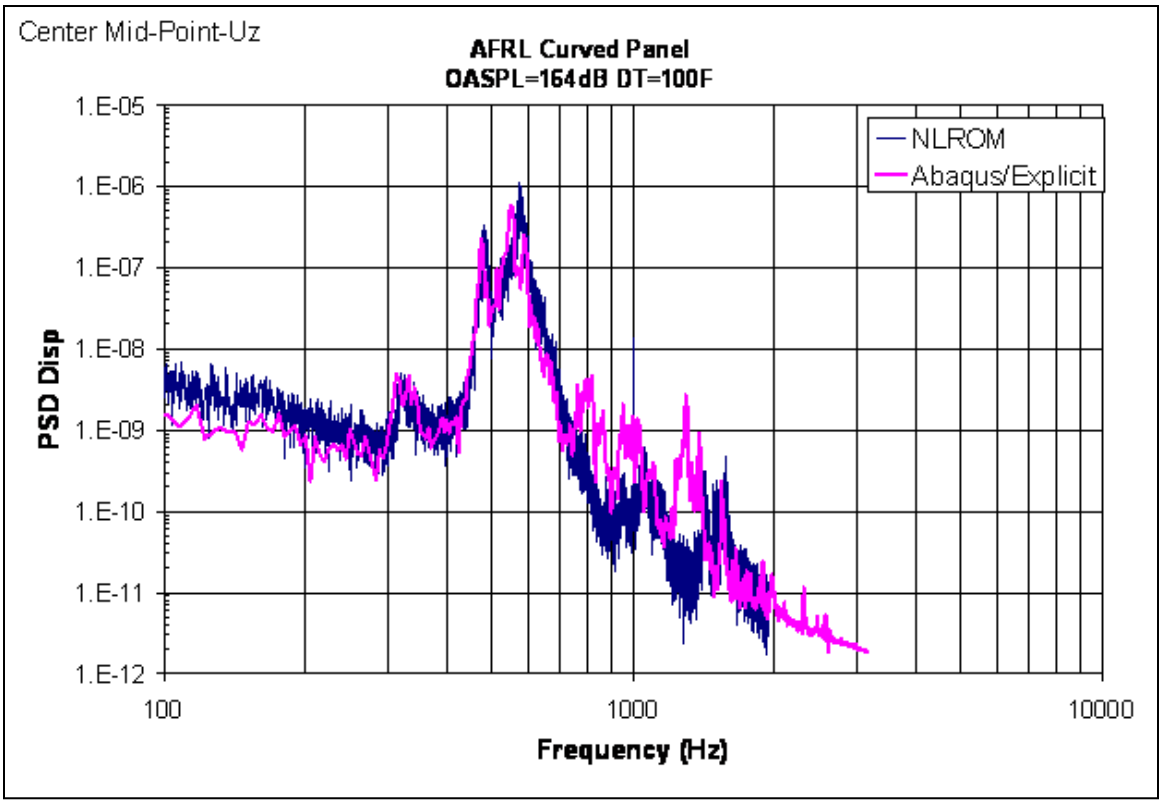

Figure 47 – Center point Uz

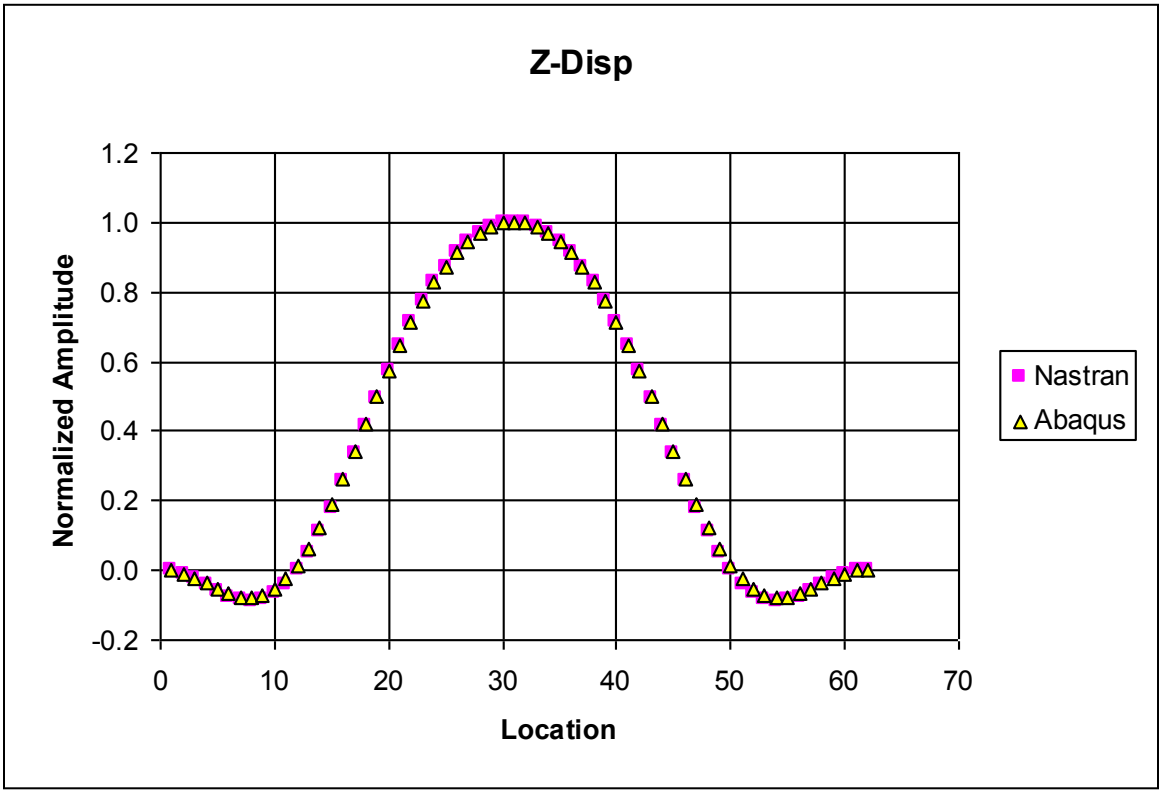

Figure 48 – Compare NASTRAN and Abaqus out-of-plane DoF mode shapes

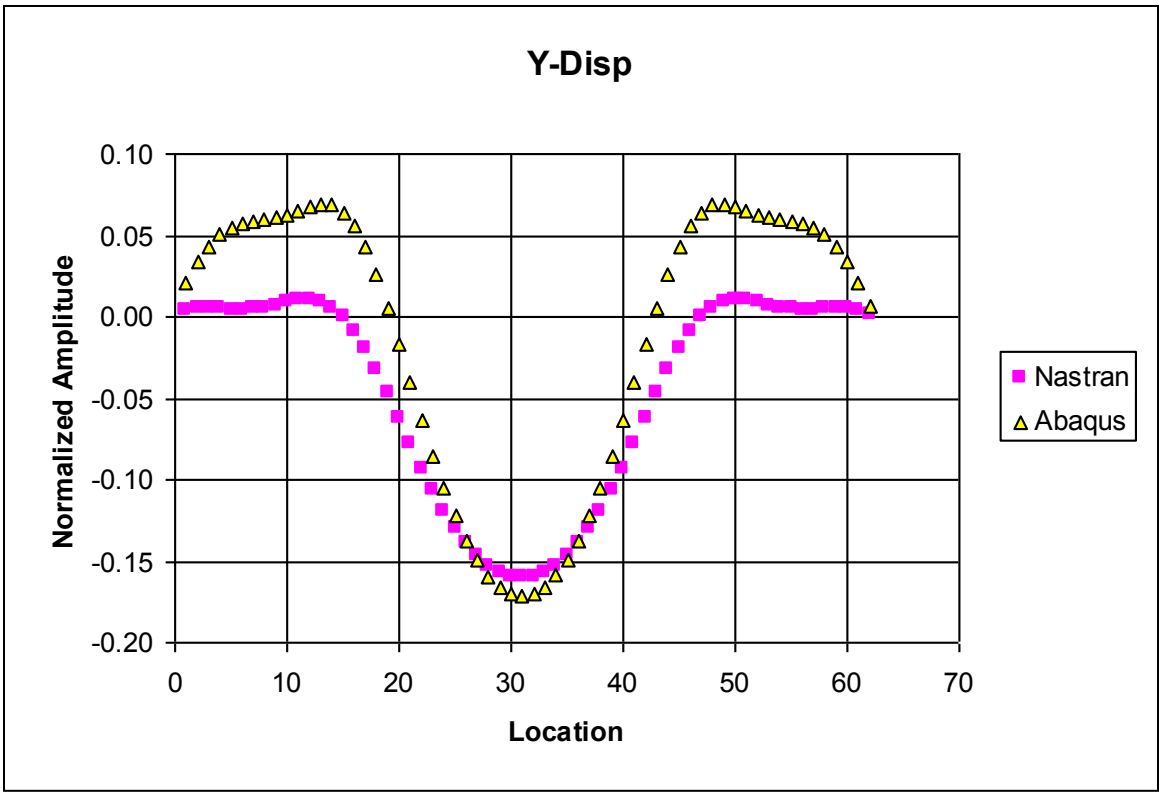

Figure 49 – Compare NASTRAN and Abaqus in-plane DoF mode shapes

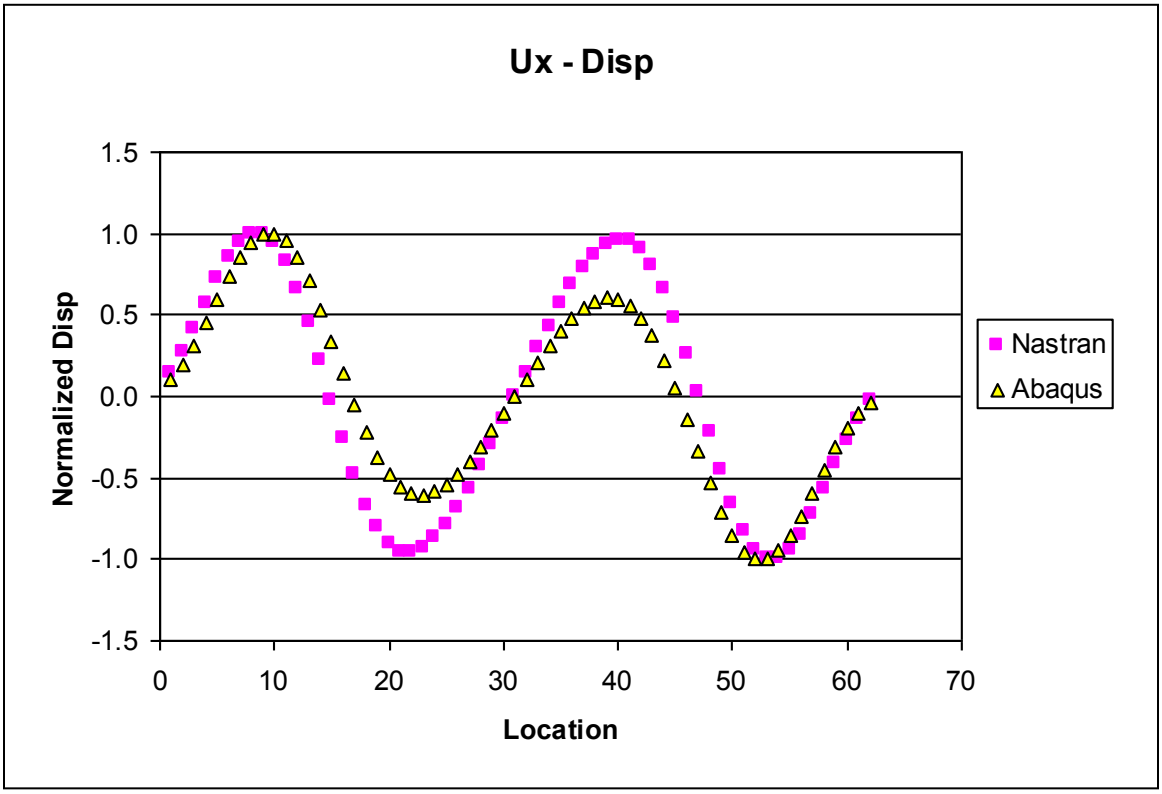

Figure 50 – Compare NASTRAN and Abaqus in-plane DoF mode shapes

5.0 Design and Analysis of a Representative Aircraft Structural Component

The NLROM technique has shown great promise on selected simplified test cases. This section of the report documents the use of NLROM as a tool to design a representative aircraft structure with nonlinear acoustic response

5.1 Design Study

The refined NLROM method was used to design a multi-bay blown flap aircraft component subjected to combined acoustic and thermal loads. For this test case, a detailed FEM of the flap test article was developed in NASTRAN, Figure 51. The flap configuration is based on the proposed test article, which are four bays wide with five supporting ribs. The overall size of the configuration was selected based on adequate replication of the interior skin bay structural dynamics. The three inner ribs and the skin were constructed of titanium. The ribs, frames, and skin are representative of the actual aircraft application.

In the initial model, the parts were "glued" together using a surface contact mechanism that is available in MD NASTRAN. Glued contacts allow dissimilar meshes to be tied together, removing the necessity of RBAR constraints or equivalence nodes. An acoustic pressure load was applied normal to the top surface of the skin. The boundary conditions were free at the trailing edge, fixed at the leading edge, and symmetric conditions on the sides of the model to best represent the dynamics in a full aircraft flap.

The first step in the study was to run the linear frequency response analysis. This was to determine the modes of interest, to be used in the NLROM solution. A normal modes analysis predicted the lowest skin panel mode to be 376 Hz, as shown in Figure 52. Also, the temperature loading was $\Delta T=0F$. The acoustic loading was representative of the actual flap engine-aero-acoustic spectrum at OASPL=168dB, and included all design factors.

The baseline model included 8 uncorrelated pressure zones. Each bay of the model had two pressure zones, stream-wise. The RMS deflections and stresses are shown below, in Figure 53 and Figure 54, respectively. The RMS displacement was dominated by the lowest flap bending mode at 125 Hz, while the RMS stress was predominately the lowest skin panel mode (shown above). The stress plot does not accurately reflect the structural Kt's. The linear reduced order model used all 17 modes up to 600 Hz. A displacement PSD of the center panel response is also shown, Figure 55. The z-displacement PSD shows the dominant modal response at 376Hz.

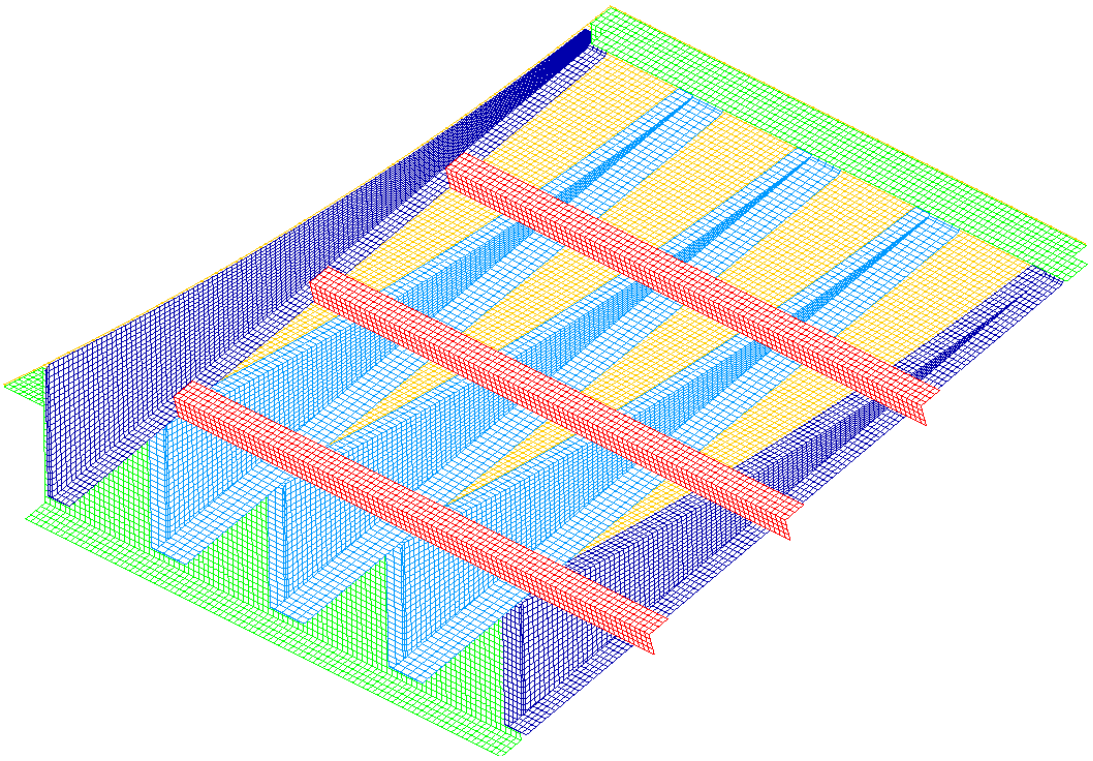

Figure 51 – Flap detailed NASTRAN FEM

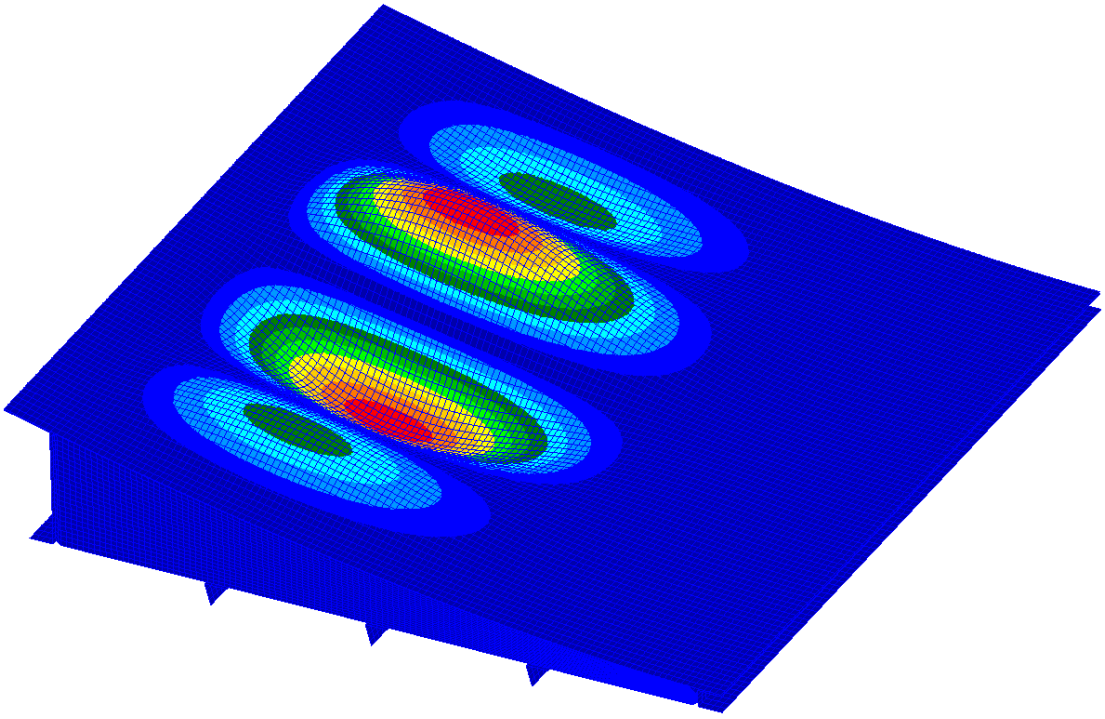

Figure 52 – Lowest panel mode at 376Hz

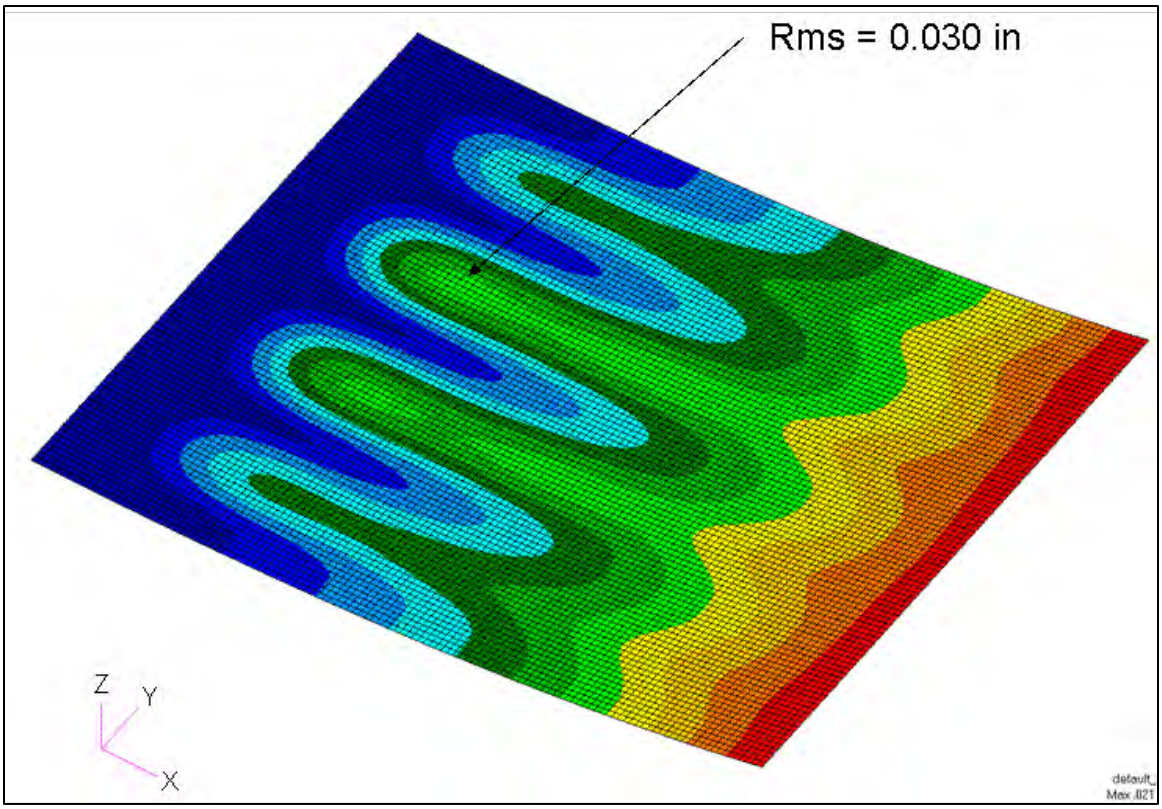

Figure 53 – RMS deflection shape

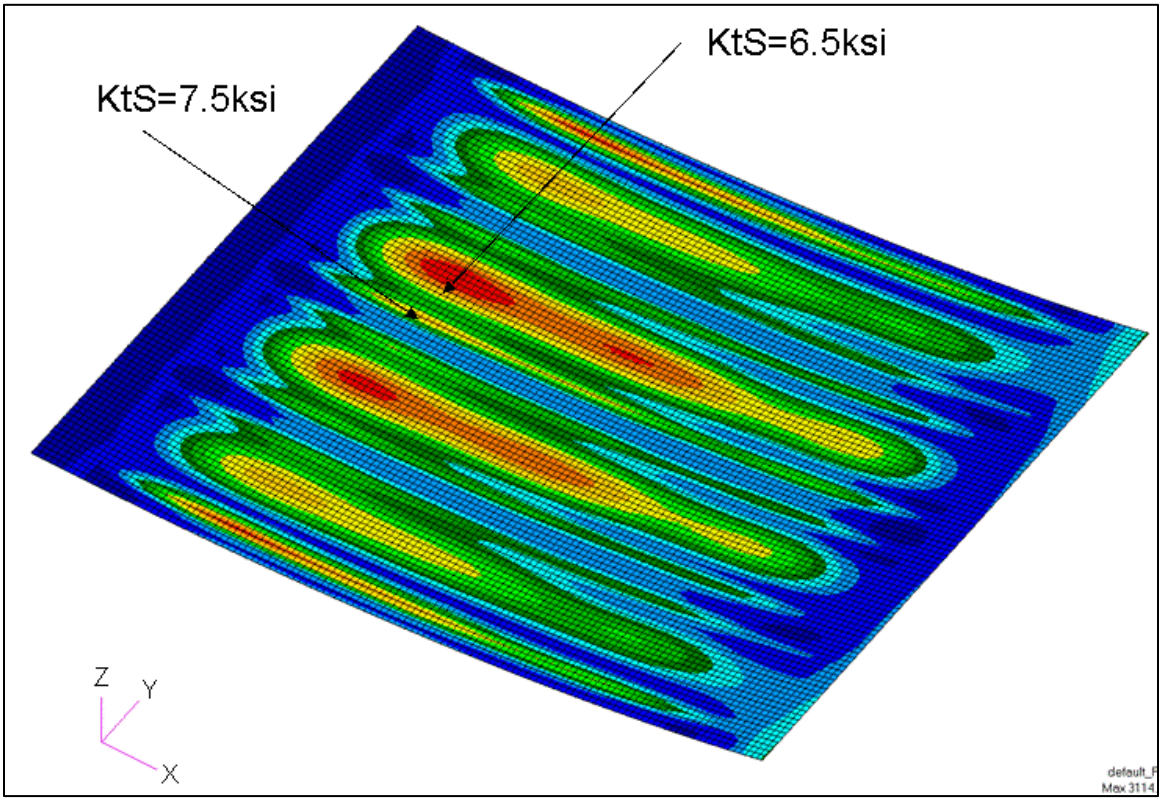

Figure 54 – RMS stresses in skin

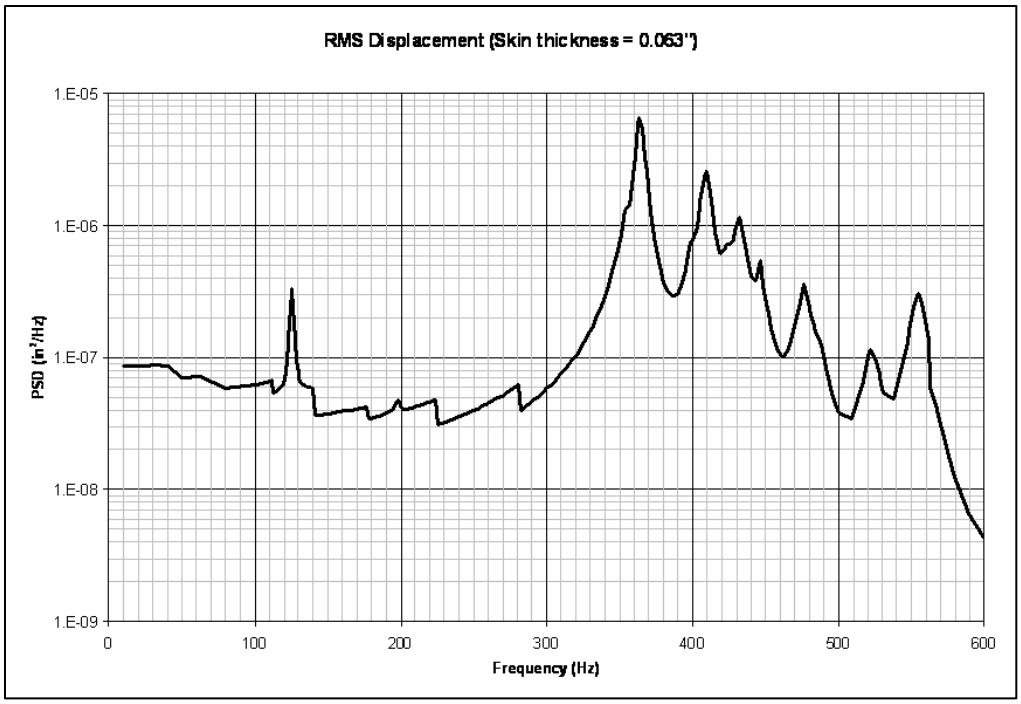

Figure 55 – Z-displacement PSD at mid bay center of panel

The flap model was run through a preliminary analysis using the Matlab NLROM GUI. This initial run did not include a thermal preload. The above linear random frequency response gave an indication of which areas of the panel would see the most stress over the test frequency range. Based on the RMS data, a node and element (4525) of interest were chosen from the location with the highest RMS stress, Figure 54. Then a linear ROM analysis was performed, using the NLROM GUI, which included all modes in the frequency range of interest. The z-displacement PSD for the center skin node is shown in Figure 56. The three modes indicated by the PSD plot for the critical node are modes 4, 6, and 14, which are shown below in Figure 57 through Figure 59, respectively.

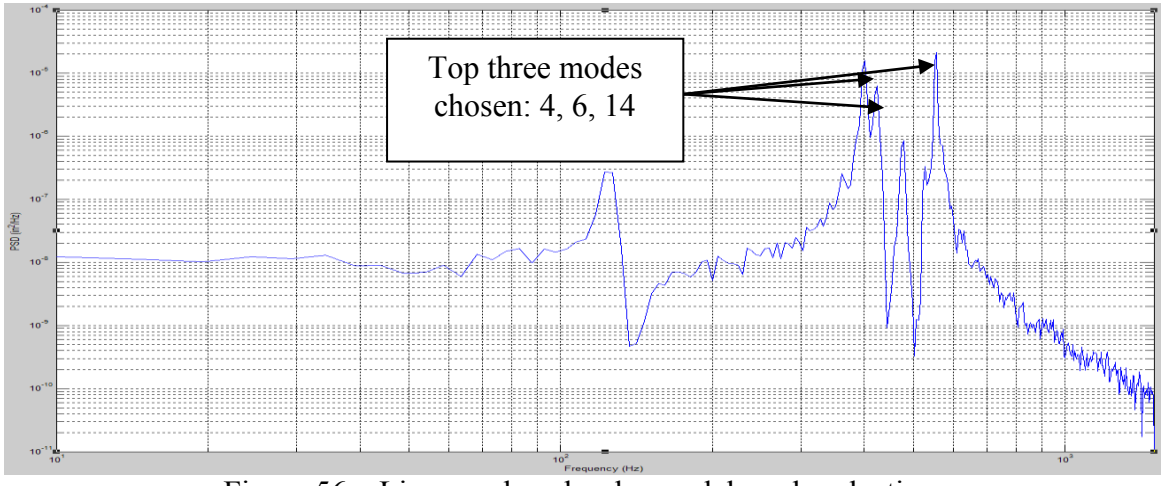

Figure 56 – Linear reduced order model mode selection

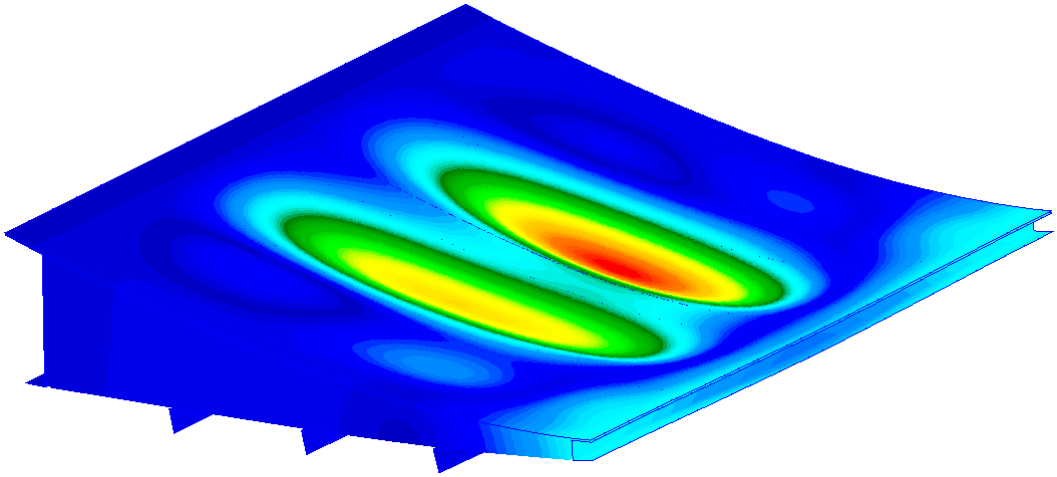

Figure 57 – Mode 4 at 399 Hz

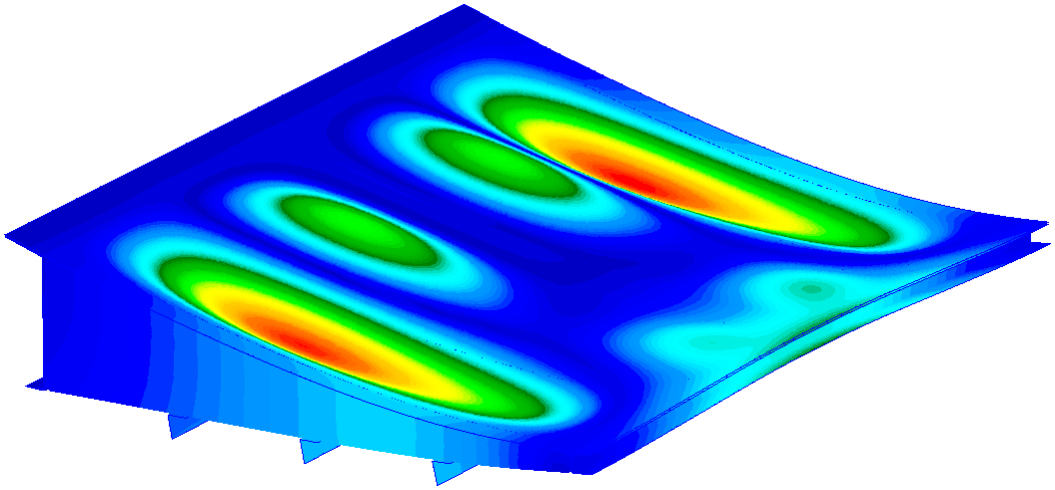

Figure 58 – Mode 6 at 423 Hz

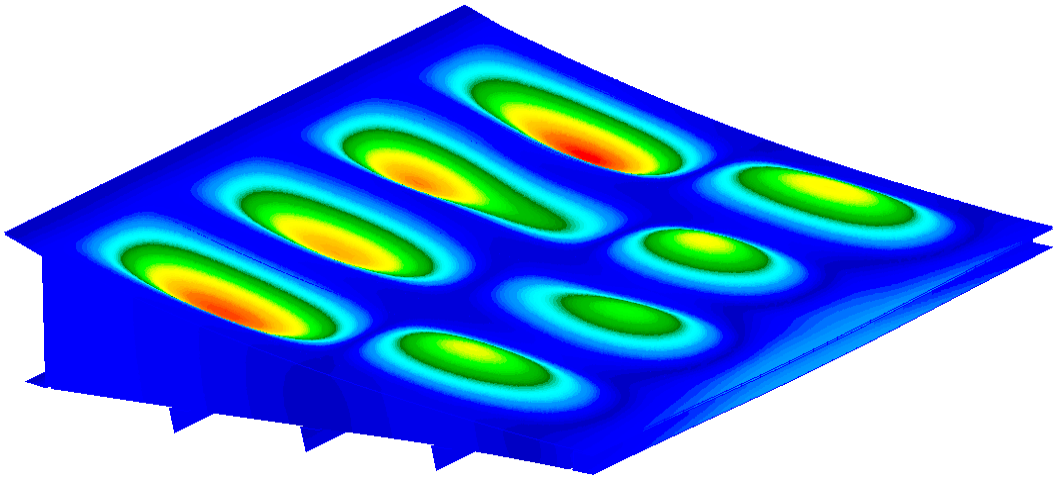

Figure 59 – Mode 14 at 555 Hz

The lowest flap bending mode was not selected for the nonlinear modal basis. It was determined that it was not a critical mode for acoustic fatigue of the skin panels. In order to calculate the nonlinear stiffness terms for the 3-mode reduced order model, a total of 26 load combination and nonlinear static analyses were run. Each nonlinear static analysis took 2.5 minutes to analyze, or about one hour clock time to run all 26 load cases. The z-displacement PSD for the critical node using the nonlinear ODE solution with the three modes selected above gives the following plot, Figure 60.

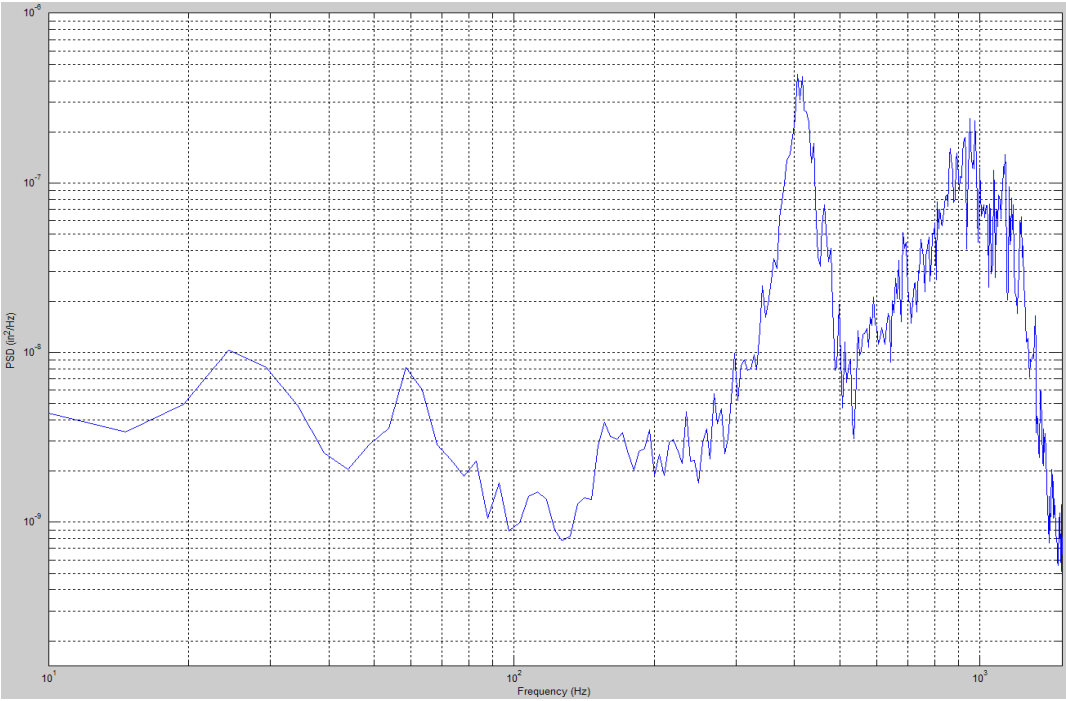

Figure 60 – NLROM center bay panel z-displacement

Stress time history post-processing was performed by selecting a shell element and outputting the displacement time history at each node degree of freedom. In this case, this was a four node shell with five DoFs per node (Ux, Uy, Uz, Rx, Ry). Then, a single element Abaqus/Explicit analysis was setup with these applied nodal displacements time histories. The Abaqus/Explicit analysis was performed and the element stress time history was output and post-processed in Abaqus/CAE. The stress time history of the element (4525) selected above is shown below in Figure 61. The plot shows the time history of the stress in the element, perpendicular to the ribs.

Post-processing stress results in a complex model for fatigue analysis from a full-order transient analysis can be tedious. Abaqus/CAE is used to extract and display the results. In CAE, the time history is saved to an ASCII file. Then, this time history is loaded into Matlab for PSD processing. For fatigue calculations, the time history is loaded into LifeWorks©, which uses a Stress-Life based cycle counting analysis. For transient analysis, results are processed for limited sets for nodes and elements and/or time steps, since very large output files can result. Hence, it's possible that the highest stressed element (i.e., most critical) is not selected. If possible, linear frequency response results are used to identify critical locations. But, if the structural response is very nonlinear, then the critical hot based on the linear analysis can be in error.

The final step was to perform Stress-Life fatigue analysis. This was performed by filtering the critical element stress time history in peak/valley pairs, and performing rain flow cycle counting analysis. The approximate design life was N=1e9 cycles. The calculated cycles to failure was N=1e13, or approximately 10,000 life times. Hence, the design was conservative. The conclusion was that the skin thickness could be decreased to minimum gauge, 0.08 inches to 0.063 inches. The response analysis was re-run with the new thinner skin gauge, Figure 61, and the stress analysis produced large positive acoustic fatigue life margins. Note the minimum gauge of 0.063 inches was set by requirements other than acoustic fatigue.

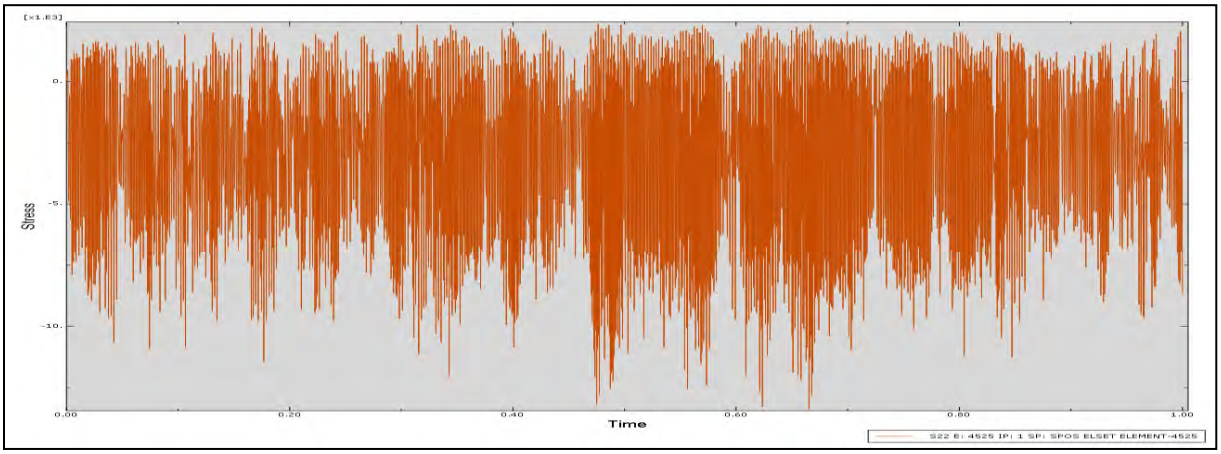

Figure 61 – NLROM post-processed element stress (4525) time history

As a comparison to the NLROM process, an Abaqus/Explicit full-order simulation was performed using a similar model (i.e., same mesh, material properties, loads and boundary conditions). The results were selectively compared to reduced-order results. Critical element #4525 was selected for output in the full order model, and PSD plots were generated to compare the out-of-plane deflection response, shown in Figure 62. The stress response in the direction perpendicular to the ribs is shown in Figure 63. In summary, this initial 3-mode solution yields reasonable comparisons to the full-order solution. There are obviously many more modes in the full-order response. There are also issues with comparing results obtained from similar models solved with different finite element codes. There is usually an assumption that the same model setup in NASTRAN and Abaqus should produce similar modal and response results. But, they can be very different as shown next.

Both models were run with no thermal preload, and the 3-mode NLROM solution used modes 4, 6, and 14. In summary, this initial 3-mode solution yields reasonable comparisons to the full-order solution in the frequency range of interest. There were obviously many more modes in the full-order response, but there were also issues with comparing similar models solved with different finite element codes. Ideally, the same model setup in NASTRAN and Abaqus should produce similar modal and frequency response results. In fact, the two analysis codes can produce rather different results for the same model, as will be discussed next.

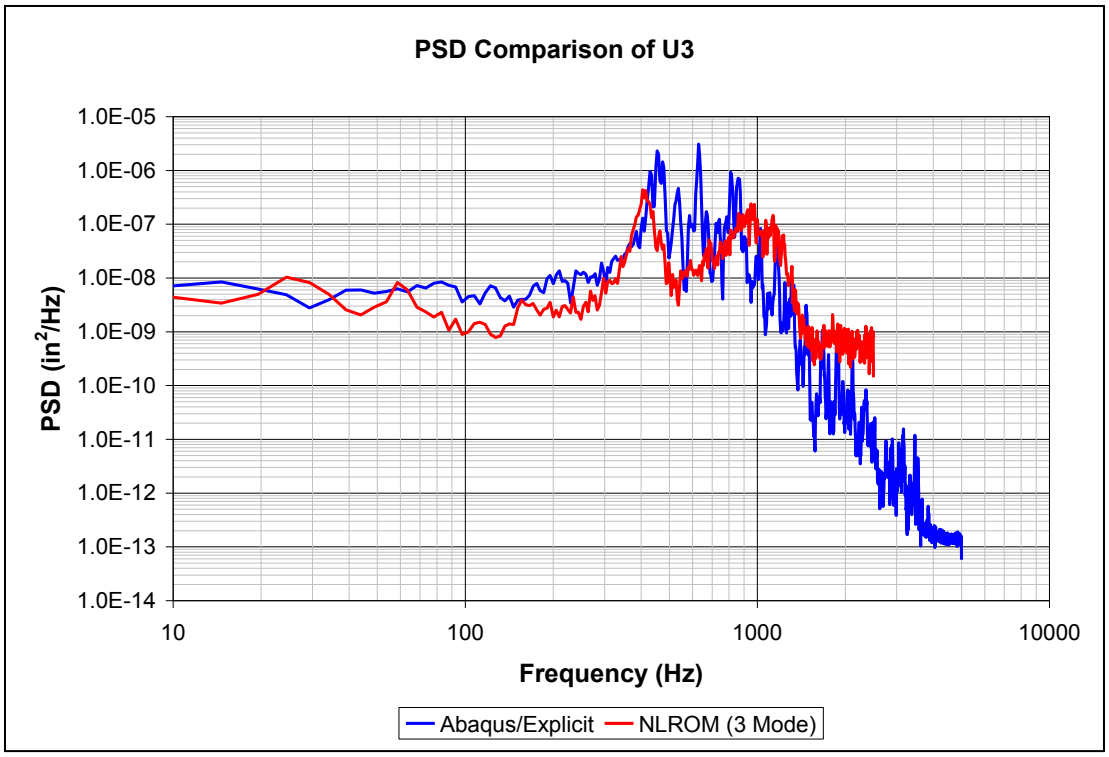

Figure 62 – PSD comparison of U_3 (or U_z)

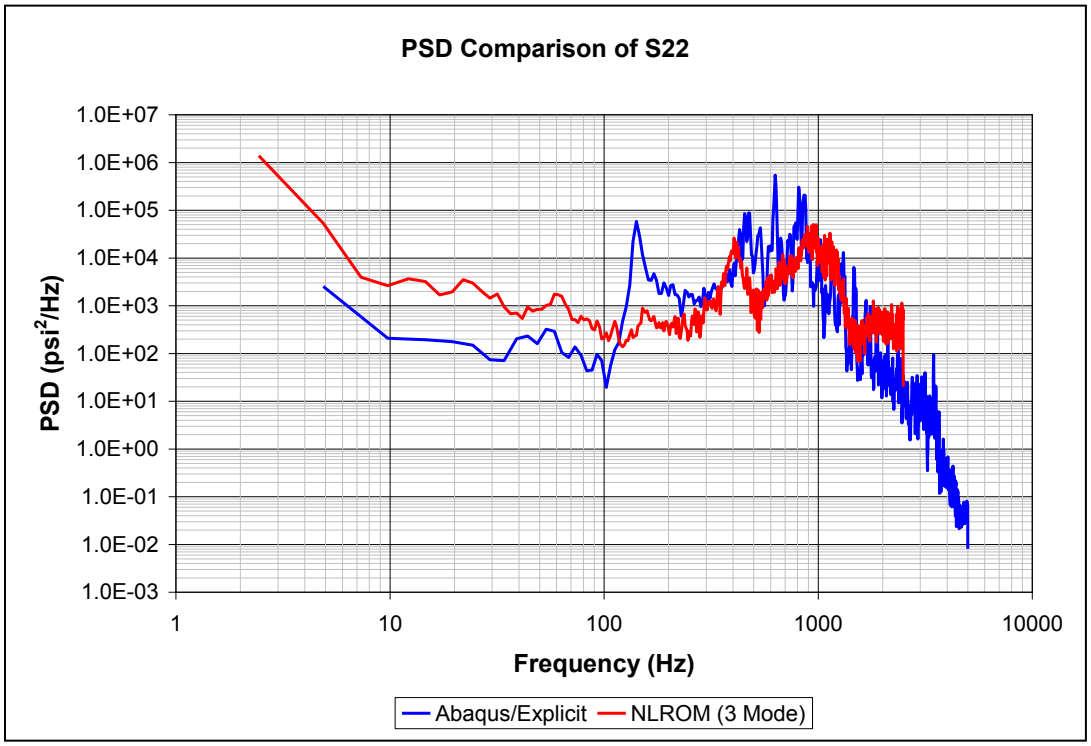

Figure 63 – PSD comparison of S_{22} (or S_y)

A comparison of the mode shapes and frequencies was performed to better understand how to interpret the PSD's from Abaqus/Explicit and NLROM. The Abaqus modes were generally higher in frequency, despite the fact that the mass properties for both models indicated that the weights were identical. There were a number of instances where Abaqus showed two modes swapped with respect to the NASTRAN solution. Also, while NASTRAN found 17 modes, Abaqus only found 15 in the frequency range up to 600 Hz. The mode shapes are shown side-by-side for comparison, in Figure 64 through Figure 76. The same Lanczos method was used for eigenvalue extractions. Beyond mode 9, there is little correlation between Abaqus and NASTRAN modes. What this means is that it would be difficult to base mode selection on the Abaqus/POD technique, or to use Abaqus/Explicit as a measure of validation to evaluate the reduced order models. The best method would be to use one analysis code for the NLROM, POD, and full-order explicit analysis.

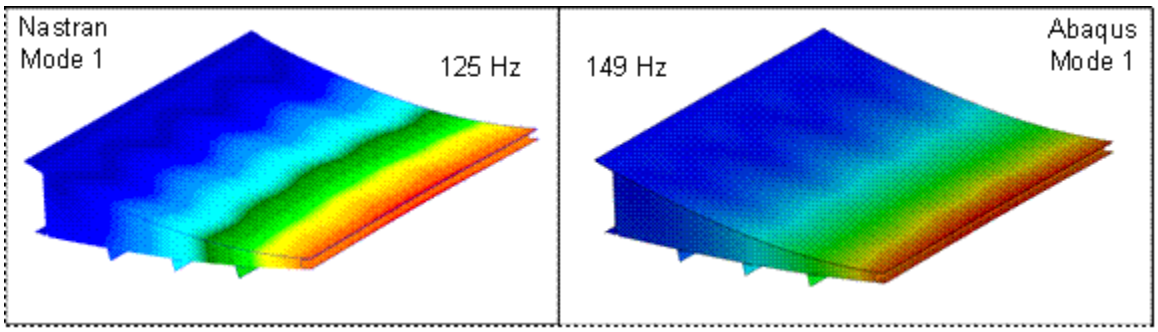

Figure 64 – Mode 1 side-by-side comparison

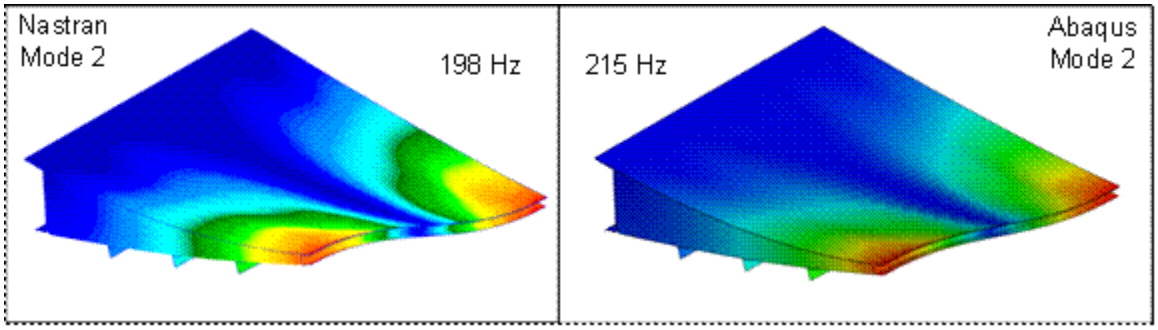

Figure 65 – Mode 2 side-by-side comparison

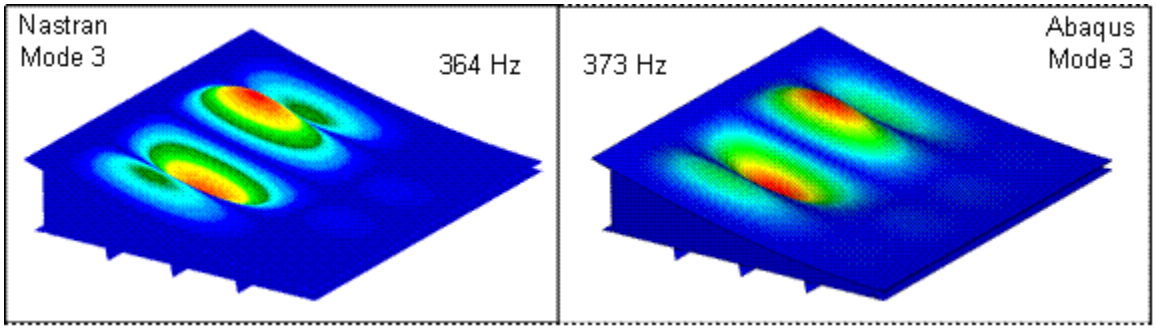

Figure 66 – Mode 3 side-by-side comparison

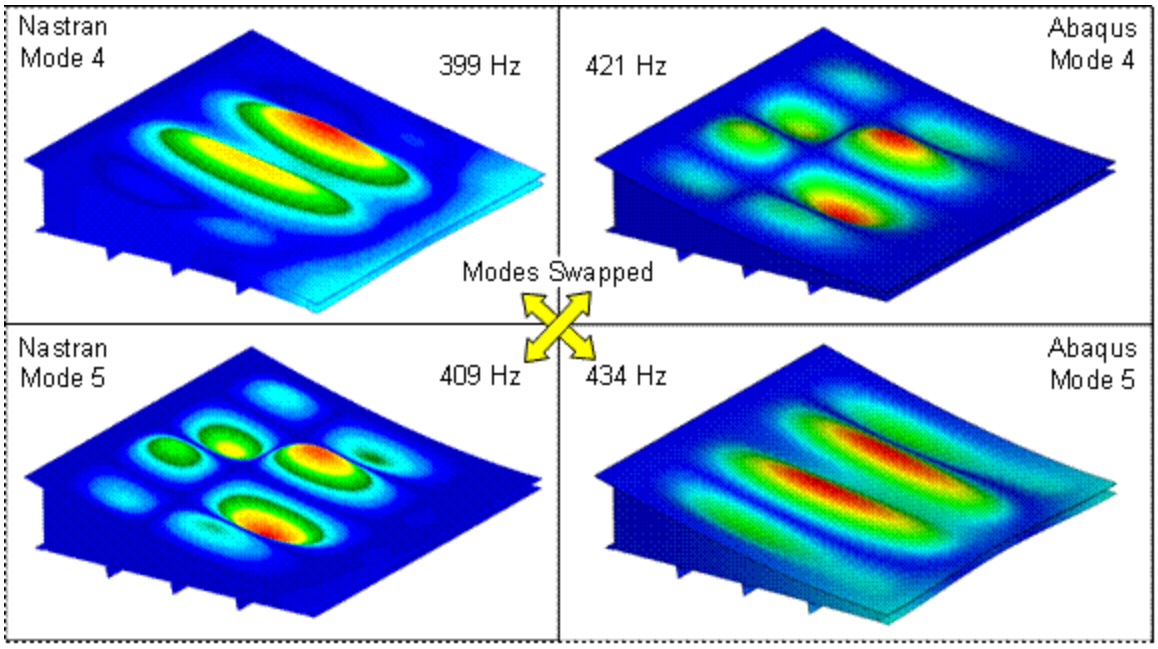

Figure 67 – Mode 4 and 5 side-by-side, modes have switched order

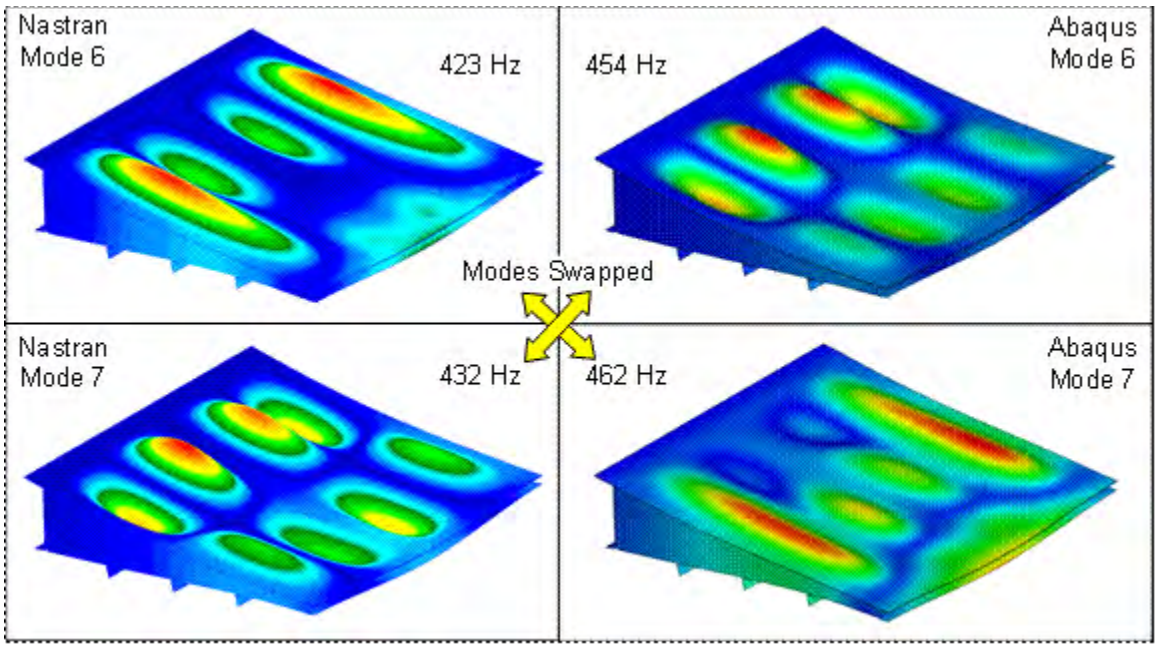

Figure 68 – Mode 6 and 7 side-by-side comparison, modes have switched order

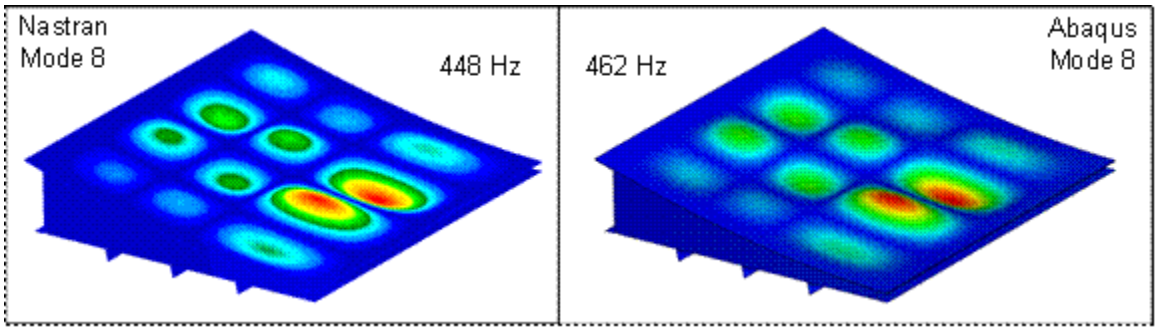

Figure 69 – Mode 8 side-by-side comparison

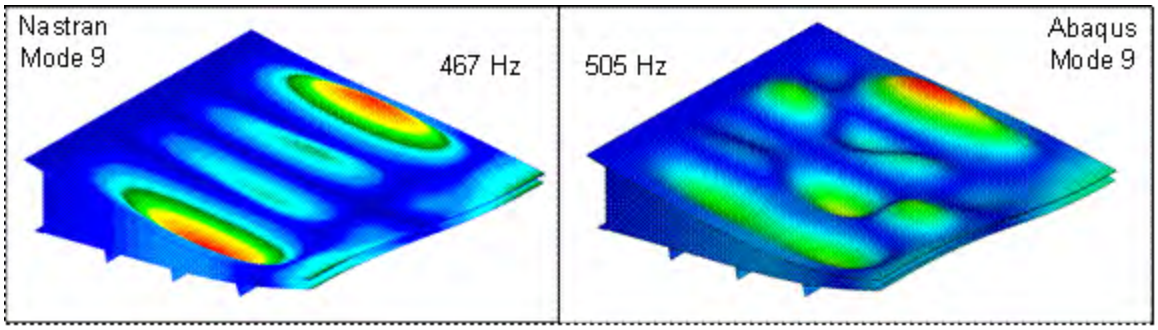

Figure 70 – Mode 9 side-by-side comparison

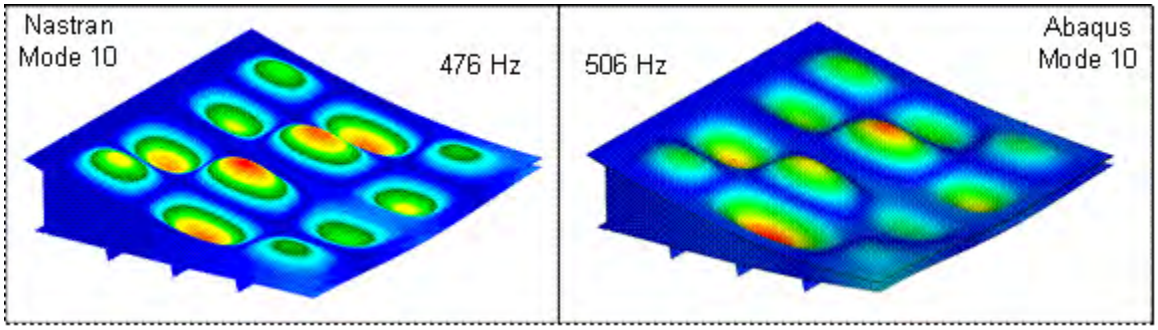

Figure 71 – Mode 10 side-by-side comparison

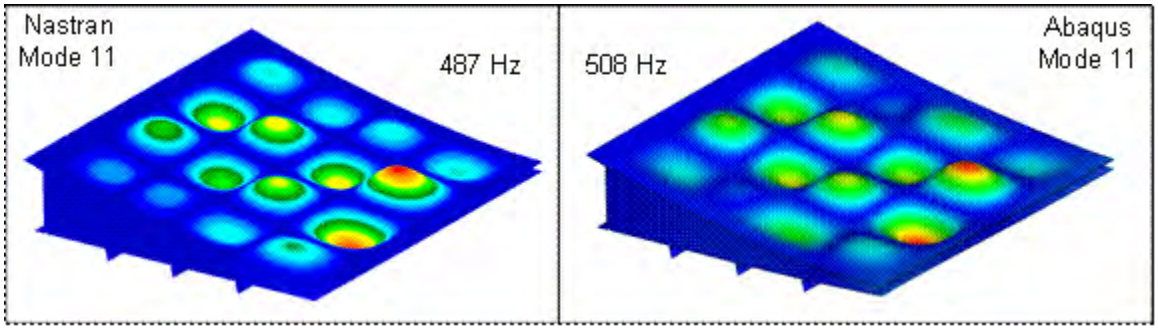

Figure 72 – Mode 11 side-by-side comparison

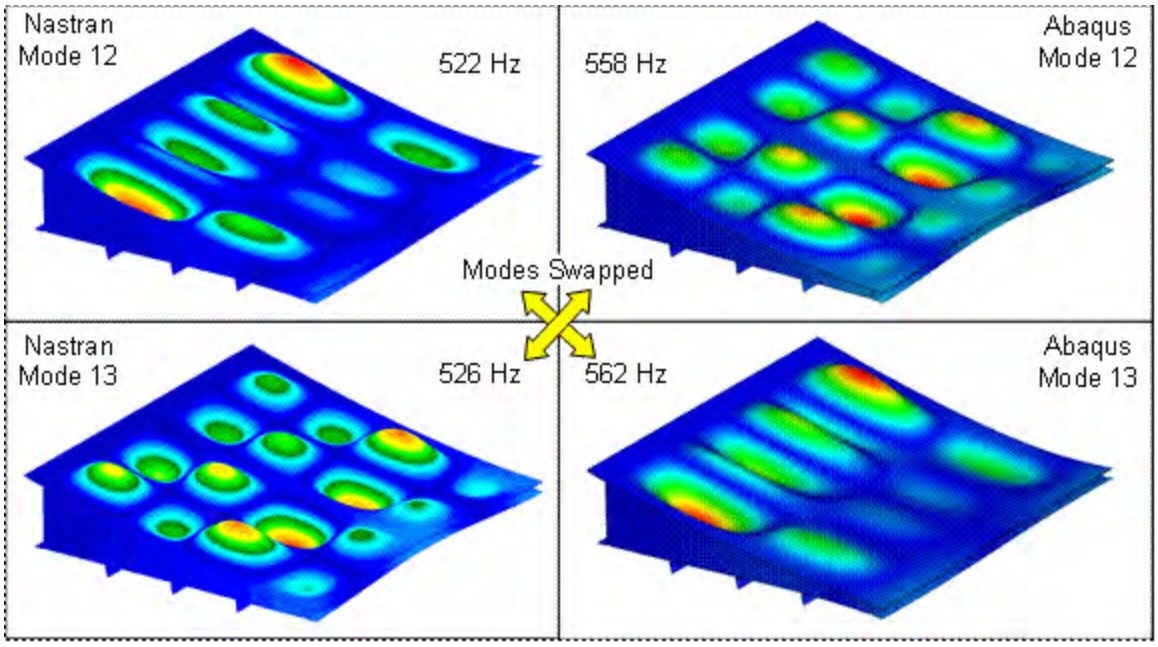

Figure 73 – Mode 12 and 13 side-by-side comparison, modes have switched order

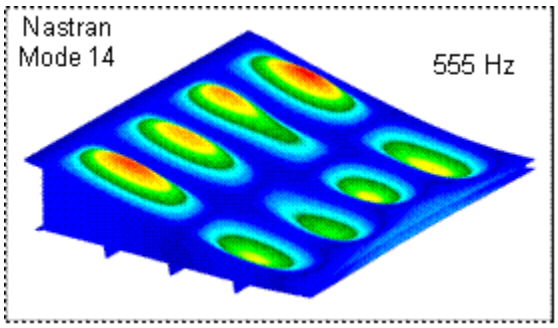

Figure 74 – Mode 14 NASTRAN only, no equivalent Abaqus mode

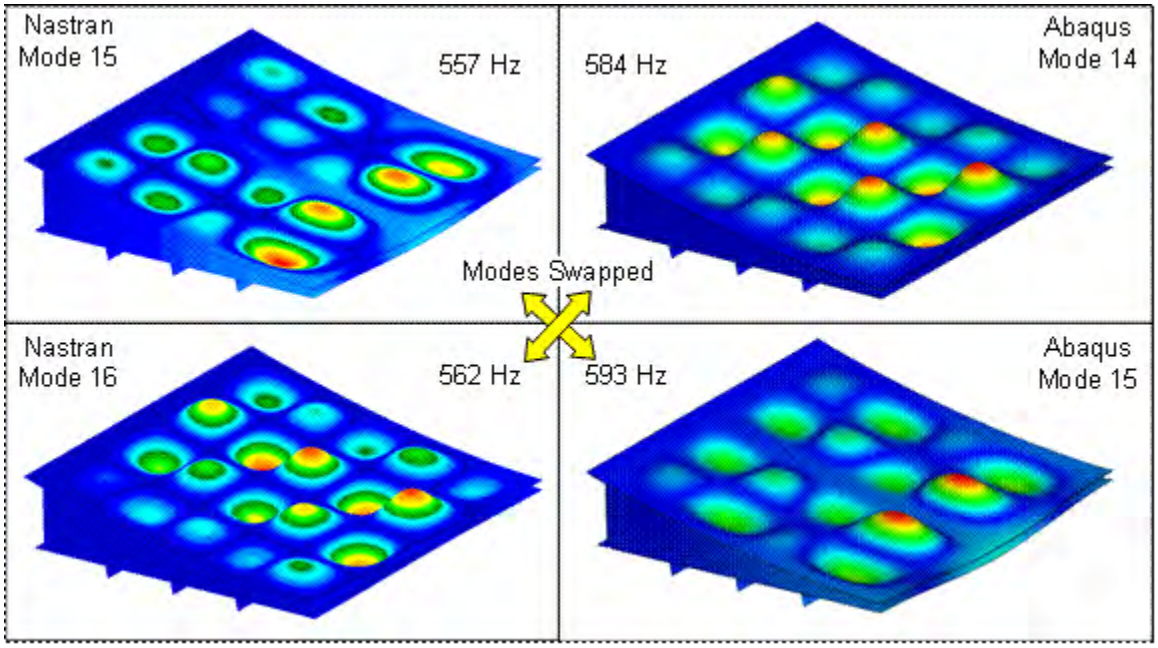

Figure 75 – Mode 15 and 16 side-by-side comparison, modes have switched order

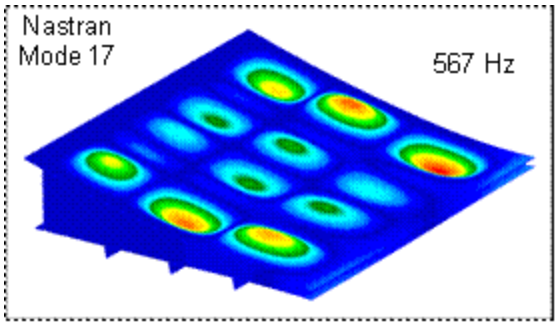

Figure 76 – Mode 17 NASTRAN only, no equivalent Abaqus mode

A separate study was performed to better understand how to reconcile the comparison issues between NLROM (based on NASTRAN) and Abaqus/Explicit. The previously described curved beam model was used with a baseline of 30 elements along its 30 inch length. Figure 77 shows a comparison between the different element types for this simple test case. The frequencies for linear elements (S4 and S4R) tended to be higher than that for NASTRAN elements, and those for quadrilateral elements (S8R) were lower. As for the NASTRAN element types, the CQUAD4 and CQUAD8 with lumped mass matched each other, as well as the CQUAD8 coupled mass solution. The CQUAD4 with coupled mass showed slightly higher frequencies.

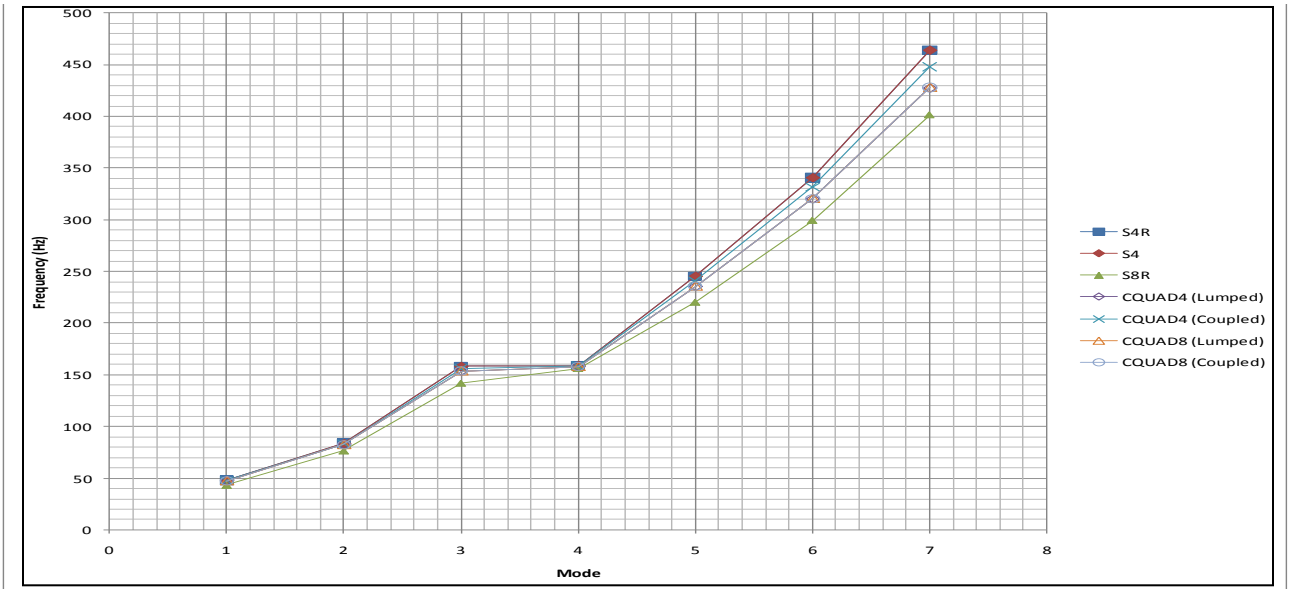

Figure 77 – Comparison of Abaqus and NASTRAN element and mass formulations

A mesh density comparison was performed for the NASTRAN CQUAD4 lumped-mass formulation and the Abaqus S4R elements, the default shell element formulations for the each code. The results indicate that the NASTRAN solution is not dependent on the mesh density, shown in Figure 78, as was the case for Abaqus S4R elements, shown in Figure 79. In light of this mesh refinement study, it appears that a much denser Abaqus model would actually be needed to achieve the same accuracy.

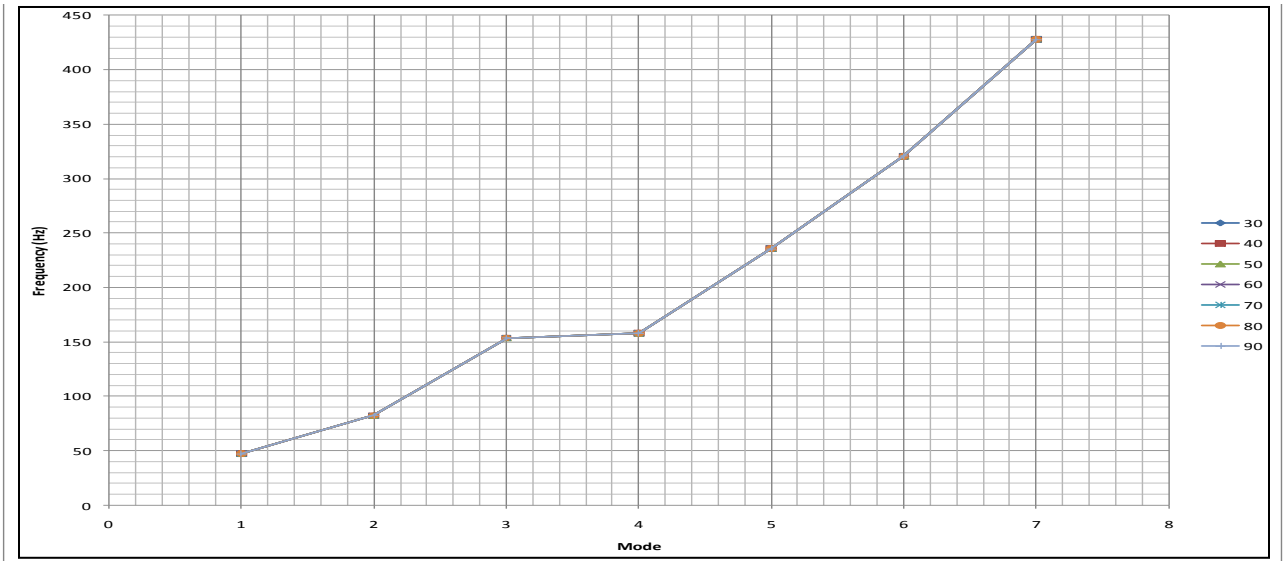

Figure 78 – Comparison of NASTRAN modal solutions with increasing mesh density

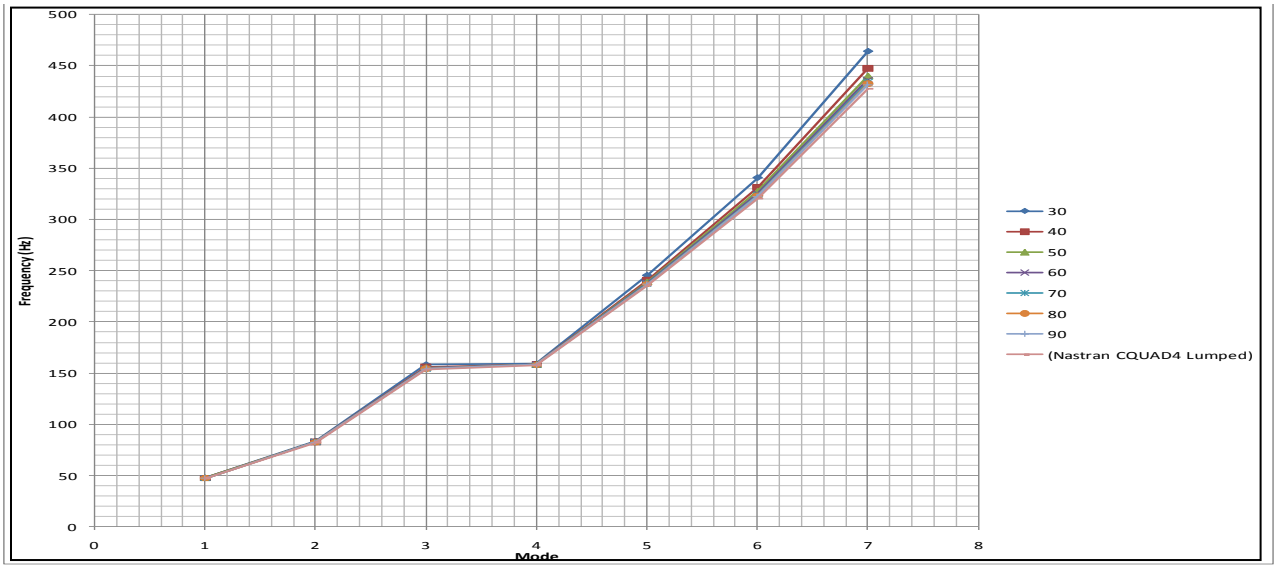

Figure 79 – Comparison of Abaqus modal solutions with increasing mesh density

The results from the element study suggest that it would be useful to change to using the NASTRAN solution 700 explicit analyses in place of the Abaqus/Explicit analysis. However, this has generated some issues of its own, as can be seen in Figure 80. Both solutions begin exactly the same, but while the Abaqus/Explicit shows essentially consistent behavior throughout, the NASTRAN SOL 700 solution exhibits what appears to be increasing high frequency participation about some presumably buckled state.

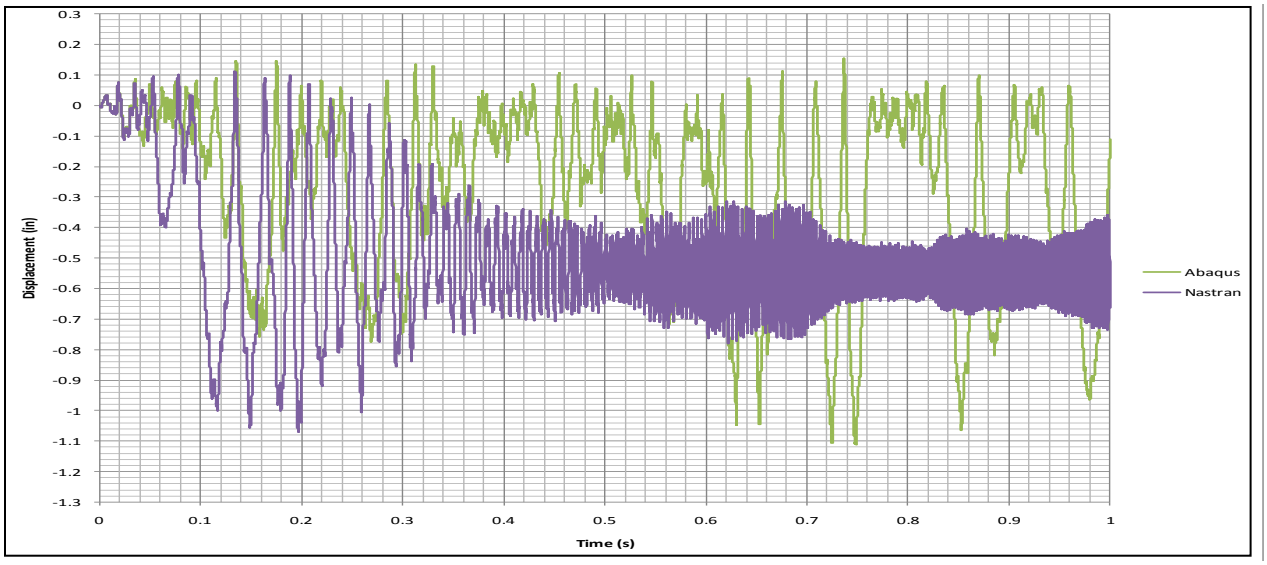

Figure 80 – Comparison of Abaqus/Explicit and NASTRAN sol700 time history for center beam node

In conclusion, the Abaqus or NASTRAN explicit analysis cannot be used as a good basis for verifying NLROM accuracy. The accuracy will be based on comparisons to the test data. However, the full-order explicit solutions do offer value in determining the computational efficiency of the NLROM solutions.

Therefore, in order to best understand these efficiency benefits of NLROM, a study was performed on the effect of number of CPU (processors) on the Abaqus/Explicit solution time. The full order Abaqus/Explicit solution was run for only 0.01s to have practical run times for the purposes of this study. It was found that the reduction in solution time began offering noticeably diminishing returns when using more than 28 processors, Figure 81. The multiples of 7, as opposed to standard powers of 2, were a limitation of the High Performance Computing (HPC) system being used for the study. This is because each 8 core node could only allocate 7 cores for Abaqus analyses.

It is interesting to note that doubling from one to two processors only gave a 33% reduction, while doubling from two to four processors gave a 50% reduction. Also, adding three more processors to the four processor solutions only gave about a 10% reduction, while doubling from seven to 14 gave roughly a 40% reduction. This suggests that there are “sweet spots” when deciding how many processors to use to solve an Abaqus/Explicit analysis. It was not determined whether these “sweet spots” were model-specific or solver-specific. For this model, a 10 sec simulation on 1-processor would take 3000 CPU hours, or on 28 processors it will take 266 CPU hrs. These are significant CPU usage times. The explicit solution described above was for only 1 sec on 28 CPUs. Therefore, the Abaqus/explicit solution time is improved with parallel processing. There are significant reductions up to four CPUs, but efficiency decreases with increasing CPUs.

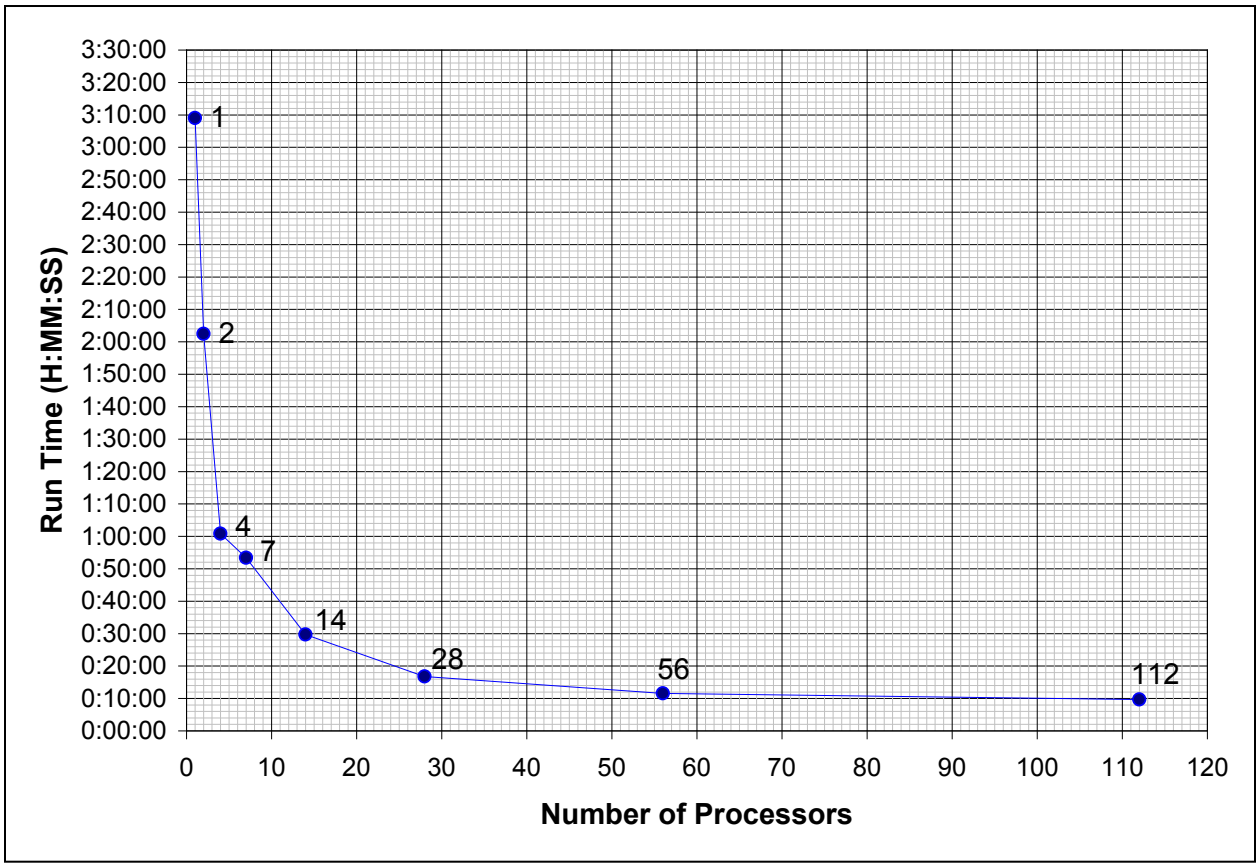

Figure 81 – CPU processor study results

5.2 Test Article Design Study

The test article was similar to the design study flap previously described, Figure 82. The interior three ribs were aircraft grade titanium, Ti-6Al-4V – AMS 4911, while the outer two ribs were stainless steel. The lower skin (hot side) was thin gauge (0.063 in) titanium. All other parts were stainless steel. The test article also consisted of cross stiffeners and leading and trailing edge frames. This extra structure helped to stabilize the test article, and provided support to the lower skin and ribs as would an upper skin in an actual aircraft flap. The upper skin was replaced with the cross stiffeners such that backside non-contacting measurements of the lower inner mold line (IML) skin were possible during the Combined Environment Acoustic Chamber (CEAC) tests. The end ribs and frames were machined stainless steel. The top cross stiffeners were standard extruded A36 steel angles.

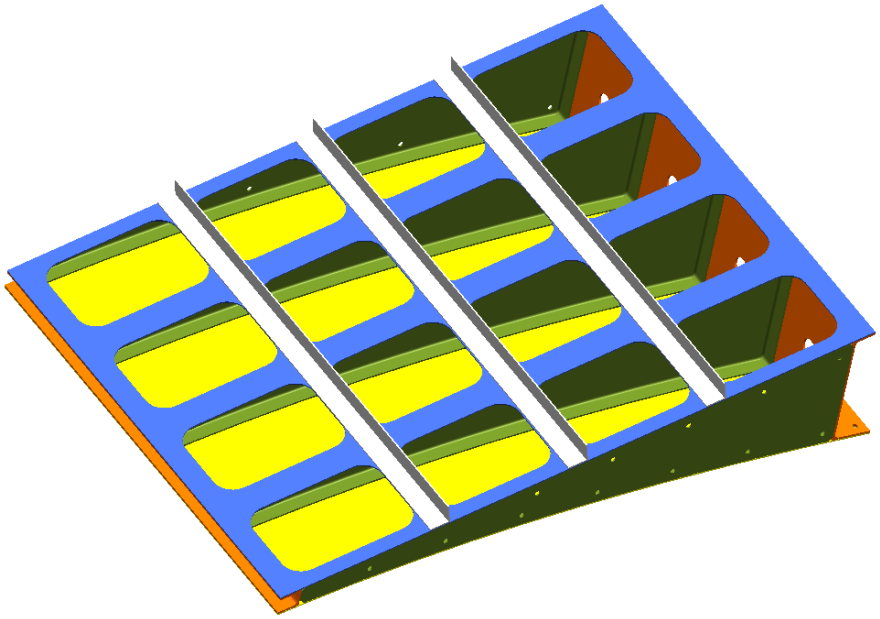

Figure 82 – Representative flap test article

The next step was to design the adapter fixture that held the flap test article in place during the CEAC and T-58 tests. Below, in Figure 83, is a drawing of the assembled test article and adapter fixture installed on the CEAC adapter cart. The adapter fixture was bolted to the end frames and outer ribs. It mated the test article to the CEAC cart as shown. When the test cart is slid into position, the test article fits through a window on the CEAC facility side wall as depicted in Figure 84. The leading edge would be flush to the interior wall with the trailing edge protruded into the chamber.

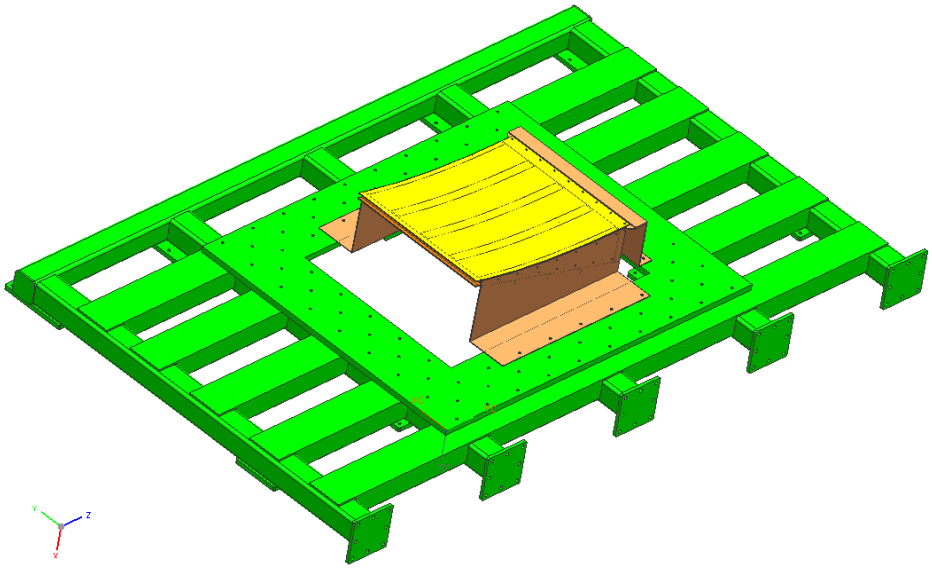

Figure 83 – Test article and fixture mounted on the CEAC cart

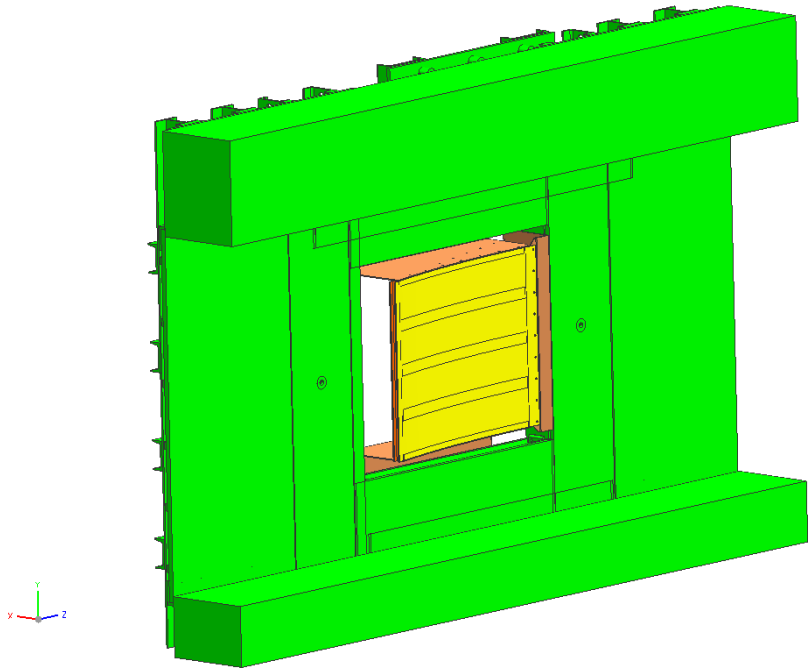

Figure 84 – Test article installation in the CEAC side wall

The second design iteration of the test article is shown in Figure 85. This design was the basis for ordering pan stock and raw materials for fabrication and assembly. Part of the effort of this task was to perform design and analysis of the test article and fixture assembly, and determine if there were any fixture modes that might influence the test article response Figure 86 is a depiction of a test article mode that resulted in a redesign of the test fixture. The goal was to remove any fixture modes from the excitation frequency range of interest. The objective is to insure that there are not any test article vibratory was to gather information about the modes that influence the test article vibratory modes, were to be test configuration Figure 87.

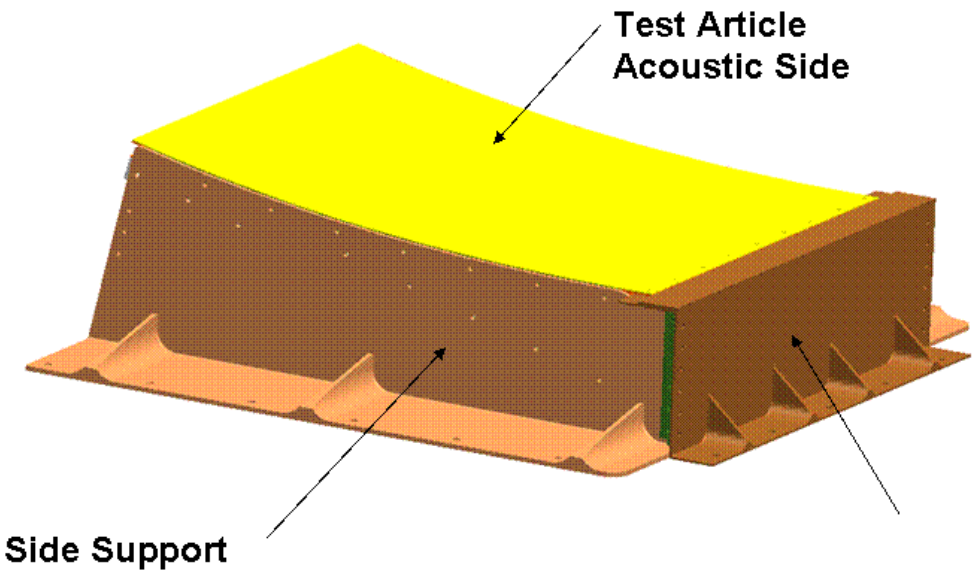

Figure 85 – Preliminary design of the test article and fixture

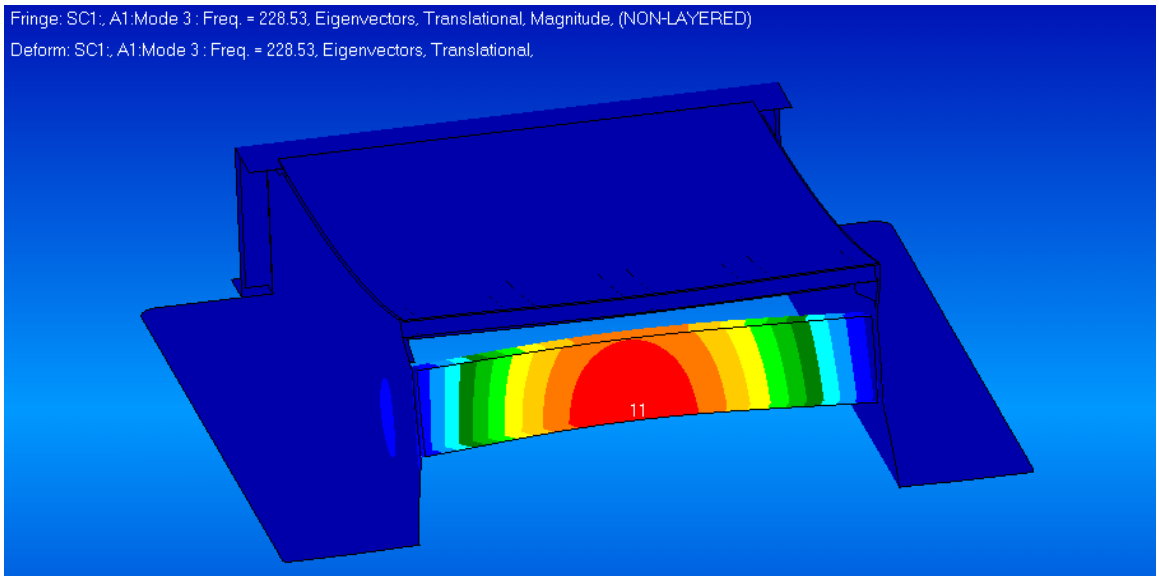

Figure 86 – Example of a fixture mode that needed to be eliminated

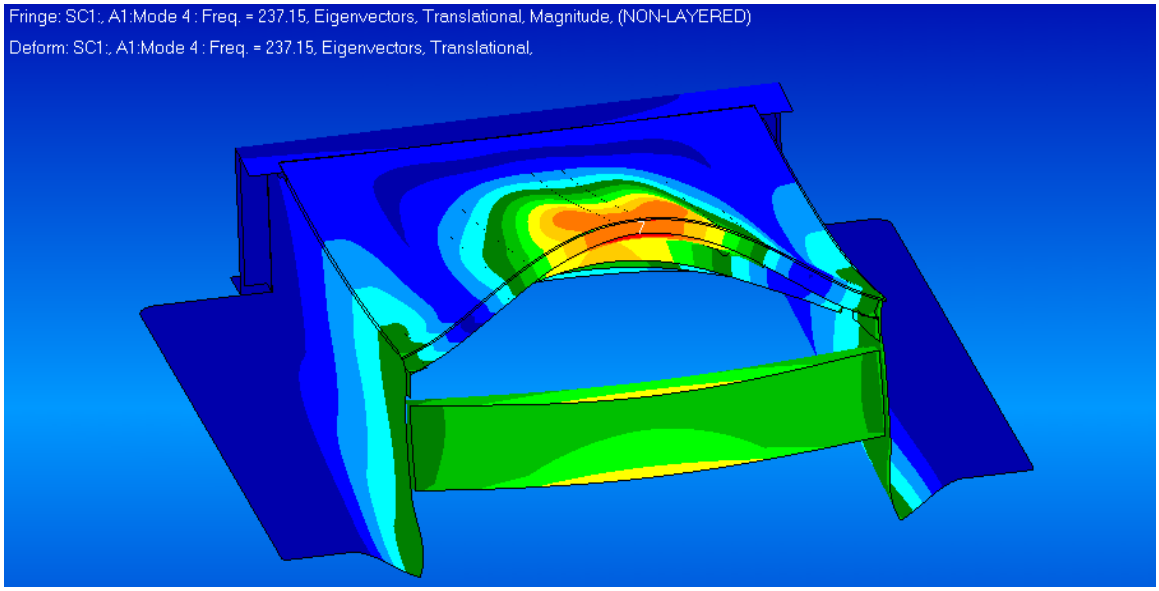

Figure 87 – Example of an expected mode similar to the actual flap

A second test article and adapter fixture was fabricated for the T-58 Burner Facility. A design constraint was that the fixtures and test articles were to be the same for the T-58 Burner Facility and the AFRL CEAC Test. Therefore, the structural modeling used in both tests should be the same. For the burner test, the fixture was mated to the test article to properly align the test article with the engine. In the figure below, the lower flat plate (in gray) is the part of the engine fixture mounting table. The blue parts are mounting hardware provided by the test facility, which was adapted to fit the fixture (in orange). The T-58 test article was identical to the CEAC test article. Hence, the test articles would have similar panel modes and frequencies for both tests. Figure 88 shows the engine, rectangular exit nozzle, test article, and the exhaust duct.

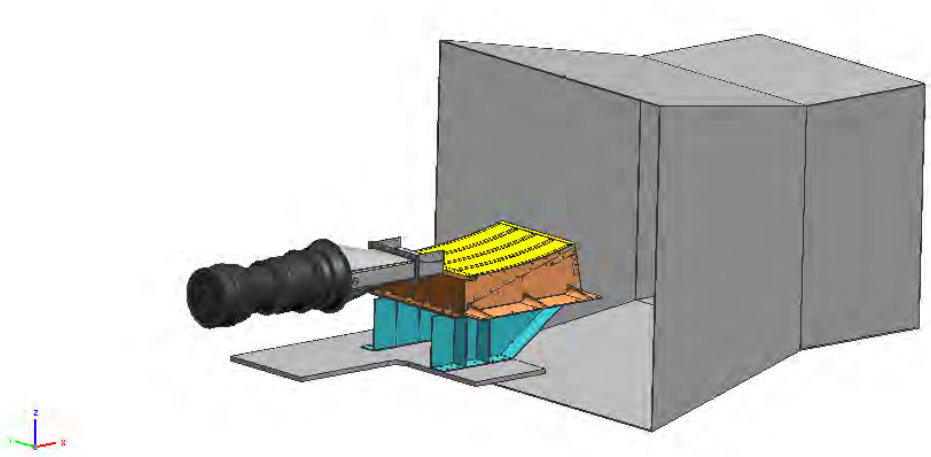

Figure 88 – Overall facility setup

6.0 Pre-test Analysis and Predictions

Analysis of the structural test component was performed using the refined nonlinear reduced order modeling methods. The response of the test component for a range and combination of acoustic and thermal loads that were expected in the test program were predicted.

6.1 Thermal Analysis

For the CEAC test, the thermal analysis was set up to mimic the test conditions. The test article fixture was included in the model and all materials were given temperature-dependent material properties. The thermal aspects included in the thermal model were radiative cooling to ambient, forced convective cooling across the skin of the test article, and open cavity radiation between a heated surface and the skin of the test article. As some of the details of the setup were unknown during the pre-test analysis the lamp bank temperature was set to 1500°F, and placed 12 inches straight out from the front edge of the test article, as shown in Figure 89.

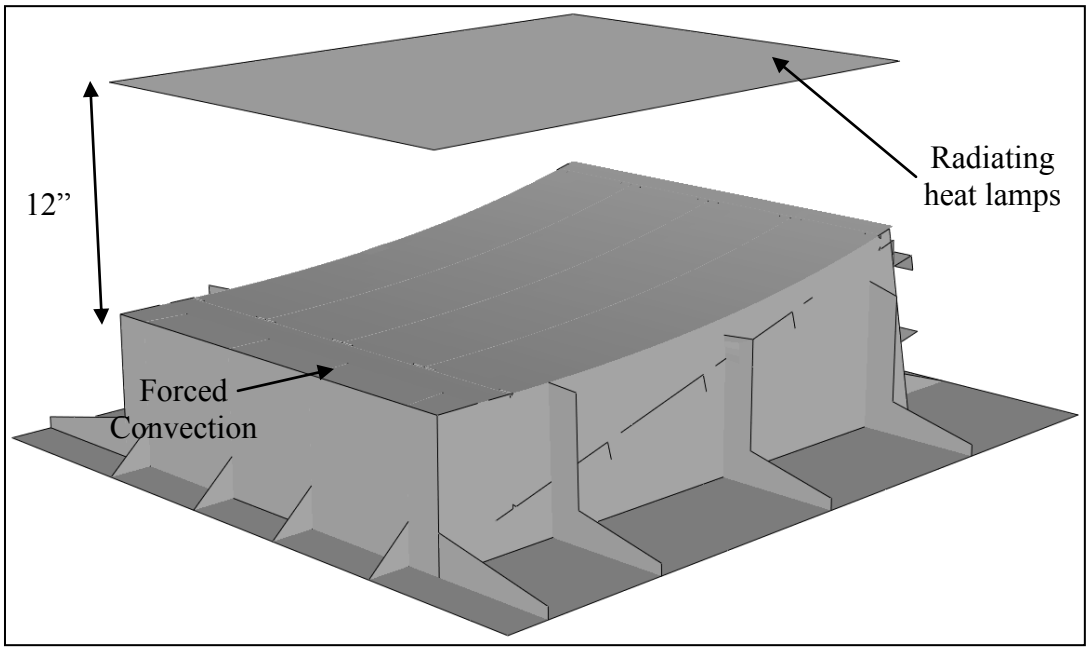

Figure 89 – Test setup with radiative surface above test article

As this was a pre-test analysis, details of certain aspects of the test were unknown. Therefore, a best estimate for many of the inputs was made to generate predictions. The heat transfer coefficient for the forced convection across the exposed surface of the skin was chosen to be 9.65×10^{-6} Btu/in^2·s·°F, corresponding to an air speed of 20 ft/s. The results from the heat transfer analysis, in Figure 90, show temperatures ranging from 75 to 500°F. This range seems in accordance with the expected temperatures for that final CEAC test.

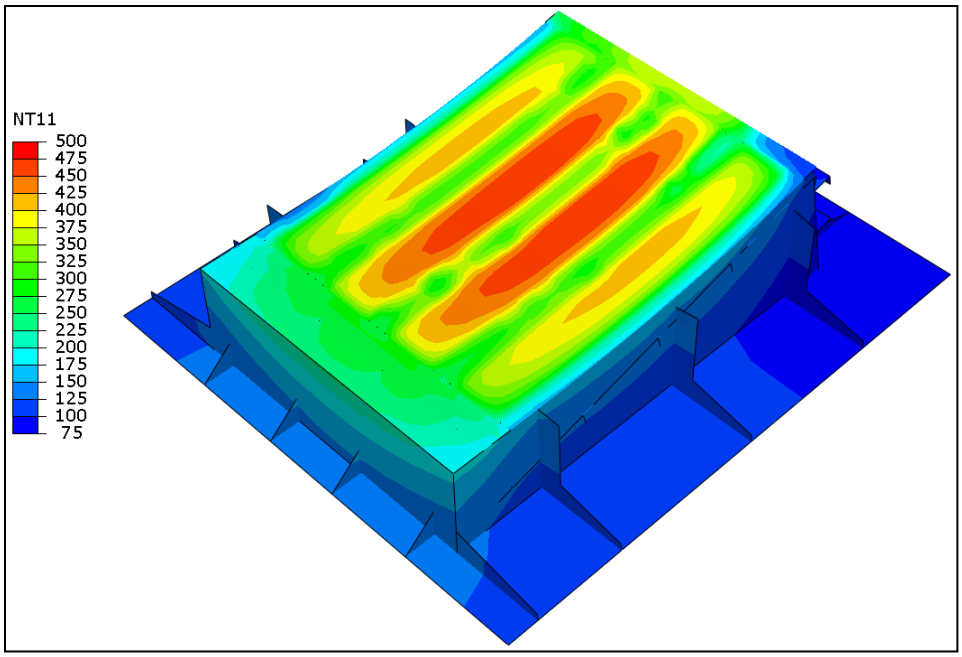

Figure 90 – Heat transfer model temperature results

The displacements and stresses for the heating profile from the thermal analysis shown above are displayed in Figure 91. These temperatures are written in NASTRAN format to facilitate a thermal preload for the hot modes analysis technique used in the NLROM process.

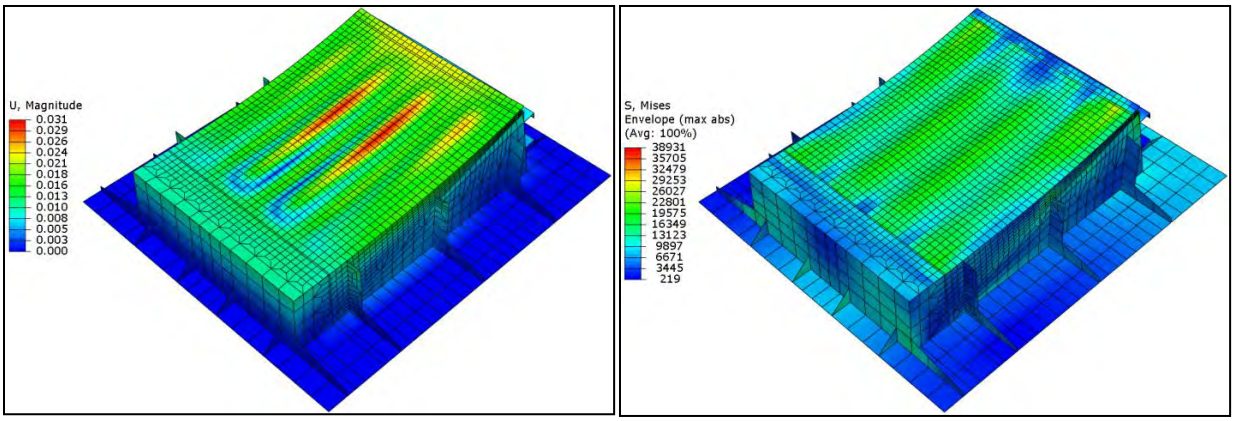

Figure 91 – Thermal displacement and stress results

The pre-test predictions of the T-58 engine test setup required a more work as the heating was not from a uniform heat source. Infrared images provided temperatures from a titanium calibration panel, but the size was different from the current test article, and therefore the temperature information outside the calibration image area was unknown. As a first approximation, the IR temperatures were placed on the test article skin as a boundary condition, and the temperatures were allowed to reach a steady state with radiation cooling to ambient air from all surfaces. Since the flow was not uniform in temperature or velocity, the convective heating from the engine exhaust was difficult to model explicitly. The plan was to take as many IR images during the test as needed to cover the whole test article skin to adjust the finite element model skin temperatures to match the test temperatures. The temperature distribution in

the T-58 engine exhaust on the calibration panel, Figure 92 and Figure 93, ranged from approximately 360 to 970°F.

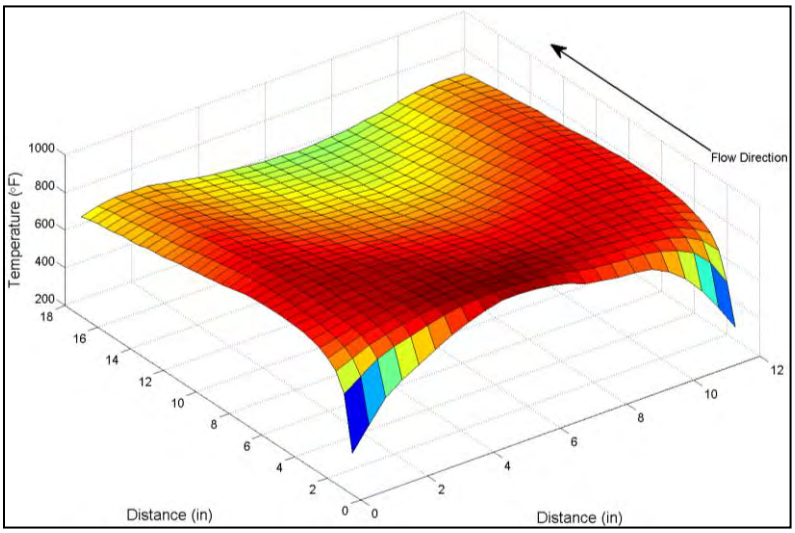

Figure 92 – Temperature distribution for Ti panel in exhaust flow of T-58 jet engine

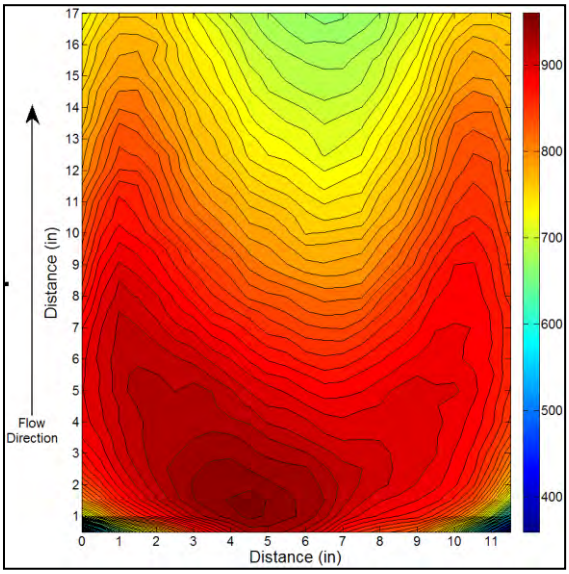

Figure 93 – Temperature distribution for Ti panel in exhaust flow of T-58 jet engine

6.2 Test Article Critical Location Studies

Initial critical location acoustic and thermal response studies were completed on the model with the fixture included. These initial linear studies were performed for the entire test article, but were performed for the thermally preloaded model for both test configurations. The model was divided into 8 pressure load cases, and uncorrelated with respect to each other. These are shown in Figure 94. Results extracted from the RMS analysis included stress, strain, acceleration, and displacement. Figure 95 and Figure 96 show the critical RMS stresses and strains in the skin, respectively. Figure 97 and Figure 98 shows the RMS acceleration and displacement results. These RMS studies indicate that the critical areas are in the center of the two middle bays, just behind the forward spar.

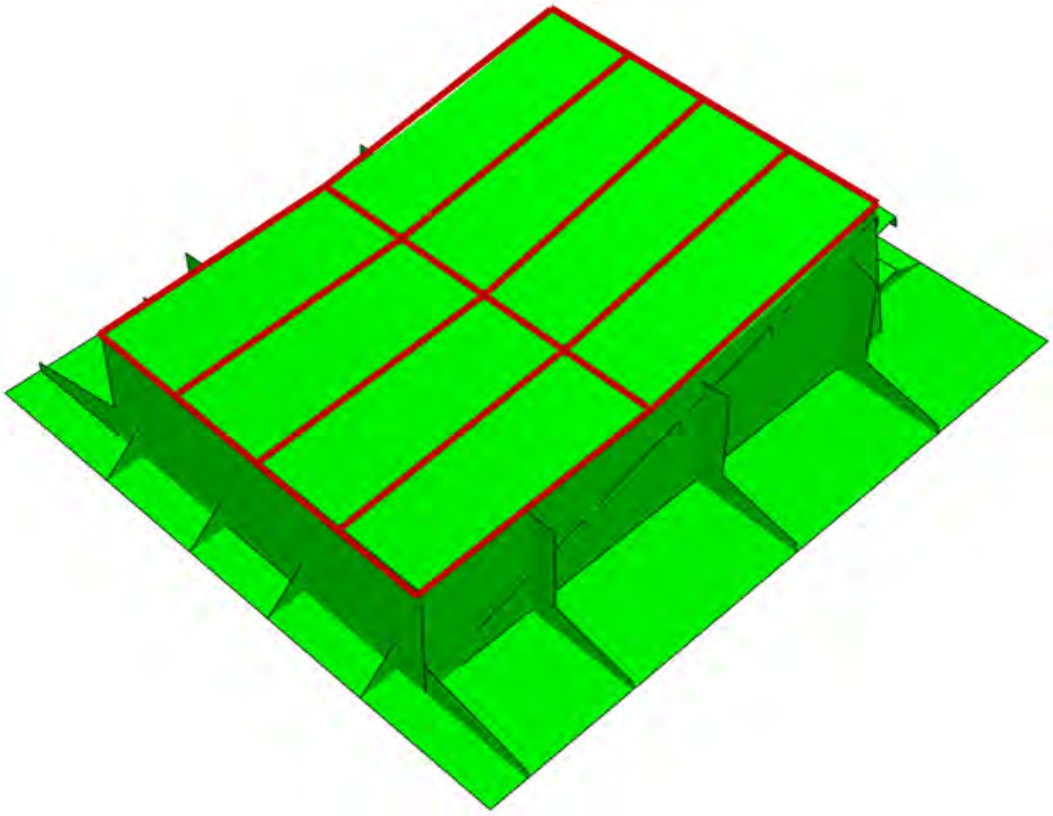

Figure 94 – Location of the eight pressure cases on the skin of the test article

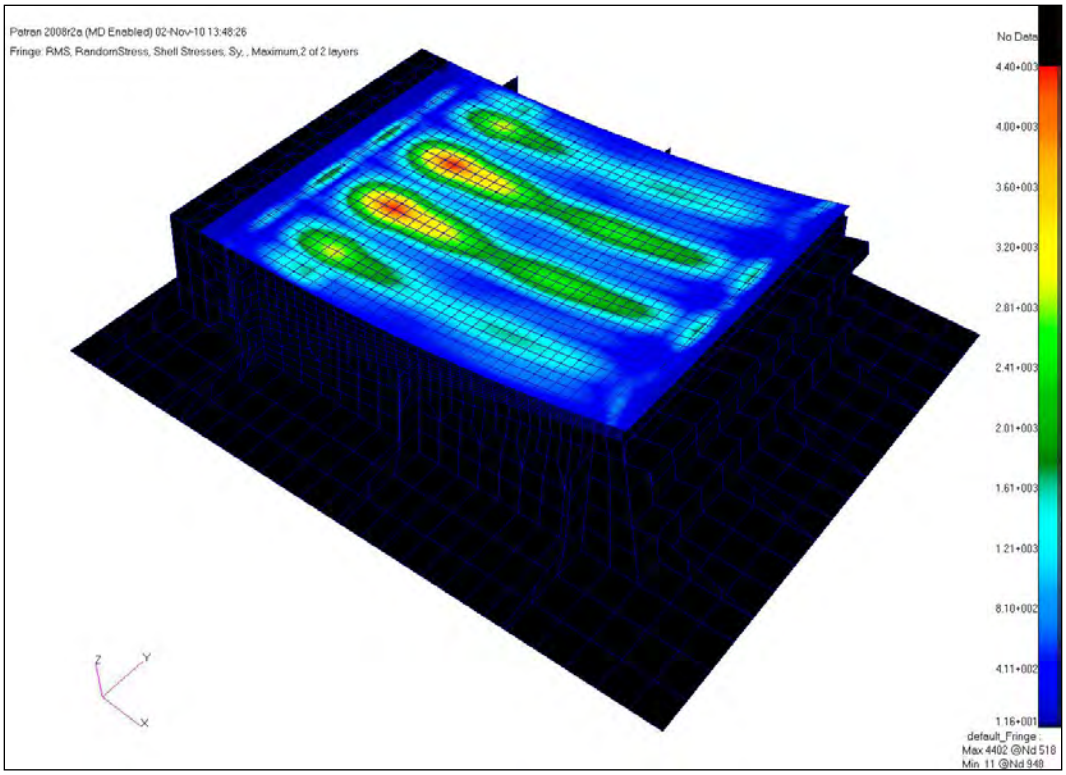

Figure 95 – RMS stress analysis of the skin showing critical locations

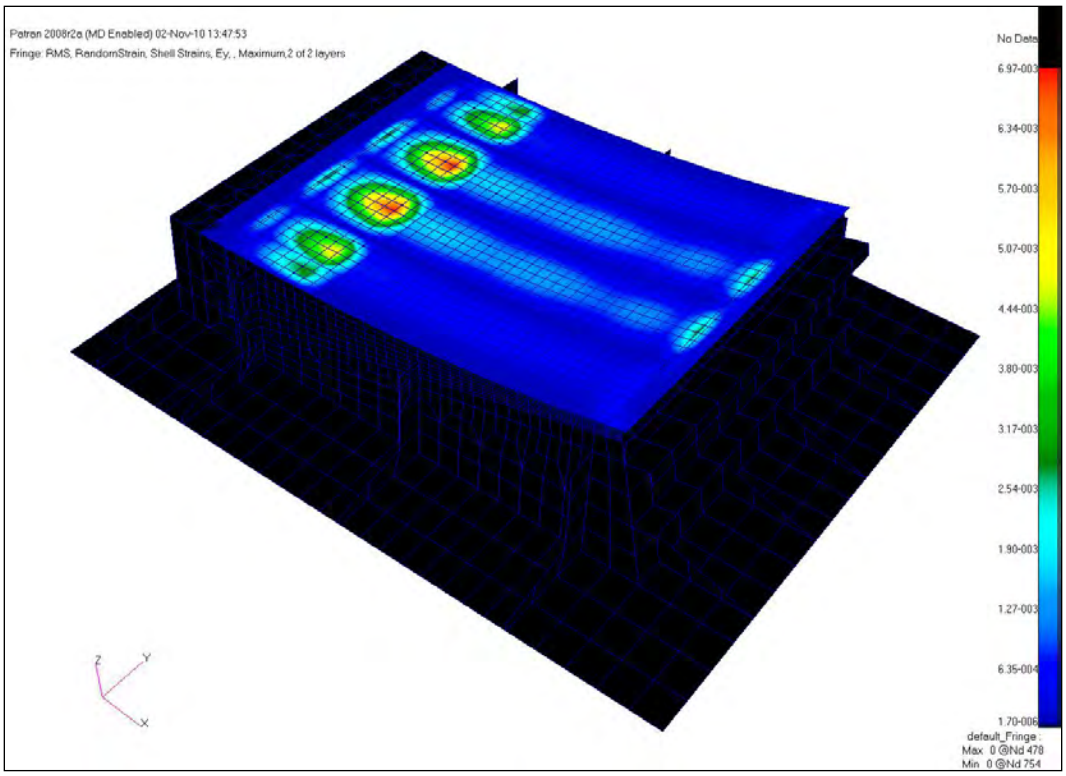

Figure 96 – RMS strain analysis of the skin showing critical locations

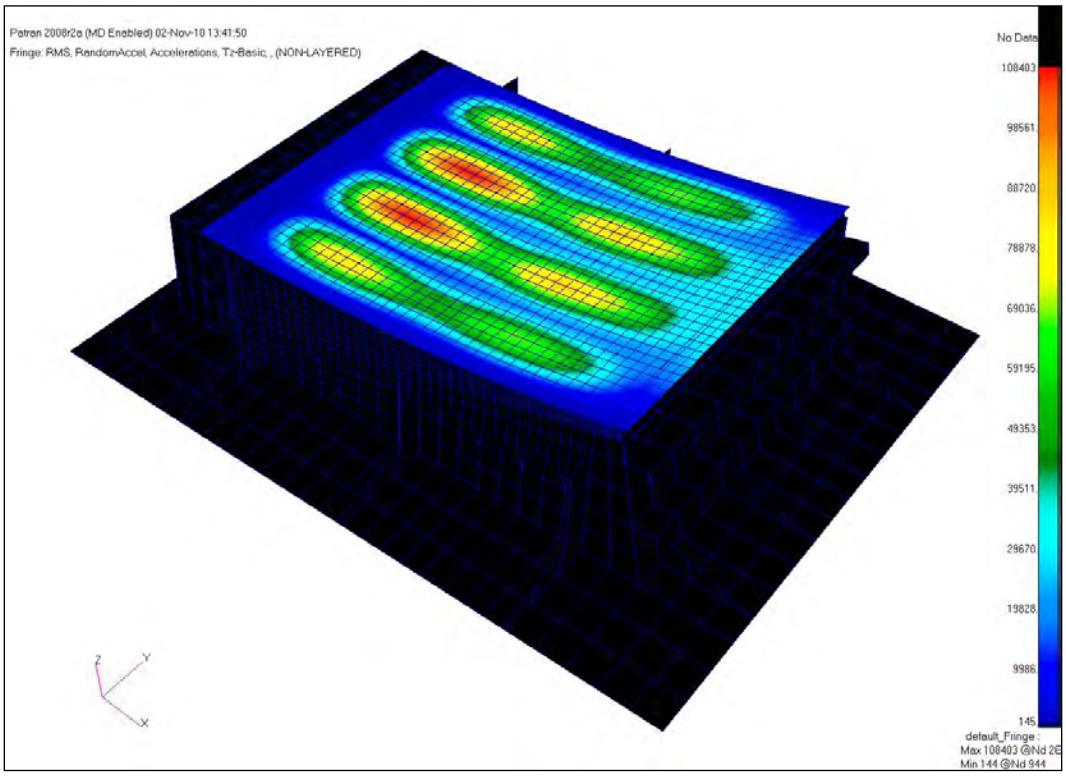

Figure 97 – RMS acceleration analysis of the skin showing critical locations

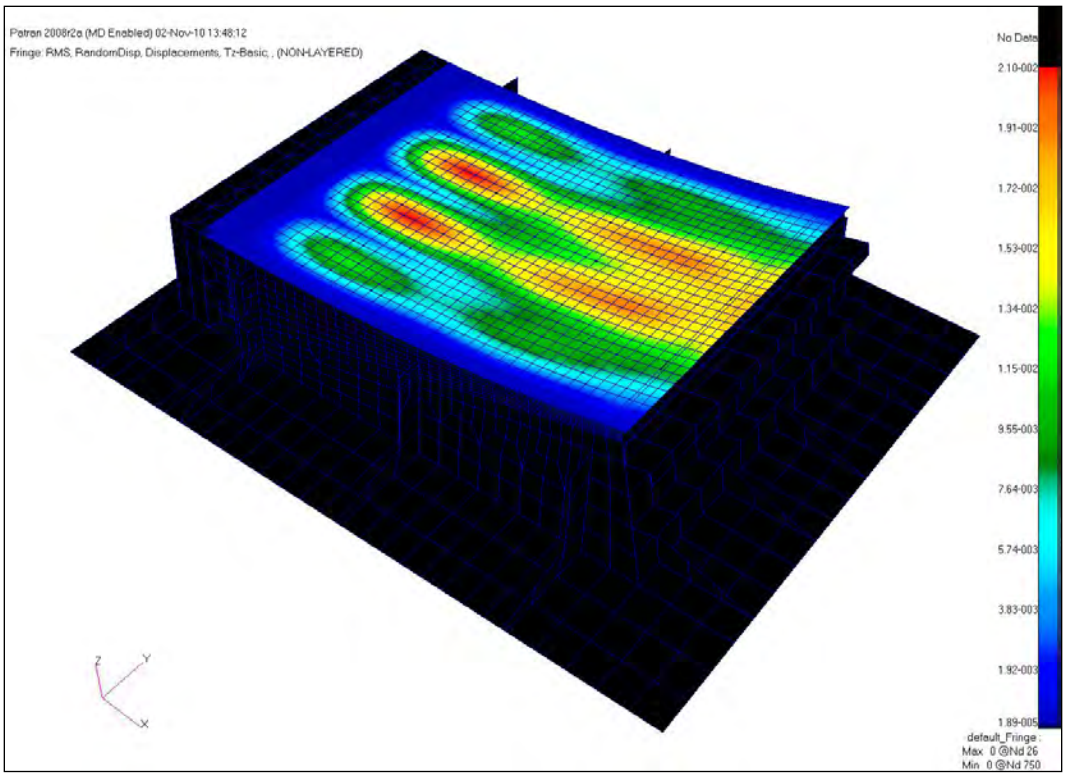

Figure 98 – RMS displacement analysis of the skin showing critical locations

For the CEAC model, a spectrum was generated to provide the pressure input to the eight skin sections. This spectrum is set to give an OASPL of 170 db, Figure 99. The displacement PSD for the critical node, chosen from the RMS stress plot, is shown Figure 100. The six top contributing modes 1, 2, 3, 4, 9, and 10 were selected for the NLROM, acoustic only, Figure 102. The mode at 200 Hz is the flap 1st bending mode.

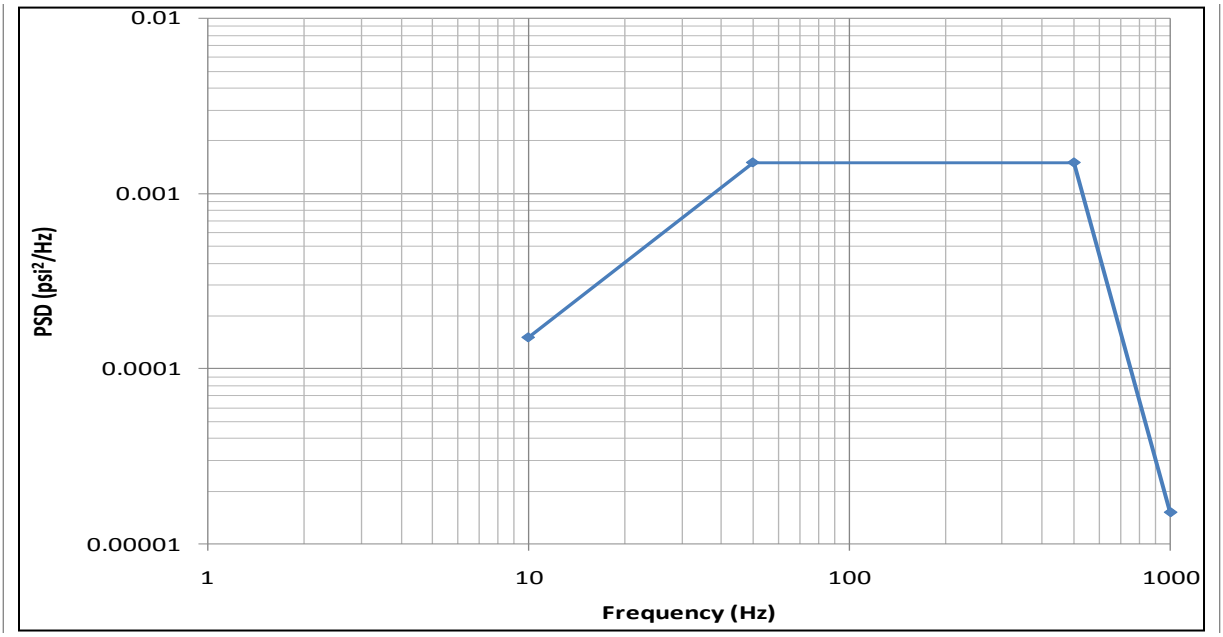

Figure 99 – Pressure input spectrum

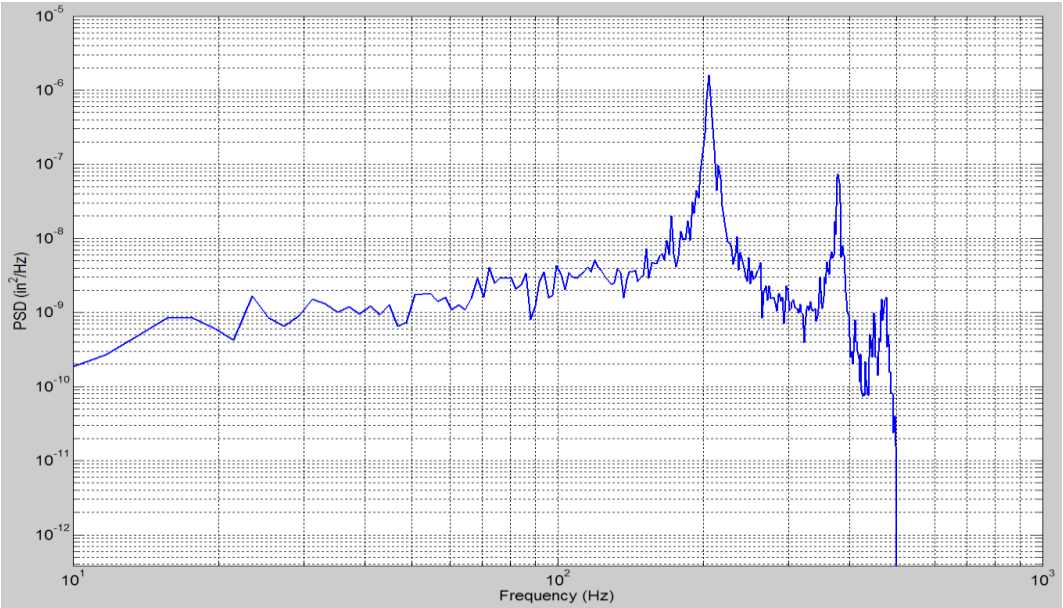

Figure 100 – Z-displacement PSD at critical RMS stress location

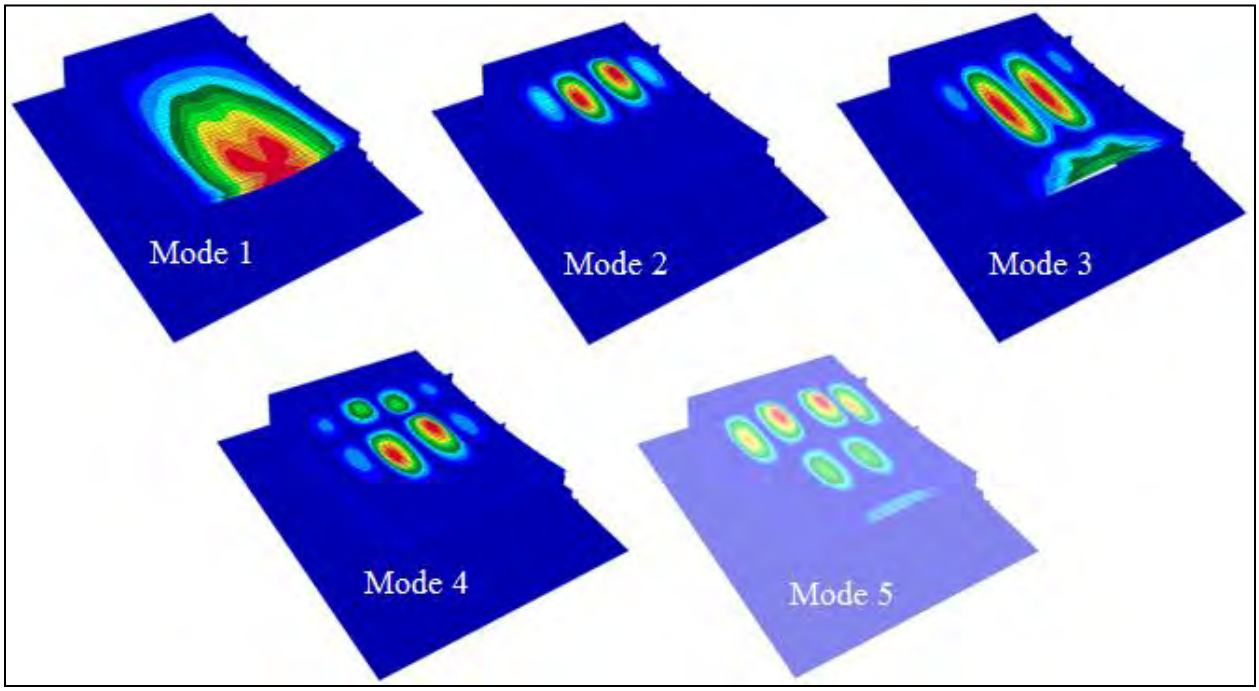

Figure 101 – First five mode shapes with selected NLROM modes highlighted

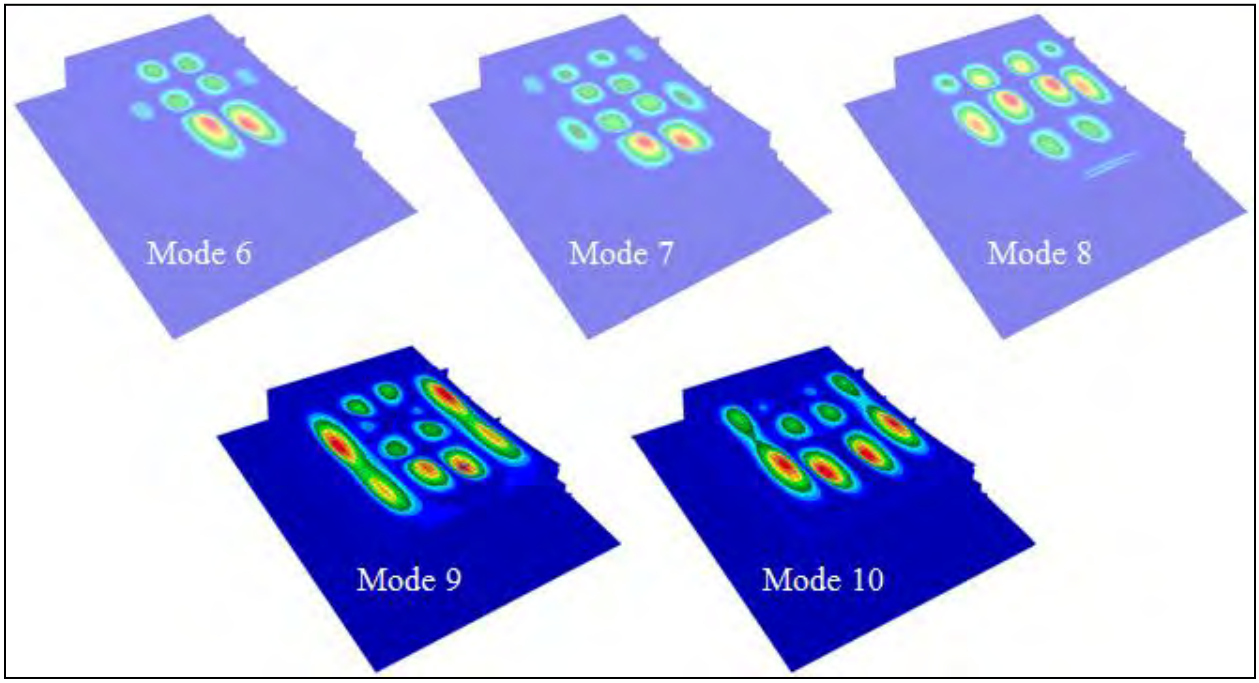

Figure 102 – Second five mode shapes with selected NLROM modes highlighted

The six modes discussed previously were assigned estimated scale factors and the NLROM process was run to completion. Also, a full-order explicit analysis was completed in NASTRAN solution 700 (explicit dynamics) for comparison. The comparison of the stress perpendicular to the ribs at the critical skin element #966 is shown in Figure 103.

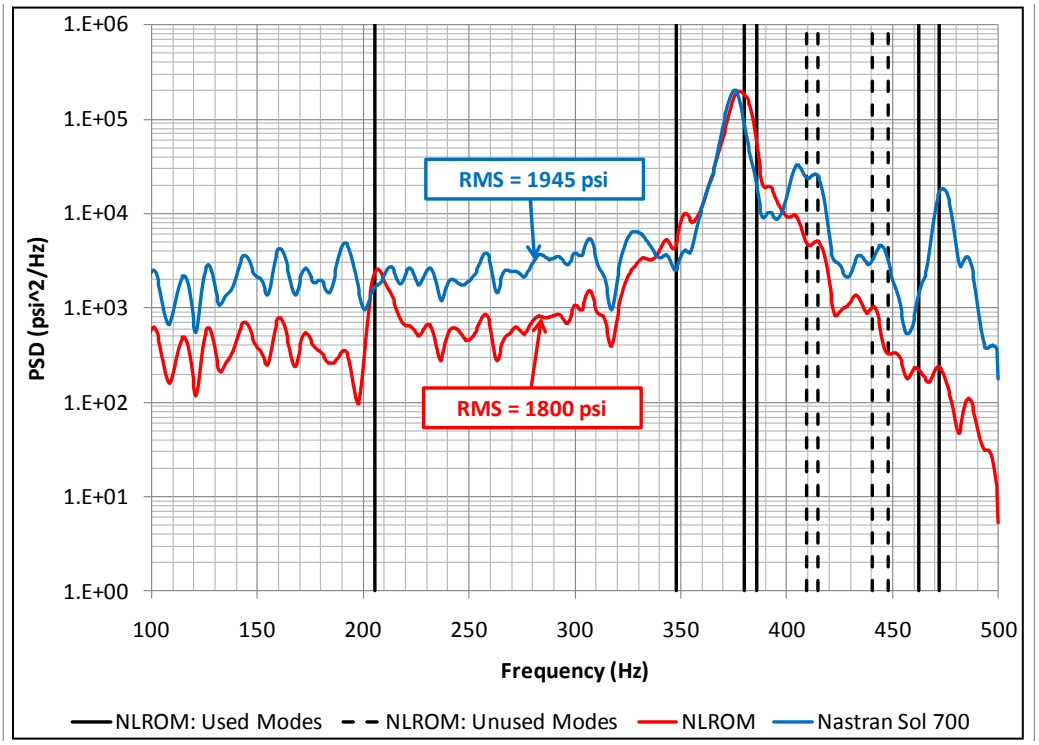

Figure 103 – PSD comparison of stress for NLROM vs. full-order explicit solution

Also given in this figure are the RMS values for the time history response of the stress for the same element in each of the analyses. In the figure, solid black lines denote the modes that were selected to be used in the NLROM solution, based on the displacement PSD for the critical node. Also shown are dashed lines at frequencies of the modes that were not selected for the NLROM solution. It is interesting to note the difference in mode importance between this stress PSD and the displacement PSD. However, it is of interest to note that there are indications that modes 5-8 do show up as small peaks in the NLROM solution, implying that the coupling between these and the selected modes does occur.

The next step included the thermal preload derived from the Abaqus thermal solution for the CEAC test configuration. After completing this thermal comparison, a decision was made toward improving the mode selection and scale factors, in order to try to make a comparison with the explicit analysis.

6.3 Pre-Test Analysis with CEAC Thermal Preload

The Abaqus heat transfer analysis was used to apply the thermal load for the CEAC model. The maximum temperature of approximately 500°F is shown in Figure 104. The steady-state temperatures from the Abaqus heat transfer analysis were extracted using a python script, and written to a NASTRAN formatted file. This file was included in the RMS analyses to determine hotspot locations. The thermal displacements shown in NASTRAN (max displacement of 0.079”) are consistent with those in Abaqus (max displacement of 0.094”), as shown in Figure 105.

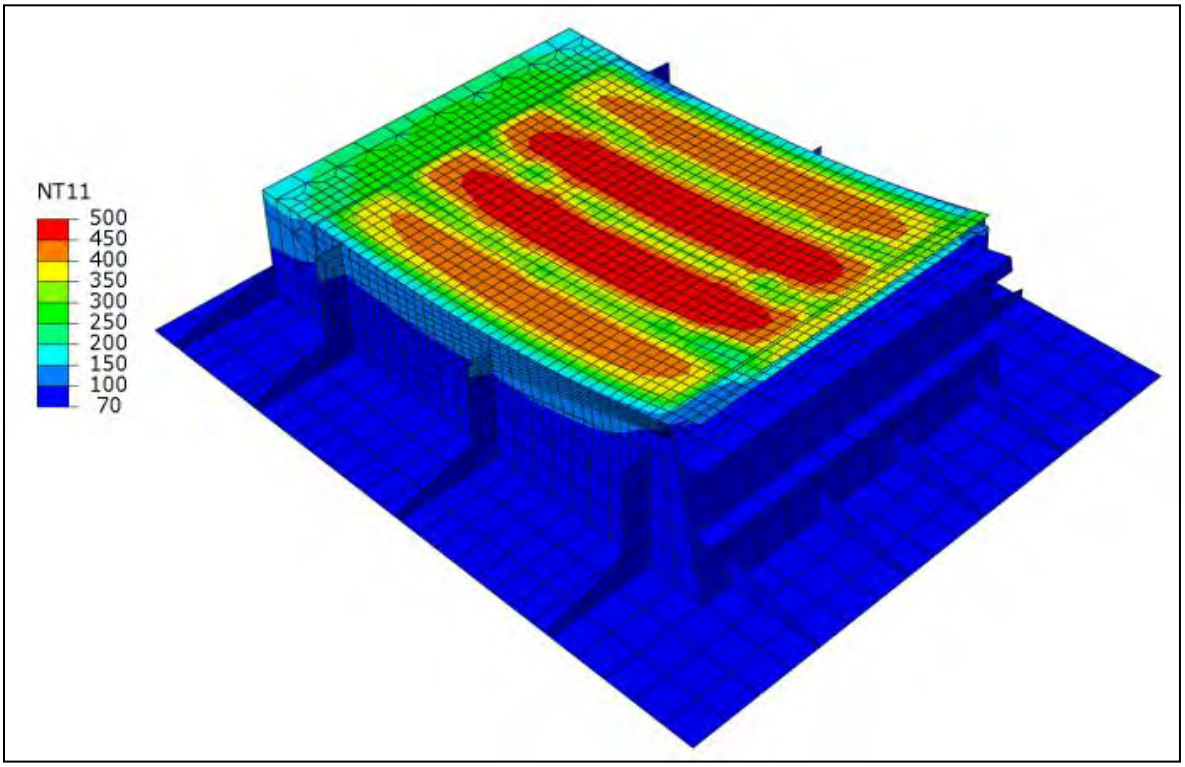

Figure 104 – Temperature distribution for CEAC thermal load

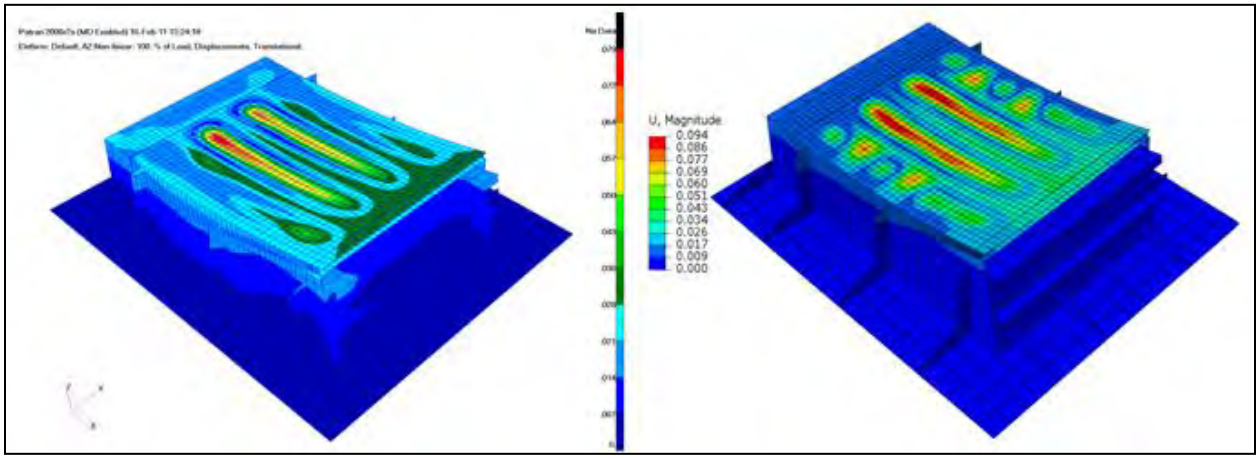

Figure 105 – Thermal displacement comparison of NASTRAN (left) and Abaqus (right)

The nonlinear thermally preloaded frequency response solution required interpretation due to differences in the modal extraction via different NASTRAN methods. The method has been to use the frequency response solution to choose critical locations from which to extract node and element responses.

The only method for achieving the nonlinear preload for the modal frequency response is to run a SOL 106 to get the nonlinear deflected shape. Then a restart is performed into a SOL 111 modal frequency response. Similarly, this SOL 106 was used to restart into a SOL 103 to get mode shapes about the deflected shape. In NLROM, the modal solution has been SOL 400 to allow for a nonlinear preload step prior to the modal analysis. These two methods give different modes, although they seem to be fairly similar at lower frequencies. One interesting note is that the SOL 400 picks up two buckling modes, while the restarted SOL 103 does not. A comparison of the two nonlinear deflected shapes is shown in Figure 106.

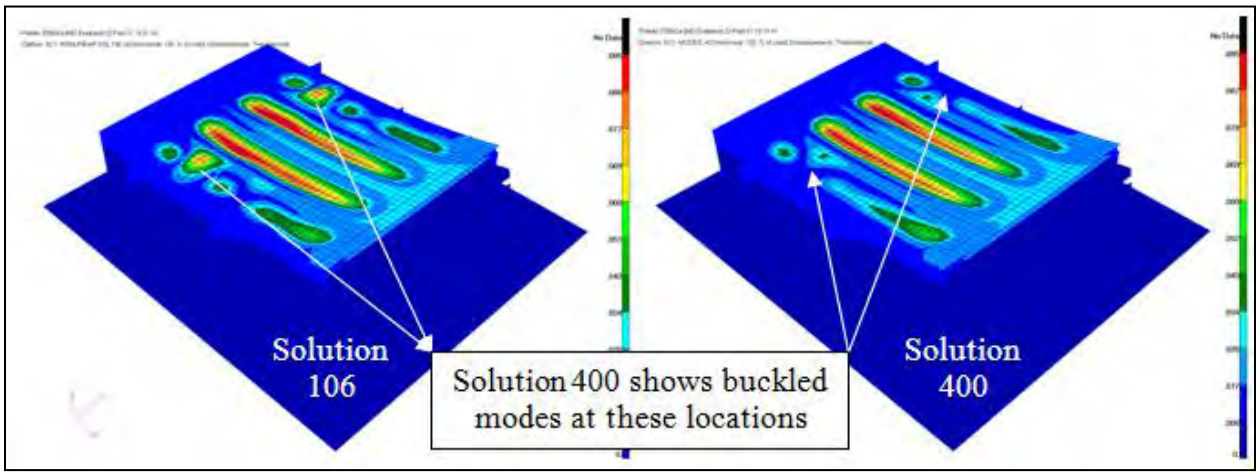

Figure 106 – Comparison of Nonlinear Deflections SOL 106 (left) and SOL 400 (right)

A separate buckling analysis using the thermal load was performed to verify the onset of buckling at less than the maximum temperature. A SOL 106 thermal buckling analysis was performed. This solution is not accurate unless the loading is near the buckling point. Therefore,

the temperatures were scaled down by a constant factor and then stepped up until the buckling point was reached. It turned out that the buckling scale factor for the temperatures was 99%. This indicated that near the temperature profile with maximum temperatures of 500°F there was a possibility of local buckling in the side panels, as indicated in Figure 106. Buckling modes observed by the modal analysis were ignored for the linear ROM by starting the modal analysis just below the first normal mode.

The instrumentation and corresponding FEM locations are shown in Figure 107. Instead of choosing a critical location as was done previously, the nodes and elements at the strain gauge locations shown in Figure 106 were used to produce PSDs of stress and strain. The stress and strain PSDs for the elements are shown in Figure 108 and Figure 109.

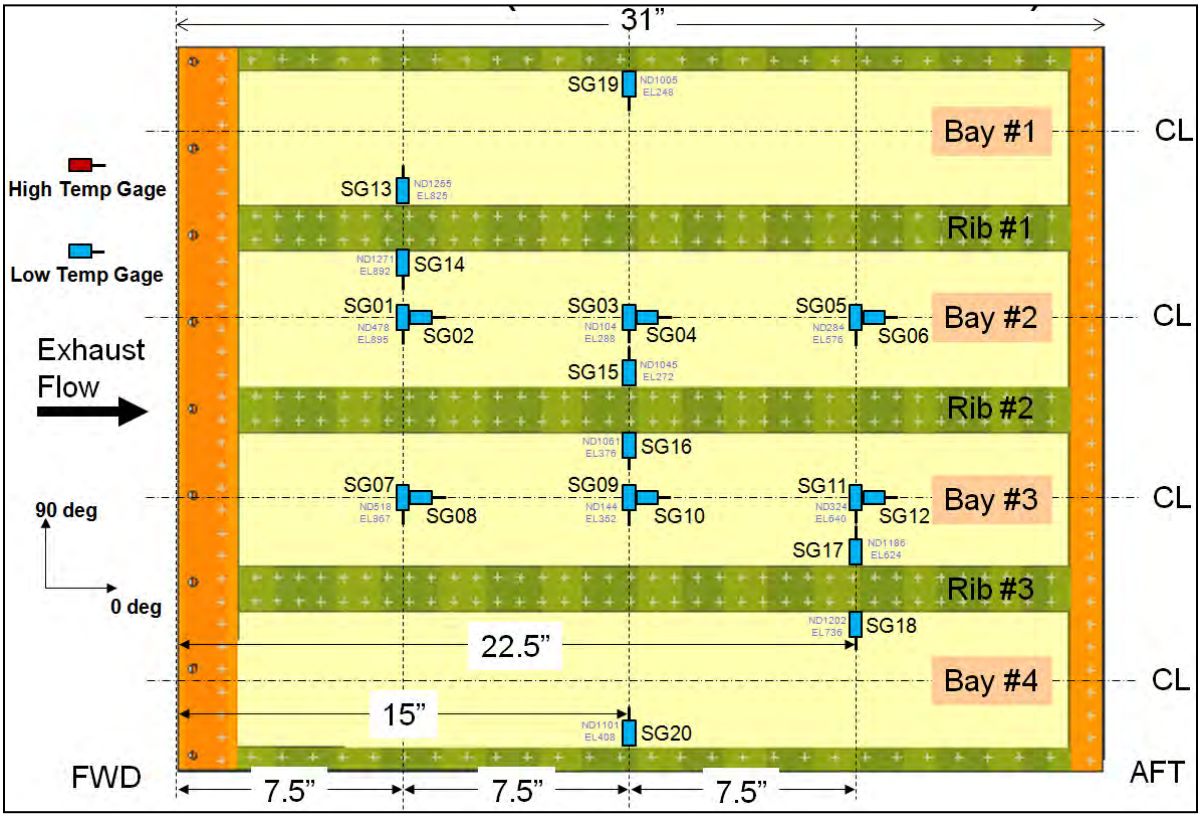

Figure 107 – Instrumentation numbering and corresponding FEM nodes and elements

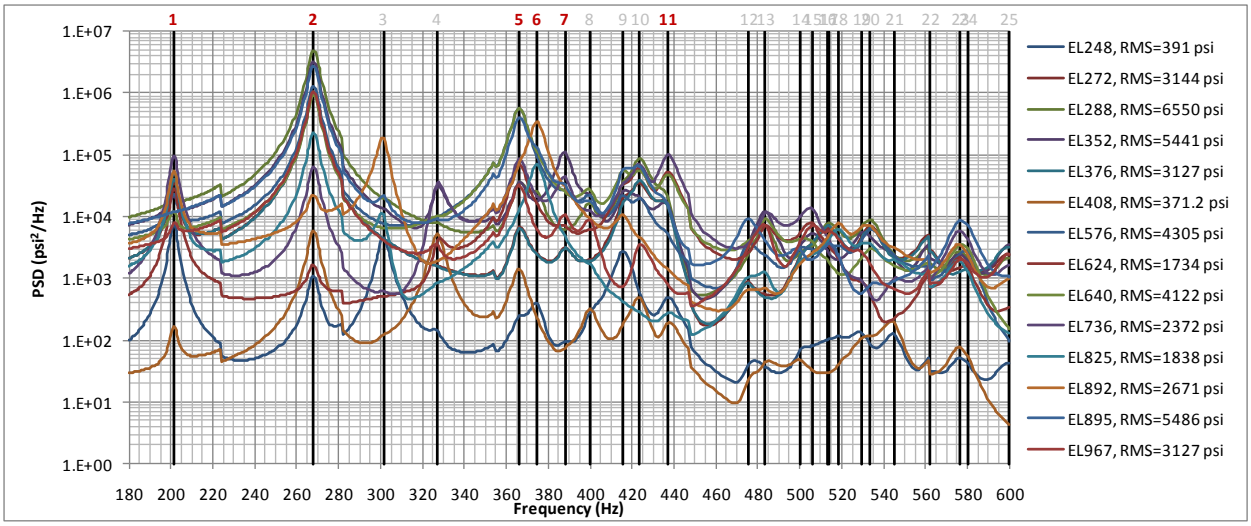

Figure 108 – Stress PSD with RMS stress and normal modes for gauge elements

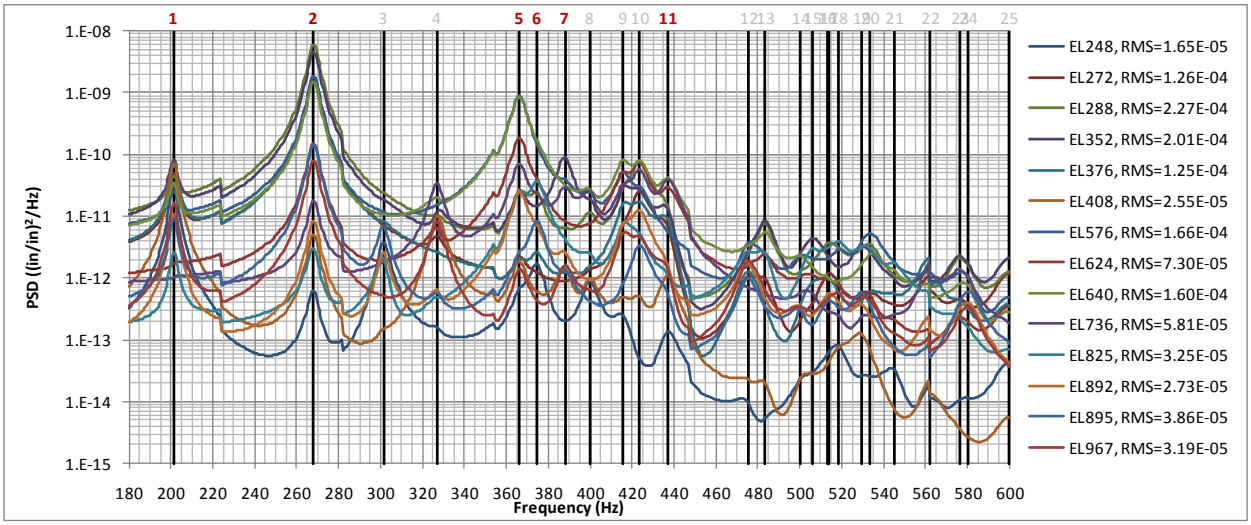

Figure 109 – Strain PSD with RMS strain and normal modes for gauge elements

From these PSDs, six modes were chosen (shown in bold red) to begin the preliminary NLROM analysis. It should be mentioned that the above plots were produced from modal frequency response analyses in SOL 111, restarted from a nonlinear SOL 106 thermal preload solution. The NLROM process uses SOL 400 to chain the nonlinear thermal and modal solutions together in sequence, without using restarts. However, as SOL 400 is formulated slightly differently (it uses a more updated nonlinear solution than 106), the preload is slightly different, as mentioned at the beginning of this section. Therefore, the modal solutions based on these preloads are slightly different as they yield different stiffness matrices at the end of the preload step. The mode shapes seem to be generally the same, but the frequencies and the order of the modes can be different. It was then necessary to look at the mode shapes selected in Figure 108 and Figure 109 to be sure the same modes were chosen from the NLROM generated set. The selected modes from the current setup are shown below in Figure 110. Table 6 makes a comparison of the two solutions with mode number and frequency listed for reference.

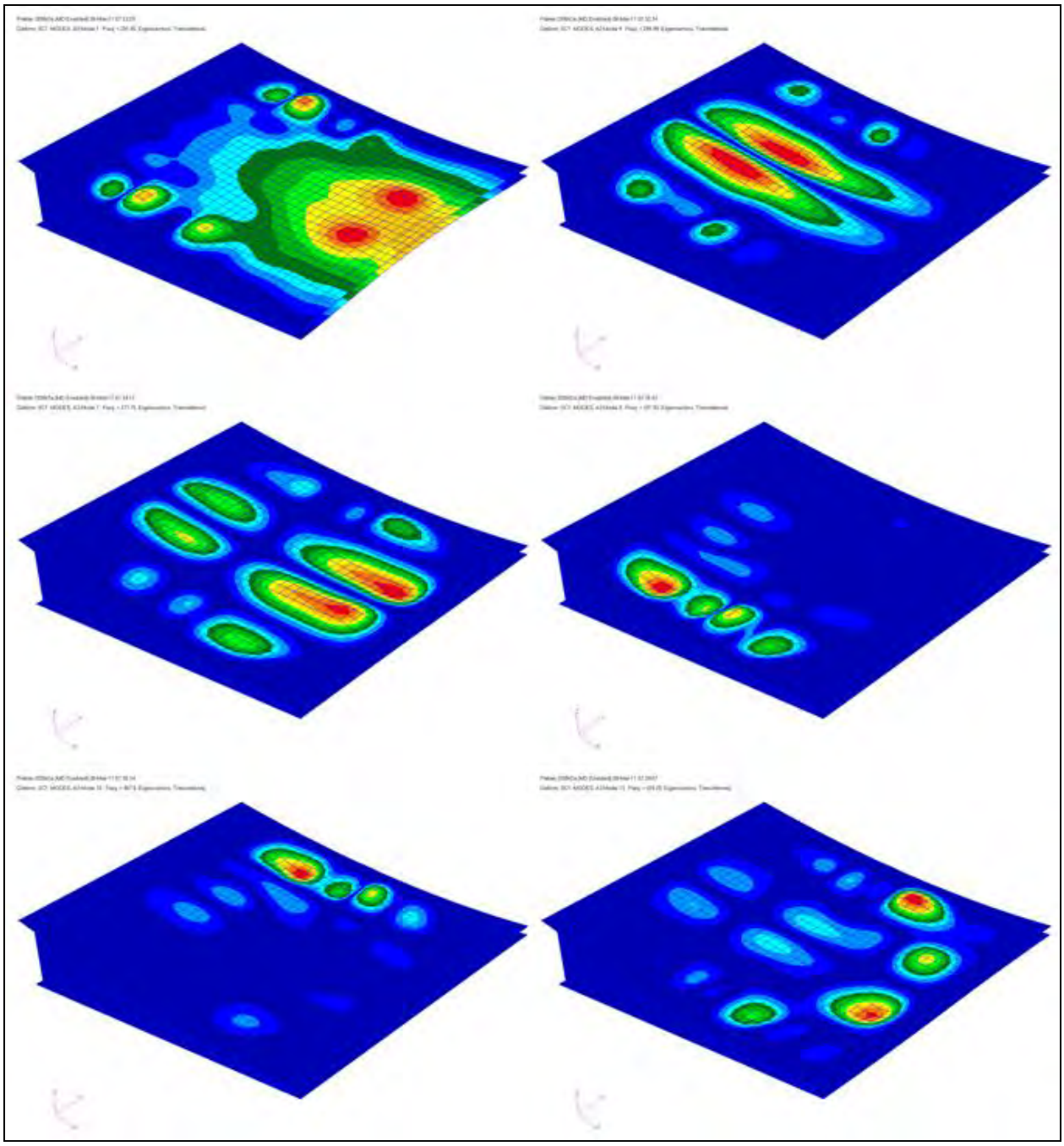

Figure 110 – Modeshapes chosen from the stress and strain modal frequency response plots

Table 6 – Selected modes from solution 111 and corresponding modes in solution 400

Solution 111			Solution 400	
Mode	Frequency (Hz)		Mode	Frequency (Hz)
1	201	→	1	202
2	268	→	4	289
5	366	→	7	378
6	375	→	8	398
7	388	→	10	408
11	437	→	13	439

The selected modes were input into the NLROM GUI, and the modal combination analysis was generated. Thermal pre-loaded ROMs have had some numerical stability issues. When this occurs, it requires re-running the nonlinear static runs with different scale factors applied to certain modes. This seems to be a trial and error process to get a set of nonlinear coefficients that will produce a stable solution. With small models this is not much of an issue, but with larger models, where there is considerable run time associated with the nonlinear static combinations, the trial and error method is inefficient. One recommendation is to develop methods to better understand which nonlinear modal coupling terms need to be determined. The goal is to reduce the number of required static runs, which will help make the model development step more efficient, and also help more rapidly resolve issues with unstable ROMs.

The six selected modes were used in a 10 second nonlinear ODE simulation to get a modal time history of reasonable length. This time history was used to write out Abaqus/Explicit files to proceed with the completion of the NLROM analysis. Once the NLROM simulation was complete, stresses and strains were post-processed from the individual element analyses at each strain gauge location. As previously mentioned, this was a post-processing operation using Abaqus. Elements were selected, and the nodal displacement time histories were output to an Abaqus model file. The displacements were applied as enforced displacements, and the output from the analysis was element stress and strain time histories, which were subsequently post-processed into PSDs. The PSDs for the stresses and strains are shown in Figure 111 and Figure 112, respectively.

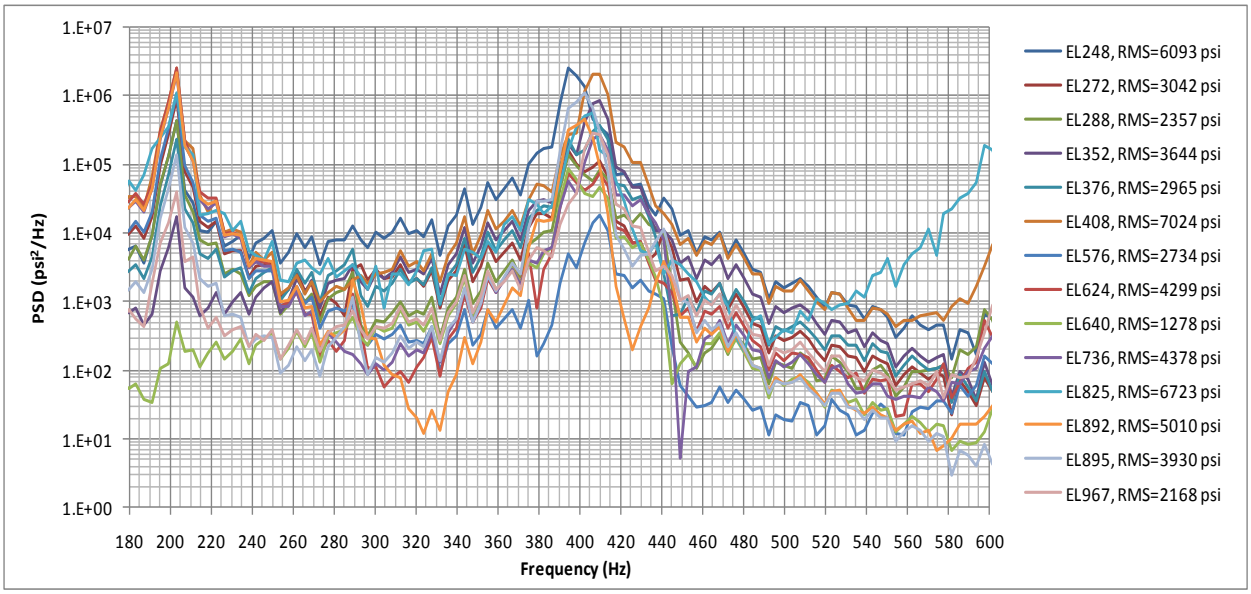

Figure 111 – Stress PSDs for single element Abaqus/Explicit analyses

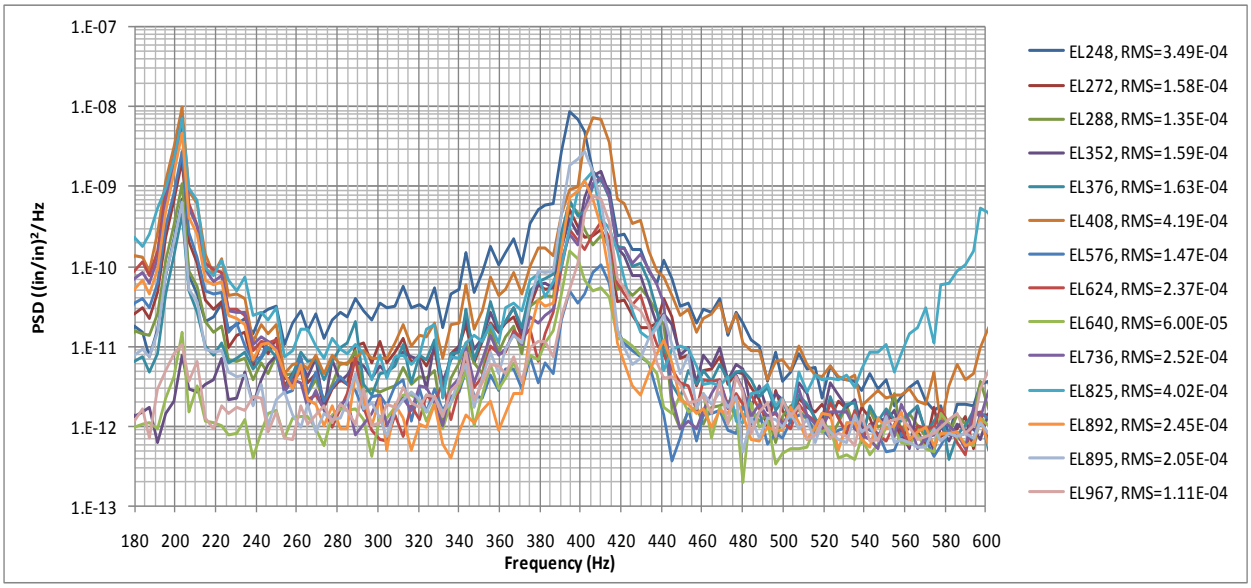

Figure 112 – Strain PSDs for single element Abaqus/Explicit analyses

6.4 LVDT Placement for CEAC Test

When performing structural acoustic response tests, it necessary to quantify the fixity of the boundary conditions. This can be accomplished by performing modal tests, which determines mode shapes, and by measuring the dynamic response on the boundary with accelerometers. However, when thermal loads are simultaneously applied with the acoustic loads, it becomes necessary to quantify the magnitude of static thermal deflections. The amount that the test article expands in the in-plane and out-of-plane directions is an indirect indication of fixity (fixture stiffness). Test data was used to correlate the model in these areas.

Therefore, four LVDT probes needed to be located for the CEAC test. The locations for the LVDT probes are shown in Figure 113. These locations were derived from the nonlinear thermal displacements from solution 400. An overall displacement magnitude plot showing the

approximate location of the probes on the test article model is shown in Figure 114. To determine the best placement for each probe, the X, Y, and Z direction plots were extracted and shown in Figure 115 through Figure 117. The in-plane X and Y-transducers will be used to verify thermal growth of test article/fixture. The Z-displacement transducers will verify out-of-plane at the max thermal displacement locations, and to capture possible side panel thermal buckling as predicted by the analysis.

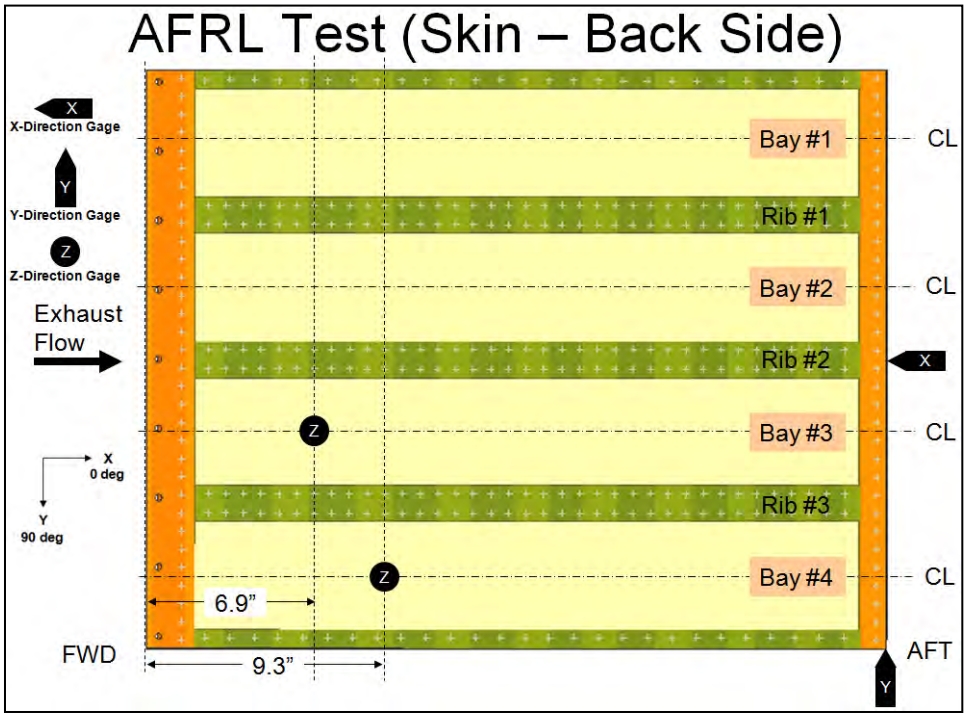

Figure 113 – LVDT placement shown with measurements

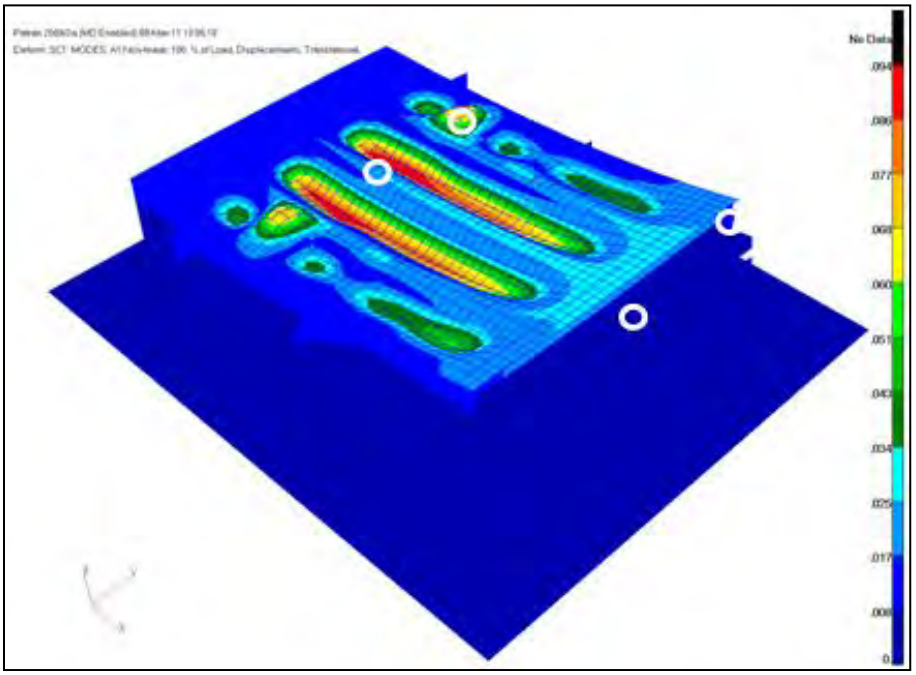
Figure 114 – LVDT placement shown on displacement magnitude results

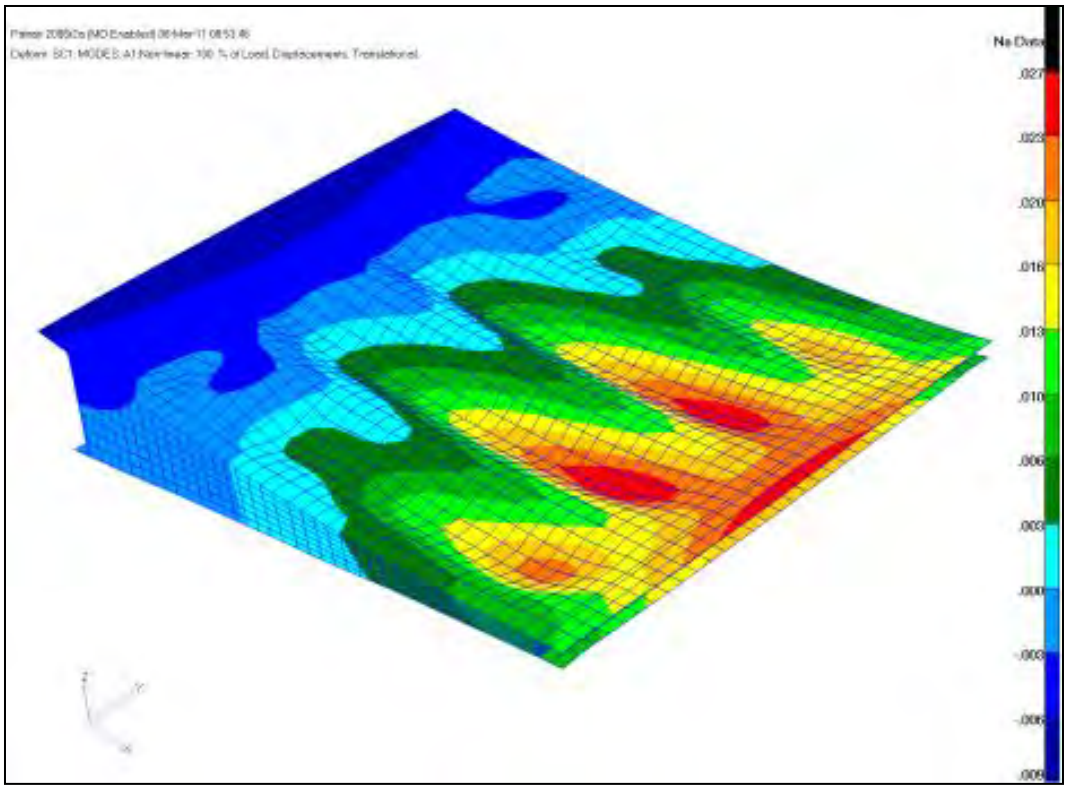

Figure 115 – Displacements in x-direction

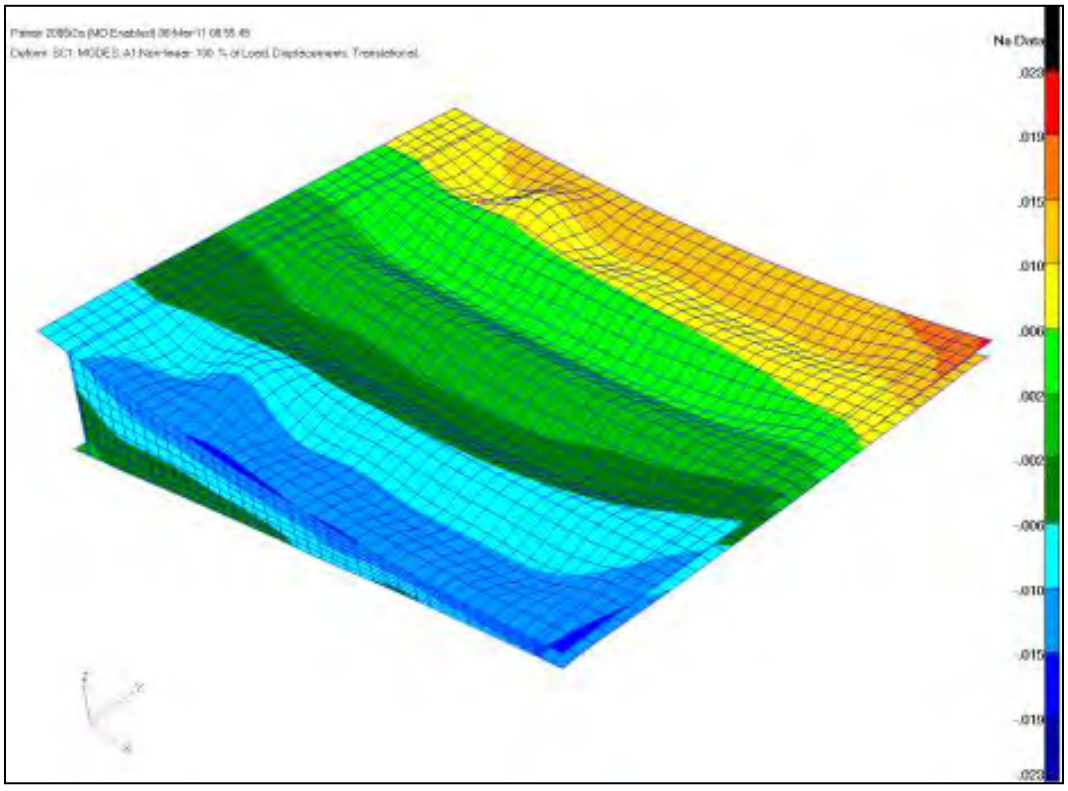

Figure 116 – Displacements in y-direction

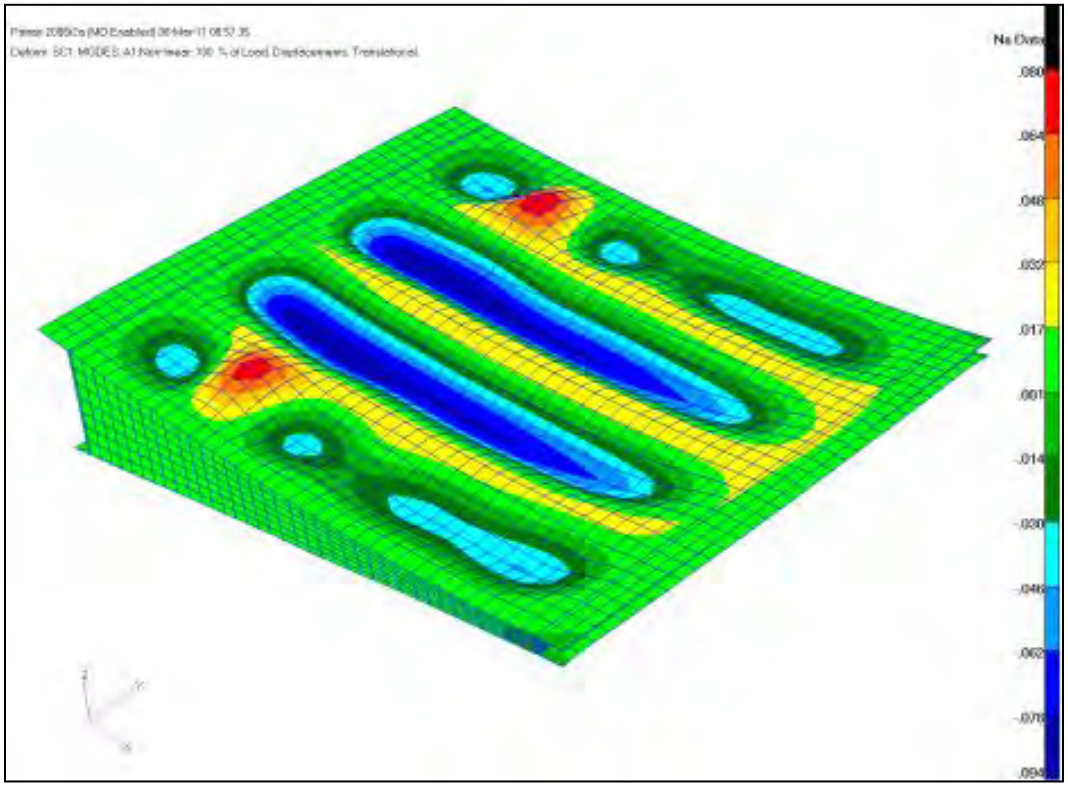

Figure 117 – Displacements in z-direction

7.0 Testing Results

Testing was performed in a thermal/acoustic test facility for the purpose of measuring response and fatigue life. The testing included modal tests of the test article in the fixture. Also, testing included acoustic testing at an elevated temperature in an acoustic facility for a range and combination of acoustic and thermal loads, and in an engine burner facility under realistic engine exhaust conditions. The test data was used to compare to the analytically predicted responses.

7.1 Test Objectives and Plan

The primary objective of the testing task was to collect sufficient data to be used to correlate, validate, and update the analytical model and NLROM response predictions. The objectives and success criteria are shown below.

Objectives	Success Criteria
Measure the resonant frequencies, damping, and mode shapes of the test articles with the test frame adapter as installed in the acoustic test facilities.	Definition of the natural frequencies, damping factors and mode shapes of panel in the fixture mounted in the test facility. Compare these modes with the analysis model modes.
Determine the thermal and acoustic response characteristics of the test articles at various temperatures and acoustic levels and/or engine power settings.	Measure time history, PSDs, CSDs, RMS values, average statistics of the critical instrumentation for every test condition.
Perform acoustic endurance/fatigue tests in the PWF at temperature and measure response.	Complete the PWF endurance/fatigue test portion of the test program, measure response and loads throughout testing, record all data channels.

The test plan included modal and acoustic testing. The modal testing was used to measure the structural dynamic characteristics (mode shapes, frequencies, and damping). Modal tests of the specimen were performed with it installed in the test adapter fixtures and in the facilities. The goal was to measure any fixture or facility influences on the modal characteristics.

For the acoustic testing, two separate thermal/acoustic tests in two separate facilities were performed. The first acoustic test was in the progressive wave facility (PWF) at the AFRL's Combined Environment Acoustic Chamber (CEAC), shown in Figure 118. The CEAC tests were a combined thermal/acoustic with the thermal load applied on the front side of the specimen through the use of a Quartz Heat Lamp system. The CEAC facility is shown in Figure 118. In this type of test, thermal and acoustic loads can be controlled separately. Sufficient data was gathered at several loading combinations in order to obtain a large database of experimental data for the NLROM correlation and for future modeling developments.

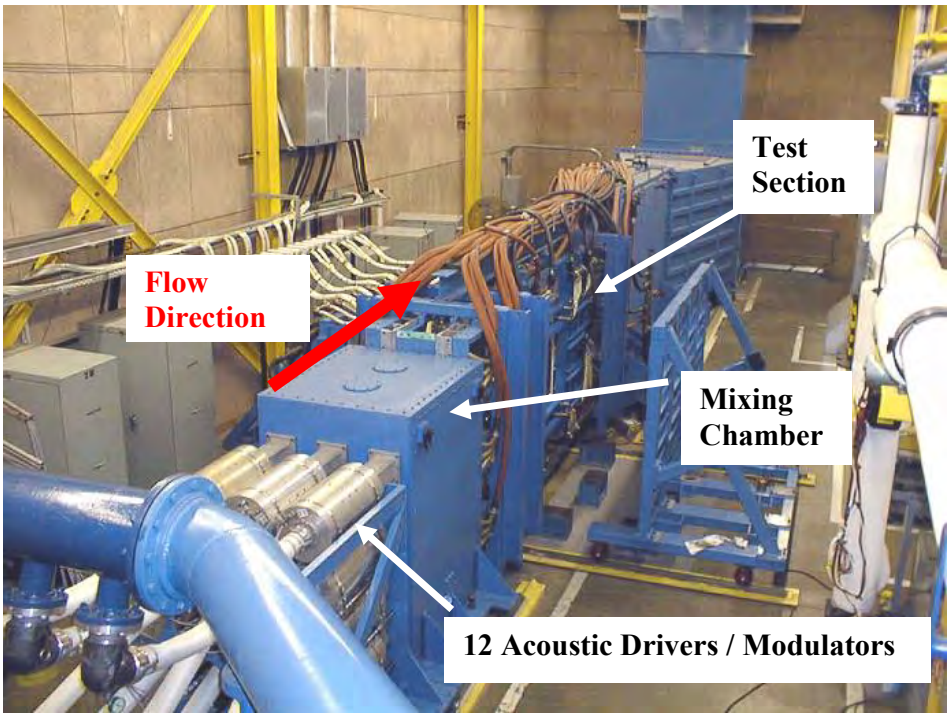

Figure 118 – AFRL Combined Environment Acoustic Chamber (CEAC)

The second test article was tested in the Boeing-St. Louis T-58 Engine Burner Facility (EBF), shown in Figure 119. The objective of this hot engine acoustic test was to quantify the response characteristics of the specimen under realistic engine flow and thermal/acoustic excitation for comparison to the CEAC testing. This type of test replicates the actual loading experienced in flight, including static pressure from exhaust impingement.

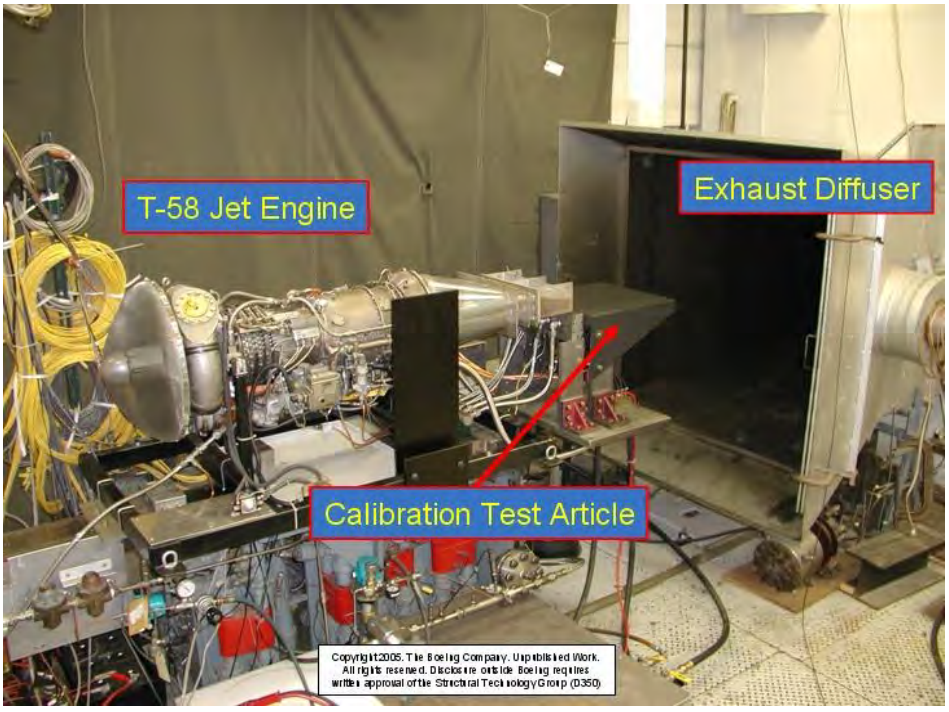

Figure 119 – Boeing T-38 Engine Burner Facility (EBF)

7.2 CEAC High Temperature Survey

Thermal surveys were performed without any acoustic loading. The objective of these surveys was to measure the structural response under steady state thermal loads. This test data was used to correlate and update the analysis model. The following is a summary of the thermal measurements taken during the survey, Test Run #16. The purpose of this test summary is to provide a technical description of the thermal measurements and to provide some technical discussion on the observations based on these measurements.

For the thermal response surveys, optical measurements were made with an ARAMIS system. ARAMIS is an optical strain and deformation measurement system for structures during loading. The system is a full-field, non-contacting strain measuring device, seen in Figure 120. The system can perform non-contact measurement of 3D-deformation and strain using 3D digital image correlation (DIC) methods via high-resolution digital cameras. In these thermal response surveys, the loaded structure was viewed by two 3D high-resolution digital cameras. The deformation of this structure under different loading conditions was recorded by the cameras and evaluated using digital image processing. The results produced from the digital imaging processing include the 3D-coordinates, 3D-displacements, surface strain and the complete strain tensor.

Figure 120 – ARAMIS high resolution camera system

The ARAMIS system used for the CEAC testing is described below:

System type:	ARAMIS 4 M
Standard measuring volume in mm:	25x20x15 to 2000x2000x2000
Camera resolution:	2048x2048 pixels
Max. Frame rate:	7 Hz (with 19" PC)
Shutter Time:	0.1 ms up to 2 s
Strain measuring range:	.01% up to > 100%
Strain accuracy:	up to .01%

For Test Run #16, the plenum pressure was set at 5 psi, with TC8 being used for temperature control. This test was a thermal survey from room temperature (RT) to 500ºF in 50° increments of 50 degrees and back down to RT. The measurements shown below were taken at a temperature of 500ºF. Each figure shows the ARAMIS deformation image and a plot of each data point, taken from the ARAMIS grid points on the test article. The deflection contour plot images were generated from thousands of ARAMIS data measurements. The results produced

from the ARAMIS measurements were images and text files that contain the un-deformed and deformed X, Y, and Z coordinates. Figure 121 shows a linear growth in the X-direction (chord-wise flow direction). Similarly, Figure 122 shows linear expansion in the Y-direction (span-wise cross flow direction). Figure 123 shows larger out-of-plane Z-deformation in the aft portion, as does Figure 124 for the middle of the test article.

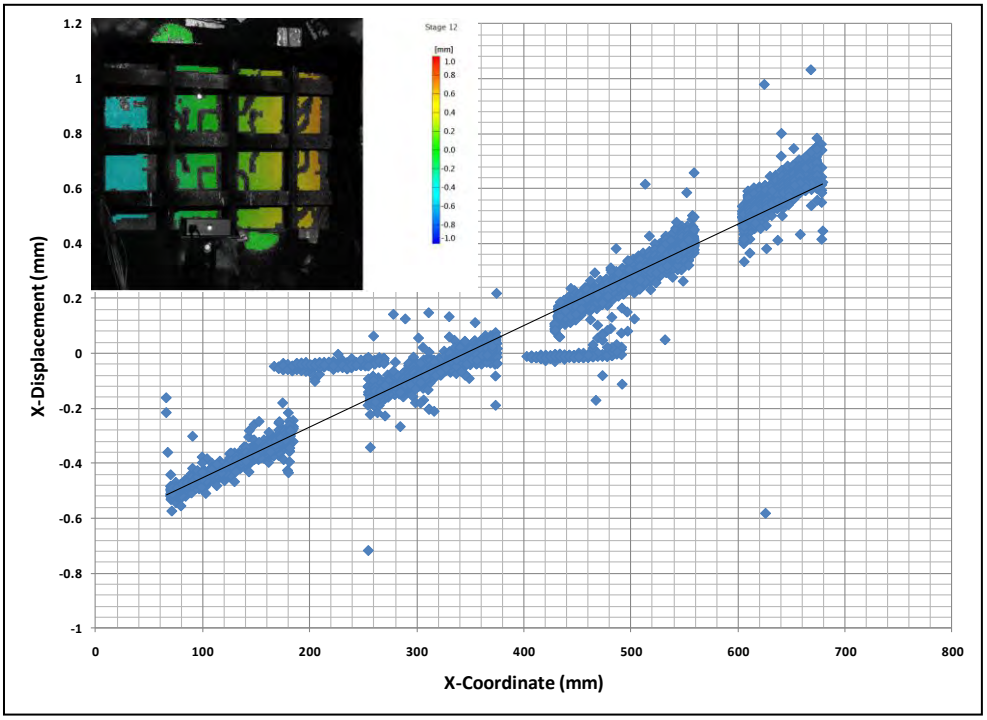

Figure 121 – ARAMIS measurement x-displacement along x-coordinate

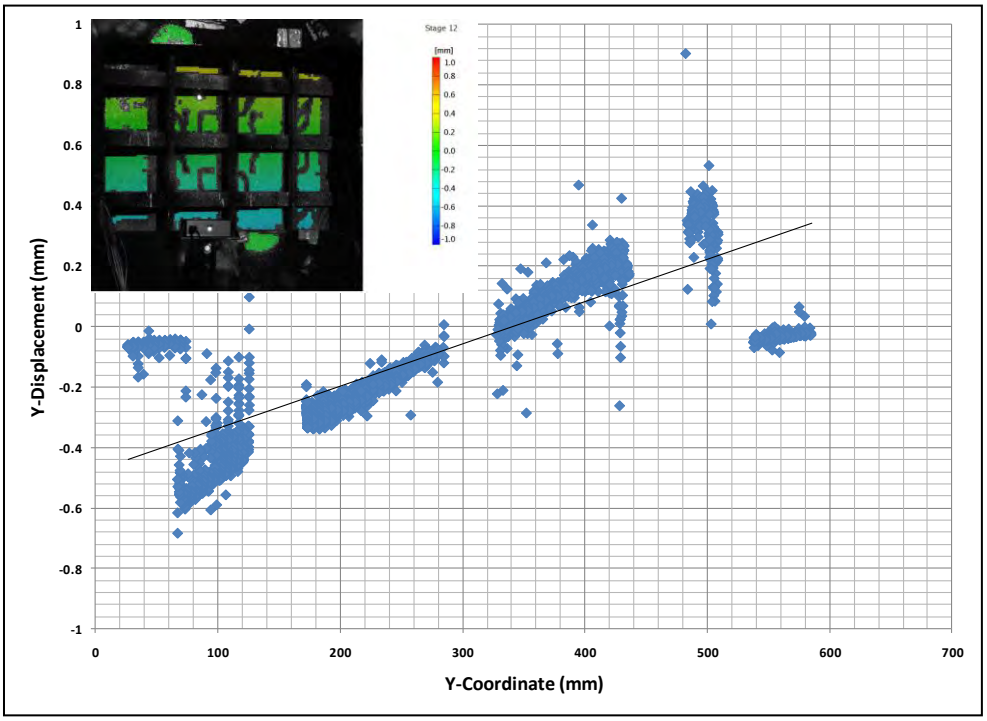

Figure 122 – ARAMIS measurement y-displacement along y-coordinate

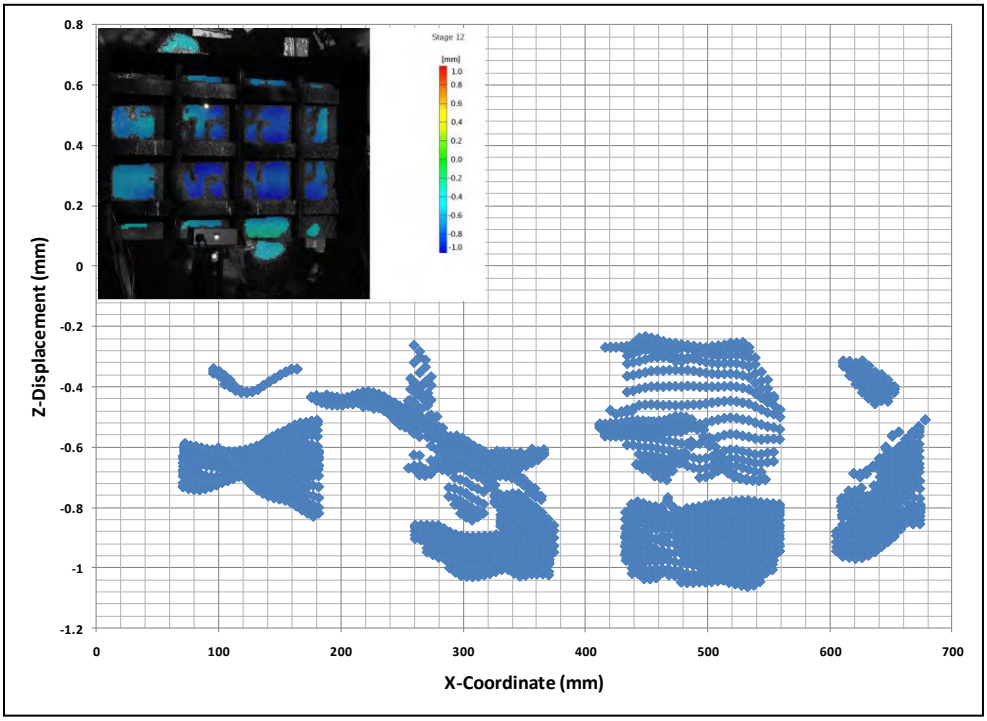

Figure 123 – ARAMIS measurement z-displacement along x-coordinate

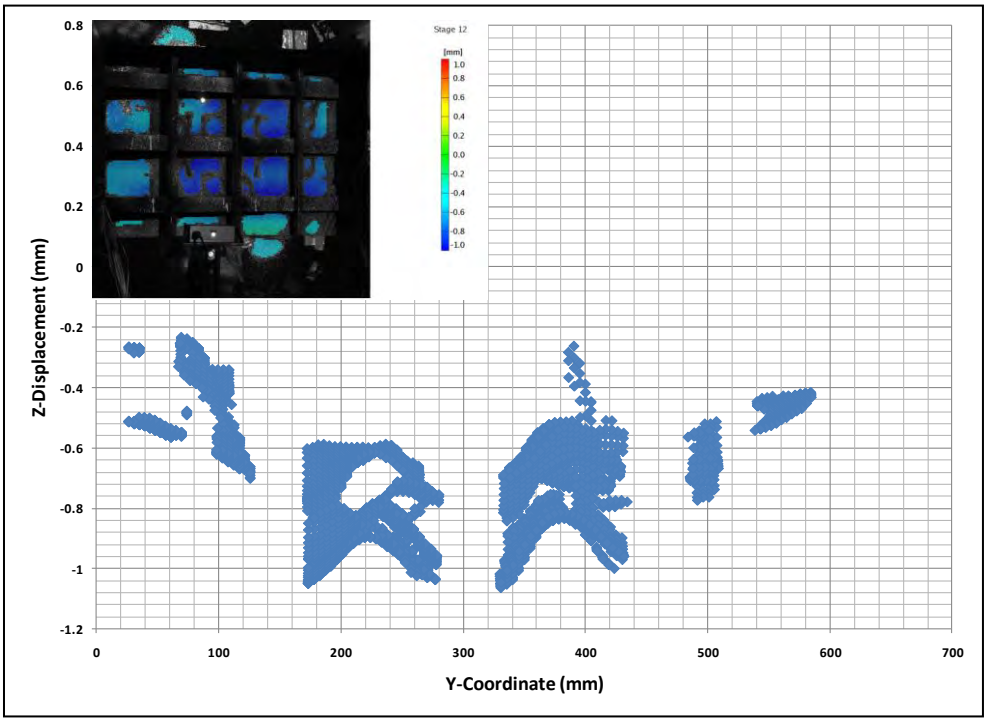

Figure 124 – ARAMIS measurement z-displacement along y-coordinate

During all thermal surveys, IR still images were taken from two different cameras; one calibrated and a second un-calibrated camera that was directed at an angle in order to image the substructure. All data was processed using the IR software, ExaminIR. The calibrated IR camera used was a FLIR SC6000 with a standard range up to 660°F, shown in Figure 125.

Figure 125 – FLIR SC 6000

The IR image in Figure 126 shows that the test article was warmer on the trailing edge (right side) than the leading edge portion of the test article. The test article was also hotter on the upper and lower sides than in the mid section. Hence, the IR data and ARAMIS deformation data correlate. The second IR image in Figure 127 shows the temperature of the substructure (i.e., top of the ribs), which was generally at 200°F to 300°F. Also, there were local gradients of temperature across the test article. Most of these local thermal effects were due to instrumentation potting on the Outer Mold-Line (OML) surface or due to air flow. The surface potting material used was Room Temperature Vulcanizing (RTV) silicone. RTV is a pretty good insulator, and it had a local effect on the underlying skin temperature. The RTV was necessary to keep the strain gauge wires securely in-place during acoustic testing. The thermal gradients were due to the heat flow into the substructure and fixture. Even though the lamp banks put out a fairly uniform heat load, there was not a uniform temperature across the test article. The conduction and radiation of heat across the test article can be relatively complex in a built-up structure like this test article. Hence, thermocouple time histories provided good point measurements and were used to calibrate IR images. However, IR images were very important for quantifying the complex thermal response. These measured temperatures were not used directly as an applied load in subsequent post-test correlation analysis, but they were used in post-test heat transfer analysis and correlation analysis. The reason for this will be discussed in the post-test correlation section of this report.

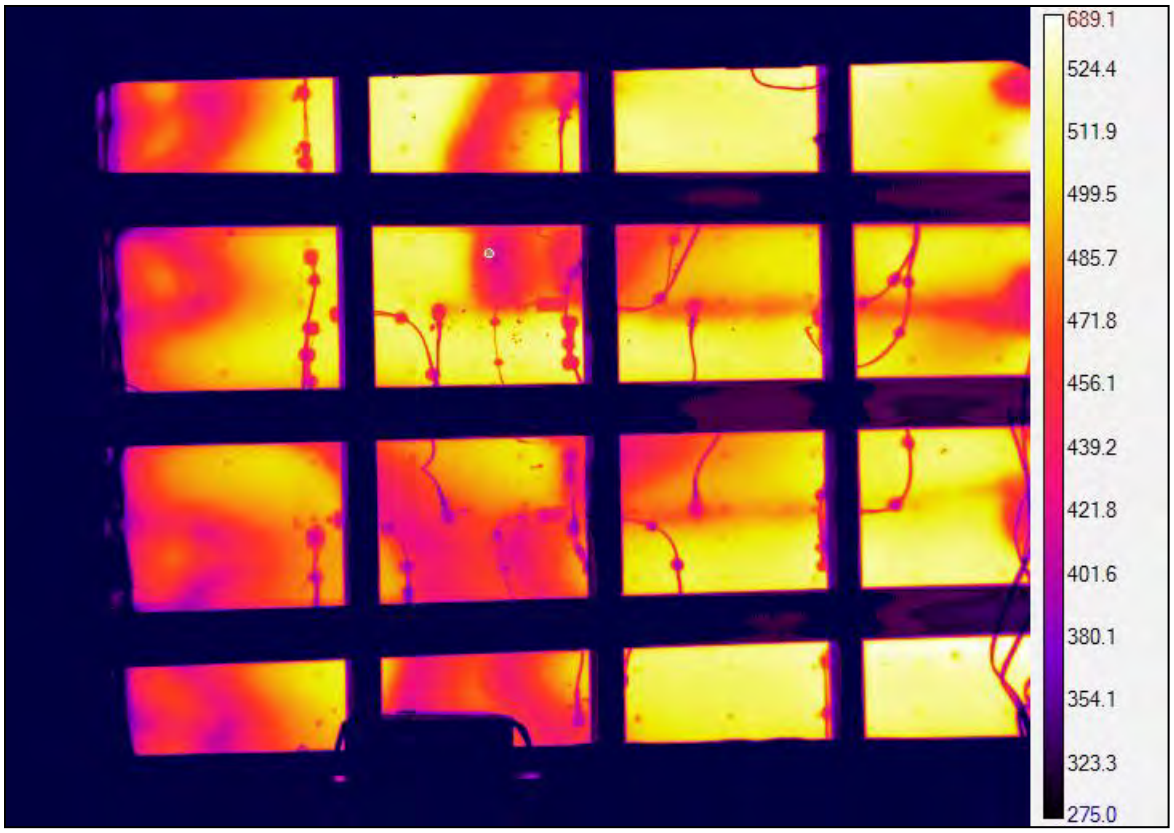

Figure 126 – IR image with temperature range 302°F to 662°F

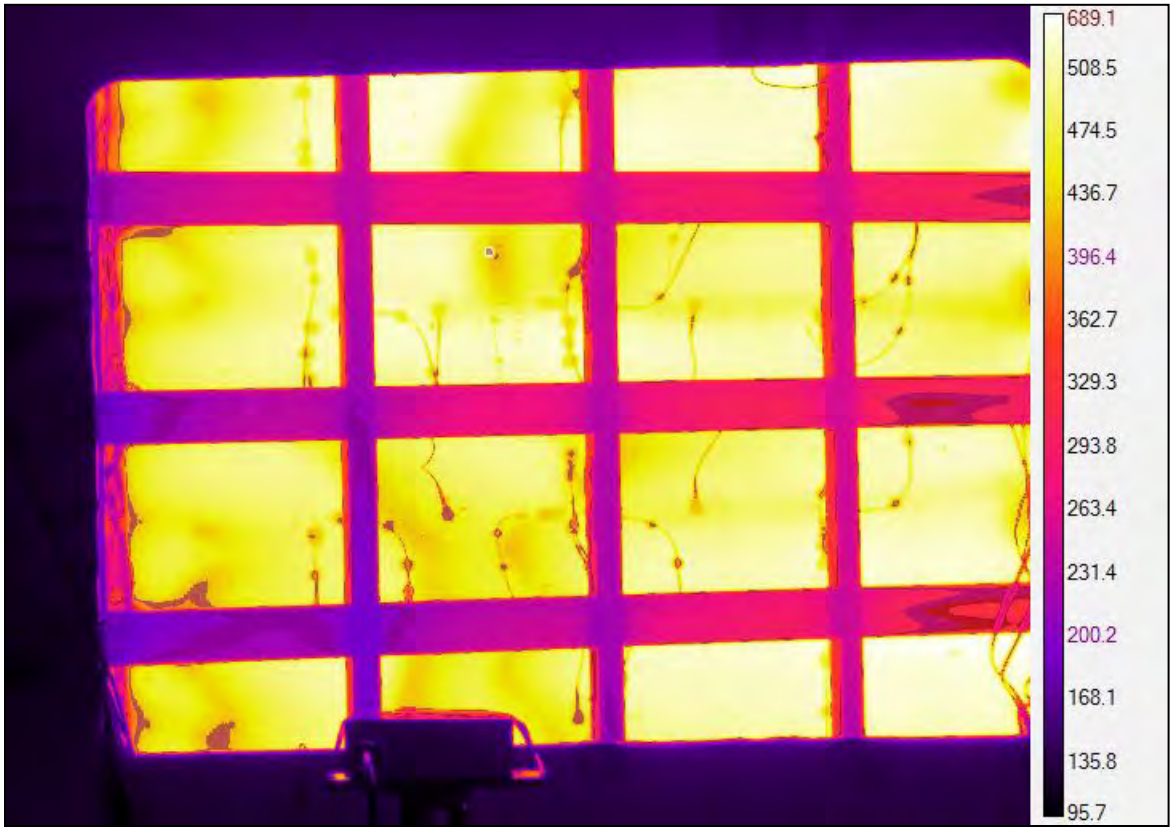

Figure 127 – Combined thermal range IR image – 50°F to 662°F

It was important that IR measurements were made with air flow. The acoustic testing was performed with some flow through the plenum, typically at about 8000 ft/min. This did have a large effect on the temperature distribution. Without any flow (or a pressurized plenum), there was back flow of outside air from the exhaust. This tended to cool the aft and lower portion of the test article, as cool outside air would flow back down the ceiling exhaust along the chamber floor. This was fairly evident, as can be seen in Figure 128, which was at a lower max temperature of 350°F with no air flow. The IR image shows the cooler lower and aft structure due to the back flow.

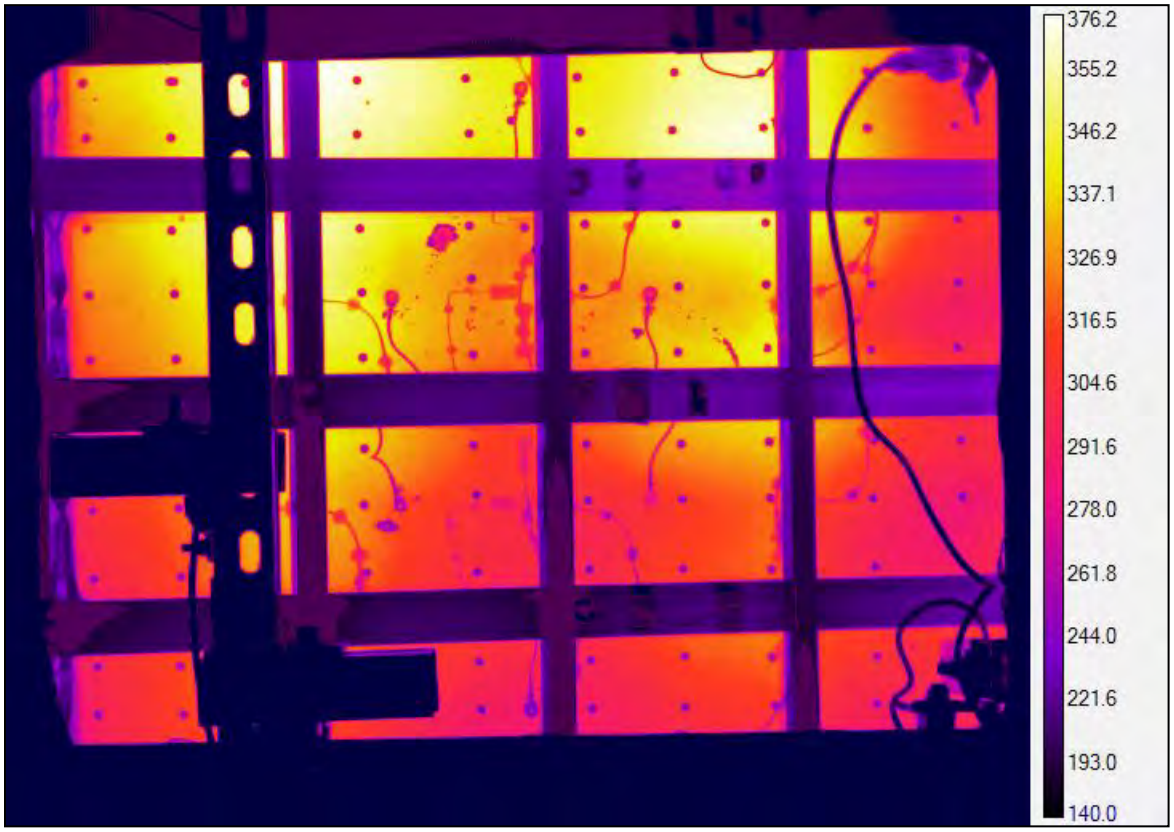

Figure 128 – IR image max temperature 350°F, no air flow

Another comparison was made with the IR image at 500°F, plenum pressure at 20 psi, at max acoustic load, and with Re OASPL = +3 dB. A plenum pressure of 20 psi equates to 9800 ft/min flow velocity in the chamber. The temperature distribution seen in Figure 129 was fairly similar to that of Figure 126.

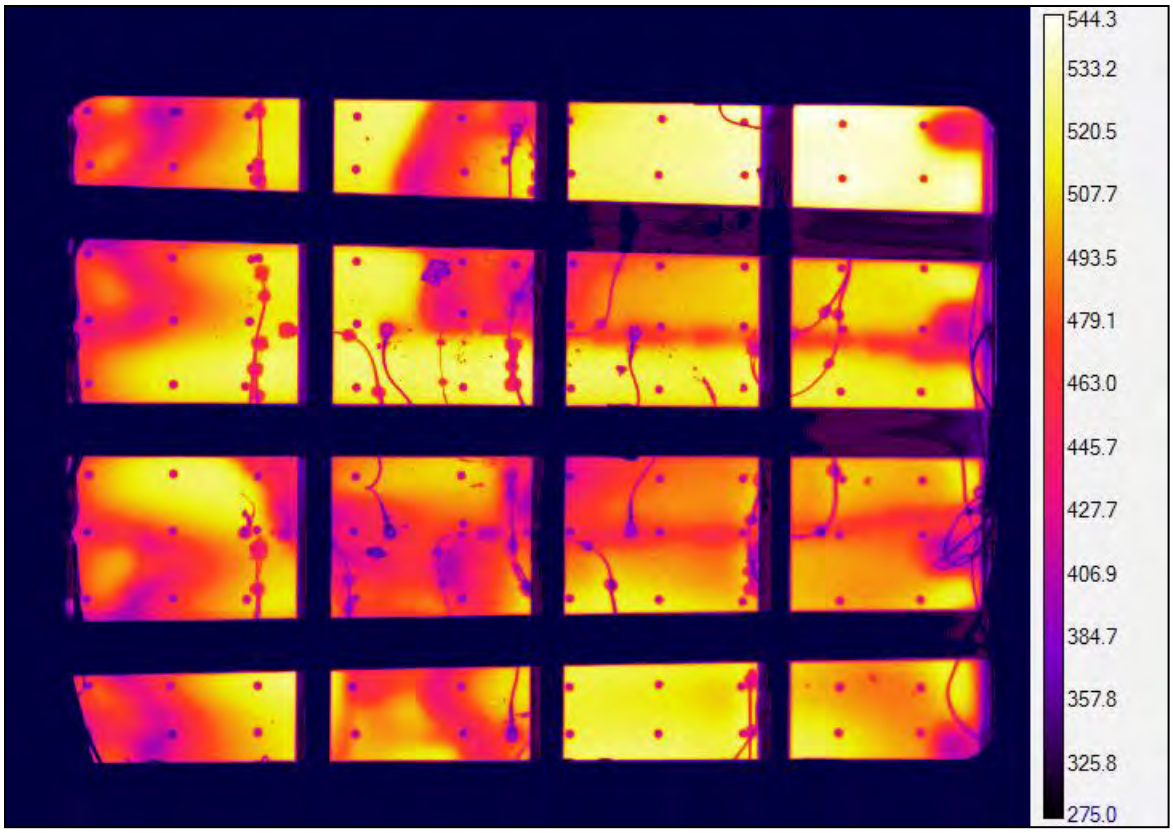

Figure 129 – IR image at max temperature 500°F, Test Run #13

7.3 CEAC Measured Acoustic Pressures

An important aspect of acoustic testing is accurate determination of the acoustic pressure over the surface of the test article. In this facility, the acoustic pressure (magnitude, spectrum, and phasing) is fairly uniform. However, since this was a validation test, it was important to quantify the acoustic pressure distribution consistent with the FEA setup. In this case, the post-test FEA would use 12 pressures zones across the OML surface. Eventually, these pressure time histories were used directly in the dynamic response simulations.

The CEAC test setup had a total of 22 acoustic sensors. The locations are shown in the CEAC Test Plan in the Appendix A. Twelve of the sensors were Flat Paks applied to the OML skin. Ten of the sensors were microphones that were positioned around the test article. Four of these sensors were chamber microphones, positioned on the upper and lower chamber walls and forward and aft on the chamber side wall. The acoustic control microphone was Mic-1, which was positioned 6 inches from the leading edge of the test article and mounted on side wall. A total of six microphones were positioned on the upper and lower sides of test article. The final two microphones were positioned on the backside of the test article on the IML side. The microphones were used for all of the test runs. However, the Flat Paks have a limited temperature and were removed after the room temperature acoustic survey, Test Run #4.

The control microphone Mic-1 had 0.217 dB variation between measurements at similar acoustic levels. There was almost a 0.08 psi-rms or 1.76 dB difference between the leading edge and trailing edge microphone. The trailing edge microphone was shadowed by the test article that sticks into the test chamber by a few inches, shown in Figure 130. The upper and lower side

panel microphones had considerable variation, shown in Figure 131. The Flat Pak sensors had a slightly higher variation of 0.29 dB. The OASPL varied by as much as 0.9 dB between the Flat Paks at the highest acoustic levels, seen in Figure 132. The noise floor in the CEAC chamber was at 0.03 psi-RMS (OASPL=140.3 dB). This was the noise level with the air flow on but with no acoustic modulation. The conclusion was that Flat Pak measurements were consistent with the control microphone Mic-1. Therefore, the Flat Pak pressure time histories were used directly in the post-test correlation. For the high temperature acoustic analysis, these pressure time histories were scaled as needed to the RMS value of the control Mic-1 during the high temperature acoustic survey.

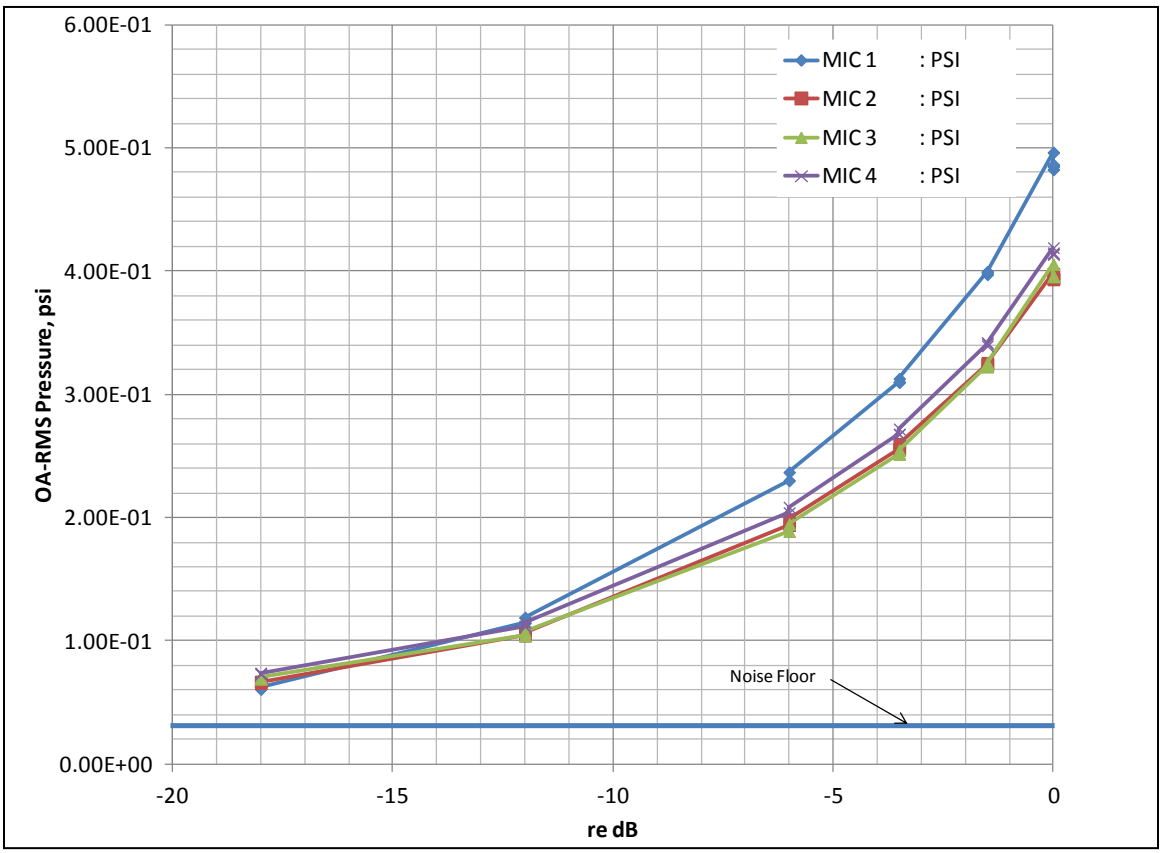

Figure 130 – Test Run #4 chamber microphones flat spectrum RMS pressure

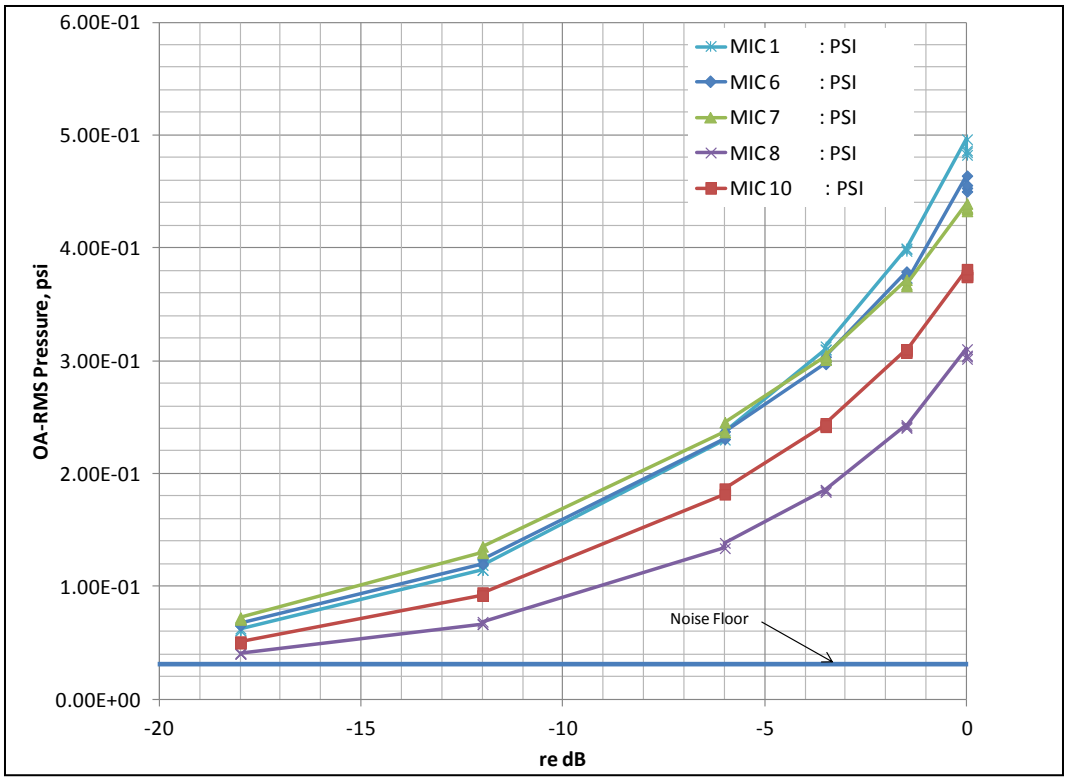

Figure 131 – Test Run #4 sidewall microphones flat spectrum RMS pressure

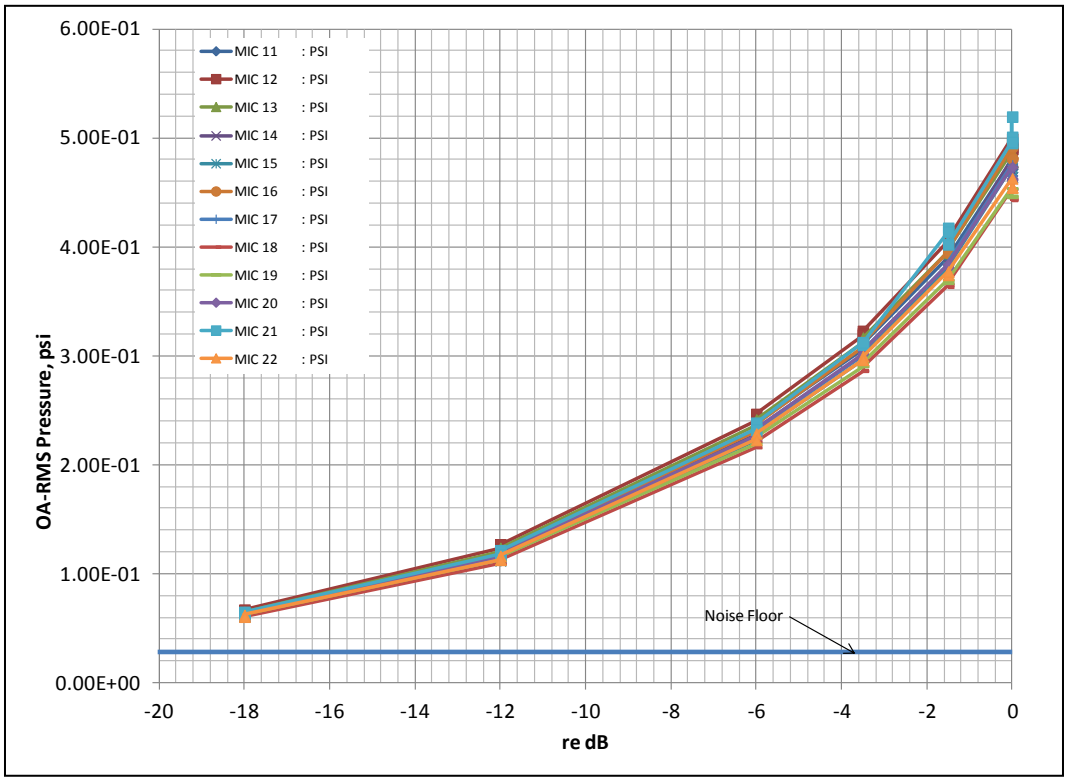

Figure 132 – Test Run #4 flat spectrum OML skin Flat Pak RMS pressure

7.4 CEAC Measured Thermal Strains

In high temperature testing, piezoelectric-type response transducers (accelerometers) cannot be used because of their temperature limitations. The typical limit for these is about 300 ºF. High temperature transducers could have been used, but they would have been fairly heavy for measuring response on thin skin panels. Therefore, strain gauges became the primary response transducer. The usual philosophy with strain gauges is to place them in location of lower strain gradients. Strain gauges measure an average strain over the small area of the wire gauge (about ¼ inch). Unfortunately, they are not very accurate at measuring strains in high gradient; i.e., K_t, locations. Also, the objective is to generally compare these strains to FEA predictions. With respect to the test article, the FEM had finite resolution on strain accuracy too. Hence, the idea was to match measurement locations to FEM locations with low strain gradients. It was also desirable to position a strain gauge at a location that was expected to initiate a crack. However, it is generally not easy to predict these locations prior to testing in a complex test article such as this flap component. The test article had 30 strain gauges distributed to measure strain on the skins and ribs. Many of the gauges were setup to provide redundancy in case the primary gauges malfunctioned.

The test article had 30 strain gauges that were setup to measure the total signal including the mean. For the acoustic surveys, the acoustic loads were increased from -18dB to +3dB relative to OASPL = 164 dB. The mean strain for gauges SG-1 through SG-12 is shown below in Figure 133 for Test Run #13 at 500°F. Note, SG-2 and SG-5 were non-functioning. These were the 0°and 90° gauges in the center two IML skin bays. In general, there is an observable effect of sound pressure level (SPL) on mean strain level. Some of the gauges increased in strain (larger magnitude), while others decreased in magnitude. Also, the effect seemed to be opposite for opposing strain gauges; e.g., SG-1 and SG-7 (Figure 134), SG-6 and SG-12 (Figure 135), and SG-4 and SG-10 (Figure 136). A similar effect was seen in the perpendicular rib edge gauges, SG-13 through SG-20 on the IML skin, Figure 137.

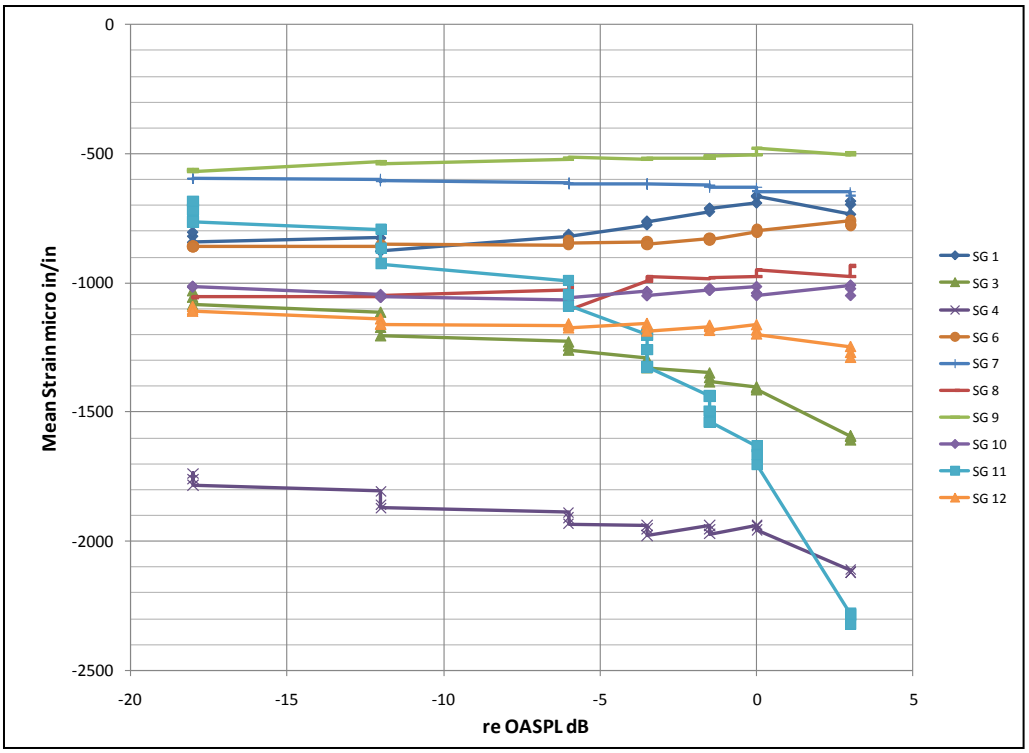

Figure 133 – Mean strains Test Run #13 at 500°F, IML center bay strain gauges

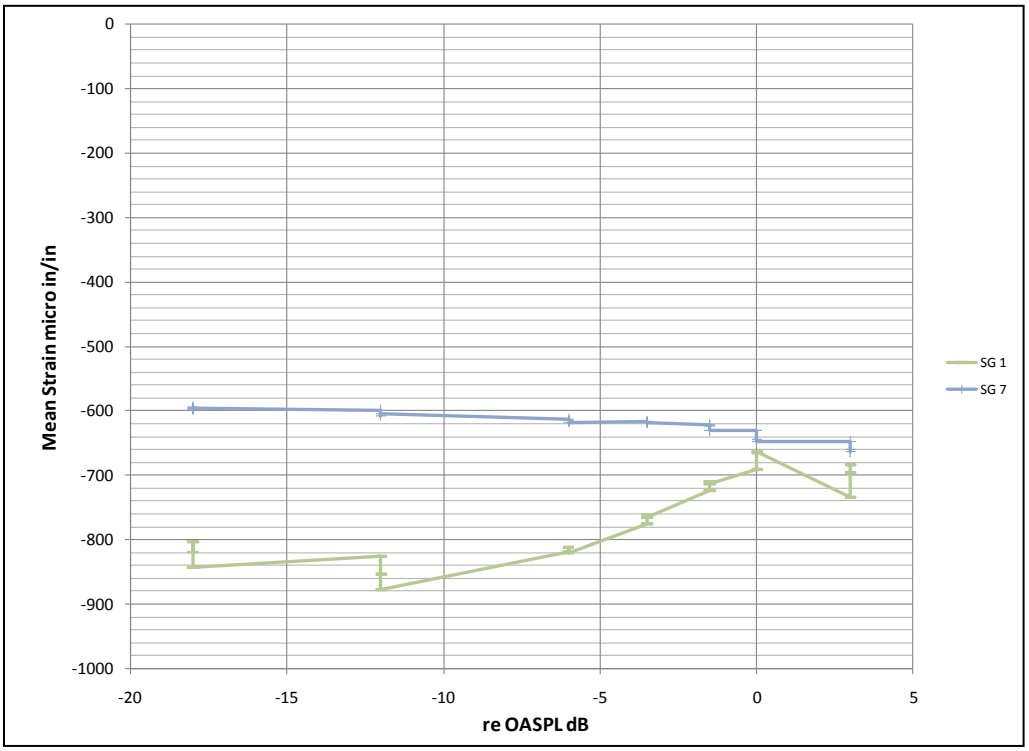

Figure 134 – Mean strains Test Run #13 at 500°F, compare SG-1 to SG-7

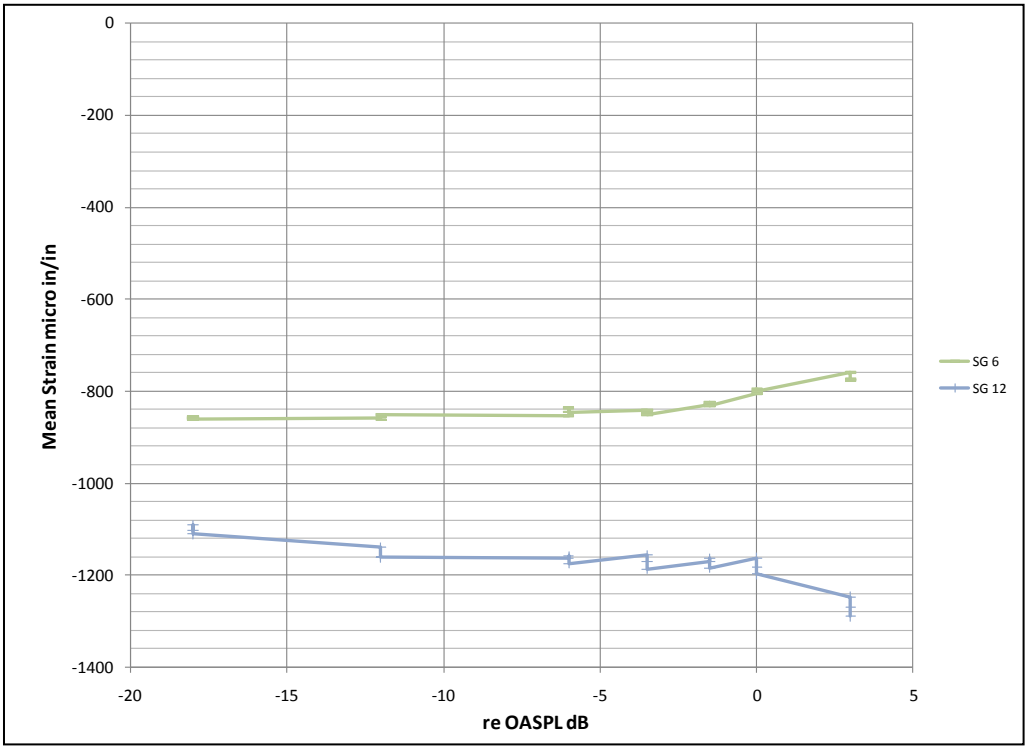

Figure 135 – Mean Strains Test Run #13 at 500°F, Compare SG-6 to SG-12

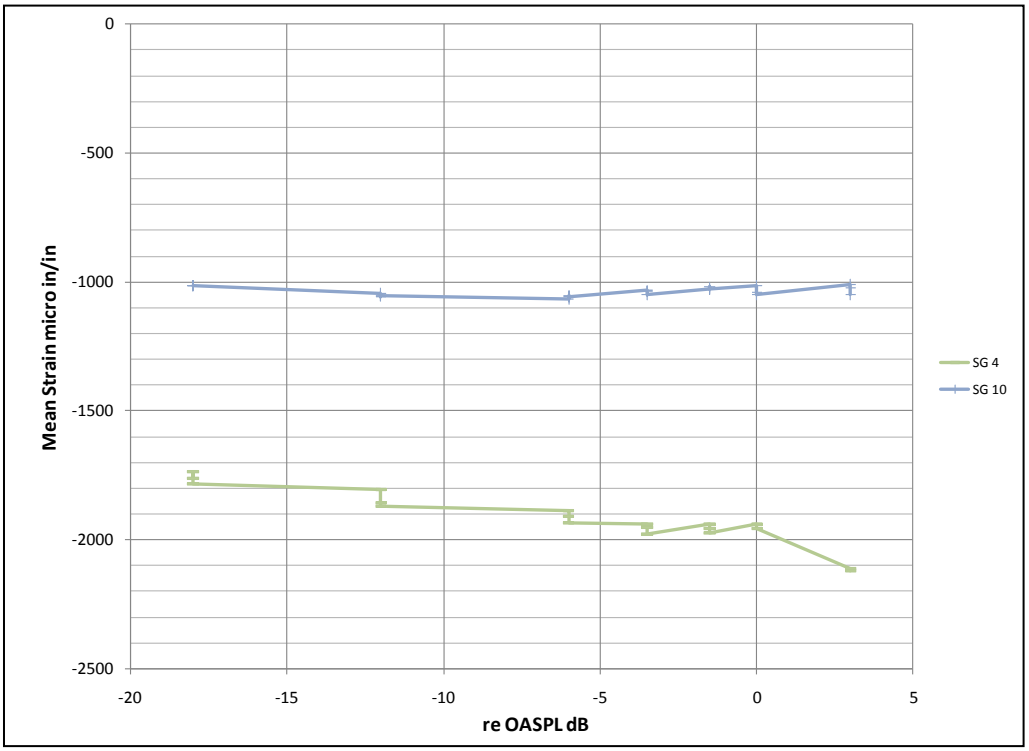

Figure 136 – Mean Strains Test Run #13 at 500°F, Compare SG-4 to SG-10

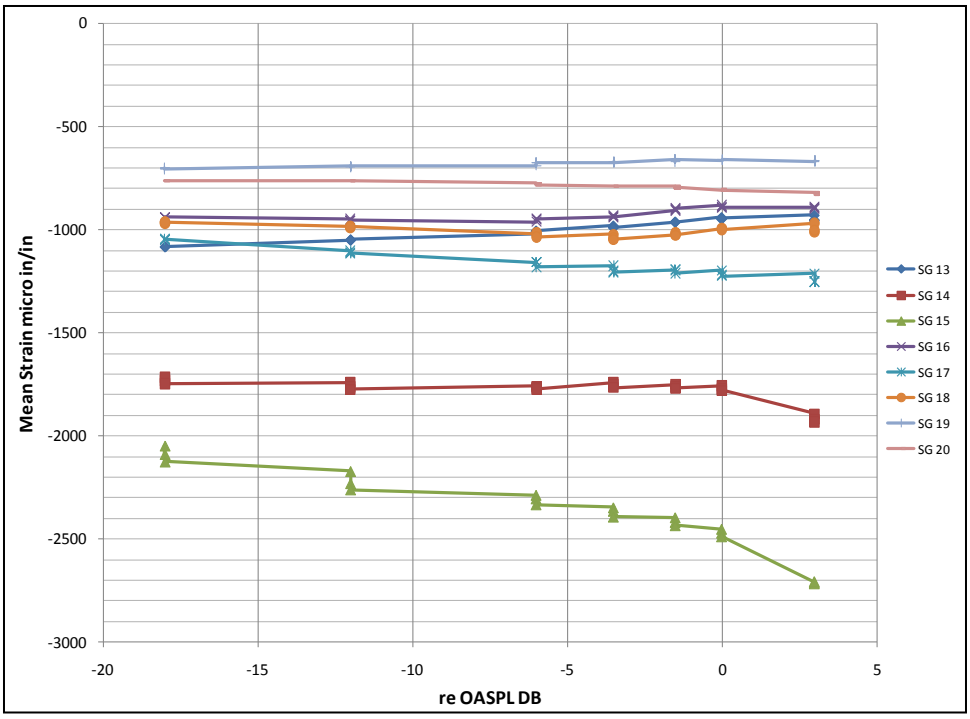

Figure 137 – Mean strains Test Run #13 at 500°F, rib edge strain gauges

Figure 138 below, shows the results from the two membrane gauges (back-to-back skin strain gauge sets.) Here, it is clear that the membrane strain was affected too. These were gauges from the two mid bays of the panel. As the membrane strain increased in one bay, it was equally decreasing in the other bay.

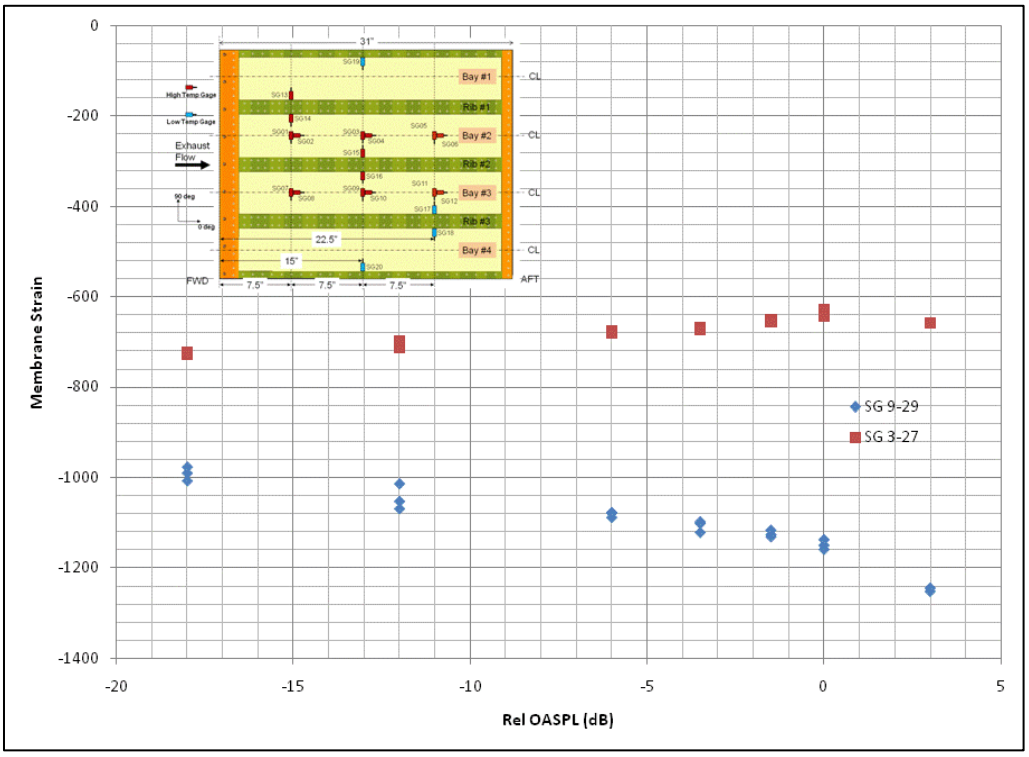

Figure 138 – CEAC Test Run 13, 500°F flat spectrum, static/thermal measurements

The sound pressure level (SPL) effect was much less at lower temperature levels. This effect can be seen in Figure 139. This figure shows the mean strain for SG-3, which was the gauge in the middle of IML skin bay. At a reference temperature of below 300°F, the sound pressure level had a minimal influence on the mean strain. Above 400°F, the SPL effect was quite noticeable. At 500°F, the effect was well-pronounced with about a 20% change in mean strain.

Test Runs 10 through 15 were performed consecutively over a single day. After the test reached a maximum reference temperature of 500°F, the temperature was decreased back to 300°F. This is the ramp-down area seen in Figure 139. The mean strain dramatically jumped at the 500°F level, but only reduced slightly when the reference temperature was reduced to 400°F on the ramp-down. However, the SPL effect diminished quite a bit. The higher mean strain at the ramp-down reference temperature of 400°F compared to the ramp-up 400°F test point was in part due to the higher substructure temperatures and fixture temperature. This can be observed in the Figure 140. The center ribs were approximately 30°F warmer during the 400°F ramp-down test point, seen in Figure 141. For reference, the OML thermocouple instrumentation locations can be seen in Figure 142.

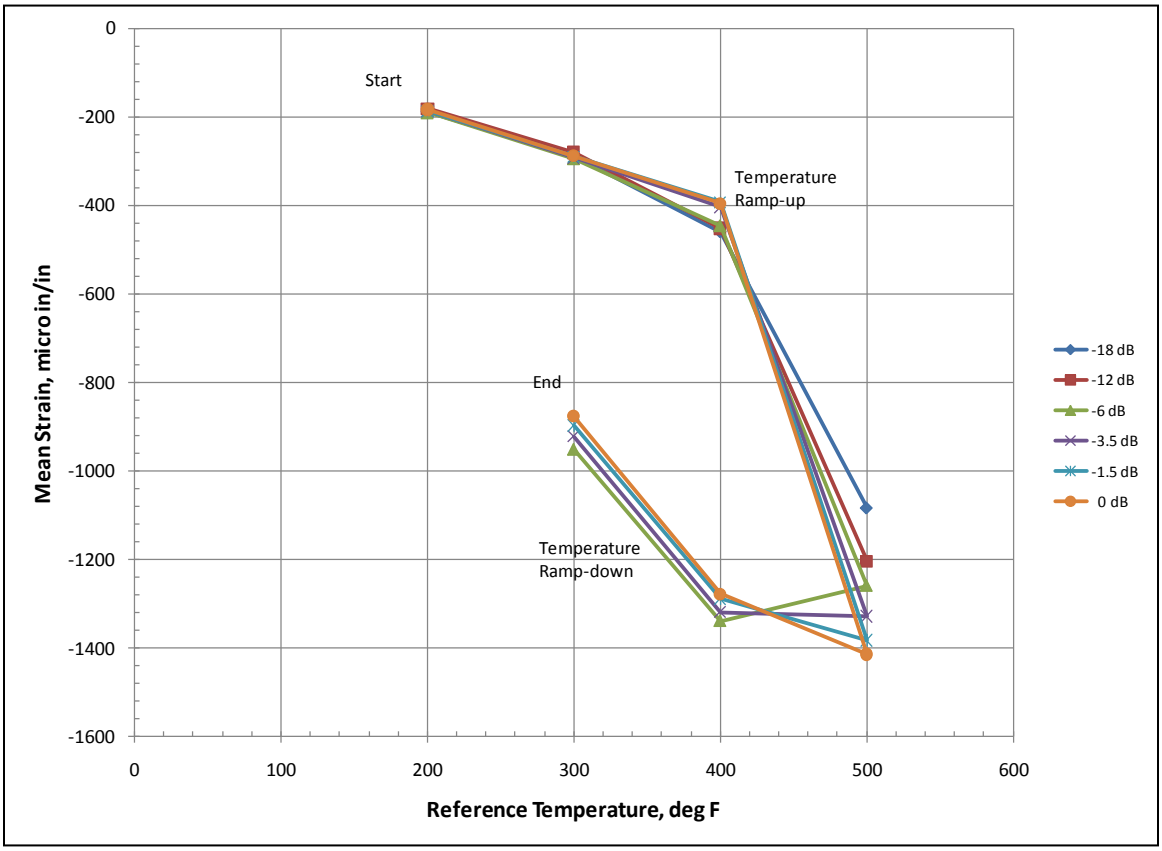

Figure 139 – Mean strain SG-3, Test Runs 10 through 15

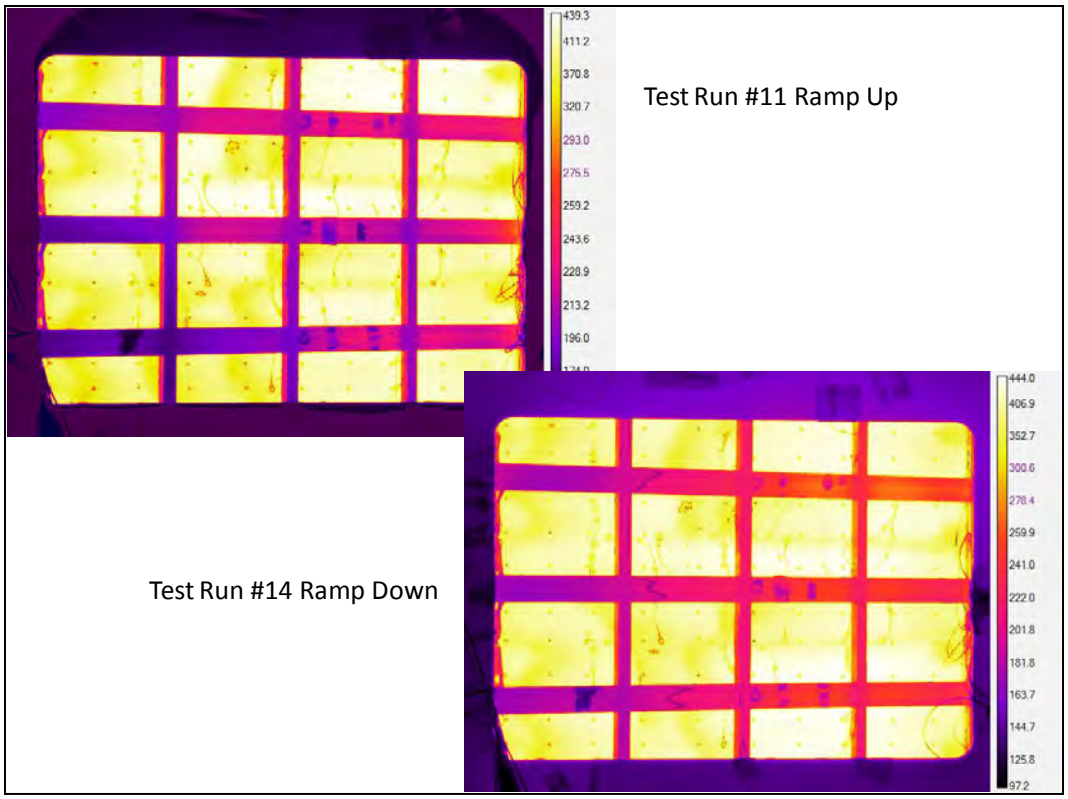

Figure 140 – Comparison of sub-structure

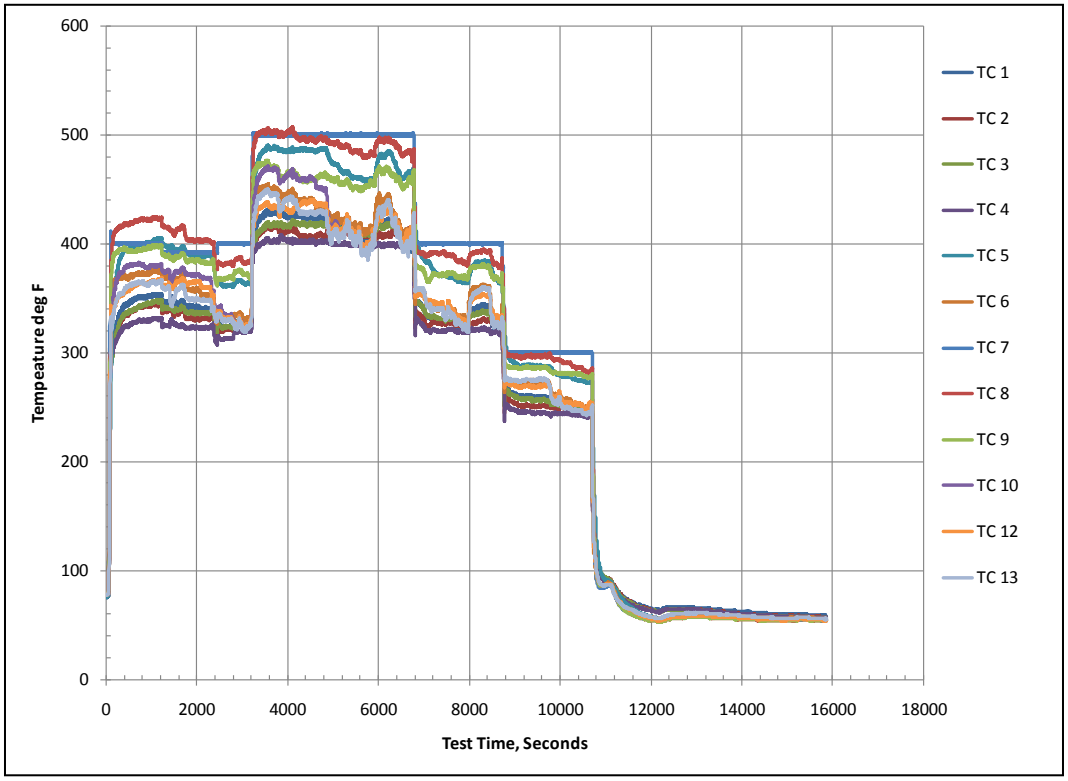

Figure 141 – Test Runs 10 through 15 temperature measurements – OML skin TCs

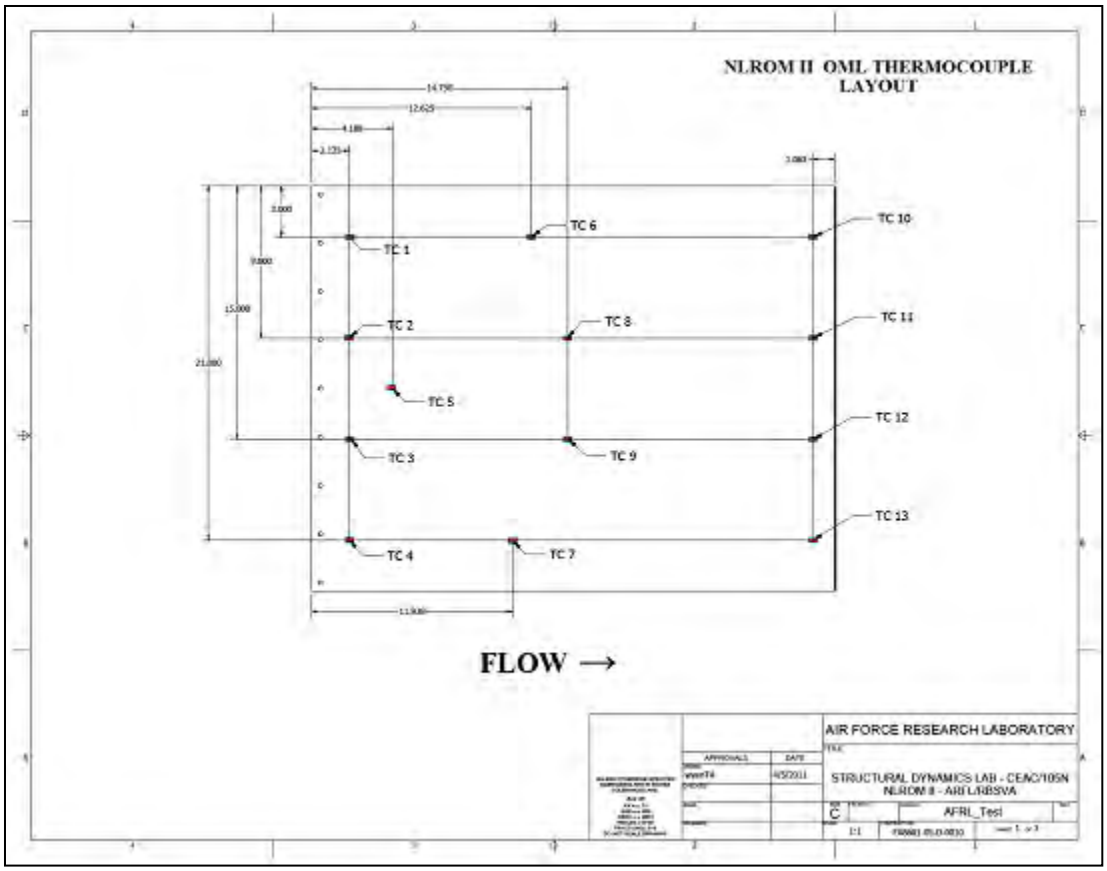

Figure 142 – OML thermocouples drawing

The next few plots show the time histories of the other thermocouples during the acoustic survey. For reference, Figure 143 and Figure 144 show the IML and fixture thermocouple locations. As seen in Figure 145, the IML temperature did vary almost 80 ºF across the skin panel in each bay. This indicated that there was considerable heat drain into the fixture and ribs, as stated earlier. Figure 146 shows that there was almost a 200 ºF difference between the top and bottom of the ribs. The top of the ribs were close in temperature to the IML skin. The fixture TCs in Figure 147 show that the fixture was fairly warm at 150 ºF, but still 100 ºF cooler than the substructure. The outer portion of fixture on the cart was nearly room temperature.

In conclusion, the heat flow from the OML to the fixture was well-characterized with thermocouples and strain gauges. In this context, this data set was sufficient in order to correlate the heat transfer analysis. This produced an accurate temperature distribution for the post-test correlation analysis. The test data presented did not show any unexpected results.

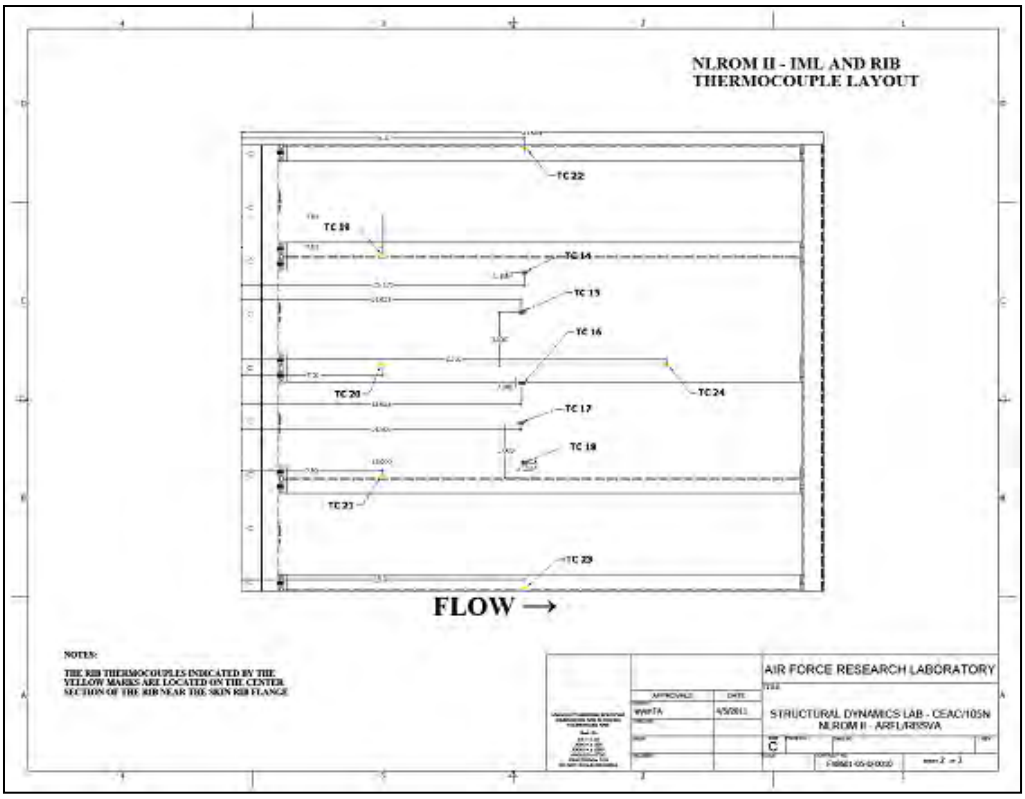

Figure 143 – IML thermocouple drawing

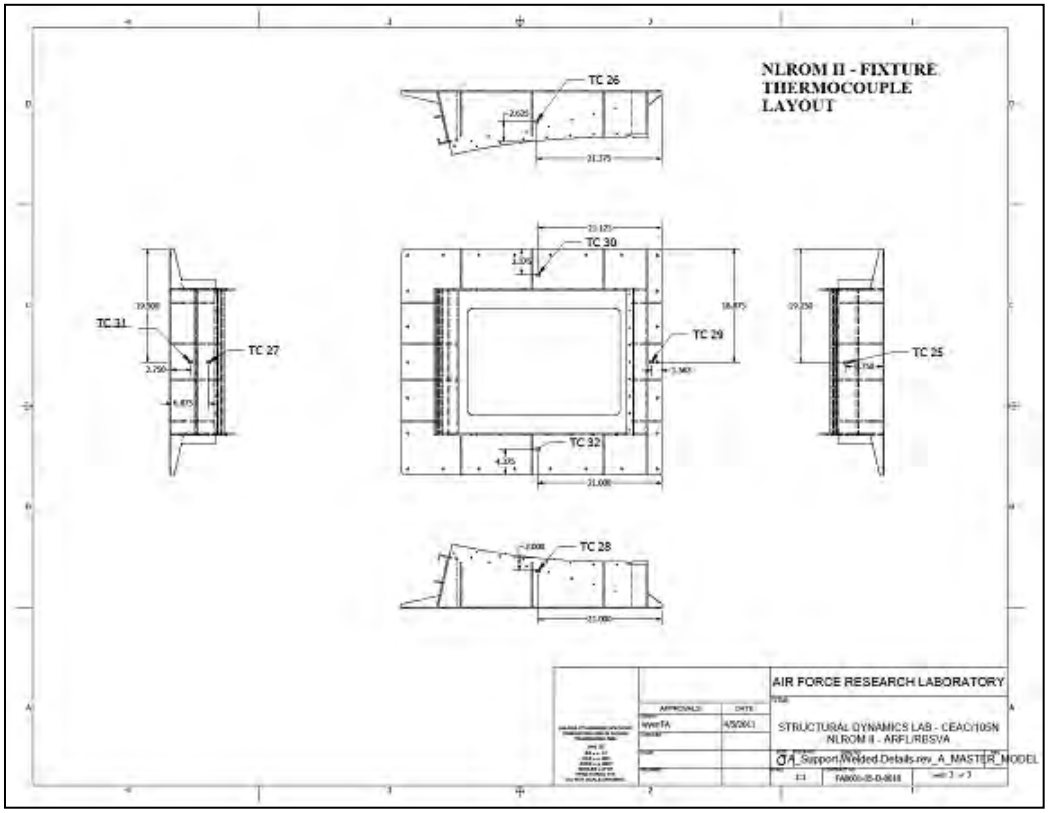

Figure 144 – Fixture thermocouple drawing

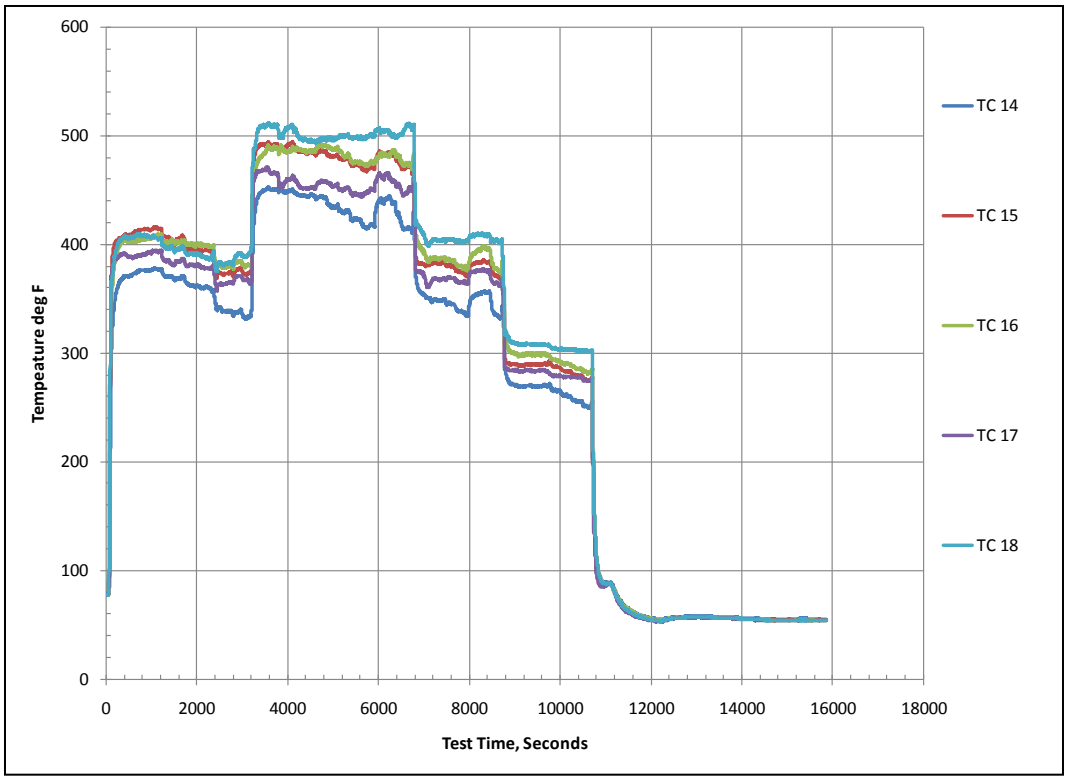

Figure 145 – Test Runs 10 through 15 temperature measurements – IML skin TCs

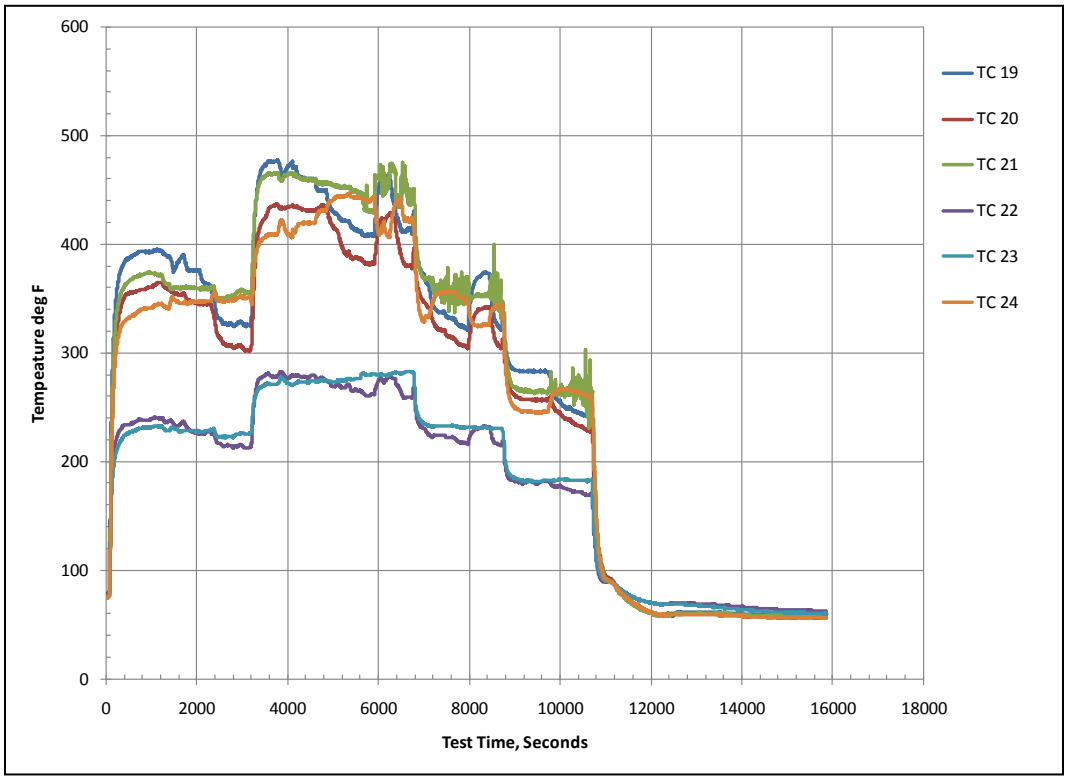

Figure 146 – Test Runs 10 through 15 temperature measurements – rib TCs

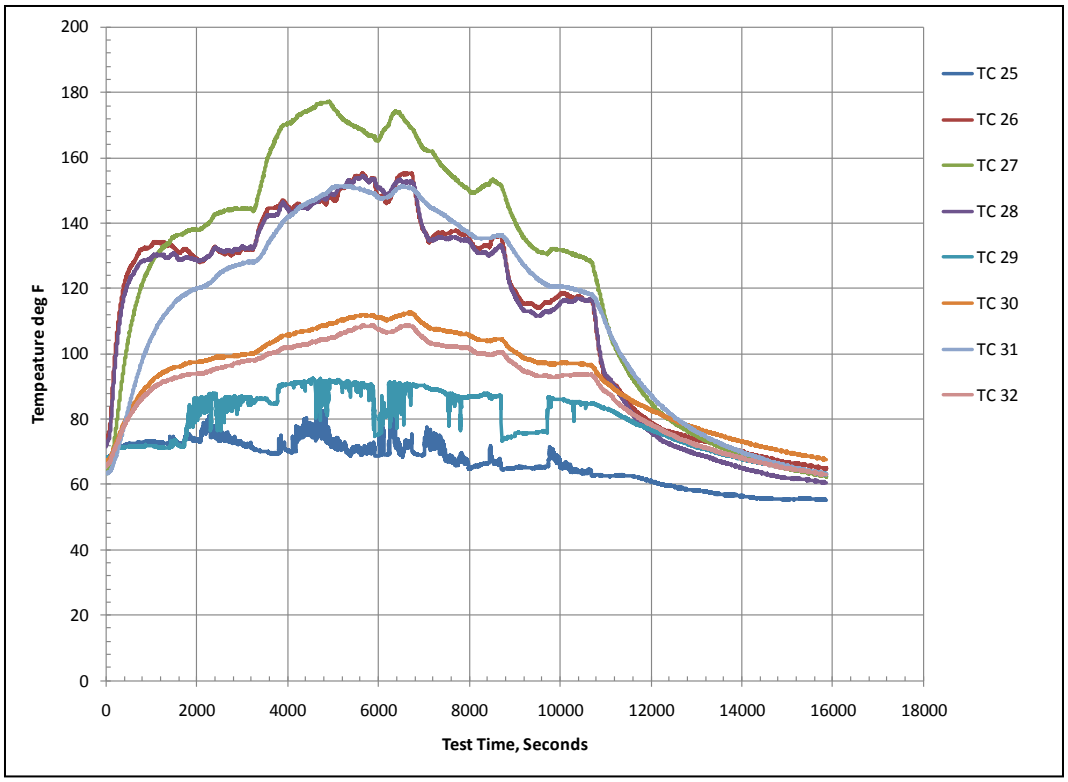

Figure 147 – Test Runs 10 through 15 temperature measurements – fixture TCs

7.5 CEAC Acoustic Sine Sweep Survey

The modal characteristics at high temperature were required for the post-test correlation. The RT modal data was only useful in correlating the reference FEM. Hence, a test method using acoustic sine sweeps was necessary to determine how the modal characteristics varied with temperature. The objective was to qualitatively observe the change in the frequency response as a function of temperature.

With the panel mounted in the chamber, the acoustic level was modulated at a constant frequency from 20Hz to 1000Hz; i.e., an acoustic sine sweep. This sine sweep was performed at several temperature levels from RT to 500 ºF. Below in Figure 148 is the frequency response function from accelerometer, A4. The characteristic frequencies changed very little below 250Hz (Figure 149), but experienced large changes above 250Hz (Figure 150) with a correlation coefficient 0.45 between RT and 500 ºF. The correlation was better between RT and 200 ºF, seen in Figure 151, but was still a large difference in the frequency response. The difference was less between 200 ºF and 300 ºF (Figure 152 and Figure 153) and between 400 ºF and 500 ºF (Figure 154).

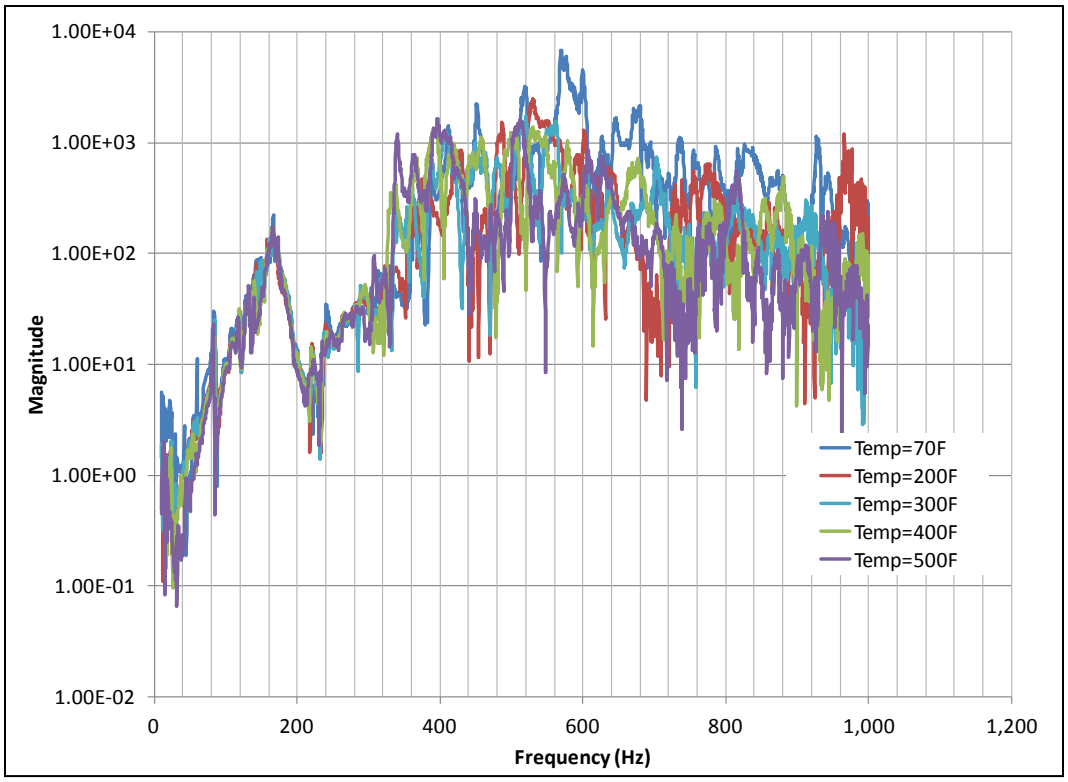

Figure 148 – Frequency Response Function (FRF), accelerometer A4

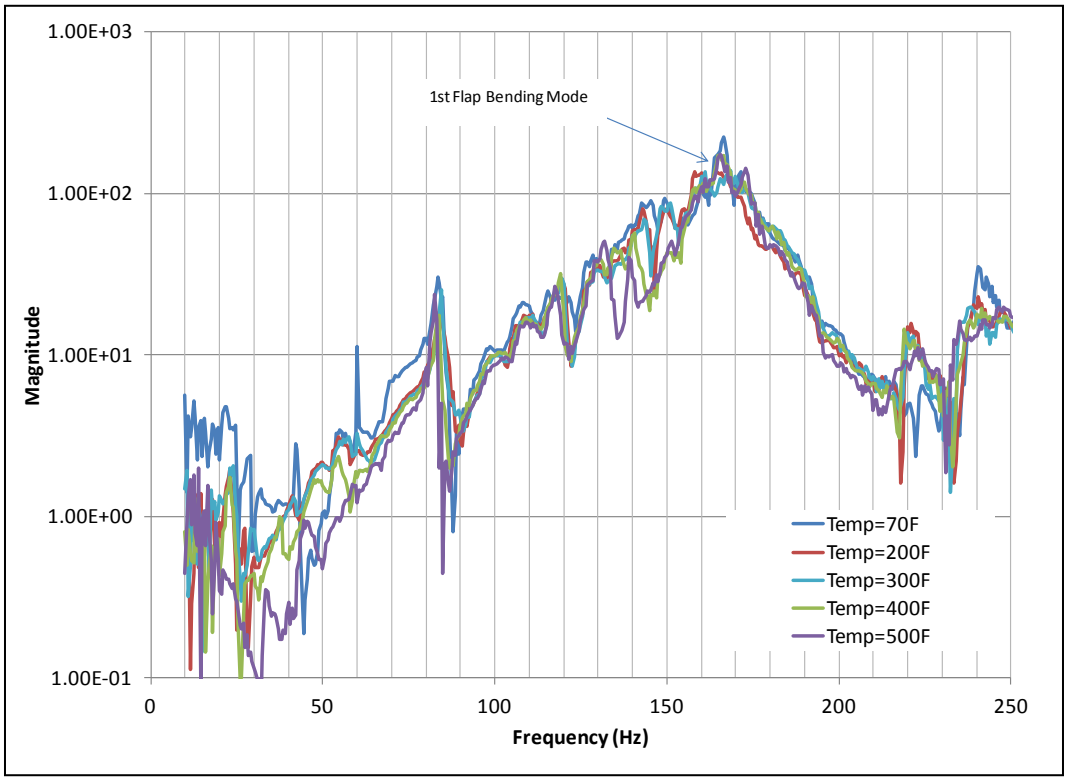

Figure 149 – Frequency zoom on FRF A4

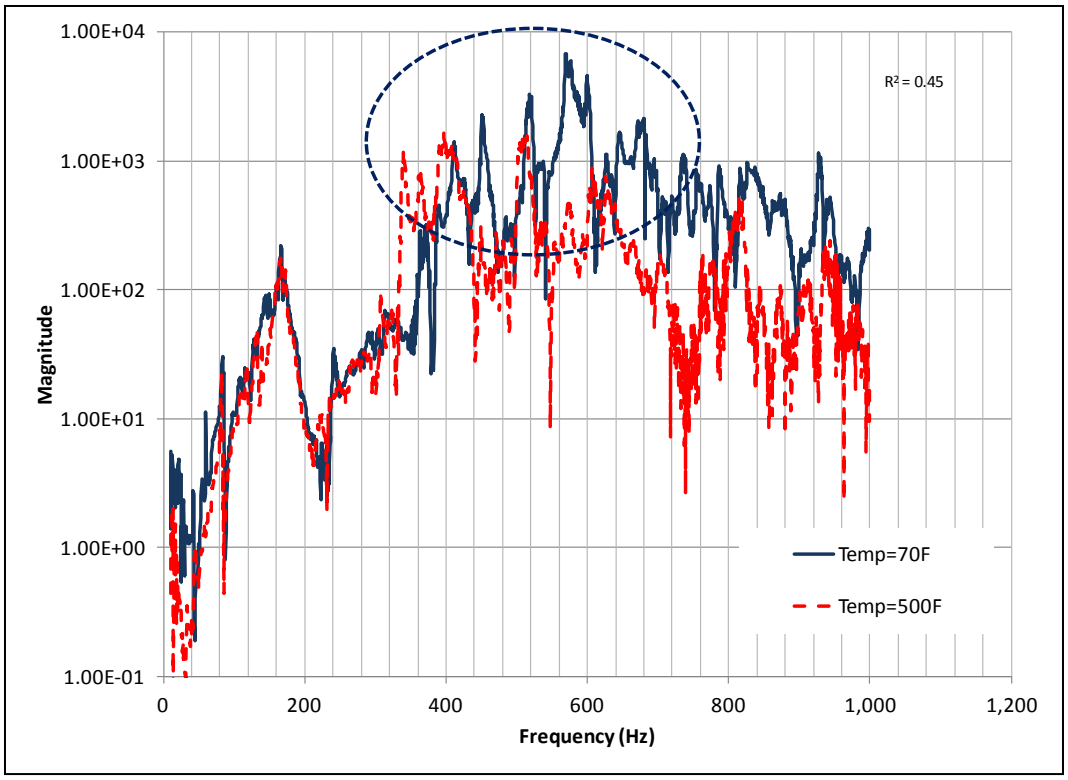

Figure 150 – FRF (A4) comparison, RT and 500°F

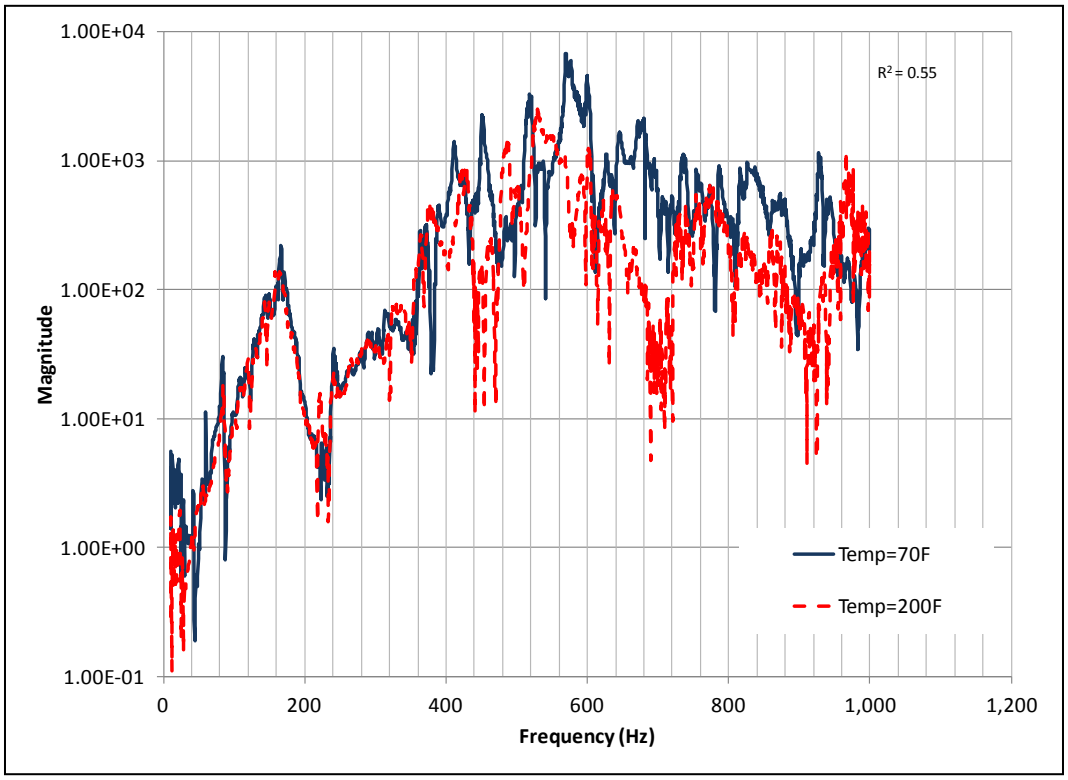

Figure 151 – FRF comparison (A4), RT and 200°F

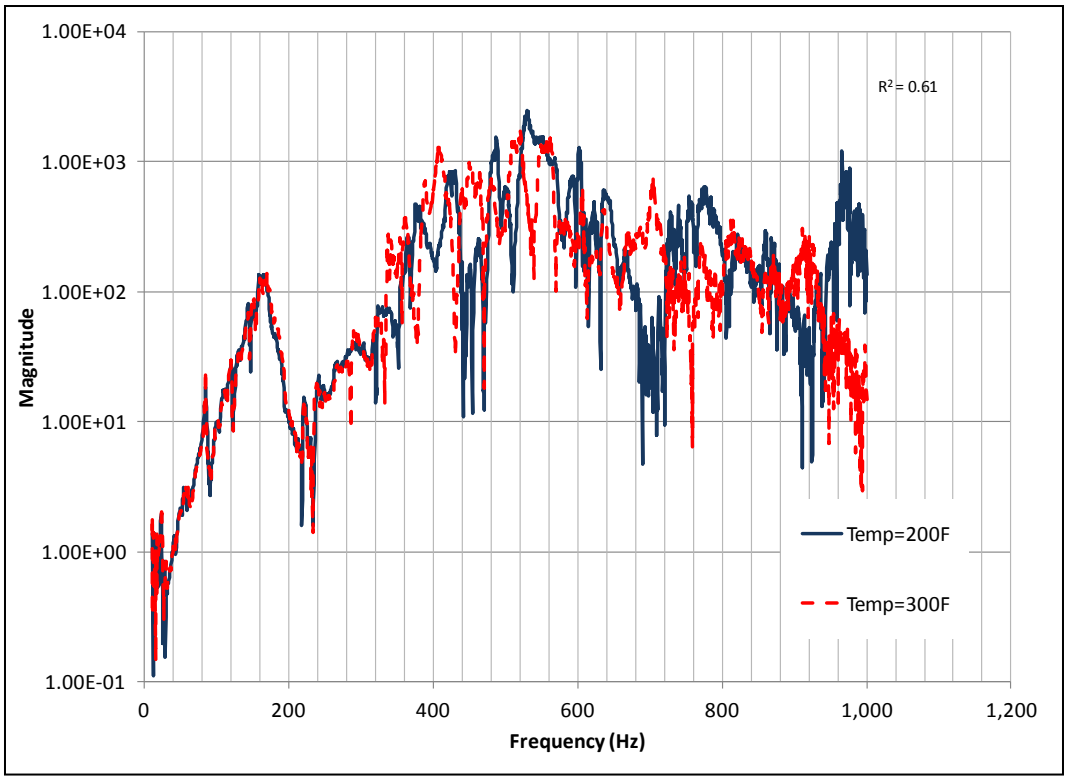

Figure 152 – FRF comparison of 200°F and 300°F

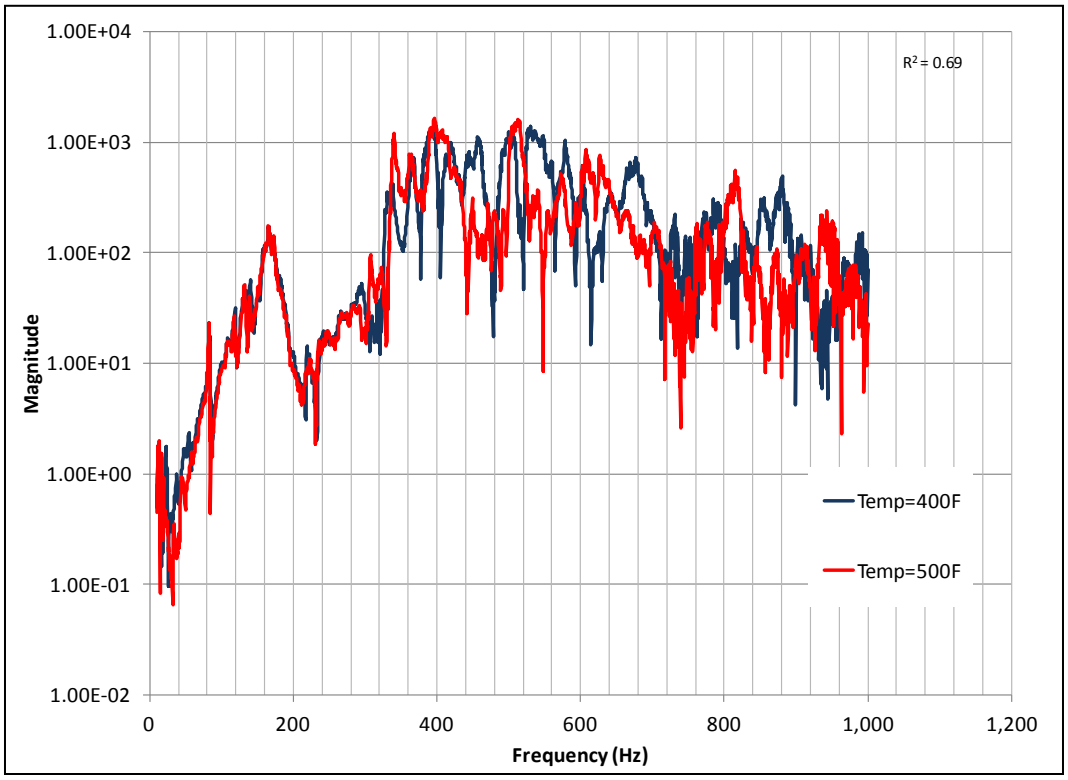

Figure 153 – FRF comparison of 200°F and 300°F

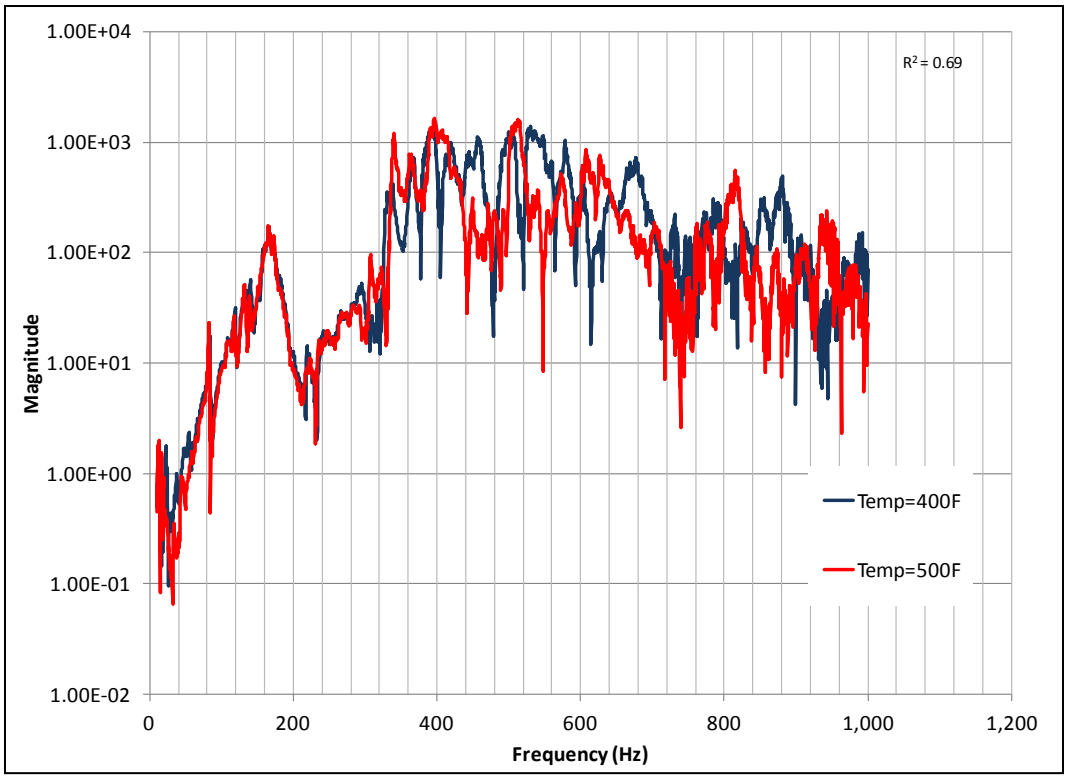

Figure 154 – FRF comparison of 400°F and 500°F

8.0 Results – Model Correlation and Updating

The two test programs were performed to gather response and loading data for use in correlating and updating the nonlinear reduced order model. The objective was to quantify and reduce the uncertainty in the inputs loads used for the response predictions through model updating. Further, it was desired to improve the structural dynamic characteristics through model correlation. The approach was to first correlate the static thermal model based on the measured data. The thermal analysis was updated from the pre-test predictions using the measured temperatures. Secondly, the model was correlated to modal test data to improve the structural dynamic response and to measure the modal damping levels that were used in the response predictions.

8.1 CEAC Model Correlation and Updating

The CEAC model correlation and updating was divided into thermal (static) and modal (dynamic) correlation. The thermal correlation used the IR, thermocouple, LVDT, and ARAMIS test data. The modal correlation used the measured mode shapes, frequencies, frequency response functions, and modal damping.

8.1.1 CEAC Thermal Model Correlation and Updating

For the CEAC test simulations, the thermal loads were predicted using a heat transfer analysis. The quartz lamp banks were modeled as radiant heat sources. The flow in the CEAC chamber was measured for input in the convection model. The thermal measurements were used to update this heat transfer analysis (Abaqus) in order to provide an accurate representation of the thermal loads in the test article. The following describes the process used to arrive at a correlated thermal model and updated temperature loads that were then used in the NLROM response predictions.

The IR data was imported into Matlab and plotted to get an understanding of the temperature distribution observed during the test, (shown in the backside image in Figure 155). As can be seen, there were significant temperature gradients on the skin. These were likely due to instrumentation, wiring, potting, and possible paint thickness variations. There was a contour for every 20°F change in temperature. The blue area in the image was the mounting fixture plate. The lighter blue was the test article substructure, and the red areas were the IML of the skin. The round object in the image was the dynamic shaker.

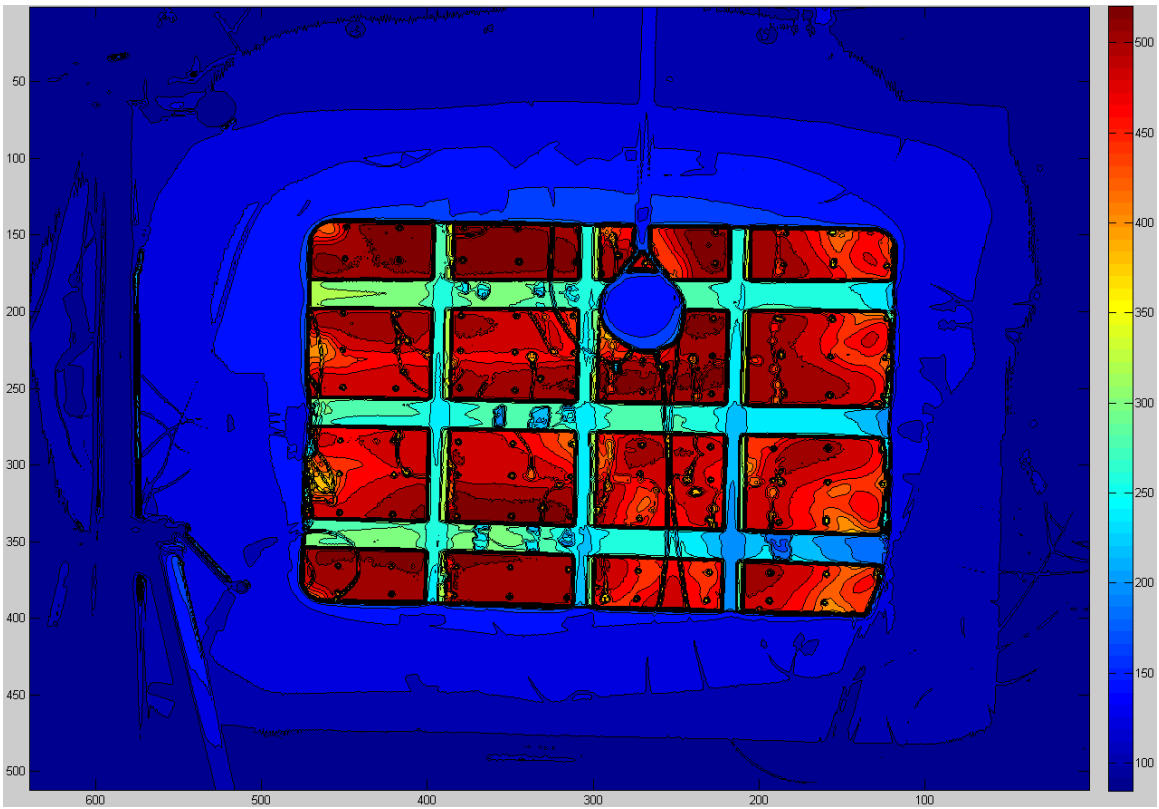

Figure 155 – IR data – temperature contours at max temperature (backside image)

The small view offered by the IR camera placement made full temperature mapping difficult, but the data was used to assist in tuning the thermal model to get a reasonable representation of the thermal profile.

After updating the existing Abaqus thermal model with the test conditions, an initial temperature comparison was done using thermocouple data and corresponding nodes on the test article. Note, the radiation lamp temperature was an input in the heat transfer analysis, but this value was not measured. Hence, a lamp bank temperature was assumed based on best available information. The overall temperature distribution for the test article is shown in Figure 156. It should be noted that to achieve a temperature profile that was more akin to the test contours, a portion of the cart backing structure was added. The comparison is shown in Table 7.

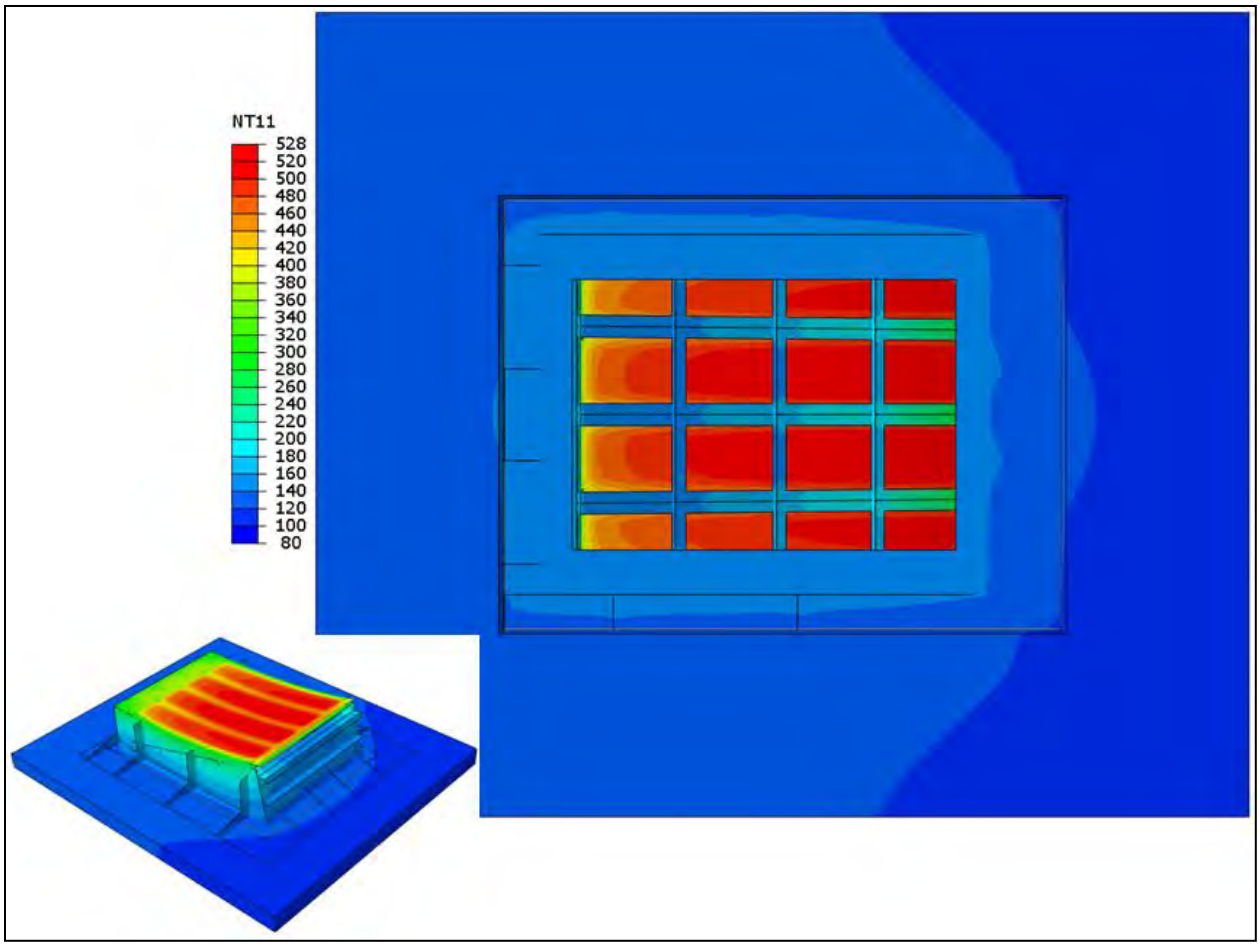

Figure 156 – Abaqus thermal model attempting to characterize the thermal profile seen in the test data

As can be seen from Table 7, the initial comparison was fairly good. For thermocouple (TC) locations, refer to Figure 142, Figure 143, and Figure 144. There were a few TC locations that seemed to have a higher disparity between the test and analysis, but most were within 10%. This initial correlation was performed with only 22 of the test article thermocouples. The other seven from the fixture were added in subsequent model correlation.

Table 7 – Initial comparison of FEM and test temperatures at thermocouple locations

	TC	Test	FEM	Node	% Diff
Skin OML	1	416	365	403	-12%
	2	404	383	443	-5%
	3	398	383	483	-4%
	4	388	366	523	-6%
	5	468	389	1284	-17%
	6	481	452	59	-6%
	7	487	452	179	-7%
	8	501	482	104	-4%
	9	500	482	144	-4%
	12	448	450	677	1%
	13	440	433	698	-2%
Skin IML	14	464	409	1029	-12%
	15	489	482	104	-1%
	16	476	417	1053	-12%
	17	492	482	144	-2%
	18	470	409	1077	-13%
Ribs	19	465	391	1263	-16%
	20	427	399	1287	-7%
	21	433	391	1311	-10%
	22	340	276	1013	-19%
	23	281	277	1093	-1%
	24	444	422	1170	-5%

After establishing a baseline starting point for the thermal correlation, a ModelCenter process was developed to correlate with 29 of the 32 thermocouples. Note, TC10, TC11, and TC25 were determined to be faulty during the high temperature modal testing. ModelCenter is a commonly used tool to enable integration of models and simulations, process automation, results visualization and data management. The ModelCenter process took 36 variables such as convection coefficients, radiation emissivity, ambient temperatures, and thermal material properties as inputs. It also used 29 points, one for each thermocouple, from a steady-state point in the thermal profile with a maximum of roughly 500°F as outputs. A Design of Experiments (DOE) was performed with the goal of creating an approximation model, and optimizing in order to reduce the error between the model and test data. The approximation model creation time was about one day. Figure 157 shows the ModelCenter process, with the "Low Fidelity" space to be filled in by the approximation model.

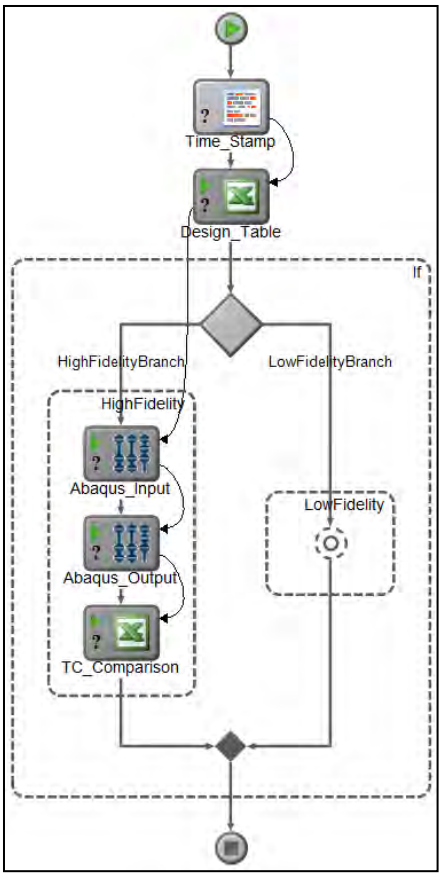

Figure 157 – ModelCenter process for correlation of FEM and test thermocouple data

The ModelCenter correlation resulted in the comparison shown in Table 8. As can be seen, the maximum percent difference was 25%, while the minimum was -17%. For the most part, the temperatures were within about ±10%. A reason for the discrepancies is likely due to a problem with using a mid-plane shell model for a thick fixture structure. Gradients through the thickness of the parts were not captured accurately, but the FEM was much simpler and solved significantly faster. The final ModelCenter implementation with the approximation model and the optimization block is shown in Figure 158.

Table 8 – Comparison of test vs. analysis temperature data at all thermocouple locations

	TC	Test	FEM	Node	% Diff
Skin OML	1	417	401	403	-4%
	2	404	413	443	2%
	3	397	414	483	4%
	4	388	403	523	4%
	5	468	419	1284	-10%
	6	480	456	59	-5%
	7	488	458	179	-6%
	8	501	471	104	-6%
	9	499	472	144	-6%
	12	447	459	677	3%
	13	441	446	698	1%
Skin IML	14	464	428	1029	-8%
	15	489	471	104	-4%
	16	475	433	1053	-9%
	17	492	472	144	-4%
	18	470	429	1077	-9%
Ribs	19	465	420	1263	-10%
	20	427	424	1287	-1%
	21	433	421	1311	-3%
	22	340	283	1013	-17%
	23	281	284	1093	1%
	24	444	404	2257	-9%
Fixture	26	184	197	6872	7%
	27	186	187	7230	0%
	28	176	199	5738	13%
	29	103	128	7990	25%
	30	123	123	8445	0%
	31	152	184	7139	21%
	32	111	123	6131	11%

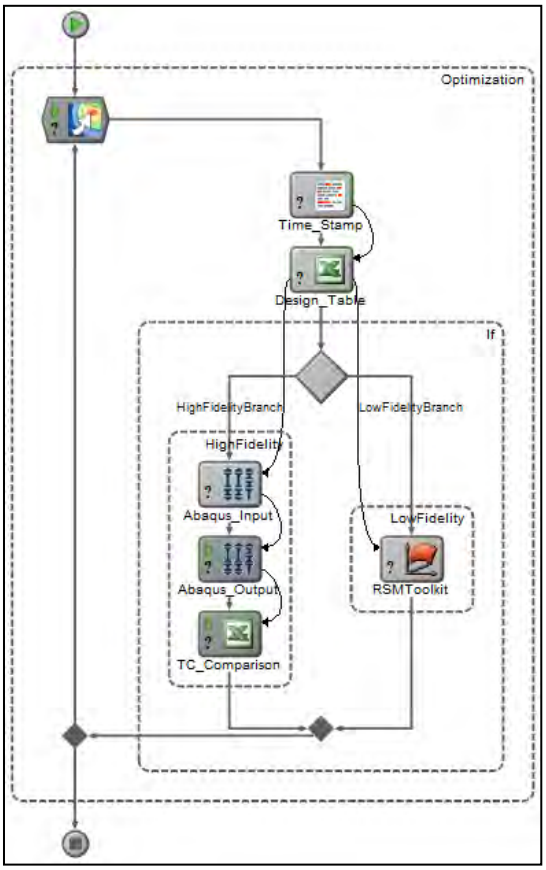

Figure 158 – Final ModelCenter implementation of the thermocouple optimization process

All of the optimization was done using the approximation model. Therefore, a final Abaqus thermal analysis was performed using the optimum point. The thermal profile from the Abaqus analysis is shown in Figure 159.

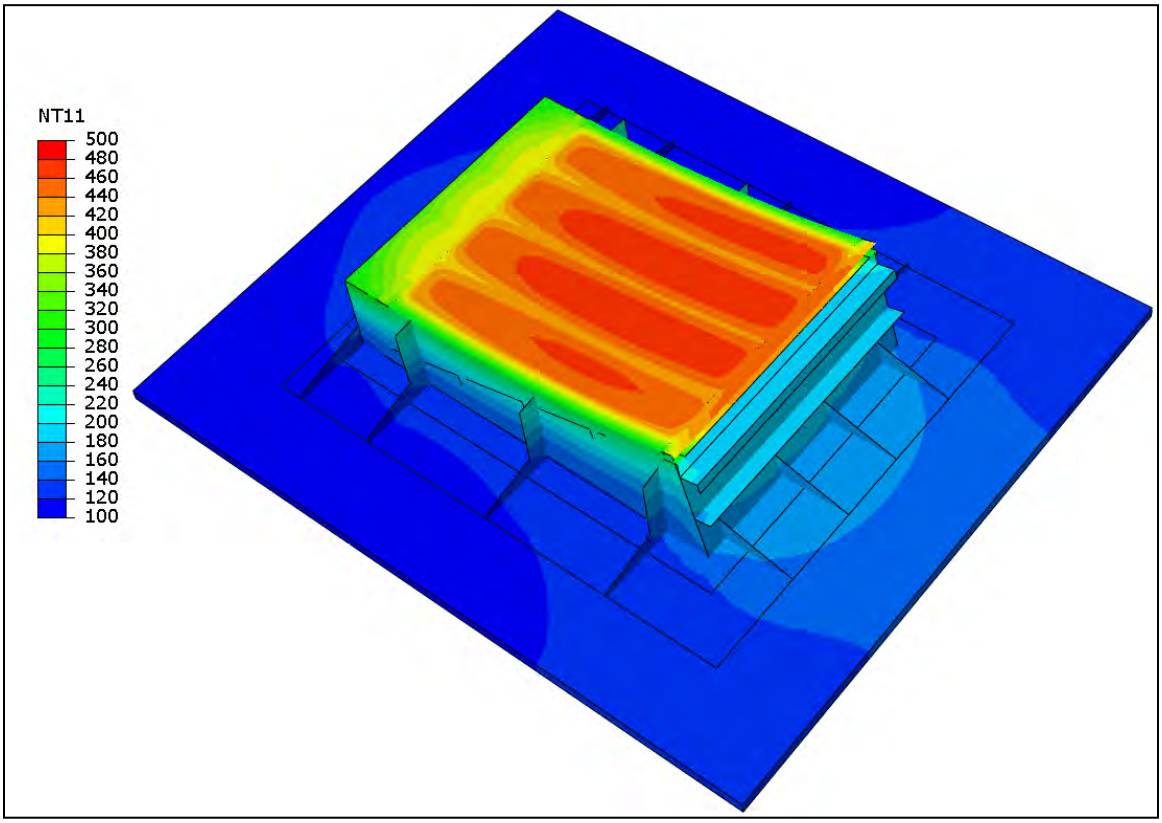

Figure 159 – Thermal profile for optimized Abaqus thermal solution

All of the temperatures from this thermal solution were written out as NASTRAN compatible temperature entries to be used in the modal correlation, which will be discussed in more detail later.

8.1.2 CEAC LVDT Correlation

The second step in the Thermal Correlation was to use the LVDT data for displacement correlation. The objective was to use the LVDT data as additional constraints to further refine the correlation of the NASTRAN thermal model setup. The CEAC model needed to be correlated to the LVDT displacement data from Test #5 – Thermal Survey. For more information on the CEAC testing refer to Appendix D. The high temperature Thermal Survey was performed after the modal and lower temperature acoustic surveys. There were four LVDTs, shown in Figure 160, along with the corresponding pictures in Figure 161. LVDT 1 and 2 measure z-displacement (in-out of the graphic), LVDT 3 measures x-displacement (side-to-side), and LVDT 4 measures y-displacement (up-down). Table 9 shows the initial relationship between the test data and the analysis prior to correlation.

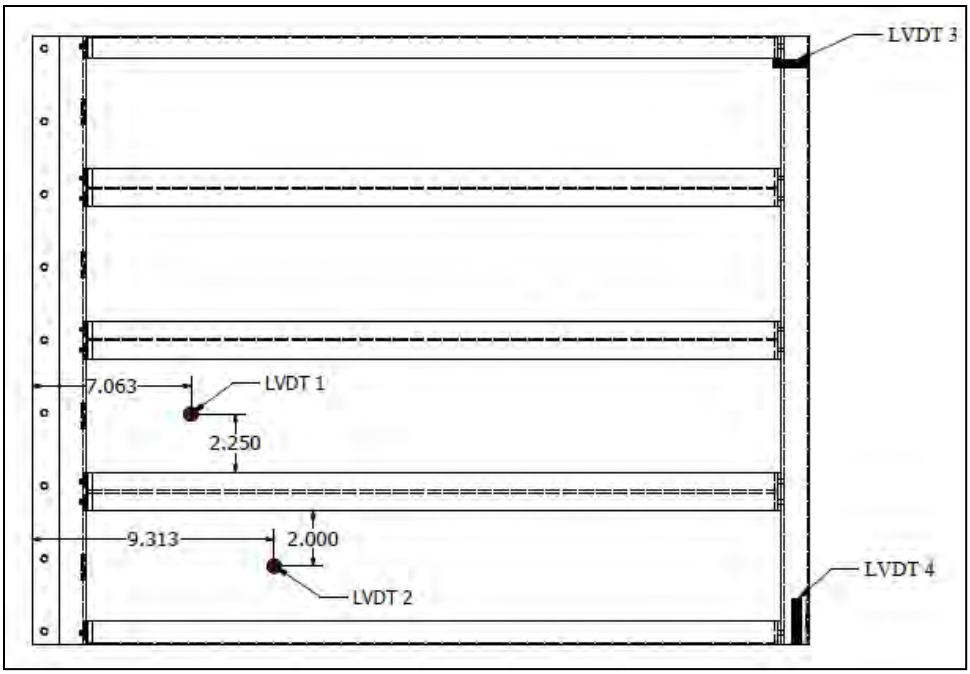

Figure 160 – LVDT locations


Figure 161 – (Clockwise, starting at top left): LVDT's 1 and 2, LVDT 3 and LVDT 4

Table 9 – Initial comparison between test data and analysis

	Test Data (in)	Analysis (in)	% Difference
LVDT1 (nd 473,z)	-0.023	-0.021	-10%
LVDT2 (nd 6,z)	-0.022	0.106	308%
LVDT3 (nd 928,x)	-0.022	0.0254	187%
LVDT4 (nd 744,y)	0.006	-0.0254	124%

In order to correlate the model, NASTRAN's SOL 200 optimization was utilized. The objective function was set to minimize the square root of the sum of the squares of the percent difference between the analysis and the test data. A constraint of +/-30% were placed on the results. The design variables used were the coefficients of thermal expansion (α) for all nine materials property cards in the model. These thermal expansion values were allowed to change between 10^{-7} and 10^{-5} (in/in)/°F. A summary of the optimization setup is shown in Table 10 below.

Table 10 – Solution 200 definition

NASTRAN Solution 200 for Model Correlation	
Objective Function	Minimize: $\sqrt{\left(\sum_{i=1}^{4}\left(\frac{\delta_{Ti}-\delta_{FEMi}}{\delta_{Ti}}\right)^2\right)}$
Constraints	$-0.30\delta_{Ti} \leq \delta_{FEMi} \leq 0.30\delta_{Ti}$
Design Variables	$10^{-7} \leq \alpha_j \leq 10^{-5}\ (in/in)/°F$ $1 \leq j \leq 9$

After several trials, a converged solution was achieved by changing the algorithm from Modified Method of Feasible Directions (MMFD) to Sequential Quadratic Programming (SQP). Adjustments to the constraints were also needed. This required that the signs of the upper and lower bounds of the test data expansion coefficient values needed to be flipped. The bounds on the design variables also needed to be increased to what are shown in Table 10. Once these changes were made, SOL 200 was able to successfully converge on a feasible solution. Table 11 summarizes the results for the coefficient of thermal expansion, while Table 12 shows the final correlation results to the LVDT data.

Table 11 – Coefficients of thermal expansion results

	Original α	Optimized α	% Difference
α1 (Ti-6Al-4V)	4.88E-06	2.09E-06	57.19%
α2 (Ti-6Al-4V)	4.88E-06	1.21E-06	75.10%
α3 (15-5Ph steel)	6.31E-06	1.00E-05	-58.48%
α4 (15-5Ph steel)	6.31E-06	1.30E-07	97.94%
α5 (4130 steel)	6.90E-06	1.00E-05	-44.90%
α6 (4130 steel)	6.90E-06	6.50E-06	5.78%
α7 (4130 steel)	6.90E-06	2.37E-06	65.71%
α8 (4130 steel)	6.90E-06	6.00E-06	13.04%
α9 (4130 steel)	6.90E-06	1.71E-06	75.16%

Table 12 – LVDT correlation results

	Test Data (in)	Test Data, Flipped Sign (in)	Optimized (in)	% Difference
LVDT1 (nd 473,z)	-0.023	0.023	0.0261	-13.54%
LVDT2 (nd 6,z)	-0.022	0.022	0.0284	-29.02%
LVDT3 (nd 928,x)	-0.022	0.022	0.0212	3.60%
LVDT4 (nd 744,y)	0.006	-0.006	-0.0042	29.99%

8.1.3 CEAC Modal Correlation

The third step in the model correlation was to improve the structural dynamic characteristics. A critical aspect of the reduced order model is an accurate representation of the modes. This correlation was performed in two steps. First, the model was correlated to the room temperature modal test data. Second, the model was correlated to the high temperature modal data.

An initial examination of the modal test data compared with that of the analysis is shown in Table 13. A stiffness knockdown of 30% for the welded steel fixture parts was an attempt to get better initial correlation of the first mode, without affecting the other modes. This appeared to be successful in achieving that goal. This can be justified in that the FEM had only rigid connections between the test article and test fixture. Thus, any compliance due to rivets and bolts was not accounted for in the FEM. The data indicated a good correlation between the model and test mode shapes at room temperature. The test condition included the test article in the chamber with the lamps in.

Table 13 – Modal comparison between room and high temperature test data and FEM temperatures

Mode Shift	Mode	Test RT Freq (Hz)	Test HT Freq (Hz)	%shift	Mode	FEA RT Freq (Hz)	FEA HT Freq (Hz)	%shift
	1	173	172	-0.6%	1	173	172	-0.6%
	2	368	359	-2.4%	2	363	269	-25.9%
	3	390	385	-1.3%	3	368	300	-18.5%
	4	414	403	-2.7%	4	403	322	-20.1%

Test vs FEA	Mode	Test RT Freq (Hz)	FEA RT Freq (Hz)	%diff	Mode	Test HT Freq (Hz)	FEA HT Freq (Hz)	%diff
	1	173	173	0.0%	1	172	172	0.0%
	2	368	363	-1.4%	2	359	269	-25.1%
	3	390	368	-5.6%	3	385	300	-22.1%
	4	414	403	-2.7%	4	403	322	-20.1%

Note: All FEA values are with a -30% knockdown to steel stiffnesses

After examining the mode shape test data, it was apparent that multiple shapes and frequencies were extracted for each "mode" of interest. Thus, as a first step in identifying the modes from the test data, a modal assurance criterion (MAC) was completed between the room temperature and high temperature data to establish the most likely mode pairs between the two tests. The MAC plot is shown in Figure 162, and the data is shown in Table 14. It should be noted that "TEST" is the room temperature results, while "FEA" is the high temperature results.

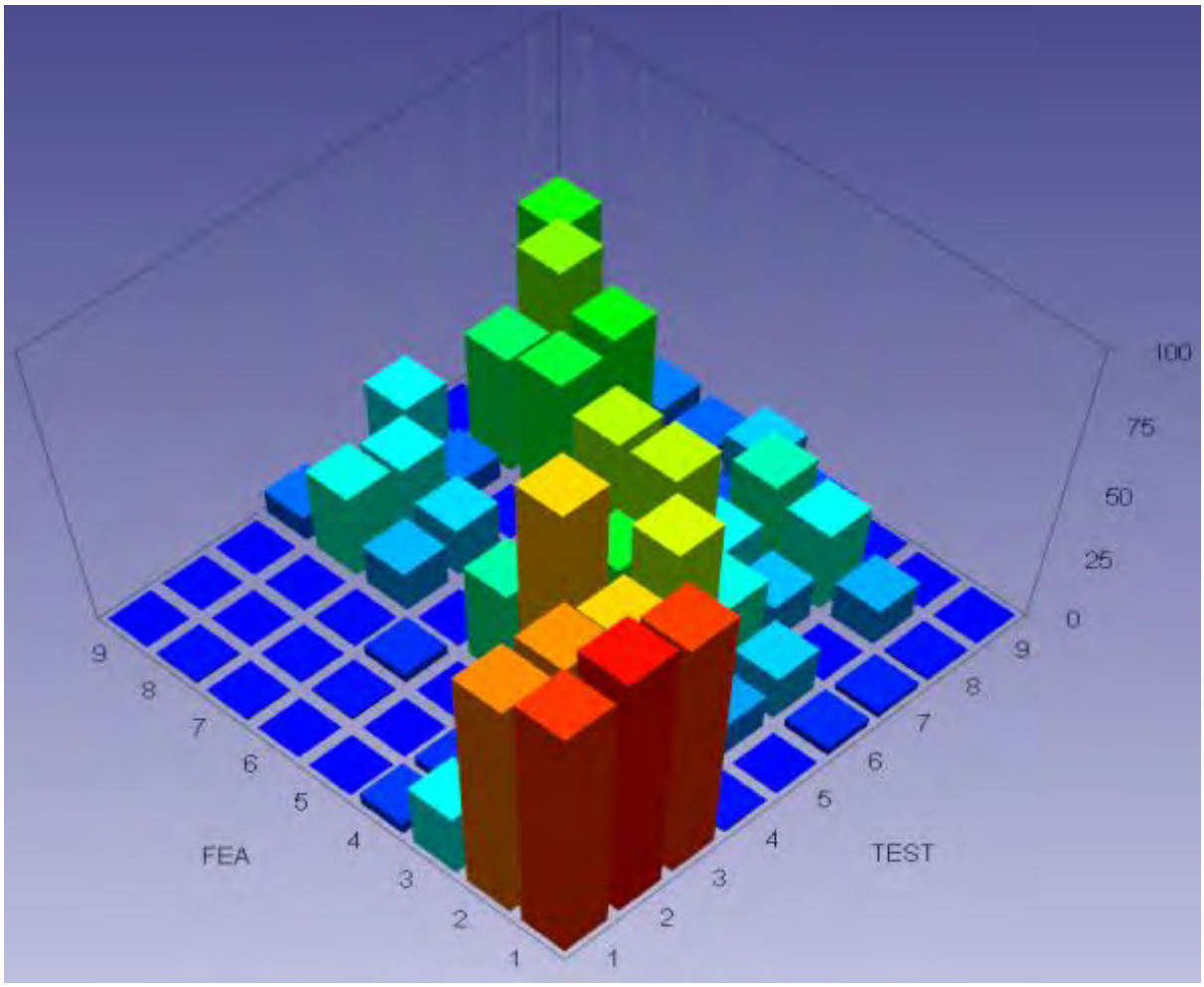

Figure 162 – MAC between room temp and high temp test data from 160 to 410 Hz

Table 14 – MAC data for matching with selected mode targets for 1st 4 modes

Room Temperature

		Shape	4	3		2	Drive		1		
		Mode	9	8	7	6	5	4	3	2	1
Shape	Mode	Freq (Hz)	414	405	390	368	307	282	181	173	160
4	9	403	51	0	0	24	0	9	0	0	0
3	8	397	5	60	42	9	28	31	0	0	1
	7	385	10	49	46	0	18	15	1	1	1
2	6	369	8	3	30	15	1	0	4	1	0
	5	359	17	7	2	65	19	36	0	0	0
Drive	4	294	7	35	23	66	47	82	5	4	5
	3	255	1	30	16	31	68	43	29	26	25
1	2	188	0	14	0	17	13	17	82	88	89
	1	172	0	1	3	3	0	1	95	99	95

High Temperature

Node-point pairs between the analysis and test were selected automatically using the Node-Point pairing tool in FEMTools. FEMTools (Finite Element Model Tools) is a multi-functional, cross-platform, solver-independent family of CAE software programs providing analysis and scripting solutions for many different types of applications. The program is developed, sold and supported by Dynamic Design Solutions Inc. The selection was based on a minimum distance criterion. A graphical representation of the Node-Point pairs is shown in Figure 163.

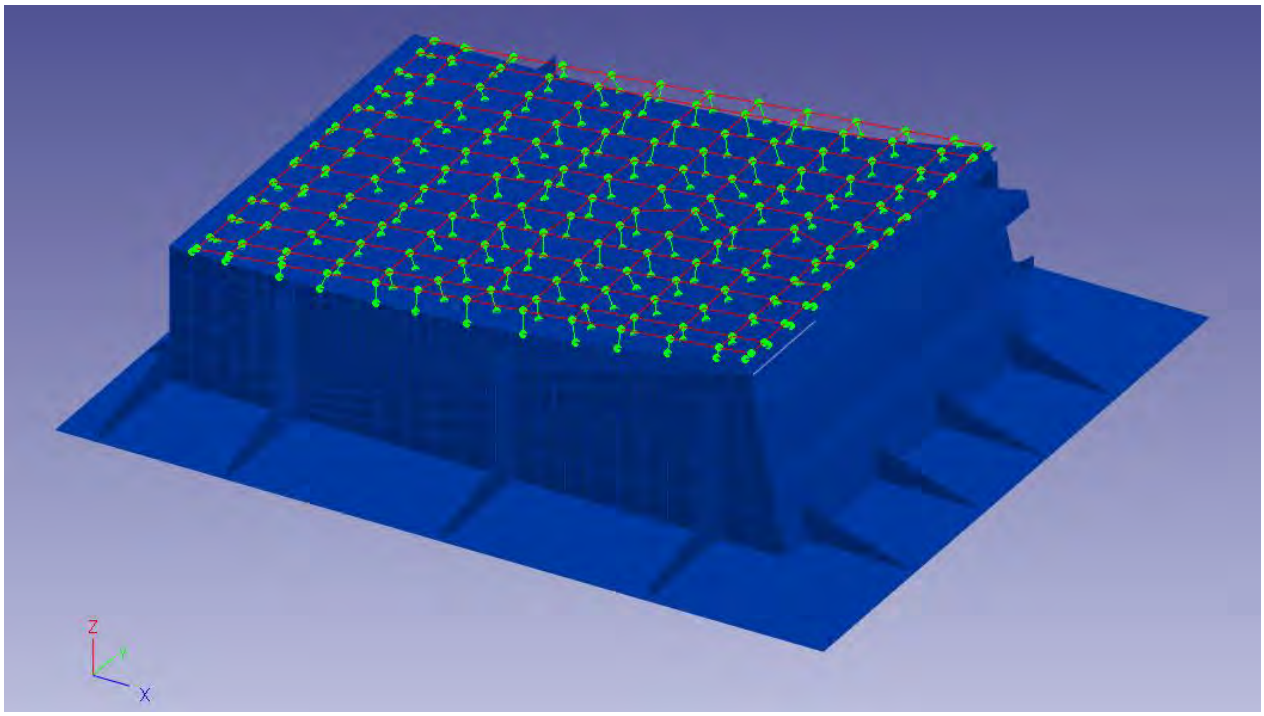

Figure 163 – Node-point pair visualization

After generating the node-point pairs, an initial Modal Assurance Criterion (MAC) matrix was generated as a comparison between the FEA and test mode shapes, Figure 164. As can be seen, the correlation between the two models was fairly low. The correlation focused on the lowest 4 modes.

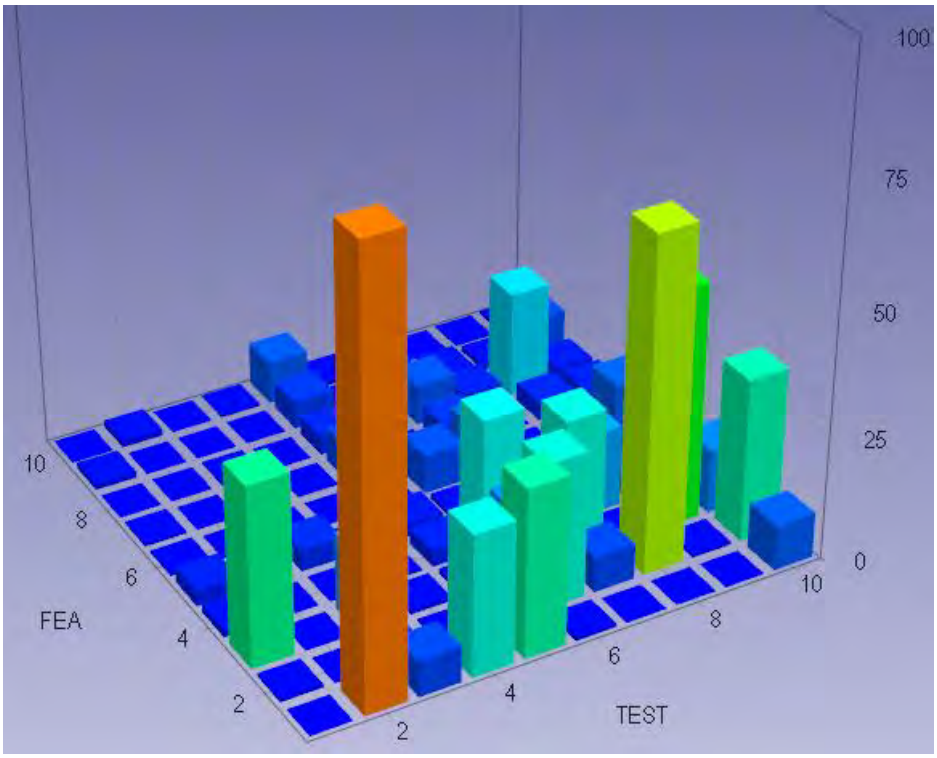

Figure 164 – Modal assurance criterion matrix plot for FEM vs. test

Some visual mode pairing was necessary in the next step of the correlation process. The room temperature mode shapes from the analysis are shown in Figure 165. These modes were observed in most of the modal test data.

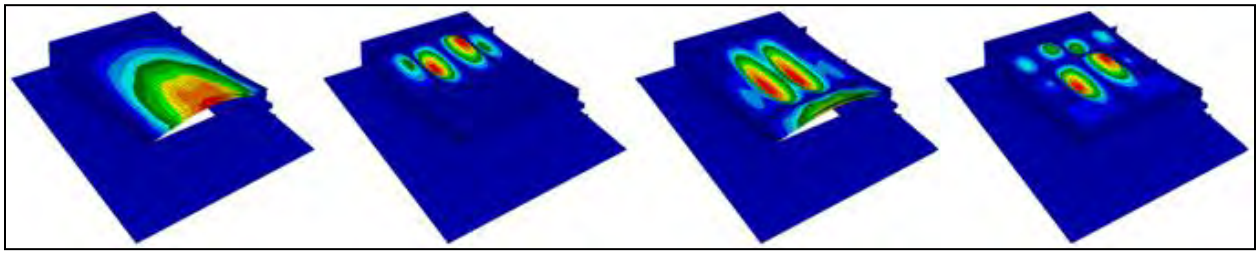

Figure 165 – FEA room temperature modes

The high temperature displacements based on the initial temperatures are shown below in Figure 166. In addition, the mode shapes for this thermal condition are shown in Figure 167. It should be noted that modes 3 and 4 are shown to have switched order. This was not observed in the test data.

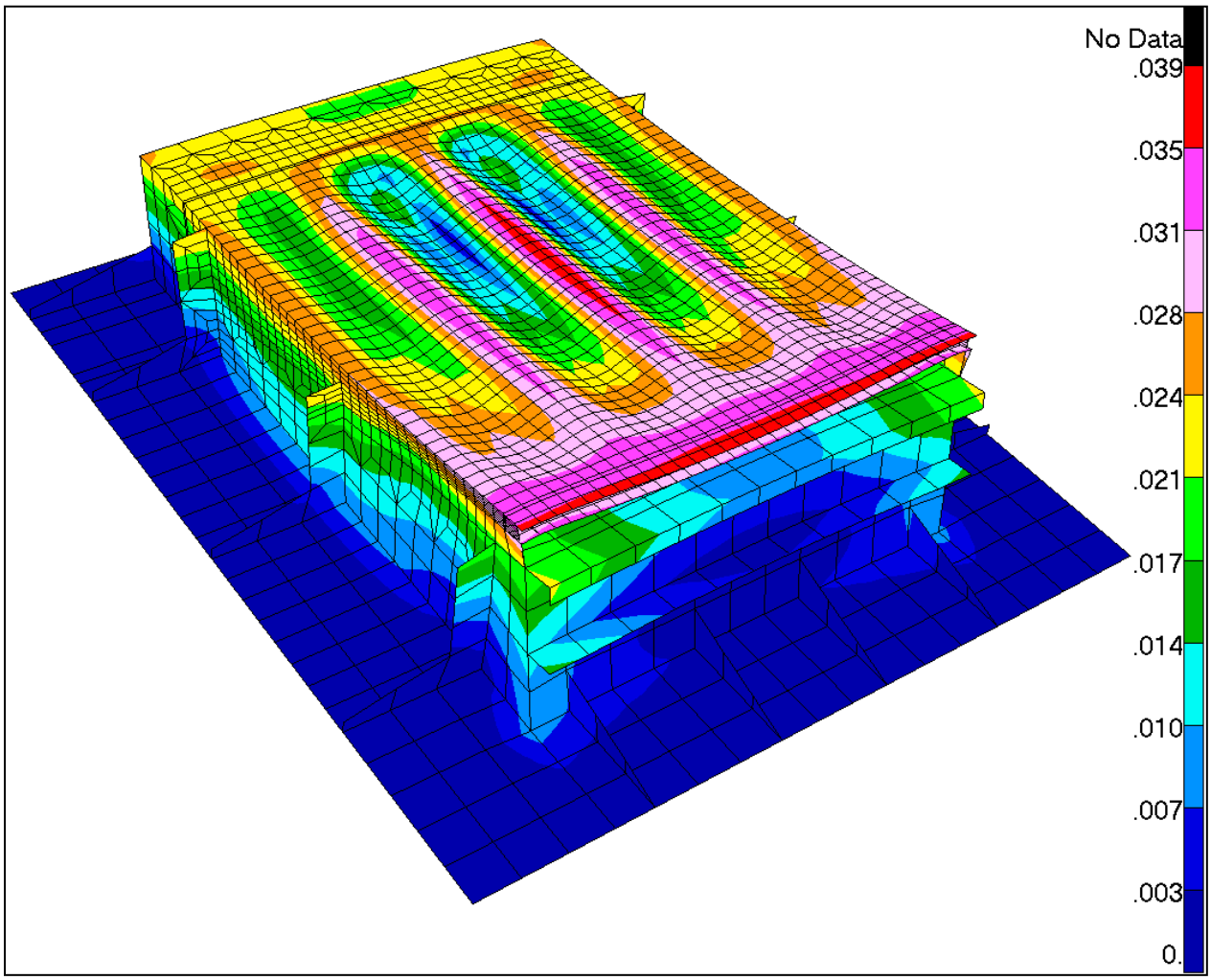

Figure 166 – FEA high temperature displacements

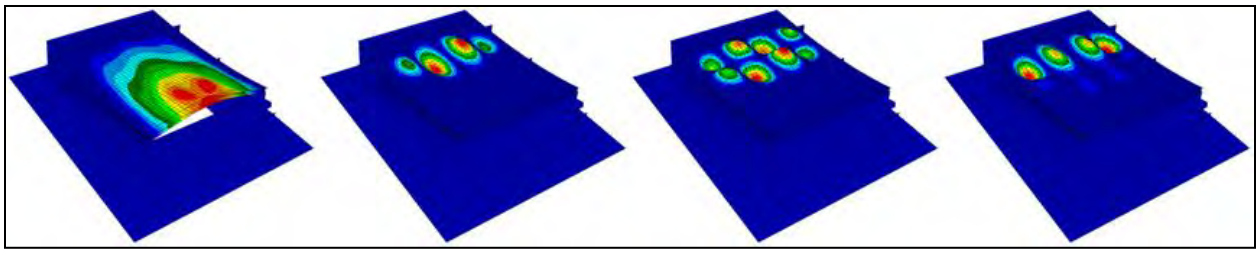

Figure 167 – FEA high temperature modes

FEMTools was used to correlate the room temperature and high temperature modal test data with the model. The stiffness of the materials in the test fixture was the primary parameter used in the model updating procedure. A correlation of the room temperature data is shown in Figure 168, with the comparison shown in Table 15.

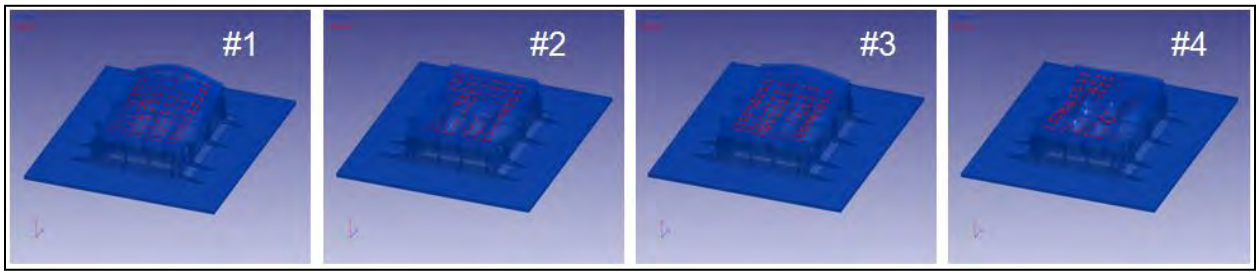

Figure 168 – Room temperature test modeshapes overlaid on corresponding FEM modeshapes

Table 15 – Modeshape comparison table for room temp test vs. correlated FEM

Mode #	FEM-Hz	MEAS-Hz	%Diff	MAC
1	179	172	3.8	99.1
2	365	359	1.6	91.3
3	368	369	-0.4	68.2
4	409	403	1.5	70.6
5	419	397	5.6	76.2

The correlation of the high temperature modal data is shown in Figure 169, with the corresponding comparison shown in Table 16. This was a large improvement over the initial test versus FEM comparison.

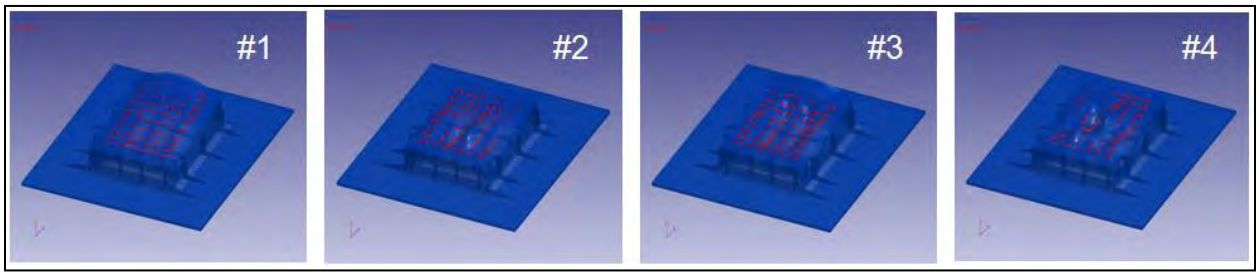

Figure 169 – High temperature test modeshapes overlaid on corresponding FEM modeshapes

Table 16 – Modeshape comparison table for high temp test vs. correlated FEM

Mode #	FEM-Hz	MEAS-Hz	%Diff	MAC
1	179	173	3.4	99.2
2	367	368	-0.2	85.8
3	377	390	-3.3	57.1
4	409	414	-1.2	69.2
5	419	405	3.5	71.0

The thermal correlation, modal correlation, and the expansion coefficients from the LVDT correlation, provided the complete post-test correlated CEAC model.

8.2 T-58 Model Correlation and Updating

With respect to the T-58 Engine Burner Test, only the thermal model was correlated and updated. Although a modal test was performed, the modal correlation was not performed, as the modes found were essentially the same as those for the CEAC test. For the thermal correlation, a similar process to the CEAC correlation was executed. The primary difference was that the measured structural temperatures were applied as steady state values in a heat transfer analysis. Unlike the CEAC test correlation, a heat transfer analysis was used to predict the structural temperatures. The reasons were two-fold. First, the IR camera could image the upper OML surface of test article. In the CEAC test, the OML surface could not be imaged through the side wall of the CEAC chamber. Second, the heat flux and thermal loading from the engine exhaust was not known. To determine the heat flux and thermal loading would have required a 3D Computational Fluid Dynamic (CFD) simulation with coupled thermal analysis. This analysis was beyond the scope of this program.

8.2.1 T-58 Thermal Model Correlation and Updating

The IR camera was placed directly above the test article looking down at the OML skin, seen in Figure 170. This provided a wide field image of the skin temperatures. This IR data was then used, along with thermocouple test data, to provide the updated temperature loads on the model during the engine run simulations. The following describes how the IR data and thermocouple test data was used to predict an updated temperature distribution.

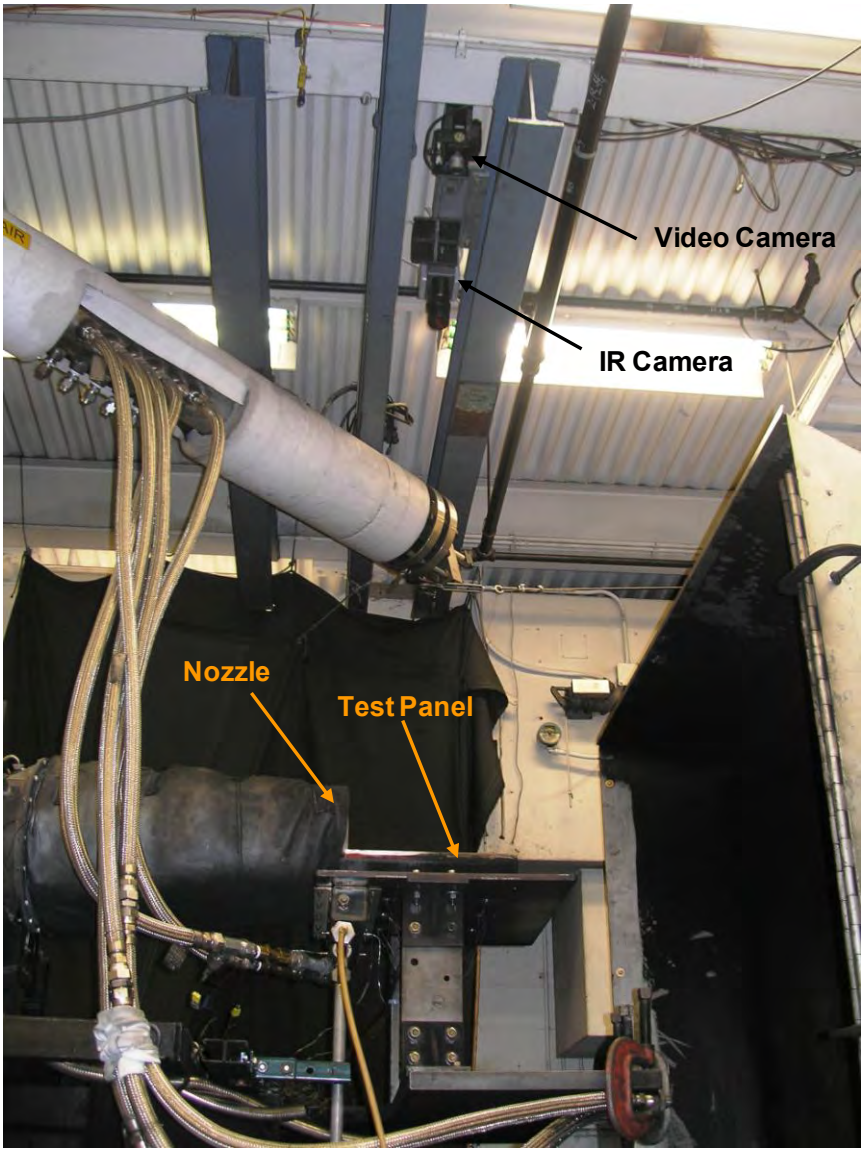

Figure 170 – T-58 test camera locations

Matlab was used to scale and extrapolate the IR data for the entire surface of the test article. The raw IR data was imported from Runs B0614 and B0615 at 85% engine throttle and 0° angle-of-attack case. The T-58 Test Run descriptions can be found in Appendix C. Run B0614 was an 11.5”x 23” snapshot of the middle of the panel beginning towards the leading edge of the panel. Run B0615 was a snapshot of the same size for the back corners of the panel. The images were positioned such that the locations of the accelerometer coincided. An overlap occurs between 9” and about 25” in the flow direction, and from about 7” to 12” and again from 14” to 18” in the transverse direction. In these areas, the temperature data was averaged between the two sets of data. Figure 171 shows the initial mapping scheme, along with the initial superposition of the skin nodes from the FEM. Note, the contour step was set at 20°F.

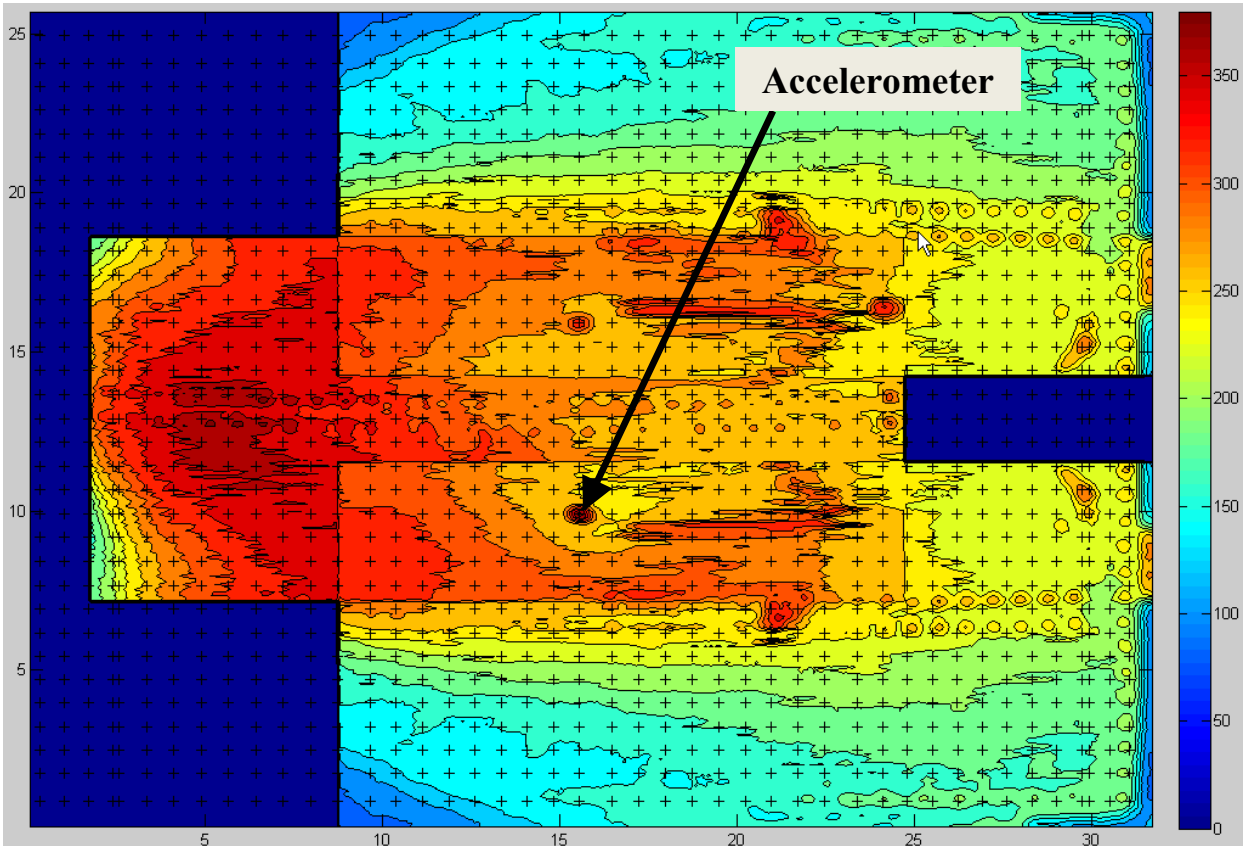

Figure 171 – Initial superposition of IR images

The data represented by Figure 171 assumed an emissivity equal to 1.0. This data needed to be scaled in order to reflect a more accurate emissivity of the panel. In order to do this, the thermocouple data was used to scale the temperatures in the IR image. TC12 was used as the reference thermocouple, boxed red in Figure 172.

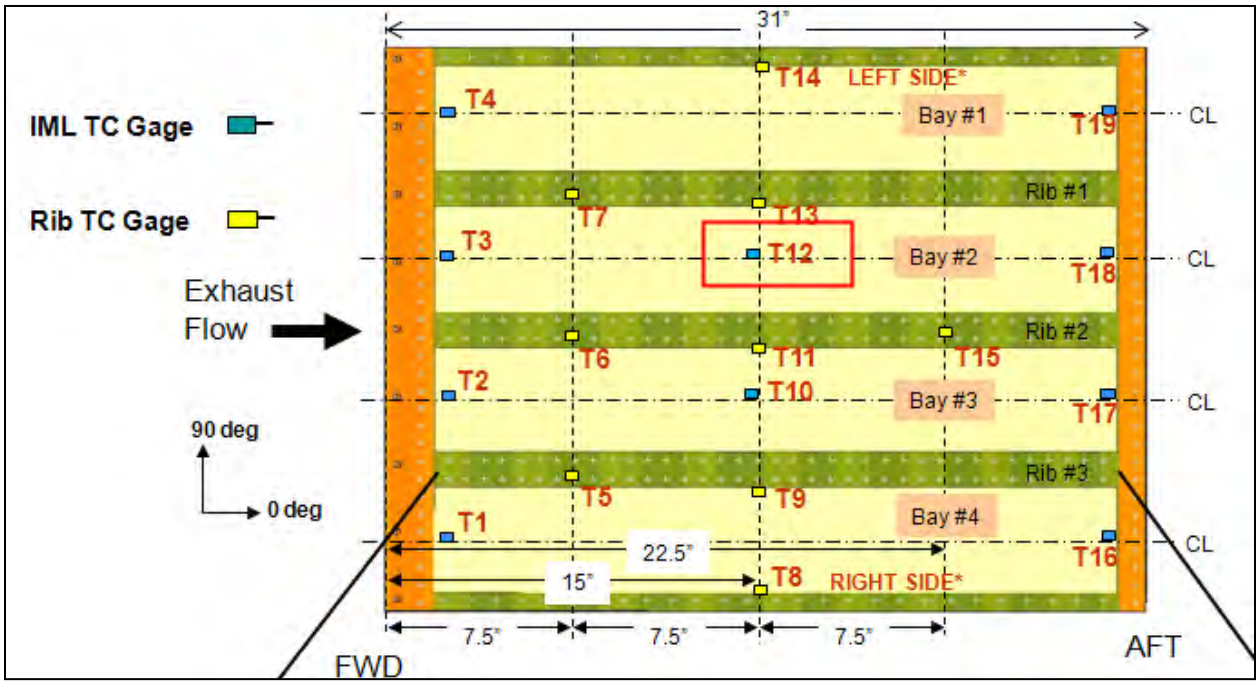

Figure 172 – Thermocouple locations

At 85% engine speed, the data for TC12 was averaged for run B0614. A factor between this average and the raw IR data for image B0614 was calculated to be 1.36. This factor was applied to the raw data for IR image B0614 in Matlab. Another factor at the common accelerometer location for the images B0614 and B0615 was then calculated to be 1.15. The TC12-B0614 factor was then multiplied by the B0614-B0615 factor and then applied to the B0615 raw IR data in Matlab. The Matlab code was re-run, producing the "Best Fit" updated temperature mapping in Figure 173, below. As can be seen, the discrete boundaries of the overlay have disappeared, producing smoother contours. In Figure 173, it was noticed that the camera produced some skewing in the images. In order to straighten these out so that the FEM nodes would line up properly and not inherit higher than expected temperatures, the fasteners had to be "pulled out" so that they would line up correctly with respect to the FEM, Figure 174.

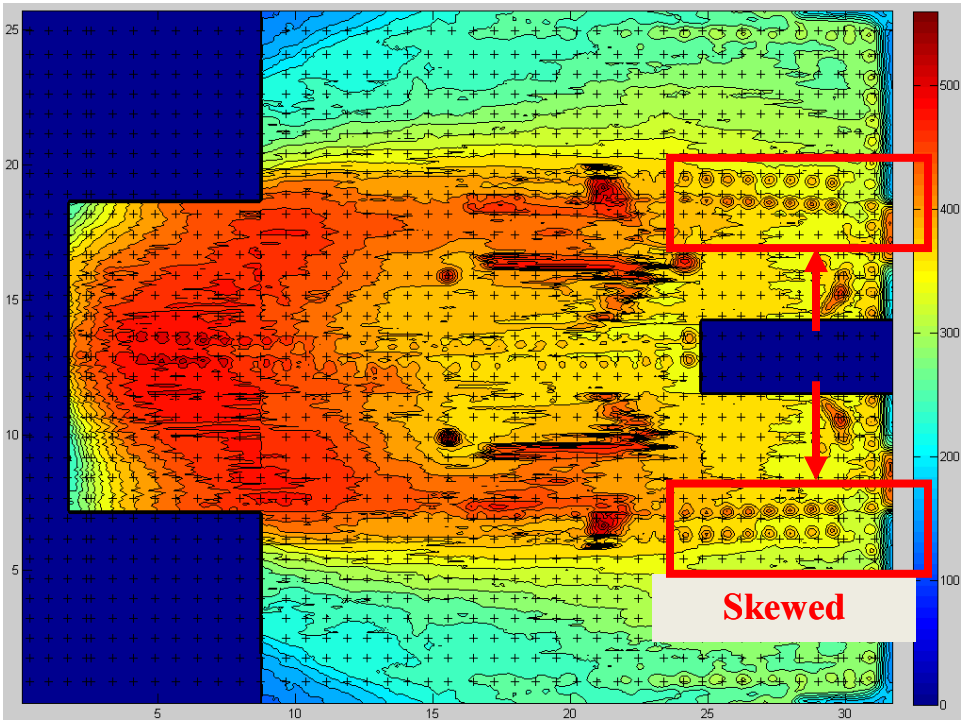

Figure 173 – Averaging scheme between B0614 and B0615 IR images; skewed areas marked

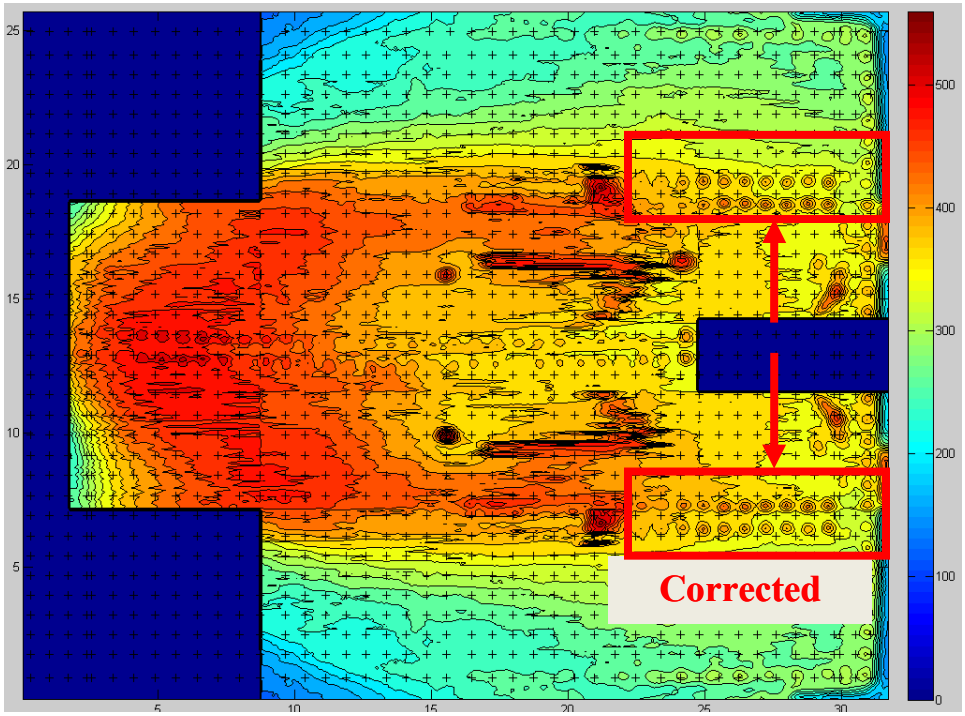

Figure 174 – Corrected fastener areas and shift of the images

The next step was to come up with a scheme to fill in the empty areas of the panel (blue areas). Matlab has a function called "TriScatteredInterp", which creates an interpolant that fits the test data. Once the interpolant was created based on the current non-zero data, it was applied to the areas where the temperature value equaled zero. Due to the triangular nature of the algorithm, it produced the results shown in Figure 175, where the white areas are "NaN". This meant that additional points needed to have prescribed temperatures assigned to them so that the algorithm

can fill in all the gaps. Also, after applying this technique, additional points in the zero-value locations were assigned temperatures so that the interpolant could apply a smoother transition between temperature zones. This was especially necessary at the back of the panel where there was an interruption in the back row of fasteners, producing incorrect interpolated values. Figure 176 is the final temperature map after these corrections were made.

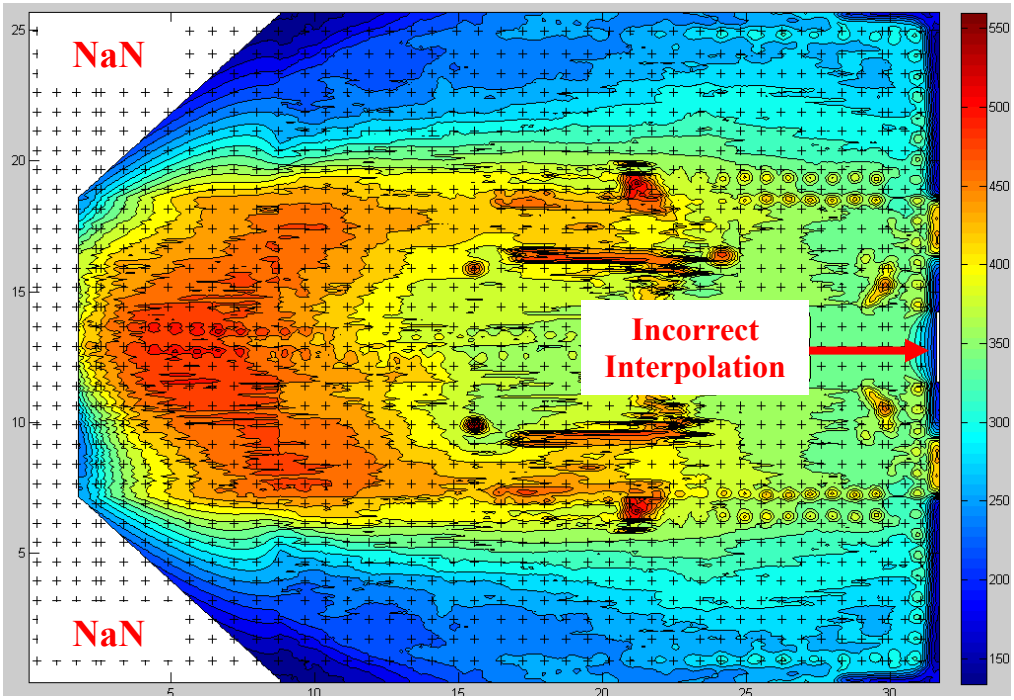

Figure 175 – First interpolation iteration

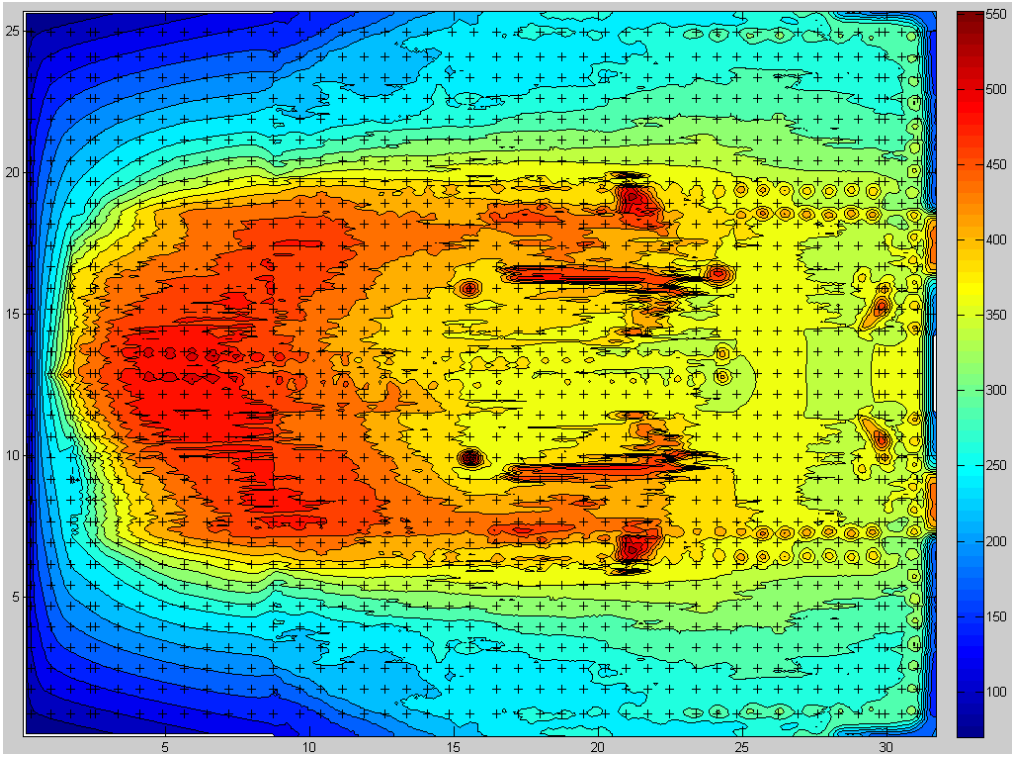
Figure 176 – Final temperature map

Now that the temperature mapping produced acceptable initial results, an Abaqus Python script had to be produced so that the nodal temperatures could be assigned as boundary conditions in the Abaqus model. Once completed, the Python script was run, creating 1452 individual boundary conditions, one for each IML skin node. A heat transfer analysis was set up, producing results shown below in Figure 177. A comparison of the thermocouple data and the corresponding skin nodes is shown in Figure 178 and Figure 179.

The emissivity and ambient temperatures for the different areas of the model were taken from a CEAC test panel model correlation. These are summarized in Table 17. These values were taken as parameters in the model correlation to produce better heat transfer results and correlation with the thermocouples.

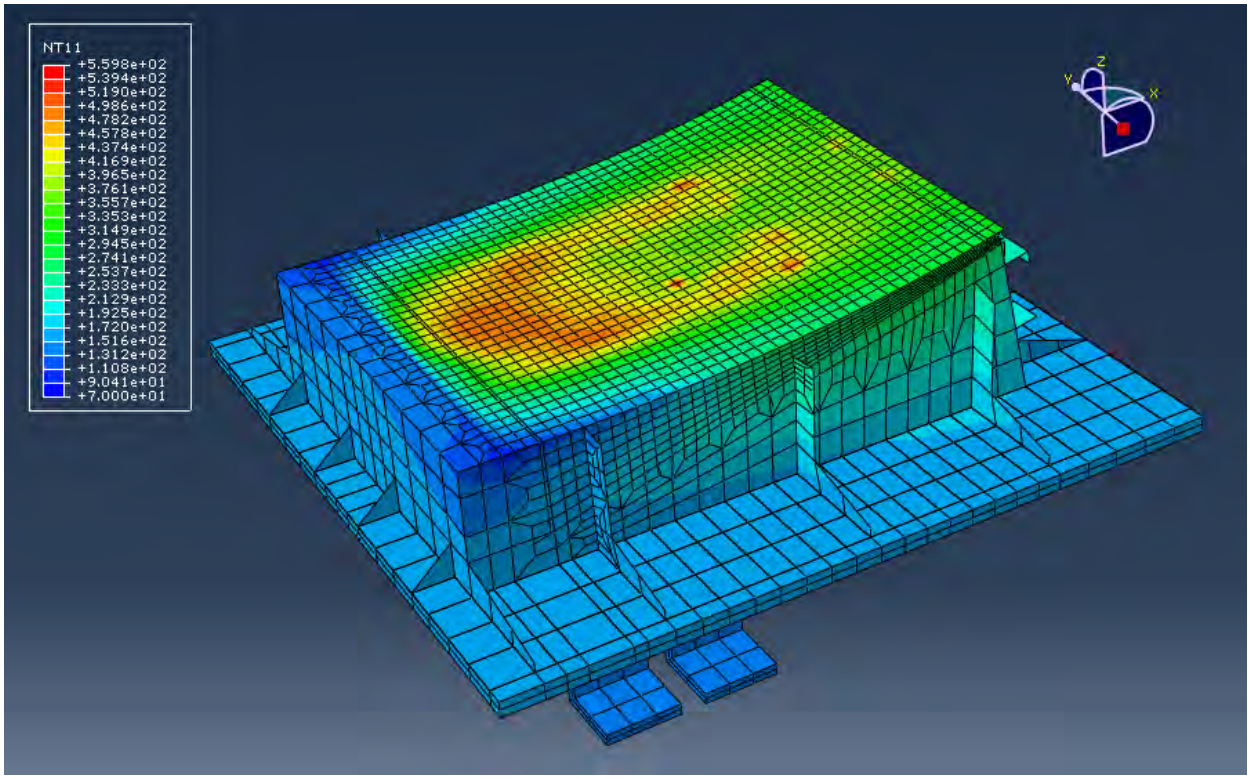

Figure 177 – Heat transfer results in Abaqus

TC	Test	FEM	Node	% Diff
T1	96	211	523	119%
T2	394	413	483	5%
T3	397	352	443	-11%
T4	86	214	403	150%
T5	376	434	990	15%
T6	342	459	984	34%
T7	312	437	978	40%
T8	132	254	1093	92%
T9	352	412	1077	17%
T10	463	486	144	5%
T11	303	376	1053	24%
T12	546	560	104	3%
T13	359	414	1029	15%
T14	132	256	1013	94%
T15	206	357	1170	74%
T16	373	293	698	-21%
T17	449	390	677	-13%
T18	444	391	632	-12%
T19	380	293	563	-23%

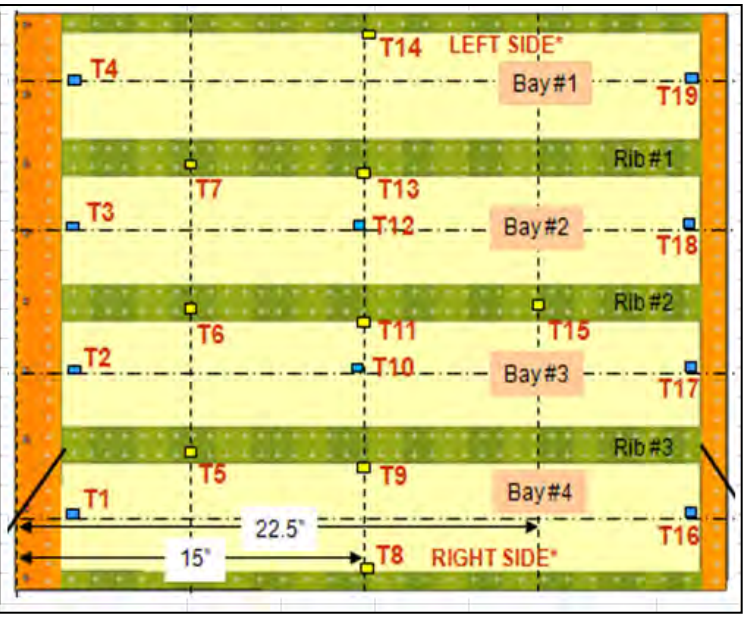

Figure 178 – T-58 test thermocouple instrumentation layout

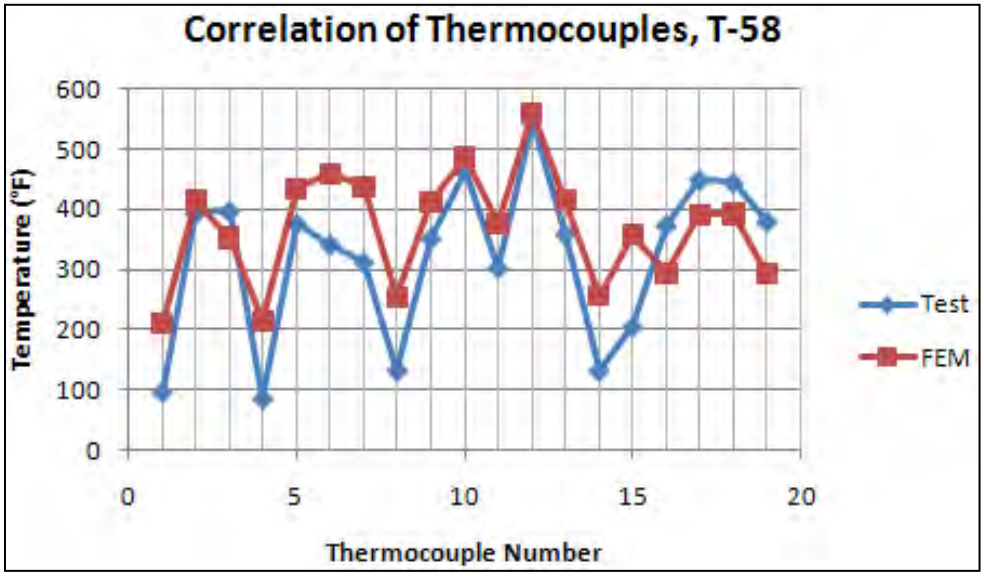

Figure 179 – T-58 thermocouple correlation

Table 17 – Emissivity and temperature data used from the CEAC thermal correlation

Component	Ambient Temp (°F)	Emissivity
Backing Structure	100	0.45
Fixture, bottom	200	0.85
Fixture, sides	200	0.85
Test Article Substructure	300	0.85

9.0 Results – Post-Test Structural Response Analysis

The post-test structural response analysis was a comparison between the final correlated and updated model with test response measurements. Two test data sets were used. The first was the CEAC room temperature acoustic tests at max levels. The second was the CEAC high temperature acoustic test at max levels. For each comparison study, all model inputs and assumptions are described. The objective was to determine any discrepancies between analysis and test to determine the accuracy of the NLROM methods as applied to thermal-acoustic response applications.

9.1 Comparison to Room Temperature Acoustic Response Results

The first comparison study was at room temperature using the CEAC Test Run #4 data set. This data set used a flat input spectrum from 50Hz to 500Hz. For all of the room temperature tests, the acoustic pressure was measured with an array of 12 Flat Pak surface transducers. The measured time histories from these transducers were used directly in the analysis simulations.

The model was setup with 12 pressure load zones (load cases) as shown in Figure 180. The center of these 12 zones aligned with the 12 Flat Pak acoustic sensors. The acoustic loads were taken from Test Run #4 at 0 dB Test Point #1.

The PSD for the control microphone (Mic #1) is shown in the Figure 181. This microphone was positioned 6 inches upstream from the leading edge of the fixture in front of the test panel along the center line. For this test run, a total of four test points were taken. Each test point was 60 seconds in length, and sampled at 40 kHz. The test points were taken consecutively. Average OASPL was 164.42 dB as measured at the control microphone. The Flat Paks had a coefficient of variation (COV) of 1% to 2% in the overall (OA) RMS pressure for the Flat Paks.

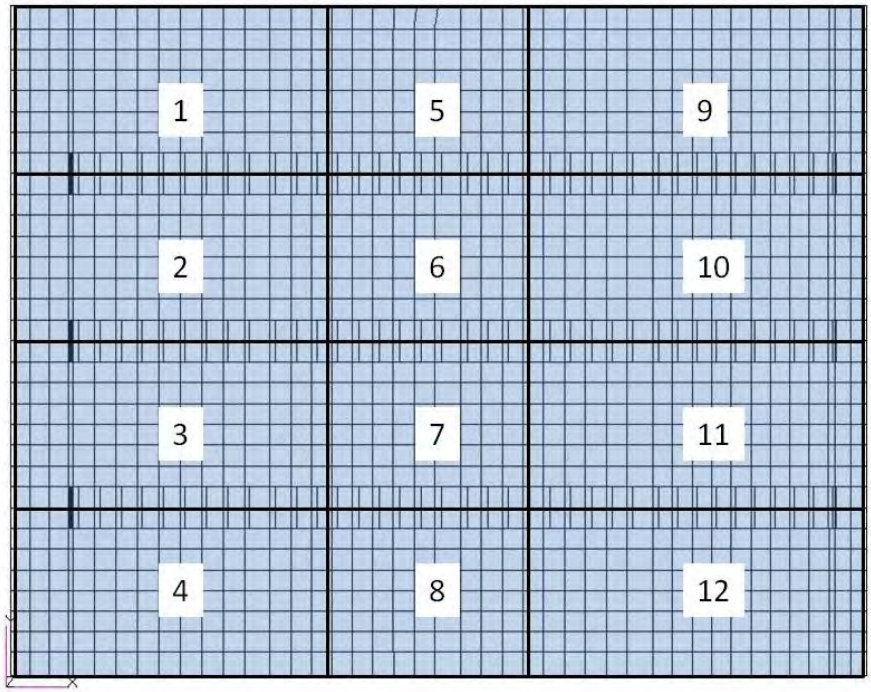

Figure 180 – Pressure zones on upper OML skin

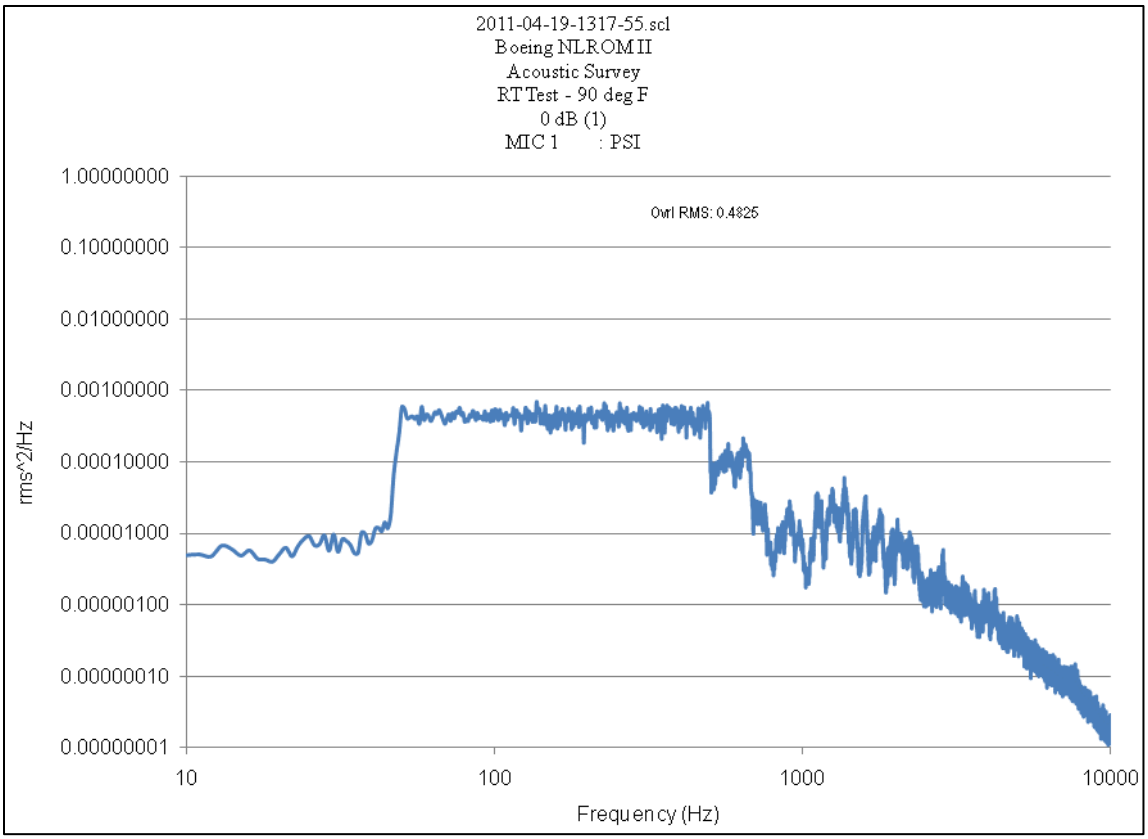

Figure 181 – Control microphone #1 from Test Run #4 Test Point #1

The room temperature nonlinear reduced order model used six modes: 1, 3, 6, 9, 11, and 14. The mode-frequencies were 1-179 Hz, 3-367 Hz, 6-410 Hz, 9-447 Hz, 11-470 Hz, and 14-493 Hz. These modes were chosen based on test data and the modal contribution (i.e., the modal load scale factor). Only six modes were used because it was found that seven or more modes generated very large output databases and the results could not be read into Matlab without causing memory issues. This was a memory limit on an 8 GB quad core PC running Matlab R2011a. Therefore the results below are for a comparison to a six-mode NLROM. Although some higher order modes were tried in the solution, this set of modes seemed to yield the most stable ROM. Selected results are shown below for various measurements. The test data is from Test Run #4. The ambient temperature was approximately 90 ºF during this survey, with the acoustic level at relative OASPL = 0 dB. The ROM used the as-measured modal damping values from the "In Closed Chamber" modal survey, Table 18. The first set of comparisons is for accelerometers A5, A7, A8, and A9 in Figure 182 through Figure 185. Accelerometers A1, A2, A3, A4, and A6 were non-functioning during this test run and are not shown in the table. The location of these transducers is shown in Figure 186. For A5, the OA-RMS was 158 g-rms compared to 166 g-rms, for analysis and test, respectively. The percent difference for the other accelerometers is below in Table 19. The analysis was generally matching the magnitudes of the peaks in the spectrums, but there was some modal content that was not being captured in the NLROM simulation due to the lack of modes in the solution. Still this was a fairly good comparison. The modes in the simulation matched the test and magnitudes of the frequency response compared well. The modes used in the ROM also seemed to capture the critical strain (or stress) response fairly well, as shown in Figure 187, with a difference of 8% in OA-RMS 20-600 Hz.

Table 18 – Measured modal frequency and modal damping factor

Modal Test Summary	Out Of Chamber		In Chamber no Lamps		In Chamber with Lamps	
Mode Number	Frequency	Damping	Frequency	Damping	Frequency	Damping
1	172	1.7	173	1.91	173	1.7
2	363	0.76	362	0.704	363	0.76
3	390	2.39	391	2.7	391	2.17
4	415	0.612	415	0.43	415	0.604
5	448	1.22	447	3.44	449	1.87
6	460	1.73	468	1.42	468	1.8
7	496	1.63	491	1.87	496	1.63

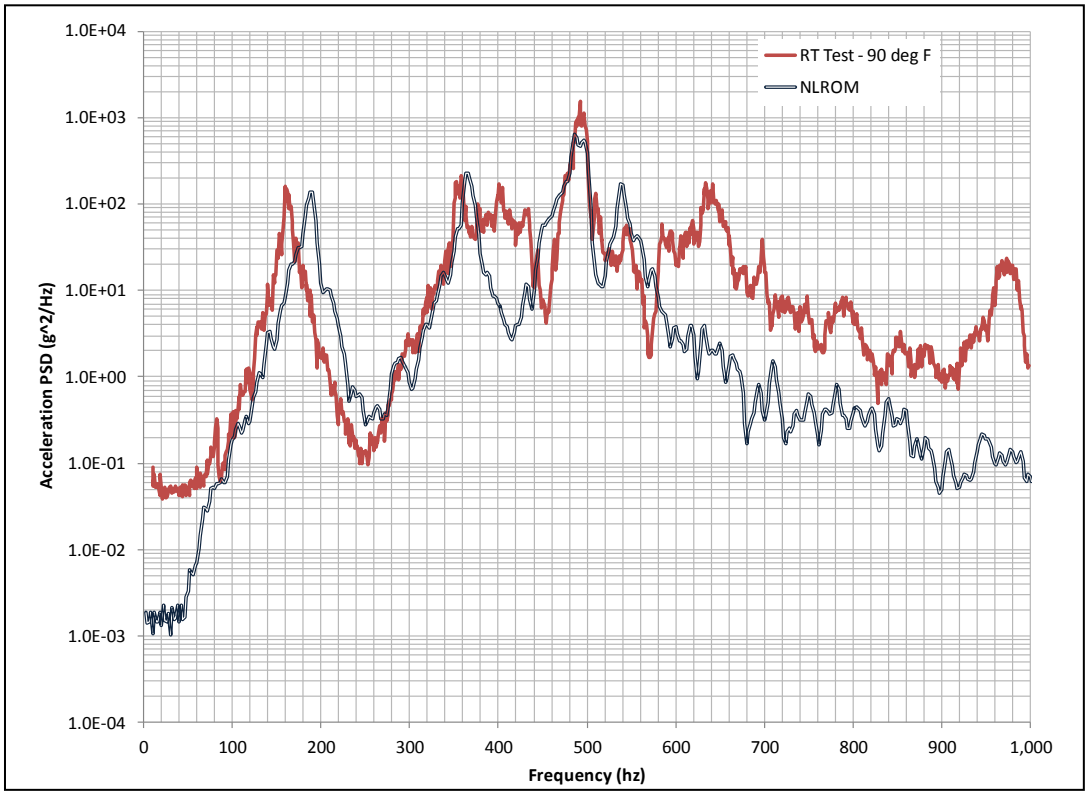

Figure 182 – Accelerometer A5 test and analysis comparison

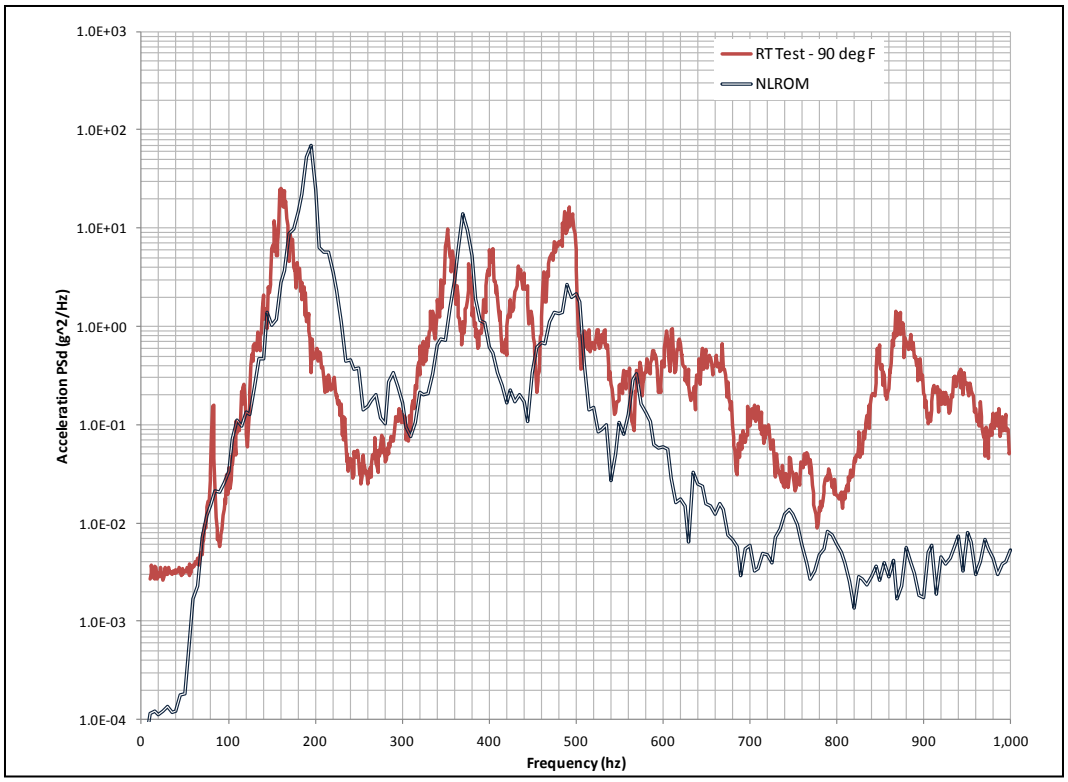

Figure 183 – Accelerometer A7 test and analysis comparison

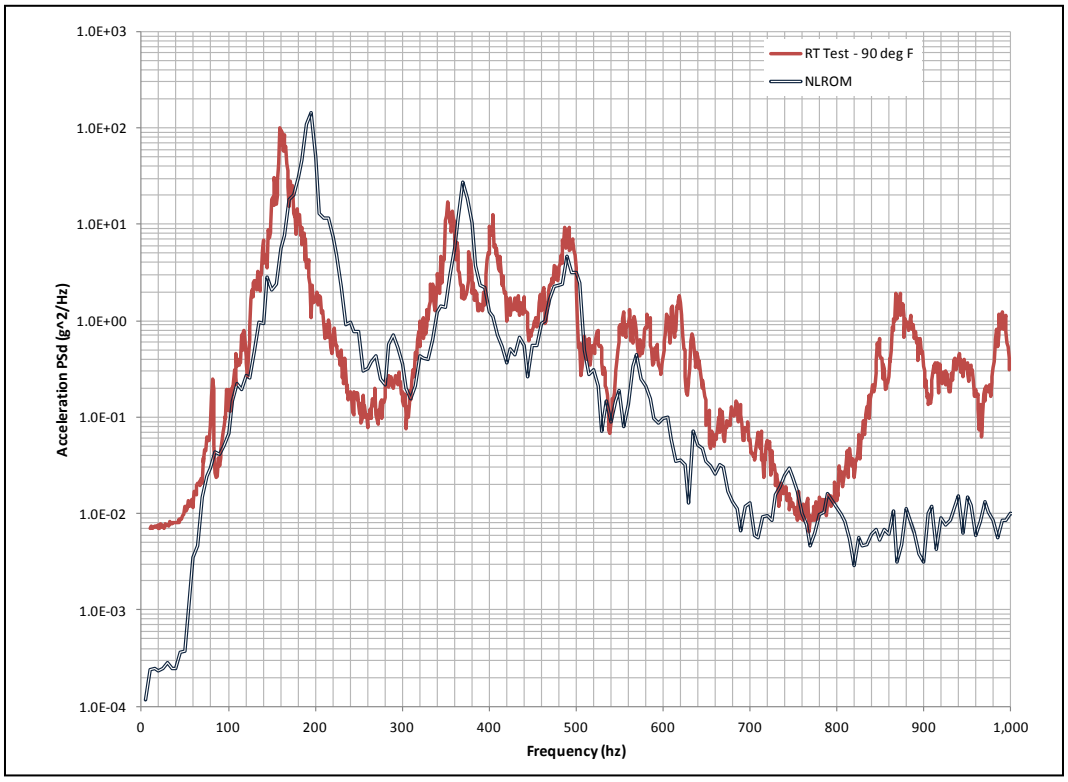

Figure 184 – Accelerometer A8 test and analysis comparison

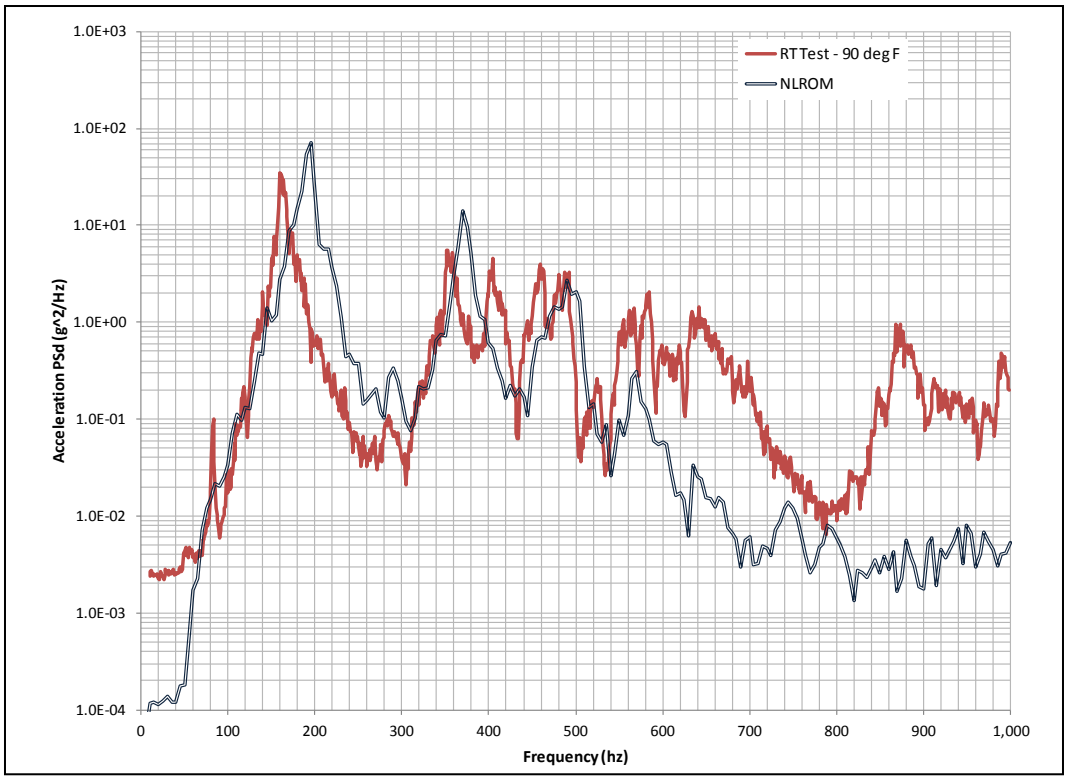

Figure 185 – Accelerometer A9 test and analysis comparison

Table 19 – Accelerometer analysis and test comparison summary

Accelerometer ID	Test OA-RMS	Analysis – NLROM OA-RMS	Percent Difference %
A5	166	158	4
A7	37	25	32
A8	44	36	19
A9	26	25	6

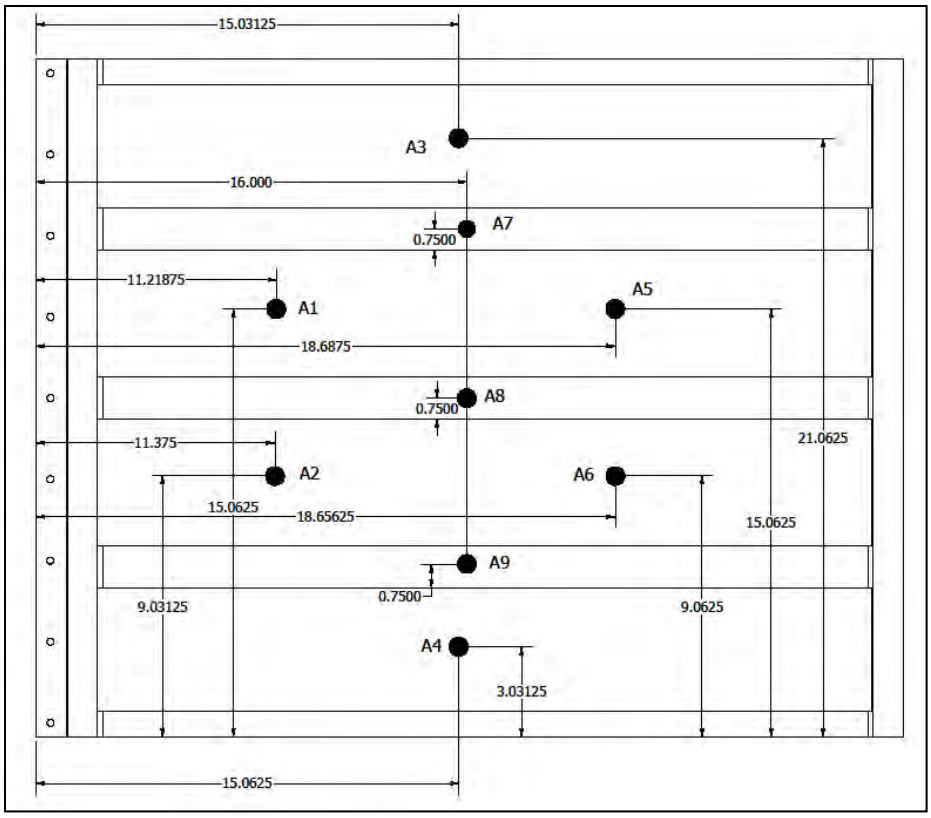

Figure 186 – CEAC test accelerometer locations

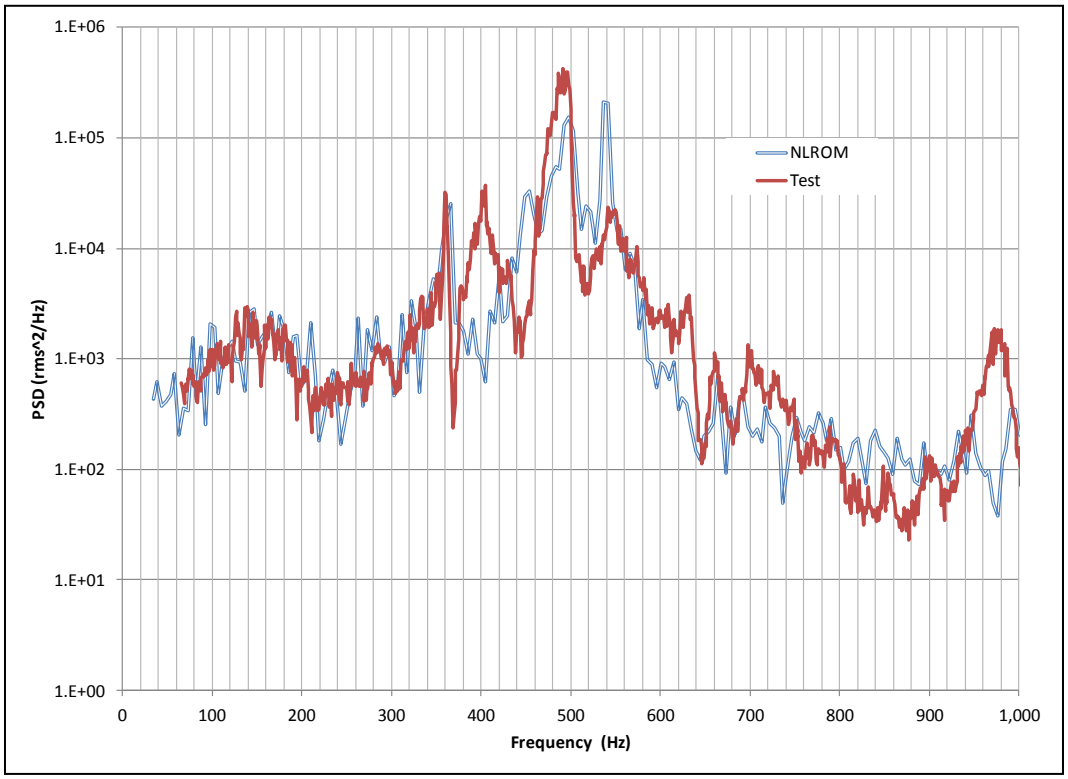

Figure 187 – Strain gauge SG 1 test and analysis comparison

9.2 Comparison to Elevated Temperature Results

The prime objective of this study was to evaluate the NLROM method for high temperature thermal-acoustic analysis of a representative aircraft test article. Therefore, testing was performed at 500 ºF and at OASPL = 167 dB (re OASPL = +3dB) with the objective to measure loads and response of the test article and compare the response to the NLROM simulation. In the previous section, 9.1, the comparison was made under acoustic load only at OASPL = 164 dB (re OASPL = 0 dB). In general, this comparison was fairly good and demonstrates that the NLROM methodology can be applied with confidence to yield engineering answers suitable for design purposes of complex assemblies such as this representative flap test article. The following takes the validation of the method one step further with the application of relatively high temperatures (at 500 ºF). These acoustic and temperature loads are representative of a near-field exhaust impinged thermal-acoustic application.

The first step in the analysis was to setup the thermal pre-load condition, which was treated as a static pre-load. The details of the thermal loading were described in Section 8.1, with an indirect measurement taken during the CEAC test. An extensive array of thermocouples was used in conjunction with an IR camera to capture thermal data for correlation of a heat transfer analysis using the finite element model of the test article. A steady state thermal response was calculated, and used as the thermal pre-load for the acoustic analysis.

As a first step, these temperatures were mapped to the FEM as a temperature boundary condition and NASTRAN SOL 400 (nonlinear static) was performed. The nonlinear thermal static Z-displacement is shown in Figure 188, with a peak displacement of 0.039 inches, which compared well with the ARAMIS measurement of 0.040 inches. Figure 189 and Figure 190 show the in-plane displacements which also compared well to test measurements. This model is the same one that has been used throughout the modeling effort, and includes temperature dependent material properties.

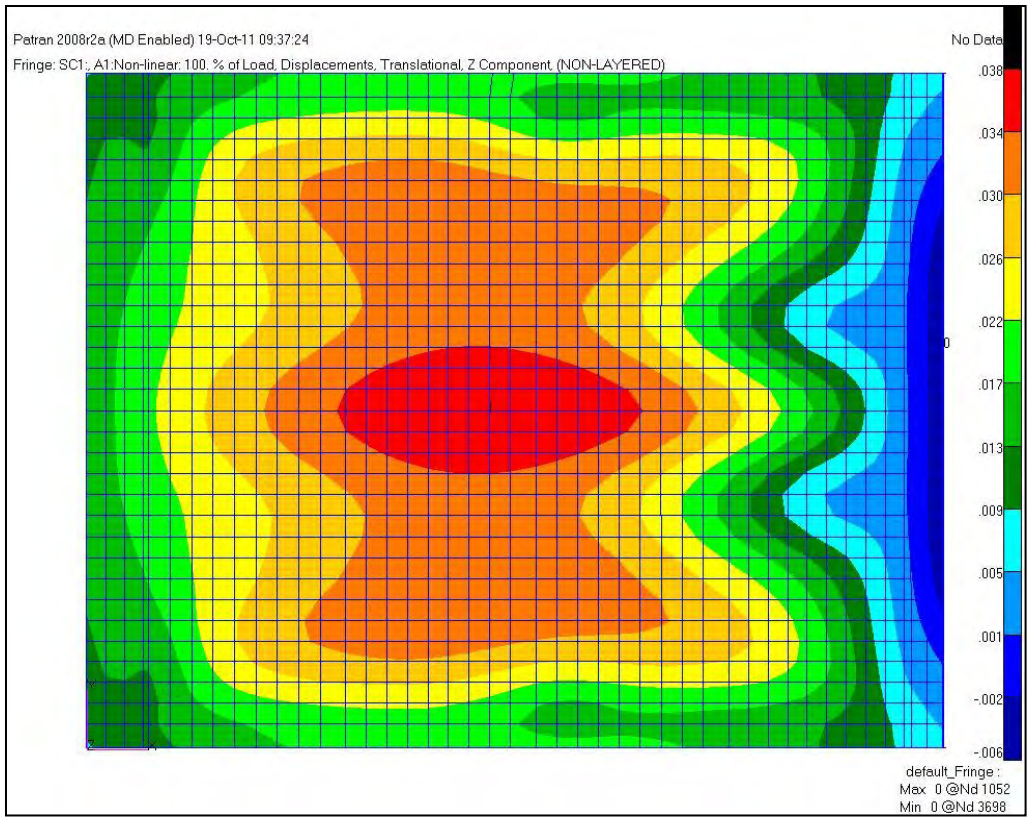

Figure 188 – Static thermal displacement Uz

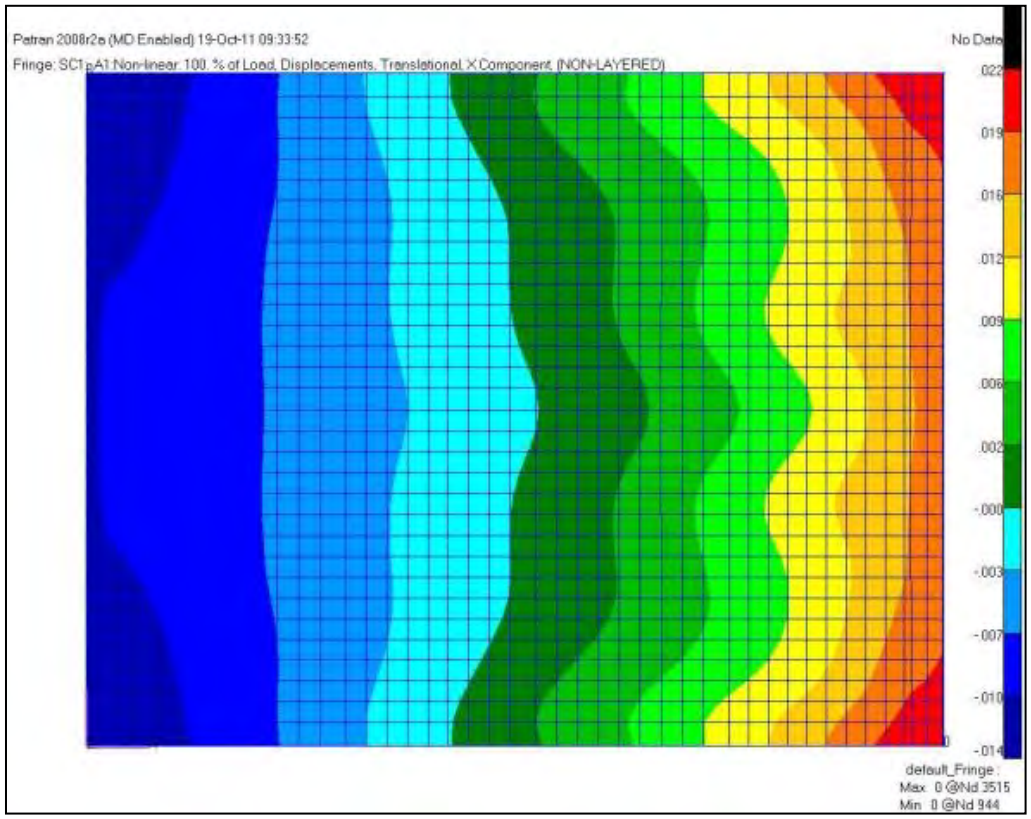

Figure 189 – Static thermal response in-plane displacement Ux

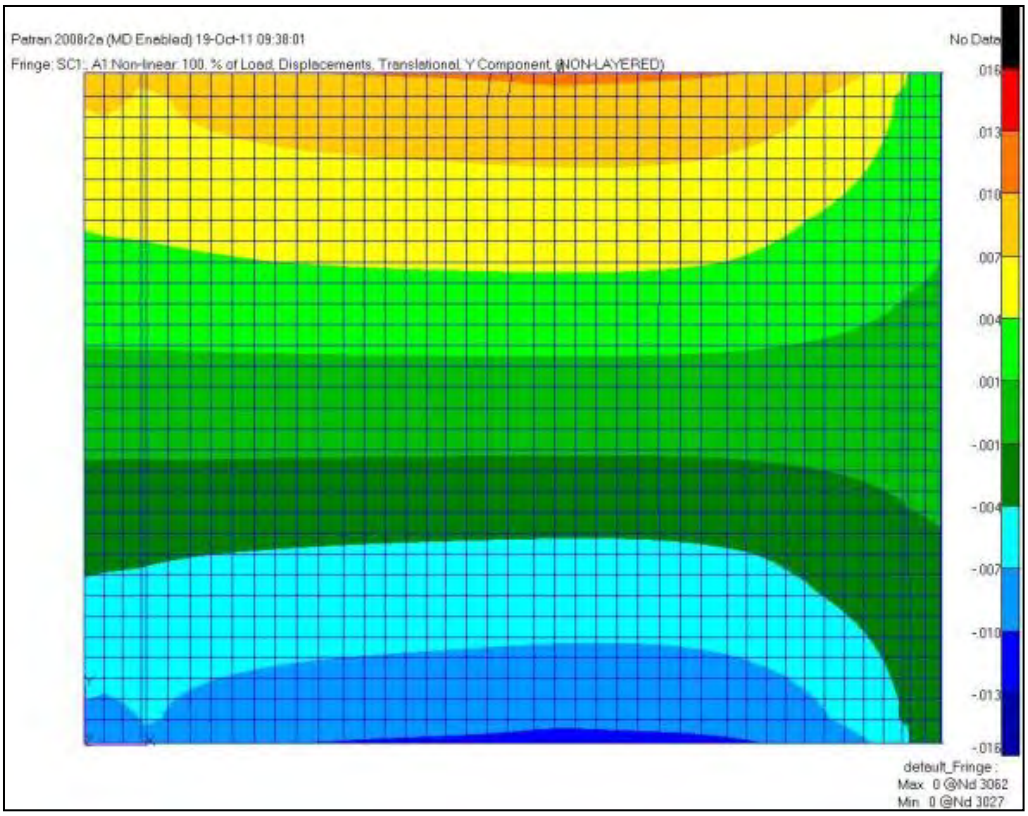

Figure 190 – Static thermal response in-plane displacement Uy

The second step was to perform a normal modes analysis and determine the adjusted modal basis, taking the thermal pre-load into account. Figure 191 through Figure 196 show the six mode shapes of interest, which were used to develop the nonlinear reduced order model.

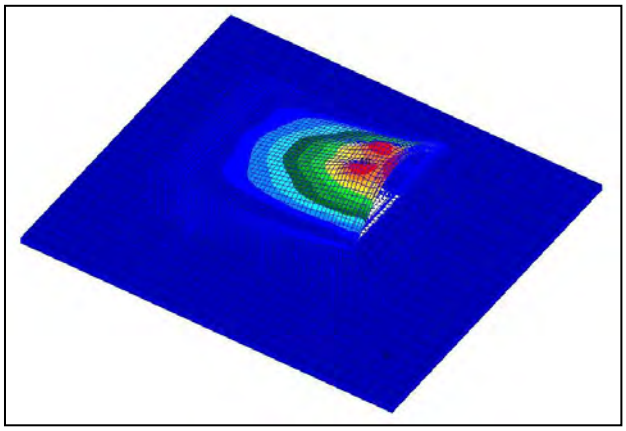
Figure 191 – Mode 1 = 176 Hz, 500 ºF

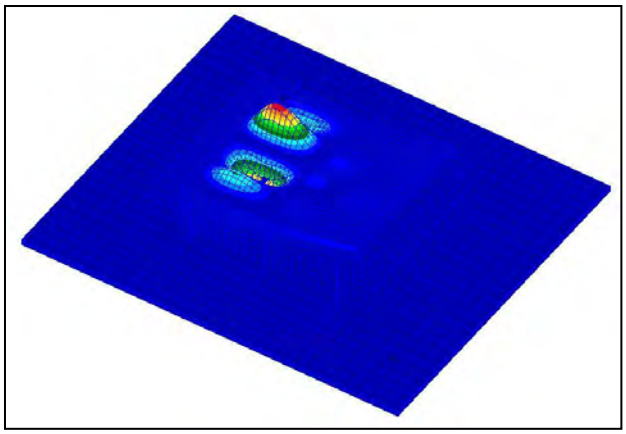

Figure 192 – Mode 2 = 347 Hz, 500 ºF

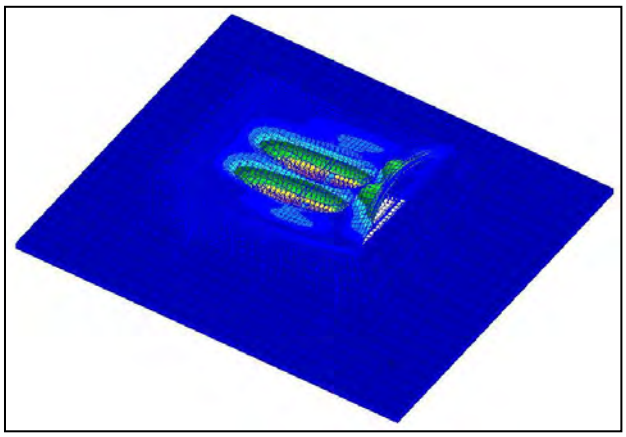

Figure 193 – Mode 3 = 358 Hz, 500 ºF

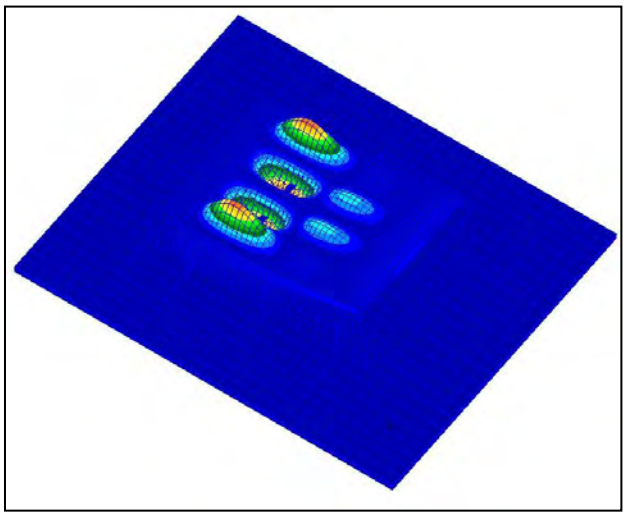

Figure 194 – Mode 8 = 398 Hz, 500 ºF

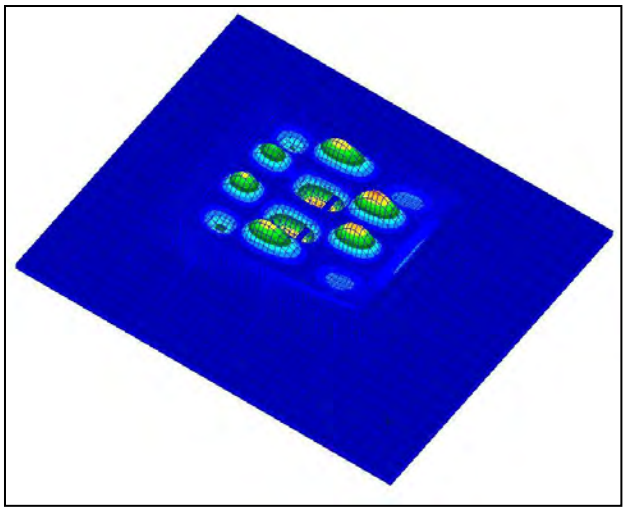

Figure 195 – Mode 11 = 426 Hz, 500 ºF

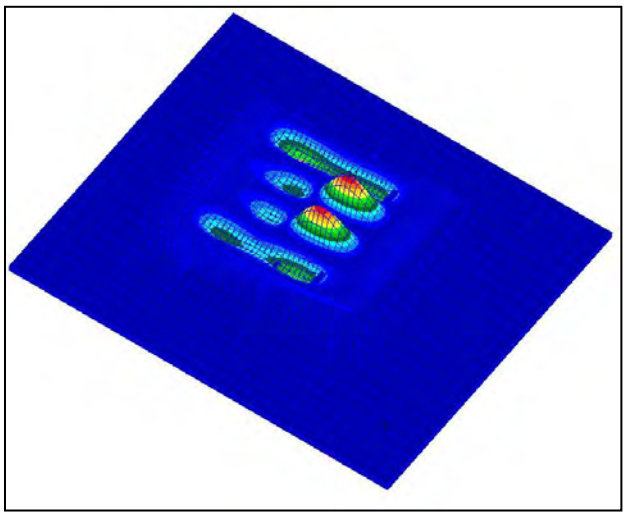

Figure 196 – Mode 13 = 452 Hz, 500 ºF

A comparison could then be made using nodes in the model corresponding to the sensor locations in the test. Test #13 was used to compare with the finite element model results, with the first comparison being made with the accelerometer data. Accelerometers A2, A4, A5, A6, A7, and A8 were the only ones active during this test run. Below are the PSDs for test compared to analysis in Figure 197 through Figure 202. The PSD units are in G^2/Hz. The red curves are the test data and the black curves are the analysis, and it should be noted that the analysis model did not include any modes greater than 500Hz. The modes that compared the closest to the test data were the modes that had the highest response.

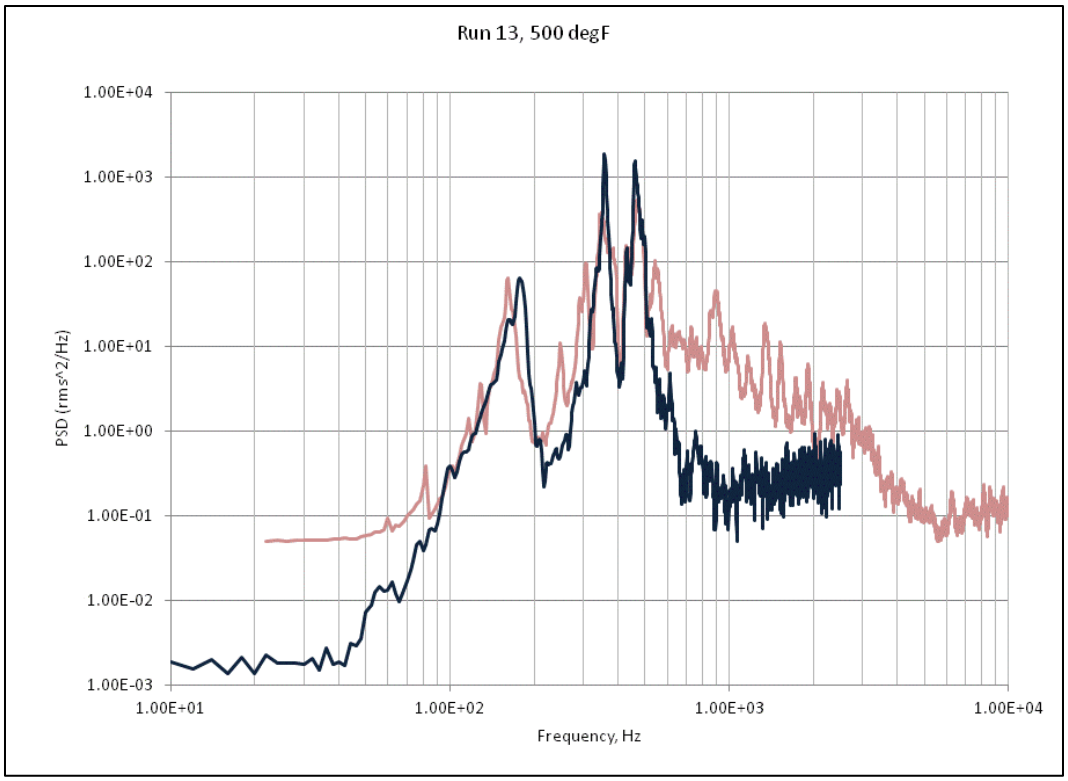

Figure 197 – Accelerometer A2, bay #3, center left

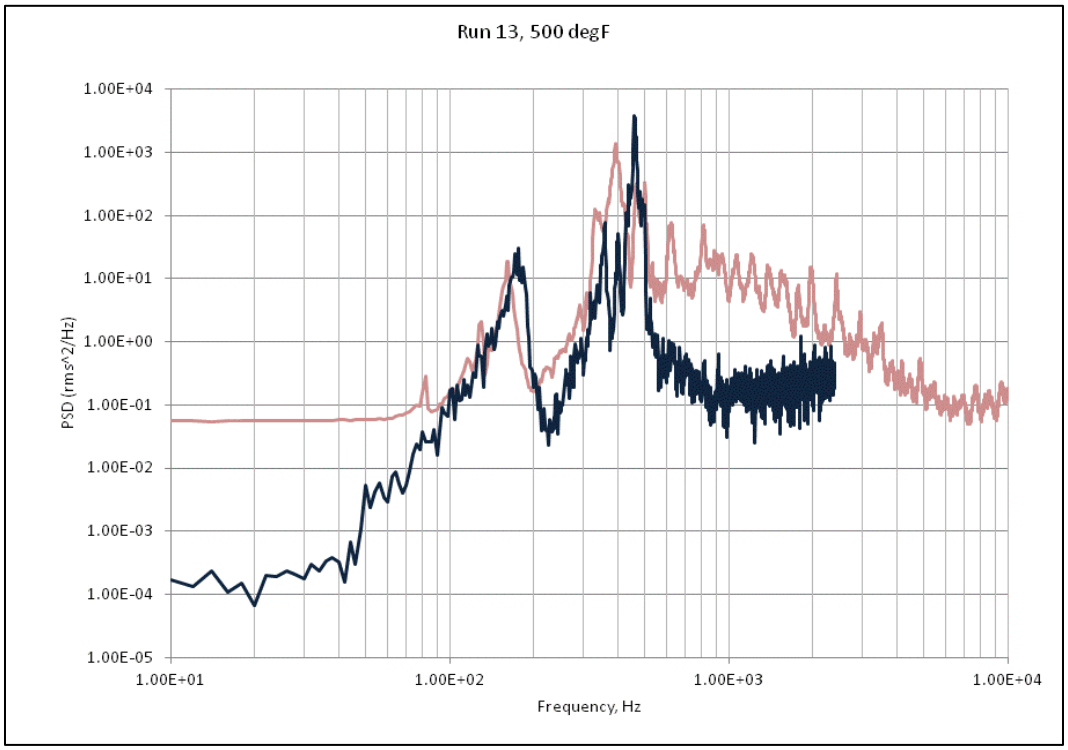

Figure 198 – Accelerometer A4, bay #4, mid center

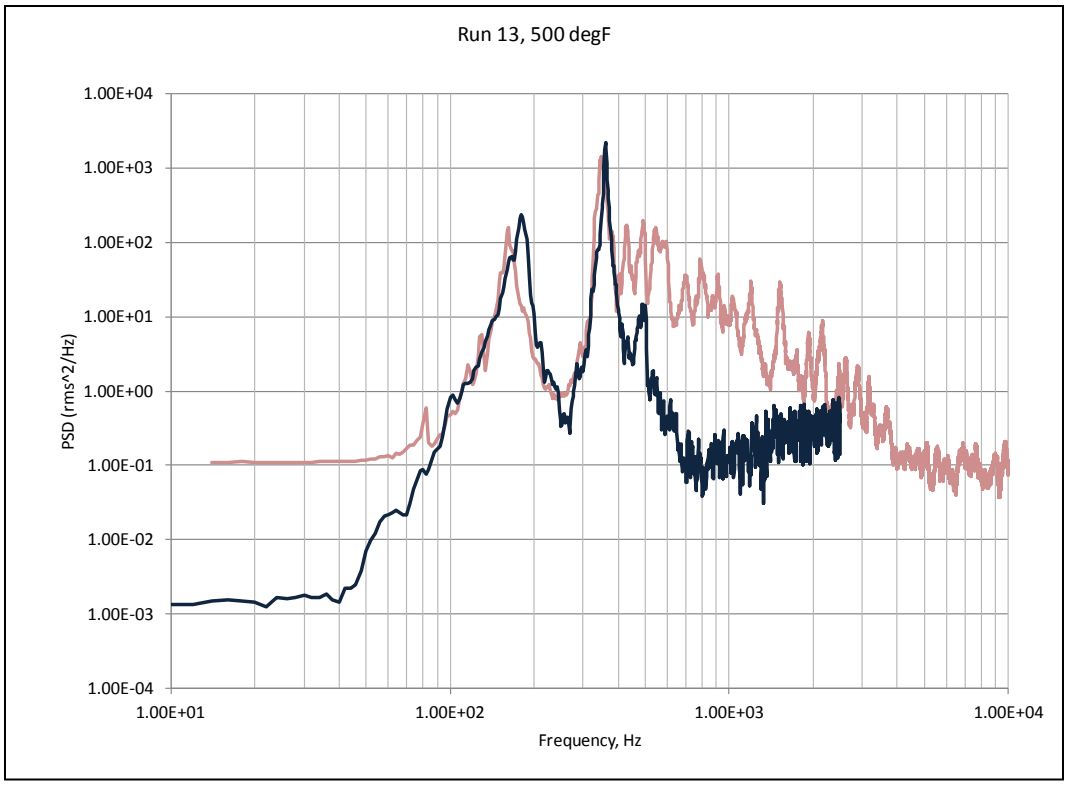

Figure 199 – Accelerometer A5, bay #2, mid right

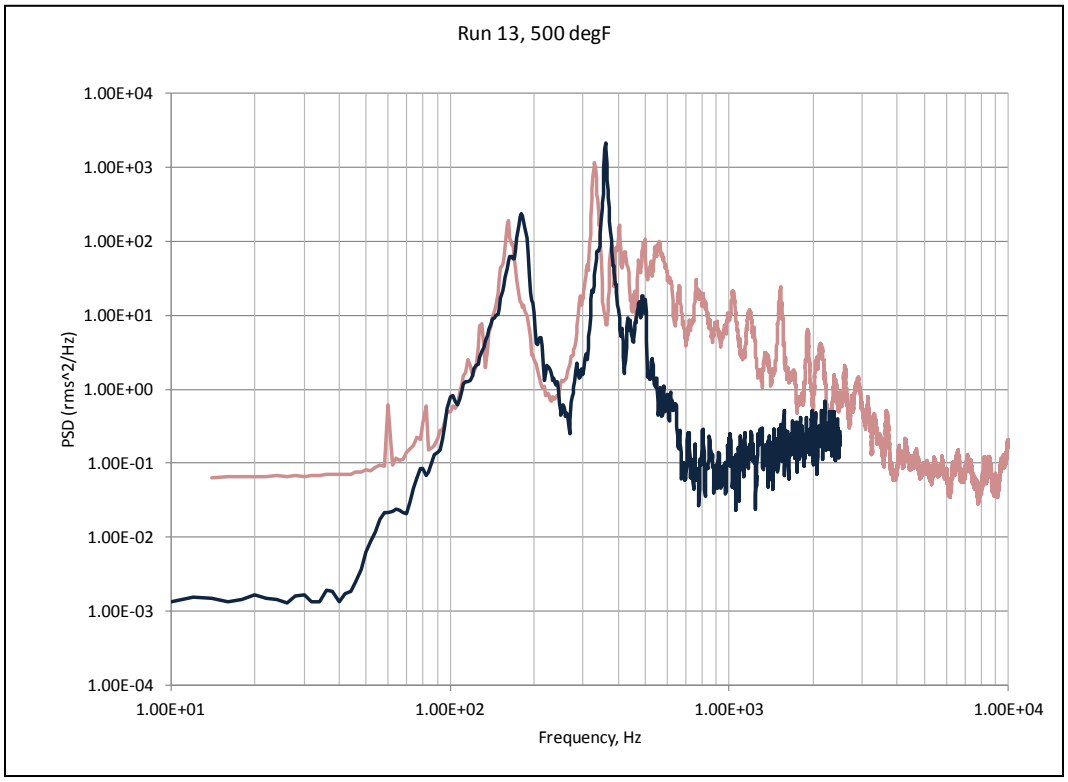

Figure 200 – Accelerometer A6, bay #4, mid right

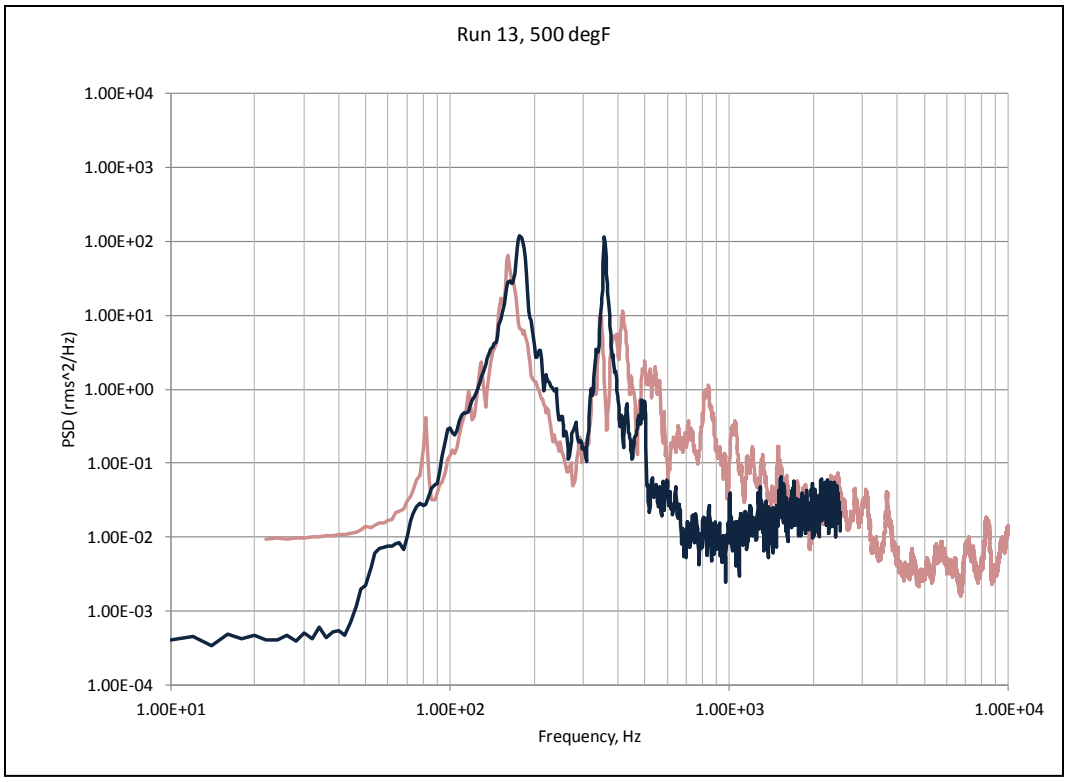

Figure 201 – Accelerometer A7, rib #2, center

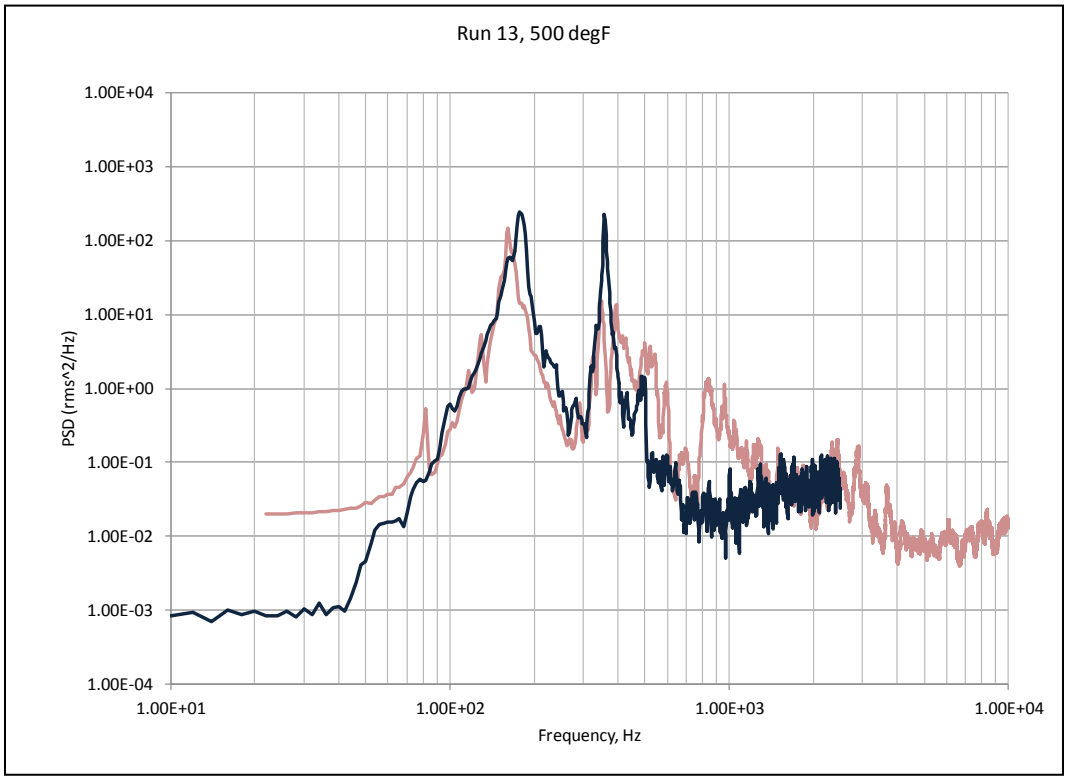

Figure 202 – Accelerometer A8, rib #3, center

RMS values were measured from 10 to 500 Hz in both the test and analysis data to make a proper comparison. The RMS values are summarized in Table 20. Acceleration is a good indicator of response correlation.

Table 20 – Test #13, 500 ºF, RMS summary 10-500Hz, test and analysis

Accel	A2	A4	A5	A6	A7	A8
NLROM	227	205	417	344	60	85
Run 1	206	224	238	190	41	55
Run 2	214	239	247	188	42	56
% Diff	7%	-13%	42%	45%	31%	35%

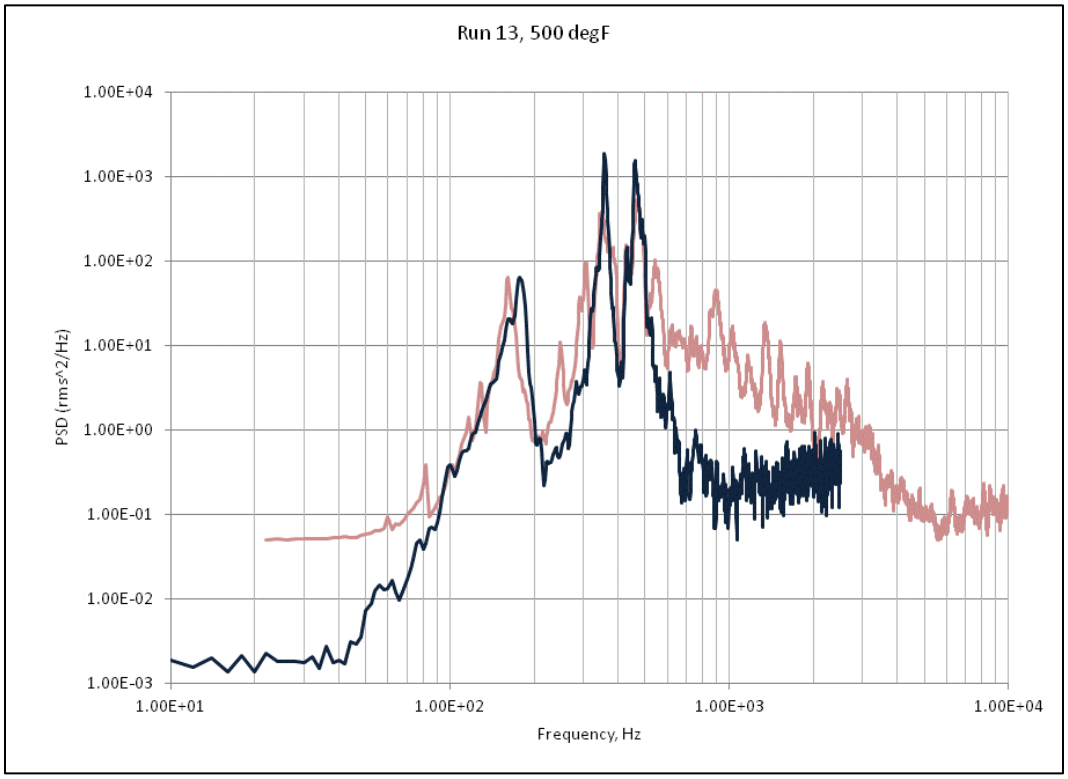

Figure 203 – Accelerometer A2, bay #3, center left

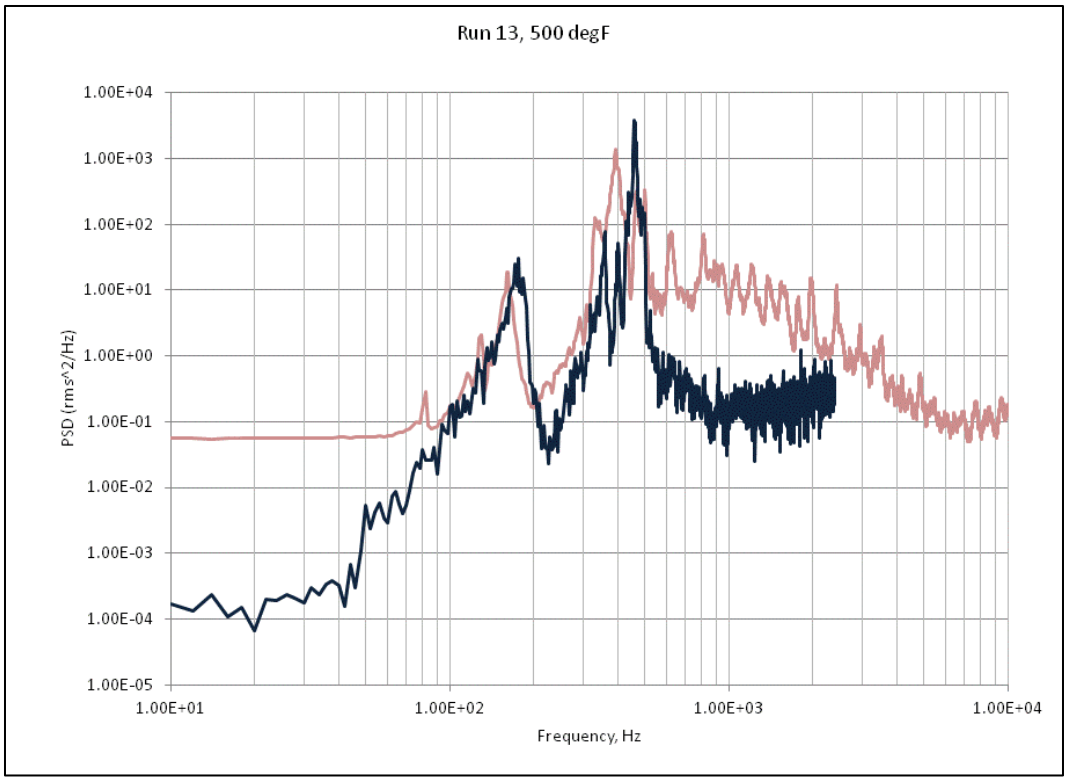

Figure 204 – Accelerometer A4, bay #4, mid center

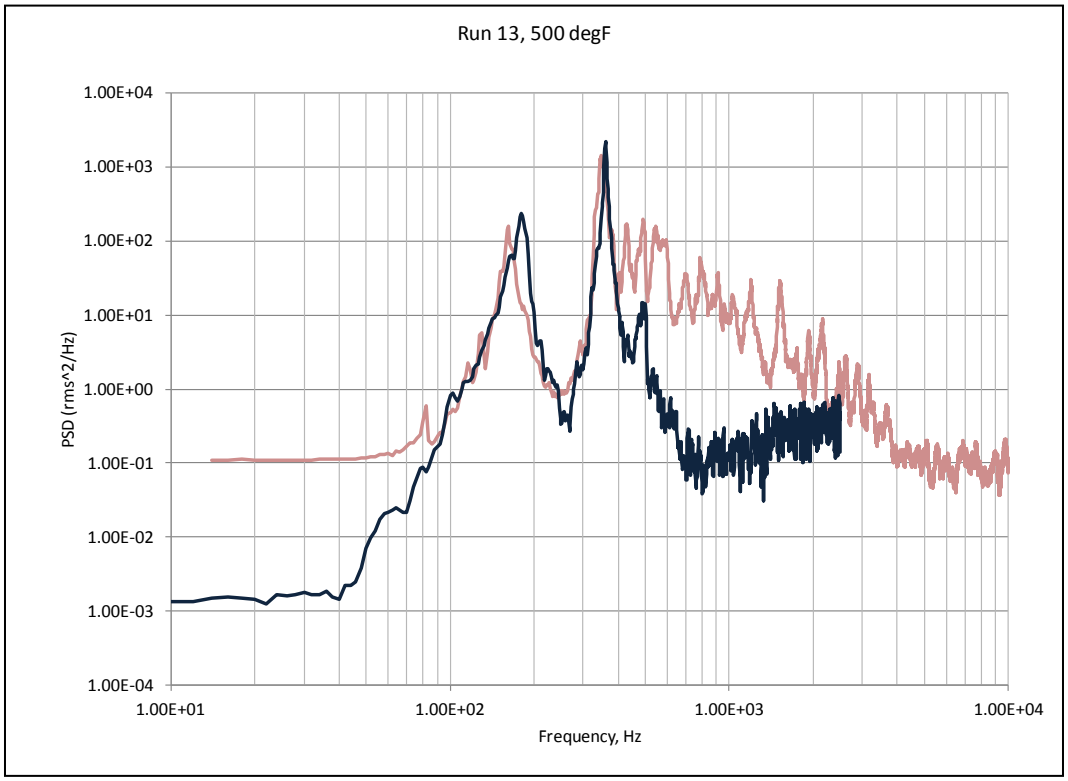

Figure 205 – Accelerometer A5, bay #2, mid right

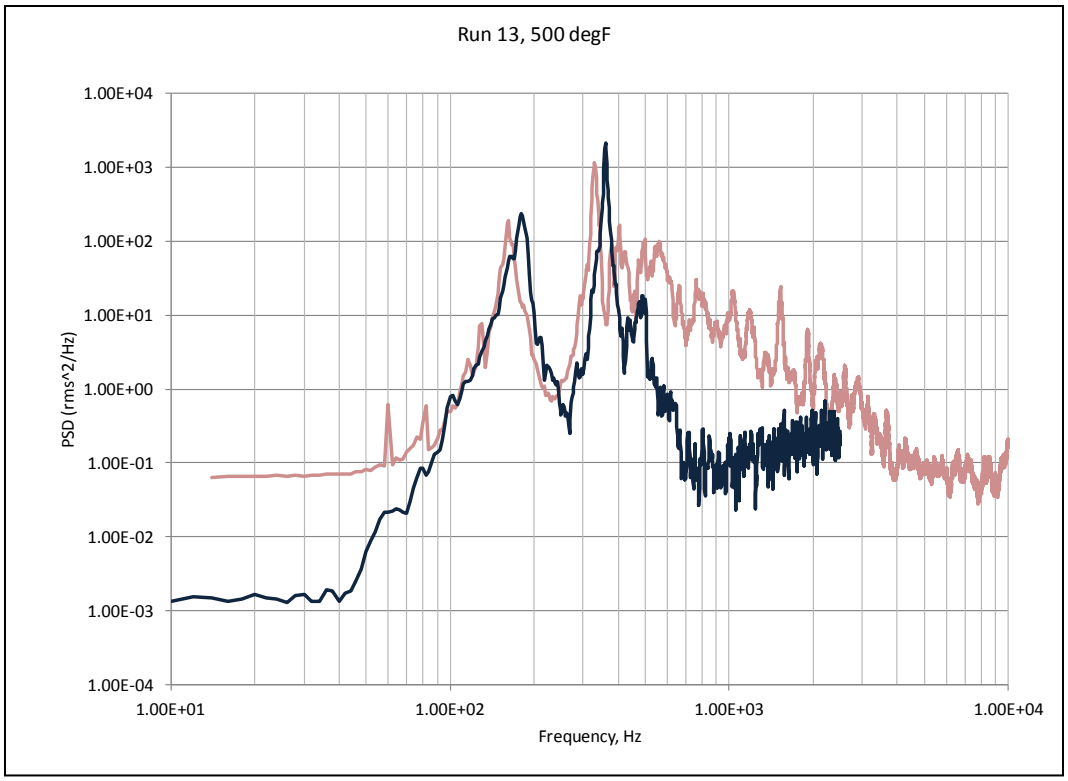

Figure 206 – Accelerometer A6, bay #4, mid right

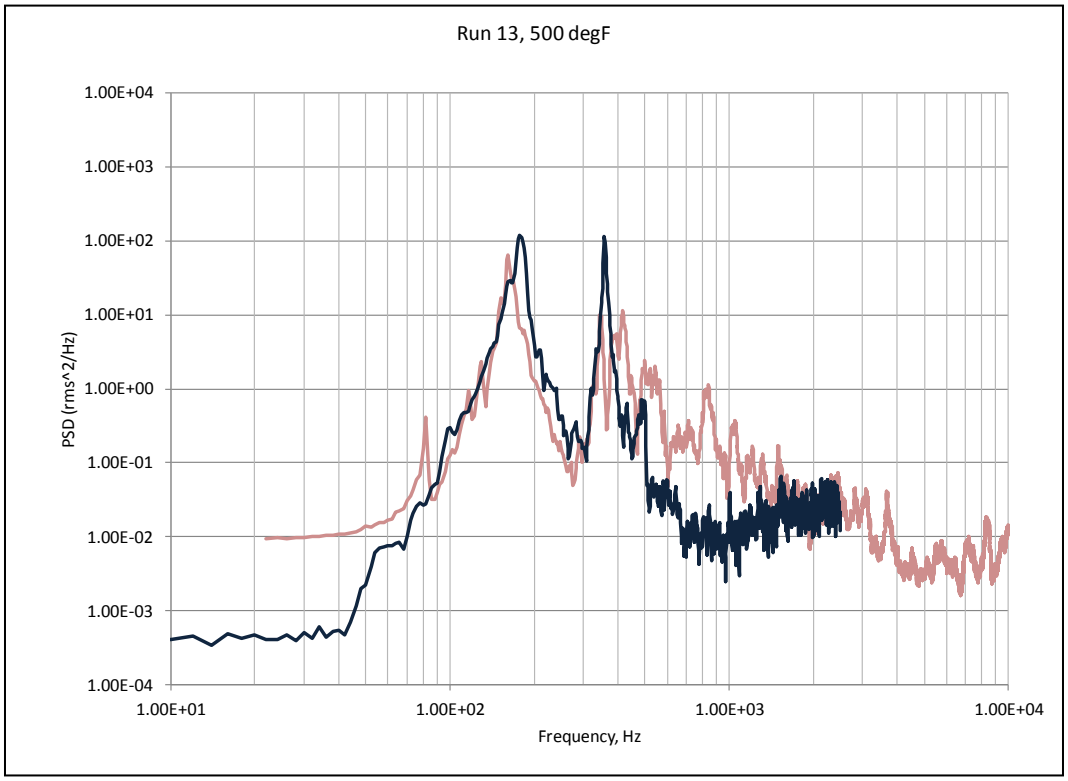

Figure 207 – Accelerometer A7, rib #2, center

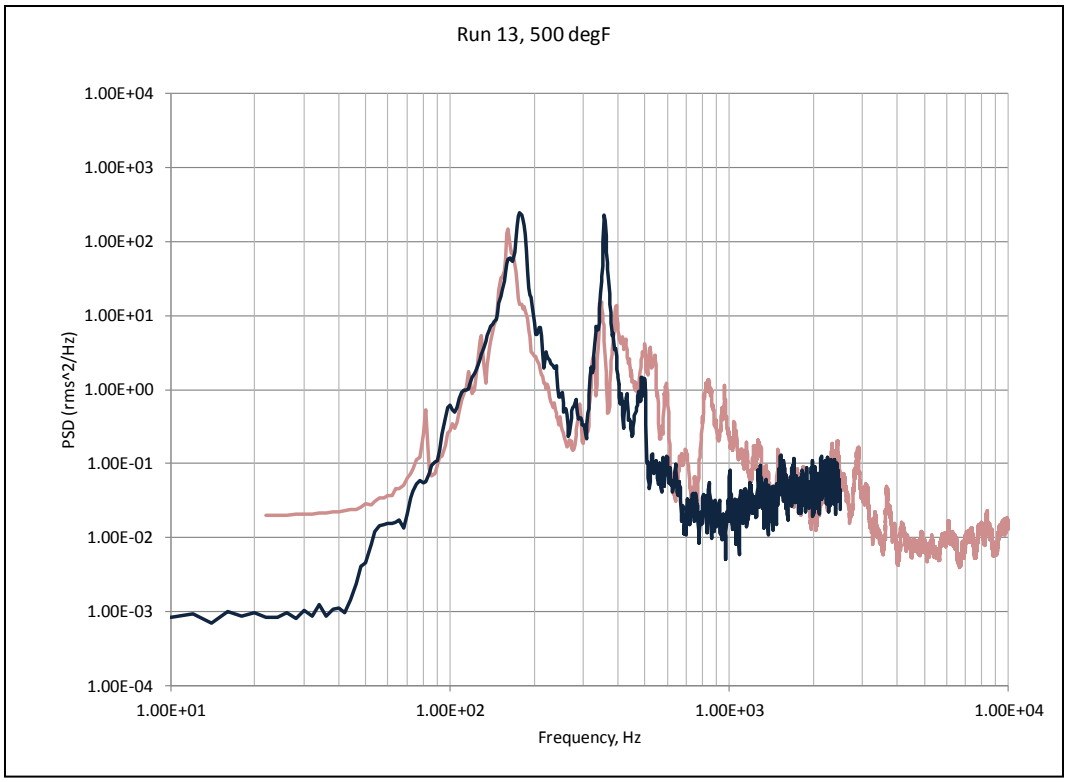

Figure 208 – Accelerometer A8, rib #3, center

The next set of data to compare with analysis was the IML skin strain gauge measurements. None of the OML strain gauges (SG27-SG30) were functioning during test run #13, and several of the IML gauges were also non-functioning or suspect (SG2, SG4, SG5, SG6, SG10, SG13, SG14, SG15, SG17, SG24). For reference, Figure 210 through Figure 213. The frequency content and magnitude is generally captured well within engineering tolerance for this type of testing. Figure 209 shows the layout of the IML strain gauges for the CEAC test.

At the acoustic level of this test run, OASPL = 164 dB, the skin bay response is slightly nonlinear (RMS < t/2) for skin panels of this width and thickness, Figure 214. The problem becomes much more nonlinear when including the thermal static response.

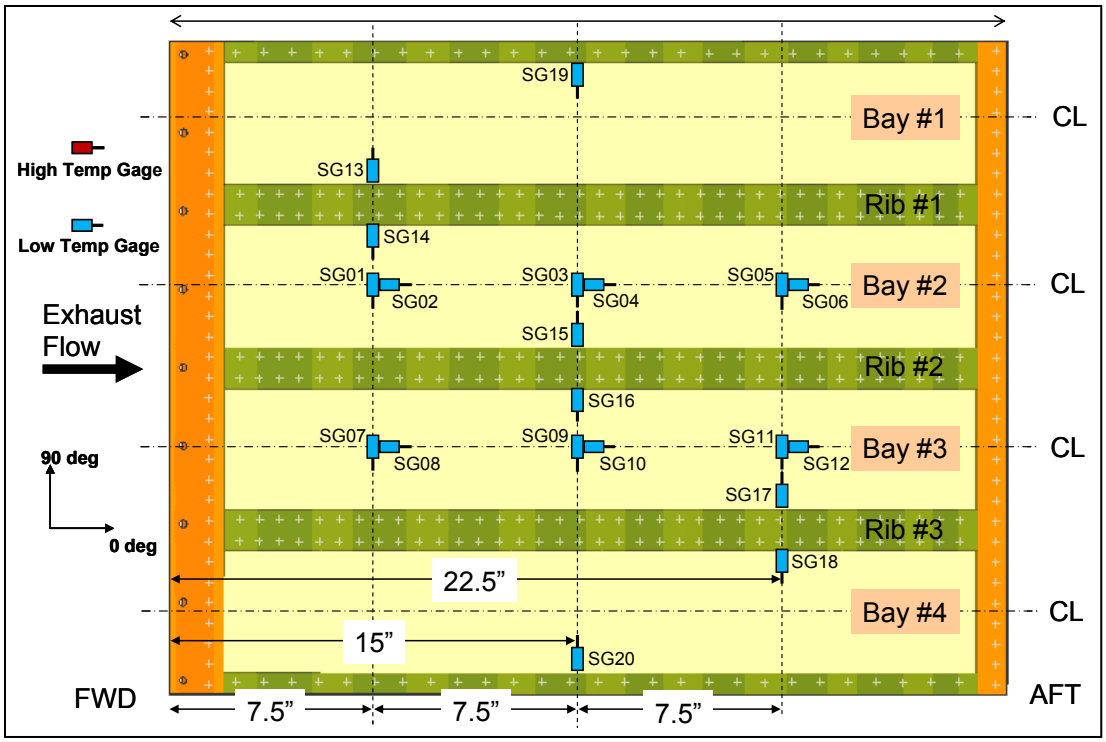

Figure 209 – CEAC IML strain gauge layout

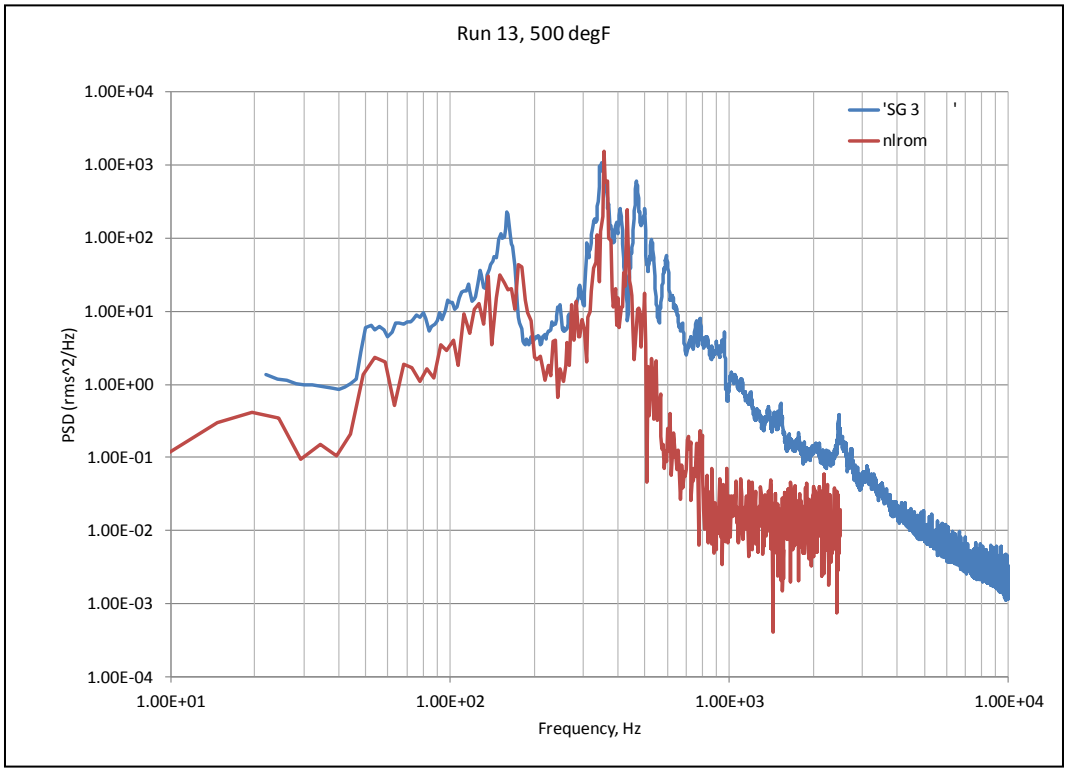

Figure 210 – Strain gauge SG-3

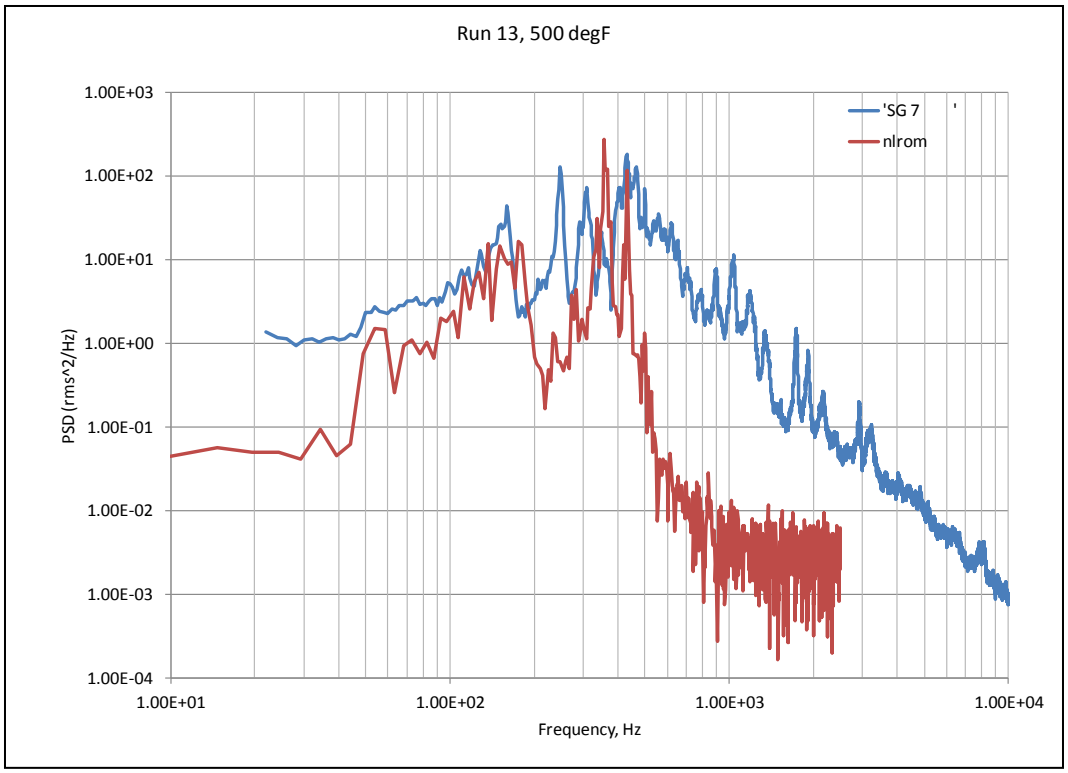

Figure 211 – Strain gauge SG-7

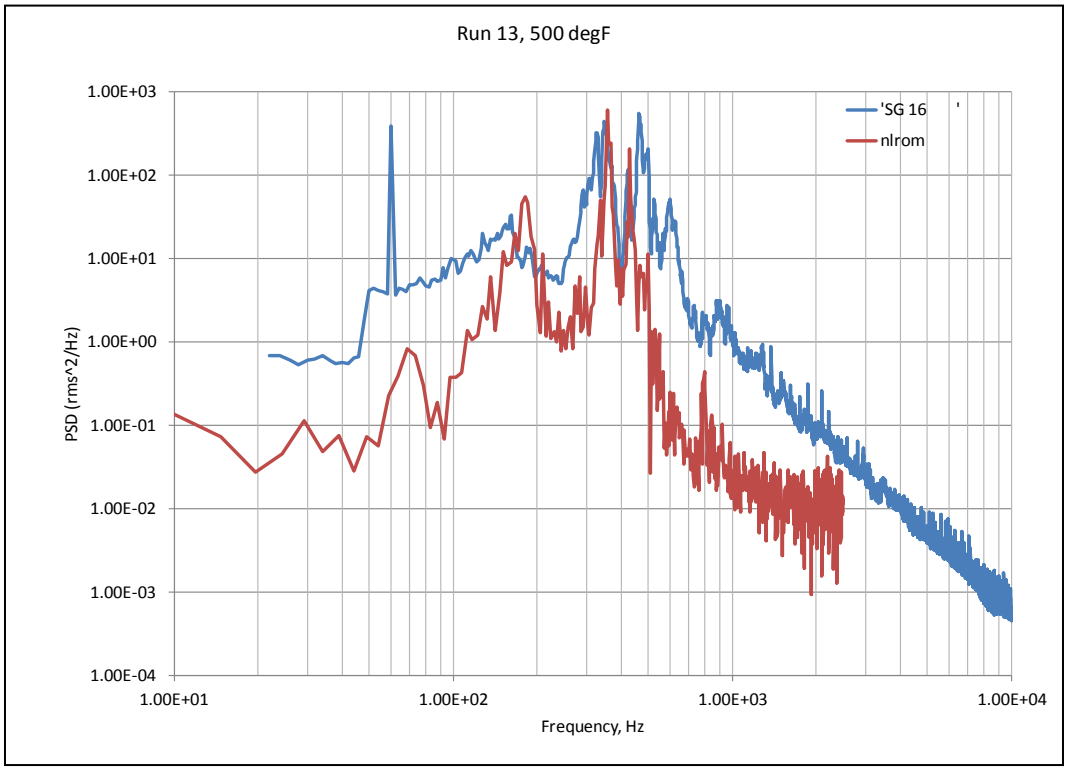

Figure 212 – Strain gauge SG-16

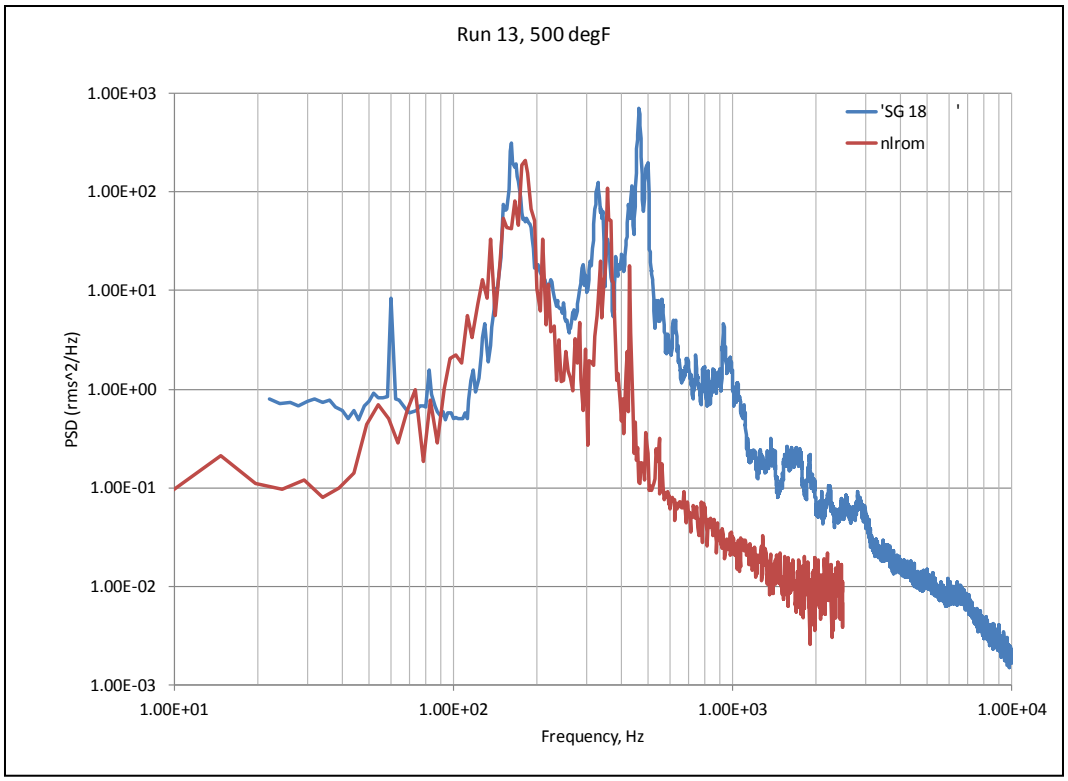

Figure 213 – Strain gauge SG-18

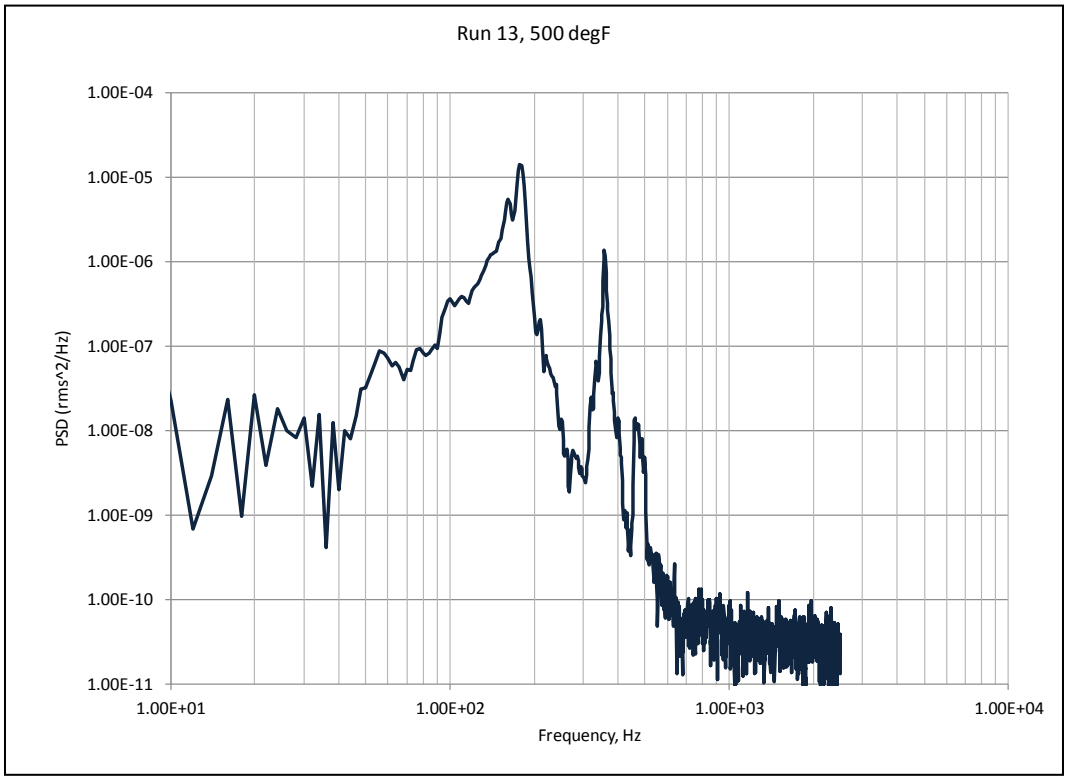

Figure 214 – Node 104 (center panel at center bay z-displacement)

Cracks were observed in the test article fixture during the endurance portion of the test. The cracking occurred in the upper surface cross stiffeners at the stiffener/rib joint, as shown in Figure 215. There were no strain or accelerometer measurements at this location. This failure occurred after 6 hr and 10 min in the Endurance Test. This is approximately 7e6 cycles to failure based on the time to failure and the crossing frequency. The part was A36 steel, and the only available s-N data is shown below in Figure 216. At a cycles to failure of N=7e6, the RMS stress is 11ksi or 384 μin/in. The crack in the stiffener did not occur at a K_t feature, but it did initiate at the interface between the edges of the rib and stiffener. A typical shape factor of 1.1 was included in the fatigue analysis. The stiffener is at approximately 150 ºF, but there is no assumed thermal knock-down, since it was not known.

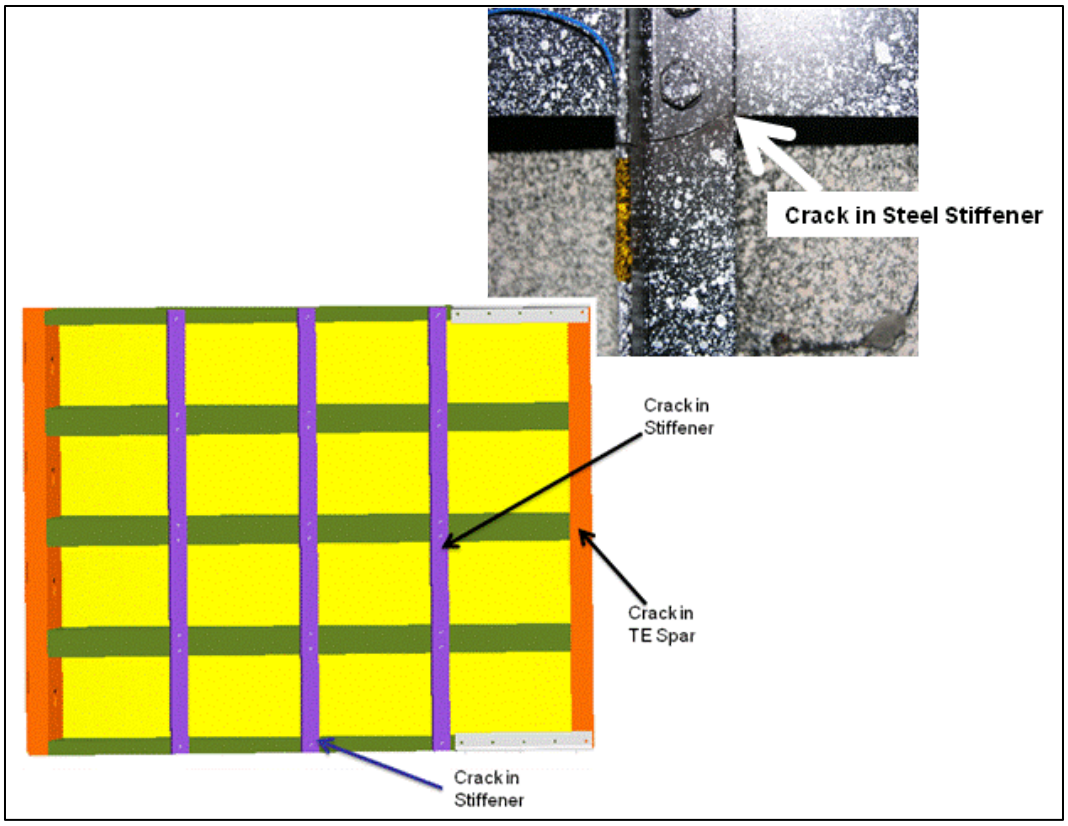

Figure 215 – Endurance test failure in center stiffener at rib interface

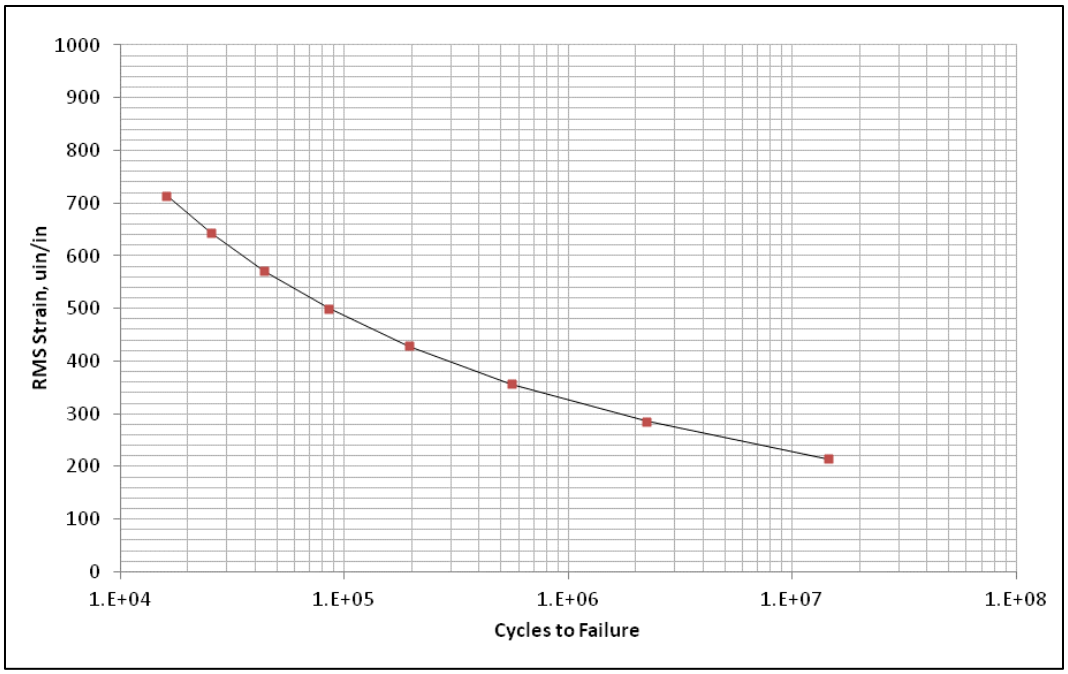

Figure 216 – Soft steel ε-N curve at RT and K_t =1.0, R=-1

The NLROM predicts the RMS strain at the crack location in aft center stiffener as $K_t\varepsilon_{11}$=155 μin/in with a mean strain of 1153 μin/in, Figure 217. Using the predicted strain and the ε-N data, the predicted time to failure is 63330 seconds (17.6 hrs). Although this is longer than the total endurance test time of 6:09:17 hrs, the test article did accumulate several hours of high temperature thermal/acoustic exposure during the response surveys.

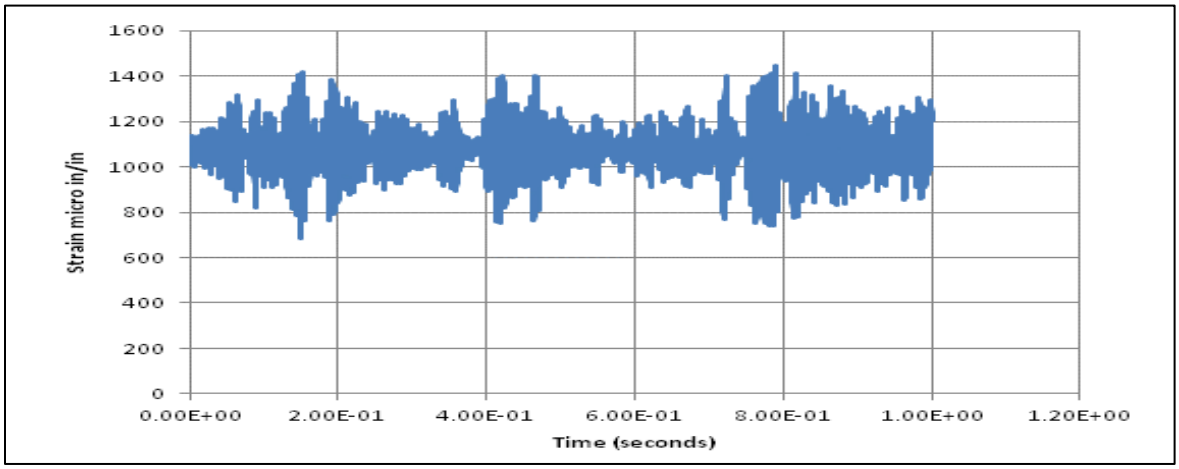

Figure 217 – Strain time history at stiffener / rib interface

10.0 Conclusions and Recommendations

The objective of this project was to advance the technology of Nonlinear Reduced Order Modeling (NLROM) as a design and analysis tool. A realistic aircraft test case was developed in order to validate the process. The NLROM process is a method to rapidly develop a nonlinear reduced order model for the purpose of dynamic response prediction of stiffened aircraft structural skins exposed to high-level aero-acoustic and thermal loading. The test case that was developed was of an aircraft blown flap exposed to high thermal and acoustic loads. The final product is a validated method with quantified benefits, a finite element model of the structural test article, and a fabricated test article. The FEM, hardware, and test data are available for future use in new methodology development studies to validate any further enhancements.

For a Verification and Validation (V&V) study, the first step was to determine if the software was coded correctly. For the verification step, the nonlinear reduced order model (NLROM) was compared to full-order analysis models. The verification test cases were a simple curved beam and plate type structures. The objective was to verify the implementation of the NLROM methodology. The implementation of the "Hot-Modes" approach was also developed and verified. For validation, the objective was to determine if the right software/process was built. In other words, is this tool useful, does it produce accurate results, and is the method scalable and stable. The validation step required comparison of the NLROM response predictions to similar test based measurements.

The first question was whether the implementation of the tool and method made it easy to use. This was addressed through the development of a graphical user interface (GUI). The GUI facilitated rapid model setup, analysis, and testing and, in general, the implementation was demonstrated to be effective on a realistic design application in which design iterations were performed. It was shown to be as accurate as full-order simulation methods. It was also determined to be much faster (less time) to setup and develop NLROM and perform nonlinear response analysis than a full-order nonlinear response analysis. Hence, the method enables more accurate analysis earlier in the design process. The general conclusion is that the method is very usable and practical.

Another concern was determining whether the method was stable. Stability has two aspects. The first is the stability of the implementation. Matlab is a very stable development platform. But, Matlab does have upper memory limits, depending on the machine. Hence, the user does have to understand memory limits of their machine in order to use this GUI. The GUI itself is very stable with plenty of error checking. Hence, if the user enters a bad number or had bad input files, the code caught many of these errors as opposed to crashing. The second aspect deals with the stability of the NLROMs during the time simulation/integration. In general, the NLROM can produce unstable results during the simulation (response divergence). The implementation of the ICE method is a least squares approximation of the nonlinear coefficients based on several nonlinear static runs. There are guidelines for setting up the nonlinear combined modes static runs in order to produce good coefficients, but this can be a trial and error process. In conclusion, Matlab is very stable, but complex models can produce unstable NLROMs due to incorrectly estimated nonlinear stiffness terms in the RON. Finally, large models with many modes can produce issues with Matlab, if memory limits are exceeded.

The third question was whether the method could be easily integrated. The method was implemented using Matlab R2011a, but it also works in R2012. The I/O routines are written in MEX. These compiled routines are machine dependent. The method is based on MD/NASTRAN. Mostly using BDF (ASCII input) or PCH file (ASCII output) formats. The method has been tested in MD/NASTRAN 2008 and 2010. The method uses Abaqus/Explicit for element stress post-processing. This has been tested in 6.9.2 and 6.10.3. In conclusion, the method was easily integrated into the latest versions of NASTRAN and Abaqus. The methodology does use SOL 400 in MD NASTRAN, which allows for chaining of multiple solutions. But, this is not unique to NASTRAN, and could be integrated into just about any general purpose FE solver. The method doesn't use DMAP in NASTRAN or python in Abaqus. Hence, no special purpose user coding is required. The same tool can be applied to any problem without requiring special modifications.

A final concern was the scalability of the NLROM method. Scalable in this context refers to model size and modal order. In this evaluation work using Matlab, there were limits to how many modes and how big of a model can be analyzed with this implementation. Hence, this is a practicality limit since the number of nonlinear static solutions goes up rapidly with number of modes. Each static solution can generate a considerable amount of output, as these solutions are analyses using the actual FEM. For the model used in this study, 3 gigabyte output files were being generated for an 8 mode solution. Also, the initial flap models had to be reduced in size because of memory limits. The conclusion is that based on user's machine memory limits, there will be a practicality limit with the number of retained modes and model size.

10.1 Analysis Observations

The primary observations were related to: (1) modeling choice, (2) mode selection, (3) model updating, (4) model correlation, and (5) model uncertainty.

Modeling Choice relates to selection of elements, mesh refinement, use of contact surfaces, and modeling of bolted connections. In general the goal when performing sub-component detailed analysis is to accurately predict internal loads. Once internal loads are determined then structural stresses can be calculated and strength and life prediction (fatigue) analyses can be performed. In order to calculate fatigue, stresses need to be accurately predicted. Accurate prediction of stresses around fasteners is performed in secondary (or break out models) analyses. These model stresses can then be used directly to predict fatigue life. Another approach uses the stresses predicted with less refined response (loads) model. But, these stresses are in reference stress locations. Traditionally, the reference stress locations are in low stress gradients areas, which are accurately predicted in a less refined model. Hence, detailed accurate stress models are nice to have but generally impractical for nonlinear dynamic analysis. There has to be a balance between modeling choice and structural stress accuracy requirements.

For this study, a model was developed that had a maximum number of degrees of freedom (DoF) that could be analyzed with the NLROM Matlab tool. This was based on output file size and memory limits in Matlab. In fact, a much more detailed FEM was initially used but memory limits in Matlab caused software stability issues in being able to manipulate such large matrices. Also, a large model results in long run times for each nonlinear static analysis. However, more detailed stress FEMs can be used if only a few modes need to be retained in the NLROM. If the problem is broad band (wide frequency) in nature and many modes need to be included in the

NLROM, then a smaller model (with less DoF) needs to be used. These are practicality gap issues that will vary from application to application and from user to user. The expense and complexity of developing NLROMs will get better with time as capability increases.

Mode Selection is one of the cruxes of the reduced order modeling (ROM). The largest cost in reduced order modeling is the development cost. Building the ROM involves running potentially hundreds of nonlinear static analyses. Each static analysis in itself can be a costly analysis, depending on the selection of modeling choices. For this study, the final analysis mode selection was performed using standard techniques. Namely a linear response analysis was performed, and the modes that attributed the most to the response were used in the NLROM response analysis. Also, modes that were identified in the modal and response testing were included. However, this isn't the best approach. The NASA POD method described in section 3.6 was found to be of use in identifying modes and presenting the modes in order of importance. For simple models, the POD method identified all bending modes as being important. This is a trivial solution for this problem. For more complex models, the POD technique did identify a set of modes that seemed to be important based on the applied loads. However, the method was implemented in Abaqus and this implementation of NLROM is in NASTRAN. The modes in Abaqus and NASTRAN differ enough to render the POD technique non-applicable for the validation study. In general, optimal mode selection methods need to be investigated further if NLROMs will be practical. This is especially true if the structure being analyzed has high modal density. It's relatively easy to identify the best modes in low modal density structures, e.g., simple plates and beams. When using the ICE approach, it is best to use all modes in the frequency range of excitation up to 2x the excitation level, if possible. This implementation of NLROM methodology using NASTRAN generates large output files, which limits how many modes can be used in the simulation due to memory limitation.

Another major objective of this program was to compare analysis predictions to test data. In order to make a best-effort comparison between analysis and test, this requires Finite Element Model Updating. Model Updating involves taking measured data (primarily loads and information about boundary conditions) and using this data directly in simulations. Direct measured data reduces discrepancies and uncertainty between model and test. For this study, the primary data used for model updates were the measured loads: temperature and pressure (steady and acoustic). For the CEAC tests, the structural temperature was not directly used in the model updating. Rather a thermal analysis was performed. The inputs to the thermal analysis were heat flux, flow conditions, conduction coefficients, and radiation coefficients. Heat flux of the CEAC quartz heat lamp bank was provided by AFRL. Air flow was measured and used in the thermal analysis. Fixture temperatures were used as thermal boundary conditions. Hence, this thermal data was used to update the model and reduce error and uncertainty. For the T-58 testing, the OML skin temperature was measured and used directly in the analysis.

Another significant source of uncertainty in response analysis is the acoustic loads. The magnitude and phasing of the acoustic loads over the OML skin is difficult to predict a priori, even in a controlled test there is significant source of uncertainty. In a progressive wave chamber, like the CEAC, the magnitude and phasing of the loads vary within the test section. Therefore, to reduce uncertainty, the acoustic loads were measured directly on the lower OML skin using Flat Pak sensors, and the pressures were correlated to the control microphone for subsequent high temperature Test Runs. The Model Updating involved using direct measured

data that would otherwise be assumed in the analysis setup; such as loads, temperature, heat flux, flow velocity, and acoustic pressures.

Model Correlation involves using measured test data and changing the model structural and material properties to best match the test data. For this study, the model correlation was only performed on the modal test data and the thermal loads data. The objective was to make sure the FEM best matched the actual test article. This reduced uncertainty to allow for response validation between test and analysis. For the CEAC analysis, modal, thermal, and LVDT data was used to correlate the model. These correlations were performed separately, and a best compromise model was used in the final NLROM comparisons. Modal test data is very important, since this is a dynamic simulation process. Modal testing provides frequencies, mode shapes, modal damping, and modal FRFs. The testing was performed at room temperature (RT) and elevated temperature conditions. Finite Element correlation software FEMTools can only perform at room temperature, and is hard-coded to use NASTAN's modal SOL 103 specifically. When running a thermal preloaded modal solution, NASTRAN's nonlinear SOL 400 was used due to its analysis chaining capabilities. Therefore, for the high temperature correlation, numerical methods were used to minimize the difference between measured and analytical frequencies and modeshapes. This resulted in the correlated hot modes NLROM. In the case of the thermal modeling, ModelCenter was used to minimize the error between the measured temperatures and predicted temperatures from the CEAC thermal analysis. The final correlation used the LVDT test data in a similar fashion. The general observation is that modal tests need to be performed at test conditions similar to that response or endurance testing. However, high temperature modal testing offers its own challenges, and there is additional uncertainty in the measured data.

Model and Test Uncertainty Quantification need to be determined when performing model validation. Differences in test versus analysis will always exist. Hence, there has to be some data analysis that quantifies the statistical scatter of the measurements. For this test program, relatively long time records (60 seconds) were recorded and all measurements were repeated three times. This provided ample data to quantify the statistical scatter and to obtain statistically significant test results. Longer time records ensure statistical confidence, and repeated measurements allows for measurement of low-order statistics (average and standard deviation). Measurements are also made before test runs at zero conditions to determine the noise floor and any measurement offsets.

10.2 Testing Lessons Learned, Observation, and Recommendations

Testing is an important part of any model validation program. A well characterized test forms the basis of quantification of the model accuracy to the physical data. A well characterized test has these features: (1) a detailed test plan, (2) accurate instrumentation drawings, (3) time sequential test logs, (4) sufficient photographic documentation, (5) documentation on all data files, (6) a description of all instrumentation, equipment, and facilities features, and (7) accurate drawing of the test articles including assembly and fastener information. The objective is to provide sufficient information; such that, others can replicate the experiment.

The test plans for both the CEAC and T-58 test are presented in Appendices A and B. Time sequential test logs are given in Appendix C and D for the T-58 and CEAC test programs. Accurate instrumentation drawings are given in Appendix E. Drawing of the test articles are

given in Appendix F. A list of lessoned learned, observations, and recommendations is given in Appendix G.

10.3 Further Development Recommendations

The primary recommendation is the continued extension, validation, and application of combined thermal-structural reduced order models for nonlinear response problems. There are two near term recommendations: (1) thermal load ROM, and (2) coupled thermal-acoustic response ROMs. The two recommended extension for the current thermal-acoustic response ROM methods are described below.

First, there is a need to determine the temperature distribution and structural response induced by a transient heat flux on OML surface panels. Heat flux is dependent on the local aerodynamic flow conditions. Both temperature distribution and structural response need to be determined using reduced order models (ROMs); such that, thermal-structural coupling is enforced. This will require separate steady-state thermal analysis to be carried out at several thermal flow conditions (i.e., snap shots). Then, for instance, POD techniques can be used to determine the thermal load ROM. The thermal load ROM can be then utilized in the structural reduced order model with and without the acoustic excitation.

Second, the recommendation is for extending the NLROM formulation to combined thermal-structural reduced order modeling method to include temperature dependent structural properties, which includes elasticity modulus and the coefficient of thermal expansion. Currently, these properties are assumed to vary linearly with structural temperature in the pre-load to determine the Hot Modes basis. Design conditions may be at a specific trajectory point or flight condition or it may be a combination of worst case conditions (max temperature, max acoustic levels, at max maneuver/flight loads.) Regardless, the analysis is assumed to be stationary, and the static temperature and mechanical loads do not change in time, and the acoustic loads are stationary too, with their statistics (mean, RMS, spectral content) assumed constant. Also, there is no interaction between the loads and response; i.e., the response does not feedback to affect the thermal, pressure, or acoustic loading. The thermal aspects of the acoustic response still need to be resolved in order develop a ROM for elevated temperature applications. The Hot Modes technique was used for this study, but it's unsure if this was the best approach. The Cold Modes approach would logically be valuable for time dependent thermal loading. For instance, it would be of interest to simulate the structural response during a high speed flight or rapid maneuvering.

Therefore, the near-term recommendation is to continue development and validation of thermo-elastic reduced order models for the geometrically nonlinear response and temperature of heated structures, which can be combined with acoustic nonlinear ROM response models. Once, the methods have been developed, and then continue with the evaluation and implementation phase. Finally, perform verification and validation testing using a full-scale aircraft component demonstration. The scope of validation testing will require improvements in the CEAC facility; refer to recommendations in Appendix G.

11.0 References

(1) Rogers, L., et al., "Durability Patch: Repair and Life Extension of High Cycle Fatigue Damage on Secondary Structures of Aging Aircraft," proceedings of the 1st Joint DoD/FAA/NASA Conference on Aging Aircraft, July 1997.
(2) Gordon, R.W., and Hollkamp, J.J., "Nonlinear Acoustic Response Prediction using Reduced-order Models," AFRL Workshop Notes, November 2007.
(3) Hollkamp, J.J., and Gordon, R.W., "Modeling Membrane Displacements in the Acoustic Fatigue Response Prediction Problem," AIAA-2005-2095, 2005.
(4) Gordon, R.W., and Hollkamp, J.J., "Reduced Order Modeling of the Random Response of Curved Beams Using Implicit Condensation," AIAA-2006-1926, 2006.
(5) Hollkamp, J.J., Gordon, R.W. and Spottswood, S.M., "Nonlinear Acoustic Fatigue Response Prediction from Finite Element Modal Models: A Comparison with Experiments," AIAA-2003-1709, 2003
(6) Hollkamp J.J., Gordon R.W., and Spottswood S.M., "Nonlinear Modal Models for Acoustic Fatigue Response Prediction: A Comparison of Methods," *J. of Sound and Vibration*, Vol. 284 (3-5), 2005, pp. 1145-1163.
(7) Liguore, S.L., Pitt, D.M., Thomas M.J., "Applied Nonlinear Low Order Response. Prediction Methods Evaluation ", AFRL-RB-WP-TR-2009-3100.
(8) Beier, T.H., "AVTIP DO #27 Identification of Dynamic Loads Problems and Solutions," December 1, 2002.
(9) Locke, J. E., "A Finite Element Formulation for the Large Deflection Random Response of Thermally Buckled Structures," Ph.D. Dissertation, Old Dominion Univ., Norfolk, VA, 1988.
(10) Mei, C., "Large Deflection Multimode Response of Clamped Rectangular Panels to Acoustic Excitation," Wright-Patterson Air Force Base, Ohio, AFWAL-TR-83-3121, Vol. I, Dec. 1983.
(11) Rizzi, S.A. and Muravyov, A.A., "Improved equivalent linearization implementations using nonlinear stiffness evaluation," NASA TM-2001-210838, March 2001.
(12) Liguore, S.L., "Identification of Uncertainties and Application of Probabilistic Analysis in Acoustic Fatigue Design, "Conference on Recent Advances in Structural Dynamics, Southampton England, UK July
(13) McEwan, M.I., "A Combined Modal/Finite Element Technique for the Nonlinear Dynamic Simulation of Aerospace Structures," Ph.D. Dissertation, School of Engineering, University of Manchester, Manchester, UK, 2001.
(14) Rizzi, S.A. and Przekop, A., "System identification-guided basis selection for reduced-order nonlinear response analysis," *Journal of Sound and Vibration*, Vol. 315, No. 3, 2008, pp. 467-485.

Appendix A. CEAC Test Plan

A.1 Introduction

This validation test was conducted as part of the Air Vehicle Integration and Technology Research (AVIATR) Delivery Order 13, Nonlinear Low Order Reduced Order Modeling Applications and Demonstration (NLROM II). This task order is focused on the application of nonlinear low order structural response methodologies to predict the structural response of a representative aircraft structure to verify to the results.

In Phase I, the AFRL NLROM methodology was implemented and evaluated. The results from Phase I can be found in reference (A1). Where it was analytically demonstrated that an 8x-100x improvement in computational efficiency while retaining the accuracy of full order nonlinear response analyses. The accuracy is critical because linear analysis methods in wide use today tend to overestimate response for most parts of a structure while underestimating or entirely missing critical stress hot spots. The result is overweight structures with critical deficiencies in design details that then suffer premature fatigue cracking. The improvement in analysis efficiency is just as critical because full order nonlinear analyses are simply not practical for large finite element models representing today's aircraft structures.

For Phase II, the NLROM methodology will be validated against test data for representative aircraft structure under thermal/acoustic loading, ref. (A2). The representative aircraft structure is a section of a full-scale blown Trailing Edge Flap (TEF). The validation testing will consist of two tests. The first test will be a progressive wave facility test in the AFRL Combined Environment Acoustic Chamber (CEAC) facility. The second test will be in the Boeing/T-58 Engine Burner Facility (EBF). The Boeing Engine Burner Facility will expose a second test article to the exhaust of a jet engine providing an entirely realistic test environment including combined thermal, acoustic and pressure loading for further validation. This Test Plan covers the AFRL CEAC testing.

A.2 Objective and Success Criteria

Our objective for this test is to accurately measure the thermal/acoustic loads and response of test article and the structural dynamics characteristics of the test article under applied thermal loads. Hence, this test article will have instrumentation and measurement systems in place to capture this data. The measured loads test data will be used to verify the thermal/acoustic loads for the predictions. The modal test data will be used to correlate the structural finite element model. The measured response data will then be used to validate the nonlinear reduced order response and full-order analyses to the measured test data. The quantification of uncertainty in all measurements will also be critical in the validation task. The uncertainty analysis will be a post-test activity but the test planning, data acquisition, sensor calibration, etc, will be important for this uncertainty quantification task.

A.3 Scope

This detailed test plan (DTP) describes the thermal/acoustic testing to be performed in the Combined Environments Acoustic Chamber (CEAC) at Wright Patterson Air Force Base (WPAFB). The actual facility operations and related procedures will be the responsibility of AFRL test personnel. The test article fabrication, test panel assembly, test panel instrumentation

(strain gauges) and the delivery are Boeing responsibilities. Installation of the test panels to the individual test facilities and instrumentation interface to the data acquisition systems are AFRL responsibilities. Changes to this plan which are within the scope of the test, may be made by "Redline" changes approved by the AFRL Responsible Engineer (RE), Travis Wyen, and documented within this DTP.

A.4 General Requirements

Handling of Test Panels – AFRL test personnel will install the test panel to the test fixture. All pre-test and post-test observations of the test panels shall be documented in a Laboratory Notebook by the AFRL RE.

Notice of Test – The AFRL RE shall be notified in advance of any scheduled test. Changes to the schedule shall be made in conjunction with the Boeing RE.

Photographs – AFRL test personnel will use a digital camera to photograph test articles and test setup before and after tests, as needed, or as requested by the Boeing RE.

Inspection – AFRL shall provide a general visual inspection of the test panel and fixture prior to the start of any test run. The AFRL RE shall conduct a complete visual inspection before and after each test run to determine any changes. The RE shall also perform any on-site measurements as necessary to document the condition and/or changes in the test articles.

Disposition of Test Hardware
At the completion of testing, the test article and fixture will be disposition per the instructions of the AFRL Program Manager: Leonard Shaw, AFRL/RBSM, (937) 904-6774.

Report – AFRL shall provide a test data package to Boeing within 30 days after completion of the test program. The Boeing RE shall release a Laboratory report to be included in the program final report.

A.5 Test Descriptions

The Combined Environment Acoustic Chamber, shown in Figure A.1, is capable of combined thermal and acoustic loads. It is capable of up to 50 BTU/ft^2-sec and 170+ dB overall sound pressure level (OASPL) at frequency range of 50-500 Hz flat spectrum. Test specimens up to 8 feet x 4 feet can be tested in this facility. A layout of the test chamber and test panel set up is shown in Figure A.1.

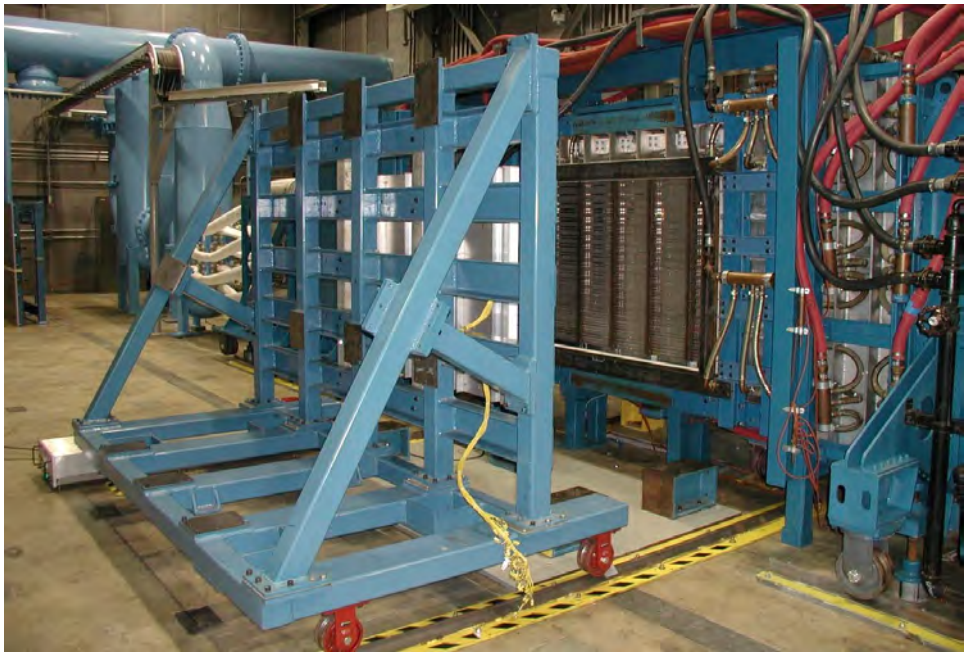

Figure A.1 – AFRL CEAC chamber for combined thermal and acoustic testing

The test facility uses a strong back cart to position the test specimen within the acoustic chamber. Illustrated in Figure A.2, a similar strong back cart is used to position the quartz lamp banks on the opposing side of the chamber. The specimen cart allows test panels to be securely mounted, independent of the test section, to minimize transmission of vibration from the chamber walls. The cart system also allows for the test specimen to be removed from the chamber between test runs for inspection. AFRL shall be responsible for integrating the test panel to the CEAC strong back cart such that the article has clearance on all sides when installed in the chamber. The front of the test panel will be installed flush with the inner surface of the acoustic chamber wall.

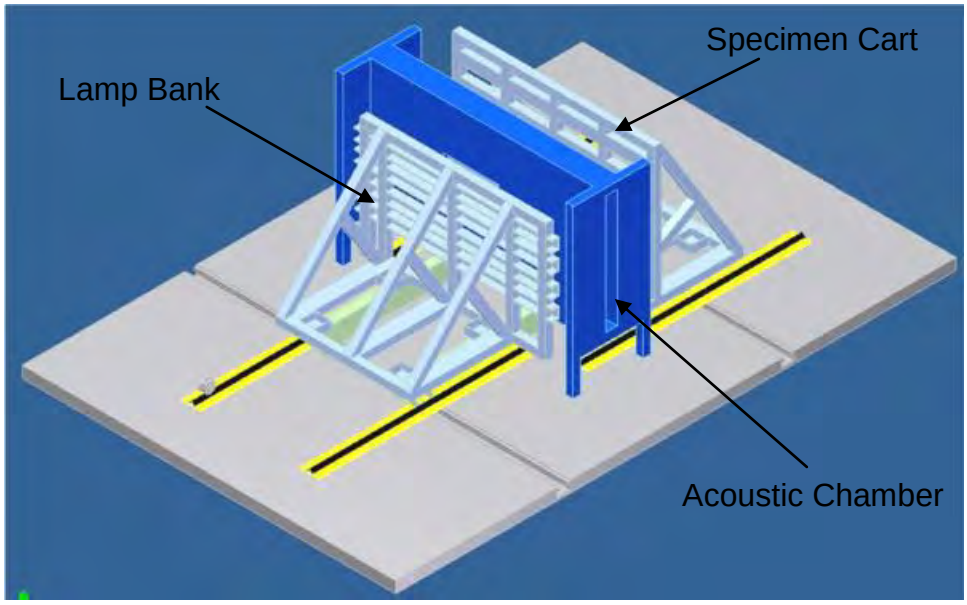

Figure A.2 – Test facility layout showing test specimen cart and lamp bank cart location relative to the test chamber

A.6 Test Panel Components

The test specimen is a representative section of a large transport aircraft trailing edge flap lower surface with substructure. The test specimen will be approximately 31”x 24”, Figure A.3. Also, there will be additional test adapter fixture, Figure A.4, which the test specimen will be bolted to and which then gets bolted to the test cart. This is the complete test article (specimen plus adapter fixture.) The test specimen consists of 5 machined ribs fastened to a skin. The adapter fixture is bolt to the movable cart. The representative aircraft structure is exposed to high thermal and acoustic loads in service. This will be simulated in the CEAC facility using combined thermal and acoustic loading. The thermal load will be accomplished through front-side heating from the quartz lamp heater system.

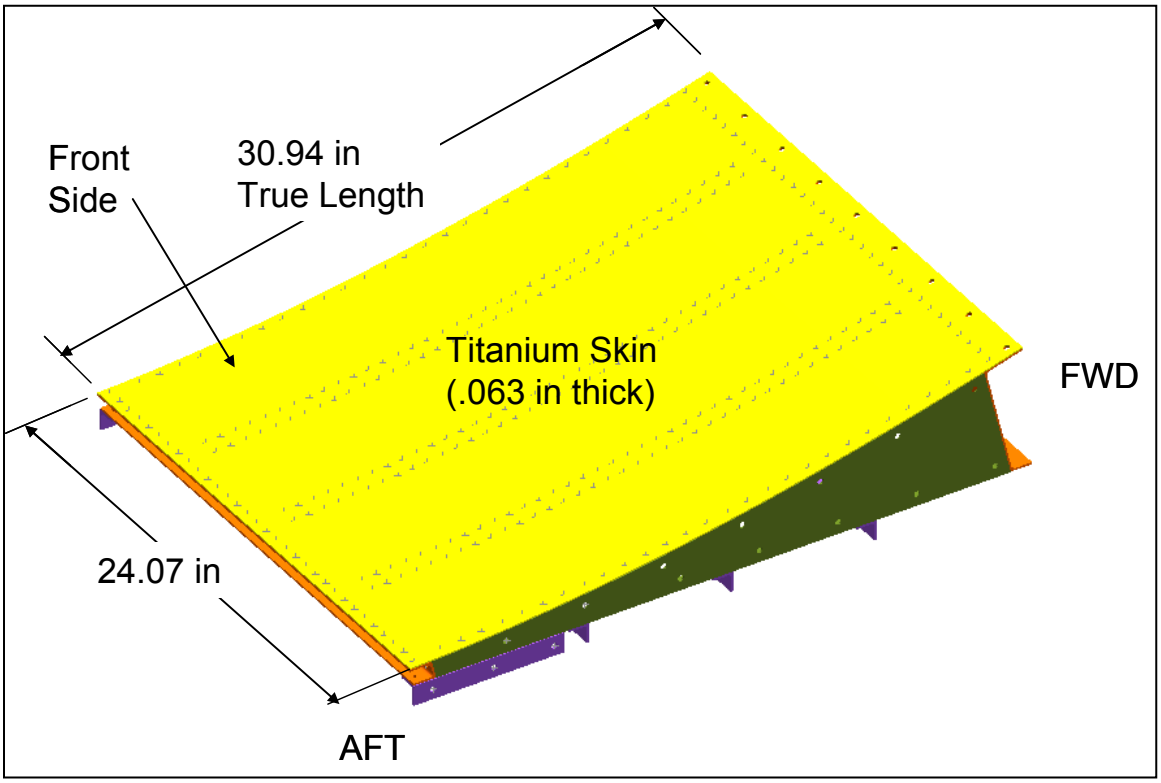

Figure A.3 – Test article

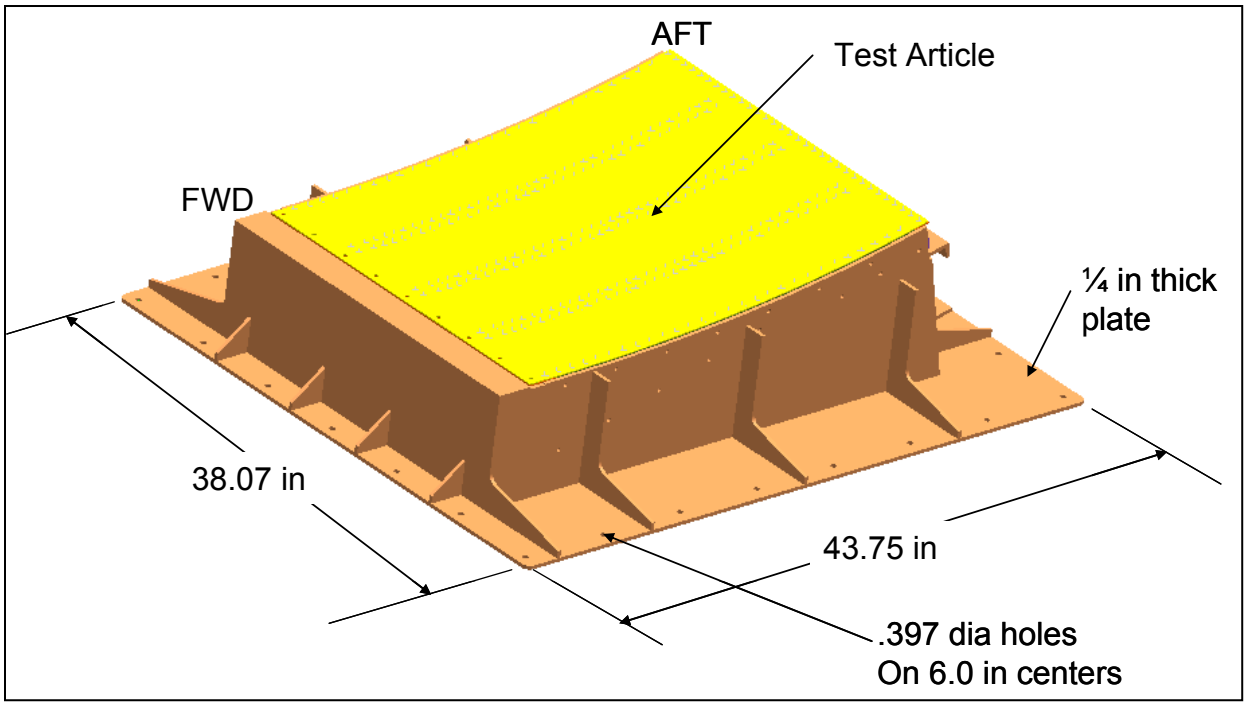

Figure A.4 – Test article with adapter fixture assembly

A.7 Test Panel Instrumentation

Instrumentation will be installed on both the test article and the fixture to measure strain, temperature, acceleration, and acoustic pressure. The following shows the type and locations of the test instrumentation to be installed by AFRL. The strain gauges will be installed by Boeing prior to delivery.

Thermal Test Instrumentation

The thermal instrumentation will be used to verify the thermal loads analysis predictions. This includes verifying the thermal loads and response. The combination of thermocouples, flow measurements, IR imaging, and displacement camera measurement system will be used. The thermal analysis uses a uniform heat flux loading. A typical heat flux loading was defined from a previous AFRL test program on a curved titanium panel. The thermal analysis is performed to predict the steady state structural temperatures. The structural temperatures are then used as a static thermal pre-load in the acoustic response analysis predictions. Hence, we need to verify the predicted temperature distribution in the test article. This will be accomplished through point temperature measurements with thermocouples (TC) and with thermal IR imaging camera. The IR cameras will be positioned behind the test article for IML temperature measurements. The TCs will be positioned to measure the temperature difference between the front and back side of the skin, the difference between the mid skin bay and skin over the ribs, the difference between the skin/rib and rib flange, and final the heat flow from the test article to the fixture. The fixture TCs will be used to verify the thermal boundary conditions.

There is a total of (28) Thermocouples (TC). A total a (13) will be installed on the OML (chamber side skin), and (5) on the IML, Figure A.5. Also, a total of (6) TC will be installed on the interior ribs, as well as, (4) on the exterior fixture, Figure A.6. The thermocouples are

sampled at a low rate. The steady state temperature will be recorded when high sample rate data is acquired.

Two IR cameras will be used. The first will be positioned directly behind the test article to get a straight on plan-view image of the IML back side. The second camera will be positioned below 1st camera to image the (3) interior titanium ribs. Digital Data reduction will be performed with the calibrated first camera. The second camera will be used for reference to thermocouples.

During the ambient acoustic surveys, measure the upstream chamber air flow velocity. Air flow data will be used for calibration of predictive model convective thermal loading setup. Position is to be determined by AFRL.

Digital Imaging Correlation (DIC) will be used to measure the steady state thermal displacement during elevated temperature test conditions. The test article can be painted with material to enhance imaging measurements.

Also, (4) Linear Variable Differential Transformer (LVDT) will be used for static displacement measurements for correlation to the DIC measurements. The placement will be on the IML skin. The specific locations will be adjusted for best correlation to the DIC.

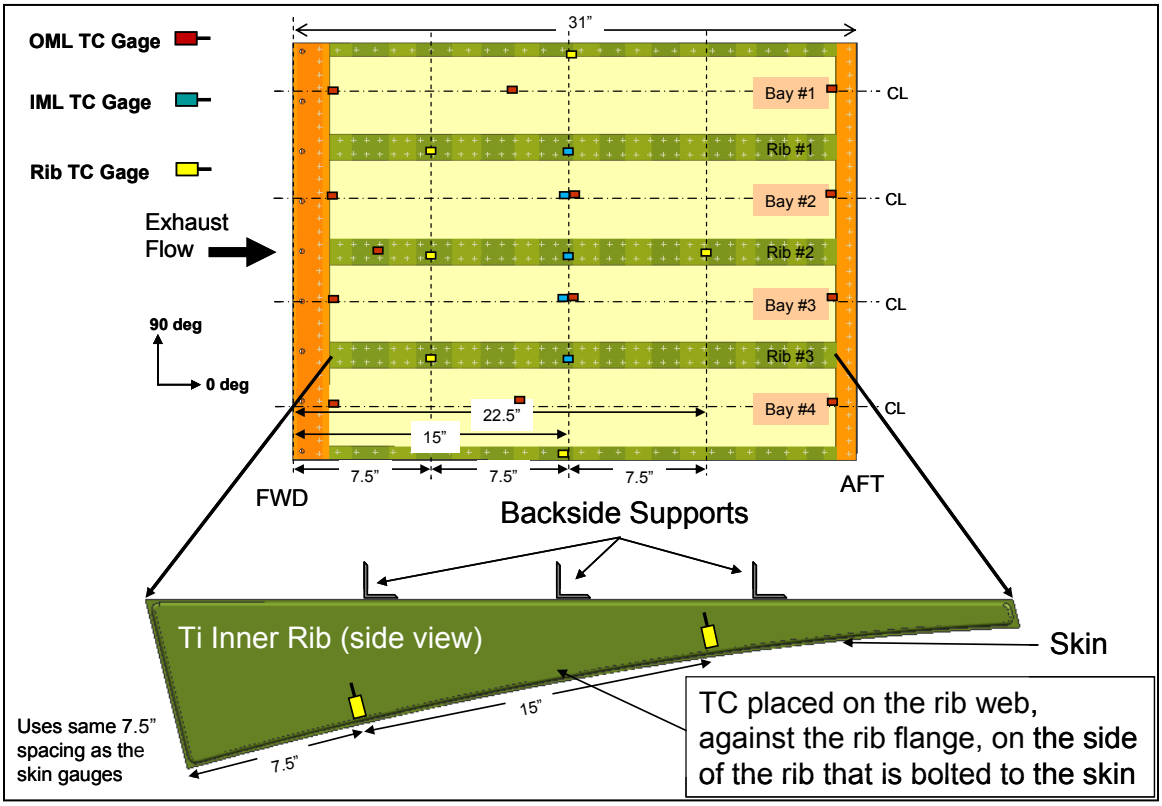

Figure A.5 – Test article thermocouple (TC) layout

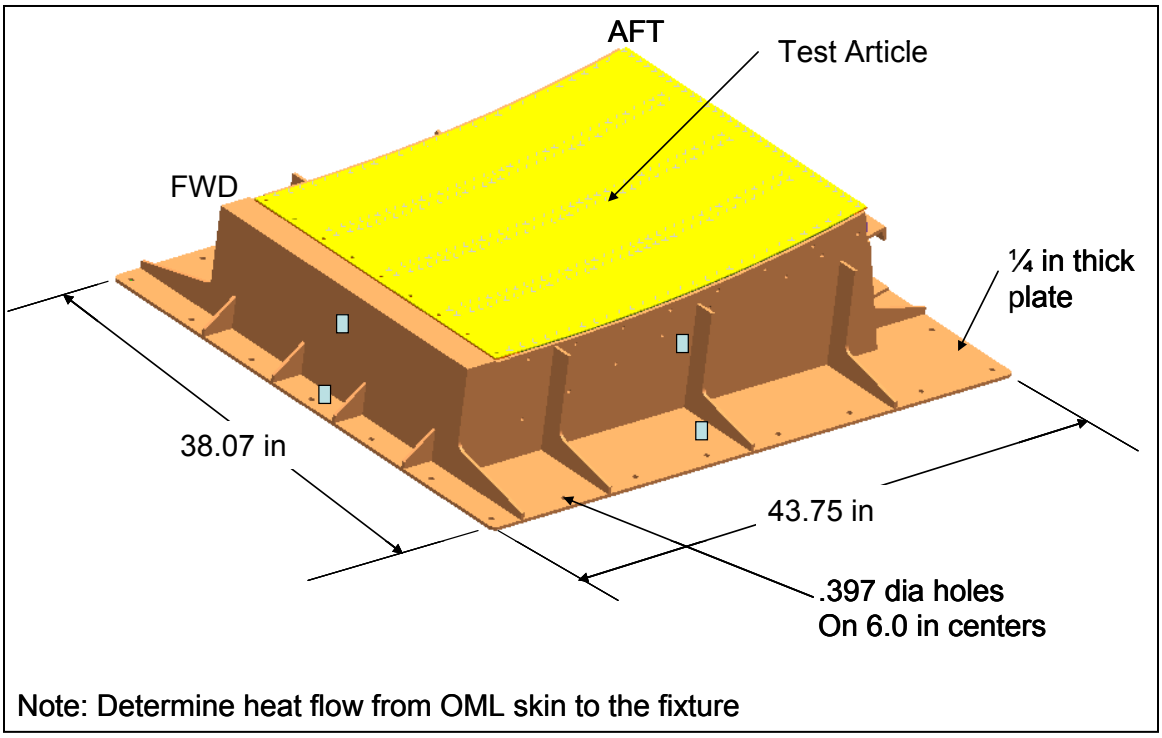

Figure A.6 – Fixture TCs

Vibration Response Instrumentation

The vibration response will be measured with a combination of accelerometers (AC), strain gauges (SG) and laser doppler vibrometer (LDV), Figure A.7. The measured response will be validating the accuracy of analysis predictions in Task 5.

A total of nine low mass accelerometers will be installed: six on the IML skin to measure out-of-plane vibration, and three on the interior ribs at mid span upper web surface to measures lateral motion. Two LDVs will be setup, as shown.

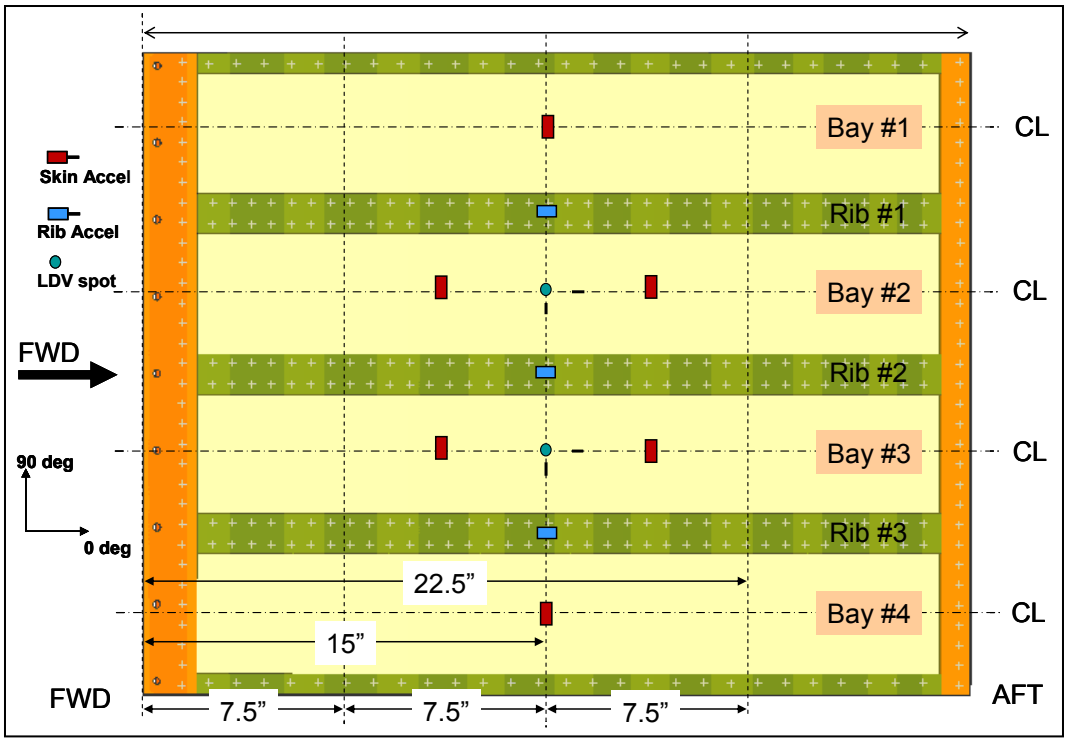

Figure A.7 – IML accelerometers instrumentation locations for acoustic testing

Strain Gauge Instrumentation

Total of (30) strain gauges will be installed on the test article, Figure A.8, Figure A.9, and Figure A.10.. The strain gauge signals will be zeroed prior to acoustic testing at all temperature levels. For the thermal survey, the total signal will be monitored. Temperature compensation will be used to measure the thermal load induced strains.

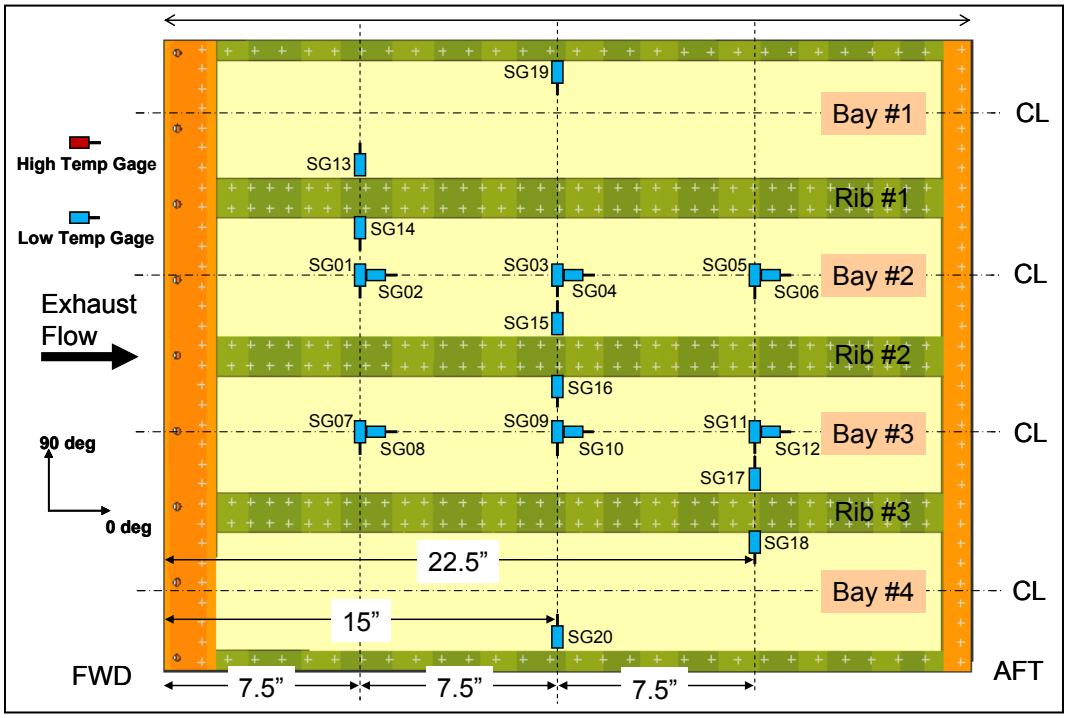

Figure A.8 – IML skin strain gauge instrumentation locations for acoustic testing

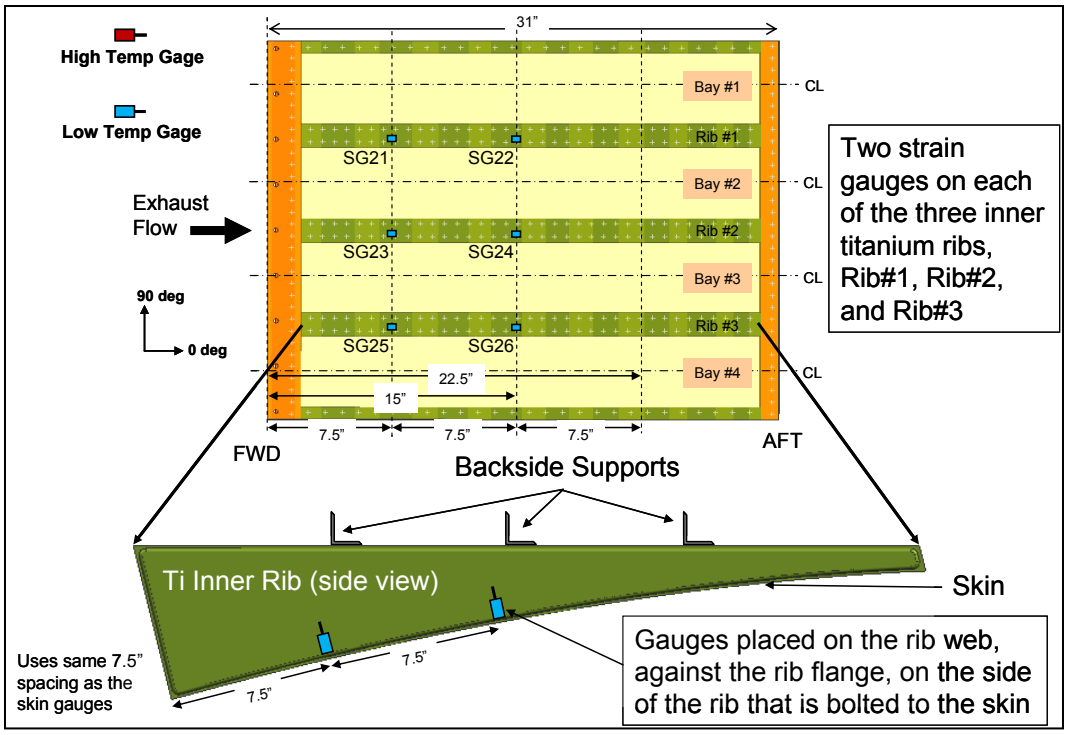

Figure A.9 – IML rib strain gauge instrumentation locations for acoustic testing

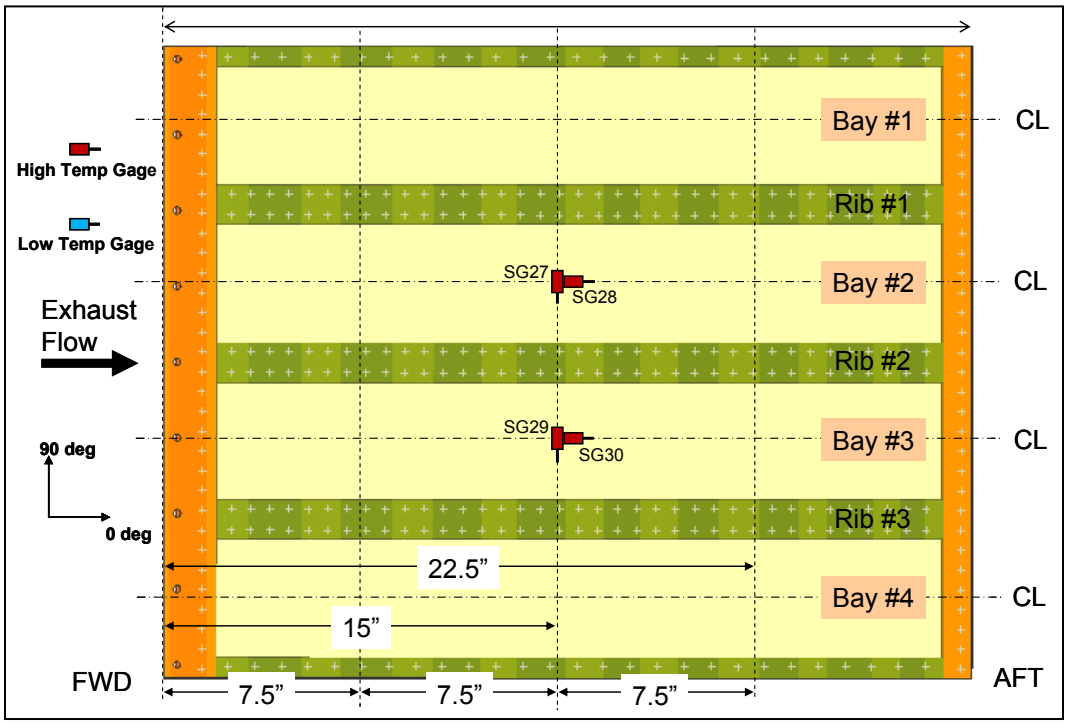

Figure A.10 – OML skin strain gauge instrumentation locations for acoustic testing

Microphone / Acoustic Measurement Instrumentation

Accurate measurement of the applied acoustic loading is critical for post-test analysis. Although the acoustic loading (spectrum and magnitude) can be controlled at one location or as an average of several locations, this is only an approximation of actual loading over the surface of the test article. The acoustic response analysis is setup as 12 separate acoustic zones on the outer mold-line (OML) skin. For the pre-test predictions we will assume the acoustic loading is the same in each zone, and that is partial correlated (phased in time).

The acoustic measurements need to measure the actual spectrum, magnitude, and phasing (spatial correlation) of the loading over the skin surface. Hence, an array of 12 Flat Pak transducers will be installed on the test article OML skin to measure these loads. These Flat Pak transducers will be used only during initial Room Temperature (RT) acoustic survey. The second set of transducers will be used during both the RT surveys and all subsequent testing.

This second set consists of a total ten high temperature walled cooled chamber microphones. The acoustic level and spectrum will be controlled using these microphones the average of the three leading edge wall mounted microphones. The microphones will be mounted in existing cooled plates upstream and above and below of the test article as shown in Figure A.11.

Also, two microphones will be placed behind the test article (inner mold-line (IML) side), Figure A.12. These microphones can be attached to the ribs or support stiffeners. These microphones will be used to determine through noise transmission characteristics, and loading on the interior ribs.

All acoustic loading will be sampled at a high rate 40khz, high pass filtered, and processed into narrow band PSDs and 1/3 Octave Spectrums.

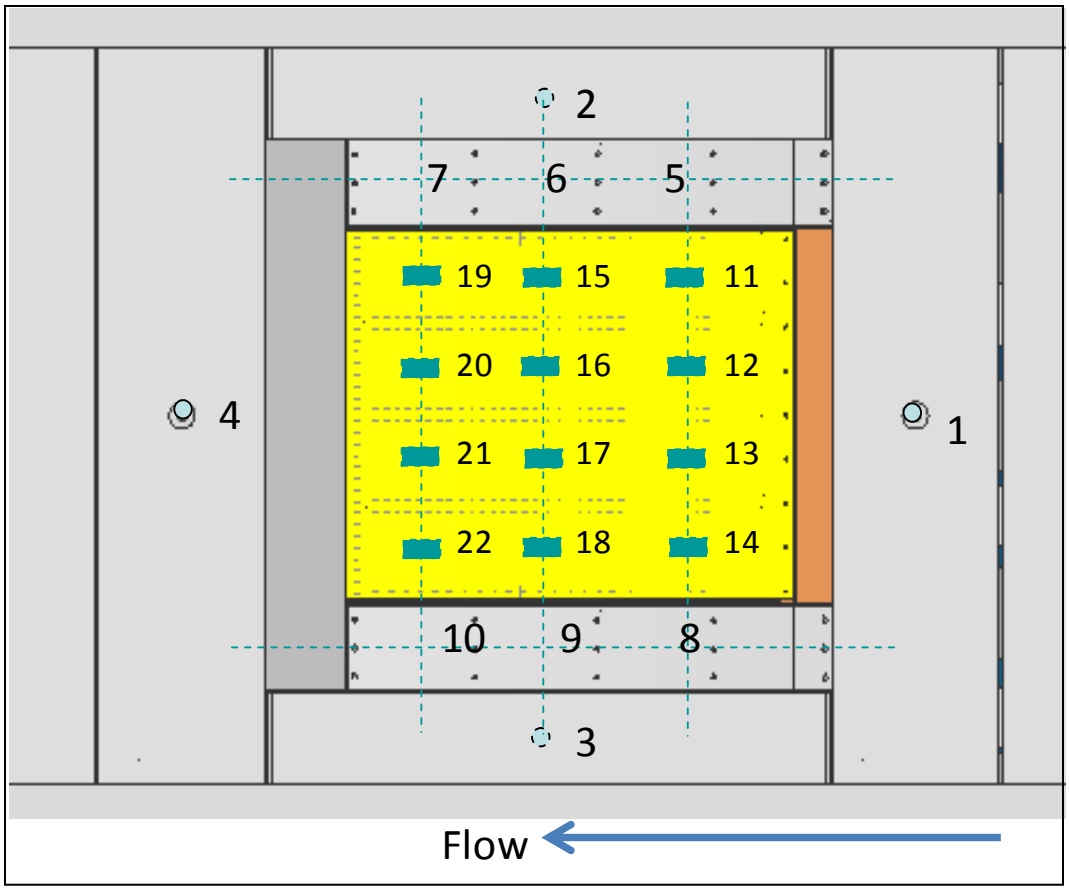

Figure A.11 – OML side - acoustic sensor locations

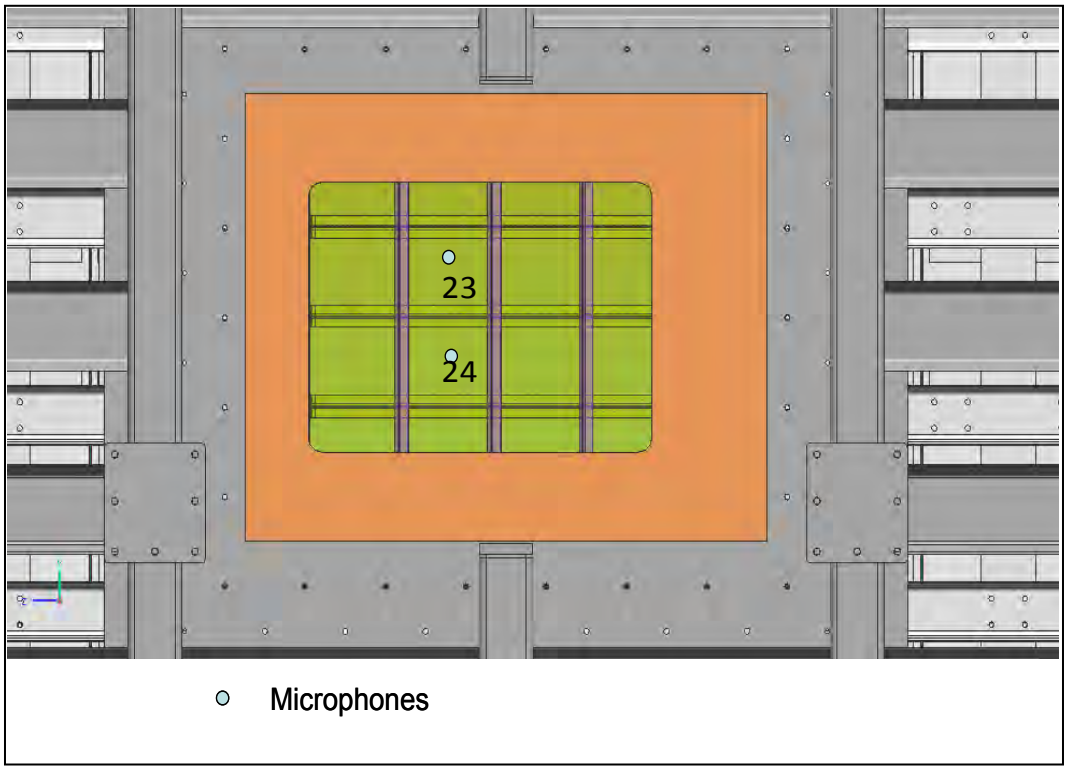

Figure A.12 – IML side acoustic sensor locations

A.8 Test Approach and Phasing

Pre-Test
AFRL will paint OML with high emissivity paint, flat –black.

Installation
Install the test specimen in the test frame adapter and mount assembly to the test Cart.

Modal Survey
Three modal surveys will be performed. The first survey will be on the Cart outside of the chamber. The second will be with the Cart rolled into the chamber side wall. The third survey will be in the chamber at elevated temperature. The first survey will be compared to the analytical model. The second test will determine the extent of acoustic coupling in the chamber. The third survey will confirm mode shapes at elevated temperatures.

Conduct a modal survey from 10 to 1000 Hz. Boeing will supply a list of modes of interest. The modal test method will use scanning laser vibrometer with shaker excitation. Data obtained from the survey shall include resonant frequencies, mode shapes, damping factors and select frequency response functions. The modal survey will include modal mapping points, on the skin, ribs, and fixture. All data will be delivered to the Boeing in electronic format, including measured reference Frequency Response Functions (FRFs) and plots of the mode shapes, and tables of the frequency and damping.

For the elevated modal survey, if the shaker excitation doesn't work, then acoustic excitation will be used.

This modal data will be used to correlate the analytical model. Boeing will use FEMTools for the correlation.

A.9 Environmental Test Survey (ETS)

The testing will be split into two tests segments. The first test segment will be a complete Environmental Test Survey (ETS), and the second test segment will be the Endurance Test (EDT). The ETS verifies the applied loads and response of the test article at different combinations of thermal and acoustic loading. The EDT is a longer duration test that will verify the sonic fatigue design, and look for at thermal degradation effects. The EDT will be performed at max conditions for ~4 hrs, and then repeated after non-destructive inspection, or until the defined fatigue failure.

The ETS will consist of the following. For each condition, all data will be recorded for 60 seconds at 40 kHz for each test condition, and repeated 3 times. The Test Phasing is shown in Table A.1. The ETS will begin with a zero condition (1) to calibrate all channels. Then, an ambient (room temperature) acoustic sine sweep survey (2) will be performed. This will be followed by a room temperature acoustic survey (3) using the flat spectrum from 50Hz to 500Hz. After the acoustic survey (3), all low temperature transducers will then be removed. The RT acoustic survey will be followed by higher temperature testing (4).

AFRL will provide real-time data monitoring on spectral analyzer for up to 8 channels.

The testing will be based on measured 1/3-octave sound pressure levels (SPL). The spectrum is defined in Table A.2 below. Feedback control is only expected between 50 to 500Hz. The Max Survey spectrum is to be used during the Environment Survey test sequence. The Endurance spectrum will be used during that portion of the test sequence. The final spectrums are TBD, but these can be used for estimating.

Acoustic Test Procedure

The acoustic testing will proceed as follows:

1. Perform acoustic only test runs to evaluate acoustic responses on the specimen surface relative to the structure. Inspect for damage, such as skin/frame cracks, broken attachments, and loose fasteners, after each run. Document condition of test panel. Document and tighten any loose fasteners.
2. If the test panel is still in good condition, precede with remaining test runs, subjecting the test panel to acoustic environment. During EDT survey, stop the run after every 30 minutes of acoustic run time to inspect for damage to the test specimen.
3. The RE shall measure, inspect, and document any damage, instrumentation changes.
4. During each run, the RE or AFRL test operator may shut down the facility immediately if any of the following should occur:
    1. Considerable damage occurs to any part of a test article (i.e., failed attachments, or rib/skin cracking).
    2. Any malfunction of the facility, which is normally defined by facility operational procedures. Perform complete inspection of panel if acoustic levels spike above planned test conditions.

Table A.1 – Environmental Test Sequence (ETS)

Test Sequence	Acoustic Level Rel OASPL (dB)	Temperature Level (deg F)	Comment
1	Ambient	ambient	Zero Condition
2	-18	Ambient – Room Temp (RT)	Sine Sweep (20 – 1000Hz)
3	-18, -12, -6, -3.5, -1.5, 0	Ambient	Calibration Test/Survey
			Remove RT Instrumentation
4	Ambient	Amb to 500 (max), then back to 100 F	Measure Steady State Thermal response every ~50F temperature levels
5	Elevated Modal Survey	500F* or highest level that can be achieved	Setup with Shakers Specimen installed in Test chamber
6	-18	100	Sine Sweep (20 – 1000Hz)
7	-18, -12, -6, -3.5, -1.5	100	Acoustic survey
8	-18	200	Sine Sweep (20 – 1000Hz)
9	-18, -12, -6, -3.5, -1.5	200	Acoustic survey
10	-18	300	Sine Sweep (20 – 1000Hz)
11	-18, -12, -6, -3.5, -1.5	300	Acoustic survey
12	-18	400	Sine Sweep (20 – 1000Hz)
13	-18, -12, -6, -3.5, -1.5	400	Acoustic survey
14	-18	500	Sine Sweep (20 – 1000Hz)
15	-18, -12, -6, -3.5, -1.5, 0	500	Acoustic survey

Table A.2 – Reference acoustic spectrums

1/3 Octave Center Band Frequency (Hz)	Max Survey Spectrum 1/3 Octave SPL (dB)	Endurance Spectrum 1/3 Octave SPL (dB)
25	151.0	154.5
31.5	150.0	153.5
40	151.5	155.0
50	154.0	157.5
63	155.5	159.0
80	155.0	158.5
100	154.5	158.0
125	153.0	156.5
160	154.0	157.5
200	153.0	156.5
250	151.5	155.0
315	150.0	153.5
400	149.0	152.5
500	148.0	151.5
630	146.0	149.5
800	145.0	148.5
1000	145.0	148.5
1250	143.0	146.5
1600	142.0	145.5
2000	138.0	141.5
OASPL	**164.0**	**167.5**

Thermal Test Procedure

A thermal survey will be performed up to 500˚F (260 ˚C) from ambient, and at every ΔT = 50˚F. Measurements will be made when reference thermocouples reach the desired temperature (center skin TC reaches desired temperature). The temperature is not expected to be uniform or the same at all transducer locations. Thermal IR imaging (video and still) of the back (IML) side will be recorded. If thermal buckling response is observed during any test condition, then additional data points may be required.

After the thermal survey, the high temperature acoustic survey (5-14) will be performed from ambient up to the max defined temperature of 500 ˚F (260 ˚C). A low level acoustic sine sweep will be performed at each temperature level. The acoustic sine sweep will be used to determine changes in test article frequencies and mode shapes with temperature.

Perform thermal only response survey at ambient acoustic conditions. Use DIC and LVDT to measure thermal deflection shape. The DIC and LVDT setups can be separate. For instance, it's expected to setup for LVDT make measurements, then remove LVDTs and setup for DIC measurement. Use thermal IR imaging to measure temperatures. Record Thermocouple data and compare to IR image data. Record IR video and stills at each thermal level.

The thermal profile to be used includes an 8 degree/second ramp rate to the target temperature. The total run time includes the ramp up period. A sample temperature profile is shown in Figure A.13.

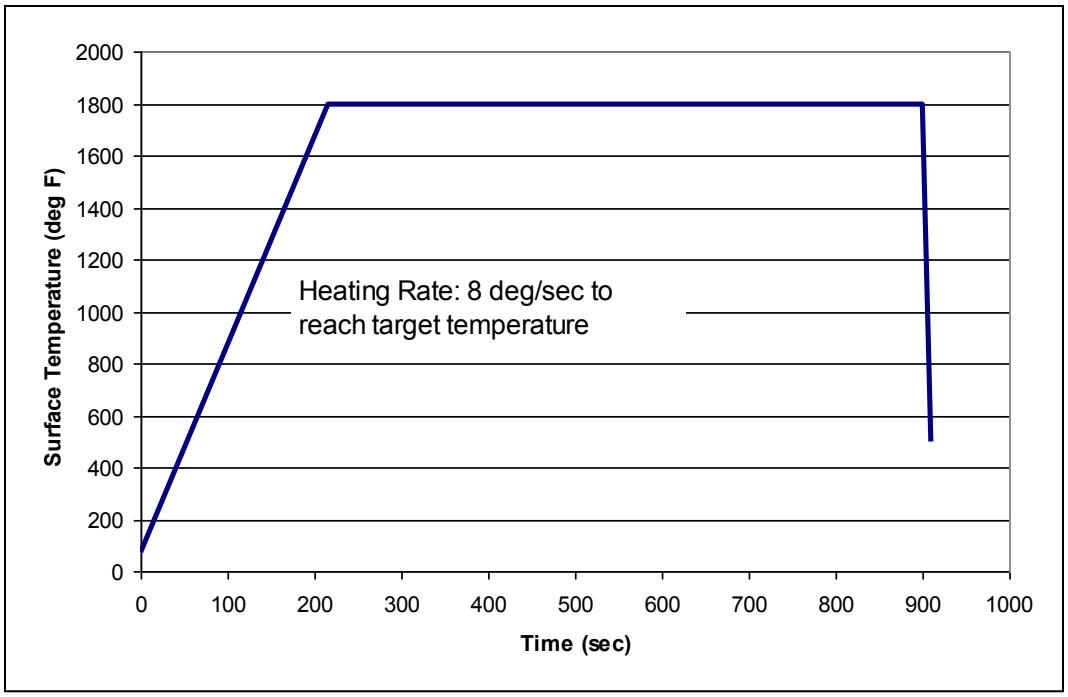

Figure A.13 – Thermal profile for thermal-structural test runs

The thermal testing will proceed as follows:

1. The test panel shall be inspected and documented in its pre-test condition.
2. The test panel shall be installed into the CEAC test fixture.
3. The lamp bank shall be positioned with the panel surface facing the heating lamps such that only the test article OML surface is heated.
4. Perform thermal only test runs. Verify the surface temperature and the back-face temperature. The specimen surface thermocouples will be used to control the lamp bank during the thermal tests. Max strain levels will also be given to AFRL such that peak thermal strains are not exceeded.
5. In the event that the thermocouples disbond from the surface or otherwise fail, a previously recorded lamp bank voltage profile can be used to continue testing. Temperature ramps should be included in time at each temperature
6. Hold temperature for 5 min after the surface TCs reach the target temperature level.
7. After maximum IML temperature 500F is reached, the test fixture and test panel shall be cooled. Post-test inspection of the test panel shall be performed by the RE with photo documentation.
8. Once all IML thermocouples approach room temperature, the test panel shall be re-verified for proper installation in the test fixture before beginning the next test run.
9. During each run, the AFRL test operator may shut down the facility immediately if any of the following should occur:
10. Panel temperatures (TC exceed 500°F) and cannot be immediately brought back under control
11. Considerable damage occurs to any part of a test article (i.e., failed attachments or cracking).
12. Any malfunction of the facility, which is normally defined by facility operational procedures. Perform complete inspection of panel if temperatures spike above planned test conditions.

13. If the test panel is still in good condition, proceed with acoustic test

A.10 Endurance Test (EDT)

After the ETS, then the Endurance Test (EDT) will be performed, Table A.3. Subject the test specimen to broadband noise per the test conditions, sequencing, exposures duration and spectra defined. All test channels will be continuously recorded. The sample rate is TBD, but it is expected to 40 kHz. Select channels of pressure, strain acceleration, and temperature will be monitored in real-time during the test on a Spectrum Analyzer. PSDs of select channels will be printed out every ½ hr during each test sequence, and all data channels will be recorded for 60 seconds.

After the first sequence, AFRL will perform an NDI. This will be a visual inspection, coin tap, and another TBD NDI inspection that will not require the specimen to be dismounted.

After the NDI test, the endurance test sequence will be repeated for an additional 4 hrs.

At the end of the second endurance test sequence, the specimen will be dismounted, all instrumentation will be removed by the lab, and a NDE will be performed. This NDE test is TBD, but it will be more than likely required dye penetrate or infrared thermography to determine any extent of damage in the titanium skins/ribs.

Deliver to Boeing all recorded data in electronic format. The final format will be agreed upon with Boeing. Also, plots of all channels at all conditions will be part of the final test documentation.

Note: At the completion of all testing, the test specimens, test fixture, and any instrumentation (unless borrowed from Boeing for this test) will be property of AFRL/RB, and do not need to be returned to Boeing.

Also, all channels should be operational to start of the acoustic testing, but it is expected that some channels will be lost during the tests. Boeing and AFRL will determine if additional instrumentation or if the data channel needs to be repaired.

Table A.3 – Endurance test sequence

Test Sequence	Acoustic Level Rel OASPL (dB) To Endurance Spectrum	Temperature Level (deg F)	Duration (Hrs)	Comment
1	0	500	4	1st Life Time
2	0	500	4	2nd Life Time

A.11 Data Requirements, Reduction, and Analysis Techniques

The data package will include post-processed time histories of all instrumentation. All data is engineering units. The data package will also include electronic and plotted PSDs of all

instrumentation during the acoustic surveys and FRF during the sine sweeps. Also, electronic and plotted Tabular data of the thermocouples will be provided.

The data should be provided on DVDs or an external USB hard drive (which would be returned to AFRL).

The AFRL Laboratory Technical Memorandum will include the following,

a. Chronological Test Log.
b. Photographs and schematic of the test setup and instrumentation locations.
c. Modal survey results including the resonant frequencies, mode shapes, damping factors and frequency response functions.
d. List of DAQ parameters for each channel. Calibration constants, sensitivity settings, data ranges, sample rates, filtering, etc.
e. All recorded data in digital format. This includes the complete time histories in engineering units. The data for each test point will be stored in separate files. The data will be converted to proper engineering units.

A.12 Support and Participation

The AFRL will be responsible for conducting the test, running the test facility, performing any safety and facility certification, installing the test specimen in the test fixture, installing the test article in the test facility, recording all data (DAQ), reducing data as required, installing instrumentation as specified.

Boeing Research and Technology (BR&T) will coordinate AFRL and witness all testing.

A.13 Facilities

All tests will be conducted at the AFRL test lab facilities at WPAFB in Dayton OH.

A.14 Security and Data requirements

This test and all data will be unclassified. The final Lab Report will not have Boeing Proprietary restrictions. Also, all data should be considered ITAR/Export Controlled until the USAF makes a determination otherwise.

A.15 References

A1. Applied Nonlinear Low Order Response Prediction Methods Evaluation, AFRL-RB-WP-TR-2009-3100, Final Report, May 2009.
A2. Nonlinear Low Order Reduced Order Modeling Applications and Demonstration, SOO, RT-09-298-0000/BAS 6727, August 24, 2009

Appendix B. T-58 Test Plan

B.1 Introduction

This validation test will be conducted as part of the Air Vehicle Integration and Technology Research (AVIATR) Delivery Order 13, Nonlinear Low Order Reduced Order Modeling Applications and Demonstration (NLROM II). This task is focused on the application of nonlinear low order structural response methodologies to predict the structural response of a representative aircraft structure to verify to the results.

In Phase I, the AFRL NLROM methodology was implemented and evaluated. The results from Phase I can be found in reference (B1). Where it was analytically demonstrated that an 8x-100x improvement in computational efficiency while retaining the accuracy of full order nonlinear response analyses. The accuracy is critical because linear analysis methods in wide use today tend to overestimate response for most parts of a structure while underestimating or entirely missing critical stress hot spots. The result is overweight structures with critical deficiencies in design details that then suffer premature fatigue cracking. The improvement in analysis efficiency is just as critical because full order nonlinear analyses are simply not practical for large finite element models representing today's aircraft structures.

For Phase II, the NLROM methodology will be validated against test data for representative aircraft structure under thermal/acoustic loading. Refer to reference (B2). The representative aircraft structure is a full-scale blown Trailing Edge Flap (TEF). The validation testing will consist of two tests. The first test will be a progressive wave facility test in the AFRL Combined Environment Acoustic Chamber (CEAC) facility. The second test will be in the Boeing/T-58 Engine Burner Facility (EBF). The Boeing Engine Burner Facility will expose a second test article to the exhaust of a jet engine providing an entirely realistic test environment including combined thermal, acoustic and pressure loading for further validation. This Test Plan covers the Boeing T-58 EBF testing.

B.2 Objective

Our objective for this test is to accurately measure the thermal/acoustic loads and response of test article and the structural dynamics characteristics of the test article under applied thermal loads. Hence, this test article will have instrumentation and measurement systems in place to capture this data. The measured loads test data will be used to verify the thermal/acoustic loads for the predictions. The modal test data will be used to correlate the structural finite element model. The measured response data will then be used to validate the nonlinear reduced order response and full-order analyses to the measured test data. The quantification of uncertainty in all measurements will also be critical in the validation task. The uncertainty analysis will be a post-test activity but the test planning, data acquisition, sensor calibration, etc, will be important for this uncertainty quantification task.

Table B.1 – Objectives and success criteria

Objectives	Success Criteria
Measure the resonant frequencies, damping, and mode shapes of the skin panel with the test frame adapter as installed in the CEAC and T-58 test facility.	Definition of the natural frequencies, damping factors and mode shapes of panel in the fixture mounted in the test facility. These modes will be consistent with the analysis model modes.
Determine the thermal and acoustic loads and response of the flap skin panel at various temperatures and acoustic levels, and/or engine speeds.	Measure time history, PSDs, CSDs, RMS values, average statistics of the critical instrumentation for every test condition.
Perform acoustic durability tests at temperature and measure response.	Complete the fatigue test portion of the test program, measure response and loads throughout testing, record all data channels

B.3 Scope

This detailed test plan (DTP) describes the thermal/acoustic testing to be performed in the Boeing T-58 Engine Burner Facility located in St. Louis, B102 laboratory complex. The actual facility operations and related procedures will be the responsibility of BTandE personnel. The test article fabrication, test panel assembly, test panel instrumentation (strain gauges) and the delivery are BR&T responsibilities. Installation of the test panels to the individual test facilities and instrumentation interface to the data acquisition systems are BTandE responsibility. Changes to this plan which are within the scope of the test, may be made by "Redline" changes approved by the BTandE Responsible Engineer (RE), and documented within this DTP.

B.4 Handling of Test Panels

Boeing St. Louis test personnel will install the test panel to the test fixture and Responsible Engineer (RE) or an authorized delegate will inspect the installation prior to testing. All pre-test and post-test observations of the test panel shall be documented in a Laboratory Notebook by the RE.

Notice of Test – The RE shall be notified in advance of any scheduled test. Changes to the schedule shall be made in conjunction with Project Engineer.

Photographs – A digital camera will be used to photograph test articles before and after tests, as needed.

Inspection – The RE or authorized delegate shall conduct a complete visual inspection before and after each test run to determine any changes.

Disposition of Test Hardware – At the completion of testing, all test specimens will be cleaned. The Test Article will be sent to B245, for shipping to USAF.

Report – Thermal and Structures Lab shall provide a test data package within 10 days after completion of the test program. Although a formal report is not required. Lab notes are required.

Changes – Changes to this plan which are within the scope of the test may be made by "Redline" changes approved by the Responsible Engineer, and documented in a Laboratory Notebook.

B.5 Engine Exposure Instrumentation

Various types of instrumentation were used to meet the objectives of this test program. The list is given in Table B.2, below.

Table B.2 – T-58 test instrumentation list

Type	Total Number	Notes
Accelerometers	9	What is temp limit?
Disp Probes	2	Mount to stiffeners
Strain gages	26	20 high temp and 6 lower temp
Microphones	6	Water cooled mounted on fixture or stand
Thermocouples	19	See chart
Pressure	6	See chart
IR Camera	1	Upper skin imaging

B.6 Thermal Instrumentation

The thermal instrumentation will include IML side thermocouples (TC), Figure B.1. An IR camera will be used for the OML temperature measurements. The TC array is shown in the figure below. The RE can adjust TC placement to best locate a transducer for ease of installation. Final placement of all TC will be documented.

In addition, an infrared camera will be focused on the top side (OML) of the test panel. For the first 10 minutes of each run, the IR camera will take images every second. For the remainder of each run, the IR camera will take images every 10 seconds (The RE can adjust this required as required.) The data will be processed to produce temperatures at or near the seven thermocouple locations. A video camera will be used to record each test.

Exhaust gas temperatures (EGTs) will be measured during each run using the engine's internal EGT thermocouple array, located just downstream of the turbine.

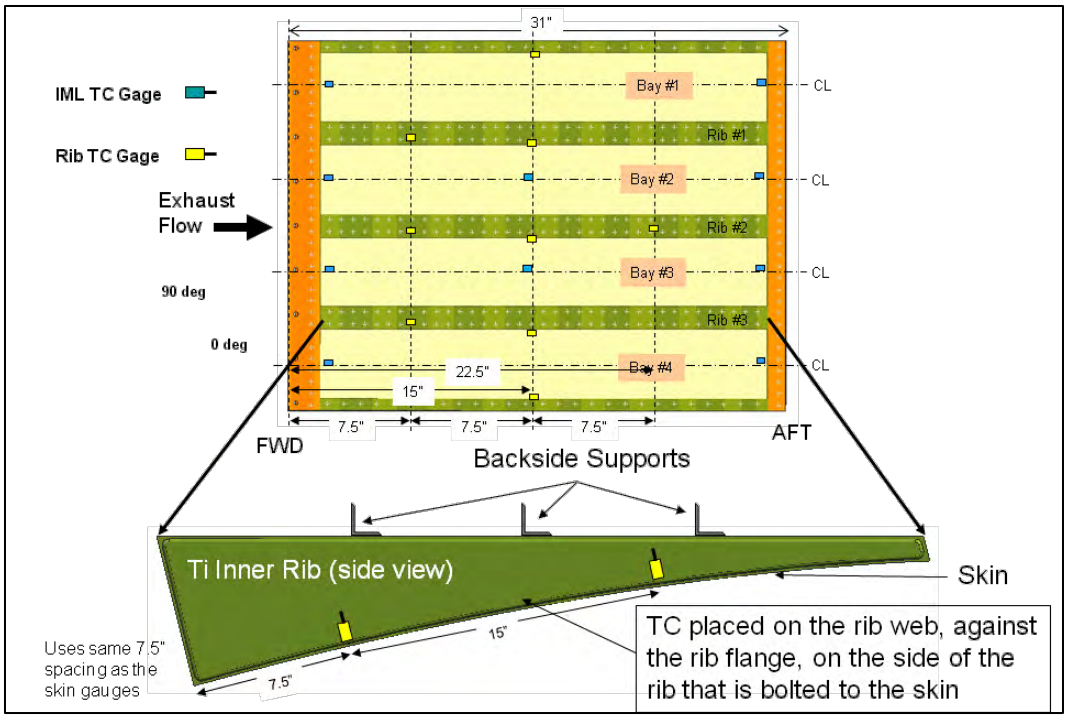

Figure B.1 – T-58 test thermocouple layout

B.7 Pressure and Acoustic Instrumentation

The static and dynamic pressure (acoustic) loads will also be measurement using (six) water cooled microphones and (six) recessed pressure taps placed as shown in the Figure B.2 and Figure B.3. The Thermal lab will design and fabricate the required mounting for the side of the fixture mounting locations.

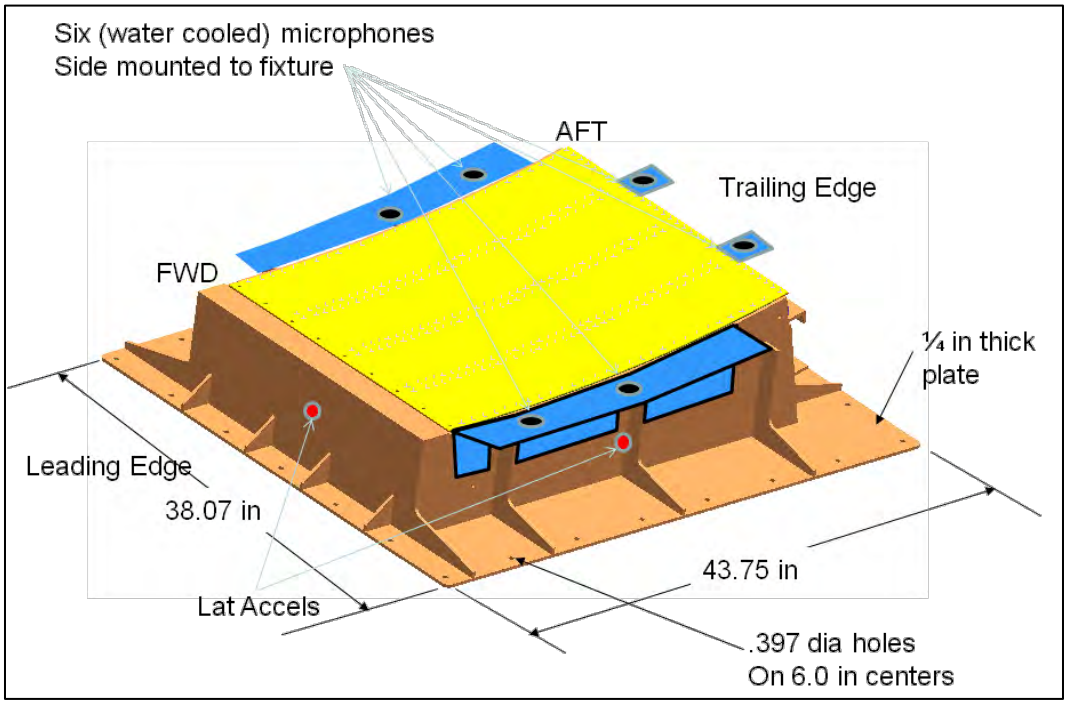

Figure B.2 – T-58 test microphone layout

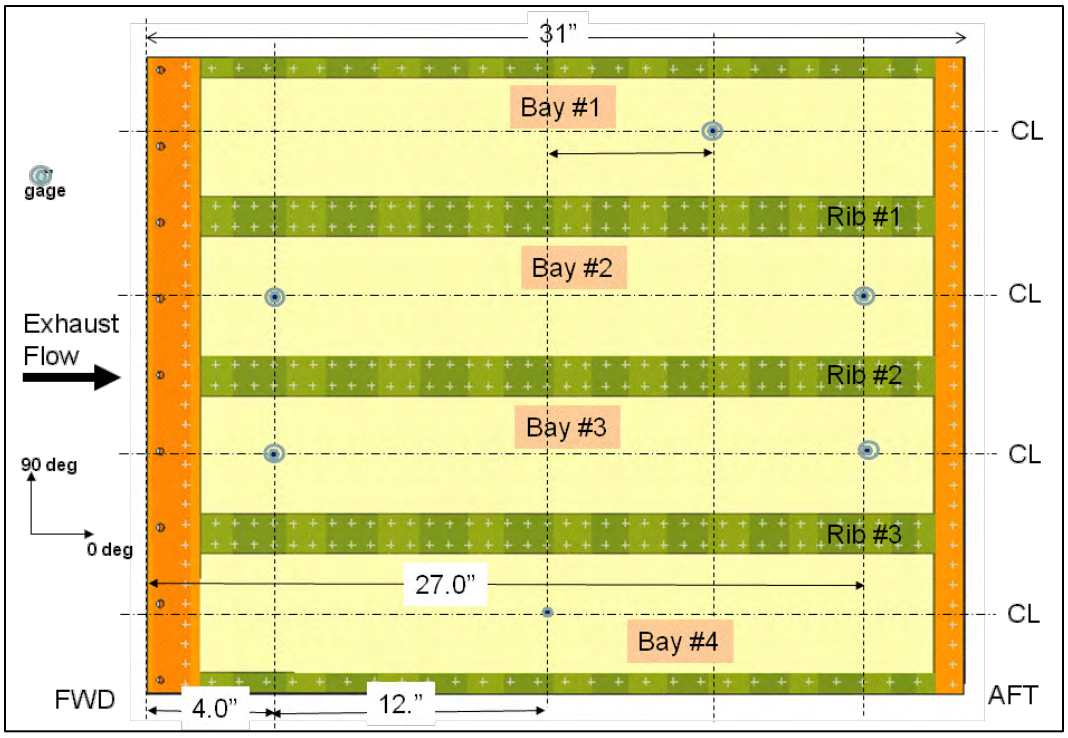

Figure B.3 – T-58 test static pressure layout

B.8 Structural Response Instrumentation

The structural response will be measured using strain gauges, accelerometers, and non contacting displacement probes. The 26 strain gauges have been installed by the structures lab as shown in the Figure B.4 and Figure B.5 below.

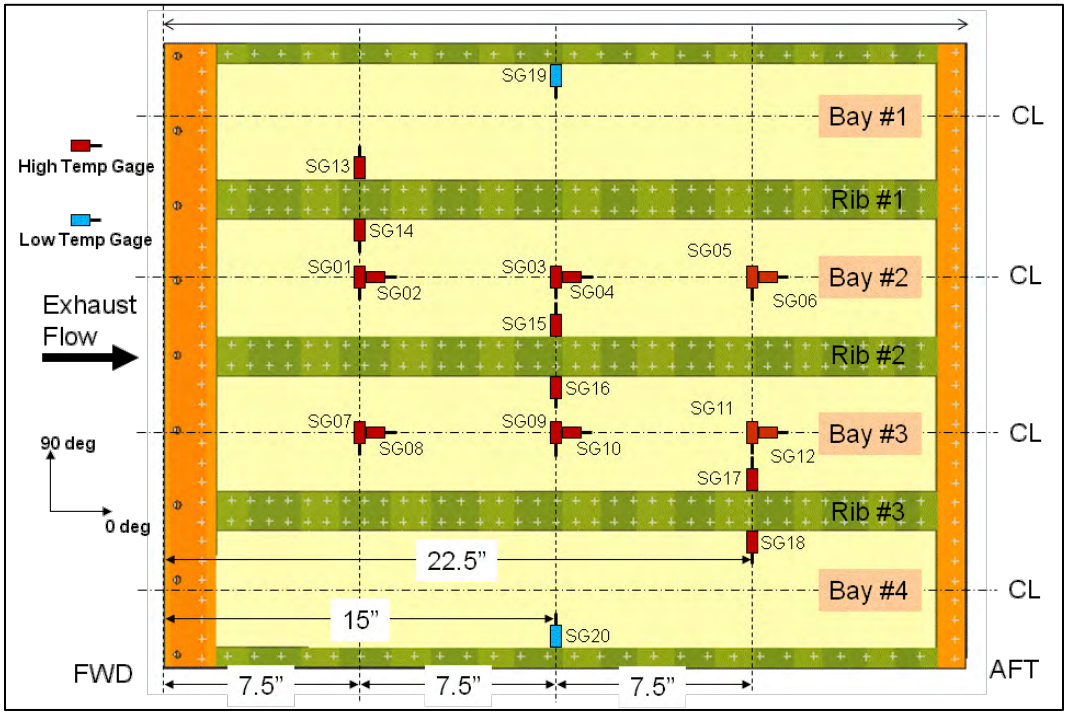

Figure B.4 – T-58 test strain gauge layout

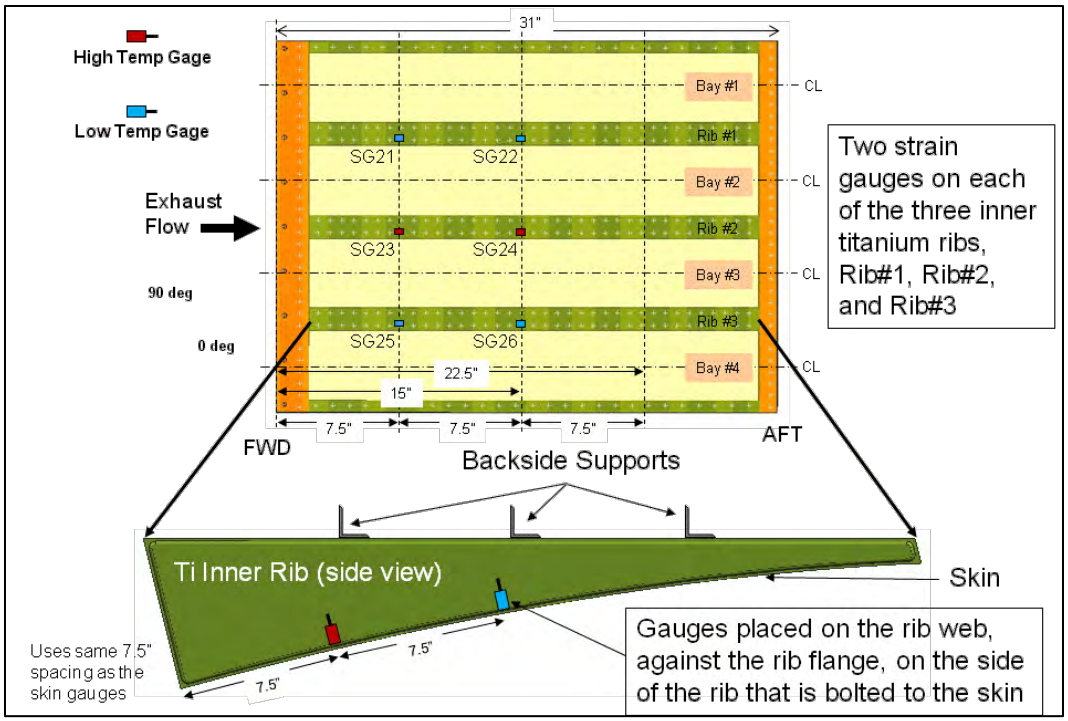

Figure B.5 – Rib strain gauges

Also a set of accelerometers and displacements transducers will be used to measure response. These are shown in the Figure B.6. The (six) rib accelerometers will be mounted to measure normal and lateral excitation as shown, and the (two) fixture accelerometers will be tri-axial accelerometers to measure the overall motion of the test setup. Finally, (two) displacement probes will be mounted on the middle stiffener to measure the skin displacement.

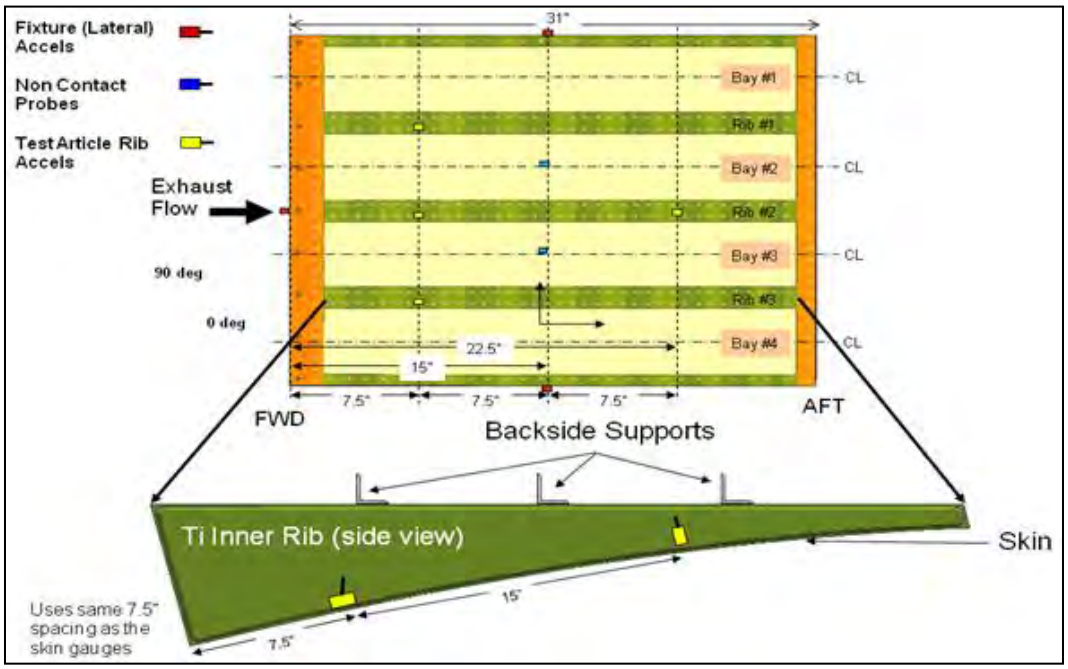

Figure B.6 – Accelerometer and displacement probe locations

B.9 Test Setup

The test setup is shown in Figure B.7. Two setups will be used to simulate zero degree and 10 degree flap orientation. The ten degree setup is shown below.

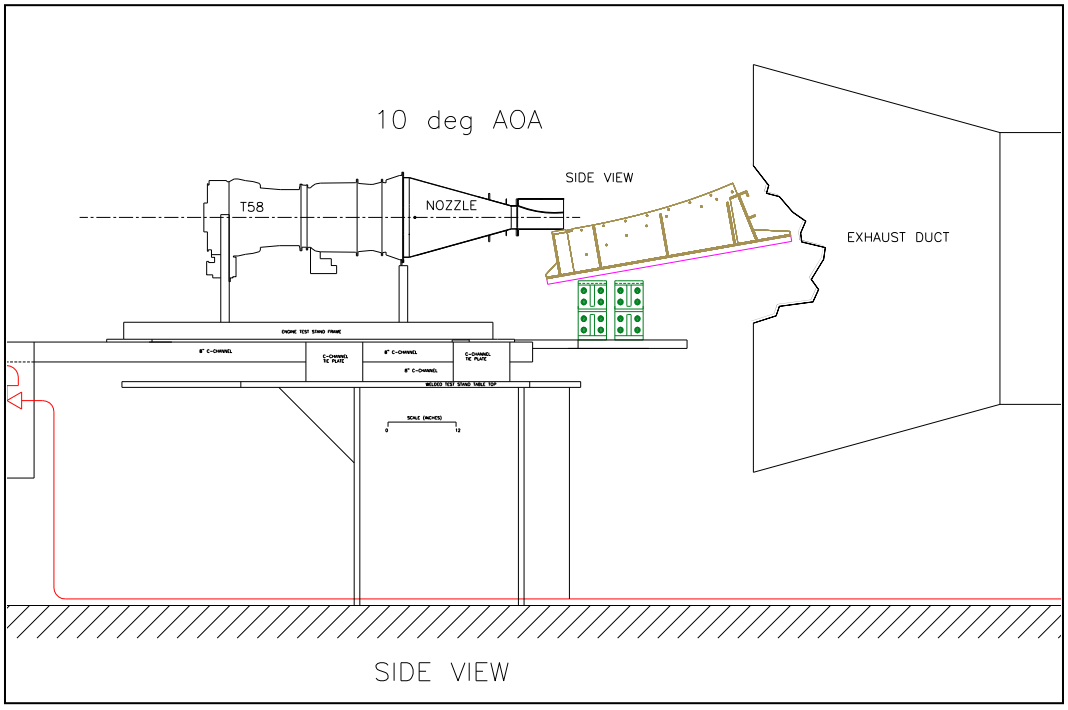

Figure B.7 – Test panel and fixture mounted behind T-58 engine

B.10 Engine Exposure Test Approach

For the EBF test, the objective is to collect response data at realistic engine flow conditions. The primary test setting is engine speed (85% of max rpm). The thermal/acoustic environment is a function of engine speed and distance from the exit nozzle. The goal will be to simulate the C-17 flap environment (max temperature 550 F, and OASPL = 166dB), but we will allow for a range of possible conditions by measuring data at different engine speeds from 50% rpm to 98% rpm (Engine Environment Survey Test).

In general, we don't want to over stress the test article (i.e., temperature > 850 F, and acoustic levels > 172 dB). First, we will collect data at several lower speeds. Then, we will proceed to high engine speeds to increase the thermal and acoustics loads, and obtain response data at these higher levels. An extended long duration test (4 hrs) at 85% engine speed will follow the engine environment survey testing.

<u>Engine Exposure Test Procedures</u>
Each test will proceed as follows:

1. Inspect, photograph, and document the test panel in its pre-test condition.
2. Attach the test panel to the test fixture. The RE shall verify panel and fittings after fixture attachment.

3. After each test sequence, visually inspect for cracks and perform tap tests to detect potential damage. Remove from test fixture and inspect flanges for damage. Document any anomalies.
4. If visible cracks, erosion, or other clearly apparent damage is observed, the testing will be stopped for engineering evaluation. Otherwise, testing will proceed with the next cycle.
5. During any cycle, the RE or test operator may shut down the facility immediately if any of the following should occur:
6. Surface temperature exceeds (1300°F) and cannot be immediately brought back under control
7. Considerable damage occurs to any part of the test article (i.e., delamination, failed attachments).
8. Any malfunction of the facility, which is normally defined by facility operational procedures.
9. Perform Modal Survey (Structural Dynamics Lab – RE Tony Hauenstein)

10. The Test Panel will be inspected by NDI Lab after test completion for post exposure evaluation (NDI and Mechanical properties).

B.11 Test Conditions

The test conditions are shown below in Table B.3. The 10°F case will be tested first. An idle (min engine speed) soak will be the first test. Then, the engine speed will be increased at increments of approximately 5%. The RE can adjust the test setting as required. The Max engine speed is 85% for the initial response survey. This first survey is critical. The RE is to make sure that all instrumentation is working properly, and being properly recorded. The high level survey will start after the test article has been inspected, and after a review of the initial low level survey test data. If the there is no damage and sufficient transducers are still working, then the 0°F setup will be performed.

Table B.3 – T-58 test proposed test matrix

Config	Test Cond #	Engine Speed	Duration (min)	Heat Flux BTU/ft2-s	Acoustic Load OASPL	EGT deg F	Comments/Instructions/Misc
	Environment Survey - Low Level						
10 deg	1	55	20	6.7	145	850	All channels, IR pictures every 5 mins, 60 sec of high rate data
	2	60	10	6.7	148	850	All channels, IR pictures , 60 secs of high rate data
	3	65	10	6.7	151	850	All channels, IR pictures , 60 secs of high rate data
	4	70	10	6.7	154	850	All channels, IR pictures , 60 secs of high rate data
	5	75	10	6.7	157	850	All channels, IR pictures , 60 secs of high rate data
	6	80	10	6.7	160	850	All channels, IR pictures , 60 secs of high rate data
	7	85	10	6.7	165	850	All channels, IR pictures , 60 secs of high rate data
	Cool Down						Visual Inspect
	Environment Survey - High Level						
	8	55	20	6.7	145	850	All channels, IR pictures every 5 mins, 60 sec of high rate data
	9	80	5	6.7	160	800	All channels, IR pictures , 60 secs of high rate data
	10	85	5	6.7	165	900	All channels, IR pictures , 60 secs of high rate data
	11	90	5	6.7	166	1000	All channels, IR pictures , 60 secs of high rate data
	12	95	5	6.7	167	1050	All channels, IR pictures , 60 secs of high rate data
	13	98	5	6.7	168	1100	All channels, IR pictures , 60 secs of high rate data
	Durability Test						
	14	85	240	6.7	165	850	All channels, IR pictures every 15 mins, 60 sec of high rate data every 15 mins.
							Inspection
0 Deg							
	Environment Survey - Low/High Level						
	15	55	20	6.7	145	850	All channels, IR pictures every 5 mins, 60 sec of high rate data
	16	60	5	6.7	148	850	All channels, IR pictures , 60 secs of high rate data
	17	65	5	6.7	151	850	All channels, IR pictures , 60 secs of high rate data
	18	70	5	6.7	154	850	All channels, IR pictures , 60 secs of high rate data
	19	75	5	6.7	157	800	All channels, IR pictures , 60 secs of high rate data
	20	80	5	6.7	160	800	All channels, IR pictures , 60 secs of high rate data
	21	85	5	6.7	165	900	All channels, IR pictures , 60 secs of high rate data
	22	90	5	6.7	166	1000	All channels, IR pictures , 60 secs of high rate data
	23	95	5	6.7	167	1050	All channels, IR pictures , 60 secs of high rate data
	24	98	5	6.7	168	1100	All channels, IR pictures , 60 secs of high rate data
	Cool Down						Final Inspection

Config	Test Cond #	Engine Speed	Duration (min)	Heat Flux BTU/ft2-s	Acoustic Load OASPL	EGT deg F	Comments/Instructions/Misc
	Environment Survey - Low Level						
10 deg	1	55	20	6.7	145	850	All channels, IR pictures every 5 mins, 60 sec of high rate data
	2	60	10	6.7	148	850	All channels, IR pictures , 60 secs of high rate data
	3	65	10	6.7	151	850	All channels, IR pictures , 60 secs of high rate data
	4	70	10	6.7	154	850	All channels, IR pictures , 60 secs of high rate data
	5	75	10	6.7	157	850	All channels, IR pictures , 60 secs of high rate data
	6	80	10	6.7	160	850	All channels, IR pictures , 60 secs of high rate data
	7	85	10	6.7	165	850	All channels, IR pictures , 60 secs of high rate data
	Cool Down						Visual Inspect
	Environment Survey - High Level						
	8	55	20	6.7	145	850	All channels, IR pictures every 5 mins, 60 sec of high rate data
	9	80	5	6.7	160	800	All channels, IR pictures , 60 secs of high rate data
	10	85	5	6.7	165	900	All channels, IR pictures , 60 secs of high rate data
	11	90	5	6.7	166	1000	All channels, IR pictures , 60 secs of high rate data
	12	95	5	6.7	167	1050	All channels, IR pictures , 60 secs of high rate data
	13	98	5	6.7	168	1100	All channels, IR pictures , 60 secs of high rate data
	Durability Test						
	14	85	240	6.7	165	850	All channels, IR pictures every 15 mins, 60 sec of high rate data every 15 mins.
							Inspection
0 Deg							
	Environment Survey - Low/High Level						
	15	55	20	6.7	145	850	All channels, IR pictures every 5 mins, 60 sec of high rate data
	16	60	5	6.7	148	850	All channels, IR pictures , 60 secs of high rate data
	17	65	5	6.7	151	850	All channels, IR pictures , 60 secs of high rate data
	18	70	5	6.7	154	850	All channels, IR pictures , 60 secs of high rate data
	19	75	5	6.7	157	800	All channels, IR pictures , 60 secs of high rate data
	20	80	5	6.7	160	800	All channels, IR pictures , 60 secs of high rate data
	21	85	5	6.7	165	900	All channels, IR pictures , 60 secs of high rate data
	22	90	5	6.7	166	1000	All channels, IR pictures , 60 secs of high rate data
	23	95	5	6.7	167	1050	All channels, IR pictures , 60 secs of high rate data
	24	98	5	6.7	168	1100	All channels, IR pictures , 60 secs of high rate data
	Cool Down						Final Inspection

B.12 Data Requirements

All dynamic data channels will have a high sample rate of (20 kHz) (except thermocouples and static pressure). Data records will be 60 seconds long for each. This data saved as ASCII time history files or some other convenient format to be determined.

The data package will include post-processed time histories of all instrumentation. All data is engineering units. The data package will also include electronic and plotted PSDs of all instrumentation during the acoustic surveys and FRF during the sine sweeps. Also, electronic and plotted Tabular data of the thermocouples will be provided.

The data should be provided on DVDs or available on a data server.

The Laboratory Technical Memorandum will include the following:

- Chronological Test Log.
- Photographs and schematic of the test setup and instrumentation locations.
- Modal survey results including the resonant frequencies, mode shapes, damping factors and frequency response functions.
- List of DAQ parameters for each channel. Calibration constants, sensitivity settings, data ranges, sample rates, filtering, etc.
- All recorded data in digital format. This includes the complete time histories in engineering units. The data for each test point will be stored in separate files. The data will be converted to proper engineering units.

B.13 Security and Data Handling

This test and all data will be unclassified. The final Lab notes will be Boeing Proprietary restrictions. Also, all data should be considered ITAR/Export Controlled.

B.14 Reference Documents

B1. Applied Nonlinear Low Order Response Prediction Methods Evaluation, AFRL-RB-WP-TR-2009-3100, Final Report, May 2009.

B2. Nonlinear Low Order Reduced Order Modeling Applications and Demonstration, SOO, RT-09-298-0000/BAS 6727, August 24, 2009

Appendix C. T-58 Test Summary

C.1 Introduction

The Boeing Engine Test Facility (ETF) was utilized to provide testing support for Phase II testing of the Air Vehicle Integration and Technology Research (AVIATR) Delivery Order 13, Nonlinear Low Order Reduced Order Modeling Applications and Demonstration (NLROM II). The Engine Test Facility was used to expose a NLROM test article to the exhaust of a jet engine, providing a test environment that included combined thermal, acoustic and pressure loading.

A primary objective for the test was to accurately measure the thermal and acoustic loads, as well as the structural dynamic characteristics, of the test article under applied test environment. As such, this test article was extensively instrumented, and measurement systems were put in place to capture this data.

C.2 Facility Description

The Boeing ETF is part of the Arc Heater Laboratory (AHL) which is located in Building 102 of the Boeing St. Louis complex and is part of the Boeing Test and Evaluation (BTandE) group. The facility is outfitted with a surplus T58 turbo shaft helicopter engine, manufactured by General Electric Company. The T58 was previously modified by removal the "free" power turbine, and modification of the third stage nozzle.

For this test series, the ETF was configured with a two dimensional (2D), rectangular exit nozzle. The 2D nozzle exit utilizes a choked throat, providing a slightly super-sonic exhaust flow at "cruise" power settings. The nozzle exit dimensions are approximately 14 inches wide by 2.73 inches high. The throat height is 2.69 inches.

When fitted with the 2D nozzle, the engine supplies a thermal/acoustic environment that is similar to that produced in much larger "dry" aircraft exhaust systems.

Operating characteristics of the facility include:

- Approximately 12 pounds per second of exhaust gas flow at 98.5% speed setting
- Exhaust gas temperature $\leq$ 1150 ºF
- Nozzle pressure ratio of slightly less than 2:1
- 165-170 dB acoustic energy
- High flow auxiliary (e.g. bypass) air sources available within the test cell at ambient or heated conditions
- Thermal imaging IR cameras for non-contact temperature measurements
- Modern PC-based data acquisition/processing systems

C.3 Test Article Instrumentation

The test panel instrumentation included strain gauges, thermocouples, pressure ports, accelerometers, and microphones. Micro-Measurements WK-06-125AD-350 general purpose linear pattern strain gauges were bonded to the test panel in the locations shown in Figure C.1 and Figure C.2. The strain measurement portion of these gauges measured 0.125" by 0.125". The maximum rated temperature for this type of gauge is 450 ºF.

The 350 ohm WK-06-125AD-350 K-alloy gauges were fully encapsulated as-supplied, and were bonded to the panel using Micro-Measurements "M-Bond 610" two-component, epoxy-phenolic strain gauge adhesive. Gauge bonding was accomplished per Micro-Measurements instruction bulletin B-130. M-Bond 610 adhesive was also applied over the topside of the gauges. All gauge terminations were silver soldered to fiberglass-insulated extension leads. Micro-Measurements ZC-NC-G1262-120 high temperature linear pattern strain gauges were applied to the test panel in the locations shown in Figure C.1 and Figure C.2. The strain measurement region of these gauges measured 0.076" by 0.062".

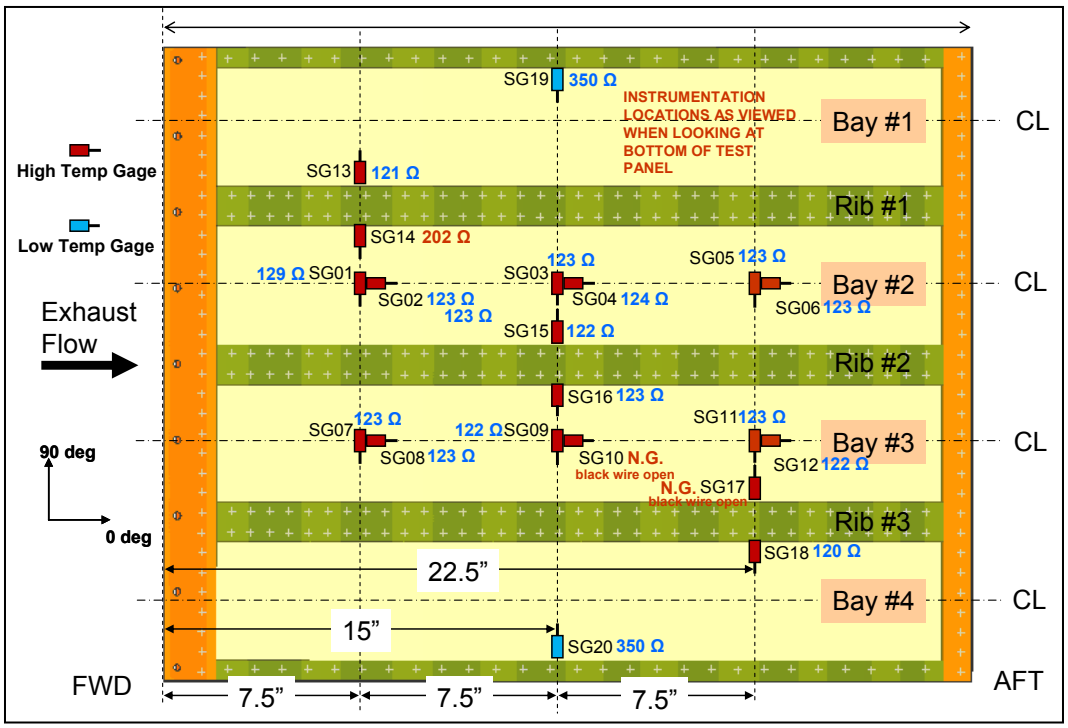

Figure C.1 – Strain gauge placement (skin, backside)

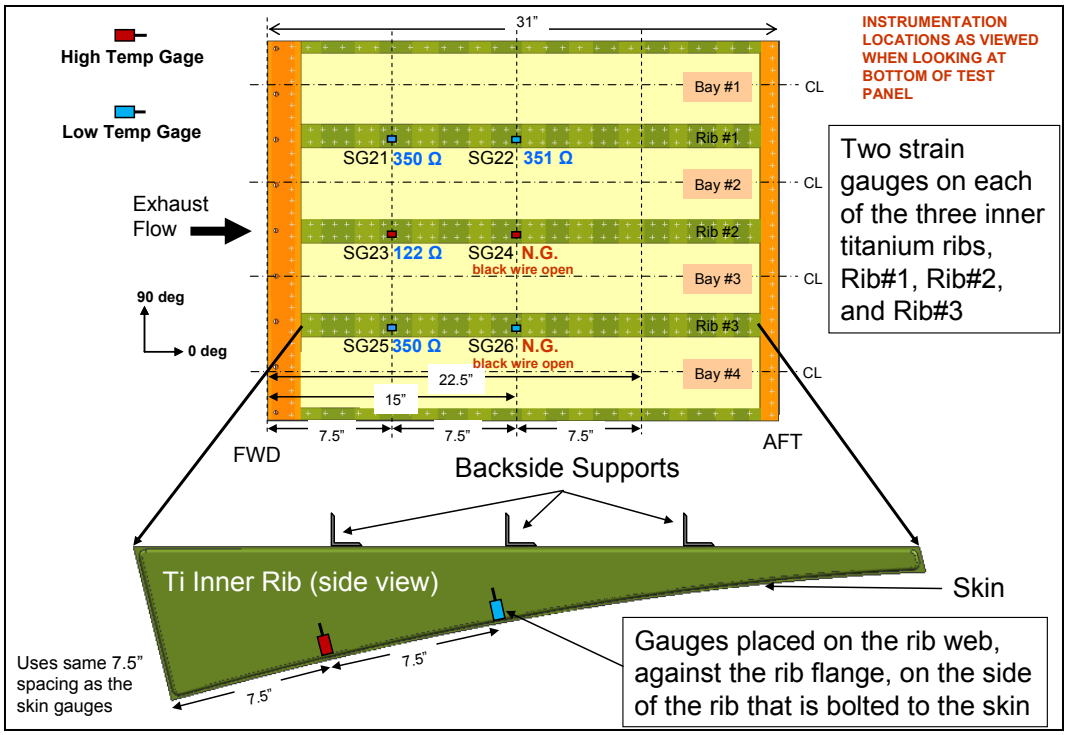

Figure C.2 – Strain gauge placement (rib side)

The120 ohm ZC-NC-G1262-120 gauges were etched Kanthal (Fe-Cr-Al alloy) foil grids in a free-filament form. The gauges were bonded to the panel using Micro-Measurements "Type H" ceramic cement, per the Micro-Measurements product instructions.

Pressure instrumentation included six static pressure measurements, which were integrated into the test panel per the locations shown in Figure C.3. The installation process involved marking the approximate location of the pressure port on the test panel, and then drilling a 0.063" clearance hole in the panel for the installation of 0.063" OD capillary tubing. Capillary tubes for each measurand were positioned in the clearance holes so as to have the measurement end of the tube sit flush with, or slightly below the flow surface of the panel. The capillary tubes were secured to the backside (non-flow side) of the titanium panel using Nichrome strips, which were tacked-welded directly to the backside surface of the titanium. Thermocouple instrumentation locations are shown in Figure C.4. A total of nineteen thermocouples were attached to the test panel. Twenty-eight gauge fiberglass insulated type "K" duplex thermocouple wire was utilized to make the thermocouples.

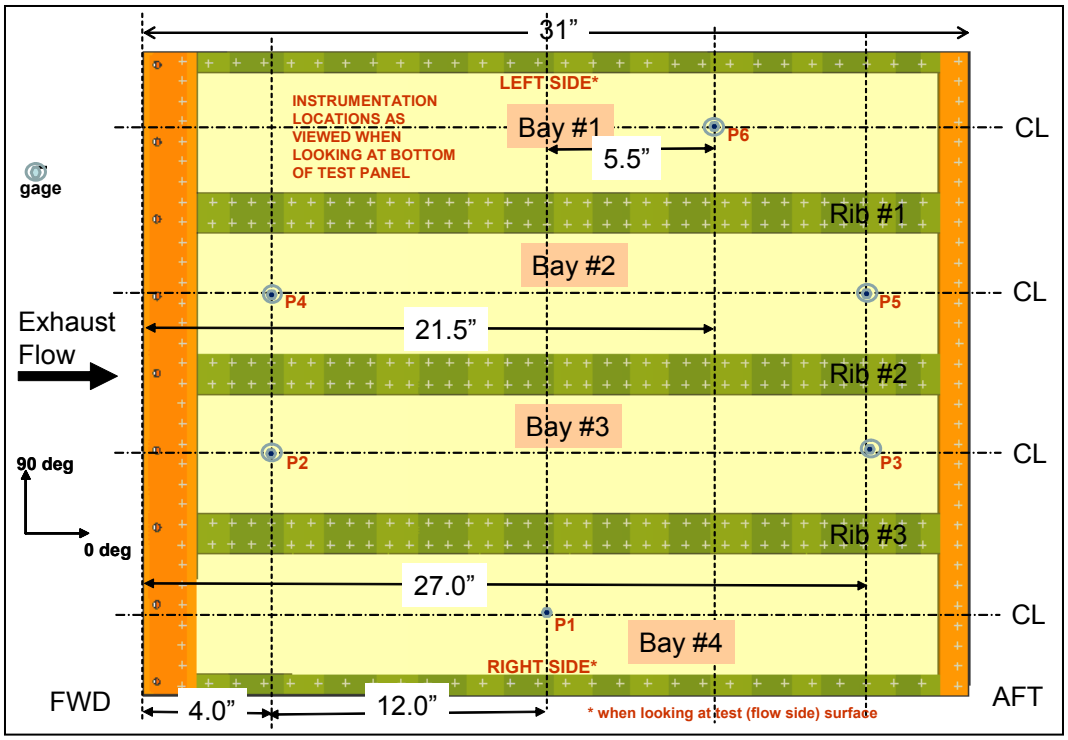

Figure C.3 – Static pressure measurements

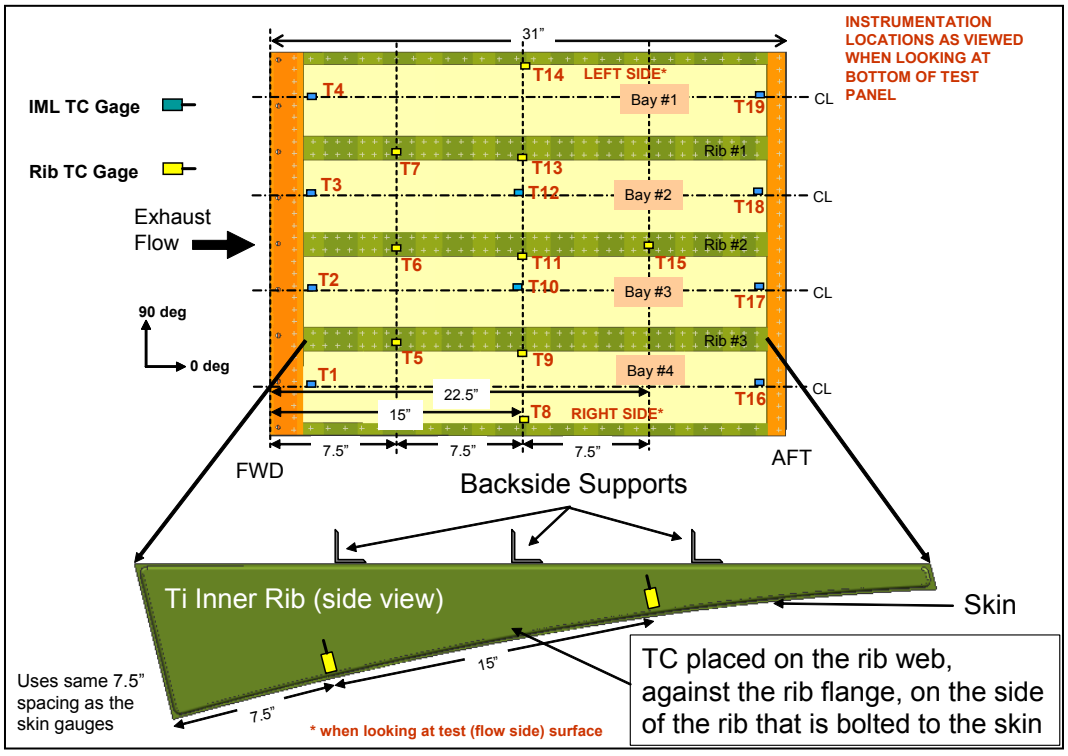

Figure C.4 – Thermocouple locations

To make the thermocouples, approximately ¼” of fiberglass insulation was stripped back at the thermocouple junction end of the duplex wire. These wire pairs were then directly tack-welded to the titanium panel to make the thermocouple junction, using the titanium itself as an “intermediate” metal conductor. The fiberglass duplex wires were further secured to the titanium

panel at discrete intervals using Nichrome strips, which were also tack-welded to the backside of the titanium panel.

A photo showing installed strain, thermocouple and pressure instrumentation is presented in Figure C.5. Steel wall extensions were attached to the outboard edges of the test article support fixture for the purpose of mounting water-cooled microphone holders and obtaining acoustic data. These extensions were located on the left- and right-hand sides (pilot's perspective) of the support fixture, as well as at the trailing edge of the fixture. PCB model 112A21 pressure sensors/microphones were installed in the water-cooled holders to obtain sound pressure measurements. The left- and right-hand wall extensions contained two microphones each. Two extensions at the trailing edge contained one microphone each. The locations of the microphones, and photos of the wall extensions and water-cooled holders, are shown in Figure C.6 through Figure C.8.

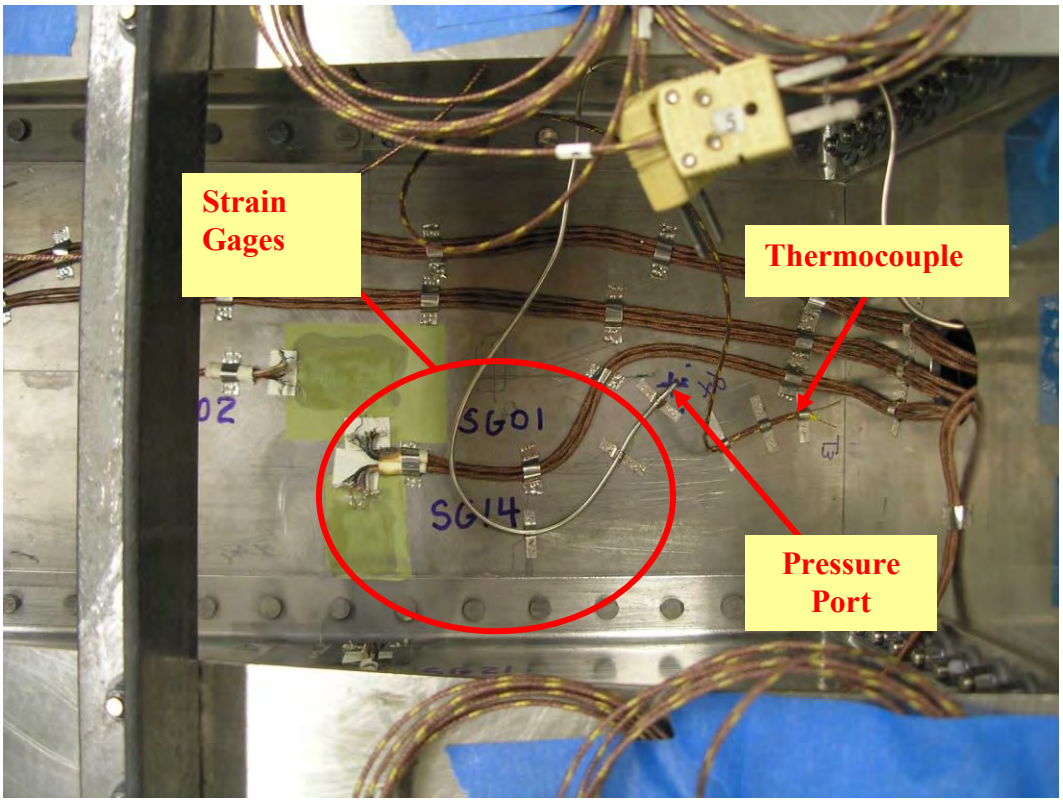

Figure C.5 – Installed strain, thermocouple, and pressure instrumentation

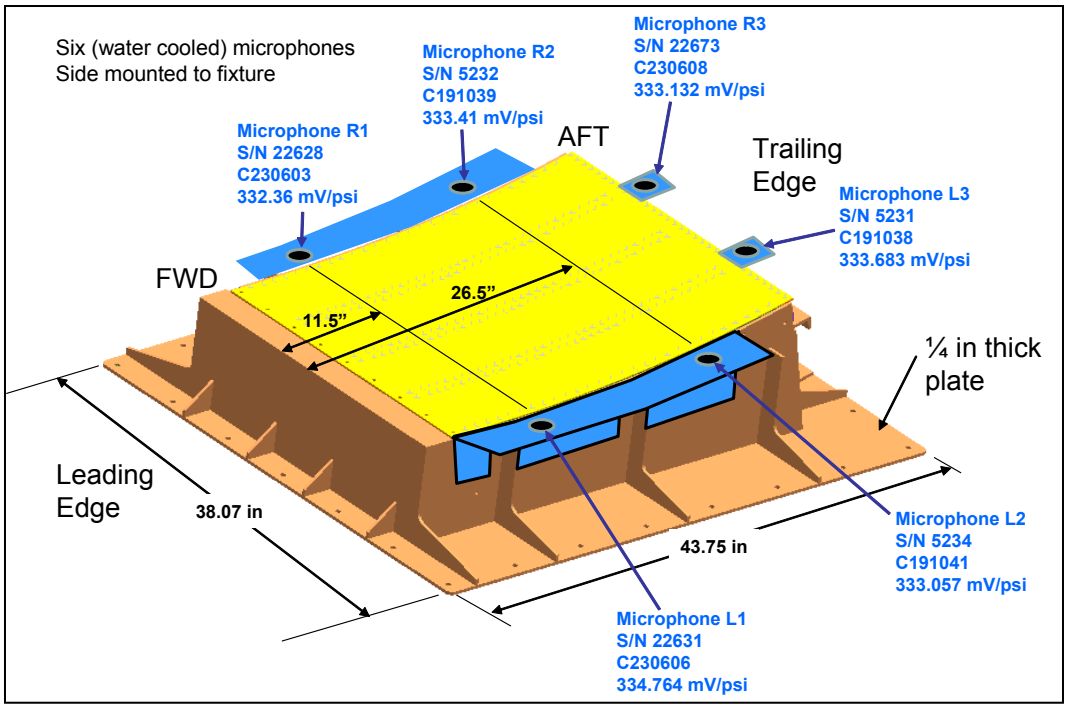

Figure C.6 – Water-cooled microphone locations

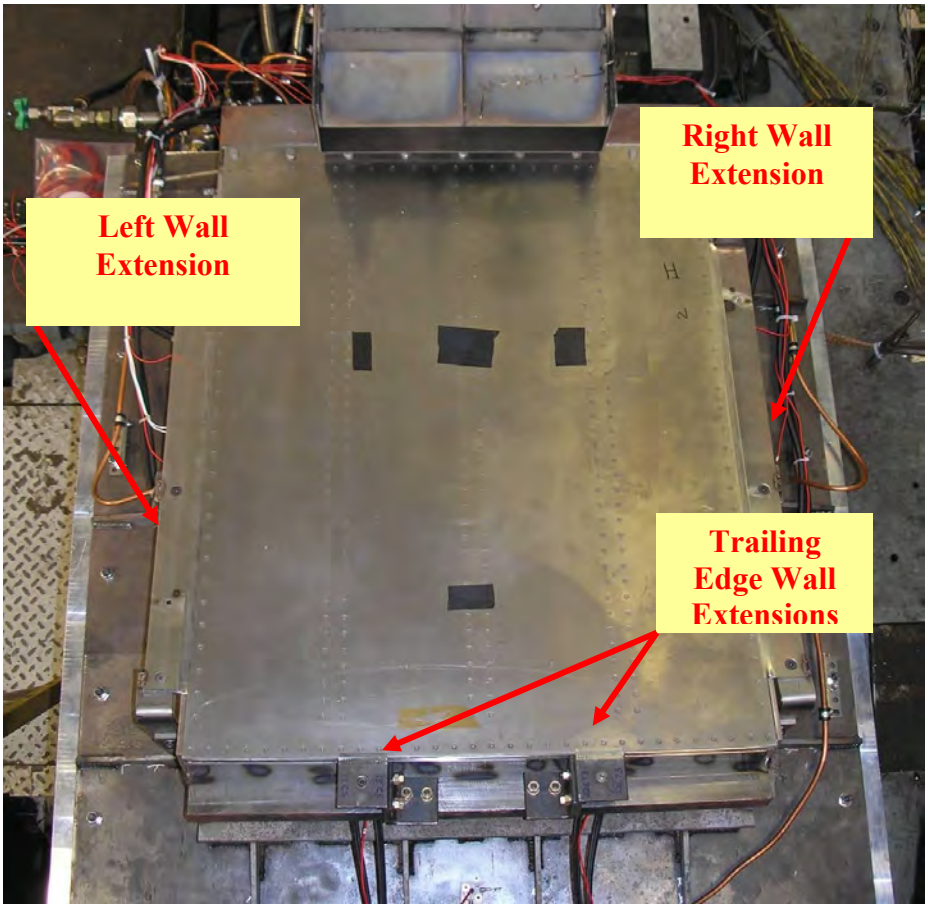

Figure C.7 – Wall extensions and microphone photo

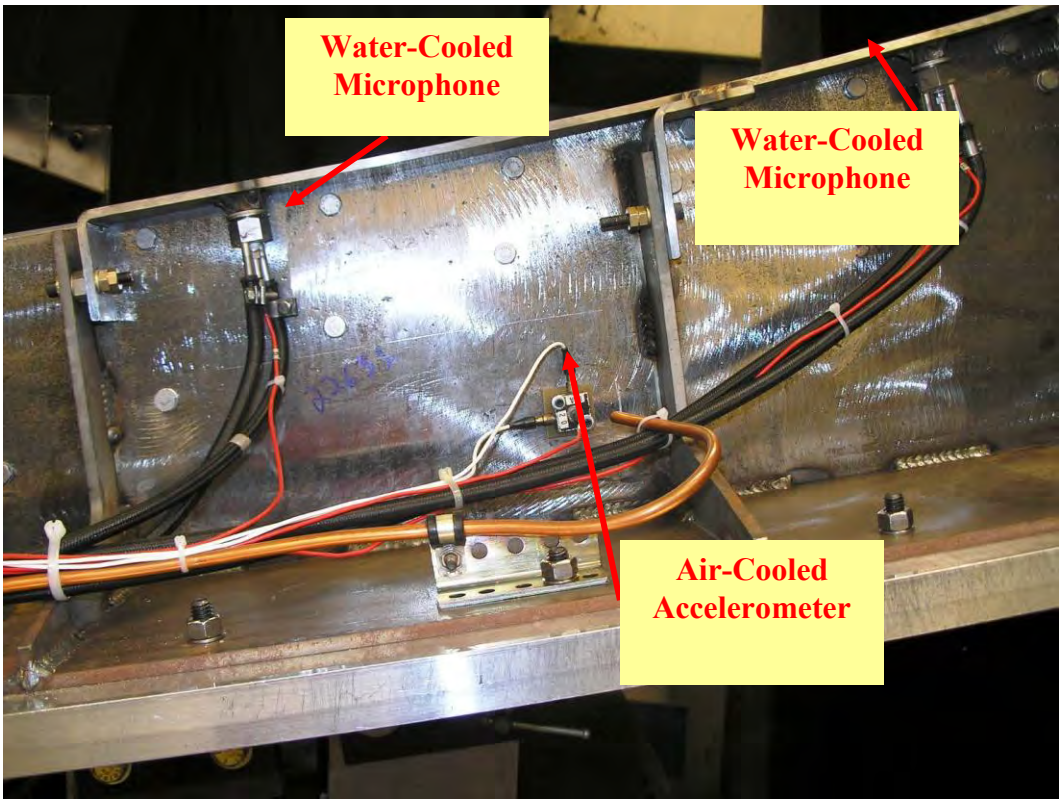

Figure C.8 – Water-cooled microphone and air-cooled accelerometer apparatus

The microphone instrumentation required charge amplifiers to produce output voltages from the piezoelectric microphone sensing elements. A PCB Piezotronics model 481A charge amplifier was utilized to provide excitation for the microphones.

Accelerometers were attached to the test fixture and test panel in the locations shown in Figures Figure C.9 and Figure C.10. A mixture of single-axis and three-axis accelerometers was utilized in order to document the test and response environment. The accelerometers were mechanically attached to phenolic or fiberglass blocks, which were in turn mechanically attached to the test fixture. To minimize temperature effects each accelerometer was air-cooled, using shop air emanating from ¼" copper tubes, and directed at the body of each accelerometer. An example of the air-cooling apparatus is depicted in Figure C.8. The accelerometer instrumentation also required charge amplifiers to produce output voltages from the piezoelectric accelerometer sensing elements.

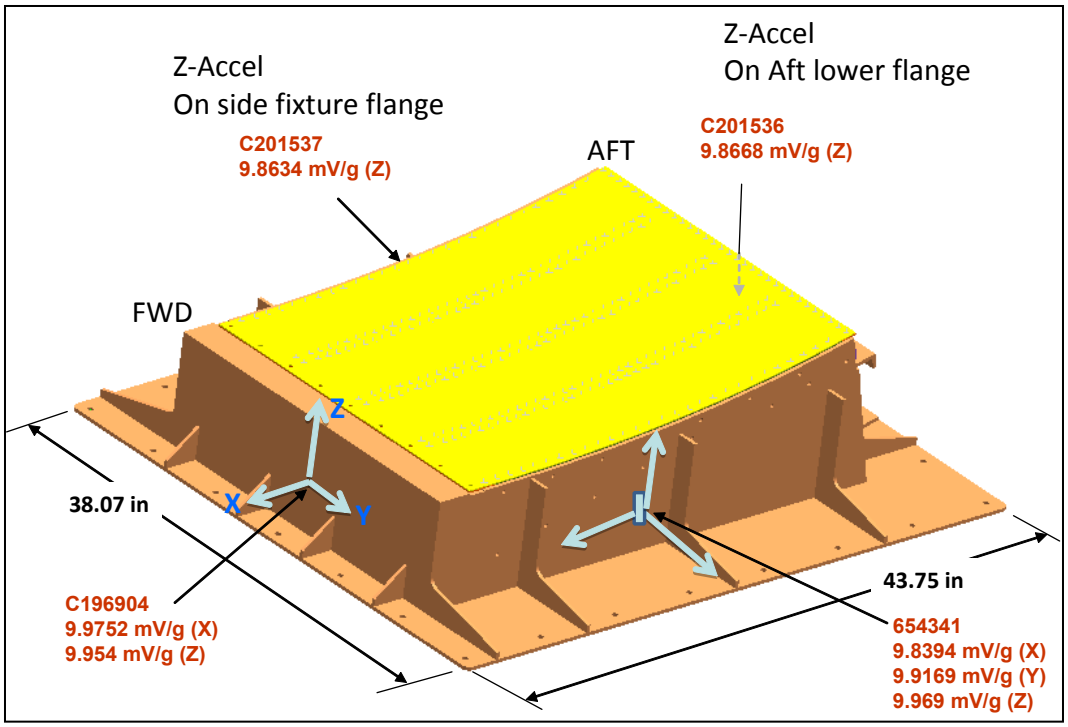

Figure C.9 – Run B0613 accelerometer locations

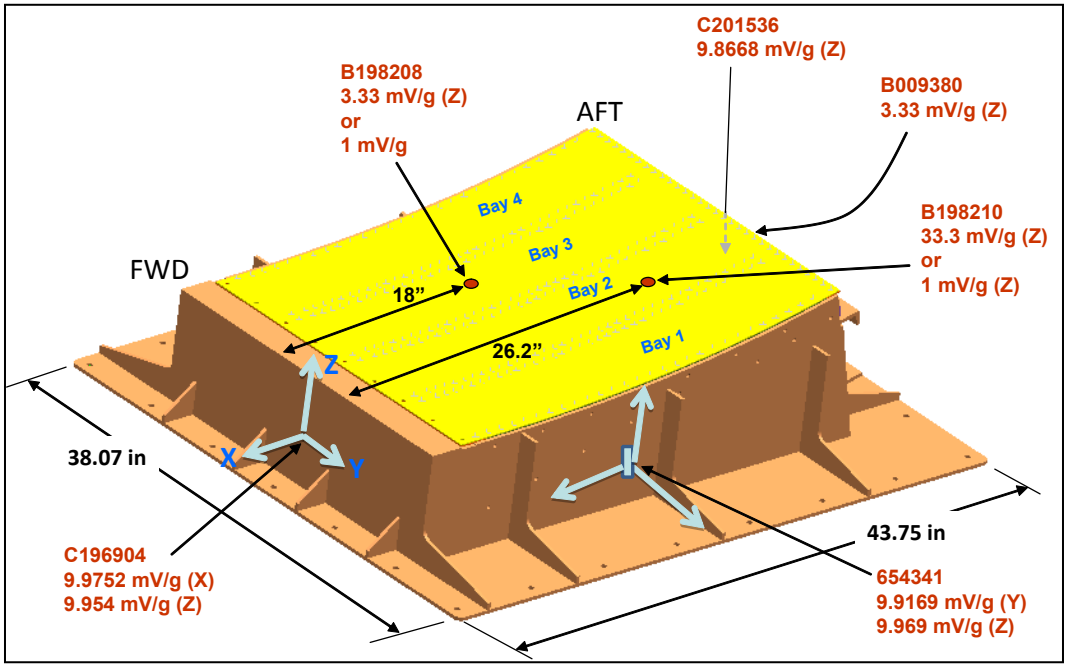

Figure C.10 – Runs B0614 and B0615 accelerometer locations

C.4 Data Acquisition Systems

Two separate data systems were utilized for this test series. The "low speed" facility data acquisition and a "high speed" system used to record the strain gauge and microphone data. ETF operating parameters were recorded and processed using the facility data acquisition system. The data acquisition system employed a Dell Precision T3400 personal computer and National Instruments LabVIEW® data acquisition software. The system was configured to acquire 72

analog data channels using a National Instruments® SCXI-1001 chassis and a mixture of SCXI 1100, 1120 and 1121 analog input modules. The multiplexed analog signals from the SCXI-1001 chassis were digitized at the computer using a National Instruments PCI-6052E analog-to-digital (A/D) board. This A/D board has 16-bit (1 in 65536) signal resolution. All data recorded with this system were recorded at a 25 Hz scan rate, and then averaged real-time within the LabVIEW software to provide recorded data at a 1 Hz interval.

All test data were recorded to hard disk for post-test processing using LabDAQ data acquisition/processing software. Selected parameters were displayed in graphical and numerical format on a real-time basis during the tests. All low speed data were output in Microsoft Excel workbook format. A second data acquisition system was set up to acquire high-rate strain gauge, accelerometer and microphone data. These data were acquired on the same data acquisition system in order to provide data on a common time base.

The Dynamic Distortion Analyzer, DDA, is a high speed data system that is used for high frequency data acquisition and analysis. The platform that the system runs on was a Kinetic Systems VXI chassis. The host computer for the system was a Dell Precision T3400 Computer running Windows® XP Pro. The application software was National Instruments LabVIEW based. The host computer acquired data from the VXI chassis over a fiber optic link.

The Kinetics Systems VXI chassis housed a model V208 500 kHz scanning A to D converter. The V208 is a 16 bit device, with simultaneous channel sampling. Five model V246-S005 eight-channel bridge conditioner cards conditioned the strain gauge outputs.

The accelerometers and microphones were routed through charge amps and also brought in through the V246 cards. The system was set to sample data at 10 kHz, with 5 kHz anti aliasing filters. 60 seconds of data were obtained at each test point and written to hard disk.

Acquired test data were converted from a binary raw format to engineering units via Matlab® software, and then written back to the hard disk. These files were then delivered to the customer in Matlab's standard format for analysis.

C.5 Optical Instrumentation

Specimen surface temperature data were collected using an Agema 900 thermal imaging camera. The Agema 900 camera was mounted above the test article, and imaged an area approximately 11.5 inches wide by 23 inches long. The imaging head on the camera obtained radiance data in an 8 to 12 μm spectral band. The peak of the spectral response band was located at approximately 11.2 μm. No filters were utilized. The accuracy of the Agema camera data is ±1% of reading, given known material emissivity (at wavelength/temperature). Lacking "at temperature" emissivity data for the test article surface exposed to the gas flow, the value was assumed to be unity (1.0). The Agema 900 IR camera data were recorded at 30 second intervals during all tests. Discrete temperature data files and images were produced for selected images. Thermal images of the test article were also recorded in real time from the video out terminal of the Agema 900 control computer using a hard drive equipped digital video recorder. The recorded videos were then transferred to DVD-R disks for archiving.

Two NTSC-format video cameras were utilized to visually document the test article performance. The "top" camera provided a view of the test article upper surface that was exposed to the hot gas flow. This camera view allowed the test engineers to monitor the test article surface conditions during testing. The "side" video camera view provided an edge view of the test surface. The side camera was mounted on a tripod nearest the control room side of the test cell.

Selected engine operating parameters from the primary data acquisition system display were dubbed with the side view video data signal as part of the displayed and recorded data.

Primary test parameters recorded with the side view video image included:

- Engine Tachometer
- Engine EGT (Exhaust Gas Temperature)
- T6
- T11
- T15
- P2
- P3

The combined video output provided a convenient means to link test conditions to panel visual performance in the event of in-test anomalies.

NTSC composite video output signals from the laboratory video cameras were recorded onto hard drive-equipped digital video recorders for temporary archiving and quick review. All video data was backed up to DVD media post-test.

C.6 Test Fixture and Assembly

Prior to installation of the thermocouple and pressure instrumentation, the NLROM test panel was mounted to a welded steel test fixture. This is same fixture as used in CEAC testing. The entire test article was then mounted to a solid mounting plate to which the steel test fixture could be attached to the ETF mounting table. The test fixture was designed to accommodate fixed angle-of-attack (AOA) settings of 0° and 10°, and the test fixture mounts were designed such that the test article leading edge deck height was the same at both the 0° and 10° settings.

The ETF mounting table was analyzed during the aluminum mounting plate design phase to ensure that sufficient structural margins were embraced. The primary load factors were the weight of the steel panel mounting fixture, the weight of the aluminum base-plate that the mounting fixture was bolted to, and the load imparted by reacted engine thrustt. Conservative engineering calculations were accomplished with the test article oriented at a 10º AOA, which was the worst-case test scenario. These calculations indicated a material stress level of approximately 2800 psi in the steel T58 mounting table, and a deflection of approximately 0.011 inches. The natural frequency of the T58 mounting table was calculated to be approximately 34 Hz.

A conservative calculation of the loads imparted to the half inch diameter bolts that secured the angle brackets to the upright mounting brackets revealed individual bolt loads of less than 150

lbs applied, in a single-shear loading mode. This resulted in bolt material stresses the order of 1100 psi. Pre-test installation and post-test removal of the test article required removal of the exhaust nozzle due to the limited amount of working space between the nozzle and the facility exhaust duct. An overhead chain hoist as well as an additional horizontally mounted come-along hoist were required to move the test article into place on the test fixture. The installation/removal set-up is shown in Figure C.11.

Table C.1 – Low speed instrumentation listing

Parameter	Channel No.	Used on Run No. B0612	B0613	B0614	B0615	Property No.	Range	Unit	DESCRIPTION	Calibration Due Date
Fuel Temp.	T0	X	X	X	X	N/A	2500	DEG F	Engine Fuel Temperature - C/A Lead 0	N/A
Coolant Temp	T1	X	X	X	X	N/A	2500	DEG F	Air Supply Temperature from Slyvania Air Heater outlet - C/A Lead 1	N/A
Oil Tank TC1	T3	X	X	X	X	N/A	2500	DEG F	Oil Tank TC1 - C/A Lead 3	N/A
Eng. Support TC1	T4	X	X	X	X	N/A	2500	DEG F	Rear Engine Support TC1 - C/A Lead 4	N/A
Eng. Support TC2	T5	X	X	X	X	N/A	2500	DEG F	Rear Engine Support TC2 - C/A Lead 5	N/A
L/H Compressor Bleed	T6	X	X	X	X	N/A	2500	DEG F	L/H Compressor Bleed Air TC - C/A Lead 6	N/A
R/H Compressor Bleed	T7	X	X	X	X	N/A	2500	DEG F	R/H Compressor Bleed Air TC - C/A Lead 7	N/A
T1	T10	X	X	X	X	N/A	2500	DEG F	Specimen T/C - C/A Lead 10	N/A
T2	T11	X	X	X	X	N/A	2500	DEG F	Specimen T/C - C/A Lead 11	N/A
T3	T12	X	X	X	X	N/A	2500	DEG F	Specimen T/C - C/A Lead 12	N/A
T4	T13	X	X	X	X	N/A	2500	DEG F	Specimen T/C - C/A Lead 13	N/A
T5	T14	X	X	X	X	N/A	2500	DEG F	Specimen T/C - C/A Lead 14	N/A
T6	T15	X	X	X	X	N/A	2500	DEG F	Specimen T/C - C/A Lead 15	N/A
T7	T16	X	X	X	X	N/A	2500	DEG F	Specimen T/C - C/A Lead 16	N/A
T8	T17	X	X	X	X	N/A	2500	DEG F	Specimen T/C - C/A Lead 17	N/A
T9	T18	X	X	X	X	N/A	2500	DEG F	Specimen T/C - C/A Lead 18	N/A
T10	T19	X	X	X	X	N/A	2500	DEG F	Specimen T/C - C/A Lead 19	N/A
T11	T20	X	X	X	X	N/A	2500	DEG F	Specimen T/C - C/A Lead 20	N/A
T12	T21	X	X	X	X	N/A	2500	DEG F	Specimen T/C - C/A Lead 21	N/A
T13	T22	X	X	X	X	N/A	2500	DEG F	Specimen T/C - C/A Lead 22	N/A
T14	T23	X	X	X	X	N/A	2500	DEG F	Specimen T/C - C/A Lead 23	N/A
T15	T24	X	X	X	X	N/A	2500	DEG F	Specimen T/C - C/A Lead 24	N/A
T16	T25	X	X	X	X	N/A	2500	DEG F	Specimen T/C - C/A Lead 25	N/A
T17	T26	X	X	X	X	N/A	2500	DEG F	Specimen T/C - C/A Lead 26	N/A
T18	T27	X	X	X	X	N/A	2500	DEG F	Specimen T/C - C/A Lead 27	N/A
T19	T28	X	X	X	X	N/A	2500	DEG F	Specimen T/C - C/A Lead 28	N/A
Bay 2, Accel T/C	T29			X	X	N/A	2500	DEG F	Bay 2, Accel T/C - C/A Lead 29	N/A
Bay 3, Accel T/C	T30			X	X	N/A	2500	DEG F	Bay 3, Accel T/C - C/A Lead 30	N/A
P1	T64	X	X	X	X	C219676	50	PSIG	Specimen Pressue P1 - C219676	3/6/2009
P2	T65	X	X	X	X	C219677	50	PSIG	Specimen Pressue P2 - C219677	3/6/2009
P3	T66	X	X	X	X	C219678	50	PSIG	Specimen Pressue P3 - C219678	3/6/2009
P4	T67	X	X	X	X	C219679	50	PSIG	Specimen Pressue P4 - C219679	3/6/2009
P5	T68	X	X	X	X	C219680	50	PSIG	Specimen Pressue P5 - C219680	3/6/2009
P6	T69	X	X	X	X	C219681	50	PSIG	Specimen Pressue P6 - C219681	3/6/2009
Venturi P (g)	T96	X	X	X	X	B172750	1000	PSIG	Venturi Inlet Pressure B172750	8/31/2007
Venturi DP	T97	X	X	X	X	C223616	30	PSID	Venturi Delta Pressure C223616 30 psid/ 5 volts FS	8/21/2008
PSWT Supply P (g)	T98	X	X	X	X	B147061	1500	PSIG	PSWT Supply Pressure - B147061	8/23/2008
Fuel (P) @ Pump	T99	X	X	X	X	703588	250	PSIG	Prop. No. 703588 - Fuel pressure at facility pump outlet	8/20/2008
Fuel (P) @ Engine	T100	X	X	X	X	B116910	25	PSIG	Fuel Pressure @ the Engine (B116910)	6/5/2007
HP Fuel @ Engine	T101	X	X	X	X	C114990	2500	PSIG	C114990 - Fuel pressure measured @ outlet of engine fuel pump	6/13/2007
P Coolant	T102	X	X	X	X	B148873	250	PSIG	B148873 Supply Pressure in heated air supply line	1/19/2009
Nozzle Static P(g)	T103	X	X	X	X	C228101	15	PSIG	Nozzle Static Pressure (g) C228101	1/1/2009
Fuel Flow	T104	X	X	X	X	B002317	2.5	GPM	Engine Fuel Flowrate B002317 FOR K1 FUEL	10/27/2007
Cell Temp	T105	X	X	X	X	C/A T/C	2500	DEG F	Cell Temp. at Ceiling	N/A
Venturi(T)	T106	X	X	X	X	C213505	125	DEG F	Venturi Inlet Air Temperature RTD Transmitter Property No. C213505	2/10/2009
Barometric P	T107	X	X	X	X	C191984	19	PSIA	Test Cell Pressure Property No. C191984	1/2/2008
Engine Tachometer	T108	X	X	X	X	Control Box	110	%	Engine Speed from Control Box Panel Meter	N/A
Engine EGT	T109	X	X	X	X	Control Box	2000	DEG F	Engine Exhaust Gas Temperature (EGT) from Control Box Panel Meter	N/A
Engine Throttle Pos.	T110	X	X	X	X	Control Box	100	%	Engine Throttle Position from Control Box Panel Meter	N/A
Spare C.O. Pv (g)	T111	X	X	X	X	B115737	500	PSIG	Spare Critical Orifice Pv (psig) - B115737	10/18/2007
Spare C.O. Pv (g)	T112	X	X	X	X	B116834	500	PSIG	Spare Critical Orifice Pv (psig) - B166834	4/9/2008
Prop. Air Feedback	T113	X	X	X	X	S/N 71337	150	PSIG	Proportion Air Controller - S/N 71337	N/A

Table C.2 – High speed data instrumentation routing and post-test condition

DDA Channel #	Measurand	Resistance (Ω)	Run B0613 Location	Post-Run B0613 Condition	Property Number	Run B0614 Location	Post-Run B0614 Condition	Property Number	Run B0615 Location	Post-Run B0615 Condition	Property Number
1	SG1	133	See Figures 1 & 2	bad	N/A	See Figures 1 & 2	bad	N/A	See Figures 1 & 2	bad	N/A
2	SG2	123	See Figures 1 & 2	bad	N/A	See Figures 1 & 2	bad	N/A	See Figures 1 & 2	bad	N/A
3	SG3	123	See Figures 1 & 2	bad	N/A	See Figures 1 & 2	bad	N/A	See Figures 1 & 2	bad	N/A
4	SG4	125	See Figures 1 & 2	bad	N/A	See Figures 1 & 2	bad	N/A	See Figures 1 & 2	bad	N/A
5	SG5	123	See Figures 1 & 2	bad	N/A	See Figures 1 & 2	bad	N/A	See Figures 1 & 2	bad	N/A
6	SG6	123	See Figures 1 & 2	bad	N/A	See Figures 1 & 2	bad	N/A	See Figures 1 & 2	bad	N/A
7	SG7	123	See Figures 1 & 2	bad	N/A	See Figures 1 & 2	bad	N/A	See Figures 1 & 2	bad	N/A
8	SG8	123	See Figures 1 & 2	bad	N/A	See Figures 1 & 2	bad	N/A	See Figures 1 & 2	bad	N/A
9	SG9	122	See Figures 1 & 2	bad	N/A	See Figures 1 & 2	bad	N/A	See Figures 1 & 2	bad	N/A
10	SG11	123	See Figures 1 & 2	bad	N/A	See Figures 1 & 2	bad	N/A	See Figures 1 & 2	bad	N/A
11	SG12	122	See Figures 1 & 2	bad	N/A	See Figures 1 & 2	bad	N/A	See Figures 1 & 2	bad	N/A
12	SG13	121	See Figures 1 & 2	bad	N/A	See Figures 1 & 2	bad	N/A	See Figures 1 & 2	bad	N/A
13	SG15	122	See Figures 1 & 2	bad	N/A	See Figures 1 & 2	bad	N/A	See Figures 1 & 2	bad	N/A
14	SG16	123	See Figures 1 & 2	bad	N/A	See Figures 1 & 2	bad	N/A	See Figures 1 & 2	bad	N/A
15	SG18	120	See Figures 1 & 2	bad	N/A	See Figures 1 & 2	bad	N/A	See Figures 1 & 2	bad	N/A
16	SG23	123	See Figures 1 & 2	OK	N/A	See Figures 1 & 2	OK?	N/A	See Figures 1 & 2	OK?	N/A
17	SG19	350	See Figures 1 & 2	bad	N/A	See Figures 1 & 2	bad	N/A	See Figures 1 & 2	bad	N/A
18	SG20	350	See Figures 1 & 2	bad	N/A	See Figures 1 & 2	bad	N/A	See Figures 1 & 2	bad	N/A
19	SG21	350	See Figures 1 & 2	OK	N/A	See Figures 1 & 2	OK?	N/A	See Figures 1 & 2	OK?	N/A
20	SG22	351	See Figures 1 & 2	OK	N/A	See Figures 1 & 2	OK?	N/A	See Figures 1 & 2	OK?	N/A
21	SG25	350	See Figures 1 & 2	bad	N/A	See Figures 1 & 2	bad	N/A	See Figures 1 & 2	bad	N/A
22											
23	accelerometer	N/A	See Figure 9, X axis	OK	C196904	See Figure 10, X axis	OK	C196904	See Figure 10, X axis	OK	C196904
24	accelerometer	N/A	See Figure 9, Y axis	OK	C196904	See Figure 10, Z axis	loose	B198208	See Figure 10, Z axis	OK	B198208
25	accelerometer	N/A	See Figure 9, Z axis	OK	C196904	See Figure 10, Z axis	OK	C196904	See Figure 10, Z axis	OK	C196904
26	accelerometer	N/A	See Figure 9, X axis	OK	654341	See Figure 10, Z axis	bad?	B198210	See Figure 10, Z axis	bad?	B198210
27	accelerometer	N/A	See Figure 9, Y axis	OK	654341	See Figure 10, Y axis	OK	654341	See Figure 10, Y axis	OK	654341
28	accelerometer	N/A	See Figure 9, Z axis	OK	654341	See Figure 10, Z axis	OK	654341	See Figure 10, Z axis	OK	654341
29	accelerometer	N/A	See Figure 9, Z axis	OK	C201537	See Figure 10, Z axis	OK	B009380	See Figure 10, Z axis	OK	B009380
30	accelerometer	N/A	See Figure 9, Z axis	OK	C201536	See Figure 10, Z axis	OK	C201536	See Figure 10, Z axis	OK	C201536
31	microphone	N/A	mic. L1 (see Fig. 6)	OK	C230606	mic. L1 (see Fig. 6)	OK	C230606	mic. L1 (see Fig. 6)	OK	C230606
32	microphone	N/A	mic. L2 (see Fig. 6)	OK	C191041	mic. L2 (see Fig. 6)	OK	C191041	mic. L2 (see Fig. 6)	OK	C191041
33	microphone	N/A	mic. L3 (see Fig. 6)	OK	C191038	mic. L3 (see Fig. 6)	OK	C191038	mic. L3 (see Fig. 6)	OK	C191038
34	microphone	N/A	mic. R1 (see Fig. 6)	OK	C230603	mic. R1 (see Fig. 6)	OK	C230603	mic. R1 (see Fig. 6)	OK	C230603
35	microphone	N/A	mic. R2 (see Fig. 6)	OK	C191039	mic. R2 (see Fig. 6)	OK	C191039	mic. R2 (see Fig. 6)	OK	C191039
36	microphone	N/A	mic. R3 (see Fig. 6)	OK	C230608	mic. R3 (see Fig. 6)	OK	C230608	mic. R3 (see Fig. 6)	OK	C230608

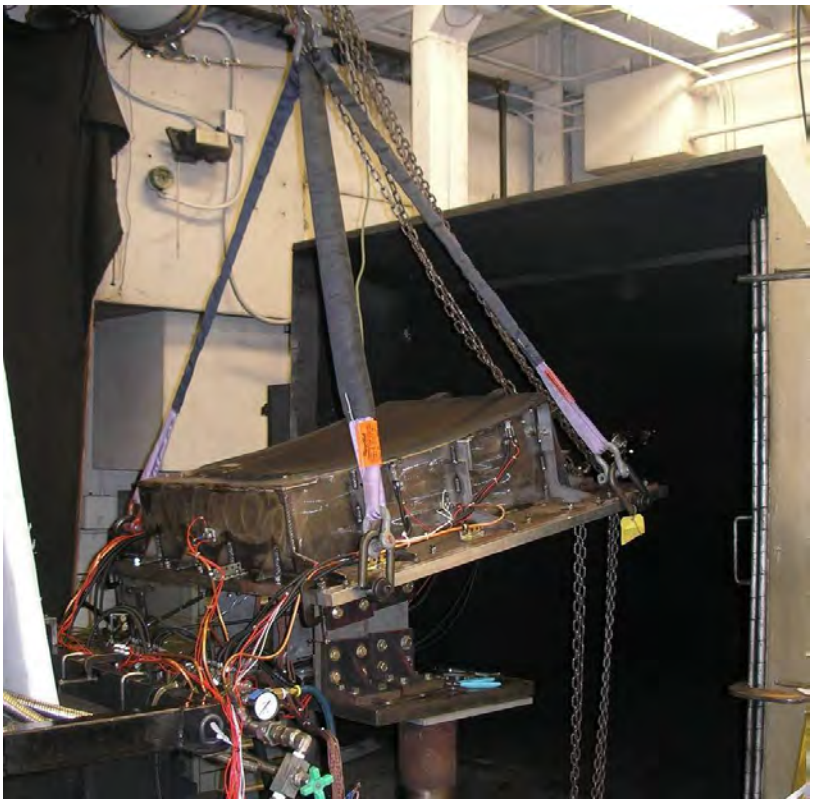

Figure C.11 – Test article installation and removal setup

Table C.3 – Test points

Run Number	Description	AOA (degrees)	High Speed Data Acquisition System Data Point	Engine Speed (%)	# seconds of data	Comments
B0613	Environmental Survey	10	1	58.0	60	
B0613	Environmental Survey	10	2	61.7	60	
B0613	Environmental Survey	10	3	65.2	60	
B0613	Environmental Survey	10	4, 5	69.1	60	
B0613	Environmental Survey	10	6, 7	76.5	60	
B0613	Environmental Survey	10	8, 9, 10	79.9	60	
B0613	Environmental Survey	10	11, 12	85.0	60	
B0613	Environmental Survey	10	13, 14	90.2	60	
B0613	Environmental Survey	10	15, 16	95.4	60	
B0613	Environmental Survey	10	17, 18	84.7	60	
B0613	Environmental Survey	10	19, 20	68.8	60	Point 19 no good?
B0614	Environmental Survey	0	1, 2	57.8	60	
B0614	Environmental Survey	0	3, 4	59.7	60	
B0614	Environmental Survey	0	5, 6	64.2	60	
B0614	Environmental Survey	0	7, 8, 9, 10	68.0	60	
B0614	Environmental Survey	0	11, 12	76.6	60	
B0614	Environmental Survey	0	13, 14	80.7	60	
B0614	Environmental Survey	0	15, 16	84.9	60	
B0614	Environmental Survey	0	17, 18	90.3	60	
B0614	Environmental Survey	0	19, 20	94.9	60	
B0614	Environmental Survey	0	21	57.6	60	
B0615	Environmental Survey	0	1	58.1	60	
B0615	Environmental Survey	0	2, 3	95.4	60	
B0615	Environmental Survey	0	4	90.0	60	Point 4 no good?
B0615	Environmental Survey	0	*	84.9	60	
B0615	Environmental Survey	0	*	80.0	60	
B0615	Environmental Survey	0	5	75.0	60	
B0615	Environmental Survey	0	6, 7	85.4	60	
B0615	Environmental Survey	0	8, 9	80.4	60	
B0615	Environmental Survey	0	10	66.5	60	
B0615	Environmental Survey	0	11	60.5	60	
B0615	Environmental Survey	0	12	57.5	60	

* High speed data acquisition system problem - no data acquired

C.7 Test Results

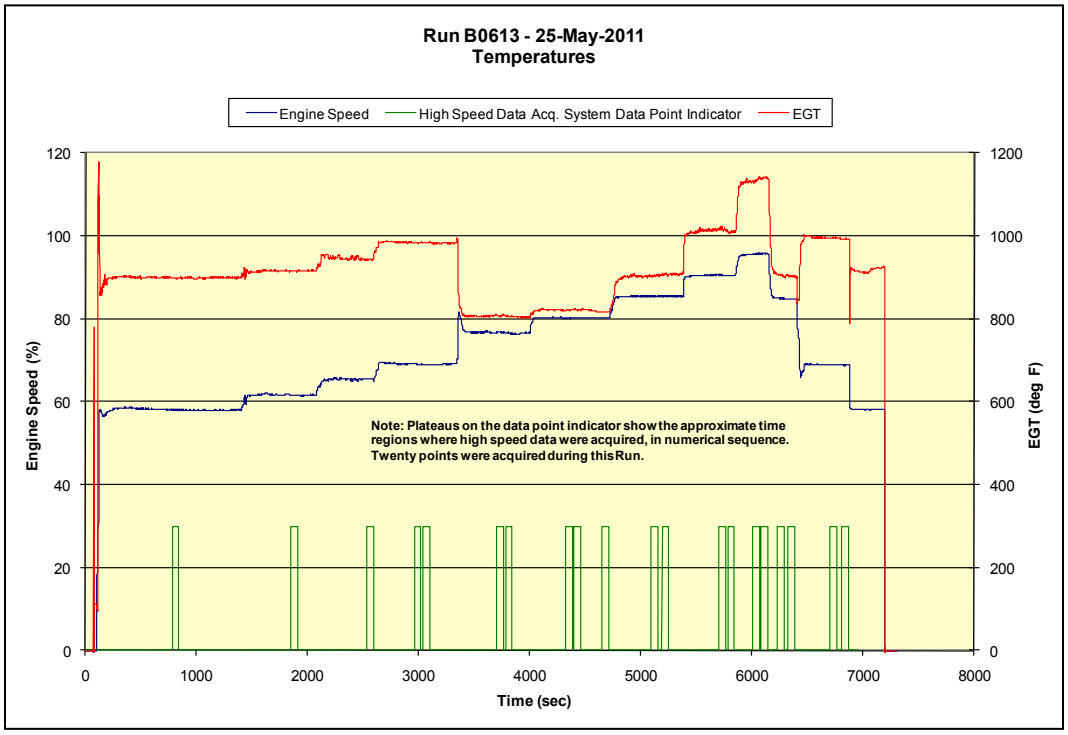

Figure C.12 – Run 613 engine conditions

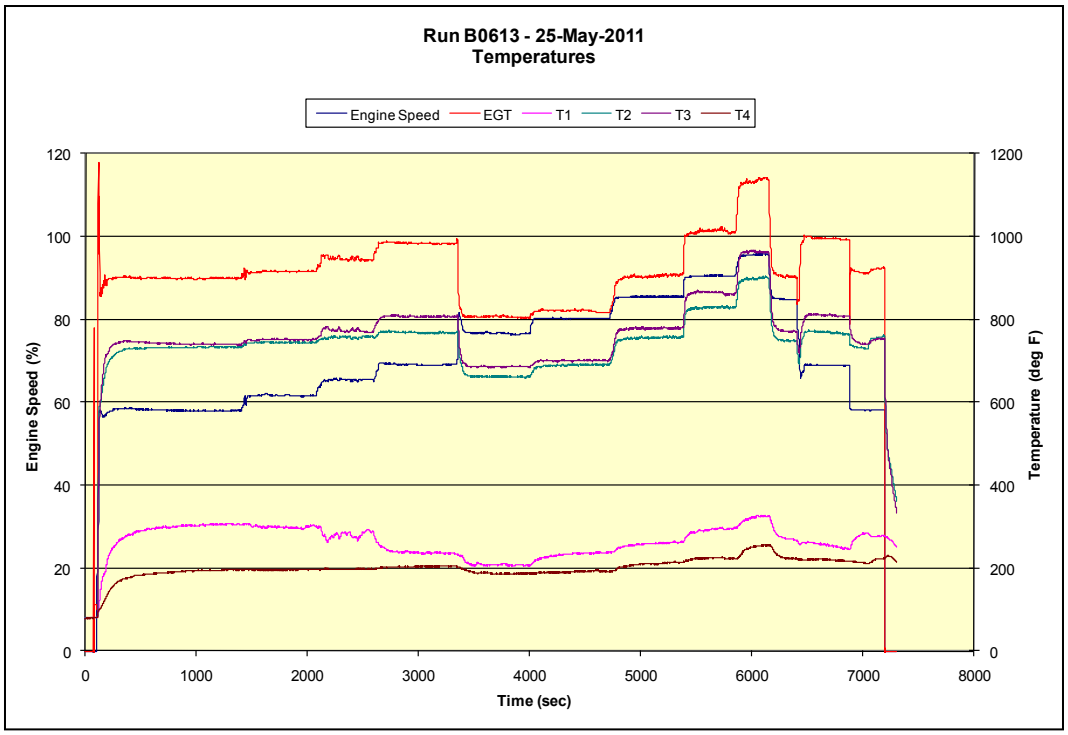

Figure C.13 – Run 613 thermocouple leading edge

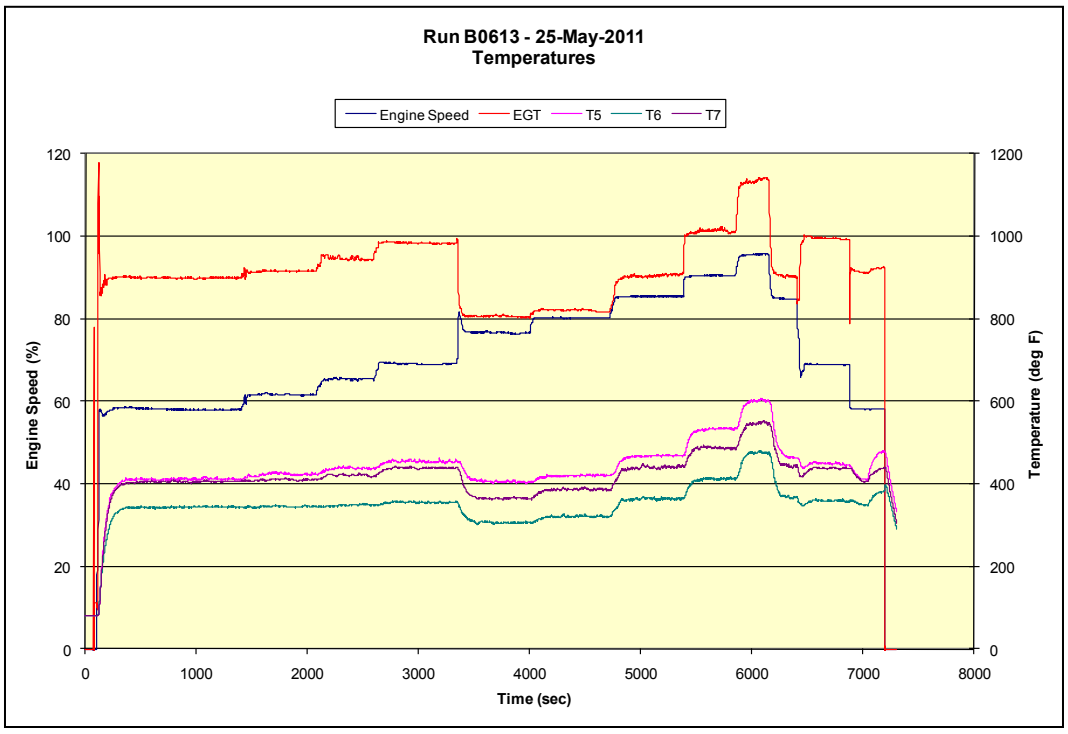

Figure C.14 – Run 613 thermocouple mid panel

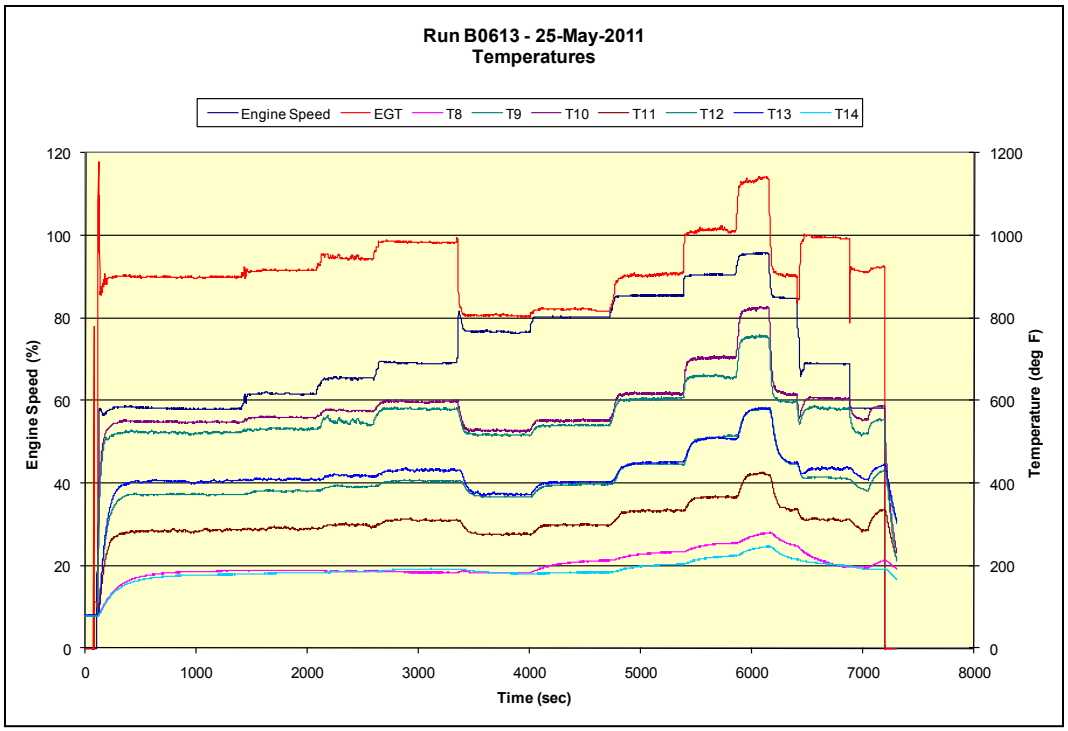

Figure C.15 – Run 613 thermocouple mid/aft panel

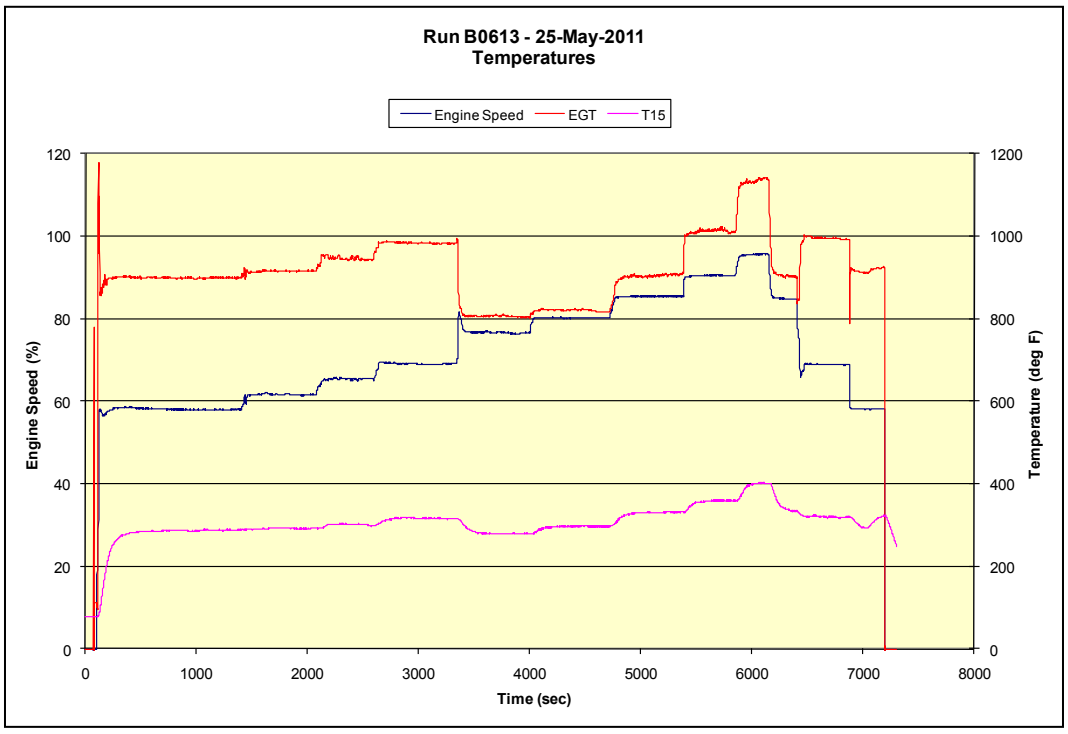

Figure C.16 – Run 613 thermocouple mid panel

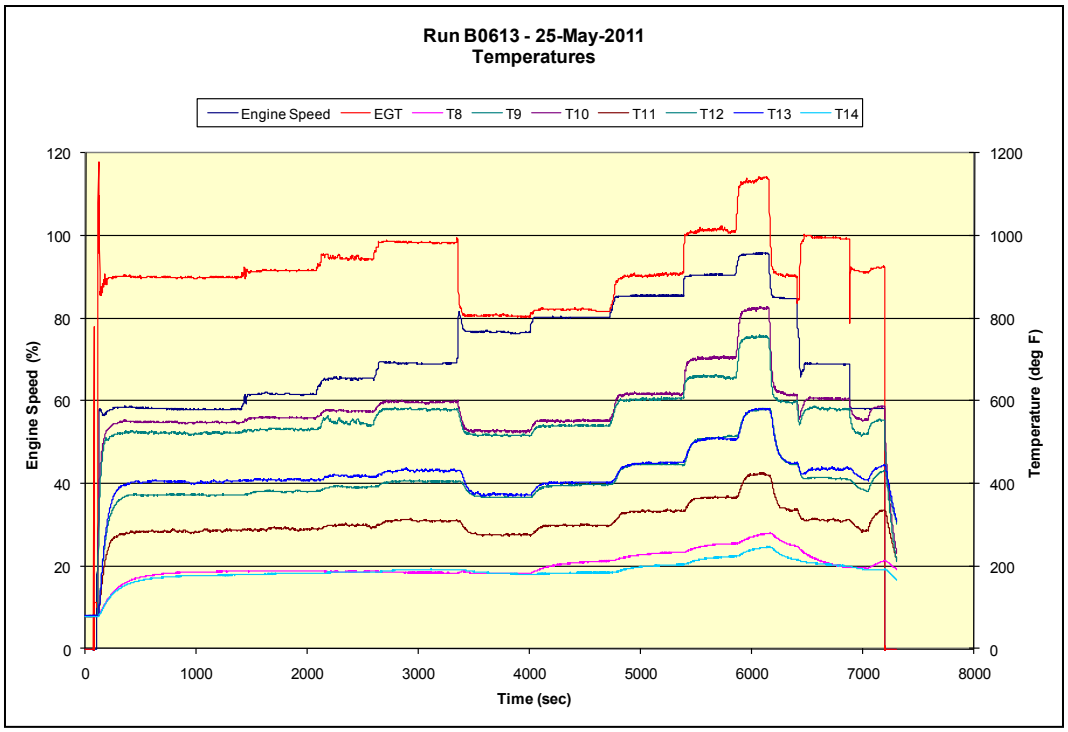

Figure C.17 – Run 613 static pressures

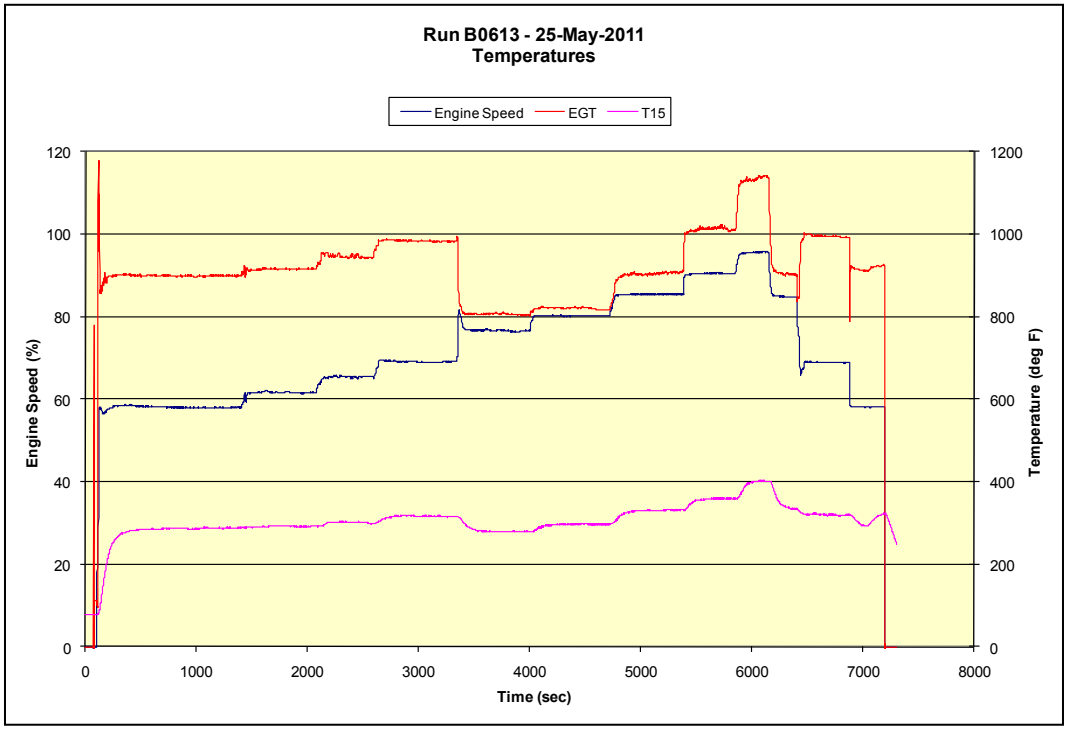

Figure C.18 – Run 613 thermocouple center rib

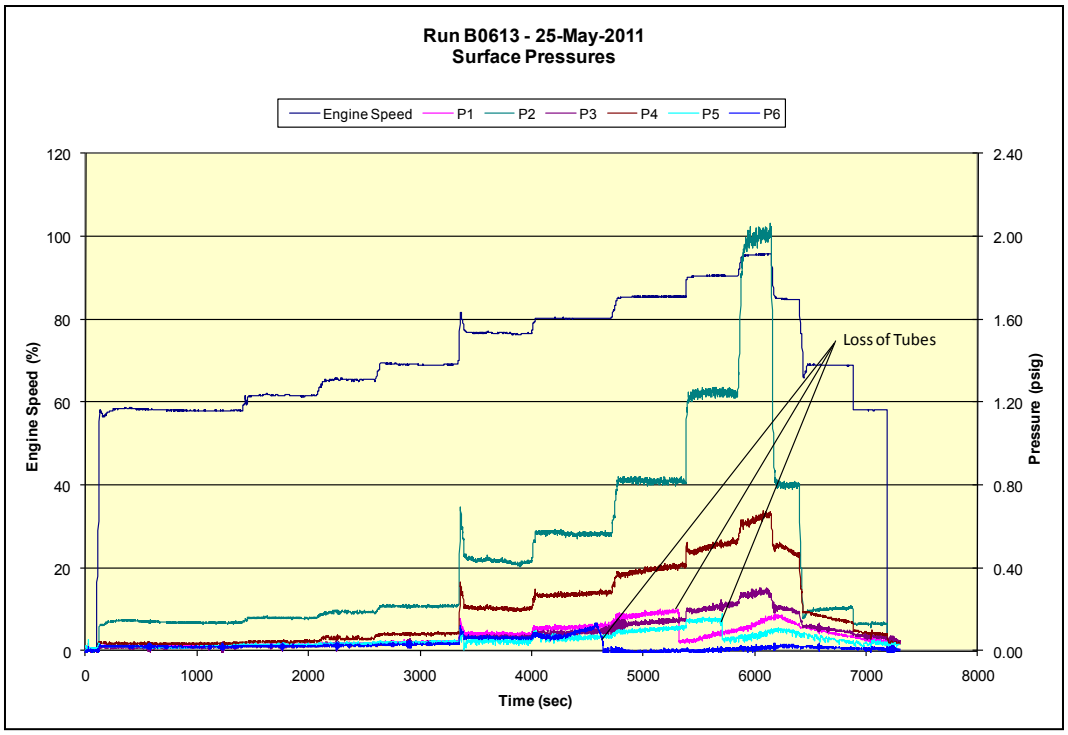

Figure C.19 – Run 613 static pressures

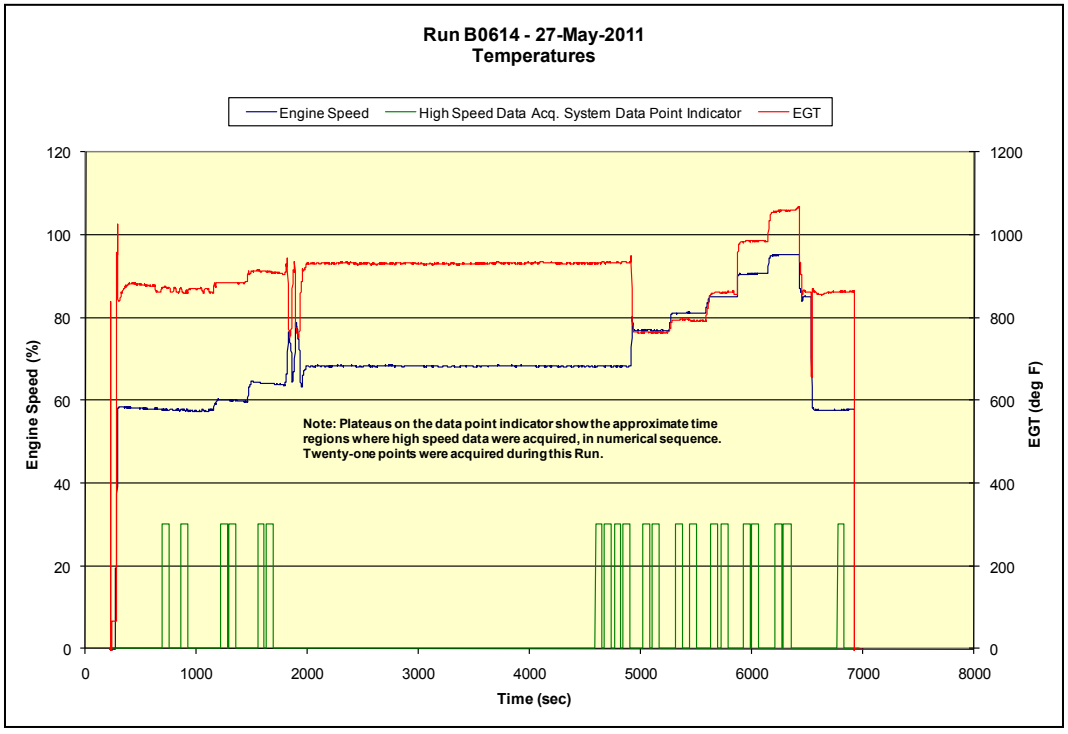

Figure C.20 – Run 614 thermocouple mid panel

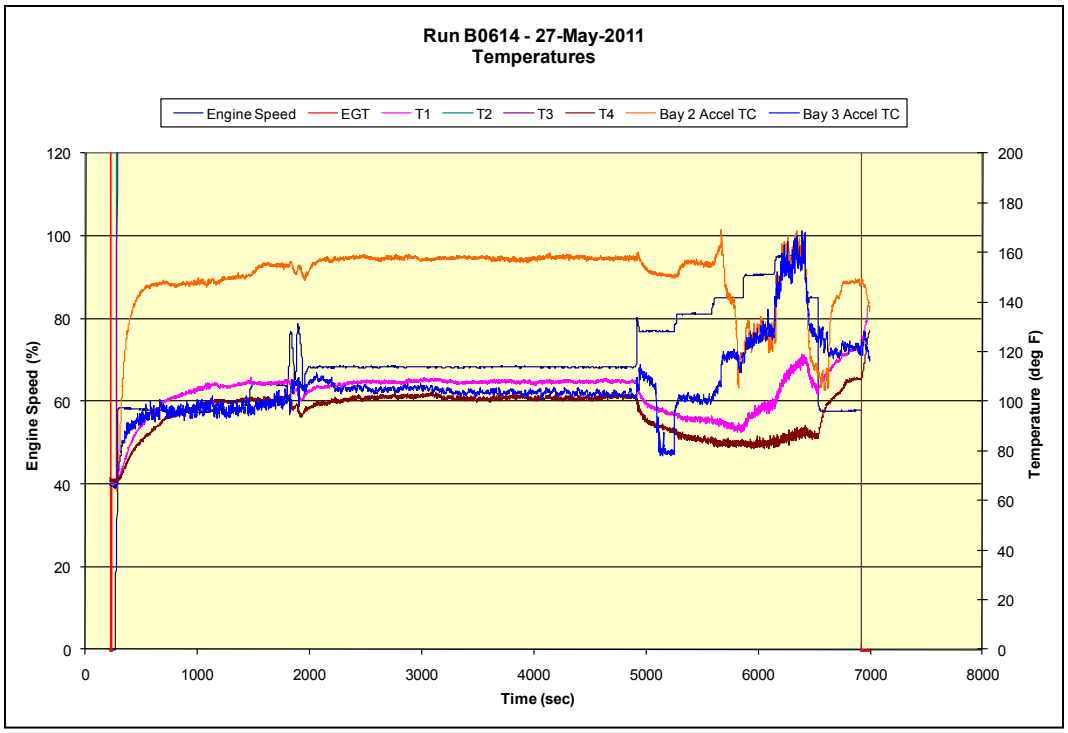

Figure C.21 – Run 614 thermocouple mid/aft panel

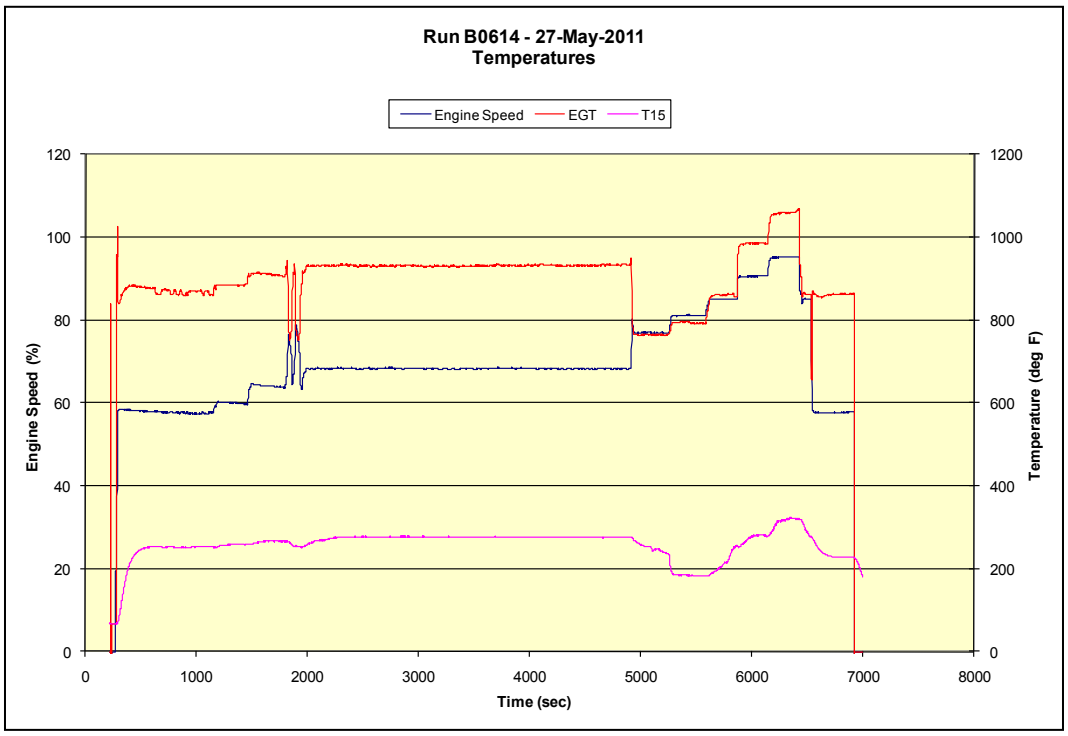

Figure C.22 – Run 614 thermocouple mid panel

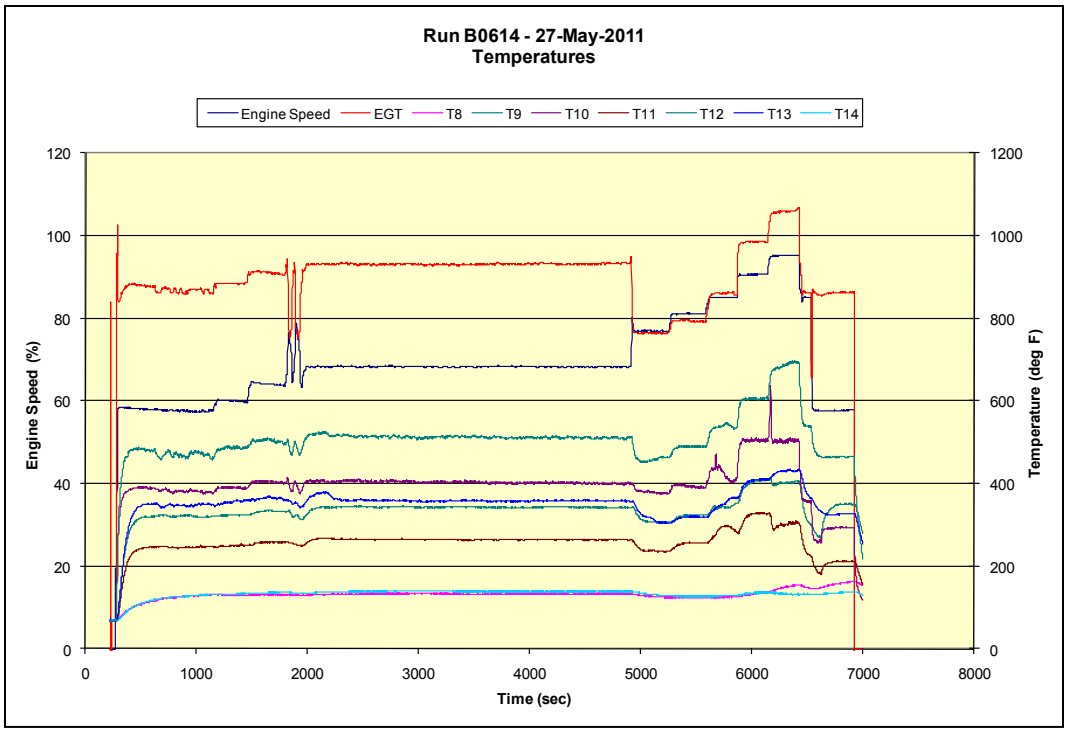

Figure C.23 – Run 614 thermocouple mid/aft panel

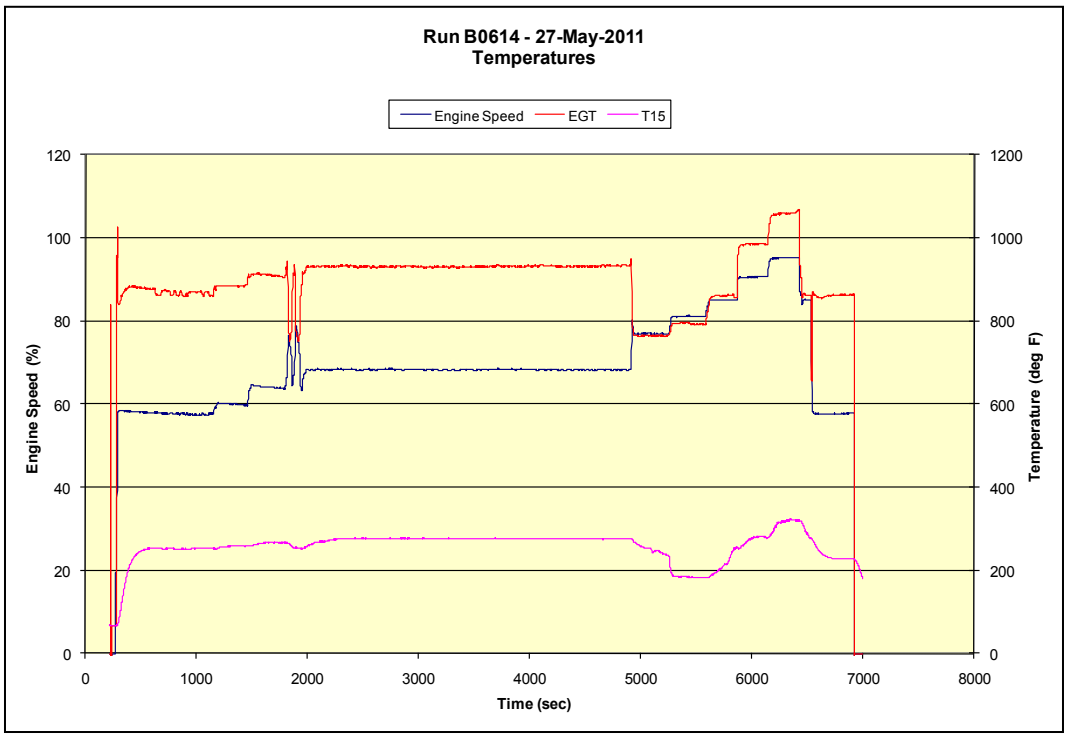

Figure C.24 – Run 614 static pressure

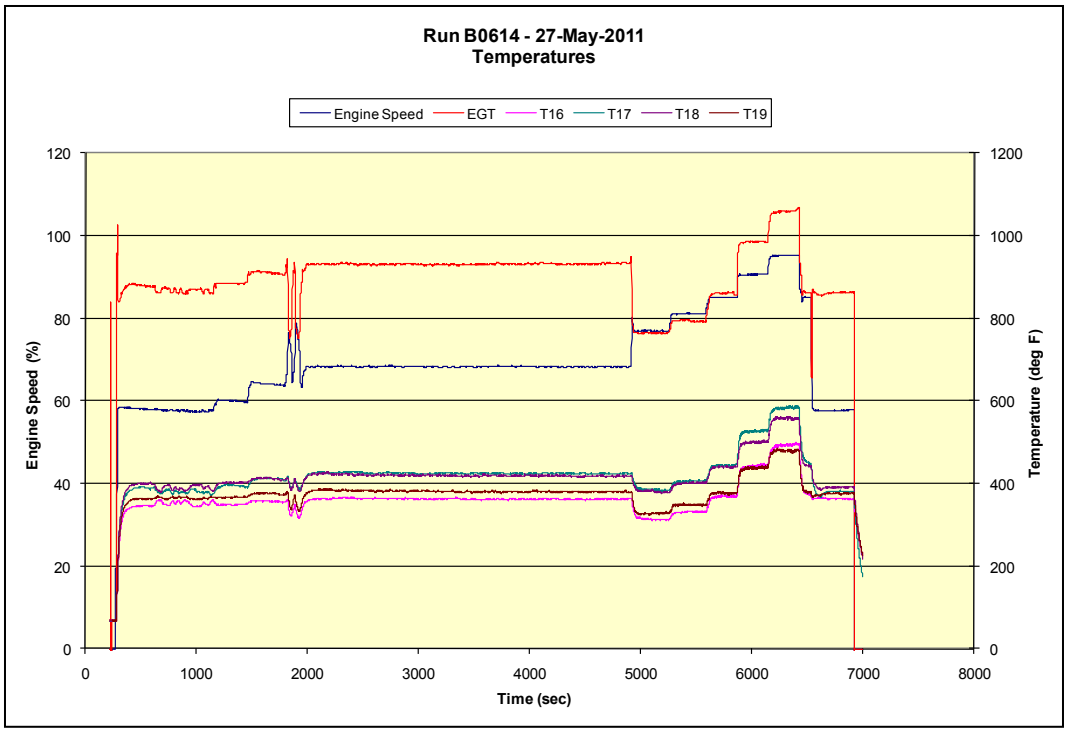

Figure C.25 – Run 614 thermocouple trailing edge

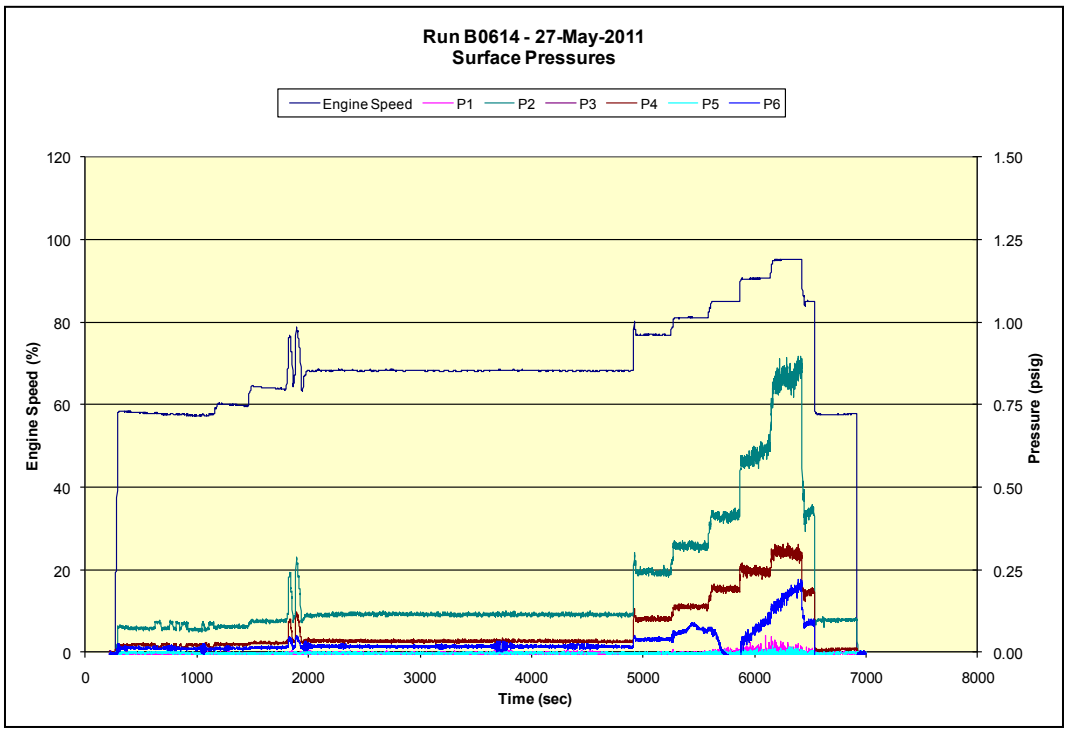

Figure C.26 – Run 614 static pressure

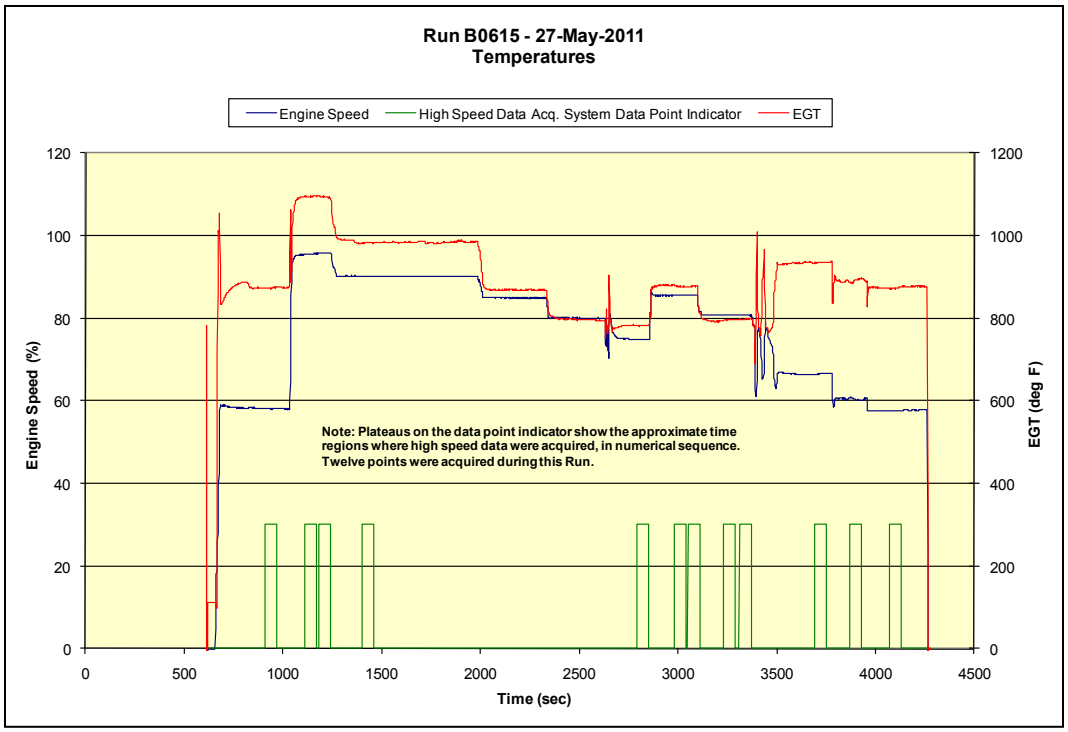

Figure C.27 – Run 615 time slots of high speed data acquisition

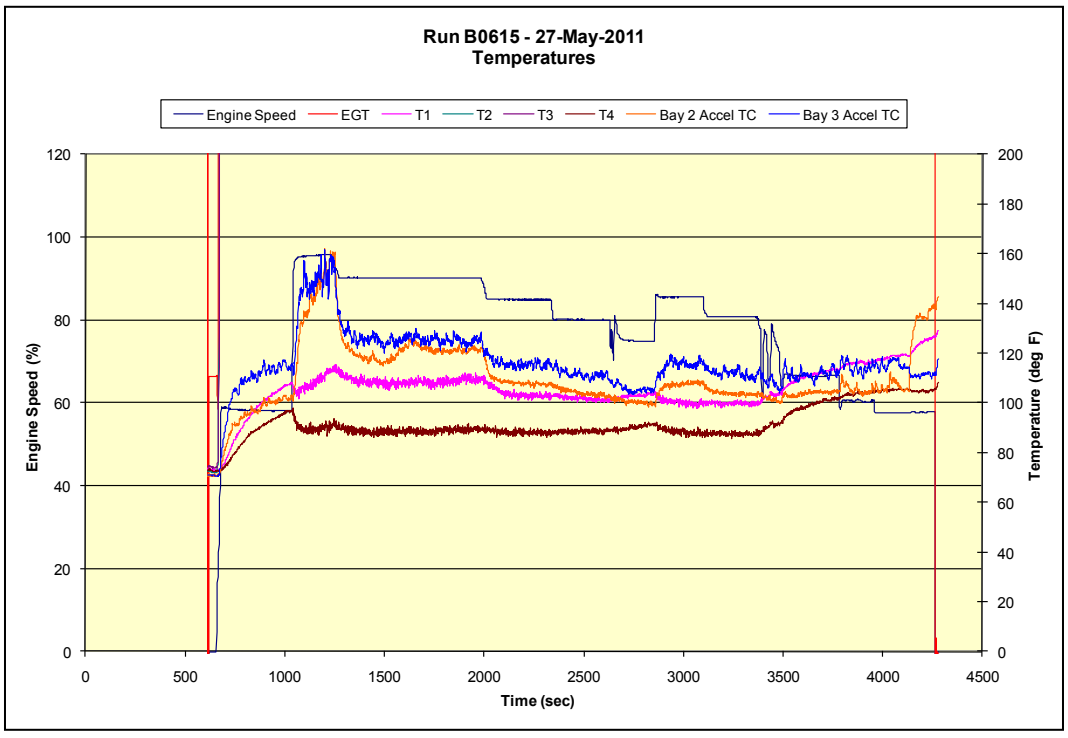

Figure C.28 – Run 615 thermocouples leading edge and at panel accelerometers

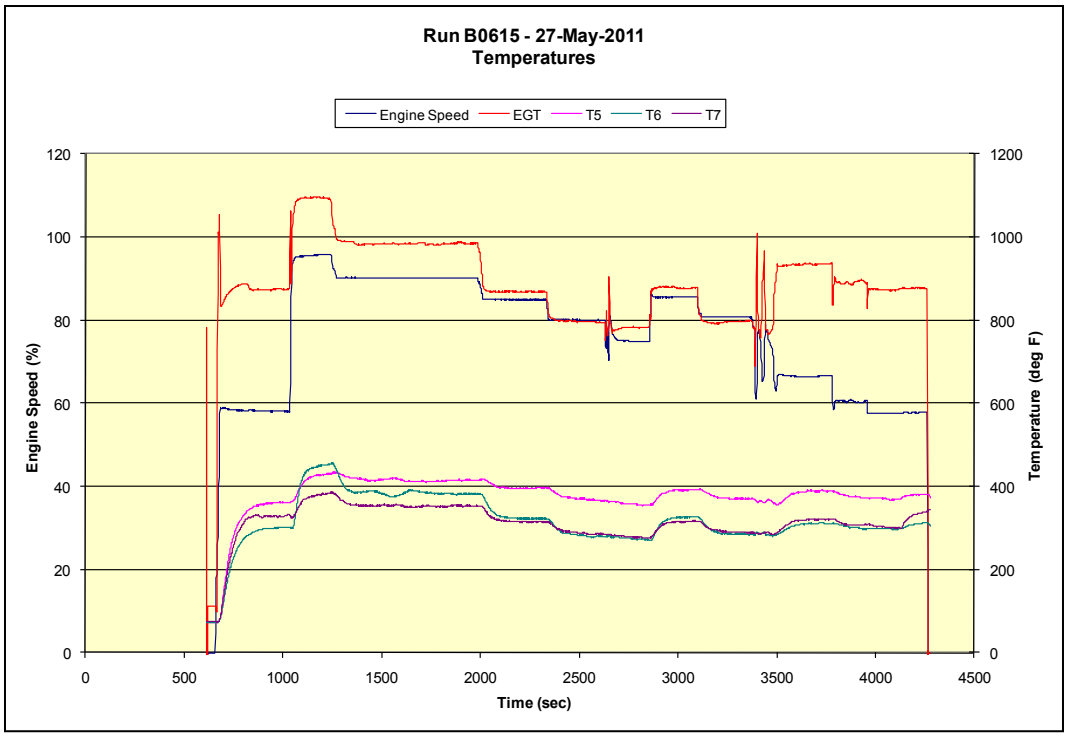

Figure C.29 – Run 615 thermocouples mid panel

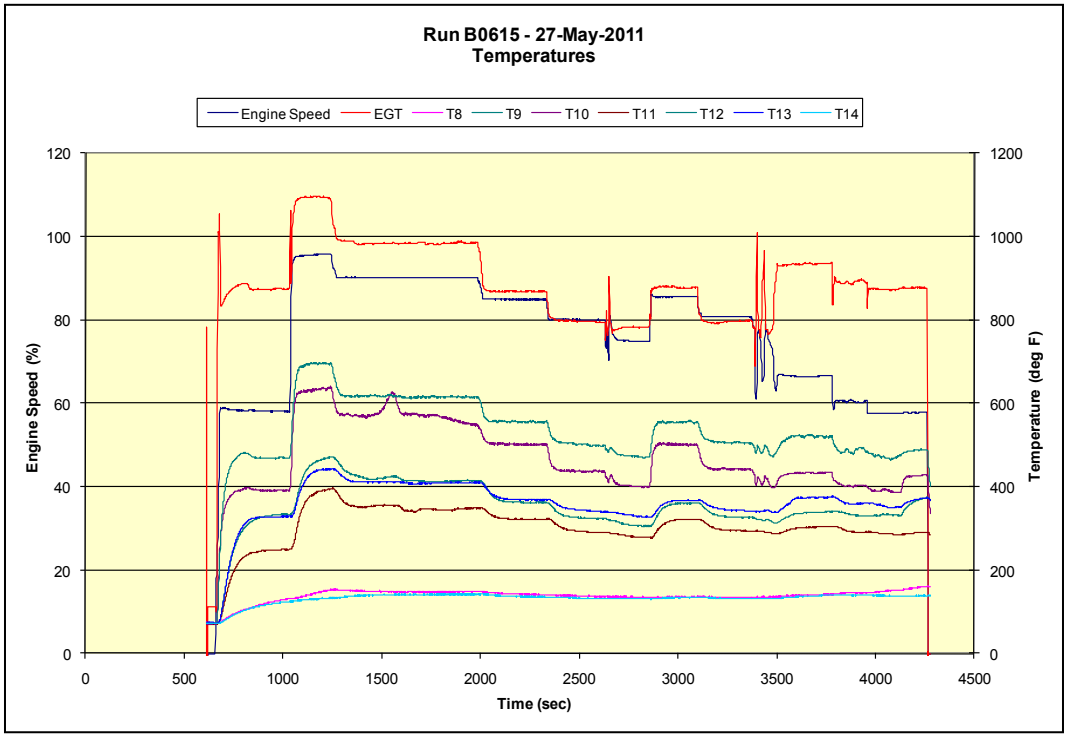

Figure C.30 – Run 615 thermocouples mid/aft panel

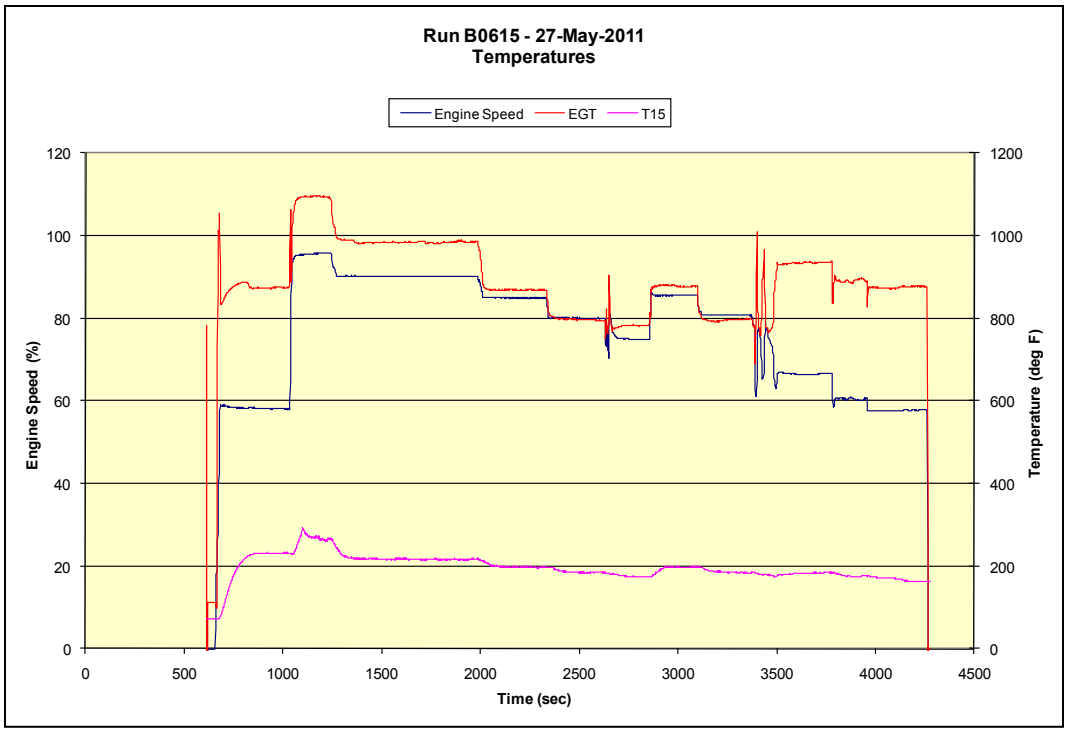

Figure C.31 – Run 615 thermocouples center rib

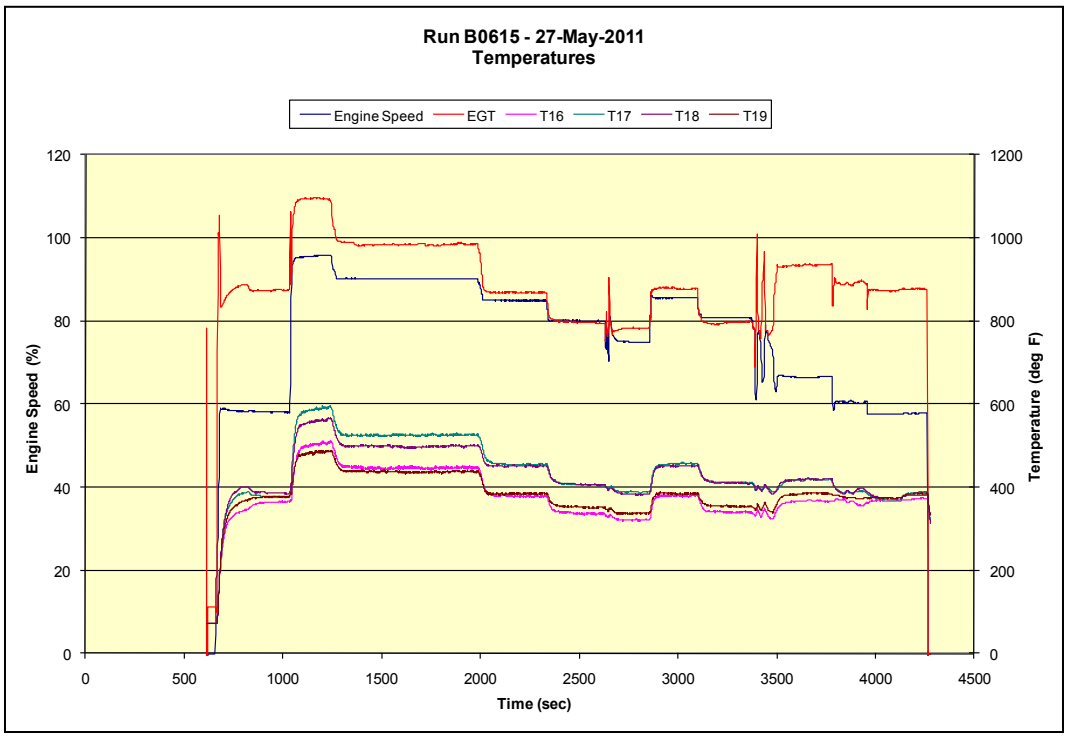

Figure C.32 – Run 615 thermocouples trailing edge

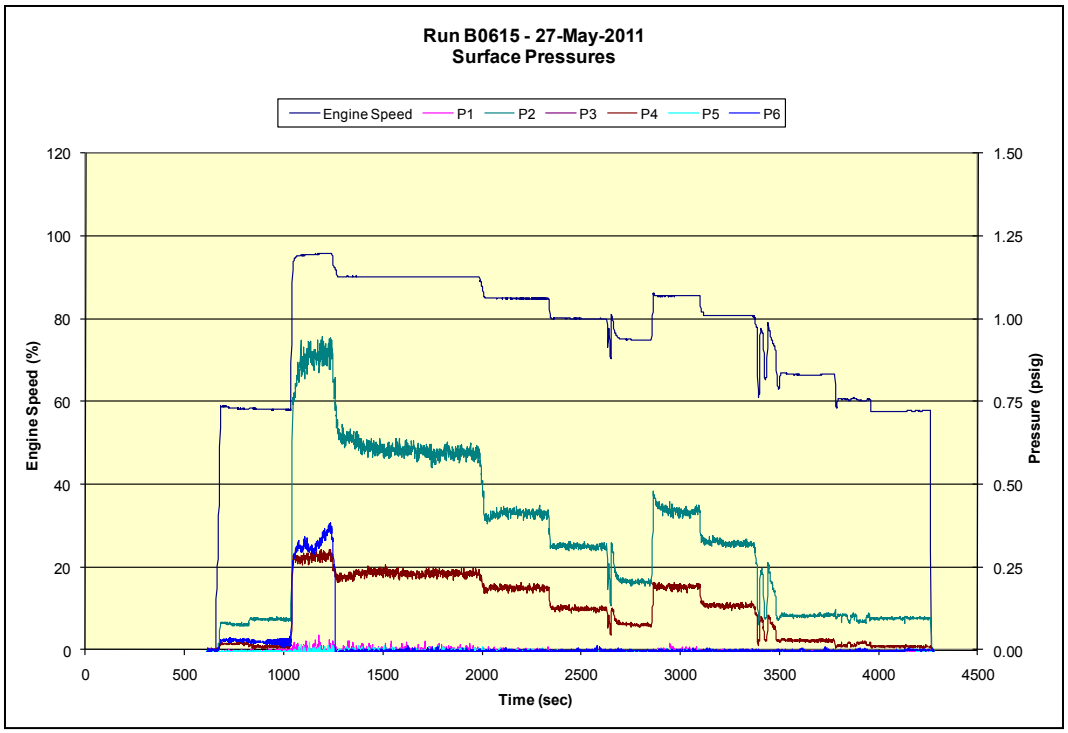

Figure C.33 – Run 615 static pressure

Appendix D. CEAC Test Notes

A summary table was created for the purposes of cataloging the test notes and providing a quick reference for understanding what data was extracted and which sensors were bad for each test. This is shown in Table D.1.

Table D.1 – Summary table for CEAC test notes

Date	Test	Type	Temp	Bad Instrumentation				Data Collected			
				Accelerometers	Strain Gauges	Microphones	Thermocouples	Pressure	Temperature	Strain	LVDT
Apr 18 2011	1	Ambient	69	1, 4, 6	3, 13, 15, 20, 27			X			
	2	Sine Sweep	73		(20)	2, 5, 9, 23, 24		X			
	2b	Sine Sweep	75	(7)		5, 9		X			
	3	Flat Spectrum	84	(3), (4), (9)	(6), (20), (27)	(5), (9), (23), (24)		X			
Apr 19 2011	4	Flat Spectrum	90	1, 2, 3, 4	27	5, 9, 24		X			
Apr 20 2011	5	Thermal Survey	100-500-150						X	X	X (4)
	6	Sine Sweep	200					X	X		X (4)
	7	Flat Spectrum	200		14			X		X	
	8	Sine Sweep	300					X			
	9	Flat Spectrum	300	1	5		5, 11	X	X	X	X (4)
Apr 21 2011	10	Sine Sweep	400					X	X		X (4)
	11	Flat Spectrum	400		5			X	X	X	X (4)
	12	Sine Sweep	500					X	X		X (4)
	13	Flat Spectrum	500		27, 28, 29, 30		10	X	X	X	X (4)
	14	Flat Spectrum	400					X	X	X	X (4)
	15	Flat Spectrum	300					X	X	X	X (4)
Apr 25 2011		Modal	500						X		
Apr 26 2011		Modal	500		2, 5, 18, 28, 29, 30			X	X		
Apr 27 2011		Modal	500						X		
Apr 28 2011	16	Thermal Survey	100-500-150		5, 9, 15, 18				X	X	
Apr 29 2011	Run 1	Endurance Test			14, 15, 28, 29, 30		12	X	X	X	
	Run 1b	Endurance Test						X	X	X	
May 02 2011	Run 1c	Endurance Test		(9)	4, 5, 9, 18, (27), (28), (29), (30)		10, 11, 12, 19, 22	X	X	X	
	Run 1d	Endurance Test			(27), (28), (29), (30)			X	X	X	
May 04 2011	Run 1e	Endurance Test			4, 5, 9, 18		10, 11, 12, 19, 22	X	X	X	
	Run 1f	Endurance Test		5, 8, 9				X	X	X	
May 05 2011	Run 1g	Endurance Test						X	X	X	
	Run 1h	Endurance Test						X	X	X	
	Run 2	Endurance Test				(1)		X	X	X	
May 06 2011	Run 2b	Endurance Test						X	X	X	
	Run 2c	Endurance Test		(2), (3), (5), (6), (8)		(1)		X	X	X	
	Run 2d	Endurance Test		2		(1)		X	X	X	
	Run 2e	Endurance Test				(1)	15	X	X	X	
	Run 2f	Endurance Test		1, 2, 3, 6	(28), (30)			X	X	X	
May 09 2011	Run 2g	Endurance Test			1, 2, 4, 5, 12, 15, 18, 24			X	X	X	
May 11 2011		Thermal Survey	200-500-200						X		X (2)
May 12 2011		Thermal Survey	500-1000				5, 6, 7, 8, 9		X		X (2)

Note: Instrumentation inside parentheses indicates a reported repair to that sensor

18 April 2011

1. Test Run #1 – Ambient Conditions
    a. Data taken for 60 seconds at 40kHz
    b. Temperature = 69°F
    c. A1, A4, A6, SG3, SG13, SG15, SG20, SG27
2. Test Run #2 – Sine Sweep (time: 1415)
    a. Test Conditions:
        i. Temperature = 73°F
        ii. Plenum Pressure = 1psi
        iii. 20-1000Hz
        iv. Sweep Rate = 10mDec/s
        v. Input Voltage = 75mV

b. Instrumentation to check:

sensor	note
SG20	fixed SG
mic 23	bad card
mic 24	bad card
mic 2	
mic 9	
mic 5	

c. DAQ module overheating – switched out.
d. Rerun sweep.

3. Test Run #2b – Sine Sweep (time: 3:28pm)
    a. Test Conditions:
        i. Temperature – 75°F
        ii. Plenum Pressure – 1psi
        iii. 20-1000Hz
        iv. Sweep Rate = 10mDec/s
        v. Input Voltage = 125mV
    b. Sweep Completed
    c. Instrumentation to check: mic 5, mic 9
    d. Inspection:
        i. A7 replaced with new accel (PCB 352C22, S/N 38979, Sensitivity = 9.717mV/g = 102.91g/V)
        ii. Ambient measurement taken @ 4:18pm
            1. Filename: 2011-04-18-1618-31.scl
4. Test Run #2 (time: 4:23pm)
    a. Test Conditions:
        i. Plenum Pressure = 16psi
        ii. Air temperature = 84°F
    b. Air Noise measurement taken
        i. Filename: 2011-04-18-???
    c. Data files:
        i. -18dB level
            1. 2011-04-18-1650.scl
            2. 2011-04-18-1651.scl
            3. 2011-04-18-1653.scl
        ii. -12dB level
            1. 2011-04-18-1654.scl
            2. 2011-04-18-????.scl
            3. 2011-04-18-1657-05.scl
        iii. -6dB level
            1. 2011-04-18-1659-22.scl
            2. 2011-04-18-1700-29.scl
            3. 2011-04-18-1701-54.scl
        iv. -3.5dB level
            1. 2011-04-18-1703-57.scl
            2. 2011-04-18-1705-02.scl
            3. 2011-04-18-1707-28.scl
        v. -1.5dB level
            1. 2011-04-18-1708-54.scl

2. 2011-04-18-1709-58.scl
3. 2011-04-18-1711-05.scl

vi. -0dB level

1. 2011-04-18-1712-54.scl
2. 2011-04-18-1714-00.scl
3. 2011-04-18-1715-12.scl

d. Test Run Completed.

e. Inspection:

i. Mic 23 and mic 24 fill off back of panel.

ii. Bad channels:

sensor	note
mic 5	
mic 9	
SG6	broken wire
SG20	loose cable
SG27	broken wire
A 3	loose cable
A 4	loose cable
A 9	loose cable

iii. Fixed all instrumentation.

19 April 2011

5. Test Run #4 (Repeat Test #3)

a. Test Conditions:

i. Use flat spectrum

ii. Air temperature = 90°F

iii. Control from mic 1

iv. Plenum Pressure = 17psi

b. Air Noise measurement

i. Filename: 2011-04-19-1240-51.scl

c. Data files:

i. -18dB level

1. 2011-04-19-1256-40.scl
2. 2011-04-19-1257-56.scl
3. 2011-04-19-1259-12.scl

ii. -12dB level

1. 2011-04-19-1301-13.scl
2. 2011-04-19-1302-54.scl
3. 2011-04-19-1304-04.scl
    a. **A3** looks bad.

iii. -6dB level

1. 2011-04-19-1305-52.scl
2. 2011-04-19-1306.scl
3. 2011-04-19-1307-20.scl
    a. **mic 5, mic 9, A3** look bad.

iv. -3.5dB level

1. 2011-04-19-1308-45.scl
2. 2011-04-19-1309-52.scl
3. 2011-04-19-1312-14.scl

a. **mic 9, A1, A2, A3** look bad.

v. -1.5dB level
1. 2011-04-19-1314-02.scl
2. 2011-04-19-1315-19.scl
3. 2011-04-19-1316-30.scl
a. **mic 5, mic 9** look bad.
b. **mic 24** fell off.

vi. 0dB level
1. 2011-04-19-1317-55.scl *error
2. 2011-04-19-1319-01.scl *error
3. 2011-04-19-1320-04.scl *error
a. File is only 38 seconds long.
b. **mic 5, mic 9, A1, A2, A3, A4** look bad. **A5, A6** are questionable.
4. 2011-04-19-1324-36.scl *error
a. **SG27** intermittent.

d. **A5** and **A6** were switched in all previous files.

20 April 2011

6. Test Run #5 – Thermal Survey
a. Test Conditions:
i. No Air.
ii. Control from TC 8.
iii. PID Parameters:
1. Kc = 0.1
2. Ti = 0.1
3. Td = 0.025

b. Data files:
i. 100°F Run
1. 2011-04-20-1038-47.scl
2. 2011-04-20-1041-14.scl

ii. 150°F Run
1. 2011-04-20-1043-31.scl
2. 2011-04-20-1046-48.scl

iii. 200°F Run
1. 2011-04-20-1048-40.scl
2. 2011-04-20-1050-38.scl

iv. 250°F Run
1. 2011-04-20-1054-27.scl
2. 2011-04-20-1056-20.scl

v. 300°F Run
1. 2011-04-20-1059-06.scl
2. 2011-04-20-1101-10.scl

vi. 350°F Run
1. 2011-04-20-1103-41.scl
2. 2011-04-20-1106-03.scl

vii. 400°F Run
1. 2011-04-20-1109-49.scl
2. 2011-04-20-1112-29.scl

viii. 450°F Run
1. 2011-04-20-1114-30.scl

2. 2011-04-20-1116-34.scl

ix. 500°F Run
1. 2011-04-20-1119-07.scl
2. 2011-04-20-1120-59.scl

x. 450°F Run
1. 2011-04-20-1124-28.scl
2. 2011-04-20-1126-59.scl

xi. 400°F Run
1. 2011-04-20-1129-17.scl
2. 2011-04-20-1132-17.scl

xii. 350°F Run
1. 2011-04-20-1135-11.scl
2. 2011-04-20-1136-46.scl

xiii. 300°F Run
1. 2011-04-20-1140-28.scl
2. 2011-04-20-1142-57.scl

xiv. 250°F Run
1. 2011-04-20-1145-42.scl
2. 2011-04-20-1147-07.scl

xv. 200°F Run
1. 2011-04-20-1152-10.scl
2. 2011-04-20-1153-53.scl

xvi. 150°F Run
1. 2011-04-20-1157-27.scl

7. <u>Test Run #6 – 200°F Sine Sweep</u> (time: 3:00pm)
   a. Test Conditions:
      i. Plenum Pressure = 18psi
      ii. 20-1000Hz
      iii. Sweep Rate = 10mDec/s
      iv. Input Voltage = 125mV
      v. Control from TC 6.
   b. RT Air Noise measurement
      i. 2011-04-20-1449-21.scl
   c. Data files:
      i. 2011-04-20-1459-55.scl
   d. Test Completed.
8. <u>Test Run #7 – 200°F – ETS</u>
   a. Test Conditions:
      i. Plenum Pressure = 18psi
      ii. Control from mic 1.
      iii. Control from TC 7.
   b. Data files: (60 second records)
      i. -18dB level
         1. 2011-04-20-1509-36.scl
         2. 2011-04-19-1511-06.scl
            a. Lots of 60 cycle noise on SG14.
         3. 2011-04-19-1512-29.scl
      ii. -12dB level
         1. 2011-04-20-1514-08.scl
         2. 2011-04-19-1516-05.scl

3. 2011-04-19-1518-14.scl

c. Stopped testing with ETS.

9. Test Run #7b – 200°F – Flat Spectrum
    a. Data files:
        i. -18dB level
            1. 2011-04-20-1523-34.scl
            2. 2011-04-20-1524-45.scl
            3. 2011-04-20-1526-12.scl
        ii. -12dB level
            1. 2011-04-20-1527-39.scl
            2. 2011-04-20-1528-48.scl
            3. 2011-04-20-1530-04.scl
        iii. -6dB level
            1. 2011-04-20-1531-41.scl
            2. 2011-04-20-1533-07.scl
            3. 2011-04-20-1534-18.scl
        iv. -3.5dB level
            1. 2011-04-20-1535-40.scl
            2. 2011-04-20-1536-54.scl
            3. 2011-04-20-1538-00.scl
        v. -1.5dB level
            1. 2011-04-20-1539-21.scl
            2. 2011-04-20-1540-30.scl
            3. 2011-04-20-1541-37.scl
        vi. 0dB level
            1. 2011-04-20-1543-04.scl
            2. 2011-04-20-1544-11.scl
            3. 2011-04-20-1545-36.scl
10. Test Run #8 – 300°F Sine Sweep
    a. Data file: 2011-04-20-1554-01.scl
11. Test Run #9 – 300°F Environmental Test – Flat Spectrum
    a. Data files:
        i. -18dB level
            1. 2011-04-20-1601-17.scl
            2. 2011-04-20-1602-24.scl *DAQ error
            3. 2011-04-20-1603-20.scl
            4. 2011-04-20-1604-28.scl
        ii. -12dB level
            1. 2011-04-20-1605-59.scl
            2. 2011-04-20-1607-05.scl
            3. 2011-04-20-1608-11.scl
        iii. -6dB level
            1. 2011-04-20-1609-35.scl
            2. 2011-04-20-1610-53.scl
            3. 2011-04-20-1612-02.scl
        iv. -3.5dB level
            1. 2011-04-20-1613-18.scl
            2. 2011-04-20-1614-24.scl
            3. 2011-04-20-1615-32.scl
        v. -1.5dB level

1. 2011-04-20-1616-49.scl
2. 2011-04-20-1617-55.scl
3. 2011-04-20-1619-03.scl

vi. 0dB level

1. 2011-04-20-1620-32.scl *error
2. 2011-04-20-1621-43.scl
    a. Seeing 200 g's on A1.
3. 2011-04-20-1622-49.scl *error
    a. TC5 and TC11 open.
4. 2011-04-20-1626-02.scl *error
5. 2011-04-20-1629-35.scl
6. 2011-04-20-1630-44.scl

b. Inspection:

i. Cleared space on DAQ hard drive.
ii. SG5 looks bad. TC11 is open.

21 April 2011

12. Test Run #10 – 400°F Sine Sweep (time: 0928)
    a. Test Conditions:
        i. Plenum Pressure = 17psi
        ii. 20-1000Hz
        iii. Sweep rate = 10mDec/s
        iv. Input Voltage = 100mV
        v. Control from TC7.
    b. Air Noise measurement: 2011-04-21-0935-06.scl
    c. Data file: 2011-04-21-0948-49.scl
    d. Test run completed.
13. Test Run #11 – 400°F EST Flat Spectrum (time: 0955)
    a. Test Conditions:
        i. Plenum Pressure = 20psi
        ii. Control from mic 1, TC7.
    b. Data files:
        i. -18dB level
            1. 2011-04-21-0956-36.scl
            2. 2011-04-21-0957-50.scl
            3. 2011-04-21-0959-00.scl
        ii. -12dB level
            1. 2011-04-21-1000-31.scl
            2. 2011-04-21-1001-41.scl
            3. 2011-04-21-1002-48.scl
        iii. -6dB level
            1. 2011-04-21-1004-24.scl
            2. 2011-04-21-1006-32.scl
            3. 2011-04-21-1006-46.scl
        iv. -3.5dB level
            1. 2011-04-21-1008-14.scl
                a. First mode appears to be decreasing in frequency.
            2. 2011-04-21-1009-21.scl
            3. 2011-04-21-1010-38.scl
        v. -1.5dB level

1. 2011-04-21-1011-57.scl
2. 2011-04-21-1013-04.scl
3. 2011-04-21-1014-11.scl

vi. 0dB level

1. 2011-04-21-1015-36.scl
2. 2011-04-21-1016-39.scl
3. 2011-04-21-1017-45.scl

c. SG5 is bad.

14. Test Run #12 – 500°F Sine Sweep
    a. Air Noise measurement: 2011-04-21-1027-11.scl
    b. Data file: 2011-04-21-1028-40.scl
15. Test Run #13 – 500°F – Flat Spectrum
    a. Data files:
        i. -18dB level
            1. 2011-04-21-1039-08.scl
            2. 2011-04-21-1040-15.scl
            3. 2011-04-21-1041-22.scl
        ii. -12dB level
            1. 2011-04-21-1042-59.scl
            2. 2011-04-21-1044-23.scl
            3. 2011-04-21-1045-31.scl
        iii. -6dB level
            1. 2011-04-21-1047-19.scl
            2. 2011-04-21-1048-26.scl
            3. 2011-04-21-1049-34.scl
        iv. -3.5dB level
            1. 2011-04-21-1051-18.scl
            2. 2011-04-21-1052-26.scl
            3. 2011-04-21-1053-50.scl
        v. -1.5dB level
            1. 2011-04-21-1055-40.scl
            2. 2011-04-21-1056-51.scl
            3. 2011-04-21-1058-02.scl
        vi. 0dB level
            1. 2011-04-21-1059-51.scl
            2. 2011-04-21-1101-06.scl
                a. TC10 went open.
            3. 2011-04-21-1102-22.scl
        vii. +3dB level (approximately 167dB)
            1. 2011-04-21-1114-42.scl
            2. 2011-04-21-1115-56.scl
            3. 2011-04-21-1117-02.scl
                a. SG29, SG30, SG27, SG28 died.
16. Test Run #14 – Repeat 400°F – Flat Spectrum
    a. Data files:
        i. -6dB level
            1. 2011-04-21-1126-43.scl
            2. 2011-04-21-1127-48.scl
            3. 2011-04-21-1128-57.scl
        ii. -3.5dB level

1. 2011-04-21-1130.scl
2. 2011-04-21-1131-29.scl
3. 2011-04-21-1132-42.scl

iii. -1.5dB level

1. 2011-04-21-1133-57.scl
2. 2011-04-21-1135-03.scl
3. 2011-04-21-1136-10.scl

iv. 0dB level

1. 2011-04-21-1147-10.scl
2. 2011-04-21-1148-17.scl
3. 2011-04-21-1149-22.scl

17. Test Run #15 – Repeat 300°F – Flat Spectrum
    a. Data files:
        i. -6dB level
            1. 2011-04-21-1208-56.scl
            2. 2011-04-21-1210-02.scl
            3. 2011-04-21-1211-12.scl
        ii. -3.5dB level
            1. 2011-04-21-1212-52.scl
            2. 2011-04-21-1214-08.scl
            3. 2011-04-21-1215-14.scl
        iii. -1.5dB level
            1. 2011-04-21-1216-34.scl
            2. 2011-04-21-1217-39.scl
            3. 2011-04-21-1219-02.scl
        iv. 0dB level
            1. 2011-04-21-1220-30.scl
            2. 2011-04-21-1221-37.scl
            3. 2011-04-21-1222-42.scl
    b. Post-Test measurement: 2011-04-21-1344-58.scl

25 April 2011

18. High Temperature Modal Test
    a. Run #1: 500°F Modal
        i. PID Parameters
            1. Kc = 0.1
            2. Ti = 0.3
            3. CV = TC6
        ii. Heat Enabled: 1100 hrs
    b. Run #2: 500°F Modal
        i. PID Parameters
            1. Kc = 0.1
            2. Ti = 0.3
            3. CV = TC9
        ii. Test Enabled: 1350 hrs
    c. Run #3: 500°F Modal
        i. PID Parameters
            1. Kc = 0.1
            2. Ti = 0.3
            3. CV = TC8

ii. Test Enabled: 1437 hrs

26 April 2011

19. High Temperature Modal Test (time: 0935)
    a. Test Conditions:
        i. 500°F modal test
        ii. Control from TC8.
        iii. Plenum Pressure = 5psi.
        iv. Modal Data Parameters:
            1. 5 averages complex
            2. 450-700Hz
            3. 1kHz bandwidth
            4. 6400 lines
    b. Data recorded at steady state:
        i. 2011-04-26-1121-31.scl
            1. Point 34 = limited signal.
        ii. 2011-04-26-1124-48.scl
    c. Instrumentation Notes:
        i. Bad: SG28, SG29, SG30, SG18, SG5, SG2
        ii. Questionable: SG27
20. High Temperature Modal Test (time: 1:38pm)
    a. Test Conditions:
        i. Control from TC8.
        ii. Plenum Pressure = 5psi.
        iii. Modal Data Parameters:
            1. 150-500Hz

27 April 2011

21. High Temperature Modal Test (time: 0852)
    a. Test Conditions:
        i. Control from TC8.
        ii. Plenum Pressure = 5psi.
        iii. Modal Data Parameters:
            1. 150-500Hz
    b. Data file: *high temp(150-500Hz)*
22. Repeat High Temperature Modal Test (time: 1242)
    a. Test Conditions:
        i. Control from TC8.
        ii. Plenum Pressure = 5psi.
        iii. Modal Data Parameters:
            1. 100-200Hz

28 April 2011

23. Test Run #16 – Repeat Thermal Survey (time: 1400)
    a. Test Conditions:
        i. Plenum Pressure = 5psi
        ii. Control from TC 8.
        iii. PID Parameters:
            1. Kc = 0.1
            2. Ti = 0.3

b. Data files: (10 second records)
    i. 100°F
        1. 2011-04-28-1408-05.scl
        2. 2011-04-20-1408-49.scl
    ii. 150°F
        1. 2011-04-28-1412-31.scl
        2. 2011-04-20-1413-56.scl
            a. Bad instrumentation: SG5, SG9, SG18
    iii. 200°F
        1. 2011-04-28-1417-39.scl
        2. 2011-04-20-1419-11.scl
    iv. 250°F
        1. 2011-04-28-1422-44.scl
        2. 2011-04-20-1425-00.scl
    v. 300°F
        1. 2011-04-28-1428-06.scl
        2. 2011-04-20-1429-53.scl
    vi. 350°F
        1. 2011-04-28-1433-09.scl
        2. 2011-04-20-1435-03.scl
            a. SG15 reading highest strain of approximately 2100με
    vii. 400°F
        1. 2011-04-28-1437-46.scl
        2. 2011-04-20-1439-22.scl
    viii. 450°F
        1. 2011-04-28-1443-20.scl
        2. 2011-04-20-1445-01.scl
    ix. 500°F
        1. 2011-04-28-1448-10.scl
        2. 2011-04-20-1450-38.scl
    x. 450°F
        1. 2011-04-28-1453-25.scl
        2. 2011-04-20-1455-38.scl
    xi. 400°F
        1. 2011-04-28-1458-21.scl
        2. 2011-04-20-1500-43.scl
c. Data files: (5 second records)
    i. 350°F
        1. 2011-04-28-1503-38.scl
        2. 2011-04-20-1505-57.scl
    ii. 300°F
        1. 2011-04-28-1508-30.scl
        2. 2011-04-20-1511-01.scl
    iii. 250°F
        1. 2011-04-28-15103-40.scl
        2. 2011-04-20-1511-01.scl
    iv. 200°F
        1. 2011-04-28-1518-51.scl
        2. 2011-04-20-1521-17.scl
    v. 150°F

1. 2011-04-28-1524-18.scl
2. 2011-04-20-1526-32.scl
    a. SG15 questionable ("stuck" at about 1260με)

d. Post-Test measurement
    i. 2011-04-28-1710-03.scl
    ii. Everything cooled to approximately 75°F.

29 April 2011

24. <u>500°F Endurance Test – Run #1</u>
    a. Pre-test inspection:
        i. A7 changed out.
        ii. Modulator valve #2 changed out.
    b. Test Conditions:
        i. Plenum Pressure = 17psi
        ii. Control from TC 8.
        iii. PID Parameters:
            1. Kc = 0.1
            2. Ti = 0.3
            3. Td = 0
    c. Heat Enabled at 1314 hrs.
    d. Air Noise measurement: 2011-04-29-1312-49.scl
    e. Valve #3 died at before reaching full load.
    f. Data Samples: (60 second records; about 167dB level)
        i. Start: 2011-04-29-1329-37.scl
        ii. 15 minutes: 2011-04-29-1342-37.scl
            1. High noise level on SG14.
            2. SG15 bad.
    g. Overload 16:43 into run. Test aborted.
    h. Inspection:
        i. Changed gain setting from 1.5psi/V to 0.5psi/V.
        ii. Modulator valves 2 and 3 dead. Replaced.
        iii. Instrumentation:
            1. TC12 dead.
            2. SG28, SG29, SG30 (previously had been repaired) have broken wires.
25. <u>Test Run #1b – Continue Endurance Test</u>
    a. Pre-test inspection: Checked wires on mic 1.
    b. Test Conditions:
        i. Plenum Pressure = 18psi
        ii. Acoustic level = 167dB
    c. Data Samples:
        i. Start [17 minutes overall]: 2011-04-29-1528-32.scl
        ii. [30 minutes]: 2011-04-29-1541-25.scl
        iii. [45 minutes]: 2011-04-29-1556-21.scl
    d. Test aborted at 29:26 run time. Total run time = 46:09.
26. <u>Test Run #1c – Continue Endurance Test</u>
    a. Pre-Test inspection:
        i. No damage detected.
        ii. Bad instrumentation:
            1. TC10, TC11, TC12, TC19
            2. SG5, SG9, SG18, SG27, SG28, SG29, SG30

b. Test Conditions:
    i. Plenum Pressure = 18psi
    ii. Acoustic level = 167dB
c. Heat enabled at 0915 hrs.
d. Data Samples:
    i. Start [46 minutes overall]: 2011-05-02-0927-45.scl
        1. TC19, TC22 questionable
        2. A9 dead, A3 questionable
    ii. [60 minutes]: 2011-05-02-0941-09.scl
    iii. [75 minutes]: 2011-05-02-0956-05.scl *partial record, DAQ error
        1. 2011-05-02-0957-36.scl *partial record
        2. 2011-05-02-0959-57.scl *full 60 second record
        3. SG4 bad.
        4. TC13 questionable.
    iv. [90 minutes]: 2011-05-02-1011-06.scl
    v. [1 hr 45 min]: 2011-05-02-1026-07.scl
    vi. [2 hrs]: 2011-05-02-1041-06.scl
e. Test aborted at 1:14:41 run time. Total run time = 2:00:50.
f. Inspection:
    i. Replaced A9 (new sensor: S/N 79730, sensitivity = 105.263g/V). A3 is questionable.
    ii. Repaired wires on SG's 27-30 (front side). SG's 4, 5, 9, 18 have broken wires.
    iii. TC's 10-12, 19, 22 are dead.
    iv. Retorqued side fasteners to 65 in-lbs.

27. Test Run #1d – Continue Endurance Test
    a. Test Conditions:
        i. Plenum Pressure = 18psi
        ii. Acoustic level = 167dB
    b. Heat enabled at 1438 hrs.
    c. Air Noise measurement: 2011-05-02-1434-06.scl
    d. Instrumentation:
        i. SG 29 questionable.
        ii. SG27 bad.
        iii. SG29, SG30 died during acoustic ramp.
    e. Data Samples:
        i. Start [2 hrs 1 min overall]: 2011-05-02-1454-06.scl
        ii. [2 hr 15 min]: 2011-05-02-1507-50.scl
    f. Observed shower of sparks at top of lamp cart.
        i. Test aborted at 20:17 run time. Total run time = 2:21:07.
    g. Inspection:
        i. Replaced SG's 27-30 on front surface.
        ii. Sparks were caused by nut plate falling from top of chamber onto lamp bank bus bars. All of these nut plates will be removed.

4 May 2011

28. Test Run #1e – Continue Endurance Test
    a. Test Conditions:
        i. Plenum Pressure = 17.5psi
        ii. Acoustic level = 167dB
    b. Heat enabled at 0934 hrs.

c. Instrumentation:
    i. SG's 4, 5, 9, 18 are bad.
    ii. TC's 10, 11, 12, 19, 22 are bad.
d. Air Noise measurement: 2011-05-04-0931-34.scl
e. Data Samples:
    i. [2 hrs 30 min overall]: 2011-05-04-0959-58.scl
    ii. [2 hr 45 min]: 2011-05-04-1014-36.scl
f. Overload at 24:13 run time (modulator valves 7, 9, 10 died). Total run time = 2:45:20.
g. Post-Test: Blown valves were replaced.

29. Test Run #1f – Continue Endurance Test
    a. Test Conditions:
        i. Plenum Pressure = 18psi
        ii. Acoustic level = 167dB
    b. Heat enabled at 1318 hrs.
    c. Data Samples:
        i. Start [2 hrs 46 min overall]: 2011-05-04-1331-32.scl
            1. A5, A8, A9 bad.
        ii. [3 hrs]: 2011-05-04-1347-05.scl
        iii. [3 hr 15 min]: 2011-05-04-1400-48.scl
        iv. [3 hr 30 min]: 2011-05-04-1415-59.scl
    d. Observed water leaking on lamp side of chamber.
        i. Test aborted at 55:19 run time. Total run time = 3:40:39.
    e. Inspection:
        i. Source of leak found to be a microphone cooling line. The hose was replaced.

5 May 2011

30. Test Run #1g – Continue Endurance Test
    a. Test Conditions:
        i. Plenum Pressure = 18psi
        ii. Acoustic level = 167dB
    b. Heat enabled at 0948 hrs.
    c. Air Noise measurement: 2011-05-05-0949-16.scl
        i. Modulator valve #1 not working.
    d. Data Samples:
        i. [3 hrs 45 min overall]: 2011-05-05-1005-36.scl
    e. Overload at 9:10 run time (modulator valve #7 died). Total run time = 3:49:49.
        i. Valves checked and changed out where needed.
31. Test Run #1h – Continue Endurance Test
    a. Test Conditions:
        i. Plenum Pressure = 18psi
        ii. Acoustic level = 167dB
    b. Heat enabled at 1100 hrs.
    c. Data Samples:
        i. [4 hrs overall]: 2011-05-05-1116-26.scl
    d. Lost modulator valve #9. Acoustic level dropped to 166dB.
        i. Test aborted at 4:50 run time. Total run time = 4:00:06.
    e. Inspection:
        i. No damage to panel observed.
        ii. Water leaking under chamber (from microphone hose).
        iii. Going to try new spectrum.

1. 89.1-562Hz
2. A2 and A4 should read 120Hz and 115Hz respectively at 167dB.
3. SG14 should show 155με (dynamic) at 167dB.

32. Test Run #2 – Endurance Test
    a. Test Conditions:
        i. Plenum Pressure = 18psi
        ii. Acoustic level = 164dB (using new spectrum)
    b. Heat enabled at 1322 hrs.
    c. Data Samples:
        i. Start [4 hrs 1 min overall]: 2011-05-05-1337-25.scl
        ii. [4 hrs 15 min]: 2011-05-05-1350-39.scl
    d. Lost valves 11, 12. Valves 6, 8 questionable.
        i. Test aborted at 29:01 run time (reduced spectrum). Total run time = 4:29:07.
    e. Inspection:
        i. A rivet from the bottom trailing edge corner is broken. Upon first observation, the fracture appears to be a fatigue failure.
        ii. Fixed the loose wire on mic 1.

6 May 2011

33. Test Run #2b – Continue Endurance Test
    a. Test Conditions:
        i. Plenum Pressure = 18psi
        ii. Acoustic level = 164dB (using new spectrum)
    b. Heat enabled at 0809 hrs.
    c. Air Noise measurement: 2011-05-06-0808-09.scl
        i. Taken during ramp up.
    d. Data Samples:
        i. [4 hrs 30 min overall]: 2011-05-06-0824-47.scl
        ii. [4 hrs 45 min]: 2011-05-06-1839-35.scl
        iii. [5 hrs]: 2011-05-06-1854-16.scl
    e. Overload at 32:31 run time (modulator valve #12 died). Total run time = 5:01:38.
    f. Inspection:
        i. Performed tap test on article and checked fasteners. Everything looks good.
        ii. Replaced modulator valves #1, 3, 12.
34. Test Run #2c – Continue Endurance Test
    a. Test Conditions:
        i. Plenum Pressure = 17psi
        ii. Acoustic level = 164dB (using new spectrum)
    b. Heat enabled at 1018 hrs.
    c. Air Noise measurement: 2011-05-06-1014-52.scl
    d. Modulator valve #4 died during ramp up.
    e. Data Samples:
        i. Start [5 hrs 2 min overall]: 2011-05-06-1031-15.scl
        ii. [5 hrs 15 min]: 2011-05-06-1044-09.scl
            1. Lost A2, A3, A5, A6, A8.
        iii. [5 hrs 30 min]: 2011-05-06-1059-07.scl
    f. Overload at 40:19 run time (modulator valve #9 died). Total run time = 5:41:57.
    g. Inspection:
        i. Changed out valves 4, 9.
        ii. Replaced cable on A8. Tightened cables on A2, A3, A5, A6.

iii. Fixed wire on mic 1.

35. Test Run #2d – Continue Endurance Test
    a. Test Conditions:
        i. Plenum Pressure = 17psi
        ii. Acoustic level = 164dB (using new spectrum)
    b. Heat enabled at 1354 hrs.
    c. A2 dead.
    d. Data Samples:
        i. [5 hrs 45 min overall]: 2011-05-06-1412-58.scl
            1. Running at about 165.5dB.
    e. Test aborted at 13:48 run time to allow modulator valves to cool. Total run time = 5:55:45.
    f. Inspection:
        i. Fixed loose wire in block for mic 1 (control).
        ii. Could hear panel popping during cool down.
36. Test Run #2e – Continue Endurance Test
    a. Test Conditions:
        i. Plenum Pressure = 18psi
        ii. Acoustic level = 164dB (using new spectrum)
    b. Heat enabled at 1450 hrs.
    c. TC 15 died.
    d. Data Samples:
        i. [6 hrs overall]: 2011-05-06-1504-44.scl *error
            1. 2011-05-06-1506-21.scl *error
            2. 2011-05-06-1507-30.scl *error
        ii. Discovered that door to the CEAC data shack was open.
    e. Test aborted at 13:32 run time to allow modulator valves to cool. Total run time = 6:09:17.
    f. Inspection:
        i. Fixed mic 1 (control).
        ii. Closed door on data shack.
37. Test Run #2f – Continue Endurance Test
    a. Test Conditions:
        i. Plenum Pressure = 17psi
        ii. Acoustic level = 164dB (using new spectrum)
    b. Heat enabled at 1536 hrs.
    c. Data Samples:
        i. Start [6 hrs 10 min overall]: 2011-05-06-1546-04.scl
            1. Running at about 165dB.
            2. A1 died. A2, A3, A6 are dying.
        ii. [6 hrs 15 min]: 2011-05-06-1551-24.scl
        iii. [6 hrs 30 min]: 2011-05-06-1606-09.scl
        iv. [6 hrs 45 min]: 2011-05-06-1621-12.scl
        v. [7 hrs]: 2011-05-06-1635-33.scl
    d. Test aborted at 50:49 run time. Total run time = 7:00:06.
    e. Inspection:
        i. Test stopped due to shift in resonant frequency of first mode from 150Hz to 100Hz.
        ii. All of the bolts on the top side were below the specified torque value. Retorqued to 70 in-lbs.

iii. No additional damage detected.
iv. Repaired SG28, SG30.

9 May 2011

38. Test Run #2g – Continue Endurance Test
    a. Test Conditions:
        i. Plenum Pressure = 18psi
        ii. 500°F profile.
        iii. Control from TC 8.
    b. Heat enabled at 1:03pm.
    c. First bending mode at 110Hz. Test aborted.
    d. Inspection:
        i. Several cracks found in the structure.
        ii. Bad SG's: 1, 2, 4, 5, 12, 15, 18, 24.

11 May 2011

39. Post Endurance Test – Thermal Survey
    a. Test Conditions:
        i. Plenum Pressure = 10psi
        ii. Control from TC 8.
        iii. 300 second holds at 200°F, 300°F, 400°F, 500°F.
    b. Data files:
        i. 200°F
            1. 2011-05-11-1505-25.scl
            2. 2011-05-11-1506-32.scl
        ii. 300°F
            1. 2011-05-11-1510-06.scl
            2. 2011-05-11-1511-23.scl
        iii. 400°F
            1. 2011-05-11-1516-02.scl
            2. 2011-05-11-1517-08.scl
        iv. 500°F
            1. 2011-05-11-1520-25.scl
            2. 2011-05-11-1522-18.scl
        v. 400°F
            1. 2011-05-11-1524-57.scl
            2. 2011-05-11-1527-44.scl
        vi. 300°F
            1. 2011-05-11-1530-21.scl
            2. 2011-05-11-1532-05.scl
        vii. 200°F
            1. 2011-05-11-1537-32.scl
            2. 2011-05-11-1538-43.scl
        viii. Cool Down
            1. 2011-05-11-1545-09.scl

12 May 2011

40. Post Endurance Test – 500°F-1000°F Thermal Survey
    a. Test Conditions:
        i. Plenum Pressure = 10psi

ii. Drive control.

b. Pre-test measurement: 2001-05-12-1000-10.scl

c. Heat Enabled at 1009 hrs.
   i. LVDT reading -0.002 inches.

d. Data files:
   i. 500°F
      1. 2011-05-12-1019-49.scl
      2. 2011-05-12-1023-25.scl
   ii. 600°F
      1. 2011-05-12-1030-16.scl
      2. 2011-05-12-1035-08.scl
   iii. 700°F
      1. 2011-05-12-1040-09.scl
      2. 2011-05-12-1044-58.scl
   iv. 750°F
      1. 2011-05-12-1049-37.scl
      2. 2011-05-12-1052-41.scl
   v. 900°F
      1. 2011-05-12-1101-42.scl
   vi. 1000°F
      1. 2011-05-12-1108-55.scl

e. Inspection:
   i. The trailing edge appeared to be rubbing against the fixture. Marks were found on the U-shaped angle in two locations.
   ii. TC's 5-9 were detached from the surface.
   iii. LVDT location (measured on back surface from upper left corner)
      1. 1.25 inches from top
      2. 5.75 inches from left edge
      3. Location noted on instrumentation drawing LVDT2

13 May 2011

41. Air Velocity Test

a. Velocity Indicator mounted in upstream microphone mounting hole.
   i. Data:

Pressure (psi)	Velocity (ft/min)
1.5	2300
5	4800
11	7150
15	8500
20	9900

b. Velocity Sensor mounted in downstream microphone hole.

i. Data:

Pressure (psi)	Velocity (ft/min)
1.5	3000
6	6330
11	8560
15	10000

17 May 2011

1. Air Velocity Test Continued
   a. Velocity Sensor mounted in center of test section, bottom microphone hole.
      i. Data:

Pressure (psi)	Velocity (ft/min)
1.5	2450
6	5440
10	7400
15	9300
18	9950

All of the measured plenum data is shown in Figure D.1.

2. Post Test Article and Fixture Weight
   a. Assembly weight = 228.6 lbs
   b. Frame/Nuts/Bolts = 193.9 lbs
   c. Panel = 34.6 lbs
   d. All weight measurements are ±0.1 lbs tolerance

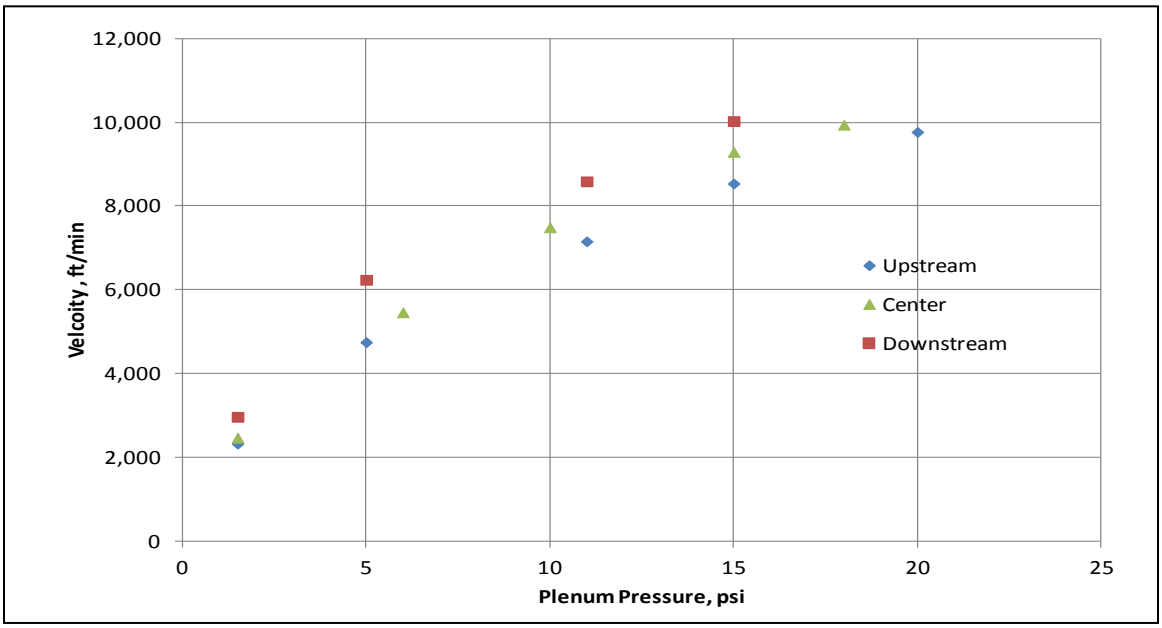

Figure D.1 – CEAC chamber plenum pressure

Appendix E. CEAC Test Instrumentation Drawings and Listing

Table E.1 – Instrumentation

NI Channel	Sensor Type	Sensor Model	Sensor S/N	CC Channel	2210 Channel	Device ID	Sensor Location
1	WC Mic	WCT-312-5 SG	Z78-53		1		Upstream 6" from center of leading edge of fixture
2	WC Mic	WCT-312-5 SG	Z78-49		2		Ceiling of test section along center line of article
3	WC Mic	WCT-312-5 SG	Z78-51		3		Floor of test article along center line of article
4	WC Mic	WCT-312-5 SG	Z78-52		4		Downstream 12" from center of trailing edge of test article
5	190HT Mic	MIC-190HT	5046-1-57		5		Top faring upstream
6	190HT Mic	MIC-190HT	J27-60		6		Top faring center
7	190HT Mic	MIC-190HT	Q27-31		7		Top faring downstream
8	190HT Mic	MIC-190HT	J27-62		8		Bottom faring upstream
9	190HT Mic	MIC-190HT	J27-63		9		Bottom faring center
10	190HT Mic	MIC-190HT	-		10		Bottom faring downstream
11	Flat Pack Prs TD	LQ-125-5 SG	250		11		See Instrumentation Drawing
12	Flat Pack Prs TD	LQ-125-5 SG	256		12		See Instrumentation Drawing
13	Flat Pack Prs TD	LQ-125-5 SG	265		13		See Instrumentation Drawing
14	Flat Pack Prs TD	LQ-125-5 SG	667		14		See Instrumentation Drawing
15	Flat Pack Prs TD	LQ-125-5 SG	266		15		See Instrumentation Drawing
16	Flat Pack Prs TD	LQ-125-5 SG	268		16		See Instrumentation Drawing
17	Flat Pack Prs TD	LQ-125-5 SG	273		17		See Instrumentation Drawing
18	Flat Pack Prs TD	LQ-125-5 SG	271		18		See Instrumentation Drawing
19	Flat Pack Prs TD	LQ-125-5 SG	259		19		See Instrumentation Drawing
20	Flat Pack Prs TD	LQ-125-5 SG	269		20		See Instrumentation Drawing
21	Flat Pack Prs TD	LQ-125-5 SG	267		21		See Instrumentation Drawing
22	Flat Pack Prs TD	LQ-125-5 SG	260		22		See Instrumentation Drawing
23	Piezoelectric Mic	Model 2510	DD47	1			Center Stiffener, Bay #2
24	Piezoelectric Mic	Model 2510	DD37	2			Center Stiffener, Bay #3
25	Strain Gage	WK-06-125AD-350			23	SG01	See Instrumentation Drawing
26	Strain Gage	WK-06-125AD-350			24	SG02	See Instrumentation Drawing
27	Strain Gage	WK-06-125AD-350			25	SG03	See Instrumentation Drawing
28	Strain Gage	WK-06-125AD-350			26	SG04	See Instrumentation Drawing
29	Strain Gage	WK-06-125AD-350			27	SG05	See Instrumentation Drawing
30	Strain Gage	WK-06-125AD-350			28	SG06	See Instrumentation Drawing
31	Strain Gage	WK-06-125AD-350			29	SG07	See Instrumentation Drawing
32	Strain Gage	WK-06-125AD-350			30	SG08	See Instrumentation Drawing
33	Strain Gage	WK-06-125AD-350			31	SG09	See Instrumentation Drawing
34	Strain Gage	WK-06-125AD-350			32	SG10	See Instrumentation Drawing
35	Strain Gage	WK-06-125AD-350			33	SG11	See Instrumentation Drawing
36	Strain Gage	WK-06-125AD-350			34	SG12	See Instrumentation Drawing
37	Strain Gage	WK-06-125AD-350			35	SG13	See Instrumentation Drawing
38	Strain Gage	WK-06-125AD-350			36	SG14	See Instrumentation Drawing
39	Strain Gage	WK-06-125AD-350			37	SG15	See Instrumentation Drawing
40	Strain Gage	WK-06-125AD-350			38	SG16	See Instrumentation Drawing
41	Strain Gage	WK-06-125AD-350			39	SG17	See Instrumentation Drawing
42	Strain Gage	WK-06-125AD-350			40	SG18	See Instrumentation Drawing
43	Strain Gage	WK-06-125AD-350			41	SG19	See Instrumentation Drawing
44	Strain Gage	WK-06-125AD-350			42	SG20	See Instrumentation Drawing
45	Strain Gage	WK-06-125AD-350			43	SG21	See Instrumentation Drawing
46	Strain Gage	WK-06-125AD-350			44	SG22	See Instrumentation Drawing
47	Strain Gage	WK-06-125AD-350			45	SG23	See Instrumentation Drawing
48	Strain Gage	WK-06-125AD-350			46	SG24	See Instrumentation Drawing
49	Strain Gage	WK-06-125AD-350			47	SG25	See Instrumentation Drawing
50	Strain Gage	WK-06-125AD-350			48	SG26	See Instrumentation Drawing
51	Strain Gage	WK-06-125AD-350			49	SG27	See Instrumentation Drawing
52	Strain Gage	WK-06-125AD-350			50	SG28	See Instrumentation Drawing
53	Strain Gage	WK-06-125AD-350			51	SG29	See Instrumentation Drawing
54	Strain Gage	WK-06-125AD-350			52	SG30	See Instrumentation Drawing
55	HT Accelerometer	2220D	DW55	3			See Instrumentation Drawing
56	HT Accelerometer	2220E	13977	4			See Instrumentation Drawing
57	HT Accelerometer	2220E	13978	5			See Instrumentation Drawing
58	HT Accelerometer	2220E	13979	6			See Instrumentation Drawing
59	HT Accelerometer	2220E	13980	7			See Instrumentation Drawing
60	HT Accelerometer	2220E	13981	8			See Instrumentation Drawing
61	Accelerometer	352C22	79236	9			See Instrumentation Drawing
62	Accelerometer	352C22	79671	10			See Instrumentation Drawing
63	Accelerometer	352C22	79232	11			See Instrumentation Drawing
64	Laser Vibrometer						Center of Bay #2, 13.50" from leading edge of test article

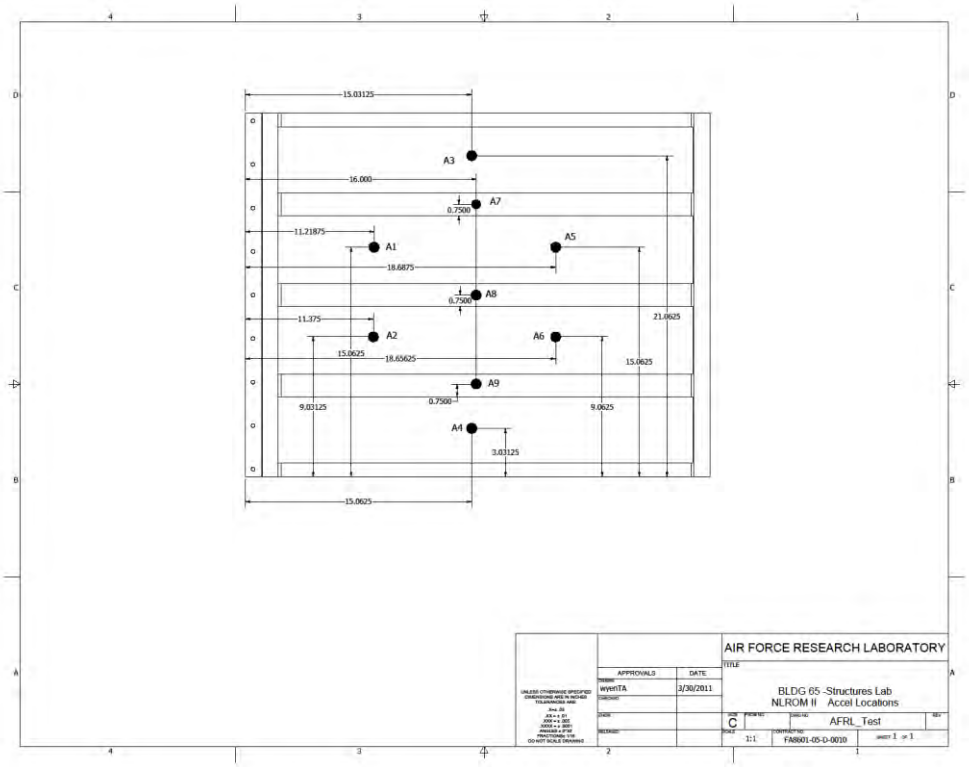

Figure E.1 – Accelerometer locations

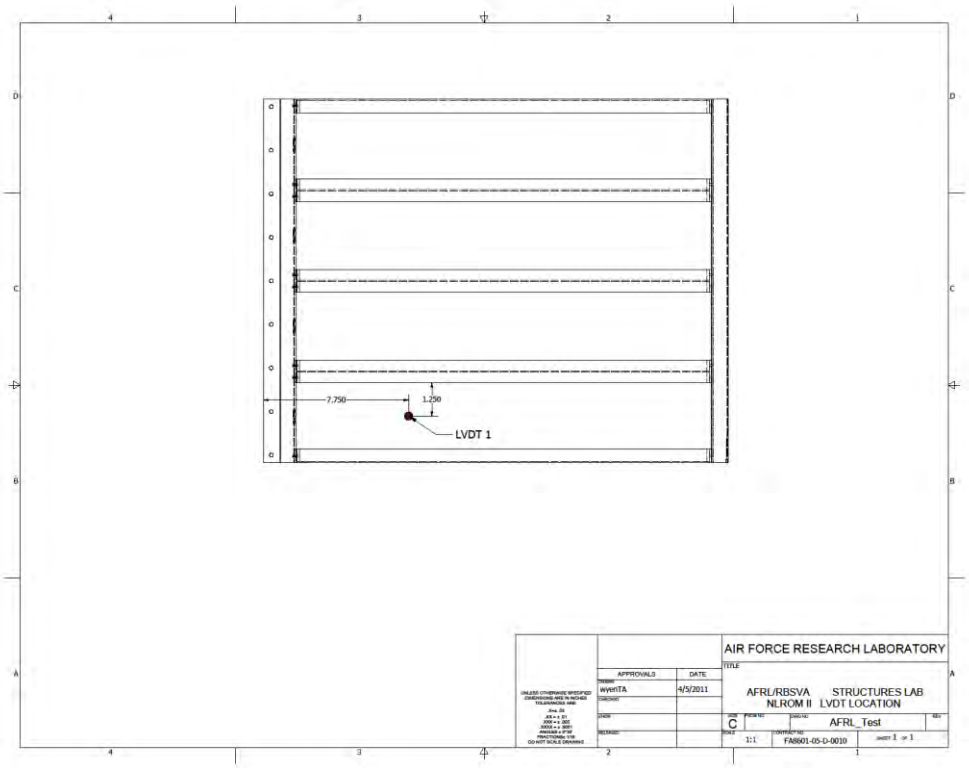

Figure E.2 – LVDT 1 location

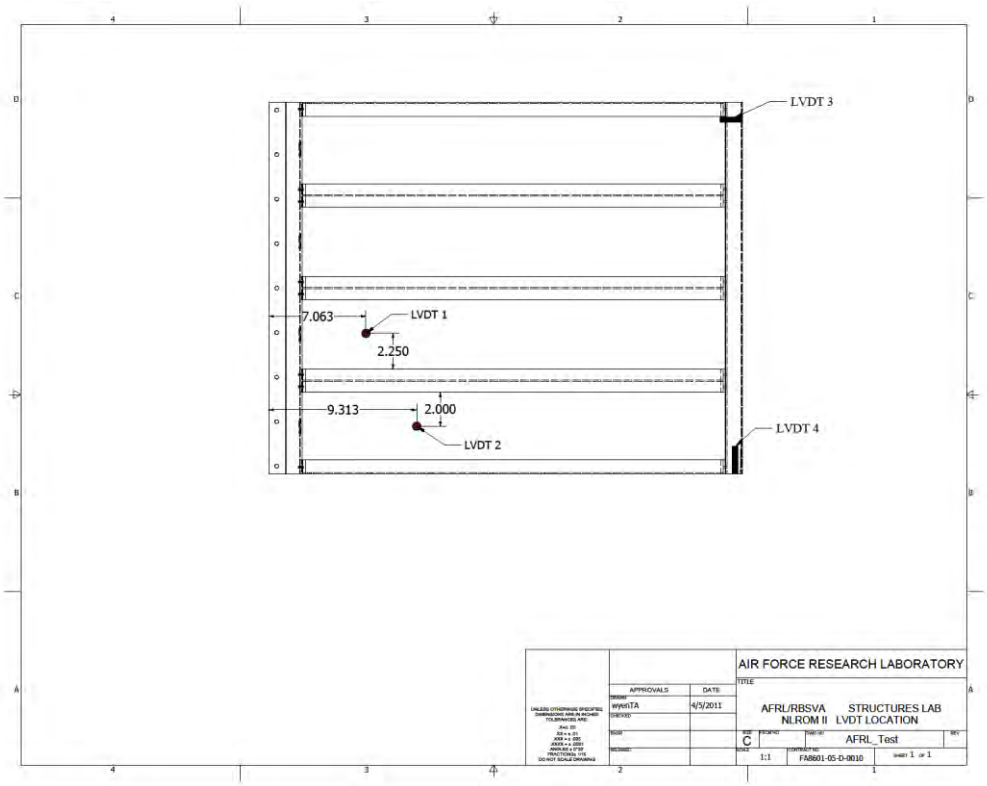

Figure E.3 – Locations of LVDTs

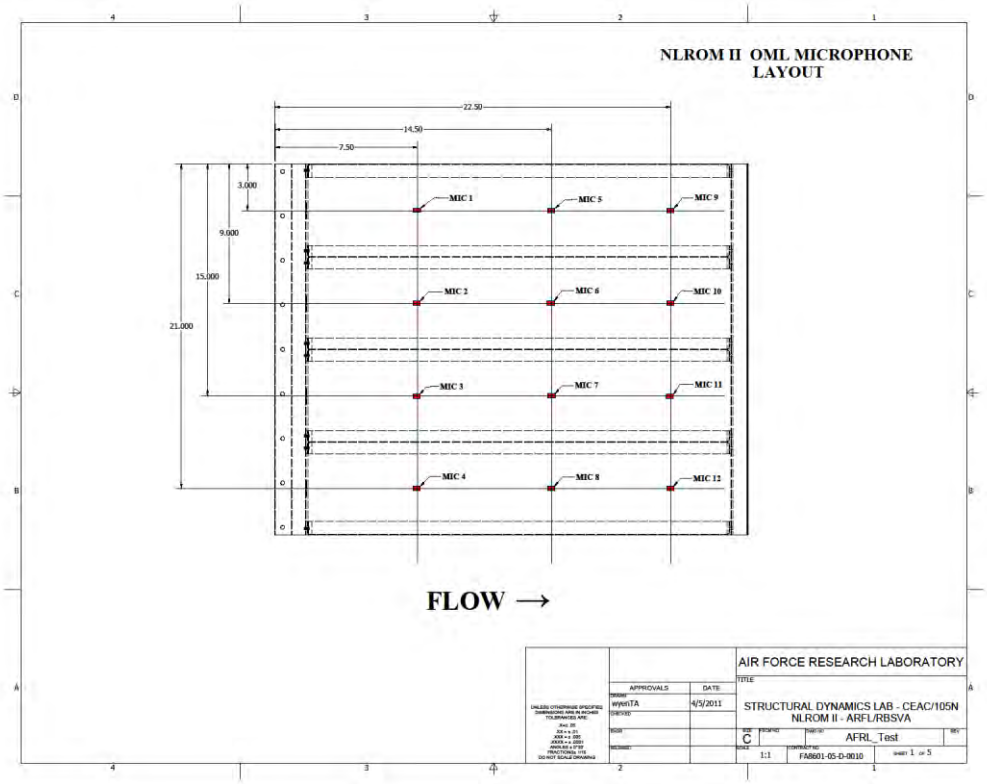

Figure E.4 – OML Microphone Layout

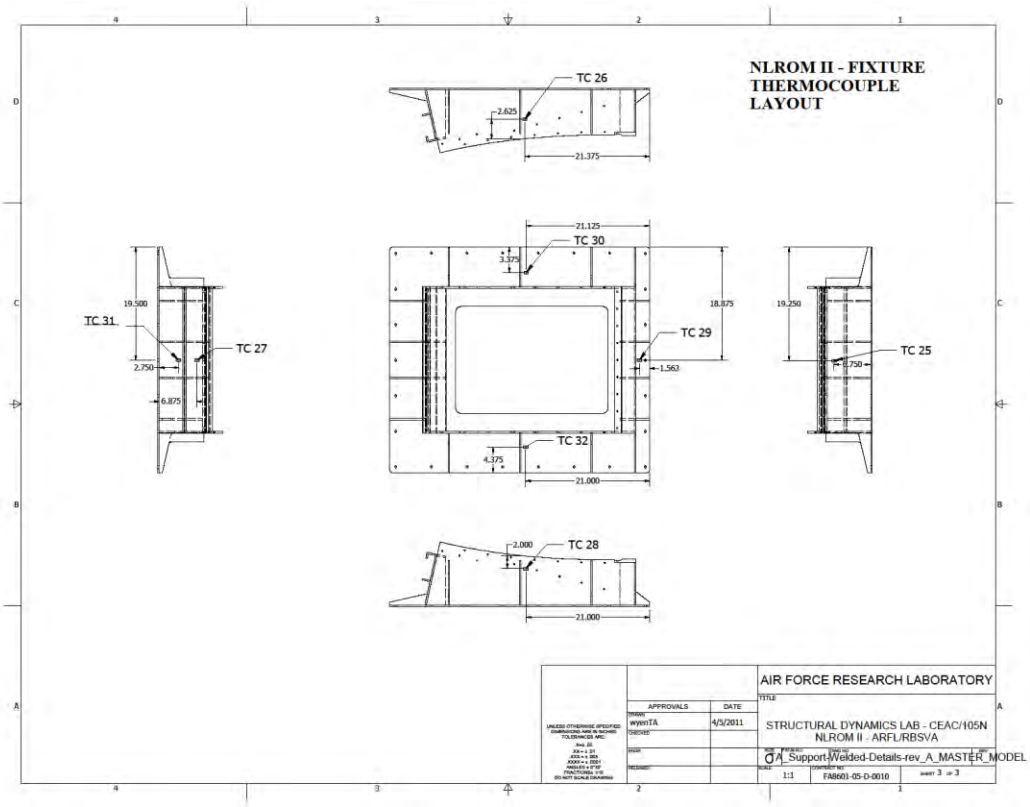

Figure E.5 – Thermocouple Layout

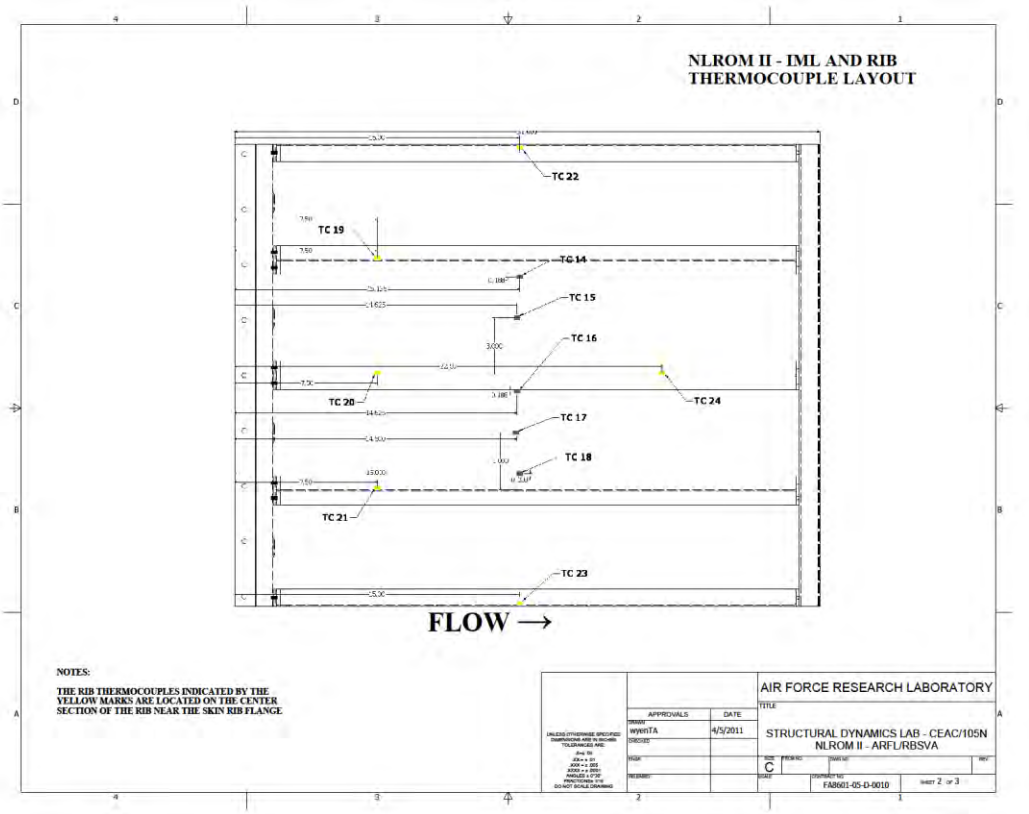

Figure E.6 – IML and Rib Thermocouple Layout

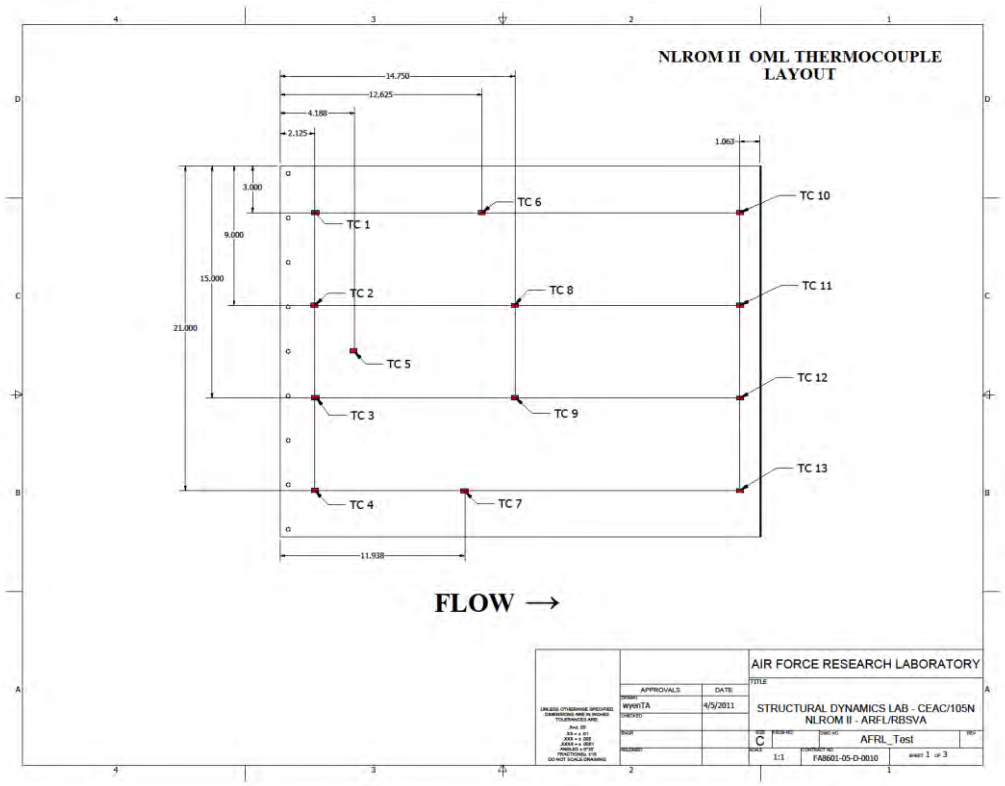

Figure E.7 – OML Thermocouple Layout

Appendix F. Test Article and Fixture Drawing

A total two test articles were fabricated, one for each test. The test article is shown below. The three interior ribs are fabricated from Titanium 6Al-4V thick plate stock. The two outer ribs are stainless steel, 15-5PH H1025. The lower skin is also Ti 6AL-4V, and was made from 0.063 inch thin sheet and rolled to the radius of curvature. The forward and aft closure spars are also stainless steel machining. On the upper side, a sheet skin was not used. Instead three cold rolled steel extrusions, steel A36 L-angles (1”x1”x0.125”), were used to brace the ribs. The lower skin is attached to the ribs using aircraft standard fasteners.

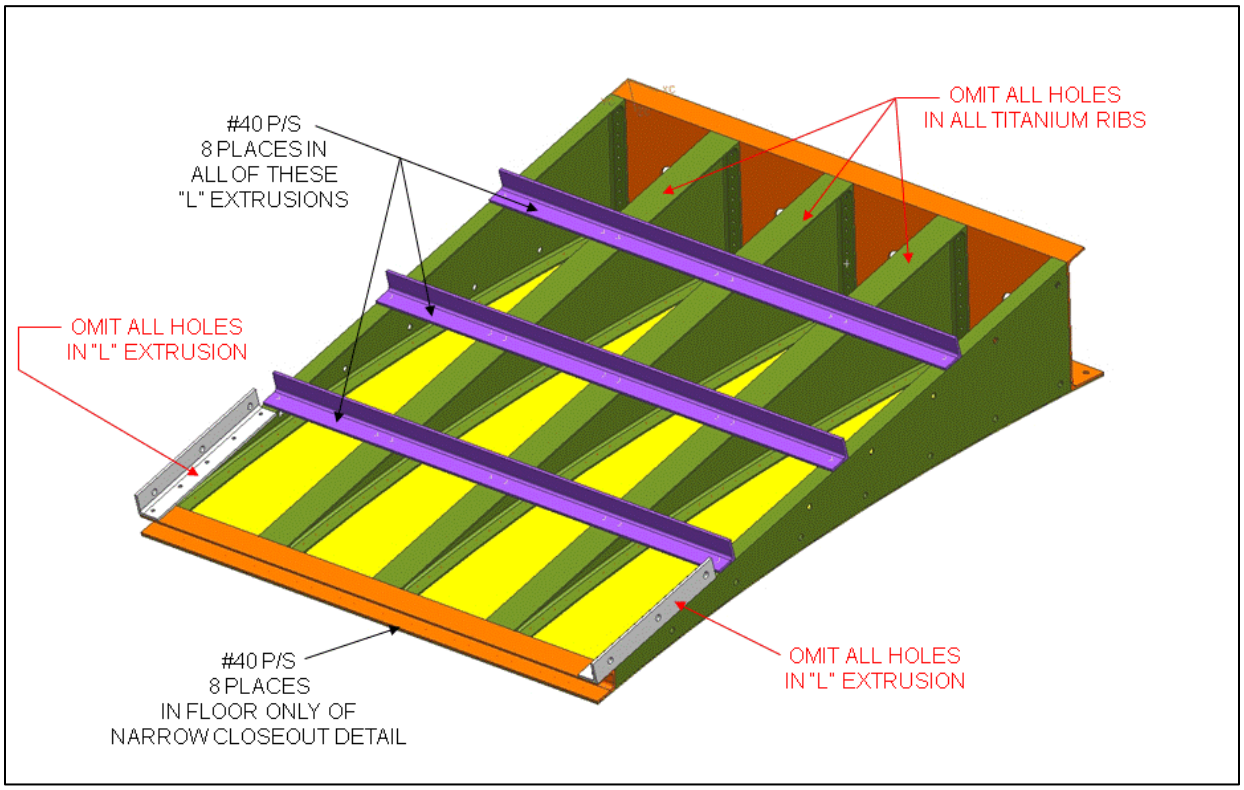

Figure F.1 – Final test article

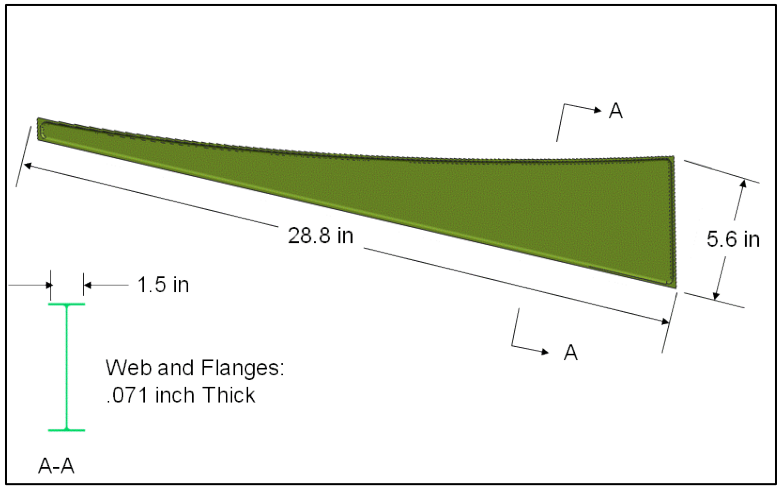

Figure F.2 – Interior Rib – Drawing

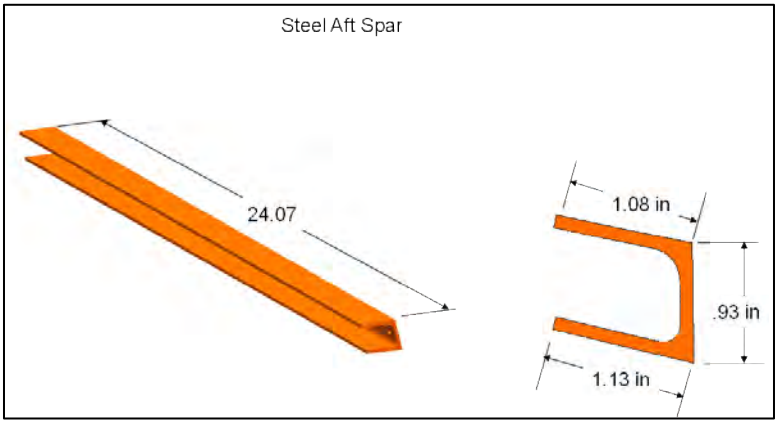

Figure F.3 – Steel aft spar – drawing

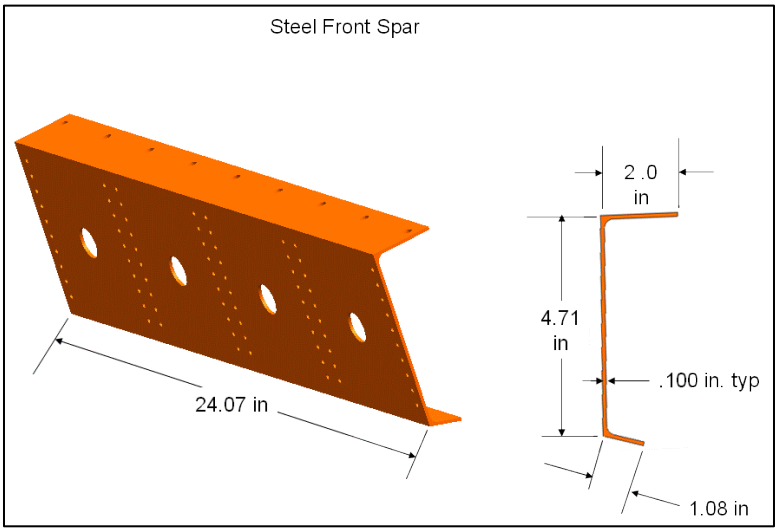

Figure F.4 – Steel front spar – drawing

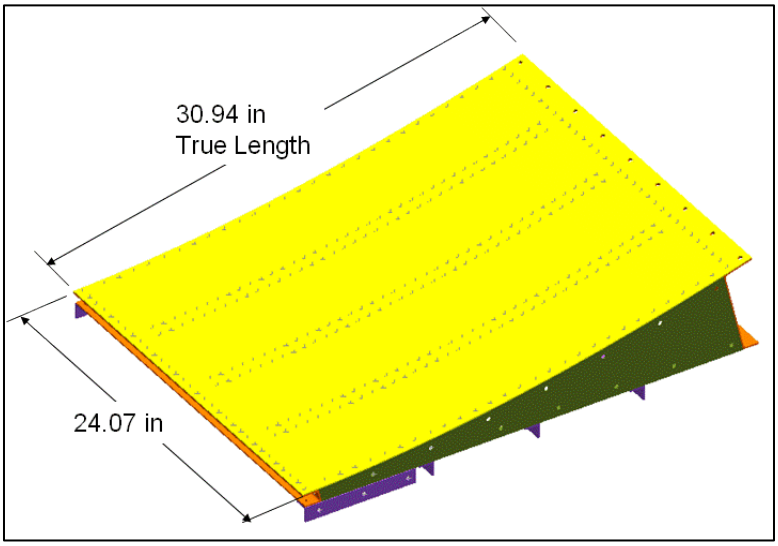

Figure F.5 – Test article final dimensions

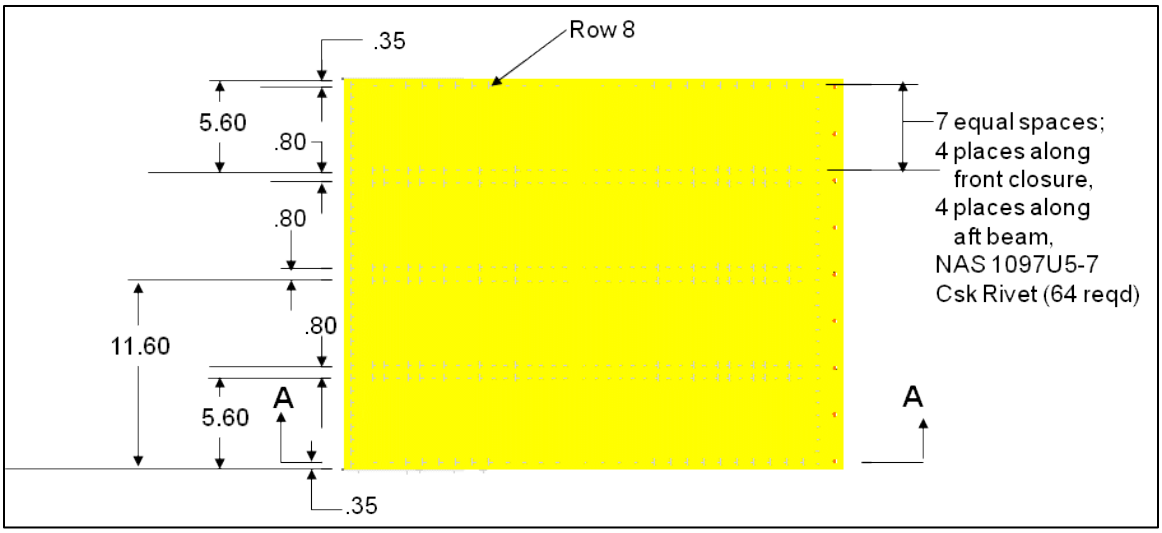

Figure F.6 – Test article skin fastener layout – drawing

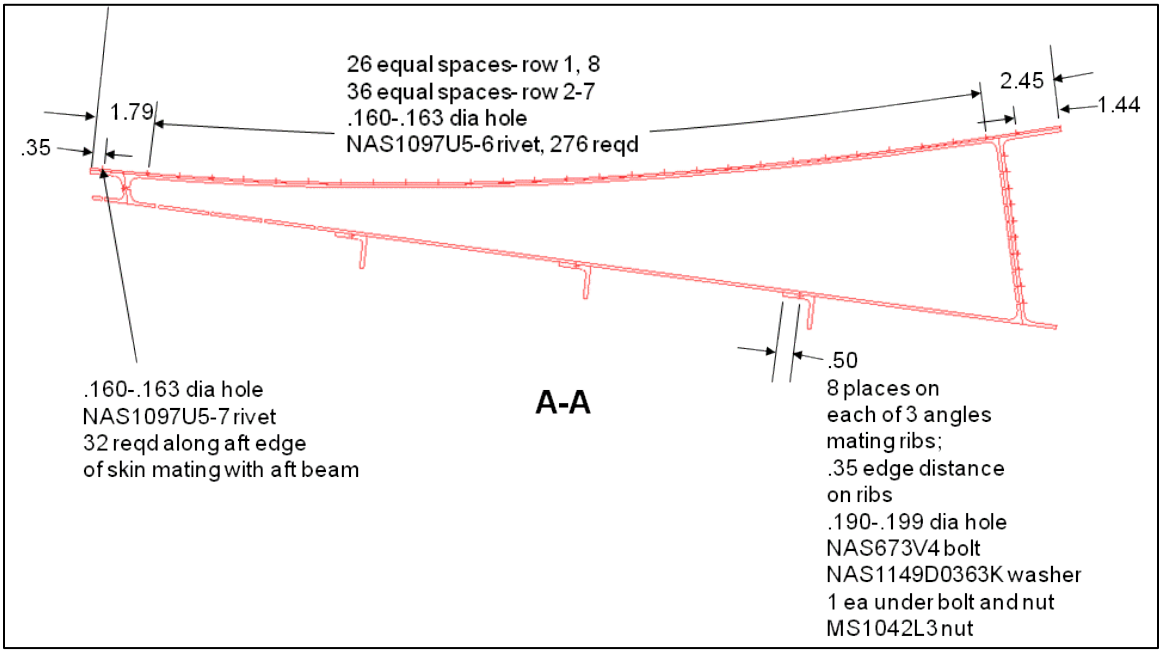

Figure F.7 – Interior rib – fastener spacing type – drawing

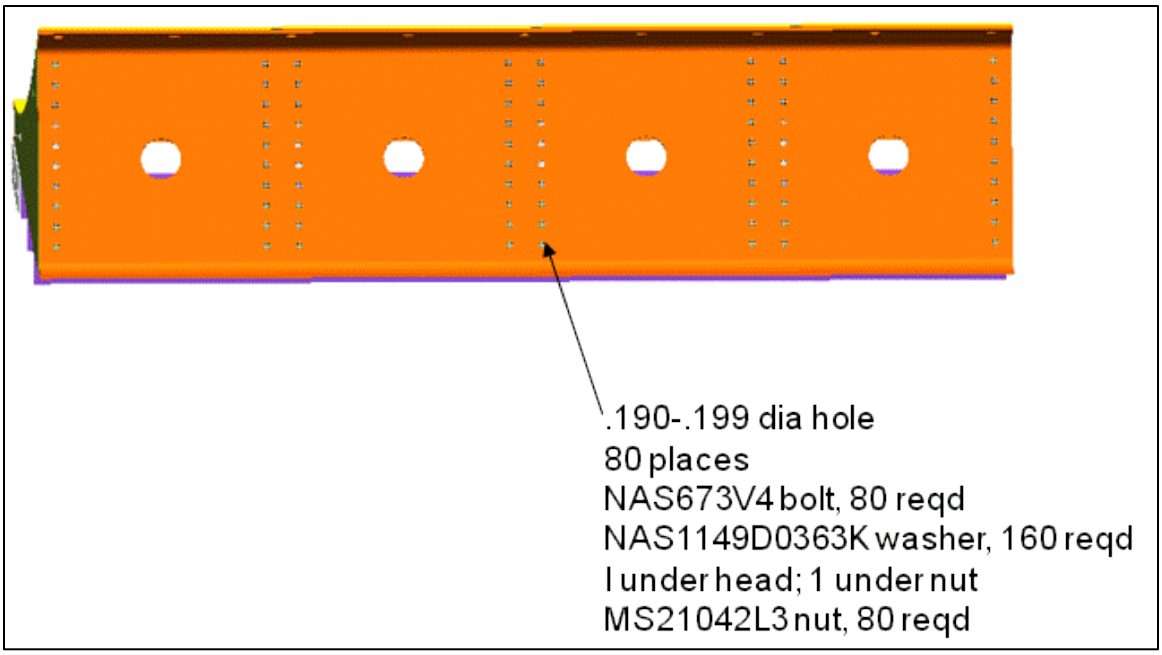

Figure F.8 – Front spar bolt hole pattern – drawing

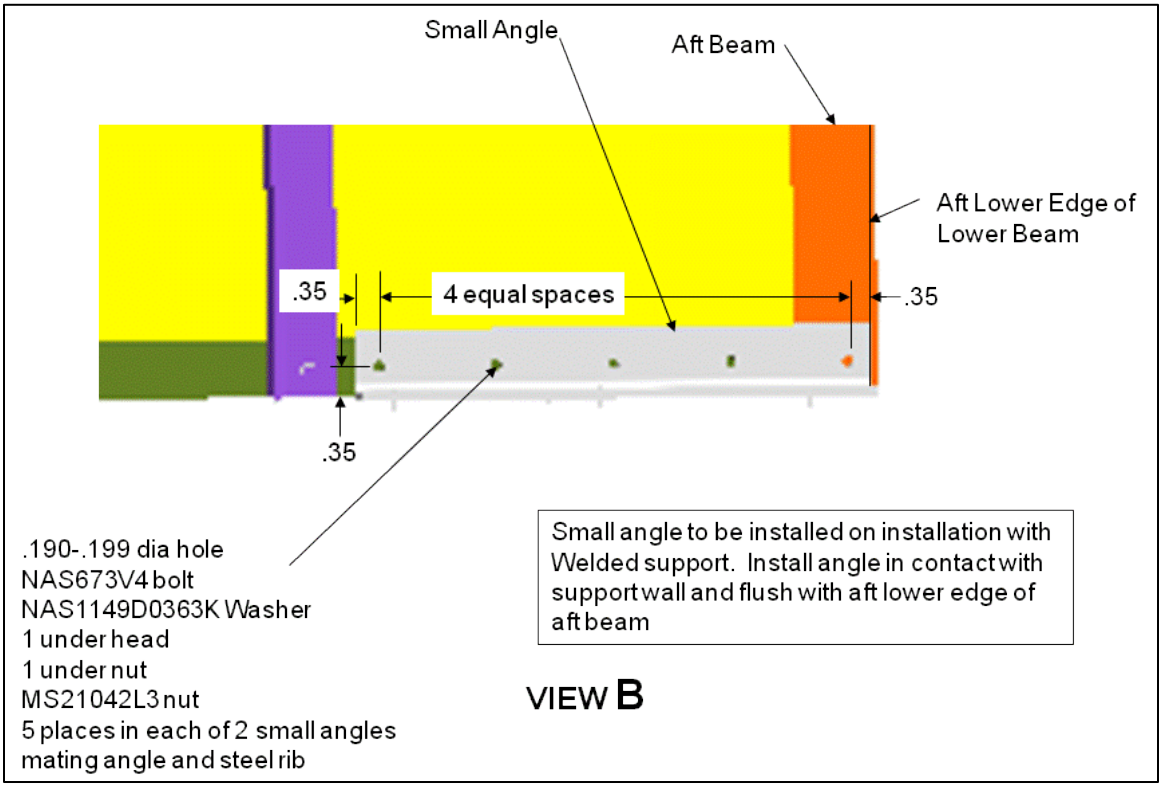

Figure F.9 – Aft support angle bolt pattern – drawing

The test fixture which supports the test article was fabricated from welded plate steel. Below is CAD model of the welded fixture. The fixture is made of 0.25 inch thick steel plate. The fixture supports the test article on 3 sides. The test article bolted on the leading edge, and both sides. The trailing edge is free, as in the actual aircraft configuration. The lower assembly of the fixture is a thick steel plate. This plate is what gets bolted to the CEAC Test Cart and the T-58 Test Stand fixtures. Below are individual parts drawings for each fixture part.

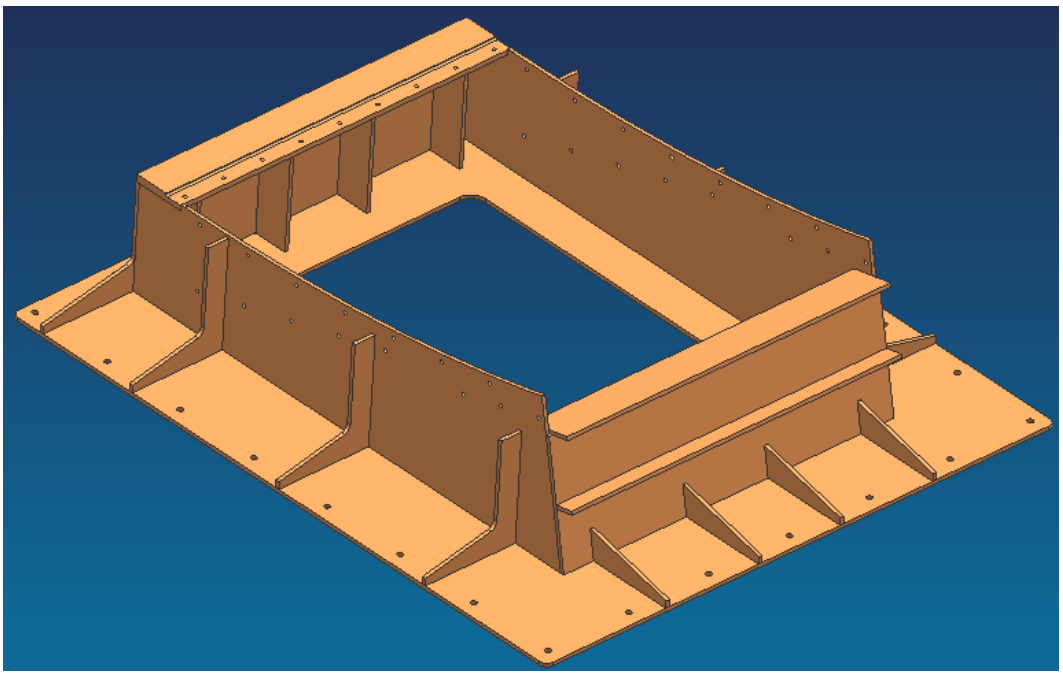

Figure F.10 – Test fixture

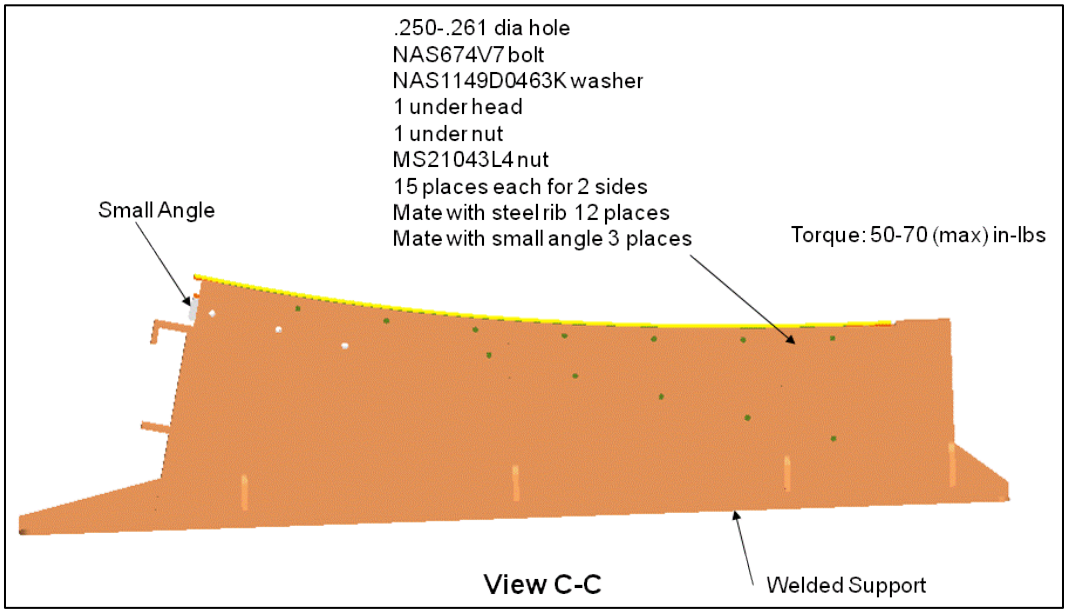

Figure F.11 – Test fixture to test article bolt pattern - drawing

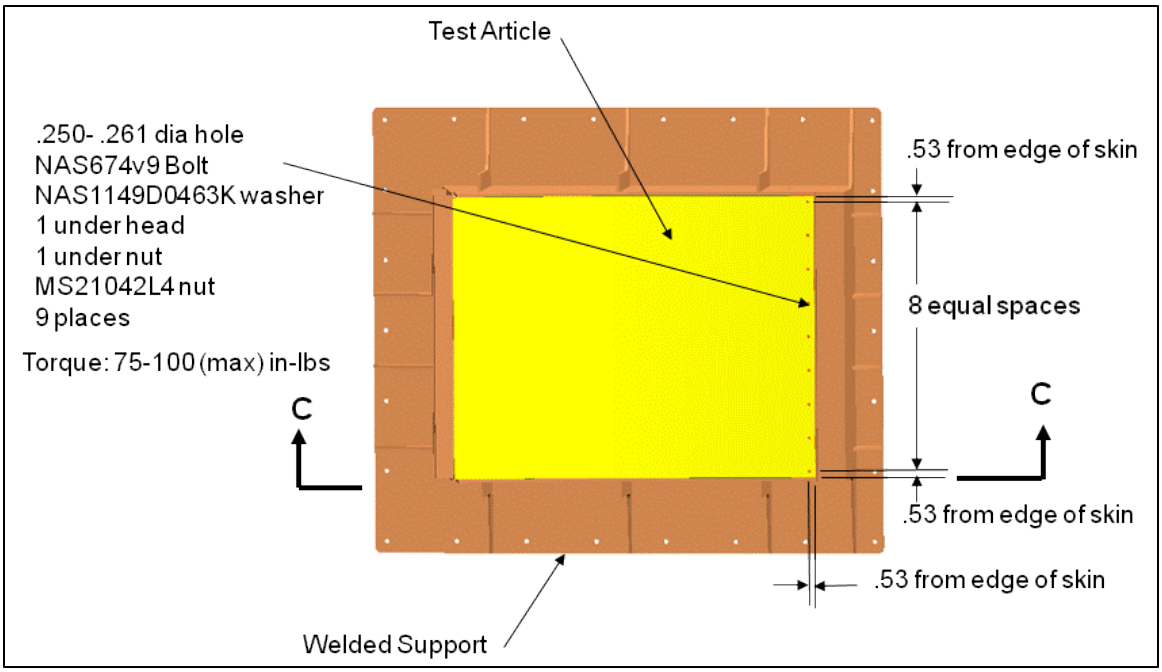

Figure F.12 – Bolt pattern to CEAC and T-58 test stands – drawing

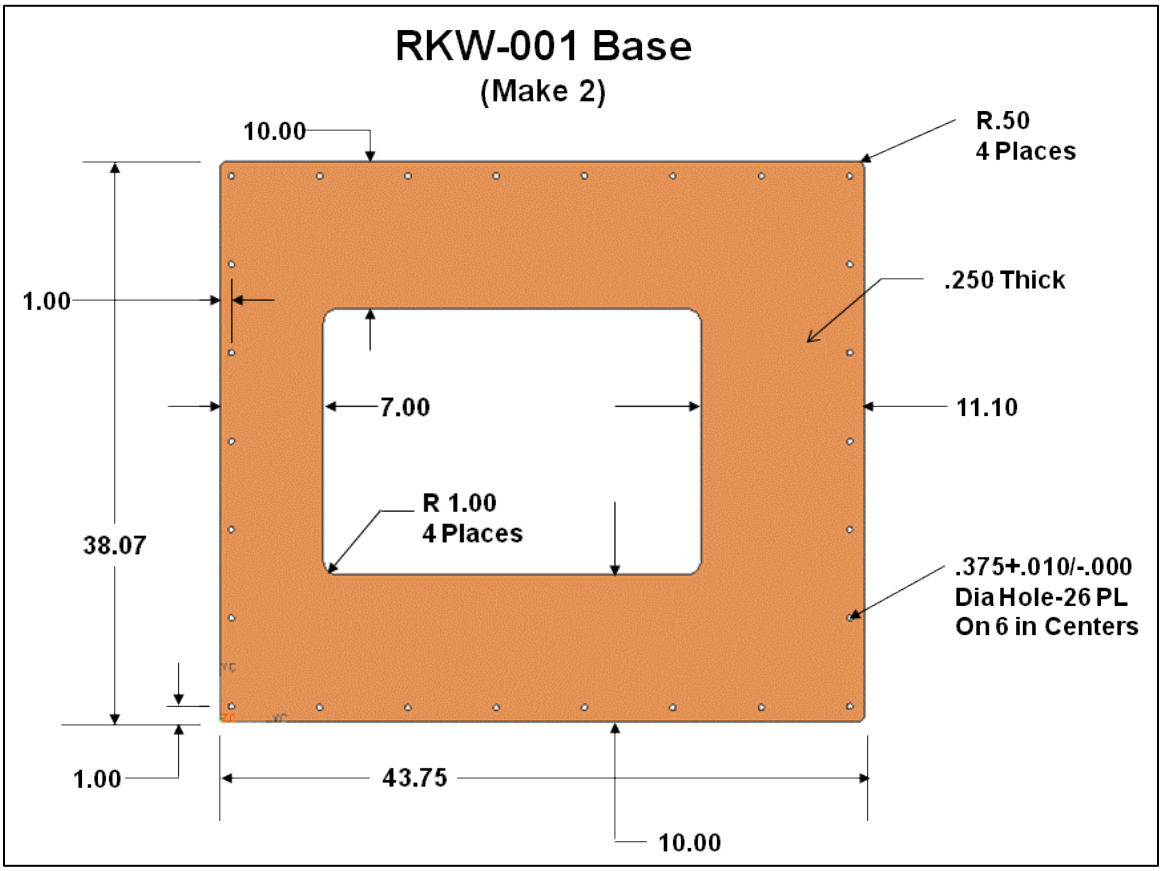

Figure F.13 – Base plate – drawing

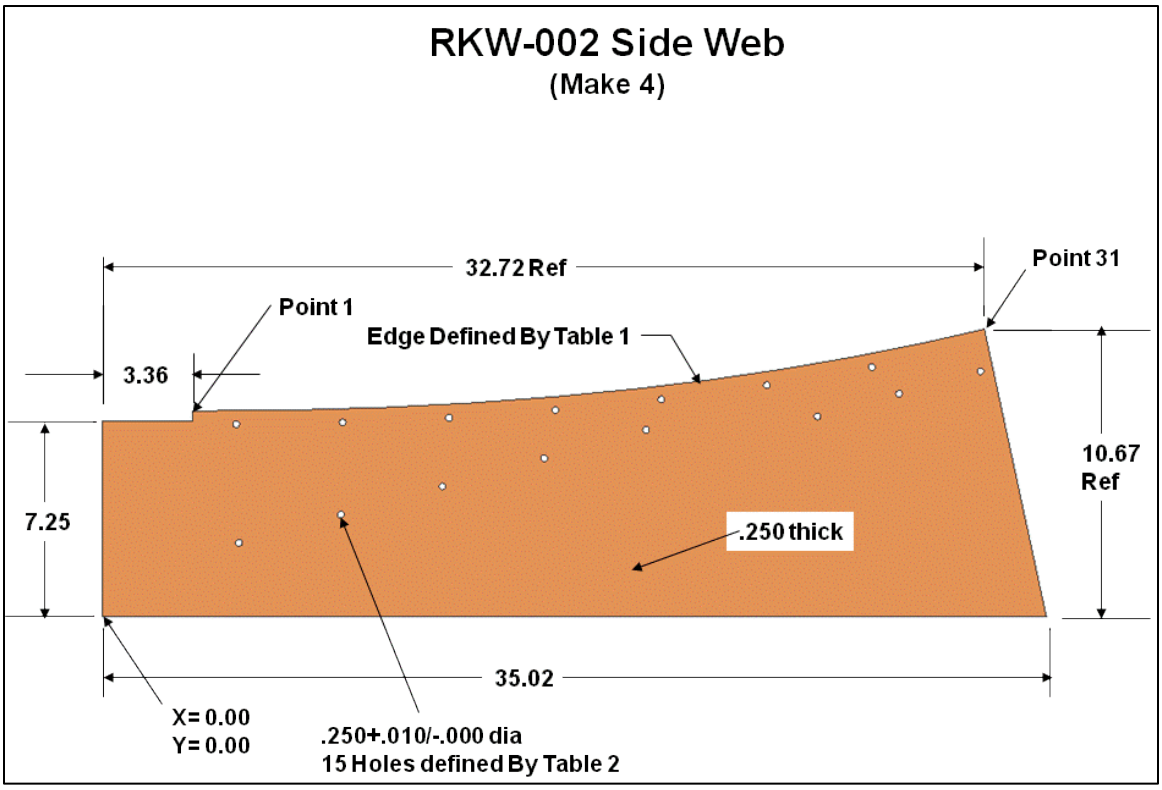

Figure F.14 – Fixture sidewall – drawing

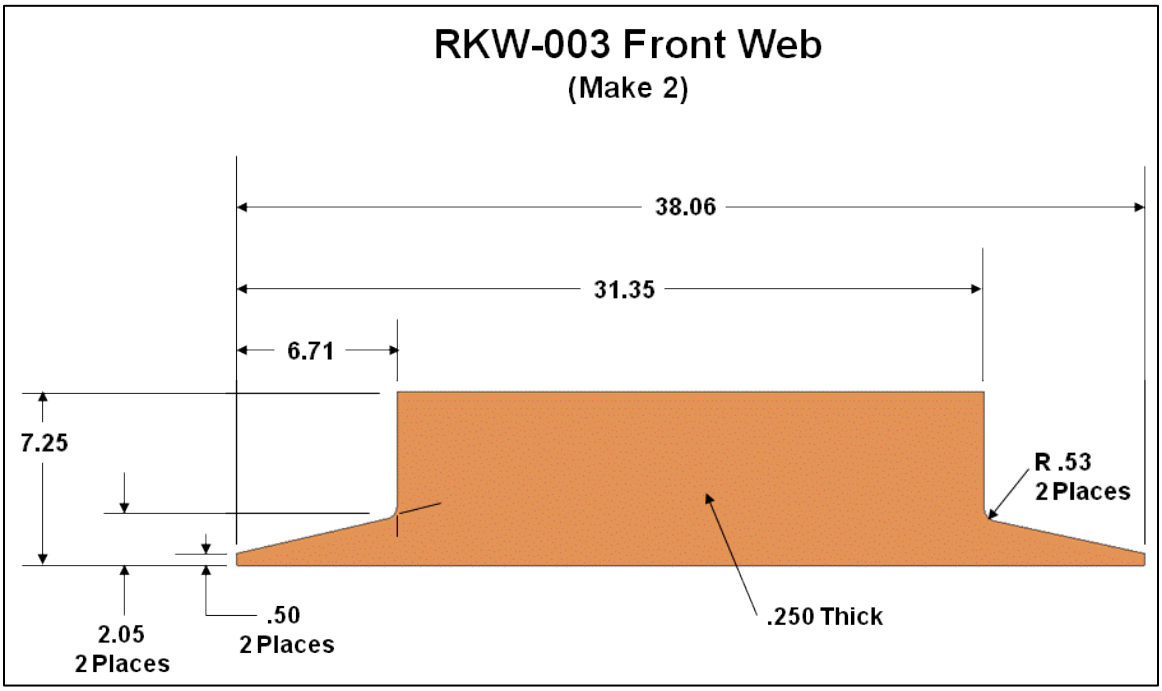

Figure F.15 – Fixture front web – drawing

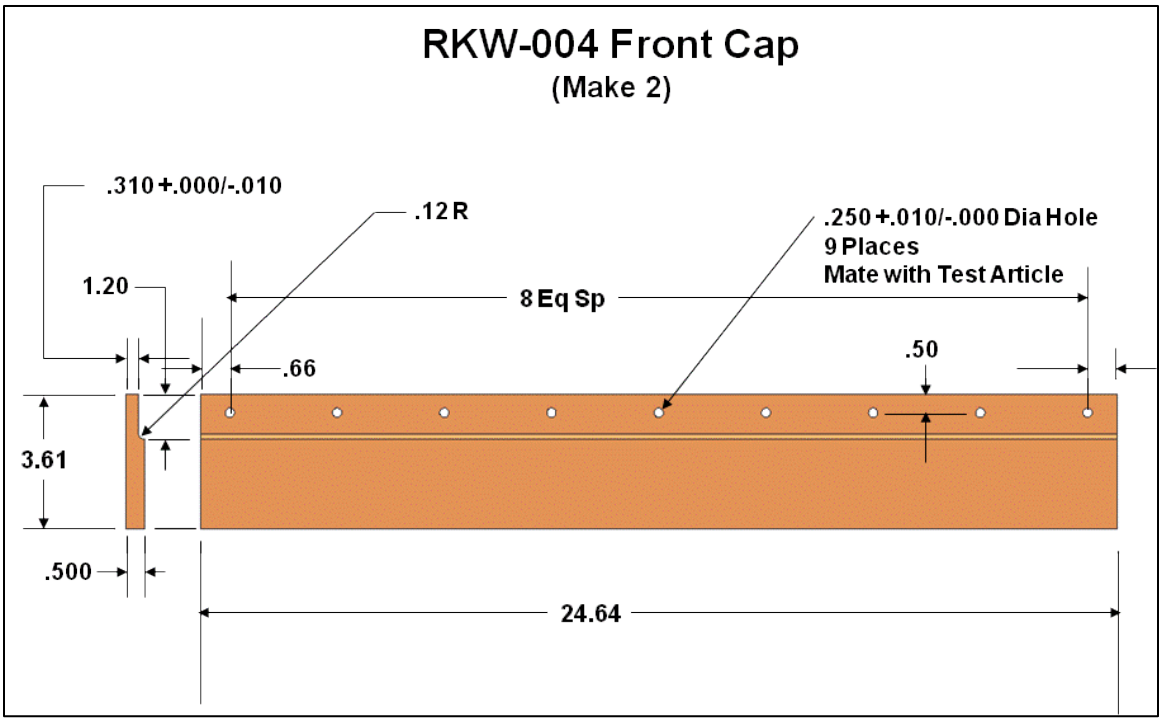

Figure F.16 – Fixture front cap – drawing

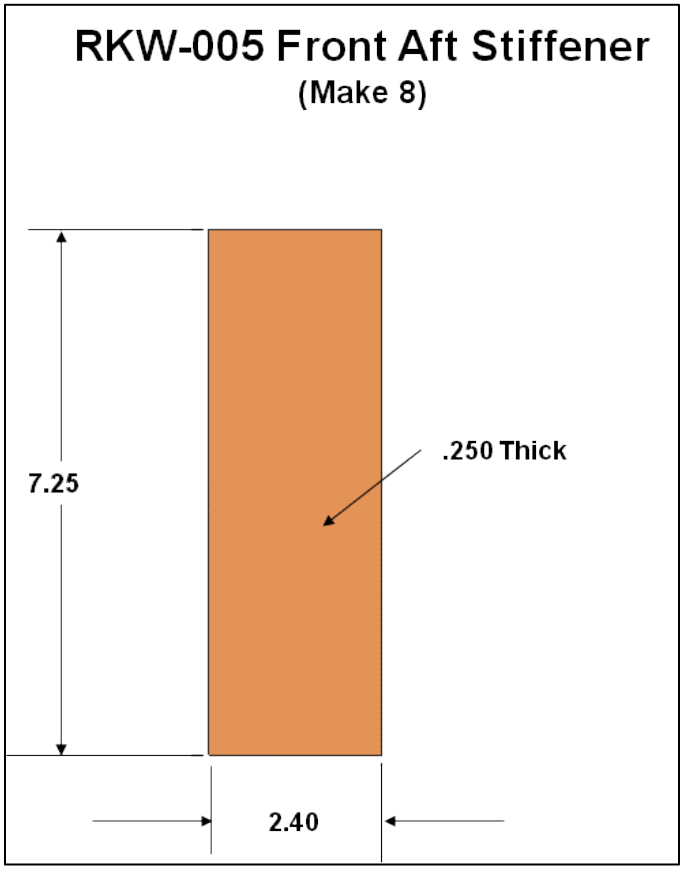

Figure F.17 – Fixture front aft stiffener – drawing

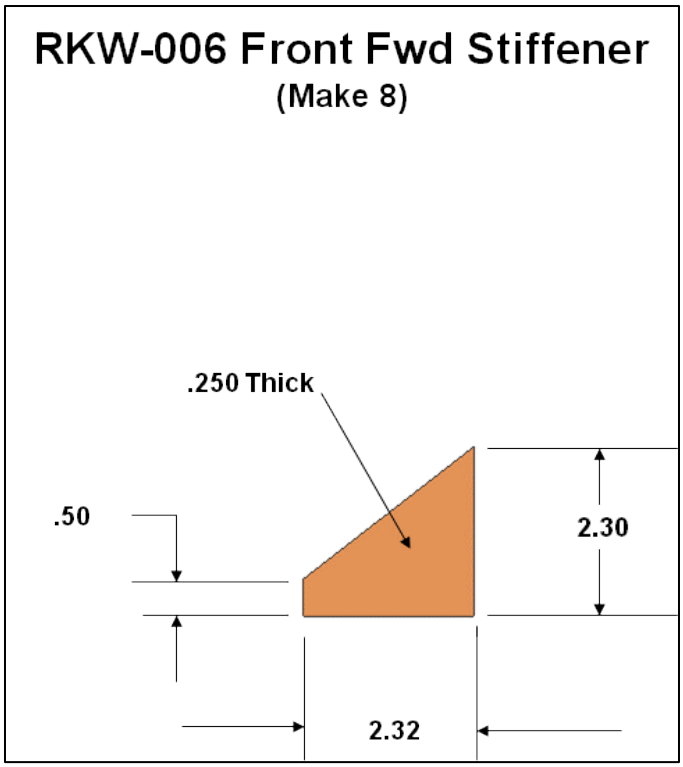

Figure F.18 – Fixture front forward stiffener – drawing

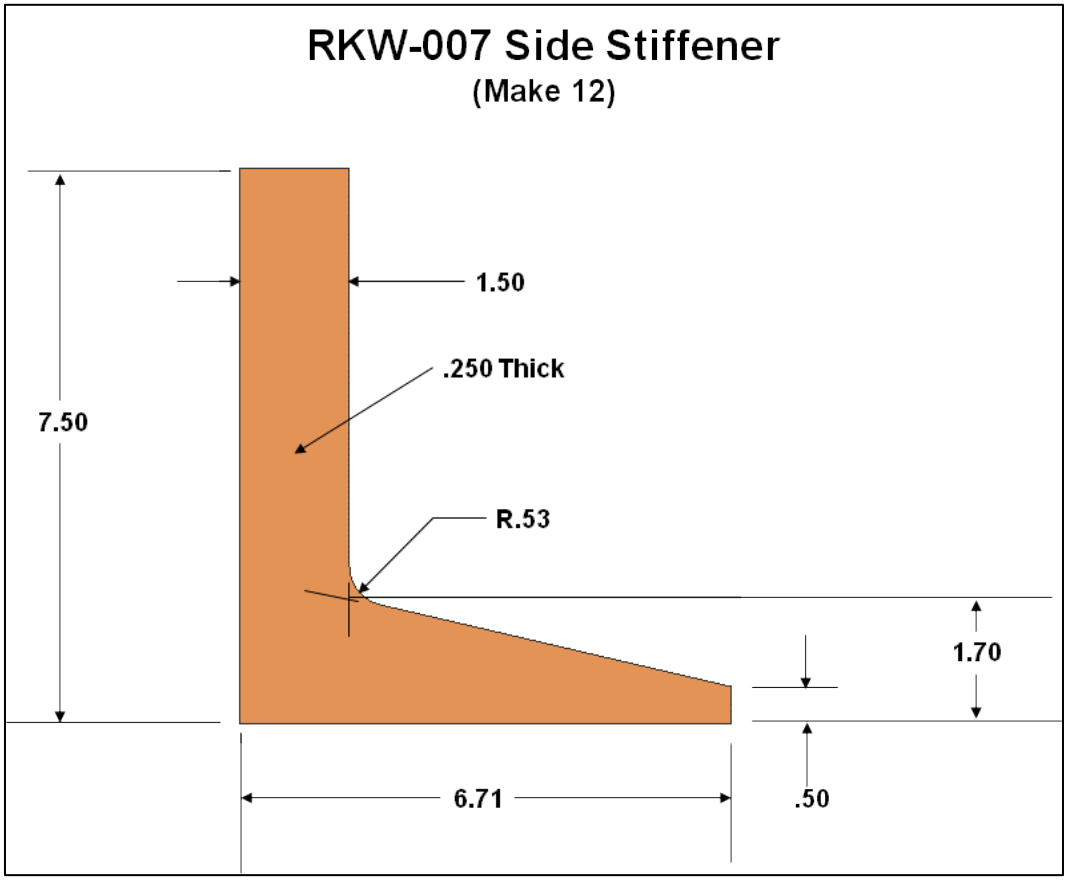

Figure F.19 – Fixture side stiffener – drawing

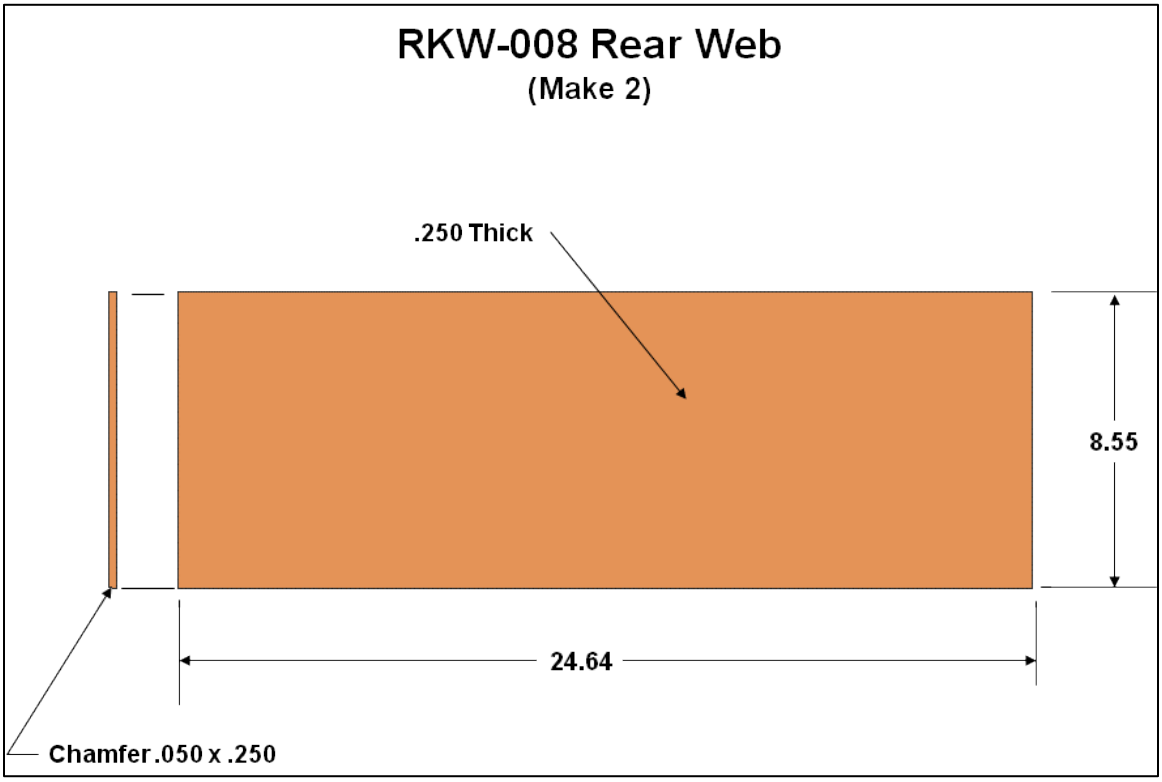

Figure F.20 – Fixture rear web – drawing

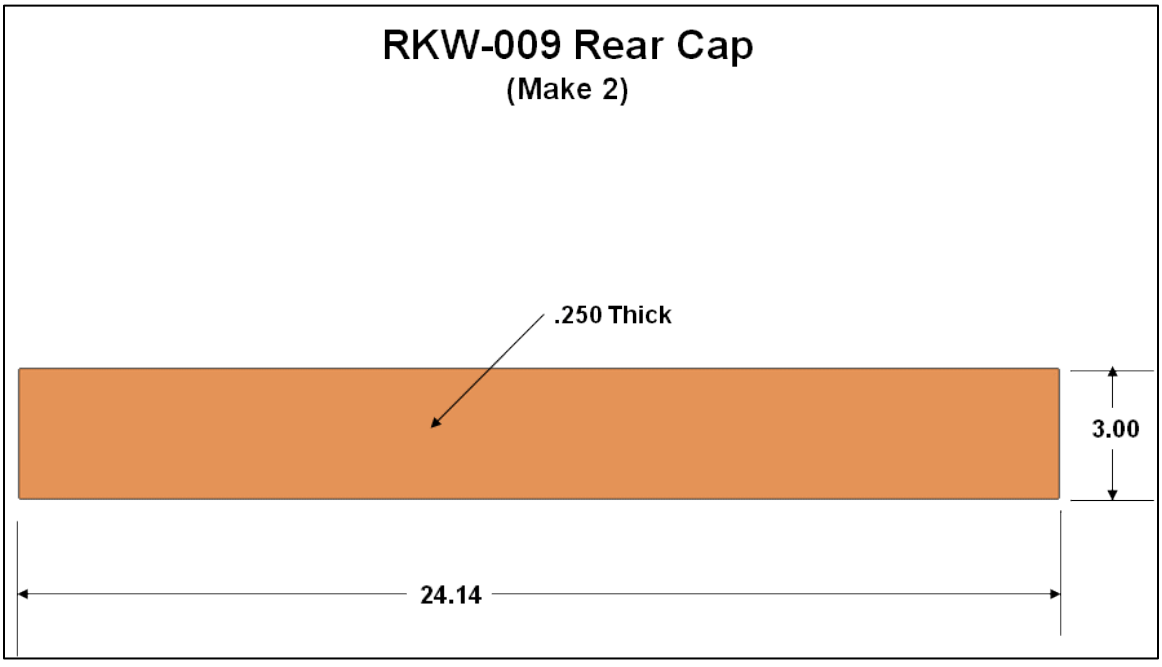

Figure F.21 – Fixture rear cap – drawing

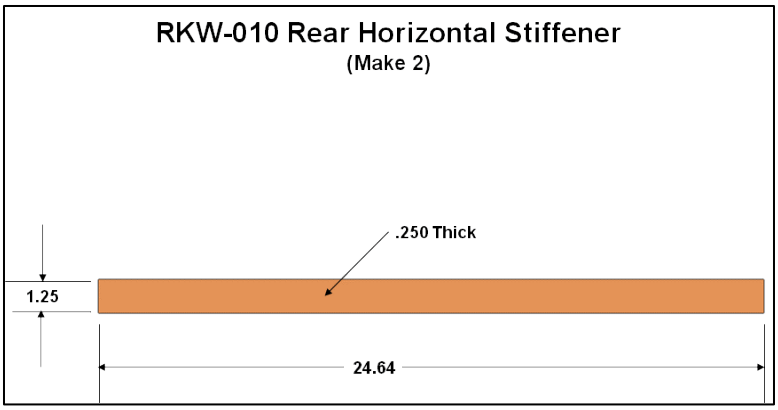

Figure F.22 – Fixture rear horizontal stiffener – drawing

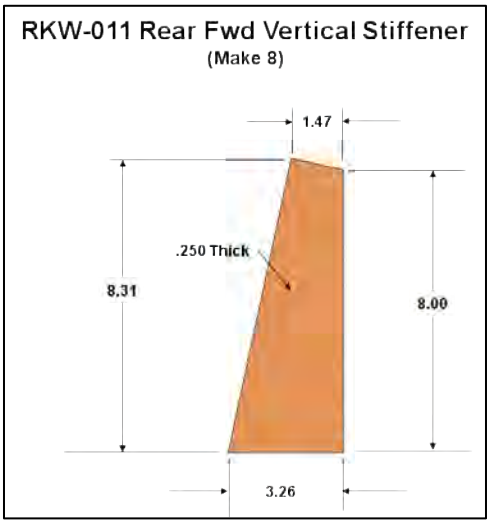

Figure F.23 – Fixture rear forward vertical stiffener – drawing

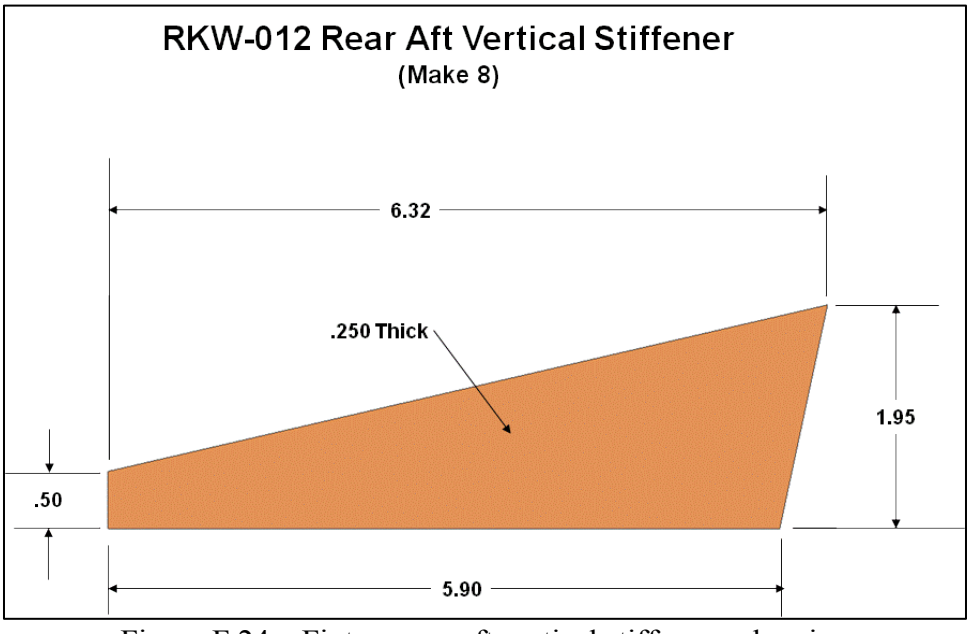

Figure F.24 – Fixture rear aft vertical stiffener – drawing

Appendix G. Testing Lessons Learned, Observations, and Recommendations

1. Why don't FEA and modal test correlate better? Pre-stress effects on mode shapes, assembly induced loads. Need to measure strain loads in assembly. Hook up strain gauges and monitor pre-load during test article assembly.
2. Make sure to use motion compensated acoustic sensors if measuring loads on a flexible surface – or use back to back transducers and measure delta pressure – motion effects cancelled out.
3. Modal testing needs to be done outside chamber, then inside chamber enclosed. Look for any chamber acoustic coupling. May need to perform analytical acoustic analysis and find the duct modes.
4. Need to measure flow velocities in chamber during acoustic runs. The flow is low ~40 mph, but this is not insignificant for heating effects.
5. Need to measure ambient air temps inside and outside chamber for heating model correlation
6. Instrumentation and wiring can cause mass and damping effects on modal response, need to take caution not to alter dynamics too much with excessive and redundant instrumentation.
7. Watch for wiring routing – place stream-wise, else it can affect heating (due to the turbulence in the flow tripping over the wiring on the panel.
8. Need weight / mass properties of test articles w/ and w/o instrumentations
9. Need some strain gauges placed back to back on skins to measure membrane loads/strains.
10. Need some thermocouples back to back on skin to measure delta temperatures and heat flux loads.
11. Need to ramp up and ramp-down heat flux/ temperatures to reduce thermal shock. Hence use thermal control.
12. Need to have temperature heating strain constraints to monitor thermal shock.
13. What happens if facility has rapid shut down at max temperature (high thermal shock)? Need to understand this facility possible failure mode affect on the test article.
14. Need to understand the cart thermal boundary condition. May need to thermally isolate cart. This is a big heat sink and test article temperature never seemed to actual reach a Steady-state.
15. Need to understand the cart dynamics. The cart dynamics were not measured through modal testing. Need to quantify the effect of cart dynamics on the response measurement at high acoustic levels.
16. Need to check all gauges after initial runs to make sure they are working – check time history, offsets, limits, PSDs,
17. Need to wring out 60Hz noise from signals. Make sure instrumentation is grounded to floor grounding cables.
18. Chamber compressor does pump out warm air. Need to make sure the test article is at steady state for zero-condition runs.
19. Compressor generates a lot of noise (140 dB), hence higher than expected baseline back ground noise – affects measurement sensitivity.
20. With compressor off, the chamber has a back flow from the exhaust. (Probably depends on outside air conditions, but this may be cool air that effects heating profile.
21. Noticed skin dynamic strain does reduce at elevated temp; this may be a thermal load effect (stiffening)?
22. Hard to control heating at low flux levels, min. test temperature is 150°F from RT ambient conditions.

23. When including substructure in the test article, this limits field of view of optical measurements. It is possible to use plexi-glass structure (or some type of IR (sapphire glass) and optically transparent material if not load bearing.)
24. IR measurements are important. RTV from wiring affects temperature gradients.
25. Need front side IR, but chamber is too narrow to get good field of view. How to expand chamber and get front and back side IR?
26. Instrumentation setup is proportional to panel size, the larger the panel, the more instrumentation is required. DAQ requirements also increase proportional. Need to consider.

Below are recommended facility needs for future extreme environment testing:

1. How to best simulate transient maneuver loading or shock oscillations effect on heating? Facility needs to control heat banks individually with separate controllers.
2. Some applications on high speed aircraft may need shaped acoustic spectrums that exceed CEAC capabilities, How to get higher loads (at low (<100Hz) and high frequency (>500Hz)?
3. Front side IR is important. The facility needs to be wider in test section to allow for a wide field view IR window on the front side. Possibly move back heat bank, add fairing and IR window.
4. Need more non-contacting instrumentation measurements. These need to be both static and high sample rate type measurements. Instrumentation effects loading and response, and need to minimize the effect and uncertainty due to contacting instrumentation.
5. Need high temp instrumentation, accelerometers are only rated to 550°F, load cells are 250°F, Flat Paks acoustic (200°F), hence need high temp transducers to 2000°F. Non-contacting may be best approach; such as, acoustic imaging and dynamic DIC.
6. Need robust equipment during high acoustic loads. The test facility acoustics level can damage cameras, lasers, computers, etc… Need robust equipment that can also survive the indirect test environment.
7. High Temp – Heating and Cooling Control to simulate trajectory loading – Do Quartz heaters have a lag? Can they simulate some transient effects – 3 deg/s temp changes.
8. Multiple independently controlled thermal zones. (Current set-up has each zone tied to same control profile with linear multiplier for each zone)
9. Since most static loads do not require real-time control, consider use of screw-jacks with in-line load cells. Adjust the screw jacks by hand until you get the desired load, lock them in-place, and then start the thermal-acoustic test (the static load is constant the whole time.)
10. Need to be able to perform high temperature modal testing, but with a thermal loading that is similar to the combined environment tests. Hence, compressor needs to be running but need to reduce noise levels.
11. Need to sample data at high rates and for a lot of channels (64 or more). Hence, high speed and large capacity data storage is needed.
12. High rate ARAMIS DIC (digital image correlation) may be a great tool for future testing to image ODS (operational deflection shapes, ID dynamic snap-through modes, etc…) But, need to acquire and transfer extremely large data files (40 gig +) and process for rapid turnaround.
13. Need to add back side static pressure for some applications (e.g. inlet structure). Internal pressure can be as high as $\Delta P = 10$psi for a fuselage application, but generally ΔP is +/-3psi or less for high speed flow (in shock zones).

14. Need to add back side heating for some applications; turbine engines, scram inlets, how to accomplish this effect without a direct quartz heat bank.
15. Some applications can have considerable mechanical (in-plane) structural loads, and how to best apply these loads in the CEAC, and make sure the equipment is not unduly affected by the acoustic/thermal loads.
16. Need to minimize the risk of a full facility shut down at high temperature, as this may cause irreparable damage to expensive test articles (also power to active cooling systems.)
17. Resolve abrupt low power thermal start-up issue. (Lamp banks have a “hard start” at lower power levels. Might be solved by not using all lamps for low power runs or by lowering gain/changing PID ratios at low power levels).
18. Closed loop signal correction for each modulator. (All 12 modulators work off the same control signal and can have small response differences. Would be nice to measure the output of each modulator before the pressure waves are mixed and adjust the input signal for each to better match the desired spectrum. This should clean up the acoustic spectrum while reducing the total power required achieving a desired noise level. Might also increase the total noise capability).

List of Acronyms, Abbreviations, and Symbols

Acronym	Description
RMS	Root Mean Square
CAA	Computational Aero-Acoustics
CEAC	Combined Environment Acoustic Chamber
CPU	Central Processing Unit
EBF	Engine Burner Facility
FEA	Finite Element Analysis
FEM	Finite Element Model(s)
LHS	Left Hand Side
RHS	Right Hand Side (in reference to terms to the equation of motion)
s-N	Stress – Cycles to Failure Data
TBL	Turbulent Boundary Layer
CSD	Cross Spectral Density
PSD	Power Spectral Density
DoF	Degrees of Freedom
IMC	Implicit Modal Condensation
BC	Boundary Condition
ROM	Reduced Order Model
NLROM	Nonlinear Reduced Order Model
NL	Nonlinear
SOL	MSC/NASTRAN Solution Sequence
EMD	Engineering Manufacturing Development
G_{rms}	RMS acceleration in units of g's
WAFO	Waves Analysis for Fatigue and Oceanography
I/O	Input / Output
ODE	Ordinary Differential Equation
PDF	Probability Density Function
V and V	Verification and Validation
POD	Proper Orthogonal Decomposition
POM	Proper Orthogonal Modes
NM	Normal Modes
POV	Proper Orthogonal Values
MAC	Modal Assurance Criteria
P/V	Peak/Valley
OML	Outer Mold-Line
IML	Inner Mold-Line

Symbol	Definition
R	R-ratio
Kt	Stress Concentration Factor
G	Gravity units equal to 386 in/s^2
Psi	Pounds per square inch
t	Skin thickness (panel or beam)
c	Nonlinear static load scalars
M	Mass matrix
K	Linear Stiffness Matrix
C	Damping Matrix
p	Modal displacements
x	Physical displacements
f	Modal Forces
F	Applied force
A	Cubic Stiffness Terms
B	Quadratic Stiffness Terms
f_n	Natural frequency (Hz)
Hz	Units of Hertz (1/second)
dB	Units of Decibels
m_0	Zero spectral moment
m_2	2^{nd} spectral moment
m_4	4^{th} spectral moment
N_{uc}	Number of upward zero crossings
N_p	Number of Peaks
ϕ	Eigenvector or Mode shape
ζ	Modal damping ratio
θ	Nonlinear stiffness terms
γ	Irregularity factor
ω	Circular frequency
σ	Standard Deviation